

**Isolating Rod Function
in the Human Eye**

A THESIS
SUBMITTED TO THE UNIVERSITY OF MANCHESTER
FOR THE DEGREE OF
DOCTOR OF PHILOSOPHY (PHD)
IN THE FACULTY OF LIFE SCIENCES

2012

Jeremiah Michael Francis Kelly

Abstract

Isolating Rod Function in the Human Eye

Jeremiah Michael Francis Kelly PhD candidate

December 2012

The first chapter explains the motivation for measuring rod function, in particular the rod's dynamic recovery from a substantial bleach which results in so-called 'rate limited' recovery of sensitivity. The physiological processes that underpin the replenishment of the rod photopigment are described and discussed, and explain the way in which rod function can act as a marker for retinal health. Overall, this chapter explains why rod function is worthy of further investigation.

Then follows a description of the experimental methods used in the study of rod function, presented in later chapters. The psychophysical procedures are described and a new method of dark adaptation measurement is presented. The key feature of this technique is a red background.

Nonlinear mathematical models are used to describe the reduction in visual thresholds with time following a bleach. Chapter three describes the difficulties associated with numerical methods of nonlinear regression and presents a novel, multi-start algorithm that extracts the parameters of interest from a model that adequately describes dark adaptation in the healthy normal subject.

Chapter 4 verifies the algorithm presented in chapter 3, which is shown to be reliable and robust. A series of numerical experiments are performed to evaluate some of the characteristics of the algorithm's performance.

In chapter five, a series of experiments are presented to investigate the possible effect of a luminous background on dark adaptation (DA). The first experiment tests whether the rod system can detect a dim red background and the second, whether the rod thresholds, when measured against light emitted by a red light emitting diode (LED), were linear. The third explores whether the background had any effect on the recovery of rod sensitivity. Finally, conventional contrast sensitivity is used to investigate the recovery from a photo bleach.

A novel laboratory-based apparatus was used to measure dark adaptation in a group of 36 subjects and the results of these measurements are presented in chapter six. The aim here was to see if the data collected were comparable with the dark adaptation data in the literature. These subjects were asked to make two visits so that an assessment of the test retest reliability of the method could be made. The method is shown to be reliable and capable of characterising the recovery of the visual system after a photo bleach.

Although inherently flexible the analogue apparatus was prone to subject driven variability. Greater consistency of measurement was achieved using a digital device developed in partnership with an industry partner, Elektron (UK). This device, described in chapter seven provided fine control of many of the experimental parameters. It was used to measure the dark adaptation of a young healthy group of 21 people.

This study uses new methodological approaches, both experimental and statistical, that are robust and reliable to facilitate investigation of rod function, and presents new find-

ings about the early phase of rod sensitivity recovery.

Declaration

No portion of the work referred to in the thesis has been submitted in support of an application for another degree or qualification of this or any other university or other institute of learning.

Copyright Statement

1. The author of this thesis (including any appendices and/or schedules to this thesis) owns certain copyright or related rights in it (the Copyright) and s/he has given The University of Manchester certain rights to use such Copyright, including for administrative purposes.
2. Copies of this thesis, either in full or in extracts and whether in hard or electronic copy, may be made only in accordance with the Copyright, Designs and Patents Act 1988 (as amended) and regulations issued under it or, where appropriate, in accordance with licensing agreements which the University has from time to time. This page must form part of any such copies made.
3. The ownership of certain Copyright, patents, designs, trade marks and other intellectual property (the Intellectual Property) and any reproductions of copyright works in the thesis, for example graphs and tables (Reproductions), which may be described in this thesis, may not be owned by the author and may be owned by third parties. Such Intellectual Property and Reproductions cannot and must not be made available for use without the prior written permission of the owner(s) of the relevant Intellectual Property and/or Reproductions.
4. Further information on the conditions under which disclosure, publication and commercialisation of this thesis, the Copyright and any Intellectual Property and/or Reproductions described in it may take place is available in the University IP Policy (see <http://www.campus.manchester.ac.uk/medialibrary/policies/intellectual-property.pdf>), in any relevant Thesis restriction declarations deposited in the University Library, The University Library's regulations (see <http://www.manchester.ac.uk/library/aboutus/regulations>) and in The University's policy on presentation of Theses

Acknowledgements

I am very grateful to Dr Ian Murray and Mr David Carden for their help, encouragement and insight.

I am thankful to Drs Maria Makridaki, Athanosios Panorgias and Humza Tahir for helping me with my ideas and thoughts as well as acting as subjects during the many calibration trials. Dr Makridaki also made her raw data available and allowed me to re-analyse it, providing an excellent opportunity to benchmark the multi start algorithm. I am especially indebted to Dr Tahir for his help with the construction of the analogue apparatus.

I would like to thank Professor Henson for his helpful comments on the literature review, which formed the basis for the introduction presented here.

I am fortunate to have been funded in this research by The College of Optometrists.

The distributed computing component of this research was achieved using the High Throughput Computing facility of the Faculty of Engineering and Physical Sciences, The University of Manchester. I would particularly like to thank Mike Croucher for his help.

The measurement of scotopic contrast sensitivity would not have been as trouble free or as enjoyable without the hard work of Mariá Cinta Puell of the School of Optics and Optometry, Complutense University, Madrid.

Stephen Lackovic of Hartest Precision Instruments was responsible for the firmware and software in the digital adaptometer and was always helpful and open to new ideas.

Dr Vincent Nourrit suggested I might enjoy using \LaTeX .

The Eurolens team especially Tracey Burgoyne, Andy Plowright and Dr Michael Read were very supportive, providing a rare coffee (1) and numerous encouraging nods while I moaned.

My sister Deborah and my wife Louise have always been encouraging.

None of the work presented here could have been done without the help of the people mentioned above, but, it is to my sons that I am most grateful. The time spent on this study could have been spent with my boys. Their patience, indulgence, forgiveness and understanding has made me both proud and humble. Proud to be the father of such fine young men, and humbled by their graciousness, Joseph and Samuel, thank you.

Dedication

For my sister Violet,
a flower ever close to my heart.

Contents

1	Rod Mediated Vision: Biophysics to Psychophysics	18
1.1	Introduction	18
1.2	Photoreceptors	20
1.2.1	How are rods and cones distributed?	21
1.2.2	Morphology	23
1.2.3	Cones and rods compared	24
1.3	Rods and the Retinal Pigment Epithelium	27
1.3.1	Rod outer segments	28
1.3.2	Inner segment, cell body and synapse	28
1.3.3	Retinal Pigment Epithelium	29
1.3.4	Bruch's membrane	32
1.3.5	Perfusion of the Retina	34
1.3.6	Between the rod and the RPE	35
1.3.7	Relationship between rods and RPE and the effects of ageing	35
1.4	Rhodopsin	37
1.4.1	Phototransduction	37
1.4.2	Steady state light and the role of the retinoid cycle	40
1.4.3	Summary of rhodopsin	41
1.5	Rhodopsin regeneration	42
1.5.1	Sensitivity control under varying light levels	42
1.5.2	Characteristics of dark adaptation	43
1.5.3	Models	45
1.5.4	The Mahroo, Lamb and Pugh Model (MLP)	46
1.6	Conclusion	50
1.7	Aims of the study	51
2	Experimental methods	52
2	Introduction	52
2.1	Subjects and ethics	54
2.2	Analogue technique	54
2.3	Calibration of the Analogue Device	59
2.3.1	Investigation of the characteristics of the light sources	60
2.3.2	Spectral Description of the Sources	63
2.3.3	Summary	67
2.3.4	LED Noise and an Ideal LED	68
2.3.5	Pre-set target screen luminance levels	77
2.3.6	Calibration of the Green LED	77

2.3.7	LED emittance spectra: a summary	79
2.4	Determination of flicker frequency	80
2.5	Flash gun calibration	81
2.5.1	Pre-calibration of the flash measurement set up	81
2.5.2	Flash calibration	85
2.5.3	Flash linearity	86
2.6	Digital device	91
2.6.1	Description	91
2.6.2	Initialisation	95
2.6.3	Experimental procedure	95
2.6.4	Verification of the digital dark adaptometer	96
2.7	Psychophysical methods	99
2.7.1	Method of limits	99
2.7.2	Constant stimuli	99
2.7.3	Method of adjustment	99
2.8	Measuring contrast sensitivity at low luminance	100
2.8.1	Definitions of contrast	100
2.8.2	Apparatus	100
2.8.3	Calibration of the screen	100
2.8.4	Experimental design	102
2.8.5	Subjects	103
2.8.6	Procedure	103
2.8.7	Model	104
2.9	Summary and outstanding issues	105
2.9.1	Detectability of red LED by rods	105
3	The Normal Dark Adaptation Function: curve fitting and modelling	107
3.1	Introduction	107
3.1.1	Fitting a model to experimental data	109
3.1.2	Variability in psychophysical data	112
3.2	Model selection	114
3.2.1	Model selection using the extra sum of squares test	115
3.2.2	Model selection using information theory	115
3.3	Methods of parameter extraction	116
3.3.1	Analytical methods	117
3.3.2	Direct search methods	119
3.4	Extraction of the Parameters	123
3.4.1	Algorithm Implementation in Matlab	124
3.5	Summary	127
4	Evaluation of an Algorithm by a Series of Numerical Experiments	128
4.1	Introduction	128
4.1.1	Aims	129
4.2	Test data and the effect of noise	129
4.2.1	Method	130
4.2.2	Results from the verification of the Matlab script	134
4.2.3	Discussion of Matlab scripts' parameter estimates	138
4.3	Calculation of confidence intervals for the slope of S2	138

4.4	Selection of starting points	139
4.4.1	Method	140
4.4.2	Comparison of objective and subjective methods	140
4.5	Summary	144
4.6	Supporting paper	145
5	The Effect of Background Luminance on Rod Sensitivity Recovery	146
5.1	Introduction	146
5.1.1	Changing the background affects the threshold increment	148
5.1.2	How might cones influence rods?	149
5.1.3	Psychophysical evidence of cone-rod interaction	150
5.1.4	Anatomical evidence of cone-rod interaction	151
5.1.5	Effect of cone-rod interaction	154
5.1.6	Rod cone interaction and contrast sensitivity	154
5.1.7	In summary	156
5.1.8	Aims	156
5.2	Method	157
5.2.1	Experiment 1: Is the background detectable by the rod system?	157
5.2.2	Experiment 2: Linearity of response with dim backgrounds	158
5.2.3	Experiment 3: The slope of the S2 phase for backgrounds of different luminance	159
5.2.4	Experiment 4: The recovery of scotopic contrast sensitivity	160
5.3	Results	161
5.3.1	Experiment 1: Is the red background detectable by the rod system?	161
5.3.2	Experiment 2: Linearity of the rod system response	162
5.3.3	Experiment 3: The slope of the S2 phase as background luminance changes and wavelength remains fixed	164
5.3.4	Experiment 4: The recovery of scotopic contrast sensitivity	165
5.3.5	Contrast sensitivity recovery using a long wavelength stimulus	168
5.4	Discussion of the four experiments	169
5.4.1	Summary	171
6	Analogue Device to Measure Dark Adaptation	172
6.1	Introduction	172
6.2	Method	175
6.2.1	Subjects	175
6.3	Results	176
6.3.1	Repeated measures	178
6.3.2	Test Retest	184
6.3.3	Summary of dark adaptation recovery parameters	185
6.3.4	The slope of the rod recovery S2: θ_4	186
6.3.5	The cone - rod break point: θ_5 (α)	187
6.3.6	The slope of the rod recovery S3: θ_6	189
6.3.7	The rod-rod transition point: θ_7 (β)	189
6.3.8	Absolute threshold	190
6.3.9	Mean squared error of the data to the fitted model	193
6.3.10	Potential outliers	194
6.4	Variability of data	197

6.4.1	Variance of residuals	198
6.4.2	Autocorrelation data	199
6.4.3	Model selection	201
6.5	Discussion and summary	204
6.5.1	Further work	205
7	A Digital Device to Measure Dark Adaptation	207
7.1	Introduction	207
7.1.1	Aims	208
7.2	Methods	208
7.2.1	Description of the device	208
7.2.2	Measurement technique	210
7.2.3	Data analysis	210
7.2.4	Subjects	211
7.3	Results	213
7.3.1	Parameters of dark adaptation and age	217
7.3.2	Comparison of noise in the data	223
7.3.3	Summary of parameter analysis	223
7.4	Effect of ramp time on data collection	225
7.5	Discussion	227
7.5.1	Further work	229
8	Discussion	231
8.1	The aims of the study	231
8.2	Main findings	232
8.2.1	Technology	232
8.2.2	Data analysis and mathematical methods	234
8.2.3	The effect of the red background revisited	237
	Bibliography	239
	Appendix	253
A	Computer Code	253
A.1	Matlab code	253
A.1.1	Numerical Experiment Code	257
A.1.2	Batch Processing	262
A.1.3	Scotopic Contrast Sensitivity	264
A.2	R code	274
A.2.1	Code listing	275
A.2.2	A method of model selection based on AIC_c values	276
A.2.3	A standard observer of the digital device	279
A.3	Shell Scripts and Condor	283
B	Further results from numerical experiment	286
C	Bootstrap Methodology and application	289
C.1	Bootstrap calculation of confidence intervals	289
C.1.1	Results	293

D Analytically derived CI are wrong	297
D.1 A pragmatic approach in R	297
D.2 Comparison of bootstrap quantiles with R SE	298
D.3 The assumption of linearity	301
E Electronic Circuit Diagrams	303
E.1 Analogue Dark Adaptometer	303
E.2 Digital Dark Adaptometer	303
F Scotopic Contrast Sensitivity Results	306
F.1 Parameter values from a bi exponential model	306
G Raw Data from Analogue Apparatus	308
G.1 Plots of raw data, with fitted curves	308
G.1.1 Comments on individual plots	308
G.2 Parameter Values for each Subject at each Visit	308
G.3 Model Fitting using Information Theory	308
H Supplementary Data for the Digital Apparatus	325
H.1 Experimental Parameter Files	325
H.2 Dark Adaptation Parameter Estimates	326
I Supporting papers	327
I.1 Confidence Intervals for Dark Adaptation via Model Comparison	327
I.2 Recovery of spatial contrast thresholds following a bleach; cone and rod components	327
I.3 A computer-based technique for assessing rod dark adaptation; age changes, data quality and reproducibility	327
J Ethical approval	363
J.1 Application for Ethical Oversight	363
J.2 Subject Information	363
J.3 Subject Consent	363
J.4 Subject Advertisement	363

Word Count 97370

List of Figures

1	Rod Mediated Vision	18
1.1.1	The Macula	19
1.2.1	Cone Density at the Fovea	21
1.2.2	Rod and Cone Count	22
1.2.3	The Change in Cone and Rod Density	23
1.2.4	Retina 9.5mm from the Fovea	24
1.2.5	CIE Human Luminous Efficiency	25
1.3.1	The Photoreceptors	27
1.3.2	RPE functions	31
1.3.3	Rod Choroid complex	33
1.3.4	The Effect of Ageing on the Rod-Choroid Complex	36
1.4.1	Conformational Changes in Rhodopsin	38
1.4.2	Phototransduction	39
1.4.3	The Retinoid Cycle	41
1.5.1	Threshold versus Intensity Curve for Rods	43
1.5.2	Dark Adaptation Recovery	44
1.5.3	Dark Adaptation Recovery Curves for a Series of Bleaches	47
1.5.4	Reduced Retinoid Cycle	48
1.5.5	Model Fitted to Dark Adaptation Data	49
2	Physical Methods and Apparatus	52
2.2.1	The analogue apparatus	55
	(a) Schematic of analogue apparatus	55
	(b) Photograph of analogue apparatus	55
2.2.2	Subject's view of Analogue Device	57
2.3.1	Characterisation of the LED light sources	61
2.3.2	Variation of optical density in a broadband diffuser against wavelength	62
2.3.3	Spectral Radiance of LEDs	63
2.3.4	Photopic luminance of the LEDs used in the test display	65
2.3.5	Scotopic luminance of the LEDs used in the test display	66
2.3.6	The spectral output of a series of narrow band filters	70
2.3.7	Linear plots of the optical density	72
2.3.8	Gaussian function fitted to the PR1500 data	76
2.3.9	Comparison of the red LED to an ideal LED	77
2.3.10	Calibration of the green LED	78
2.4.1	Flicker sensitivity log-log plot for subject aged 46 years	80

2.5.1	Apparatus to calibrate the Flashgun	82
2.5.2	Radiometric to photometric linearity	83
2.5.3	Relationship between radiometric reading and output voltage	84
2.5.4	Eight traces from flash setting 1/1	85
2.5.5	The relationship between area under the signal spike and the flash setting	87
2.5.6	The variation in spike for each flash setting.	88
2.6.1	The digital dark adaptometer	91
2.6.2	The target board of the digital dark adaptometer	93
2.6.3	The operation screen	94
2.6.4	The calibration screen	95
2.6.5	Linearity of LEDs for varying voltages	97
2.6.6	Change in the LED intensity	98
2.8.1	Contrast calibration screen, not to scale.	101
2.8.2	Contrast as a function of look up table.	102
2.8.3	How the parameters of the bi exponential model	104
3	The Normal Dark Adaptation Function	107
3.1.1	Difficulty of parameter estimation	108
	(a) Raw data collected for a young subject.	108
	(b) Raw data collected for an older subject.	108
3.1.2	The seven-parameter model	110
3.2.1	A series of nested models to represent the recovery of sensitivity.	116
3.3.1	Comparison of logistic to step function	118
3.3.2	The Nelder Mead Simplex Method	121
4	Evaluation of an Algorithm by a Series of Numerical Experiments	128
4.2.1	A summary of the numerical experiment	131
4.2.2	Illustration of Test Data	132
4.2.3	Histograms of the parameter estimates of the S2 phase	136
4.2.4	Changes in the estimate of the slope S2 as input noise varies.	137
4.4.1	The distribution of the values of S2	141
4.4.2	Measures of agreement, Equality	142
4.4.3	Measures of agreement, BA	143
5	The Effect of Background Luminance	146
5.1.1	The effect of the red background	147
5.1.2	The principle of the red background	148
5.1.3	Threshold versus intensity	149
5.1.4	Summary of the rod pathway	153
5.1.5	Rods influence cone flicker thresholds	154
5.3.1	Threshold elevation in the dark adapted eye for differing wavelengths and scotopic intensities	161
5.3.2	Threshold versus Intensity for series of backgrounds	163
5.3.3	Slope of the S2 phase against background luminance	165
5.3.4	Slope of the S2 phase for increasing background luminance	166
5.3.5	Contrast sensitivity recovery following photo bleach.	167

5.3.6	Contrast sensitivity recovery following photo bleach.	168
5.3.7	Recovery of scotopic sensitivity for a red stimulus.	169
6	Analogue Device to Measure Dark Adaptation	172
6.1.1	The principle of the red background	174
6.2.1	Age distribution of subjects	176
6.3.1	Summary of the data collected using the analogue device	177
6.3.2	Individual plots of data collected at the first visit.	179
6.3.3	Data of subjects who returned for a second visit.	180
6.3.4	A histogram of the values of the slope of the S2	181
6.3.5	Comparison of the two estimates of the slope of the S2 phase	182
6.3.6	Bland Altman plot of two estimates of S2.	183
6.3.7	Distribution of S2 with ‘box and whisker’ plot overlaid.	187
6.3.8	The effect of age on S2.	188
6.3.9	Box and whisker plots of Cone Rod Breakpoint	189
6.3.10	Distribution of calculated threshold at the rod-rod transition time.	191
6.3.11	Post β thresholds	192
6.3.12	Box and whisker plots of Mean Squared Error	194
6.3.13	Detail of cone threshold outliers	195
6.3.14	Detail of cone phase for subjects with extreme cone coefficients	197
6.4.1	Auto correlation count against time interval between thresholds	200
6.4.2	Liberal classification of data	202
6.4.3	Conservative classification of data	203
7	A Digital Device to Measure Dark Adaptation	207
7.2.1	Digital Device	210
7.2.2	A schematic view of the target board	211
7.2.3	Age distribution of recruited subjects.	212
7.2.4	Data from subject 18, excluded for reasons discussed in the text.	213
7.3.1	Summary of all data	215
7.3.2	Individual plots for each subject.	216
7.3.3	Summary histograms of the age and parameters of dark adaptation	218
7.3.4	Boxplot comparison of the cone phase parameters	219
7.3.5	Boxplot comparison of the S2 phase of rod sensitivity recovery	220
7.3.6	Boxplot comparison of the S3 phases	222
7.3.7	Threshold after the rod-rod transition point.	223
7.3.8	Boxplot comparison of the noise in sensitivity recovery	224
7.4.1	Dark adaptation curves for different ramp times	226
7.4.2	Poisson regression of the Ramp time to the autocorrelation count data	227
7.5.1	The effect of raising the cone threshold on the cone rod breakpoint	229
8	Discussion	231
8.2.1	Simulated data for a standard observer of the digital device.	235
8.2.2	Summary of all data compared	237
	Appendix	253

B.0.1	Changes in cone parameter estimates	287
B.0.2	Histograms of the parameters defining S3	288
C.1.1	Bootstrap estimates of the mean and standard error of each parameter component	291
C.1.2	The process of HTC	294
C.1.3	Comparison of parameter estimates and confidence intervals	295
C.1.4	The linear relationship between the CI	296
D.2.1	Bootstrap and nls compared	299
D.3.1	Linearity of parameter estimates	302
D.3.2	Linearity of parameter estimates	302
E.2.1	Block diagram of Analogue Apparatus	304
E.2.2	Circuit Diagram of the Target Board	304
E.2.3	Circuit Diagram of the Illumination Board	305
G.1.1	Subjects 1 to 3	309
G.1.2	Subjects 4 to 6	310
G.1.3	Subjects 7 to 9	311
G.1.4	Subjects 10 to 12	312
G.1.5	Subjects 13 to 15	313
G.1.6	Subjects 16 to 18	314
G.1.7	Subjects 19 to 21	315
G.1.8	Subjects 22 to 24	316
G.1.9	Subjects 25 to 27	317
G.1.10	Subjects 28 to 30	318
G.1.11	Subjects 31 to 33	319
G.1.12	Subjects 34 to 36	320
J.4.1	Emergency Information card for subjects	392

List of Tables

2	Physical Methods and Apparatus	52
2.3.1	Comparison of measured broadband luminance with narrowband calculated values	68
2.3.2	Summary of the filter characteristics.	73
2.3.3	The method of calculating the scotopic luminance of the red LED	74
2.3.4	Photopic and Scotopic Values of Background Luminance	77
2.3.5	Voltage luminance equivalences	79
2.5.1	Area under the curve converted to photopic and scotopic energy values.	86
2.5.2	Calculated percentage bleach	90
3	The Normal Dark Adaptation Function	107
3.1.1	Parameter values of the data	110
3.4.1	Comparison of Matlab and R	124
4	Evaluation of an Algorithm by a Series of Numerical Experiments	128
4.2.1	Starting parameter values passed to the function <code>fminsearch</code>	133
4.2.2	Summary statistics for the two sets of test data.	135
5	The Effect of Background Luminance	146
5.2.1	Photopic and Equivalent Scotopic Luminances	158
5.3.1	Conversion of photopic luminance to scotopic luminance	162
5.3.2	Summary of the parameter estimates for each light source.	163
5.3.3	Parameters of the simple exponential model	167
6	Analogue Device to Measure Dark Adaptation	172
6.3.1	Summary statistics for the parameter values of the dark adaptation curve for 35 subjects.	178
6.4.1	Variance of the residuals as the phase changes	199
6.4.2	Summary of coding for model selection.	201
7	A Digital Device to Measure Dark Adaptation	207
7.3.1	Summary of the parameters of dark adaptation	217

8 Discussion	231
Appendix	253
D.1.1 Summary statistics for nls	298
F.1.1 Parameters of the bi-exponential model	307
G.2.1 Summary of parameters from the first visit	321
G.2.2 Summary of parameters from the second visit	322
G.3.1 Classification of data according to model fit	323
G.3.2 Classification of data according to model fit	324
H.2.1 Summary of the parameters for the data found using the digital device . .	326

ROD MEDIATED VISION: BIOPHYSICS TO PSYCHOPHYSICS

the darkest night is ignorance

Buddha

1.1 Introduction

This mini-review will concentrate on the structure and function of the rod system. In particular the changes that occur in the rod and surrounding anatomy with age and how those changes affect the visual performance of the rod system.

Interest in rod-mediated vision is growing, driven partly by its link with age related maculopathy (AMD). This disease is alarmingly common, on the increase and is responsible for vision loss in 30% of the over 65s in the western world (Klein, Peto, Bird & Vannewirk 2004). Initially, AMD is a disease of the retinal pigment epithelium (RPE), a layer of cells intimately related to the photoreceptors, eventually resulting in photoreceptor damage and loss. Early RPE dysfunction has an effect upon photoreceptor function (Liang & Godley 2003).

Although the most obvious and debilitating consequences of maculopathy are a result of damage to the cone system, there is convincing evidence that rod health is a vital prerequisite of cone health (Leveillard, Mohand-Said, Lorentz, Hicks, Fintz, Clerin, Simonutti, Forster, Cavusoglu, Chalmel, Dolle, Poch, Lambrou & Sahel 2004, Lorentz, Sa-

hel, Mohand-Saïd & Leveillard 2006, Yang, Mohand-Saïd, Danan, Simonutti, Fontaine, Clerin, Picaud, Léveillard & Sahel 2009, Fridlich, Delalande, Jaillard, Lu, Poidevin, Cronin, Perrocheau, Millet-Puel, Niepon, Poch et al. 2009, Cronin, Raffelsberger, Lee-Rivera, Jaillard, Niepon, Kinzel, Clérin, Petrosian, Picaud, Poch et al. 2010).

Furthermore, rods in the central retina are preferentially vulnerable to ageing (Curcio, Millican, Allen & Kalina 1993), and it has been shown that the kinetic parameters of rod vision are a sensitive assay of retinal health (Owsley, Jackson, White, Feist & Edwards 2001, Dimitrov, Robman, Varsamidis, Aung, Makeyeva, Guymer & Vingrys 2011)

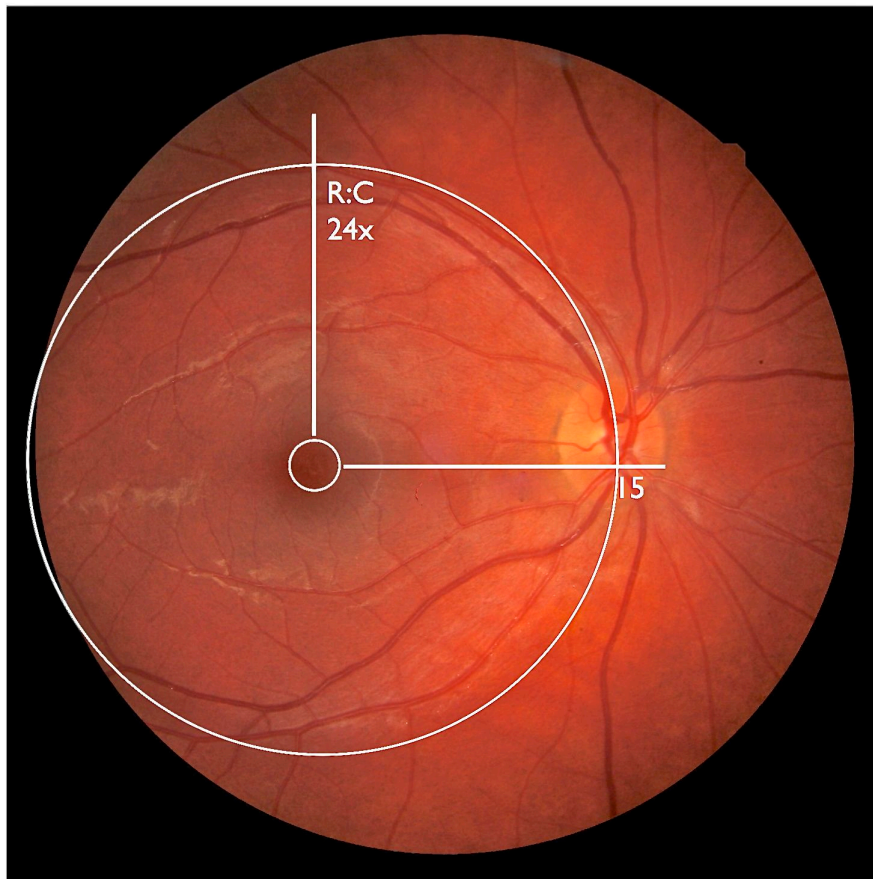


Figure 1.1.1: The macula is the region contained in the large white circle, notice the much smaller circle that describes the cone dominated region. The rod to cone ratio at the outer circle, with diameter 15° is 24:1.

The human retina is rod dominated, apart from a small area at the fovea. In figure 1.1.1 we can see that the cone dominated region is a small part of the macula.

Rods signal increasing light levels by falling levels of neurotransmitter, glutamate. At light levels in excess of 1000 td*, rods saturate, i.e. the release of the neurotransmitter reaches a minimum and the rods are unable to signal any further increase in light levels. The evolutionary advantage of this situation is still unclear, one suggestion is that this provides a mechanism by which energy demand can be balanced over the diurnal cycle. Most energy expenditure is in photopigment recycling during daylight, while at night the greater effort is on neurotransmitter production and release. Another suggestion is that the sudden reduction of light, e.g. by the appearance of an overhead predator, leading to a sudden rise in neurotransmitter release may more accurately signal the change and confer a survival advantage.

The first section presented here discusses the distribution and morphology of photoreceptors across the retina and compares and contrasts the rods and cones. There then follows a description of retinal anatomy and physiology as they affect rod function, with particular reference to ageing. The central process of rod physiology is photo-transduction and this will be briefly described, in particular concentrating on the understanding of the role of rhodopsin, its mode of action in transduction, and its replenishment. A more detailed discussion, particularly of the kinetics of the recovery of rod sensitivity following a photo-bleach is provided in later chapters. Finally, the features of rod-mediated vision, as revealed by psychophysical measurement will be discussed. In particular, the features of rod vision when presented with low luminance stimuli and how these can be used to provide an insight into dynamical mechanisms of rod vision will be discussed.

1.2 Photoreceptors

Rod photoreceptor structure and function are interdependent. The distribution of photoreceptors along with their interrelationships with other tissues and the characteristics of those surrounding tissues circumscribe rod performance. Here the density, distribution, and then the structure of the rod photoreceptor are considered.

The duplex nature of the retina, i.e. two separable cone and rod mechanisms, is well established (Schultze 1866). These two systems along with nonlinear coding strategies, account for the efficiency and the large dynamic range achieved by the retina (Wark, Lundstrom & Fairhall 2007). The retina encodes light signals in a biologically challeng-

*The troland is a unit of retinal illuminance and is defined as the product of the incident luminance (cd.m⁻²) and pupil area (mm²). Luminance can be scotopic or photopic.

ing environment; light energy focussed by anterior ocular components falls on the retina, where a small avascular area is responsible for detailed vision (Ham, Mueller, Ruffolo, Millen, Cleary, Guerry & Guerry 1984). The retina is rich in oxygen and liable to extremes of temperature. These two features demand that the retina, if it is to avoid photic damage, must be able to quench free radicals, effect rapid repair, sustain prolonged turn over of photoreceptor outer segments and recycle highly unstable photo-labile components. That this system is capable of good vision for seven decades or more is evidence of the robust mechanisms used to protect the retina in general and the photoreceptors in particular.

1.2.1 How are rods and cones distributed?

The density of cone photoreceptors is greatest in the central 1mm, yet varies greatly between individuals. The density of cone photoreceptors in the fovea, for example, is known to vary by 2.9 fold between subjects with a range of 150 K to 500 K cones.mm⁻² (Curcio, Sloan Jr, Packer, Hendrickson & Kalina 1987), the variation in central cone density can be clearly seen in the two panels of 1.2.1, where both photographs are taken at the same magnification yet the cell sizes are different.

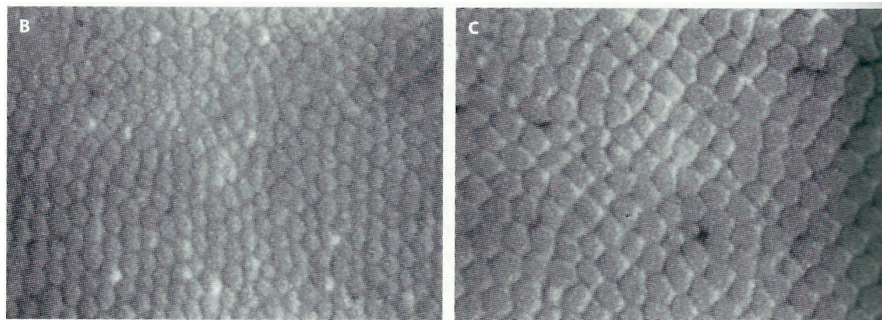


Figure 1.2.1: The variation in cone density between individuals, photographs taken at the same magnification. Figure taken from Hendrickson (Hendrickson 2005) after Curcio (1990)

The highest rod density is found along an ellipse that passes through the optic nerve head ($\sim 15^\circ$) and extends into the nasal retina, the point of peak density being superior-nasally. The rod density falls by ~ 20 fold as the ellipse crosses the horizontal, and there is a further fall in rod density from the rod ring to the far periphery (Curcio & Allen 1990).

The estimates for total numbers of receptors are subject also to wide variation between

studies, but between subjects in each study the total numbers remain relatively constant. What is clear from many human studies is that there is a ratio of ~ 20 rods to each cone throughout the peripheral retina, 9 to 1 in the macula, and a central rod free area at the fovea about 1.25° in diameter. The ratio reaches parity at $\sim 450 \mu\text{m}$ and only the central $300 \mu\text{m}$ is rod free, see figure 1.2.2.

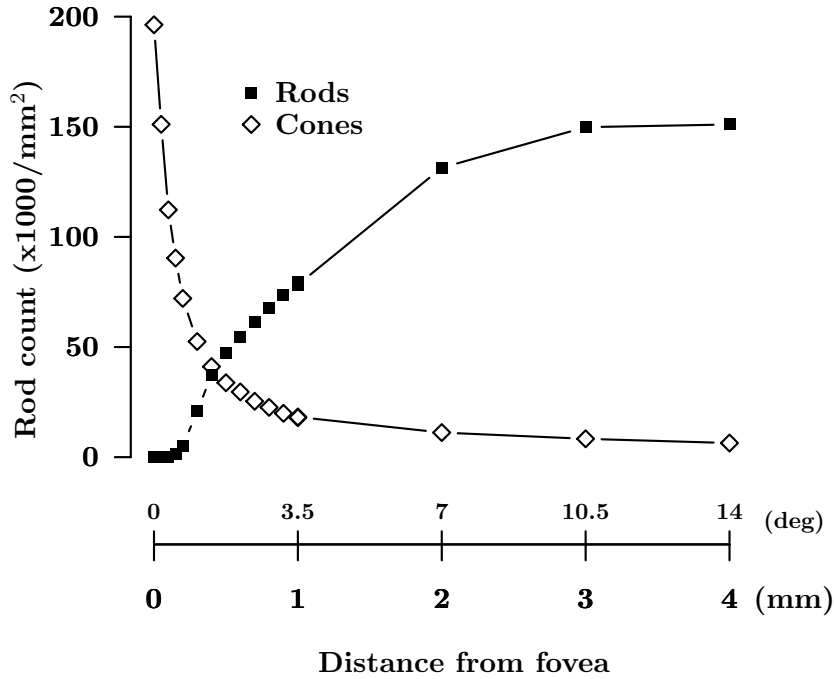


Figure 1.2.2: Rod and cone count as a eccentricity varies. Taken from Curcio et al.(1990)

Overall it is thought that there are around 6 million cones and 120 million rods in the average human retina (Østerberg 1935, Curcio & Allen 1990, Jonas, Schneider & Naumann 1992, Masland 2001, Wang & Kefalov 2011).

Of particular importance for the present study is the differential susceptibility of the each photoreceptor type to aging. While overall cone numbers remain relatively constant throughout life, the rod cell count falls by 30%. As rod numbers fall, the inner segments become larger but the overall rhodopsin content of the retina remains constant (Curcio et al. 1993). Rhodopsin is the photopigment exclusive to rods. What is not known is

whether the changes in scotopic vision found with increasing age are due to the fall in rod numbers and changes to rod morphology, altered post receptor processes, or if changes in other factors e.g. metabolite delivery, waste elimination, growth factor regulation or the accumulation of photo-toxic residues, account for the phenomenon.

1.2.2 Morphology

As the density varies with eccentricity so does the diameter of the receptors as illustrated in the four plots of 1.2.3. Cone diameter increases from the centre to the periphery with the peripheral cones up to three times larger, at $10\ \mu\text{m}$, than those at the fovea, $3\ \mu\text{m}$. Rod size also varies with eccentricity, they have their maximal density at $\sim 15^\circ$ from the fovea and their smallest size, $3\ \mu\text{m}$, increasing to $5\ \mu\text{m}$ at the periphery (Jonas et al. 1992).

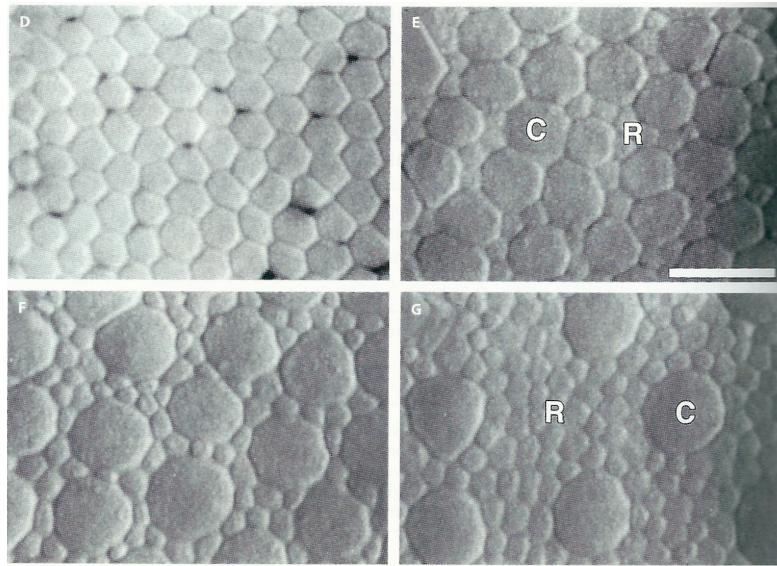


Figure 1.2.3: The change in Cone and Rod density with eccentricity. Micrographs obtained from post-mortem samples. From top left by row the panels show the change in cone size with increasing distance from the fovea, the fall in cone density and the concomitant rise in rod density. Upper left is at $125\ \mu\text{m}$, although rods are found here, none appear in this image. Upper right at $\sim 660\ \mu\text{m}$ where rod superiority begins. Lower left, $1.4\ \text{mm}$, rods exceed cone by 6:1, Lower right, $5\ \text{mm}$, the peak of rod density. Scale bar = $10\ \mu\text{m}$. C=cone, R=rod. Figure taken from Hendrickson (Hendrickson 2005) after Curcio (1990)

The variation in number and size with respect to location can be seen in figure 1.2.3. The honeycomb pattern of the rod mosaic and the regularly spaced cones can be seen

in figure 1.2.4 (from Jonas 1992).

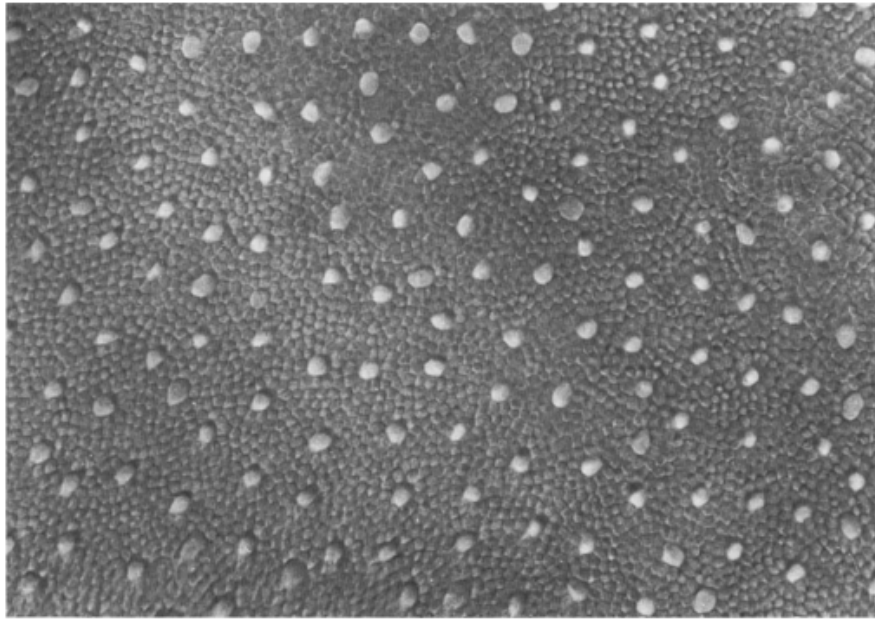


Figure 1.2.4: Retina 9.5 mm from the fovea, rod density 58 000 rod.mm⁻², cone density 2 000 cone.mm⁻². The isolated larger cells are cones. From Jonas 1992.

1.2.3 Cones and rods compared

Cones can function at very high light intensities and are specialized for rapid detection of stimuli, in contrast, rods are slower and can only operate at lower light intensities. The extreme sensitivity of the rods is in part due to the higher thermal stability of the rod photopigment compared to that of the cones (Gozem, Schapiro, Ferré & Olivucci 2012). The cone visual pigment dissociates into opsin and chromophore more readily than the rod photopigment, generating signals to thermal rather than photic stimuli. This means that rods can more reliably signal single photon events (Lamb & Pugh Jr 2006).

Photopigment The rods contain only one type of photopigment, rhodopsin, while cones contain different photopigments (iodopsins) (Baylor 1987). Each opsin type when exposed to light has different probabilities of photon absorption, dependant upon wavelength, resulting in different spectral sensitivity. Replenishment of the chromophore in the two types of photopigment is also different; the rods exclusively rely upon the retinal

pigment epithelial cells, while the cones use both the RPE and Müller cells to restore sensitivity to the opsin molecule (Wang & Kefalov 2011).

Luminous efficiency Rhodopsin is ~ 2.5 times more efficient than iodopsin at photon capture. This partly explains the different luminous efficiency profiles published by the CIE and shown in figure 1.2.5. In humans, the photopic luminosity function is formally regarded as due to the activity of the L-(long wavelength) and M-(medium wavelength) cone types (Wyszecki & Stiles 1967).

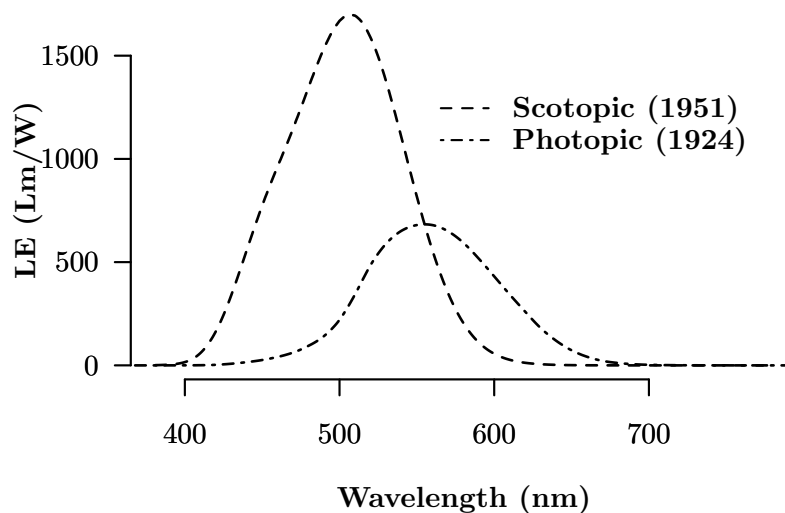


Figure 1.2.5: The CIE Human Luminous Efficiency functions for scotopic and photopic vision.

Surface area Although rods are much longer than cones, the surface area of the rod outer segment (OS) is much smaller than that of the cone outer segment. The discs in the rod are surrounded by the plasma membrane of the cell and are not in direct contact with the extracellular matrix, also known as the inter photoreceptor matrix (IPM), see figure 1.3.1. In contrast, the cone outer segment is in direct contact with the IPM and therefore able to rapidly exchange nutrients and metabolites (Mustafi, Engel & Palczewski 2009). This difference between rod and cone outer segments is crucial and is an important factor in explaining the differences in the sensitivity recovery dynamics between rod and

cone-mediated vision as discussed in later chapters.

Temporal stimuli The more intimate relation between cone OS and IPM leads to a 20-fold faster deactivation of the photopigment in cones over rods, with a correspondingly shorter life for the activated photopigment. This difference in deactivation means that the response of the rod to a dim flash is slow. The flicker fusion frequency for rod mediated human vision is ~ 3 Hz rising with increasing background level to ~ 18 Hz, in contrast the cone system rises to ~ 55 Hz in a bright background (Hecht, Shlaer & Verrijp 1933).

Spatial stimuli The response to spatial stimuli is also different; cone mediated sensitivity to a sinusoidal grating has its peak ~ 4 cycles per degree (cpd). The sensitivity response has a band pass profile and resolution limit ~ 55 cpd. As the light level falls and the sensitivity becomes rod mediated the profile becomes low pass in character with a resolution limit of ~ 3.5 cpd (Van Nes, Bouman et al. 1967). This difference is attributed to differences in post-receptoral processing, and is discussed further in section 5.1.6 on page 155. As light levels fall, the number of rods recruited by ganglion cells rises, this increases the sensitivity but reduces spatial resolution (Nelson & Kolb 1985, Kolb & Nelson 1983).

Photoproducts The cone system seems to be unaffected by the presence of photoproducts following a bleach, unlike the rods whose persistent insensitivity following a photo bleach is attributed to photoproducts downstream of the event of photon capture (Lamb & Pugh Jr 2006).

Physiology The dramatic differences in luminance sensitivity between rod and cone photoreceptors can be partly summarised at a receptor level by the following factors:

- Rods have a greater number of discs than cones
- Dense packing of rhodopsin in those discs
- Highly mobile rhodopsin in disc membrane
- Rhodopsin better able to capture a photons

- Low dark current noise

These features at a cellular level in concert with post-receptoral mechanisms that pool responses make the rod system over 1000 times more sensitive to luminance than the cone system (Rieke & Baylor 1998).

1.3 Rods and the Retinal Pigment Epithelium

Each type of photoreceptor, rod and cone, has four distinct regions; outer segment, inner segment, cell body and a synaptic terminal. A schematic comparison of the two photoreceptor types is shown in figure 1.3.1. An important difference between the rod and cone outer segment is that the rod discs containing the photopigment rhodopsin, are enclosed within the outer segments plasma membrane, while the cone discs are shelf like invaginations of the plasma membrane.

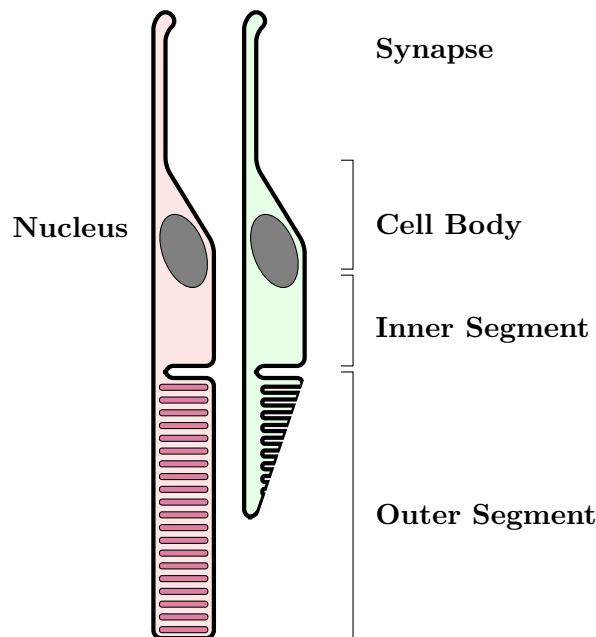


Figure 1.3.1: The photoreceptor, rod on the left, cone on the right, showing the outer segment containing the rhodopsin packed disks, linked to the inner segment and its organelles, by a cilium, the nucleus and the extension to the synapse.

1.3.1 Rod outer segments

The rod outer segment is specialized for light capture and amplification. This is achieved by having long cylindrical outer segments containing ~ 1000 discs. Embedded in the surface of each disc is a light sensitive photopigment, rhodopsin. The discs are spaced at ~ 30 nm, each packed with rhodopsin at a density of $\sim 25,000 \mu\text{m}^{-2}$. With a diameter of $2 \mu\text{m}$ each disc would contain 10^8 rhodopsin molecules. The molecules of rhodopsin move freely and rapidly in the disc by Brownian motion and the dense packing increases the probability of absorption of light, while the high mobility maximises the gain of the first step in the photo-transduction cascade, the activation of transducin (Lamb & Pugh 2004).

The outer segment undergoes a continual renewal and disposal process in which newly synthesised discs are added at the base and distal packets of outer segment membrane are phagocytised by the retinal pigment epithelial. The time course of this cycle is around two weeks (Young 1967). There is evidence that the rate of renewal in humans remains constant through life, while the rate of phagocytosis falls. This causes lengthening and loops in the distal outer segment with age (Marshall, Grindle, Ansell & Borwein 1979). Marshall et al. suggest that these morphological changes may, in part, be responsible for the changes in scotopic vision seen with increasing age. However, Cunea et al. (2007) argue that these may be methodological artefacts. Evidence from the mouse model suggests the opposite, here rod outer segments shorten with increasing age, suggesting that shortening of the rod may be responsible for reduced scotopic sensitivity with increasing age. It is nevertheless important, since in general there is very little understanding of why rod function should decline with age in humans and a physiological explanation of this sort could provide the basis for explaining the phenomenon.

1.3.2 Inner segment, cell body and synapse

In all photoreceptors the outer segment is connected to the inner segment by a thin cilium, as seen in figure 1.3.1, the inner segment is a cellular compartment that contains the organelles for normal cellular function and the nucleus. The inner segment further extends into the synaptic region.

Central to the signalling of photon capture by the rod photoreceptor is the circulating current generated in the cell. The inner and outer segments of both types of photorecep-

tor have energy dependent ion* pumps that create a standing current that is maximal when in a darkened state. In this state the rod cell is depolarized (-40 mV) and there is a constant release of glutamate from the synaptic region of the cell (Molday 1998, Pugh & Lamb 2000).

Absorption of light reduces the flow of positive ions through the cell membrane and reduces this current. The fall in this current and subsequent hyperpolarization of the plasma membrane leads to a fall in neurotransmitter release at the synaptic cleft. Hence, perhaps surprisingly, as the light levels rise the neurotransmitter release falls. This change is then transmitted to other neurons of the downstream retina (Baylor, Lamb & Yau 1979).

1.3.3 Retinal Pigment Epithelium

The retinal pigment epithelium (RPE) and the photoreceptors are often considered to be a single functional unit, since they are interdependent for their mutual health and function (Han, Giese, Schmitz-Valckenberg, Bindewald-Wittich, Holz, Yu, Bille & Niemz 2007) .

The RPE is a monolayer of post-mitotic cells located between Bruch's membrane and the photoreceptor outer segments. The sizes of the cells vary with eccentricity; those near the fovea being taller but thinner, while those in the periphery are broader and flatter. In the adult, the average size is reported as varying between 10 to 16 μm diameter and 7 to 10 μm in thickness (Garron 1963, Sakuragawa & Kuwabara 1976). Each RPE cell at the fovea is in contact with 20 to 30 rod outer segments (Ts'o & Friedman 1968) and 30 to 40 elsewhere (Robinson & Hendrickson 1995). Up to the age of 40 years the cell density is relatively uniform throughout the retina at about 4000 cells. mm^{-2} , after this age the numbers fall to ~ 2000 cells. mm^{-2} (LaCour 2008).

Invaginations on both the apical and basal surfaces increase the surface area available to the photoreceptor outer segment in the former and to Bruch's membrane in the latter. The apical invagination encircle the outer third of the rod outer segment (Sakuragawa & Kuwabara 1976). Between RPE cells there are tight junctions that ensure a blood-retina barrier. Each cell has a basal nucleus and a large number of organelles, reflecting the high metabolic activity of the cells. Large numbers of melanin containing organelles are found at the apex of the cell.

*positive ions

The RPE has a multiplicity of functions, including

- Light absorption and consequent reduction in stray-light, the melanin granules also have a role in free radical scavenging (LaCour 2008).
- Establishment of a blood retinal barrier that allows for regulated trans-epithelial transport of nutrients and waste products to and from the photoreceptors; e.g. glucose, ions, water and lactate. Metabolite exchange is mediated by both active transport and diffusion gradients. The presence of tight junctions between cells means that there is no extracellular route for transport and all metabolite and fluid transport is cell mediated.
- The visual cycle; uptake, recycling, transport and release of retinol (vitamin A) and some visual cycle intermediary compounds (retinoids). Retinol uptake occurs at both the base and the apex of the cell. The release of the crucial retinoid, *cis*-retinal, only occurs at the apical membrane. The movement of retinol across the basal membrane is mediated by a retinol binding protein (RBP), which is produced in the liver. Release of *cis*-retinal and the uptake of retinol across the apical membrane is by active transport facilitated by an inter-receptor binding protein (IRBP) (Bok 1993).
- Phagocytosis of the rod and cone outer segments that are shed from their distal ends and following their digestion, the reuse of proteins, fatty acids and lipids. Phagocytosis takes place at the apex of the cell using membrane receptor mediated processes and appears to be under circadian control, being greater in the morning upon waking (Besharse, Hollyfield & Rayborn 1977).
- Protection of the outer retina from damage by reactive oxygen species by melanin, lutein and zeaxanthin.
- Co-ordination of growth factors; two important growth factors are vascular endothelial growth factor (VEGF) and pigment epithelium-derived factor (PEDF), their interaction is important in the prevention of choroidal neo-vascularisation (Ohno-Matsui, Yoshida, Uetama, Mochizuki & Morita 2003).
- Regulate ion buffering, and maintain receptor excitability.

These functions are summarised in figure 1.3.2.

Work with the Rhesus monkey model demonstrated that the amount of membrane material ingested and processed by RPE cells is substantial. For example, it has been calcu-

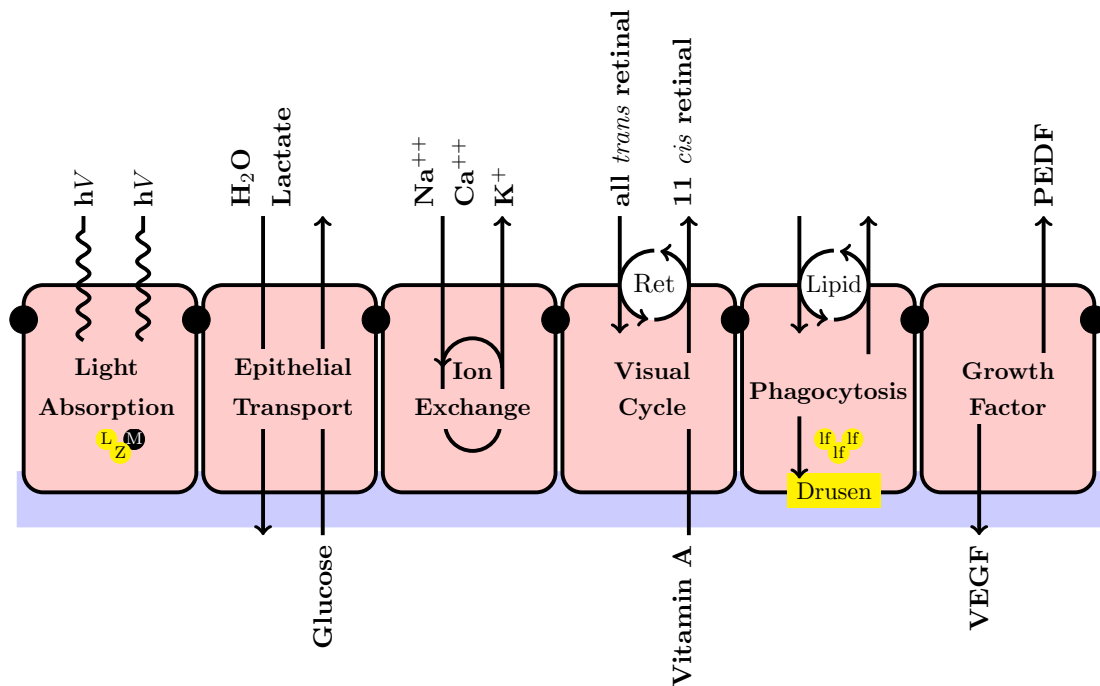


Figure 1.3.2: RPE functions. Summarised as straylight absorption, epithelial and ion regulation and mineral transport, the visual cycle, disc phagocytosis and growth factor regulation. Black circles represent tight junction, and $h\nu$ a photon, Ret, retinoid cycle, Lipid, lipid cycle, M, melanocytes, lf, lipofuscin, L, lutein, Z, Zeaxanthin, VEGF, vegative endothelial growth factor, PEDF, pigment epithelium derived factor. The coloured base representing the basement membrane of the RPE, part of Bruch's membrane. Figure adapted after Strauss 2005.

lated that each extra-foveal RPE cell must ingest and process a volume of rod outer segment that corresponds to 7% of the volume of the RPE cell itself (Young 1971). As post mitotic cells this means that RPE cells process a quantity of membrane far in excess of any other phagocytic cell. It has been suggested that this large phagocytic load is responsible for the accumulation of lipofuscin (Nilsson, Sundelin, Wihlmark & Brunk 2003), furthermore, exocytosis of lipofuscin and other waste products may lead to the accumulation of hydrophobic material in Bruch's membrane (described below) and therefore reduce its permeability for essential nutrients (Marshall et al. 1979, LaCour 2008).

Drusen

Drusen appear at the interface of the RPE and Bruchs membrane and their origin is still not clear. They are hydrophobic and may be the result of exocytosis of incompletely

digested material from the overlying RPE cells, or they may result from the incomplete clearance following RPE cell death, the subsequent surrounding RPE cells enlarging and laying on top of the residue. They have however, been shown to interrupt the flow of material between the choriocappilaris and the RPE (Booij, Baas, Beisekeeva, Gorgels & Bergen 2010, Scholl, Bellmann, Dandekar, Bird & Fitzke 2004).

Age effects on RPE

Through life the RPE layer changes in significant ways, in particular, the following are found:

- Build up of lipofuscin, a incompletely understood complex with a likely composition of partially metabolised retinoids and outer segment membranes. Lipofuscin is photo reactive and therefore a source of oxidative stress for the enclosing RPE cell. Furthermore, in aged RPE the cytoplasm is largely occupied by lipofuscin aggregates (Han et al. 2007).
- Drop in the number of RPE cells, this increases the phagocytic load on the remaining cells. Furthermore, the rate of RPE cell loss is faster than that for the overlying rod photoreceptors. This means that with increasing age each remaining RPE cell is in contact with a growing number of photoreceptor OS (Dorey, Wu, Ebenstein, Garsd & Weiter 1989).

What is not clear is the effect these age-related changes have on RPE function and therefore rod function. It is suggested that intracellular congestion by lipofuscin may have an effect on retinoid recycling and phagocytosis (Boulton 2008). The fall in cell density with age may not have an effect or it may reduce the efficiency of one or all RPE functions e.g. phagocytosis.

1.3.4 Bruch's membrane

Bruch's membrane is an acellular pentalaminar structure that separates the retinal pigment epithelium from the choriocappilaris and has a thickness that varies from 2 to 6 μm (Boulton 2008). The five layers: the RPE basement membrane, inner collagenous layer, elastic layer, outer collagenous layer, and choriocapillary endothelium basement membrane are shown in figure 1.3.3, Bruch's membrane is located between the two arrowheads.

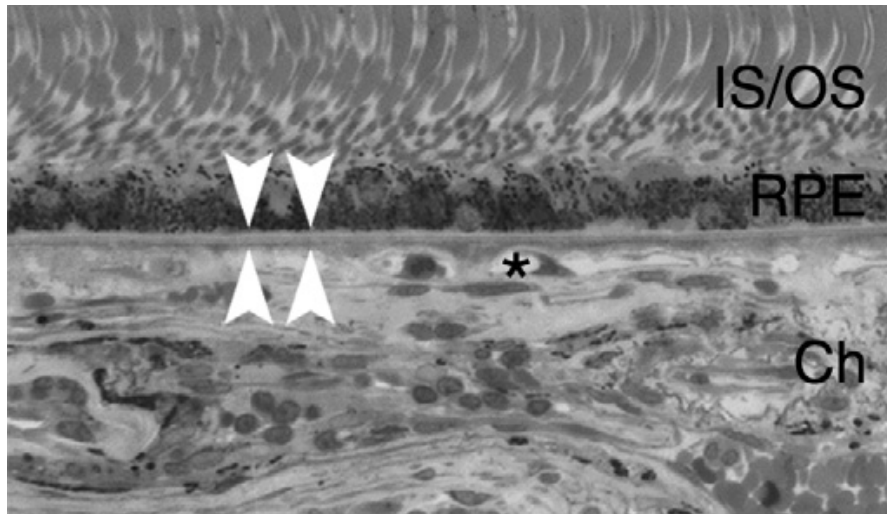


Figure 1.3.3: The relationship between choriocapillaris Ch, Bruch's membrane between white arrows, and RPE. IS/OS inner and outer segments (Curcio et al. 2009).

There are three main functions for Bruch's membrane (Booij et al. 2010);

- regulate the diffusion of molecules between choroid and RPE
- provide structural support for RPE cell adhesion, migration and perhaps differentiation
- act as a division barrier, restricting choroidal and retinal cellular migration

All nutrients to and metabolites from the RPE and photoreceptors must cross Bruch's membrane (Curcio, Bradley, Guidry, Kirk, Wilson, Barnes, Kruth, Chang & Chang 2002). The collagen layers of the membrane are composed of collagen types I, III, IV and V. The distribution of collagen types does not vary significantly between macular and peripheral sites or with age. However, the solubility of the collagen declines markedly with age, from 100% in the first decade to ~50% in the ninth across all sites. There is also a significant increase in non-collagen protein at the macula with age (Karwatowski, Jeffries, Duance, Albon, Bailey & Easty 1995).

The thickness of Bruch's membrane increases with age, with peripheral thickening preceding macula changes (Newsome, Huh & Green 1987). However, the macular portion later becomes the thicker part (Guymer, Luthert & Bird 1999), with the result that the membrane in the ninth decade is over twice the thickness of that of the infant human (Ramrattan, van der Schaft, Mooy, De Bruijn, Mulder & De Jong 1994). Molecules and cellular debris accumulate in Bruch's membrane throughout life (Guymer et al. 1999).

These changes in Bruch's membrane with age act to reduce the free flow of molecules between the choriocapillaris and the photoreceptors (Boulton 2008).

1.3.5 Perfusion of the Retina

Choroid

The inner retina relies on the retinal vasculature while the outer retina is served by the choriocapillaris, a part of the choroidal circulation next to Bruch's membrane (Singh-Hayreh 1974). An exception to this is at the fovea, where the inner retina is highly modified, with post receptor cell and capillary displacement resulting in a thinner avascular zone.

Branches of the ophthalmic artery, a branch of the internal carotid, enter through the sclera near the optic nerve as the short and long posterior ciliary arteries. They branch to form the choroid and the choriocapillaris, a dense capillary bed that is about 200-300 μm thick. The choroid has the highest blood flow per unit tissue perfused of any in the body, with 7-fold greater flow in the macula relative to the periphery (Curcio et al. 2009).

Choriocapillaris

The choriocapillaris is a vascular network of freely branching flat and wide capillaries that are highly permeable. These vessels are next to Bruch's membrane and have a fenestrated endothelium. There is a very high blood perfusion rate in the choriocapillaris, this high blood flow acts to stabilize temperature and provide nutrients and oxygen to the retinal pigment epithelial cells and the outer parts of the retina (Strauss 2005, Alm & Bill 1970). The capillary walls are permeable to proteins and large molecules and provide the only route for such molecules, e.g. vitamin A. Both active transport and diffusion gradients allow the movement of nutrients from the choriocapillaris to the outer segments of the receptors (Bill, Sperber & Ujiie 1983, Delaey & Van De Voorde 2000). The retina has a very high oxygen demand at $31 \text{ ml} \cdot \text{mg}^{-1} \cdot \text{hour}^{-1}$, and there is a substantial oxygen tension gradient from the choroid to the photoreceptor inner segments (Arden & Sivaprasad 2012).*

*The brain also consumes large quantities of oxygen $\sim 20\%$ of the total uptake of the body, but the retinal requirements per unit mass are even higher.

There is only a small change in partial pressure of oxygen (PO_2) from the arterial to venous side of the choroid when compared to other tissues, yet there is very high level of blood flow. This high blood flow explains the large oxygen tension across the tissues and the small change in PO_2 as the blood passes through the choriocapillaris and allows for a thicker outer retina to be sustained than would be the case otherwise (Bill et al. 1983). Further roles, besides oxygenation, nutrition and thermoregulation, for this high blood flow are volume buffer and aqueous production (Delaey & Van De Voorde 2000). Strict temperature stability is important for the photoreceptor outer segments as it is known that the circulating dark current, generated by the cation pumps, is very sensitive to temperature changes. Any small changes in temperature could generate anomalous signals in the photoreceptors (Lamb 1984).

With increasing age the choroid and choriocapillaris thin to less than half the thickness found in youth. Furthermore, the size of the choriocapillaris lumen falls by a third (Ramrattan et al. 1994). The narrower lumen is liable to occlusion by red blood cells further reducing the ability of the serum to act as a medium for nutrient and gas exchange (Han et al. 2007). The overall effect of these changes is to reduce the blood flow; compromising oxygen tension, metabolite delivery, waste clearance, and temperature regulation.

1.3.6 Between the rod and the RPE

The rod is not in direct contact with its associated RPE cell; rather it is separated from it by the IPM. This matrix has two likely roles; firstly, coordinating the location and density of a variety of soluble proteins. For example IRBP and metallo-proteases, which have an important role in rhodopsin replenishment. A second probable role of the IPM is mediation by the insoluble components, in particular the glycosaminoglycans (GAGs), of retina to RPE binding. The dominant type of GAG in the IPM is hyaluronan. Evidence for this attaching rôle comes from the identification of binding sites for hyaluronan on photoreceptors (Hollyfield 1999).

1.3.7 Relationship between rods and RPE and the effects of ageing

The journey of nutrients from the circulation to the rod outer segment is from the fenestrated choriocapillaris through Bruch's membrane, then following uptake and processing by the RPE, subsequent release to the IPM, and finally to the plasma membrane of the

rod before incorporation and use in the cytoplasm or disc. The reverse journey must be made by metabolites that are to be cleared from the rod-RPE complex. Each structure traversed on this journey changes through life. These changes have an impact on the performance of the rod system and they are summarised in figure 1.3.4.

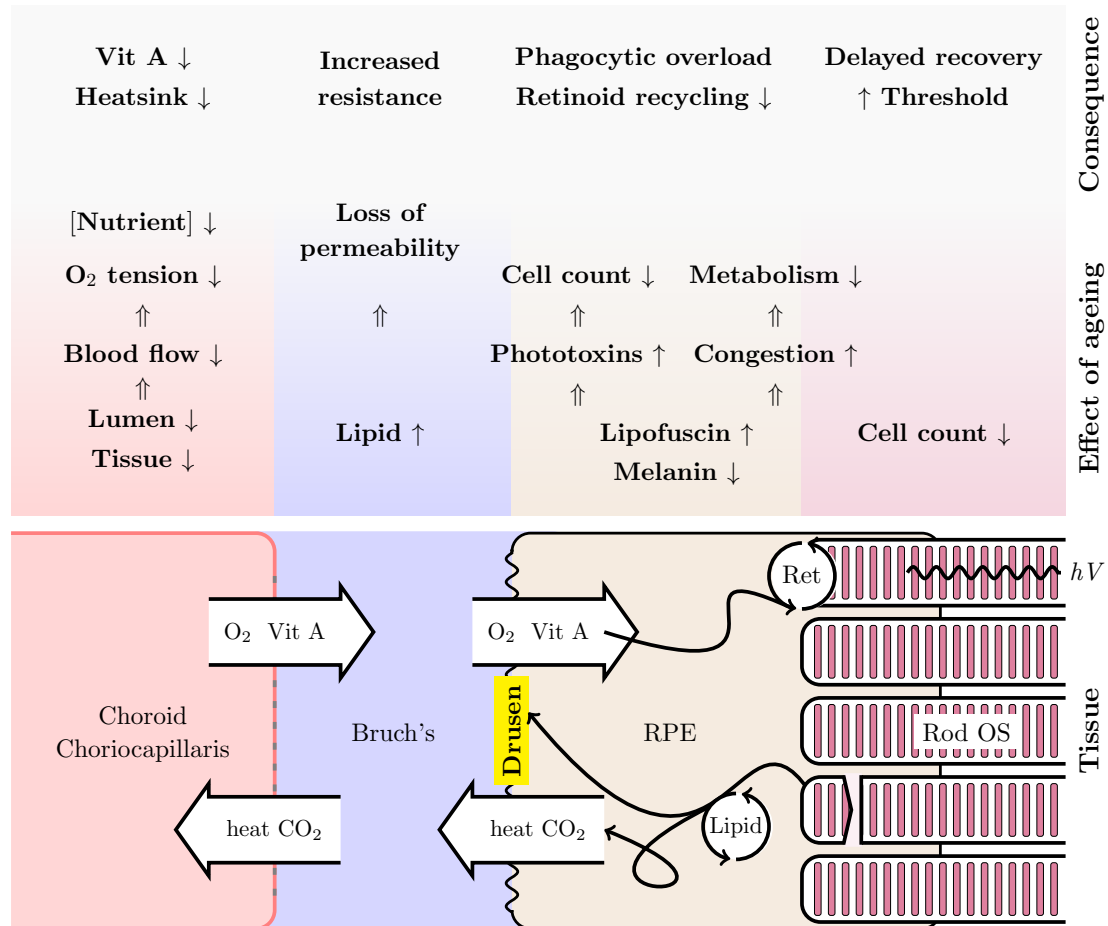


Figure 1.3.4: The effect of ageing on the rod-choroid complex. Atrophy of the chorio-capillaris reduces the blood flow and hence the concentration of available nutrients and ability to remove heat. The build up of hydrophobic material in Bruch's increases its resistance to the flow of solutes. The complex age related changes to the RPE compromise retinoid recycling. The result of these changes is to elevate absolute thresholds and reduce the rate at which the rod photoreceptor can recover from a photic challenge. Ret means retinoid, [] concentration, hV a photon.

The overall effect of these changes to the rod photoreceptor is to reduce the availability of metabolites, lose the benefits of heat stability, and compromise clearance of waste products. This in turn reduces the efficiency of rhodopsin maintenance and recycling.

1.4 Rhodopsin

The photopigment rhodopsin belongs to a class of sensory macromolecules known as G protein-coupled receptors (GPCR); they are widespread in the body and have a key role in the regulation of cellular function.* GPCRs control a wide range of cellular processes, e.g. the senses of vision, smell and taste, and also a myriad of intercellular signalling systems in response to external stimuli. For a review of this ubiquitous family of receptors see Pierce, Premont & Lefkowitz (2002)

Rhodopsin has been widely studied as it is an easily obtained example of this class of protein. GPCRs are usually activated by attachment of a specific molecule, a ligand. This ligand changes the shape of the GPCR exposing an active site, which then initiates an amplification cascade of chemical activity (Strader, Fong, Tota, Underwood & Dixon 1994). Although ligand binding is the commonest form of molecular activation for GPCRs, this is not the case for rhodopsin. The conformational change arises when the molecule of retinal embedded in the opsin molecule absorbs a photon and changes shape from its *cis* to its *trans* isomer, see figure 1.4.1.

Rhodopsin has two components, a large trans-membrane protein termed opsin and a chromophore that is a derivative of vitamin A, 11-*cis*-retinal. The rhodopsin macromolecule, see inset figure 1.4.2, penetrates the disc membrane. The light sensitive compound embedded within it, *cis*-retinal, has peak absorption at about 500nm. In the case of rhodopsin the G protein is transducin and it is the activation of transducin that initiates a cascade of cellular activity, called phototransduction.

1.4.1 Phototransduction

Rhodopsin is responsible for the process of photo transduction, the transformation of light energy to electrical activity, illustrated in figure 1.4.2. The outer columns depict the outer plasma membrane of the rod outer segment; with positive ions (cations) being expelled from the cytoplasm by an energy dependent pump. The inner space pierced by ellipses represents a disc and trans-membrane macromolecules of rhodopsin (R), metarhodopsin (R*) and guanosine cyclase (GC). Absorption of light by the chromophore *cis*-retinal in rhodopsin (R) leads to near instantaneous isomerisation to *trans*-retinal, this causes a conformational change in the opsin producing metarhodopsin II (R*).

*a lecture on the history of GPCRs was delivered by Nobel Laureate Robert J. Lefkowitz, see <http://www.nobelprize.org/mediaplayer/index.php?id=1875> 16 Dec 2012

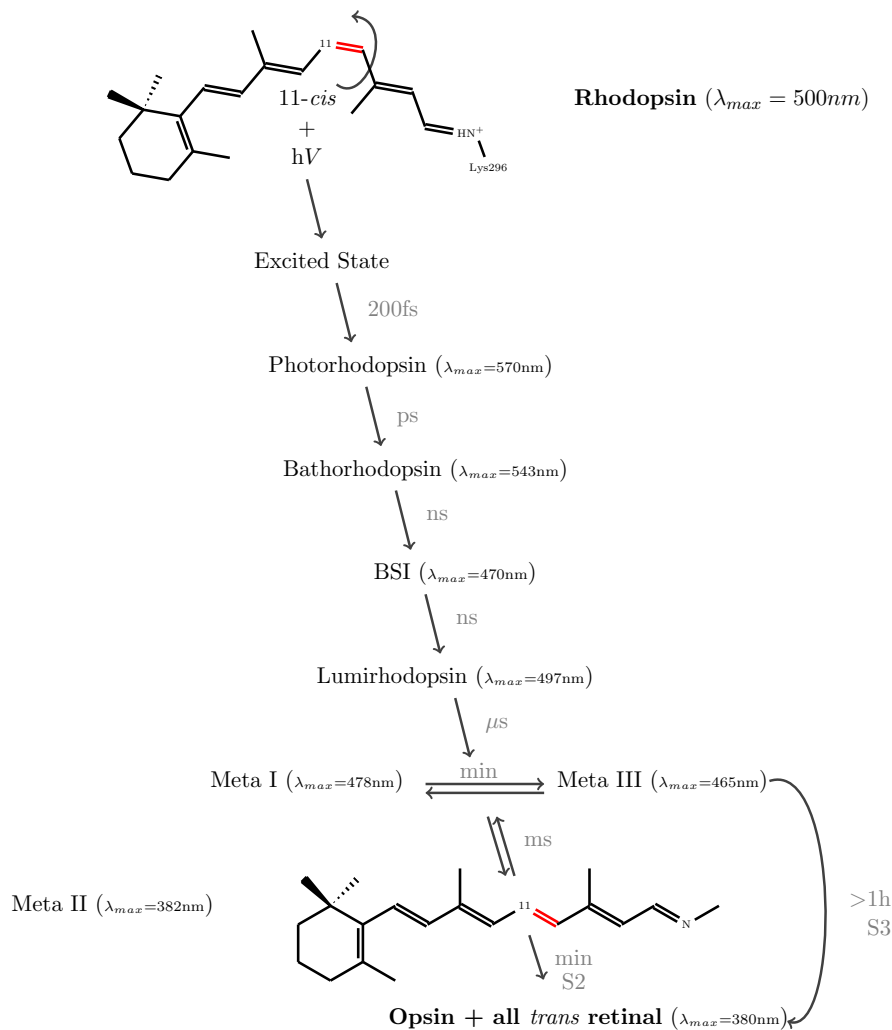


Figure 1.4.1: Conformational changes in Rhodopsin following absorption of a photon($h\nu$). Following absorption of light, the 11-*cis*-retinal chromophore isomerizes to the all-*trans* configuration within 200 fs and then relaxes thermally through a series of spectrally well-defined intermediates to the active Meta II state, which binds and activates the G protein transducin. Hydrolysis of the Schiff's base linkage generates opsin and frees all-*trans* retinal. BSI blue light sensitive intermediate. Adapted from Smith (2010)

Metarhodopsin II has an 'active site' that catalyses the exchange of GTP to GDP in the G-protein transducin (T) activating the transducin.*† The activated transducin (T*) then stimulates the effector protein cyclic-GMP-phosphodiesterase (PDE) in the disc

*GTP: guanosine triphosphate

†GDP: guanosine diphosphate

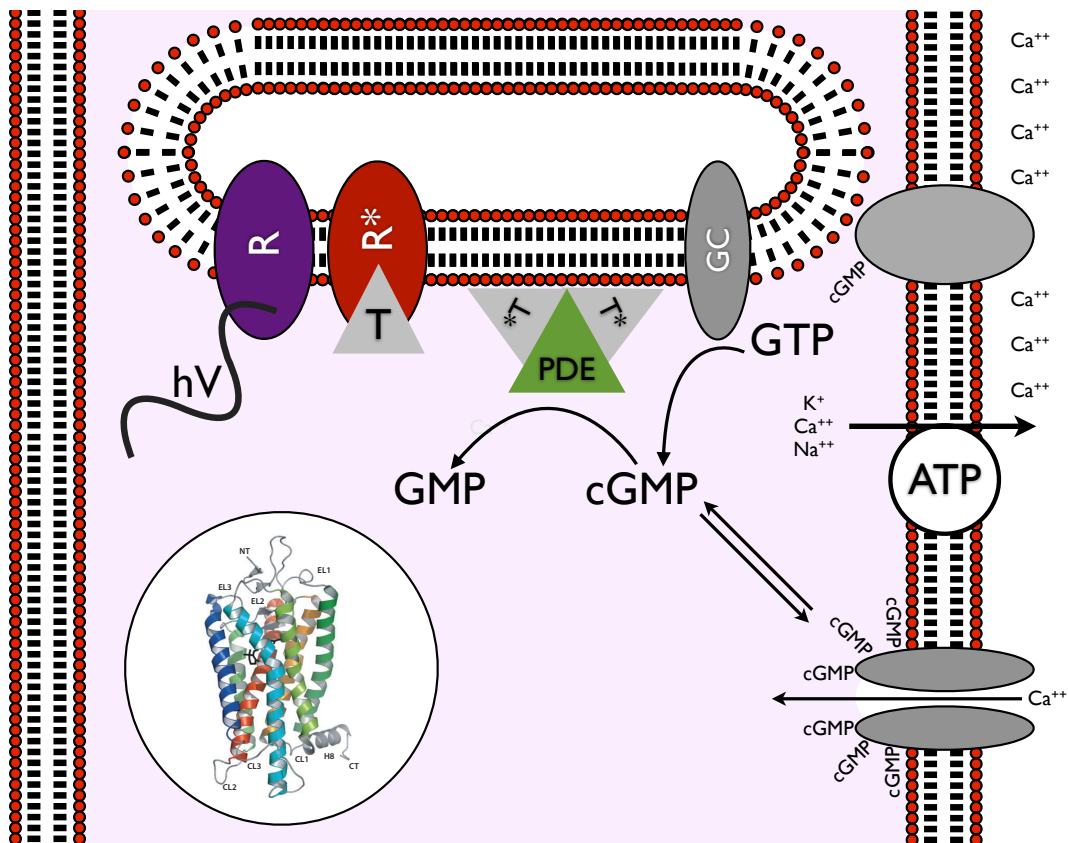


Figure 1.4.2: Phototransduction. Rhodopsin is a seven helix transmembrane macromolecule, inset, (R) that captures a photon and undergoes a conformational change, exposing an active site that interacts with transducin (T) which then reacts with phosphodiesterase (PDE) to reduce the intracellular concentration of cGMP, leading to the closure of the Ca^{++} gated channels. Further detail is provided in the main text.

membrane.* The phosphodiesterase hydrolyses cyclic-GMP (cGMP) to GMP and as the amount of cGMP in the cytoplasm falls the gated ion channels on the outer segment membrane close, causing a build up of Ca^{++} on the outside of the segment. This hyperpolarization reduces the amount of neurotransmitter glutamate that is released at the synaptic cleft and signals an increase in the light level to the downstream neuronal pathway.

Phototransduction also requires reliable deactivation of the receptor protein cGMP-phosphodiesterase and subsequent regeneration to the light sensitive rhodopsin. Without reliable deactivation of the cascade, the rod would have unpredictably variable amplification of photon capture. A first step in deactivation is an interaction between

*GMP: guanosine monophosphate

metarhodopsin II and the enzyme rhodopsin kinase that adds phosphate to residues at the C terminus of the metarhodopsin II. The phosphorylated site is tightly bound by the protein arrestin, preventing further activation of transducin (Pugh & Lamb 2000). With the R* deactivated, the enzyme guanosine cyclase (GC) restores the levels of cyclic GMP and allows the gated calcium channels to re-open.

The isomerisation of rhodopsin from *cis*- to *trans*-form is extremely rapid, of the order of microseconds, the time scale of the numerous intermediates is shown in figure 1.4.1 (adapted from a figure in Smith (2010)). However, the time from isomerisation to free opsin and retinal is of the order of minutes (Wang & Kefalov 2011). The free opsin can weakly trigger the transduction cascade (Cornwall & Fain 1994). The return to the inactive state (rhodopsin) is through the retinoid cycle and can take up to an hour. The rods are saturated at daylight light levels and are therefore largely inactive. When saturated their photopigment regeneration is maximal while their neurotransmitter release is minimal, it has been suggested that this is an energy balancing mechanism over a circadian cycle (Pugh & Lamb 2000). However, this has been called into question by a supposition that when dark adapted the rods have a greater oxygen demand and may present a risk to the compromised retina in people with diabetes (Arden, Sidman, Arap & Schlingemann 2005).

1.4.2 Steady state light and the role of the retinoid cycle

So far the response to a single photon has been discussed, however a sustained response to light requires a continually replenished supply of the active constituent of the rhodopsin. That is, the *cis*-retinal that is isomerised by absorption of a photon must be replaced. This is achieved by a biochemical cycle, which transforms the retinol expelled from the rod to the RPE, and thence from the RPE as *cis*-retinal, back to the rod. This so-called visual cycle is illustrated in figure 1.4.3. It has been known for many years that the RPE is the major site of *cis*-retinal production (Fulton & Rando 1987). Within the RPE the all-*trans*-retinol, received from the IPM and the choroidal circulation is bound to cellular retinol binding protein (CRBP) and converted to 11-*cis*-retinal, by enzyme activity, see figure 1.4.3.

At the end of the sequence, the *cis*-retinal leaves the RPE, crosses the sub-retinal space and enters the photoreceptor outer segment where it combines with free opsin to form visual pigment. The inter-photoreceptor matrix contains a high affinity retinoid binding

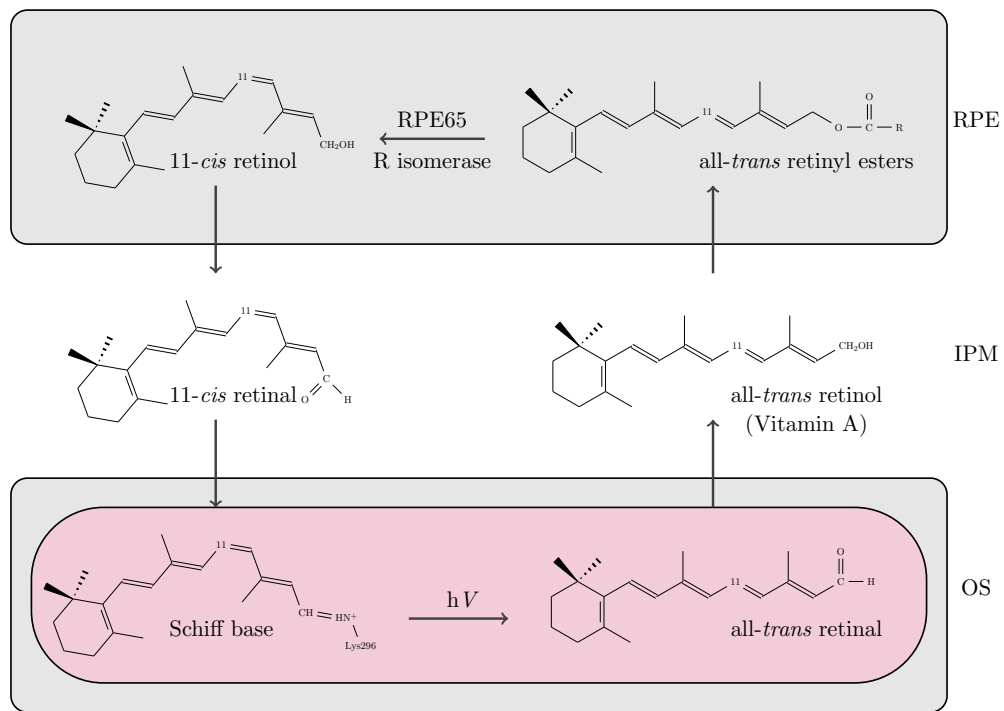


Figure 1.4.3: The retinoid cycle, OS rod outer segment, RPE retinal pigment epithelium, IPM inter photoreceptor matrix

protein.* This protein is necessary for receptor survival and may act as a buffer to protect the retina against extracellular retinoid (Ho, Massey, Pownall, Anderson & Hollyfield 1989).

1.4.3 Summary of rhodopsin

Rhodopsin is central to the process of photo-transduction; its regeneration is dependent upon the transport of material from the choriocappillaris, via uptake and processing in the RPE and active transport across the IPM to the rod outer segment. The availability of vitamin A (retinol) and other nutrients to the RPE cell and the RPE cell's ability to recycle retinoids are the limiting factors in maintenance of rod sensitivity.

*interstitial retinoid binding protein (IRBP)

1.5 Rhodopsin regeneration and the recovery of scotopic sensitivity

Having shown above the intricate systems necessary for the healthy maintenance of rod function, the process of dark adaptation will be discussed and in particular how this mechanism can provide insight into rod performance and hence the efficiency and health of the chorio-rod complex, in particular the RPE.

1.5.1 Sensitivity control under varying light levels

The eye is constantly adapting to varying light levels and is sensitive over a range of some 10 log units (Arshavsky & Burns 2012). This adaptation usually occurs quickly, both when changing from a light to dark environment and the reverse. The sensitivity of the rod system can be described by a threshold versus field intensity plot, where the just noticeable increment in scotopic threshold is measured against a series of background field intensities. This sensitivity was measured by Aguilar and Stiles (1954), see figure 1.5.1.

They describe four distinct regions. At low background intensities the threshold measured is the absolute threshold of the fully dark adapted eye, called the dark light phase, which is due to random fluctuations in the circulating dark current. As the field intensity increases there follows a transition phase when the increase follows a square root law, or the deVries Rose Law, related to the ability of the system to respond to infrequent photon capture. There then follows a linear phase where the ratio of stimulus to background remains constant, Webers law. As the background intensity continues to increase the rod system is unable to detect the stimulus and the system is described as saturated. This is a measure of the static performance of the rod system.

Dark adaptation

Dark adaptation is the recovery of sensitivity upon moving from a light to a dark environment. Technically, the term dark adaptation is usually defined as the recovery of sensitivity following a photo-bleaching light. That is, a light of sufficient intensity to bleach a significant fraction of the photopigment (Leibrock, Reuter & Lamb 1998). A significant level of bleaching is rarely experienced in everyday life.

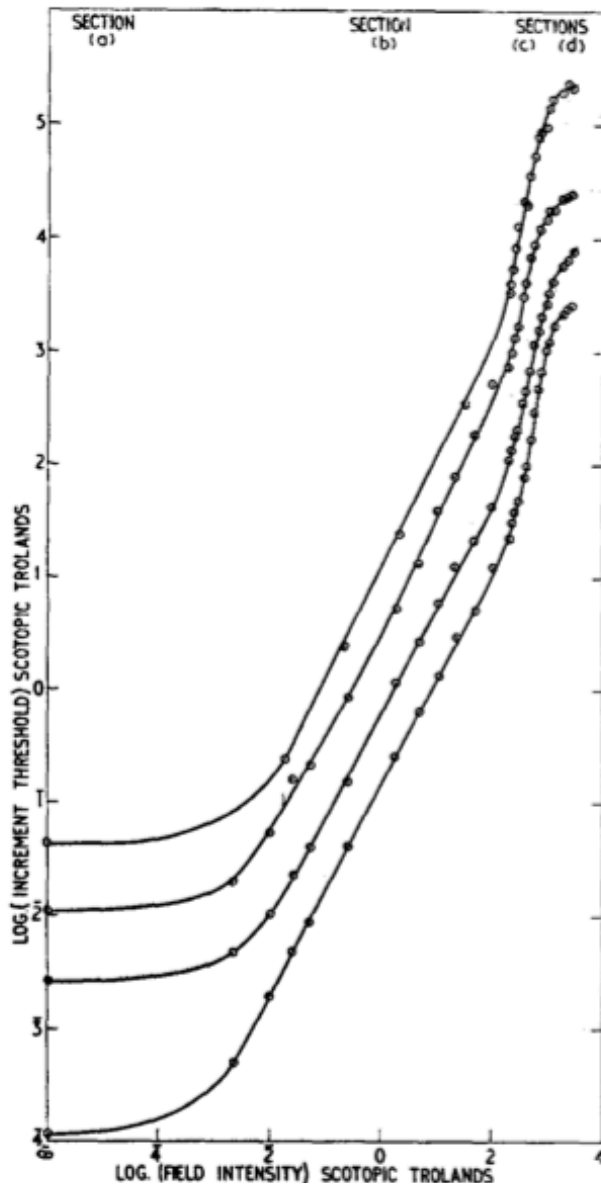


Figure 1.5.1: Threshold versus intensity curve for rod photoreceptors, showing four regions of performance, from very low field intensity to saturation; (a) Dark light, (b) deVries Rose, (c) Weber and (d) Saturated (from Aguilar & Stiles (1954)).

1.5.2 Characteristics of dark adaptation

Following an intense light that bleaches the photo pigment there is a characteristic recovery of sensitivity in the healthy human (Hecht, Haig & Chase 1937), see figure 1.5.2.

The biphasic recovery consists of two exponential phases; the first is the recovery of cone sensitivity, which reaches a plateau until the rods become sufficiently sensitive, whereupon the second phase begins. The transition point between these two phases is often referred to as the alpha point. The slower recovery of rod sensitivity continues until the absolute threshold is reached some 40 mins after the extinction of the bleaching light. The question we address is what biochemical event(s) control this rate of recovery.

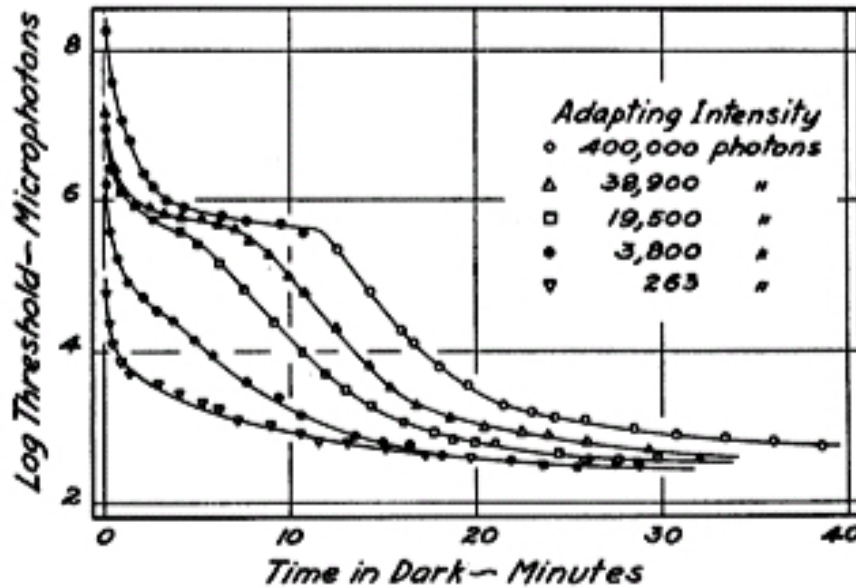


Figure 1.5.2: Dark adaptation recovery for small and large bleaches. (Hecht et al. 1935).

It is worth mentioning here some features of dark adaptation. Firstly, dark adaptation is a measurement of the visual systems ability to recover from a challenge to its equilibrium. Secondly, adaptation suggests that this phenomenon is in some way beneficial and improves the performance of the visual system, this is not the case, the inability to see for several minutes has no benefit. Furthermore the desensitisation of the visual system caused by bleaching is far in excess of the fraction of pigment bleached.

Lamb (2004) elaborates on this using Hecht's figure; in figure 1.5.2 the plot for 3,800 photons* is equivalent to a 20% bleach, initially the threshold is raised 1000 fold and even after several minutes there is still a 100 fold elevation, yet 80% of the photopigment is available for photo-transduction. This suggests that rather than the lack of photopigment causing the desensitisation; it is the presence of a photoproduct that elevates

*an historical term for scotopic trolands

threshold.

In addition, it is well established that the recovery of sensitivity is associated with the visual cycle of pigment regeneration. Hippocrates is reported to have known that night blindness was improved by the consumption of fish oils. More recently, Holm (1925) demonstrated that Vitamin A deficient rats were reluctant to step off a pedestal in low light, while well nourished rats had no difficulty. While in humans, low levels of vitamin A result in prolonged elevation of the absolute threshold of vision (Tansley 1931) and subsequent dietary supplementation results in a marked improvement (Owsley, McGwin, Jackson, Heimbürger, Piyathilake, Klein, White & Kallies 2006).

1.5.3 Models

To account for the characteristic shape of the dark adaptation curve, two subtly different approaches have been followed; one method is to choose a model that fits the data and use that model to reveal insights in to the recovery of sensitivity, a second is to attempt to understand the underlying biological mechanisms and create a mathematical model that is representative of the underlying events. These two approaches are not mutually exclusive.

Hecht et al.(1937) proposed a two exponent model, which both fitted the data and was consistent with the theory at the time, see figure 1.5.2. This proved to be an example the first type of model. Although the prevailing theory was that the sensitivity of the eye was directly related to the amount of unbleached photopigment, Crawford and Stiles' (1932) work on 'equivalent light' and Granit's later work using reflective densitometry (1938), demonstrated that this was too simplistic. The presence of an intermediate compound that continues to stimulate the photo-transduction cascade once the initial light is extinguished became a more useful theory (Pugh 1975).

Other mathematical models of the first type have been used, for example, Jackson et al.(1999) used a four exponent model for heuristic reasons rather than theoretical. This model allows for the parameters to be determined in a simple manner, a variation on this model; an exponential and bilinear is described by McGwin et al.(1999) and can be considered an example of the second model type. This is discussed below in relation to the Mahroo, Lamb and Pugh model.

Dimitrov et al.(2008, 2011) used a bi-exponential method; they were particularly interested in the final thresholds of the cone and rod systems, however, they argue that

the second time constant (rod phase) is equivalent to the second phase (S2) of Lamb's (1981) model. Mahroo, Lamb and Pugh (2004) created a biological model, where they considered the biological events and created a mathematical model that could represent those events.

1.5.4 The Mahroo, Lamb and Pugh Model (MLP)

Lamb (1981) when discussing the recovery of sensitivity following a photo-bleach described three phases of rod recovery. An early phase (S1) with slope $5.3 \log_{10}(\text{td}) \cdot \text{min}^{-1}$ equivalent to an exponential time constant of 5.7s. This phase can be seen when the bleach is weak ($<2\%$) and does not elevate the cone threshold. The second component (S2) has a longer time constant of 104.6s. The component S2 is identified in figure 1.5.3 by the series of parallel red lines. The final component (S3) has a time constant of 6.8 min. The first two components are, for small bleaches, linearly dependent upon the flash intensity. For larger bleaches ($>20\%$) the second phase exhibits rate limited behaviour.

In explaining the significance of these components Lamb adopted the Stiles Crawford (1932) equivalent light model and assumed that the equivalent light was proportional to the presumed photoproduct responsible for threshold elevation. He suggests that each component represents the exponential decay in the concentration of a hypothetical threshold elevating photoproduct.

Pigment regeneration hypothesis

Mahroo and Lamb (2004) re-examined the work of Pugh (1975) on the significance of the photo-bleach and its affect on the recovery of sensitivity and described a biological model. Pugh presented a series of measurements of dark adaptation for varying levels of bleach, see figure 1.5.3, where the leftmost curve is following a bleach of 0.5%, and has features typical of a small bleach; no discernible cone phase and very rapid approach to absolute threshold. The rightmost plot, 98% bleach, shows the typical biphasic recovery.

Mahroo and Lamb (2004) proposed a dark adaptation and pigment regeneration hypothesis; following activation of rhodopsin and its subsequent release of *trans*-retinal, an unknown substance, sometimes referred to as naked opsin, reduces the circulating rod current and elevates the psychophysical threshold by activating the cascade of photo-transduction.

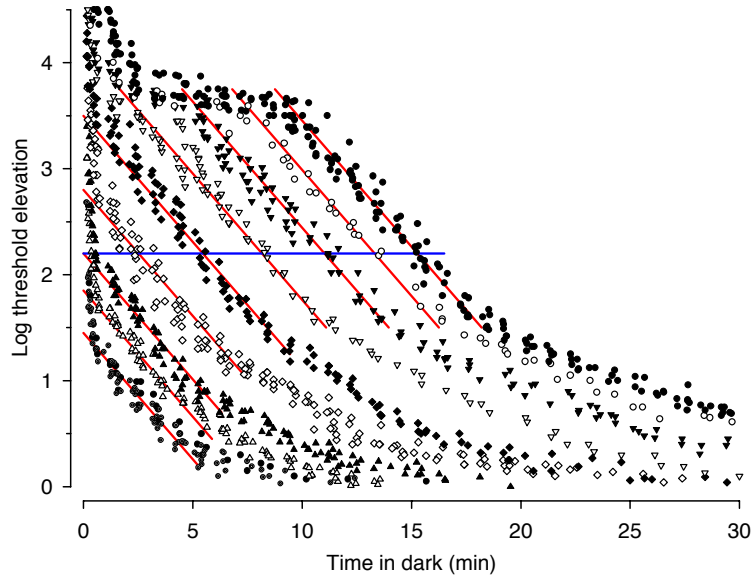


Figure 1.5.3: Dark adaptation recovery curves for a series of bleaches, from 0.5% (left closed circles) to 98% (right closed circles) taken from Pugh (1975).

The work of Mahroo, Lamb and Pugh (MLP) lead to the MLP model, derived from a series of differential equations, based on a simplified retinoid cycle shown in figure 1.5.4. The solutions to these differential equations using the Lambert function (Lambert 1758), they argue, satisfactorily explain the effect of both small and large bleaches. The essence of the model is that one single factor, the delivery of 11 *cis*-retinal, controls the sensitivity recovery in the scotopic section of the post bleach dark adaptation curve. Furthermore, Lamb and Pugh (2004) provide examples from healthy and abnormal human visual systems, as well as animal models where the MLP model is sufficient to explain the changes found in dark adaptation for the examples chosen.

The MLP model explains the effect of bleaches of varying intensities. For small bleaches, less than 8%, the threshold recovery is mediated by a process governed by first order kinetics, i.e. the rate of recovery is determined solely by the rate at which *cis*-retinal can combine with opsin to reform rhodopsin, since there is sufficient *cis*-retinal available locally. The reaction rate is labelled $V(t)$ in figure 1.5.4, and the resultant threshold elevation is proportional to the bleach. The level at which recovery ceases to be governed by first order kinetics is determined by the local concentration of *cis*-retinal, $[c]$. For larger bleaches, greater than 20%, the recovery is characteristic of a rate-limited mechanism. In other words, there is some restriction in the chain of *cis*-retinal supply,

labelled R , which limits the rate at which rhodopsin can reform. A small bleach partially depletes the supply of *cis*-retinal in or near the outer segment, that is reduces $[c]$, but not sufficiently to be the limiting factor, while a large bleach causes a significant reduction necessitating transfer from the RPE to the outer segment, whereupon the limit is the rate of transfer.

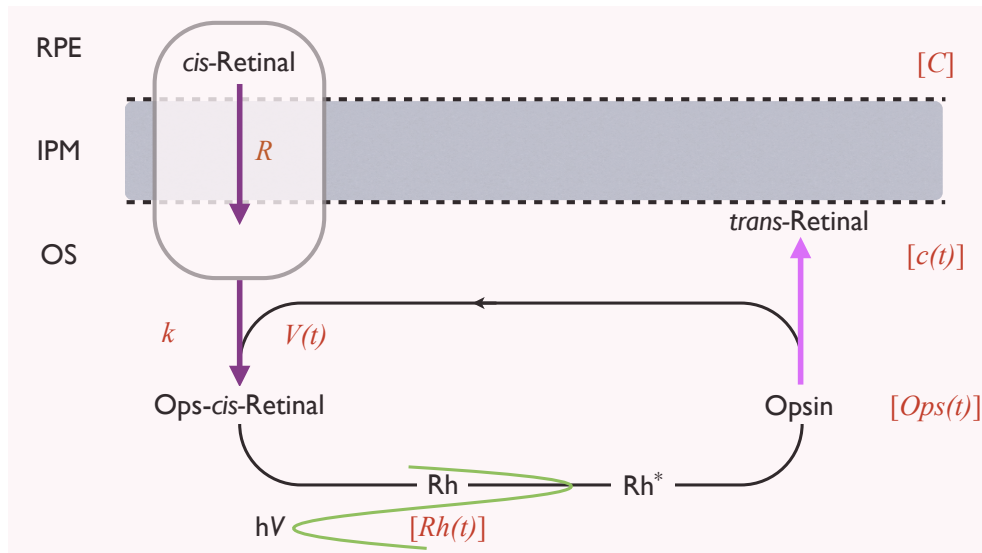


Figure 1.5.4: RPE is the retinal pigment epithelium, IPM the interphotoreceptor matrix and OS the outer segment of the rod. A summary of the retinoid cycle, where R is the resistance to molecular flow, k is the bimolecular constant, $V(t)$ is the rate of reaction, hV a photon, $[Rh(t)]$ the concentration of rhodopsin at time t , Rh^* the transformed rhodopsin, metarhodopsin, $[Ops(t)]$, $[c(t)]$, and $[C]$ the concentrations of opsin, retinal in neuroretina and retinal pigment epithelium respectively. After Lamb and Pugh (2004).

Hypoxic retina hypothesis

In addition to the retinoid deficiency hypothesis, there is an argument that the thickening of Bruch's membrane causes ischaemia of the outer retina and that this reduces the oxygen available to the layers of the retina intermediate to the choroidal and retinal blood supplies. This raises the possibility that the earliest signs of vision loss would be caused by post receptor changes (Feigl, Brown, Lovie-Kitchin & Swann 2006). This is discussed further in section 5.4 on page 170.

Mathematical model

An exponential and bi-linear function (McGwin Jr, Jackson & Owsley 1999), shown in figure 1.5.5, can describe the MLP model and is discussed in detail in chapter 3. The data shown were collected following a flash that bleached $>30\%$ of the photopigment, note the semi logarithmic plot. Three phases of sensitivity recovery can be seen, an early cone phase and two rod phases.

An exponential model, with parameters $\theta_{1,2,3}$, models the early cone phase. The cone threshold $\theta_1(\log_{10}(\text{cd.m}^{-2}))$, θ_2 is the threshold at time zero ($\log_{10}(\text{cd.m}^{-2})$), called the cone coefficient in figure 1.5.5, and θ_3 is the cone time constant, tau (min).

The first rod phase, S2, is modelled by two parameters $\theta_4(\log_{10}(\text{cd.m}^{-2}).\text{min}^{-1})$ the slope of this component, and θ_5 (min) the time at which the phase begins, or α point. The final rod phase, S3 is similarly modelled by two parameters, $\theta_6(\log_{10}(\text{cd.m}^{-2}).\text{min}^{-1})$, the sum of the slopes of the two rod phases and the second transition time, θ_7 (min) or β point.

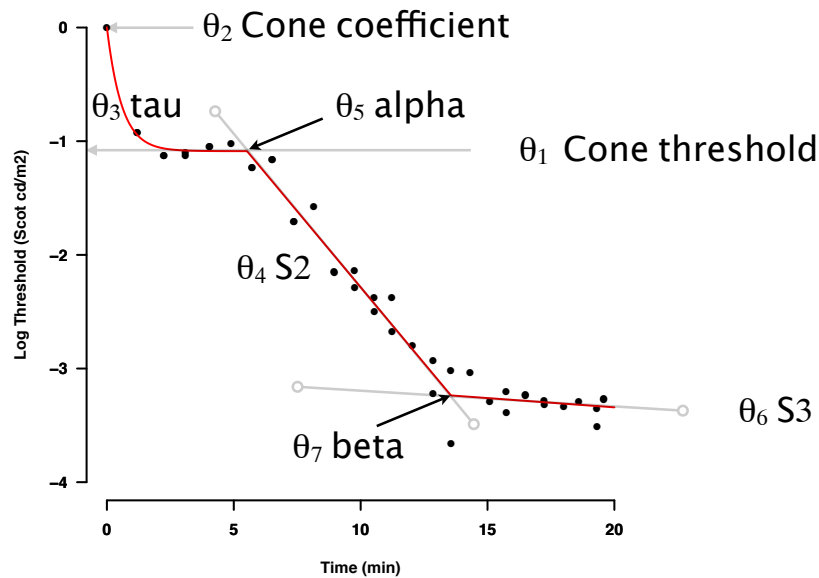


Figure 1.5.5: Model fitted to dark adaptation data, showing the seven parameters; Cone threshold, the cone coefficient, i.e. initial threshold, the cone time constant, tau, the first transition point, alpha, then the slope of the first rod phase, S2, the second transition point beta and then the final rod phase slope, S3.

The threshold can be summarised by the exponential bilinear model where threshold $Thres$, a function of time t , for a parameter θ such that:

$$Thres(t) = \theta_1 + \theta_2 \cdot \exp(-t/\theta_3) + \theta_4 \cdot h(t, \theta_5) + \theta_6 \cdot h(t, \theta_7) \quad (1.5.1)$$

where $h(t, \theta)$ is a step function

$$h(t, \theta_{5,7}) \begin{cases} 0 & \text{if } t - \theta_{5,7} \leq 0, \\ t - \theta_{5,7} & \text{if } t - \theta_{5,7} > 0. \end{cases}$$

This model allows for the extraction of the slope of the S2 phase.

1.6 Conclusion

Features of rod physiology and function have been described; some parts of the above will be highlighted here.

Age related macular disease is ostensibly a disease of the cone system with its pathogenesis in RPE function. Yet the retina is rod dominated and the continued health of cones depends on the viability of the rod system. The photoreceptors are highly specialised post-mitotic cells and are intimately dependent upon the surrounding anatomy, in particular the RPE. Furthermore, rods are preferentially vulnerable to ageing and disease. The recovery of rod sensitivity following a challenge to their equilibrium is a sensitive index of the rod system health. The recovery is often measured using a psychophysical method called dark adaptation, where typically an intense light is used to bleach a significant fraction of the photopigment and the recovery of sensitivity is measured over time.

A mathematical model, based on the retinoid deficiency hypothesis, of the underlying biological events has been presented and the rod phase S2 can be identified in the model (θ_4); this phase reveals the performance of the rod-choroid complex in restoring *cis*-retinal to the outer segment and is therefore a useful measure of the health of that complex. Any intervention that aims to improve retinal health might usefully be monitored and evaluated by measuring dark adaptation.

1.7 Aims of the study

The overarching objective of this study was to understand rod function in the normal and aged eye in terms of the physiology of the outer retina. This understanding would be informed by psychophysical measurement of rod performance in the human eye. To this end a desktop device to measure dark adaptation was developed.

Vision turns on the absorption of light by a photopigment. This absorption brings about a transformation in the photo-pigment, which is then signalled to the organism by a biological cascade. The absorption of light changes the photopigment and it is the restoration of this photopigment and the mechanisms that serve this process in rod mediated vision that are of interest here.

The aims:

1. develop a reliable and accurate device to measure rod function in the human
2. derive robust mathematical methods of model selection and parameter extraction
3. investigate methods of confidence interval calculation for parameters derived by numerical methods of non-linear regression
4. calibrate and characterise the components of two devices to measure dark adaptation
5. investigate the parameters of dark adaptation using the above techniques
6. present the results of these investigations

EXPERIMENTAL METHODS

If you can not measure it, you can not
improve it

Kelvin

Introduction

As described in Chapter 1 the process by which scotopic sensitivity increases when an observer encounters almost total darkness, is called dark adaptation. The speed with which we become responsive to low light levels is now regarded as a sensitive assay of retinal health.

Conventionally, the kinetics of scotopic recovery are measured by exposing observers to a bright light called a photopic bleach. This instantly reduces sensitivity and vision is impeded by a strong afterimage that gradually subsides as vision recovers. During this recovery period observers are required to detect a small flashing light. Typically a button press is required when the flickering stimulus is detected and the level at which it is noticed gradually reduces in intensity as sensitivity increases.

Outline

This chapter presents the experimental apparatus, procedures and calibrations carried out in this study. The first section describes the selection of subjects and ethical approval.

The second section describes a laboratory based technique to measure dark adaptation. The measurement of the static attributes of rod function is well established and the method used here adapts the technique of Aguilar & Stiles (1954). They measured the rod threshold increment versus field intensity.

The essence of their technique was to select wavelengths so that the rod and cone systems could be separated, they used a red background to elevate the cone threshold and measured rod function using a green probe. This allowed rod measurements at higher luminance. In the method presented here a red background elevates the cone threshold, shortening the cone phase of sensitivity recovery and should enable the measurement of rod sensitivity recovery at higher luminance. This in turn will shorten the time taken to measure dark adaptation.

The next section discusses the characterisation of the apparatus, in particular the physical attributes of the light sources. This is followed in the fourth section by a description of how the flicker frequency for the test stimulus was chosen.

In the fifth section the calibration of the flash gun used to photo bleach the subjects is presented along with a table relating flash intensity and pupil size to percentage of photopigment bleached.

A table top digital device was developed in association with industry partners, Tinsley Precision Instruments. This device is described and the methods used to calibrate are presented in the sixth section.

In the next section the technique used to measure contrast sensitivity at low light levels is presented.

Finally there is a summary and discussion of outstanding issues.

2.1 Subjects and ethics

Subjects were recruited by a campus wide call for volunteers. Other subjects were post-graduate colleagues and members of staff from the Faculty of Life Sciences.

Inclusion and exclusion criteria

A subject was considered suitable if they had had an eye examination within the last year and had a best corrected acuity of better than 6/9 Snellen. A result was initially considered acceptable if the subject was able to complete the task required. Subsequent exclusion criteria if any, are discussed in detail, where applied.

Ethics

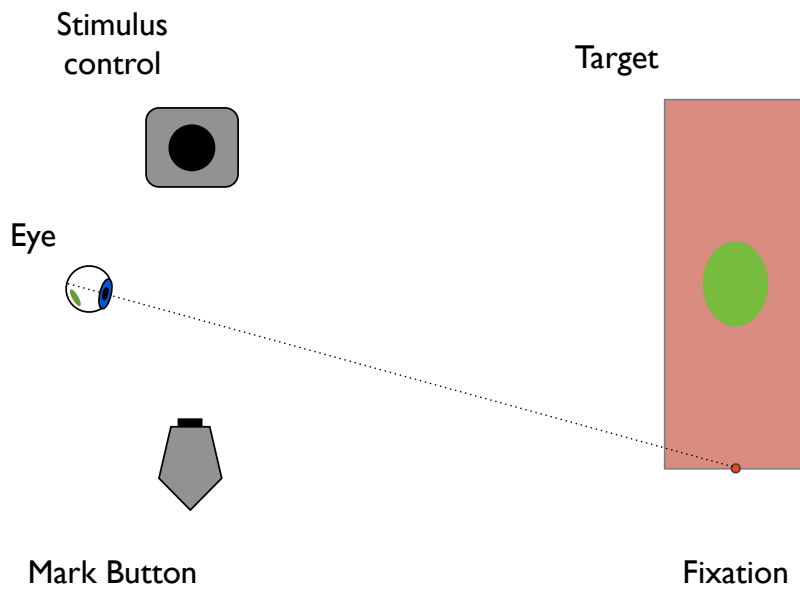
This study was granted ethical approval by the Ethics Research Committee for the Experimentation on Humans at The University of Manchester (reference 09169). The experiment was carried out in accordance with the tenets of the Declaration of Helsinki (World Medical Association:1964 – 2008). The full application for ethical oversight is presented in Appendix J.4 on page 363

2.2 A new analogue technique for measuring scotopic recovery

A laboratory based apparatus was constructed to measure rod sensitivity, shown in figure 2.2.1. The conventional method of measuring dark adaptation uses a zero luminance background. However, the method used here has a luminous background to which the rods are relatively insensitive. Once the stimulus intensity is below the photopic luminance of the background it can only be detected by the rods and therefore any further change in stimulus threshold is due to the rod response alone.

Apparatus

A schematic of the apparatus is shown in figure 2.2.1a and a photograph in 2.2.1b, the target screen is 30cm by 13cm and is set 57cm from the subject. The subject is lightly



(a) Schematic of analogue apparatus



(b) Photograph of analogue apparatus

Figure 2.2.1: The analogue apparatus, showing the chin rest, the stimulus and its controller, time stamp button and apparatus required to generate the stimulus. The grey box on the right with three switches controls the wavelength of both stimulus and background, along with the intensity of the background.

constrained using the chin rest. The stimulus, which is 4cm in diameter, flickers as a square wave at 4Hz controlled by a function generator TWG501 (Feedback,UK), see appendix E.2.1 on page 304 for a schematic of the electronic components.

Stimulus The stimulus is in the form of a pedestal. The background is at constant luminance and the stimulus is presented over this, see figure 2.2.2. This was achieved by using an enclosing cylinder, which contained both background and stimulus LEDs. The background LEDs were matched to the surrounding background.

The view seen by the subject is shown in figure 2.2.2. The subject attends to the eccentric fixation point, a red LED* ($\lambda_{max}=655\text{ nm}$) with the preset luminance of 8.4 cd.m^{-2} . The background is red ($\lambda_{max}=655\text{ nm}$) and has a preset luminance of 0.05 cd.m^{-2} (photopic). The central green stimulus ($\lambda_{max}=530\text{ nm}$) on a red pedestal subtends 4° at 15° horizontal eccentricity to the fovea in the temporal retina.

Measurement technique

The subject's right eye was exposed to a brief flash of light from a flashgun (Speedlight SB800, Nikon, Japan). The use of a flash of light is well established (Hecht et al. 1935, Campbell & Rushton 1955, Rushton & Powell 1972) So that accurate fixation could be maintained, care was taken to not expose the fovea to the flash. The intensity of the flashgun was one quarter the maximum and bleached the photopigment, dependant upon pupil size, from 23 to 98% (Rushton & Powell 1972). The left eye was occluded, and natural pupils were used.

The subject was then lightly constrained using a chin rest and instructed to maintain fixation upon the small LED to their right hand side, see figure 2.2.2. A method of adjustment was used to set thresholds. The subject was prompted aurally to set a threshold, using the stimulus control, by the operator approximately every 20 to 30 seconds. They were told to set the threshold in one direction only, from 'unseen to seen' by turning the controller clockwise. Once the stimulus was seen by the subject they stopped turning the controller and pressed the marker switch, and then returned the stimulus to its zero value.

The voltages across these two devices, the controller and switch, were tracked and recorded using a high-resolution data logger (PICO 20ADC, UK) and a laptop computer

*light emitting diode

(Sony Vaio, Japan), which displayed the voltages to the experimenter throughout. This enabled the subject to be monitored for compliance to instructions and attention. Then the data were stored on an Excel spreadsheet (Microsoft, USA), for subsequent analysis. Some experienced observers were able to set threshold without supervision.

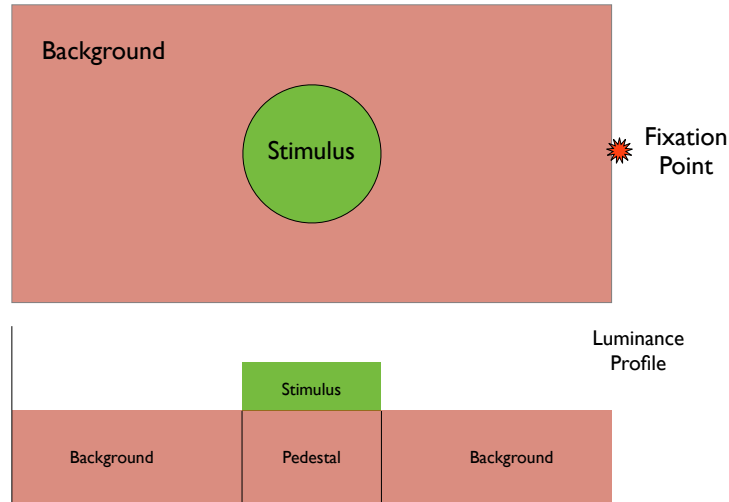


Figure 2.2.2: The apparatus as seen from the subject's perspective, lower panel the luminance profile of the display.

Data analysis

The analysis of the data and methods of curve fitting will be discussed at length in the next chapter, but are briefly mentioned here for completeness. A version of the exponential bi-linear parametric model proposed by McGwin et al. (McGwin Jr et al. 1999), was fitted to the data, see section 3.4 on page 123 and figure 3.1.2 on page 110. To determine the parameters a non-linear regression was applied using a multi start algorithm with the Nelder-Mead (Nelder & Mead 1965) simplex method as its kernel in both MATLAB and R. This simplex based method was chosen as the behaviour of the parameters, i.e. how they vary, is unknown and this method is useful when the derivatives of the parameters are unavailable (Wright 1995). The model can be represented as the threshold $Thres$ as a function of time t

$$Thres(t) = \theta_1 + \theta_2 \cdot \exp\left(\frac{-t}{\theta_3}\right) + \theta_4 \cdot h(t, \theta_5) + \theta_6 \cdot h(t, \theta_7) \quad (2.2.1)$$

where $h(t, \theta)$ is a step function

$$h(t, \theta) \begin{cases} 0 & \text{if } t - \theta \leq 0, \\ t - \theta & \text{if } t - \theta > 0. \end{cases} \quad (2.2.2)$$

Further detail regarding the algorithm used, along with other statistical methods used are described more fully in the next two chapters. Appendix A.1 on page 253 contains the computer code used.

Statistical significance was set at the traditional 5% level (Johnson 1999, Poole 2001). Data were initially stored as spreadsheets and subject to preliminary analysis, e.g. plotting of the threshold over time, in Excel (Microsoft, USA) and then subject to further analysis using scripts written in MATLAB (Nantick, USA) or the open source statistical programming language R [www.cran.org](R Development Core Team 2010).

Summary statistics; mean, median, variance and inter-quartile range (IQR) were calculated for parameters of interest. Non-symmetrically distributed parameters are quoted as median and IQR, while symmetric parameters are quoted as mean and standard deviation. When comparing repeated measurements of biological phenomena Altman and Bland have presented elementary statistical methods. They compare the difference between the two measurements to the the mean of the measurements. They also propose the coefficient of repeatability (CoR) as a statistic, which is defined as the standard deviation of the differences multiplied by ± 1.96 (Bland & Altman 1986).

The red background

The red background has some benefits. Theory suggests (Aguilar & Stiles 1954) that the red background minimises the cone phase of the dark adaptation recovery curve and allows the rods' increase in sensitivity to be rapidly identified in the data. This should shorten the time required to establish the slope of the S2 phase. A second benefit is that the subject is more comfortable when not in complete darkness.

Central to this method is an assumption that the rods are insensitive to the red light and that their recovery is unaffected by the background. This was considered in two ways, a physical approach presented in the next section and an empirical one. The empirical investigation of the red LED light is the basis for chapter 5 and will be discussed there.

2.3 Calibration of the Analogue Device

In order to characterise the light sources two photometers were used.

Photometers

The characteristics of the LEDs, the flashgun, and optical density of filters and diffusers in the apparatus were measured using a combination of two photometers; the PR1500 and the PR650 (Photo Research, Calif. USA).

The PR1500 is a spot photometer which uses a photomultiplier tube. The device has a dynamic range of 7 log units, from 1×10^{-3} to 1×10^4 $\text{mW.cm}^{-2}.\text{steradian}^{-1}$ using variable gain and internal neutral density filters, over the range 375 to 1100 nm (PR1500 Operating Manual). The PR1500 also has an analogue output jack, which returns values in volts within microseconds, allowing connection to a data logger or smart interface e.g. CED1401 (CED Cambridge, UK). The output voltage needs to be calibrated against a known source and subsequent values calculated. This feature was used to measure the light emitted by the flashgun.

The PR650 has a quoted sensitivity range of 3.4 to 17,000 cd.m^{-2} and can be controlled remotely by a computer and Matlab scripts using functions from the psychtoolbox (Brainard 1997). The PR650 uses an array of 81 silicon cells to measure the radiometric output of a source. The incoming light is split using a prism and the light then directed at the silicon cell array. Each cell measures the radiance for a narrow band about a particular wavelength. Measurements can be made in the range 380 to 780 nm. The bandwidth of each measurement is 8 ± 2 nm. Photopic measurements are rendered using internal conversion factors. When connected to the computer the PR650 can be used to measure the spectral composition of the light source in radiometric units. The PR650 has a dynamic range of 4 log units and uses a system of Automatic Adaptive Sensitivity. This feature of the PR650 automatically determines the optimal dynamic range to maximise the signal to noise ratio by varying the integration time (PR650 Operating Manual). The larger the signal measured, the shorter the integration time required. This becomes important in the characterisation of the light emitting diodes, where the light emitted at non-dominant wavelengths is a small fraction of the maximum.

To summarise, both instruments can be connected to external devices to obtain measurements over brief time intervals in the case of the PR1500 or in the case of the PR650

to yield wavelength spectra. The PR1500 is more sensitive than the PR650 but cannot provide detailed wavelength information.

2.3.1 Investigation of the characteristics of the light sources

Two light sources were used red ($\lambda_{max}= 655$ nm) and green ($\lambda_{max}= 530$ nm). Each light source could be used either for the background or the stimulus. The analogue apparatus, see figure 2.2.1, was constructed to produce light at low luminance; the stimulus varies from zero to 0.5 cd.m^{-2} (phot), while the background has four preset levels; ‘off’, 0.05, 0.1 and 0.2 cd.m^{-2} (phot). The light generated by the LED is reflected from the internal walls of the stimulus housing and travels through the diffuser then to the eye. Measurements of dark adaptation were made with a red background and a green stimulus.

Method

As discussed above the PR650 is unable to measure very low light levels, therefore when measuring the light produced by the LEDs the diffuser was removed and the LED light reflected from the internal wall of the apparatus measured directly. Having measured the radiometric output of each LED type, it was necessary to convert the radiometric values to photometric values, figure 2.3.1 summarises the various methods used to determine the scotopic and photopic outputs of each LED.

The first factor to consider was the absorption characteristics of the diffuser. The optical density was found and is shown in figure 2.3.2.

The sensitivity of the eye depends upon its state of adaptation, therefore it is important that measurements can be rendered in both scotopic and photopic units. The photopic and scotopic sensitivity of the human eye as defined by CIE standards was used in this study: photopic (CIE:1924) and scotopic (CIE:1951), see figure 1.2.5.

To measure the spectral output of a source the PR650 was connected to an Apple MacBook (Apple, CA, USA) and controlled using a script operated through Matlab (Mathworks, MA, USA) using Psychophysics Toolbox extensions (Brainard 1997, Pelli 1997).

Analogue Device

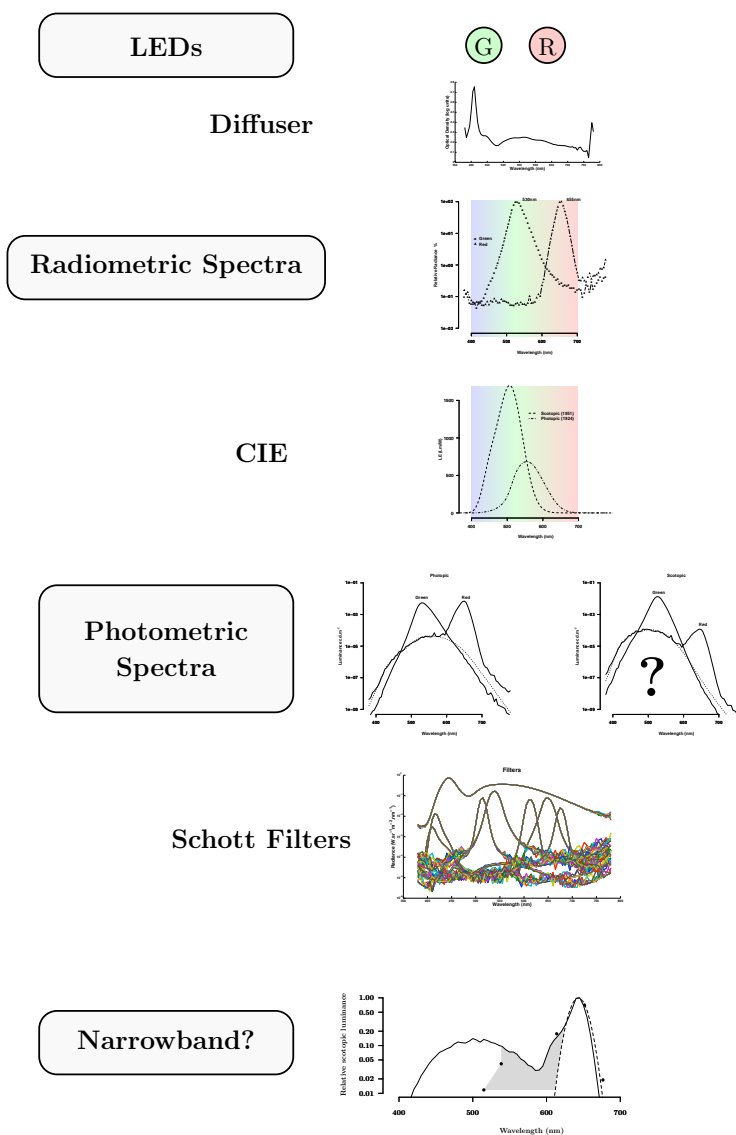


Figure 2.3.1: The characterisation of the LED light sources. Initially the optical density of the diffuser was found, then the radiometric spectra of each LED. These spectra were then weighted by the diffuser and the CIE luminous efficiency spectra to find the photopic and scotopic spectra for each LED. This raised a question about the scotopic light emitted by the red LED at wavelengths of ~ 500 nm. Using narrowband filters the light emitted by the red LED was measured.

Optical Density of the Diffuser

The light from the LEDs is viewed through a broadband diffuser (Xerox, White Paper, 80gsm). The amount of light absorbed by a filter is described by its optical density d , this is defined as the logarithm (base 10) of the transmission of the filter.

$$d = -\log_{10} \frac{I}{I_0} \quad (2.3.1)$$

where I is the intensity through the filter and I_0 is the intensity without a filter.

Using the PR650 and a broadband reference light source of luminance 4820 cd.m^{-2} , the spectral composition of the reference source was found. Then the diffuser was introduced into the light path and the spectral output of the broadband source again measured.

The optical density plotted against wavelength is shown in figure 2.3.2. The highest absorption is at the shorter wavelengths ($<450 \text{ nm}$) reaching a peak of 2.76 log units at 410 nm , at wavelengths greater than 450 nm the optical density is of the order of $2.2 \pm 0.05 \text{ log units}$. For all wavelengths measured the optical density is $2.2 \pm 0.1 \text{ log units}$.

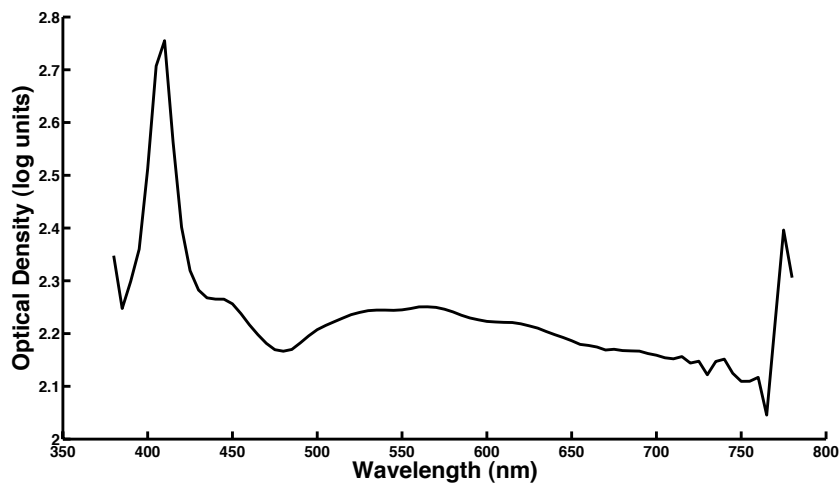


Figure 2.3.2: Variation of optical density in a broadband diffuser against wavelength

The optical density at each wavelength measured was used as a weighting factor when calculating the luminance of the screen.

2.3.2 Spectral Description of the Sources

If the red LED has significant output at short wavelengths it will stimulate the rod photoreceptors. It follows therefore that the spectral output needs to be clearly described; the fundamental principle of this dark adaptation measurement technique is that there is a separation between the rod and cone systems that can be exploited by careful selection of test wavelengths.

The PR650 cannot measure spectra with total luminance below 3.4 cd.m^{-2} , so to measure the spectral radiances the diffuser was removed and the LEDs measured directly. Further characterisation was carried out using the PR1500 and seven Schott narrow band filters (Schott, Mainz, Germany) and is described below.

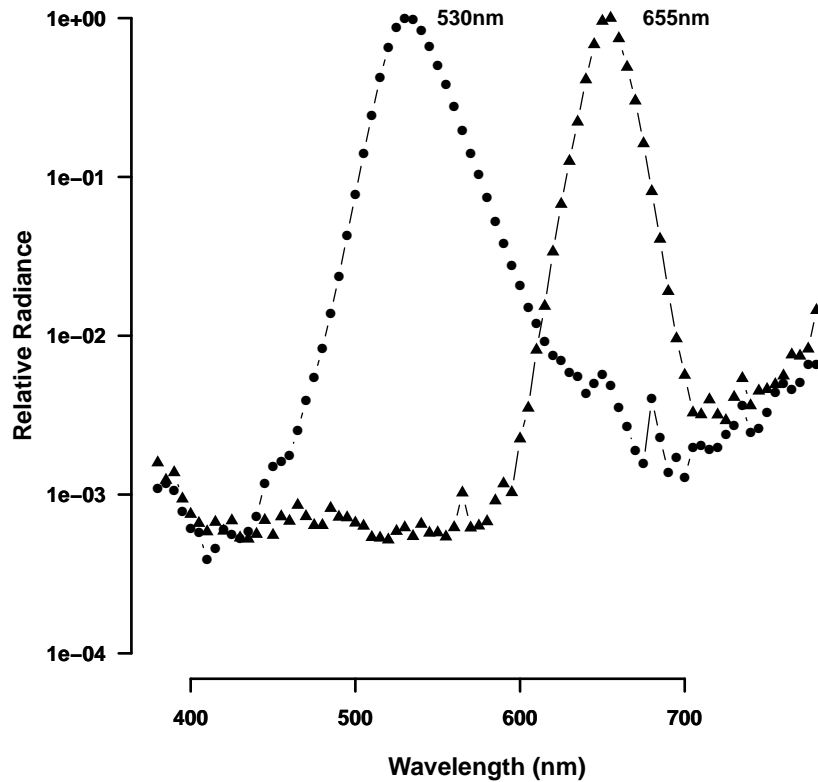


Figure 2.3.3: The spectral radiance of the red and the green LEDs, filled circles are green, filled triangles are red. The ordinate axis is logarithmic.

Two types of LED were used to produce the light in the apparatus. Five radiometric measurements of the spectral output of each LED were made using the PR650 connected to a computer. The green LED had a peak wavelength 530 nm and full width half maxima (FWHM) of 30 nm, and the red had a peak wavelength 655 nm and FWHM of 20 nm. Figure 2.3.3 shows the output of the green and the red LED. Both radiance spectra are approximately symmetric about their peak wavelength with a slight elevation in the far red. At wavelengths far from the peak the noise levels become more evident. The noise may be attributed to straylight, noise generated by the PR650 or noise from the LED. This question of noise was addressed and the details follow below.

Calculating the Photopic Scaling Factor

The photopic luminance spectra of the screen in the apparatus was found by measuring the spectral radiance of each LED weighted by the photopic sensitivity function (V_λ CIE (1924)) and corrected for the optical transmission of the diffuser. This gave a spectrum in photopic $\text{cd.m}^{-2}.\text{nm}^{-1}$. However, this was not equal to the directly measured luminance rather it represented the distribution of light output from the screen.

Then the area under the data points was scaled to have an area corresponding to a photopic luminance of 0.2 cd.m^{-2} , the maximum luminance of the background used in this study. The initial measurements of total radiance were; green $0.047(\pm 4.8 \times 10^{-5}) \text{ mW.cm}^{-2}$ and red $0.564(\pm 0.001) \text{ mW.cm}^{-2}$, equivalent to $0.2(\pm 0.001) \text{ cd.m}^{-2}$ for green and $0.2(\pm 0.002) \text{ cd.m}^{-2}$ for red.

The scaling factor is necessary since the background is illuminated by 4 LEDs in the apparatus and measurements were taken from only one LED. A logarithmic plot of the calculated photopic spectral luminance of each LED can be seen in figure 2.3.4. The green background remains quite symmetric about its peak wavelength, however the red background is skewed by the photopic sensitivity function, with an apparently large amount of energy for wavelengths less than 600 nm.

Calculating the Scotopic Luminance

In order to consider the scotopic luminance of the background the unweighted radiometric measurements were converted to photometric units. The radiometric values were multiplied by the scotopic sensitivity function (V'_λ CIE (1951)), corrected for the trans-

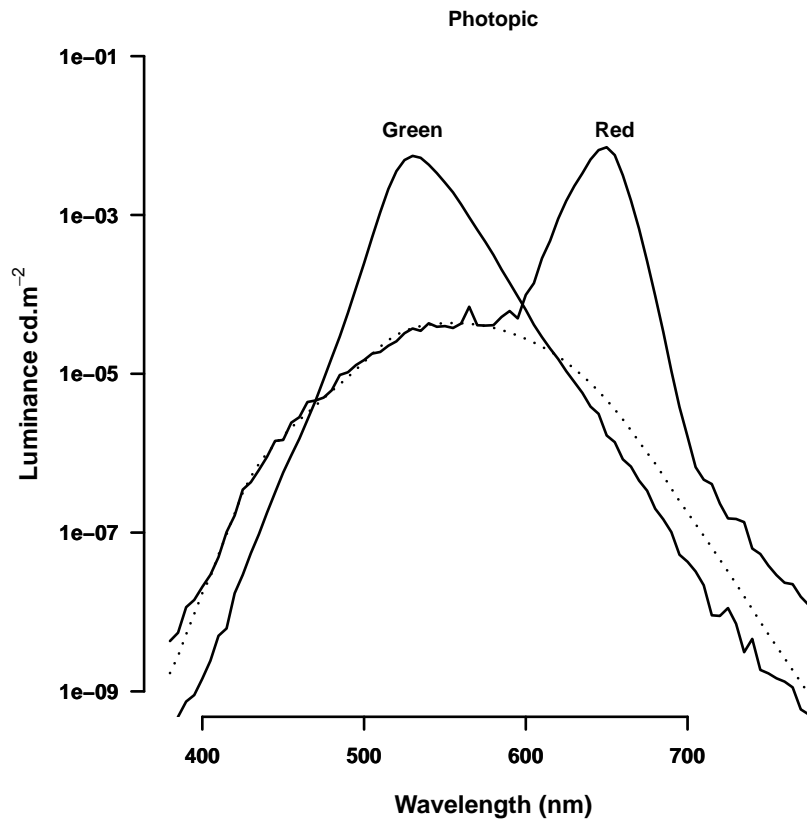


Figure 2.3.4: Photopic luminance of the LEDs used in the test display obtained by weighting with V_λ and the transmittance of the diffuser. The green LED is shown with a peak at 530 nm, the red LED with a peak at 655 nm. The dotted line is the zero value of the PR650, scaled for the red LED. A log plot is used to show the contribution from the skirts of the distributions.

mittance of the diffuser and multiplied by the scaling factor found above, see figure 2.3.5 and equations 2.3.2 and 2.3.3.

The CIE luminous efficiency functions are relative, so a further scaling factor of 2.489 was used, this is the ratio of scotopic luminance to photopic luminance for a broad band source, and compensates for the difference in absolute values between photopic and scotopic sensitivity curves.*

The area under the resulting curves gave the scotopic luminance of the backgrounds. Figure 2.3.5 suggests that for wavelengths less than 600 nm, the red LED contributes to scotopic luminance. However, this may be an artefact, the method of repeatedly scaling

* $\left(\frac{1700}{683}\right)$

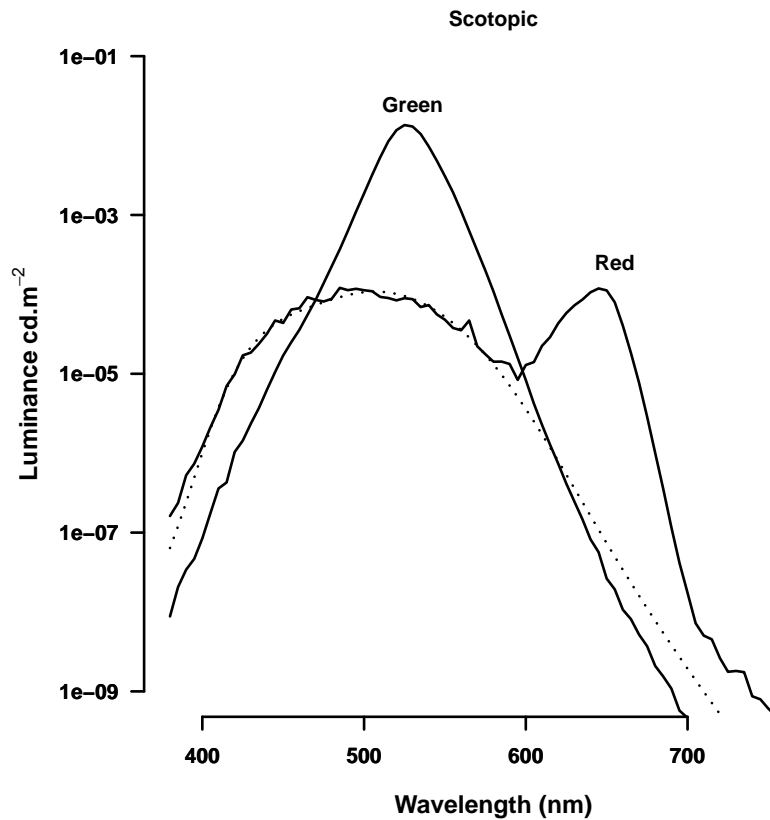


Figure 2.3.5: Scotopic luminance of the LEDs used in the test display, following weighting with V'_λ . The green LED is shown with a peak at 530 nm, the red LED with a peak at 655 nm. The dotted line is the zero value of the PR650, scaled for the red LED.

very small values might be misleading. Nevertheless, this is important when considering rod sensitivity measurements, as this is maximal in the region of 500 nm. The rod is sensitive to light levels as low as 1×10^{-7} cd.m⁻²(scotopic), and if the red LED has a significant output at 500 nm then the rod will respond to the sum of both the stimulus and the background.

Summary of the algebra

The repeated measurements and scalings are summarised by the following equations. The first equation shows how a constant specific to the instrument was found. The second equation uses this constant to calculate the scotopic luminance of the background for

the two LED types.

$$\frac{Rad}{Trans}.V(\lambda).k = 0.2\text{cd.m}^{-2}_{photopic} \quad (2.3.2)$$

where *Rad* (radiometric units, W) is the radiometric output of the source, *Trans* (no units %) the transmittance of the diffuser, *V*(λ) (Lm/W) the relative photopic luminous efficiency function and *k*(no units) the instrument specific constant.

$$2.489 \times \frac{Rad}{Trans}.V'(\lambda).k = Luminance_{scotopic} \quad (2.3.3)$$

Equation (2.3.2) was used to find *k*, then using equation 2.3.3, where *V'*(λ) is the relative scotopic luminous efficacy function, the scotopic output was calculated.

2.3.3 Summary

The experimentally determined broadband and narrowband values along with the narrow band equivalents calculated using Wyszecki & Stiles (1967) reference data are presented in table 2.3.1. A narrow band source at 655 nm with photopic luminance of 0.2 cd.m⁻² has a scotopic luminance of 2.8×10⁻³ cd.m⁻². In our apparatus the luminance returned by the PR650, which has measured across a wide spectrum, is 1.31×10⁻² cd.m⁻². If the wavelengths chosen for the calculation are restricted to the interval 10 nm about the peak wavelength, (645 – 665) then the scotopic luminance is 2.9×10⁻³ cd.m⁻². This suggests that the light sources are narrowband and that we have scaled the noise of the PR650 and added that to the total.

The measurements with the PR650 suggest that a third of the scotopic luminance for the red LED is generated by wavelengths shorter than 600 nm. If the source has a broadband nature, that is, has significant light levels at wavelengths of ~500 nm, then the shorter wavelengths may affect the assumption that the rods are relatively insensitive to the background.

A similar argument applies to the green LED, however, as the peak of the scotopic sensitivity function is near to the peak of the green LED, there is less distortion of the spectral distribution.

This raises two questions, does the red LED emit light at shorter wavelengths, and what level of scotopic luminance is there at the shorter wavelengths?

Table 2.3.1: To convert from photopic to scotopic luminance at 655 nm, a factor of 0.014 was used, at 530 nm, a factor of 2.34. (Wyszecki & Stiles 1967, page 104). The measured values use the whole spectrum for the broadband figure, and a restricted spectrum for the narrow band figure. The measured narrowband and calculated figures are in good agreement, however, the broadband figures differ by a factor of ~ 2 to 3 fold.

Scotopic cd.m ⁻²	Red	Green
Measured		
Broadband	0.0131	0.8844
Narrow band	0.0029	0.4671
Calculated	0.0028	0.468

We can see from this that the PR650, although able to define the peak wavelengths and FWHM, cannot provide the information we need. The insensitivity of the PR650 to low light means that a different strategy had to be adopted.

2.3.4 LED Noise and an Ideal LED

In order to investigate the nature of the noise in the measurements of the red LED, a further series of measurements were made. Any noise could be derived from the measurement apparatus, the LED itself, straylight or a combination of all three. The causes of noise within an LED, are beyond the scope of this work, further details are discussed in Bürmen, Pernuš & Likar (2008).

The PR1500 which is based on a photo-multiplier, is very sensitive and has a lower measurement level of 1×10^{-2} cd.m⁻² in the range 350 to 1060 nm. This range can be extended by altering the sensitivity of the device. This increases the sensitivity by a log unit (PR650 manual).

Measurements made with the PR1500 do not have to be made over the entire spectrum. The PR1500 photo-spectrometer will measure a narrow band spectrum and use an open ended integration time. This gives a hundred fold increase in sensitivity over the PR650. This greater sensitivity means that measurement with narrow band filters and the PR1500 will provide information about the red LED at wavelengths less than 600 nm.

The Use of Schott Narrow Band Filters to Measure Emitted Light

In order to measure the red LED with greater precision a series of narrow band filters were used in conjunction with the PR1500.

The exact optical characteristics of the filters were determined as follows. A reference light source with luminance 4135 cd.m^{-2} was used; the source was an array of ultra bright LEDs (Lumiled Luxeon colour temp. 5500k, Phillips, NL) with a diffuser (Lee Filter no 216, UK). The reference broadband source was first measured with the PR650, and then each filter was introduced into the light path in turn and the spectral output of the source re-measured. A total of seven measurements for each filter were taken.

The spectral radiance of the source and spectral radiance measured for each filter are shown in figure 2.3.6. The amplitude of the source has a range of less than 3 log units, with a spike at 440 nm, the logarithmic plot tends to compress values giving a reduced impression of the elevated area. The spike at shorter wavelengths allows the manufacturer to claim a colour temperature of 5500k.

The amplitude of the reference source is well within the claimed dynamic range of the photometer, yet there was measurable noise at the extremes of the spectra measured for the narrowband filters. This suggests that the dynamic sensitivity mechanism, described in section 2.3, has a dynamic range ~ 3 log units when measuring these sources rather than the 4 log units claimed by the manufacturers.

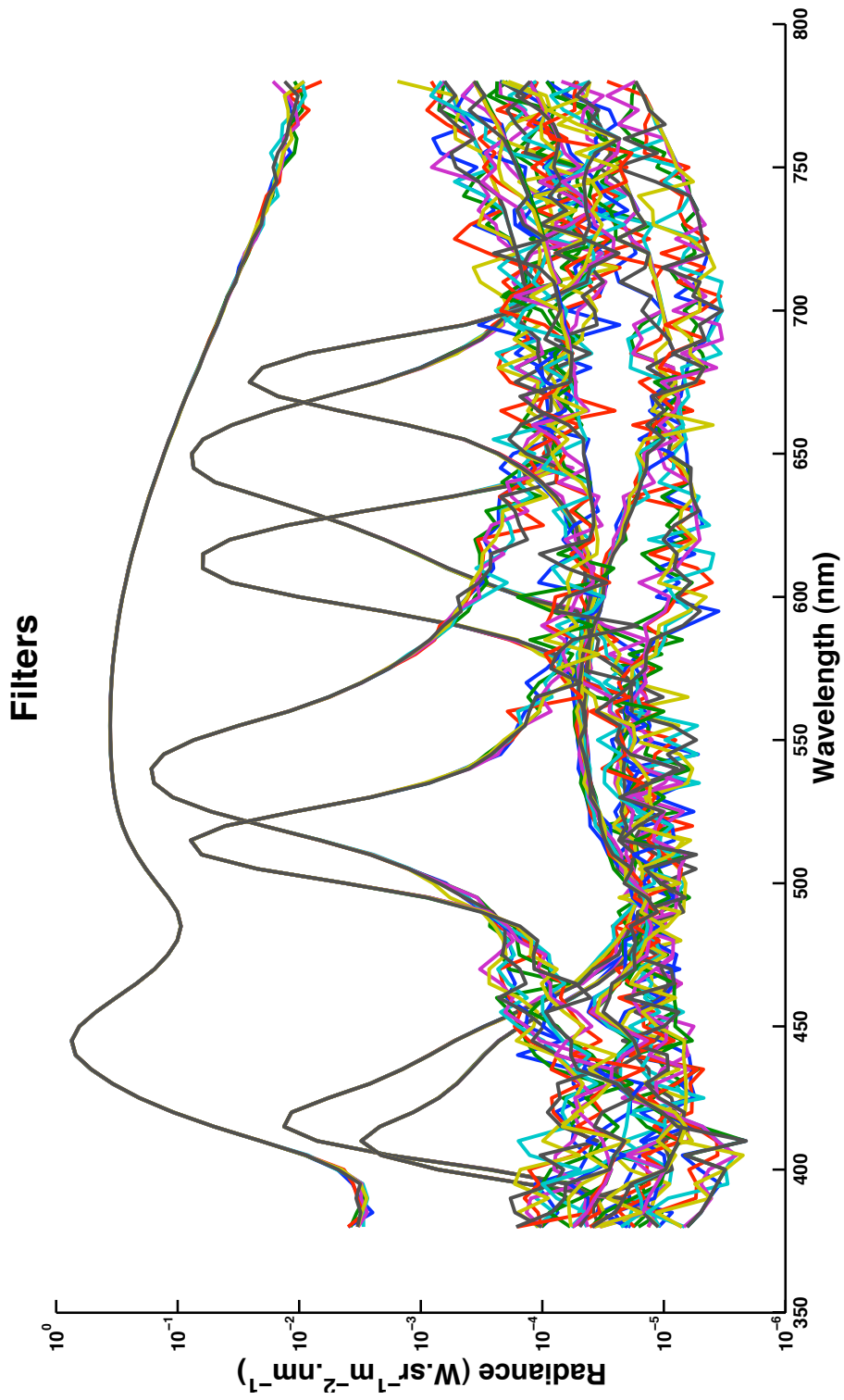


Figure 2.3.6: The spectral output of a series of narrow band filters shown with the reference broadband source at the top, note the use of the log scale. The measurements shown are the raw data, averaging would have hidden the noise at the extremes of the spectra.

The transmission and half height widths varied for each filter and are summarised in table 2.3.2. A linear plot of the optical density more clearly reveals the narrow band nature of the filters and facilitates determination of the peak transmittance and can be seen in figure 2.3.7.

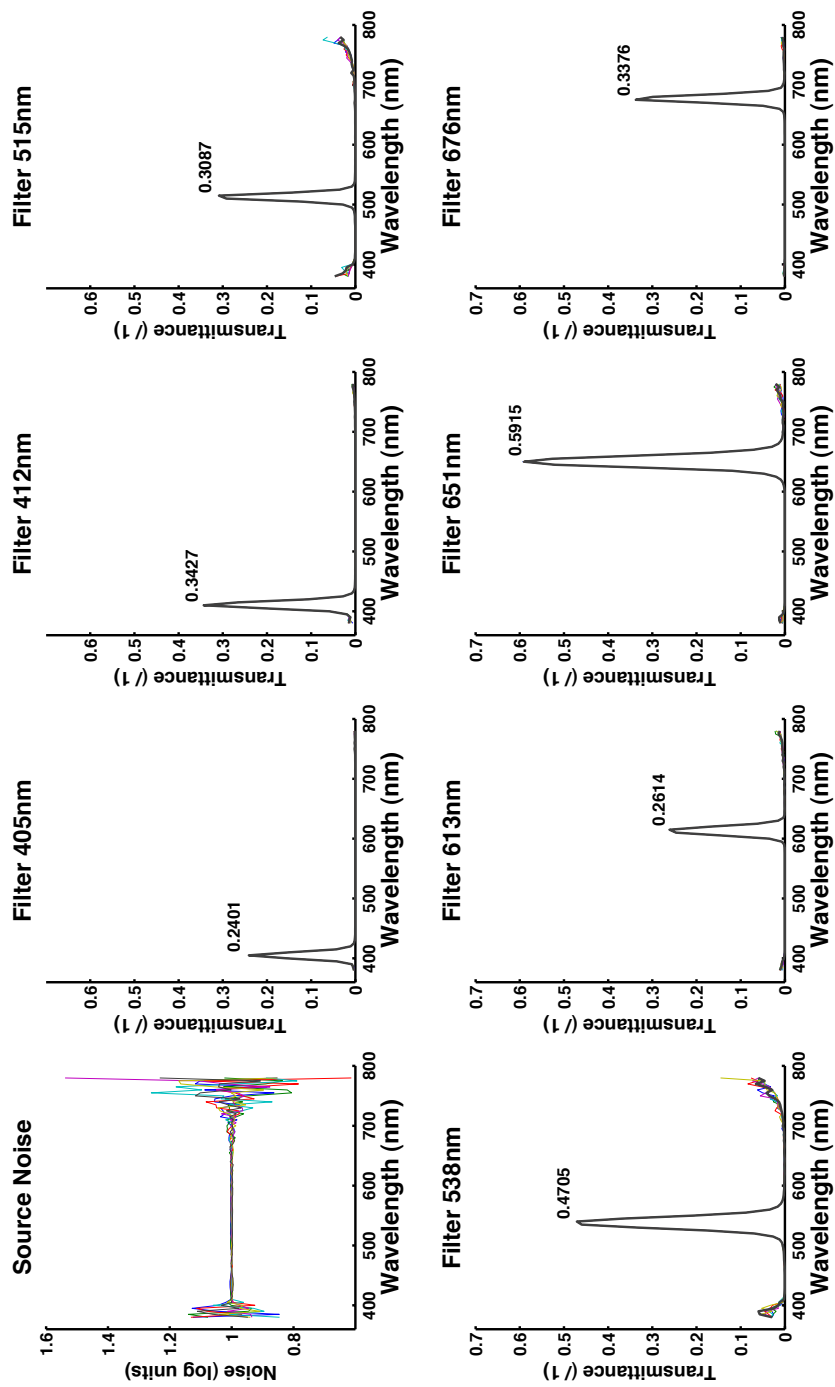


Figure 2.3.7: Linear plots of the optical density functions of the narrow band filters. The first plot is of the source, subsequent plots indicate the peak transmittance of each filter. The measured values are summarized in table 2.3.2

Measurement of the Red LED with the PR1500 and Schott Filters

The characteristics of the filters are summarised in table 2.3.2, in the second column the wavelength of the peak transmission (nm) is shown, then the calculated full width half maxima measure (nm) is shown, this is a reflection of how wide the transmission spectrum is for each filter. Notice that the values are not uniform with filter 4 having the widest transmission spectra (20.5 nm), and filter 7 the narrowest (11.1nm).

The peak transmittance is the amount of incident light that is transmitted through the filter, this value was used to normalise the measured light intensity. So, for example, if the incident light has luminance 10 cd.m^{-2} at wavelength 405.1nm we would expect to measure 2.401 cd.m^{-2} with filter 1. Dividing this value by the transmittance yields the true value.

In the final column are the correction factors for the photomultiplier tube in the PR 1500. The photomultiplier tube has a linear but non uniform response to light in the range measured here. Therefore the normalised measurements should be multiplied by the correction factor to yield the true light intensity.

Table 2.3.2: Summary of the filter characteristics. **Peak Trans** is the measured transmission using a broadband source, not corrected for the sensitivity of the photomultiplier tube. **Correction Factor** is the factor required to correct for the sensitivity of the photomultiplier tube, taken from the manual.

Filter	Peak λ measured (nm)	FWHM (nm)	Peak Trans 1^{-1}	Correction Factor (no units)
1	405.1	12.2	0.2401	0.614
2	412.9	12.3	0.3427	0.575
3	515.0	12.3	0.3087	0.758
4	538.9	20.5	0.4705	0.821
5	613.8	15.0	0.2614	1.273
6	651.6	20.1	0.5915	1.770
7	676.5	11.1	0.3376	2.451

Procedure Using the radiance mode, the PR1500 was set to its maximum sensitivity and re-calibrated in accordance with the manufacturer’s instructions. The objective lens was adjusted to bring an image of light from the red LED reflected from within the device

into focus. A measurement was first made without any filter in place, then each filter was placed in the light path and the radiance value noted for each filter. The sensitivity was then increased ten fold, the calibration checked and the initial measurements were repeated. The radiance was again recorded for each filter.

Table 2.3.3 shows the values as the scotopic luminance at each wavelength was calculated from the radiance measurements. The mean radiance was corrected for the sensitivity of the photomultiplier, then corrected for the transmittance of the filter. This gave the true radiance, which was then multiplied by the scotopic luminance efficiency value for that wavelength. Only integer wavelengths were available so the decimal values were interpolated linearly. The values were then normalised to the peak value at 651.6nm. The radiance measured for the first two filters is very close to the zero measure of the PR1500, and may be artefacts.

Table 2.3.3: The method of calculating the scotopic luminance of the red LED ($\lambda_{max}=655$ nm), at a variety of wavelengths. For each column; **Photosensitivity**, **Peak Trans** the value shown is the radiance after adjustment for that factor. **Relative Scot Lum** is the calculated radiance converted to scotopic luminance and normalised to $\lambda=651.6$ nm

Peak λ nm	Radiance mW.cm ⁻²	Mean mW.cm ⁻² ($\times 10^{-1}$)	Photo Sensitivity mW.cm ⁻²	Peak Trans	Relative Scot Lum
Open	2.45×10^2	2.55×10^3	2.50×10^2		
405.1	1.00×10^{-4}	4.00×10^{-2}	2.05×10^{-3}	1.26×10^{-3}	5.24×10^{-3}
412.9	1.00×10^{-4}	7.00×10^{-3}	4.00×10^{-4}	2.30×10^{-4}	6.71×10^{-4}
515.0	1.30×10^{-3}	1.30×10^{-2}	1.30×10^{-3}	9.86×10^{-4}	3.19×10^{-3}
538.6	0.90×10^{-2}	1.03×10^{-1}	0.97×10^{-2}	7.92×10^{-3}	1.68×10^{-2}
613.8	5.1×10^{-1}	5.3	0.52	6.60×10^{-1}	2.52
651.6	9.94×10^1	8.40×10^2	9.17×10^1	1.62×10^2	2.74
676.5	6.74	8.87×10^1	7.81	1.91×10^1	5.67×10^1

Characteristics of the Red LED; does it generate scotopic light?

The measurements shown in table 2.3.3 and in figure 2.3.8 support the supposition that the red LED is narrow band. The literature suggests that the LEDs can be considered narrow band, if they have nominal FWHM of ≤ 50 nm (Lee, Sundar, Heine, Bawendi & Jensen 2000, Dodabalapur 1997, Bergh & Dean 1972). It follows therefore, that the spectral distributions can be modelled by a Gaussian function (Chhajed, Xi, Li, Gessmann & Schubert 2005). The model is summarised in equations 2.3.4 and 2.3.5. The

power density distribution is described as

$$P(\lambda) = P \frac{1}{\sigma\sqrt{2\pi}} \exp \left[-\frac{1}{2} \left(\frac{\lambda - \lambda_{peak}}{\sigma} \right)^2 \right] \quad (2.3.4)$$

where

$$\sigma = \frac{\lambda_{peak}^2 \Delta E}{2hc\sqrt{2 \ln 2}} \quad (2.3.5)$$

and where ΔE is the FWHM value of the emission spectrum and P is the total power of the LED, h is Planck's constant and c the velocity of light. A constrained non-linear regression gives a best fit at $\lambda = 651.6$ nm, of $P = 107.3 \pm 0.03$ mW.cm⁻² for $\sigma = 13.867 \pm 0.001$, this gives a FWHM value of 30.53 nm and an $R^2 = 0.99$. This is larger than the value of the FWHM measured with the PR650, which was 20 nm.

The method described here using the PR1500 and narrow band filters samples seven points whereas the PR650 samples 81 points. Further, the derived peak wavelength is 651.6 nm, this corresponds to the peak wavelength of the available filters rather than 655 nm as found by the PR650. These two factors may account for the difference in bandwidth. Figure 2.3.9 shows the Gaussian fit, derived from the PR1500 data compared to the data measured with the PR650. The relative power is of most interest here, rather than the absolute value of the power P , since we are comparing the output for differing wavelengths of the same LED.

The measurements using the narrowband filters are shown against a idealised narrow-band source with a Gaussian output, see figure 2.3.8. The measurements match the narrow band part of the spectrum, and therefore the measurements made by the PR650 at the lower wavelengths (400 – 600 nm) are likely to be overestimates. By how much they over estimate the output is shown below.

The process of estimating the values at these low light levels is essentially a series of linear scalings of the raw data. Moreover, the scotopic luminous efficiency function is maximal at ~ 507 nm and is 3.4log units larger at its peak than at 655 nm. The dynamic range of the PR650 is three log units and therefore it is likely we will have intrinsic noise for low luminance measurements. In other words, we might be amplifying the zero error of the PR650. We can therefore take the estimates of light at the lower wavelengths, using the filters and the PR1500 as upper limits.

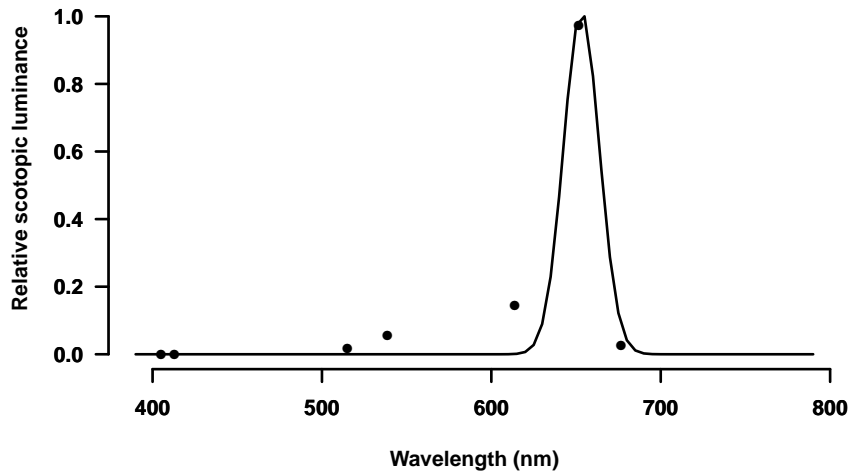


Figure 2.3.8: The constrained fit of a Gaussian function (peak $\lambda = 650$ nm) to the PR1500 data, solid line is the Gaussian model, filled circles mark the red LED measured values using the PR1500 combined with the Schott filters

How much light is there at 515 nm? The scotopic luminance of the red LED when measured with a the PR650 and PR1500 in combination with narrowband filters is shown in figure 2.3.9 and compares them to an ideal narrowband source. The shaded area indicates the light that might be emitted and be capable of stimulating the rods. From table 2.3.3 we can see that at 515 nm the scotopic luminance of the background is at least two log units less than at the peak luminance of the background LED.

From table 2.3.1 the background scotopic luminance at 655 nm is 2.9×10^{-3} cd.m⁻², therefore at 515 nm the scotopic luminance of the red LED is no more than $\sim 3 \times 10^{-5}$ cd.m⁻²(scot) and could be lower. We therefore have an upper bound for the amount of light emitted at 515 nm.

The minimum detectable luminance of the PR1500 is given as 1×10^{-2} cd.m⁻²(phot). The technique described above has enabled an estimate of low light levels to be made, but the light emitted by the red LED might still be detectable by the rods. The question of the whether the rods are stimulated by the red LED light cannot be answered categorically using the measurement techniques available here, therefore an empirical approach is needed and this is explored further in chapter 5.

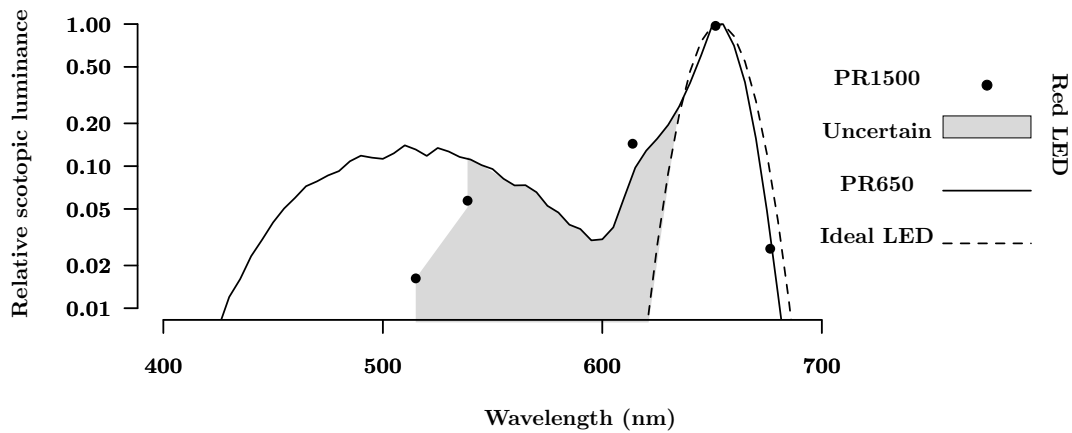


Figure 2.3.9: Comparison of the red LED measured with the PR650 (solid line), and the PR1500 (filled circles) to an ideal narrow band LED (dashed line). The shaded area is the region we are concerned may be affecting the rods.

2.3.5 Pre-set target screen luminance levels

The preset luminance levels were characterised as follows. The photopic levels were measured directly and the scotopic levels calculated assuming narrowband light is emitted by the LEDs, both are given in table 2.3.4. The pre-set levels were set using variable resistors and the PR1500.

Table 2.3.4: Photopic and scotopic values of background luminance. To convert from photopic to scotopic luminance at red (655 nm) a factor of 0.014 was used, at green (530 nm), 2.34. These are both narrow band values (Wyszecki & Stiles 1967, page 104).

Photopic	(cd.m ⁻²)	0.05	0.10	0.20
Scotopic	(cd.m ⁻²)			
Red		0.0007	0.0014	0.0028
Green		0.117	0.234	0.468

2.3.6 Calibration of the Green LED

In this study a green LED was used as a stimulus. The values returned by the data logger for the stimulus are in volts, which need to be converted to scotopic units.

The technique to calibrate the green stimulus was as follows: The PR1500 was calibrated

and set to radiometric mode; so as to allow measurements at lower light levels. The diffuser was removed and the PR1500 was focussed on a patch illuminated by the a green LED. The data logger was initialised and the voltage across the LED noted for a range of radiances. The potentiometer was adjusted across its full range, noting the extreme values as well as 14 intermediate points.

The diffuser was replaced and the photopic luminance measured at three values, these values were used to scale the original radiometric data to photopic data, as will be demonstrated the relationship between radiometric and photometric measurements is linear for the PR1500, see figure 2.5.2.

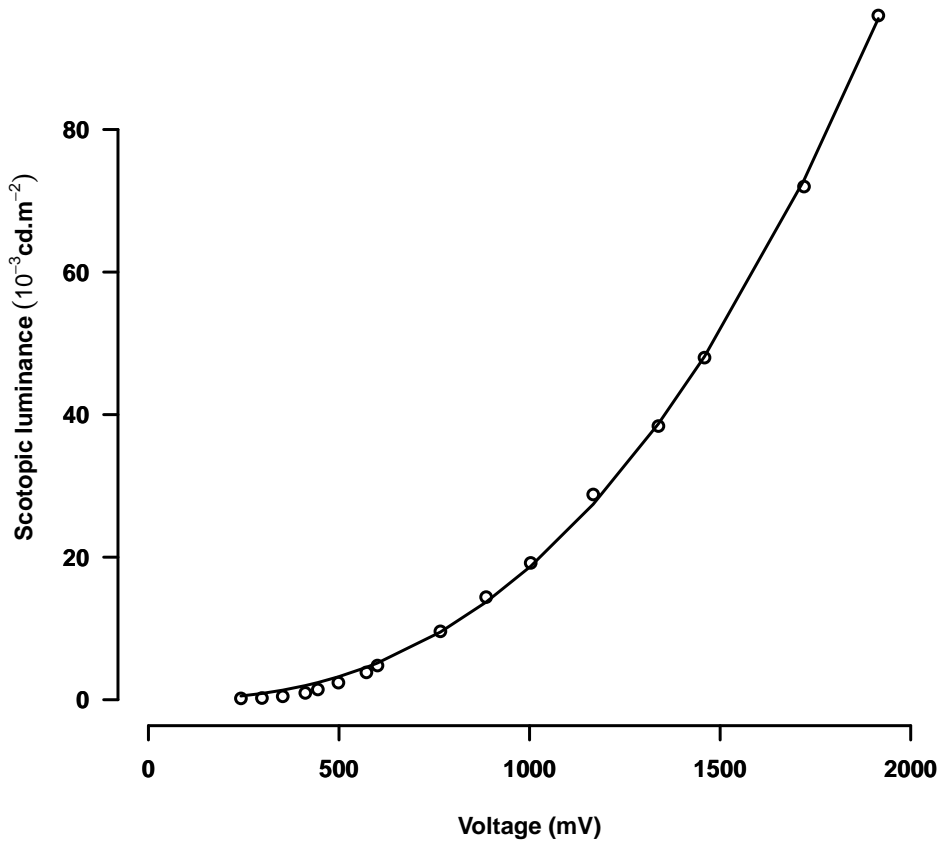


Figure 2.3.10: The scotopic luminance in $\times 10^{-3} \text{ cd.m}^{-2}$ of the green LED as a function of voltage.

The three luminance values equated to a particular voltage (see table 2.3.5) and the

Table 2.3.5: Voltage luminance equivalences. The luminance that corresponds to a particular voltage across the stimulus LED

Luminance	Voltage
cd.m ⁻²	mV
3.00×10 ⁻²	1945
2.05×10 ⁻²	1724
1.02×10 ⁻²	1297

data was rescaled appropriately. For example, if the voltage was 1500mV and this corresponded to 0.2 cd.m⁻², then the radiometric reading at 1500mV was scaled to match this reference. This scaling factor was then applied to all the data.

To convert from radiance (volts) to photopic luminance (cd.m⁻²) at the screen for the green LED the factor was 1/408.6. For green light of wavelength 530 nm, the scotopic luminance is 2.34 times larger than the photopic luminance (Wyszecki & Stiles 1967). Therefore the factor needed to scale from radiance to scotopic luminance for the green LED was 1/174.6.

This is permissible as the transformations effected by the diffuser and the photometer are linear. Figure 2.3.10 shows the relationship between the voltage across the LED and the scotopic luminance of the stimulus, the relation can be summarised as

$$Scotopic = 9 \times 10^{-13}(mV)^{3.45}.$$

2.3.7 LED emittance spectra: a summary

1. The red LED emits light maximally at 655 nm, at 515 nm the light emitted is less than 3×10⁻⁵ cd.m⁻²(scotopic), this is less than 1% of the maximum output, and at 500 nm the light emitted is less than this.
2. The green LED when used as a stimulus varies from 0 to 42×10⁻³ cd.m⁻² photopic, or from 0 to 96×10⁻³ cd.m⁻² scotopic.

2.4 Determination of flicker frequency

Using the author as a subject the absolute threshold for a range of flicker frequencies was measured.

Using the analogue apparatus with a red background with luminance 0.05 cd.m^{-2} the absolute threshold after 20 minutes was found for a range of flicker frequencies. No photo bleach was used. The results are shown in figure 2.4.1. The sensitivity appears to be reaching a plateau at 4Hz and therefore this was the frequency chosen for the final version of the device. The low pass nature is to be expected and has been found by others (Lange 1954).

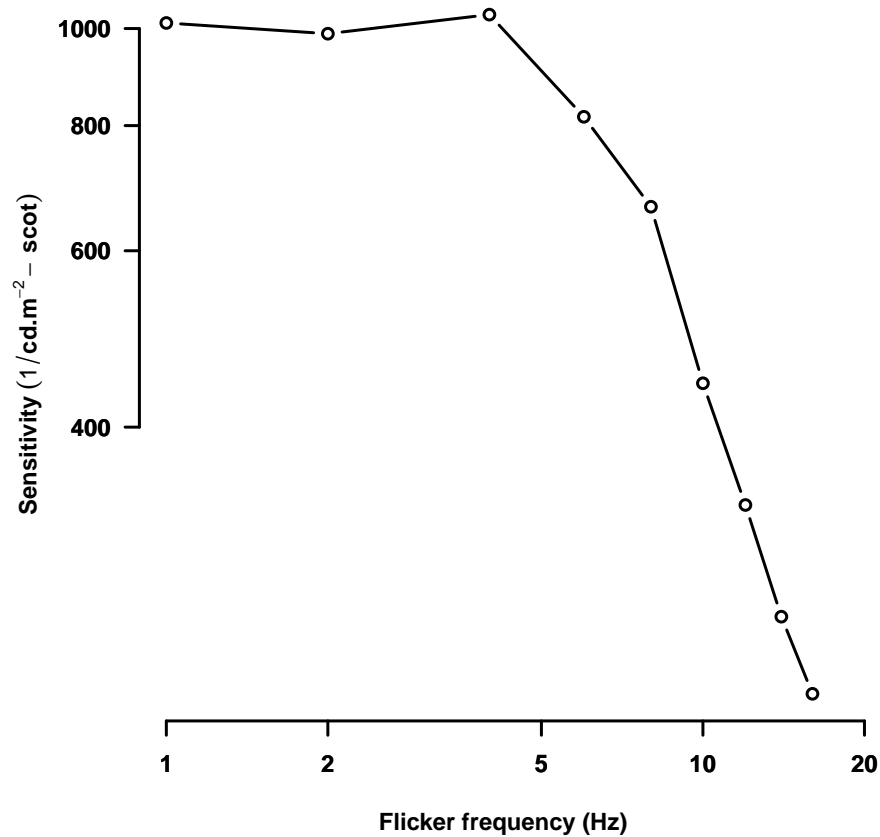


Figure 2.4.1: Flicker sensitivity log-log plot for subject aged 46 years

2.5 Flash gun calibration

Typically when measuring rod recovery the eye is subjected to a flash of light that causes a proportion of the photo-pigment in the eye to be transformed, often referred to as a bleach. The amount of photo-pigment bleached is dependent upon the energy incident upon the retina; this is a function of the incident light, pupil size and ocular absorption*.

A Nikon Speedlight SB800 (Nikon, Japan) flashgun was used to bleach the retina. To calculate the level of bleach it was necessary to determine the scotopic luminance incident at the cornea. Measurements of the intensity over time of the flash for each setting available were made. The PR1500 is able to measure brief flashes of light and return a voltage proportional to the intensity of the light. When connected to the CED1401 smart interface (CED,UK) and its proprietary software (Signal, version 1.9) a time series can be collected of intensity against time.

The process of calibration takes the output voltage of the PR1500 and scales it to scotopic luminance (cd.m^{-2}). First, the linearity of photopic to radiometric measurements made by the PR1500 was checked. This established that there were no internal processes that could distort the readings. Then the radiometric to voltage linearity was checked. It was found that for high radiometric values the photomultiplier saturated. The output voltage was calibrated so that a relationship could be found between output voltage and photopic measurement derived with the built-in photopic filter. Finally the photopic measurements were scaled to scotopic values.

2.5.1 Pre-calibration of the flash measurement set up

Radiometric to photometric linearity

The PR1500 has an ‘open’ radiometric facility and a ‘photopic’ mode. The relationship between the two was first checked for linearity across a range of luminances. The PR1500 was aligned to measure an illuminated area on the matt screen viewed through a neutral density (ND) wedge, as shown in figure 2.5.1, The ND filter was mounted on a spindle so that rotation about its axis, changed the density of the filter and hence the apparent

*The introduction explains that the flash must bleach at least 20% of the photopigment if the recovery of rod sensitivity is to be independent of bleach intensity, this ‘rate limited’ recovery reflects the performance of the ‘rod choroid’ complex, see section 1.5.4 on page 46

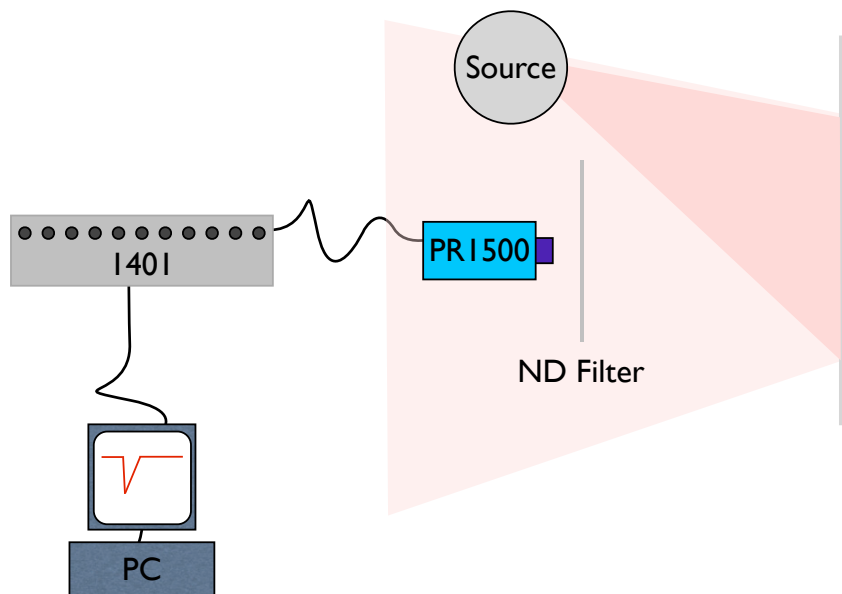


Figure 2.5.1: Apparatus to calibrate the flashgun using the PR1500; showing the relative positions of the source illuminating the matt white screen, a PR1500 focussed on the screen through an ND filter, or wedge, and connected to a CED 1401 and sampled using PC software.

luminance of the area of the screen. The illumination was provided by a tungsten halogen lamp, (BHS, UK) and without the ND filter, the screen had a luminance of 9345 cd.m^{-2} . For each of 23 luminance levels a note was made of the ‘open’ reading and the ‘photopic’ measurement. This was repeated three times for each luminance.

The results are shown in figure 2.5.2. The high correlation coefficient ($R^2=0.996$) suggests a high degree of linearity between ‘open’ and ‘photopic’ modes, for a broadband source, unaffected by the electronics of the device.

Radiometric to voltage linearity

Repeated measurements were made to determine the relationship between radiometric mode and the output voltage of the photometer for varying luminances. The voltage

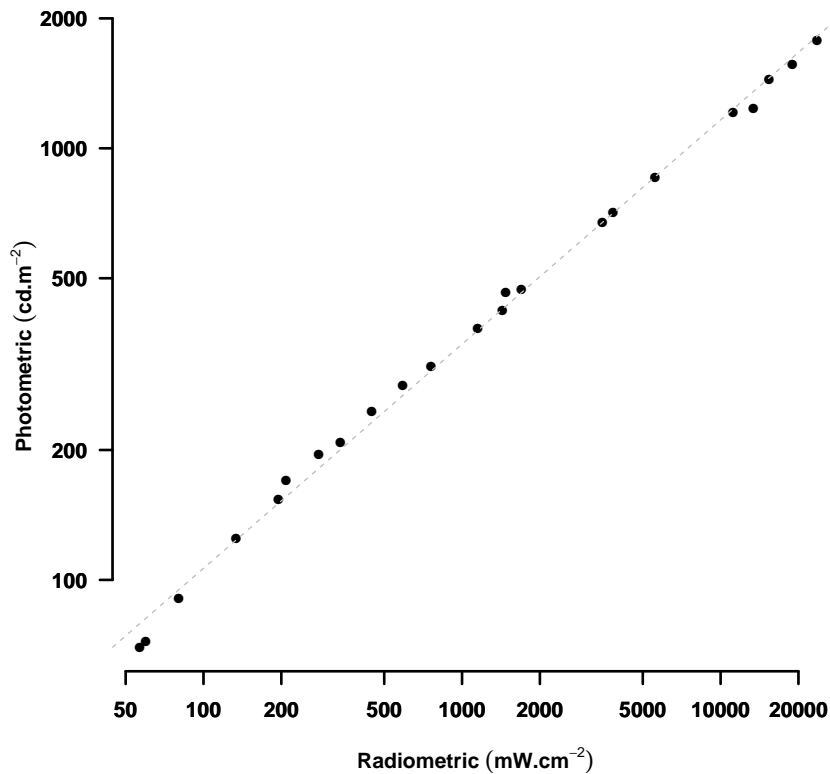


Figure 2.5.2: Radiometric to photometric linearity

output jack of the PR1500 was connected to the CED 1401 smart interface using its specialist software ‘Signal’ (CED, Cambridge, version 1.9) installed on a PC (Dell, Windows XP, USA). The software was set to sample the voltage at 25Hz for 40ms over 8s, this gave 200 sweeps of the output.

Three measurements were taken at each of 15 luminance levels controlled by the neutral density wedge and the average of 200 sweeps taken as an estimate of the output voltage. The photo-spectrometer saturated when the output voltage was driven lower than -166.67mV , see figure 2.5.3. The response is linear in the range 0 to 1200 mW.cm^{-2} , and the neutral density filter and the internal attenuator were adjusted so that the output voltage of the flash, at its maximum setting, did not saturate the photometer.

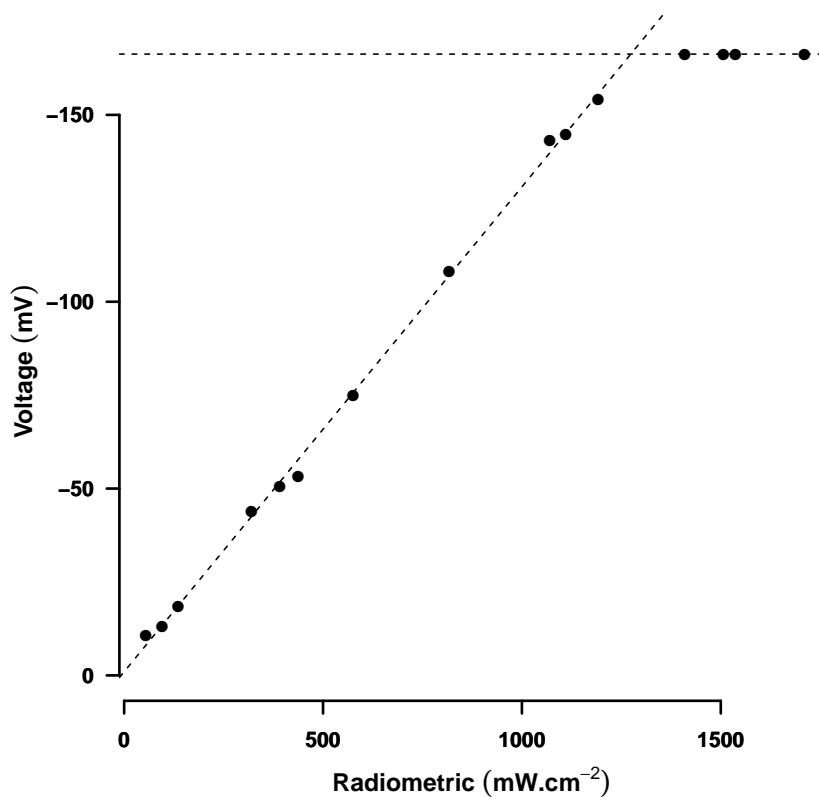


Figure 2.5.3: Relationship between radiometric reading and output voltage, for the PR1500 photometer

Converting volt•seconds to Luminance•seconds

The measurements described above confirmed the range over which the photometer returns linear measurements and the need to remain below saturation level. The internal attenuator facility on the device (X100) and an external ND filter were used so that the maximum flash intensity did not saturate the PR1500.

Then the voltage output for a given luminance and neutral density filter combination was found using a broadband reference source (Tungsten Halogen lamp, BHS,UK). The photopic luminance 9572 cd.m^{-2} was found after attenuation to be equivalent to -8.371mV and therefore a scaling factor of $-1177\text{cd.m}^{-2}.\text{mV}^{-1}$ could be used to calculate the photopic $\text{cd.m}^{-2}.\text{sec}$ equivalence of the $\text{mV}.\text{sec}$ value.

2.5.2 Flash calibration

The PR1500 photo-spectrometer was connected to the CED1401 (CED, Cambridge UK), as illustrated in figure 2.5.1. The CED1401 was configured using its bespoke ‘Signal’ software to peri-trigger at values less than -7mV, sampling at 8 kHz and reporting the 20 pre-trigger values and the next 762 values. All measurements were taken with the room lights and computer monitors extinguished.

For each flash setting measured, eight measurements were taken, each measurement gave rise to a 782 by 2 array. The first column reported the time points sampled and the second column the output voltage at each sampling point. The final 200 points were used to calculate an average noise (or dark light) value and this was used to zero the data. For each array the first 200 points were used to calculate the area under the curve. A trapezoidal numerical integration method was used. Figure 2.5.4 illustrates the eight spikes for the flash setting ‘1/1’ (maximum), the area under the curve is 1029 mV.s.

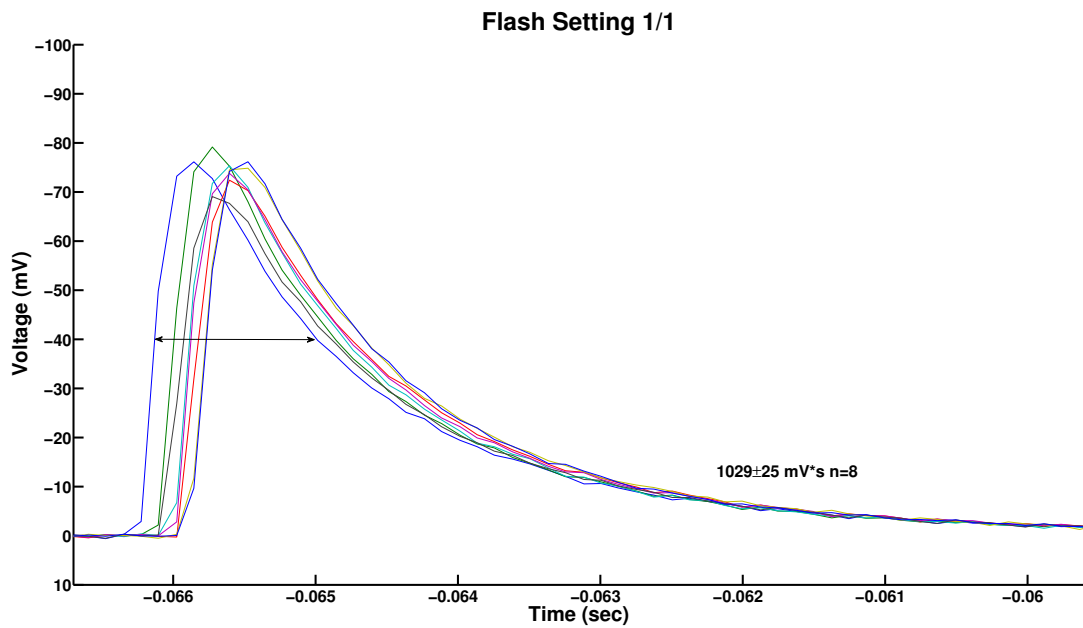


Figure 2.5.4: Eight traces from flash setting 1/1. Note that the time scale is in 5ms intervals, recorded during the peri-trigger phase, hence the negative values. The bar is the half-height bandwidth and is 6ms long.

2.5.3 Flash linearity

Measurements were taken at flash settings, 1/16, 1/8, 1/4, 1/2 and 1/1. The linearity of the relationship between flash energy (intensity x time) and flash setting is shown in figure 2.5.5. A summary of the measurements at each flash setting can be seen in figure 2.5.6. It is clear that for higher flash settings the variation in intensity is achieved by altering the flash duration, while for smaller flashes, '1/16' and '1/8', changes to the pulse height are also used.

In table 2.5.1 the area of each flash is scaled to photopic energy using the conversion factor found in section 2.5.2 and scotopic energy levels. To transform broadband photopic luminance to scotopic luminance a scaling factor of 2.489* was used (Wyszecki & Stiles 1967, p104).

Setting	Area mV.sec	photopic cd.m ⁻² .sec	scotopic cd.m ⁻² .sec
1/16	-62.24	73 200	182 200
1/8	-111.21	130 900	325 800
1/4	-279.73	329 100	819 100
1/2	-497.56	585 400	1 457 100
1/1	-1028.70	1 210 400	3 012 700

Table 2.5.1: Area under the curve converted to photopic and scotopic energy values.

*1700/683

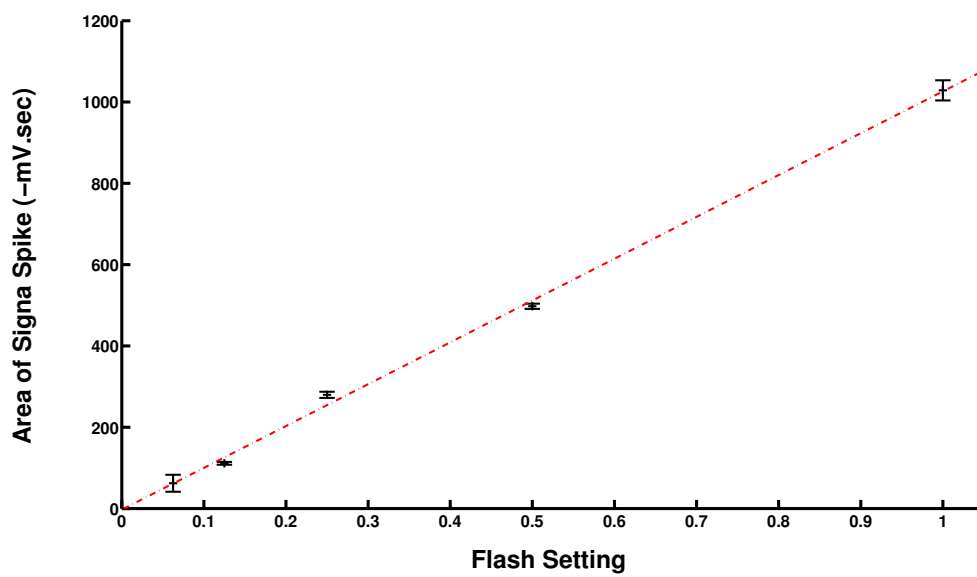


Figure 2.5.5: The relationship between area under the signal spike and the flash setting; error bars are one standard deviation ($R^2 = 0.998$)

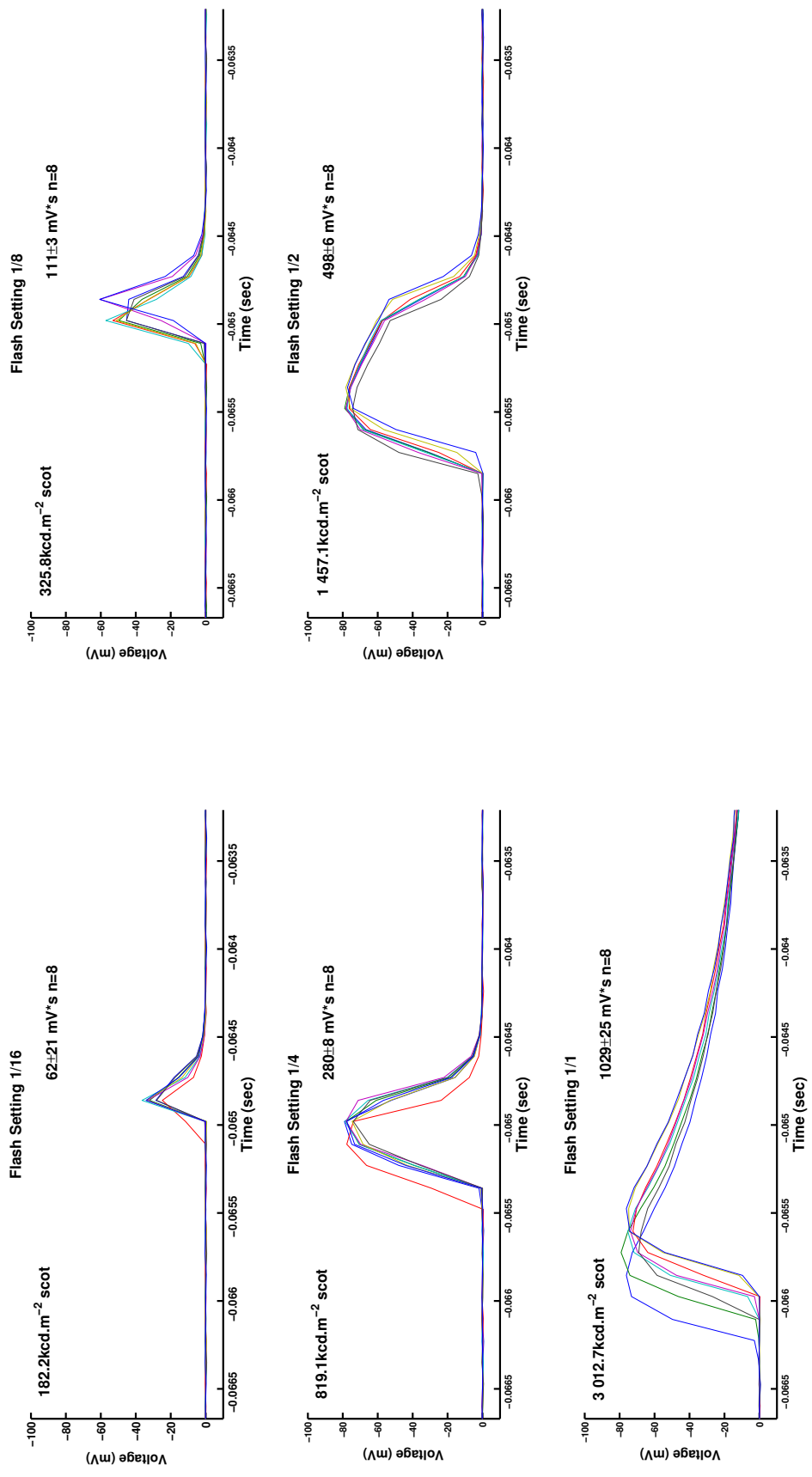


Figure 2.5.6: The variation in spike for each flash setting. For all the measurements apart from the '1/16' setting the most significant change is the pulse width, the pulse height in the '1/16' graph may be underestimated by the sampling rate of 8 kHz.

The bleach achieved by each flash setting is dependent upon the pupil size. The scotopic energy (cd.m⁻².s) for each flash setting was converted to scotopic trolands × time for a range of pupil sizes, from 2 mm diameter to 8 mm in 0.5 steps. Rushton (1956) describes a relationship between the pigment remaining p_0 following a bleach produced by a brief (less than 40 seconds) flash, of time t_0 seconds and intensity I scotopic trolands, see equation 2.5.1, and provides a worked example (Rushton & Powell 1972).

$$\log_{10}(\log_{10}(\frac{1}{p_0})) = \log_{10}(It_0) - 7.3 \quad (2.5.1)$$

This equation was used to produce table 2.5.2. The table describes the percentage of photopigment bleached for each condition. The values for flash settings 1/128, 1/64 and 1/32 were extrapolated from the data.

Table 2.5.2: Calculated percentage bleach for a given pupil diameter and flash setting, the values for 1/128, 1/64, and 1/32 are extrapolated from the experimental data

Pupil Diam (mm)	2	3	4	5	6	7	8						
Setting													
1/128	0.54	0.85	1.22	1.66	2.16	2.72	3.35	4.04	4.79	5.60	6.46	7.38	8.36
1/64	1.39	2.16	3.10	4.19	5.44	6.84	8.37	10.04	11.83	13.74	15.75	17.86	20.06
1/32	3.06	4.74	6.75	9.07	11.68	14.55	17.65	20.94	24.39	27.97	31.65	35.39	39.17
1/16	6.31	9.69	13.65	18.10	22.96	28.12	33.47	38.93	44.39	49.78	55.01	60.03	64.77
1/8	12.50	18.83	25.95	33.56	41.38	49.13	56.59	63.56	69.93	75.59	80.51	84.70	88.19
1/4	23.67	34.43	45.54	56.27	66.05	74.52	81.51	87.03	91.20	94.23	96.34	97.76	98.67
1/2	41.91	57.21	70.55	81.06	88.62	93.61	96.65	98.36	99.25	99.68	99.87	99.95	99.98
1/1	66.37	81.78	91.38	96.45	98.72	99.60	99.89	99.97	99.99	100.00	100.00	100.00	100.00

2.6 A digital device to measure scotopic recovery

Having collected data with the analogue device described above, greater control of the experimental parameters was desired. In particular the rate at which the stimulus increases in intensity and the time between threshold settings. The analogue equipment is largely controlled by the subject and is liable to the subjects interpretation of what is desired. For example, some subjects felt that rapid collection of data was an objective, and they increased the stimulus intensity too rapidly leading to transient changes in adaptation and therefore noisy data. For this reason and because computer control of other parameters was required, a device as described below was developed.

2.6.1 Description

The digital device is a modified MPS9000 (Van Der Veen, Berendschot, Hendrikse, Carden, Makridaki & Murray 2009) see figure 2.6.1, manufactured by Hartest Precision Instruments (HPI, Crawley, UK), and controlled by firmware that is written to an erasable programmable read only memory chip (EPROM). In its standard form the MPS9000 uses two LEDs (λ_{max} 450 and 520 nm) to measure macular pigment optical density.



Figure 2.6.1: The digital dark adaptometer, a modified MPS9000 (Hartest Precision Instruments, Crawley, UK)

The standard device was modified. Changes were made to the target board, the illumination board and the control software. The target board is where the subject looks when measurements are made and is shown in figure 2.6.2. The central aperture is used for fixation and the 3° targets 8° either side of fixation provide the stimulus, one for testing the right eye the other the for the left. The LEDs in the target board were replaced, with a red LED (dominant $\lambda=655$ nm), and a green LED (dominant $\lambda=530$ nm) fitted to each aperture in the target board. The control software determined which LED was used in each location. Although the device is capable of presenting either red or green stimuli on either a red or green background, red background and fixation with a green stimulus were used through out the study.

The resistors in the LED circuits were altered so that the output over the desired range was linear. In appendix E.2 on page 303, the circuit diagrams for the original apparatus are shown and the modified resistors and LEDs are highlighted. Two diffusers were added to the target board, a sheet of white paper (Xerox, $80\text{g}\cdot\text{m}^{-2}$) and a diffusing acetate gel (Lee filters No. 216), both cut to shape, attenuated the output . The paper and the gel where not glued together, this allowed a small gap between the two layers and caused the outline of the stimulus to be blurred.

The illumination board provides the light for the background. To obtain the red background an illumination board was made using the existing board, but altering the existing white ultra-bright LEDs to the same red as the fixation LEDs. These modifications were made at the University of Manchester by the author.

The control software was supplied by Mr S Lacovic, of HPI, who altered the proprietary MPS9000 software, originally written in Access (Microsoft, USA). The modified and compiled software was sent to the author in the form of an executable binary. This was written to an EPROM chip using a Galep-IV programmer and 28/32 way adaptor (Conitec, Farnell,UK) connected to a PC (Dell USA). The chip was mounted on the control board of the MPS9000.

The new software also has a graphical user interface (GUI) that is used to make the measurement of dark adaptation and calibrate and set the operating parameters for each measurement. The new software enabled the following parameters of the stimulus and background to be varied;

- background luminance: zero to $0.3\text{ cd}\cdot\text{m}^{-2}$
- background wavelength: either red or green

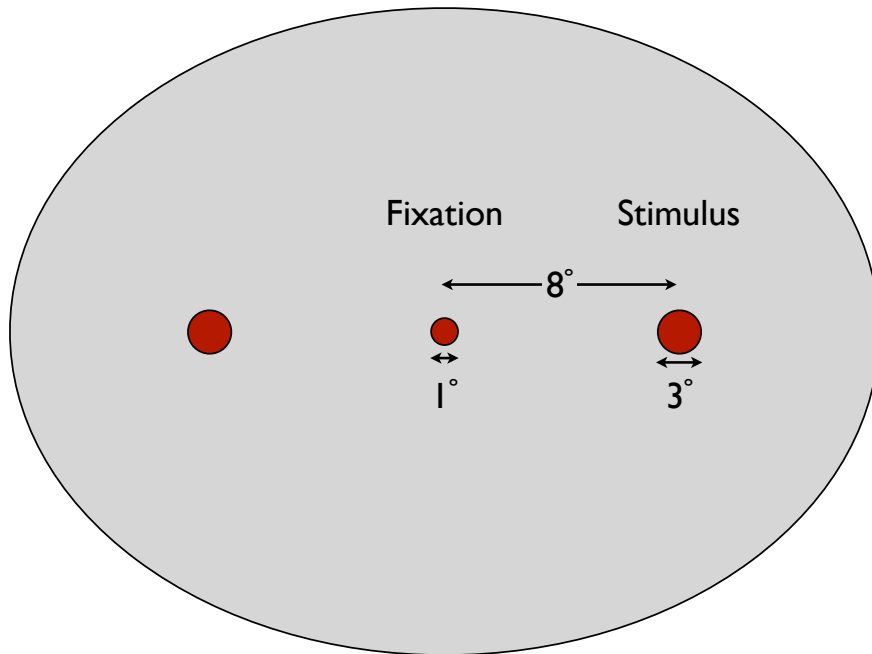


Figure 2.6.2: The target board of the digital dark adaptometer

- initial stimulus intensity
- stimulus luminance range: from zero to 0.5 cd.m^{-2}
- rate of stimulus increase, or ramp time
- stimulus wavelength; either red or green
- time between stimulus presentations
- stimulus start level following a response.

The parameters are controlled by editing a parameter file either directly or using the GUI. Further fine control and calibration can be achieved by use of voltage controls and calibration factors accessible through the GUI and also by direct alteration of the resistors in the circuitry.

In figure 2.6.3 the default settings are shown, starting from the upper left corner; **Start** is the attenuation of the stimulus at first presentation (10dB), **Frequency** is the flicker frequency of the stimulus (4Hz). **Ramp time** is the time taken to move from the **Start** attenuation level to the **Stop** (40s). **Interval** is the time between threshold measurements(5s). The **Retest step** value (9.5dB) is the amount by which the stimulus is

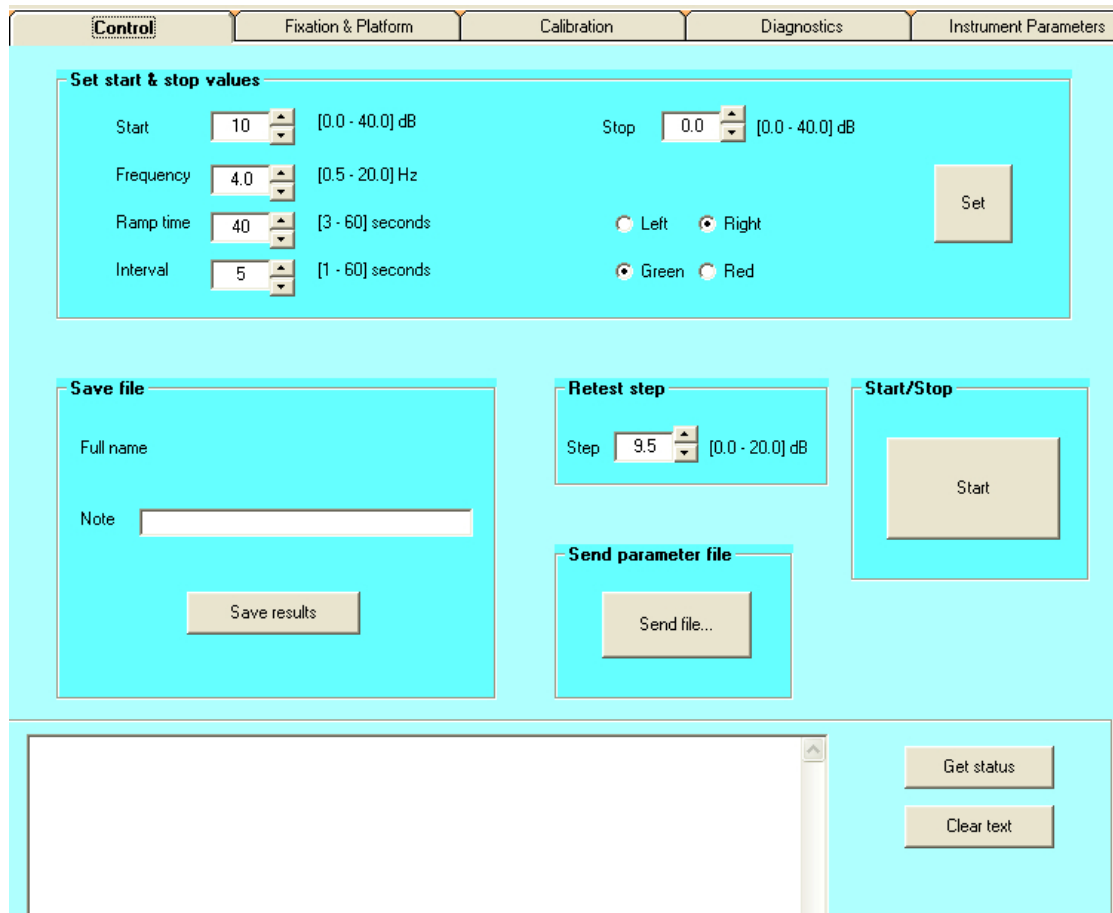


Figure 2.6.3: The control screen.

attenuated before being re-presented following a button press.

If any values are changed these are communicated to the device by pressing the **Set** button on the upper right hand side. During the measurement the results are shown in the lower left white field, and once completed they can be saved by adding a note to the **Note** field and pressing the **Save results** button. On the lower right side are two buttons, **Clear text** which clears the results field, and **Get status** which recovers the details of the parameters of that measurement. The measurement begins when the button **Start** is pressed.

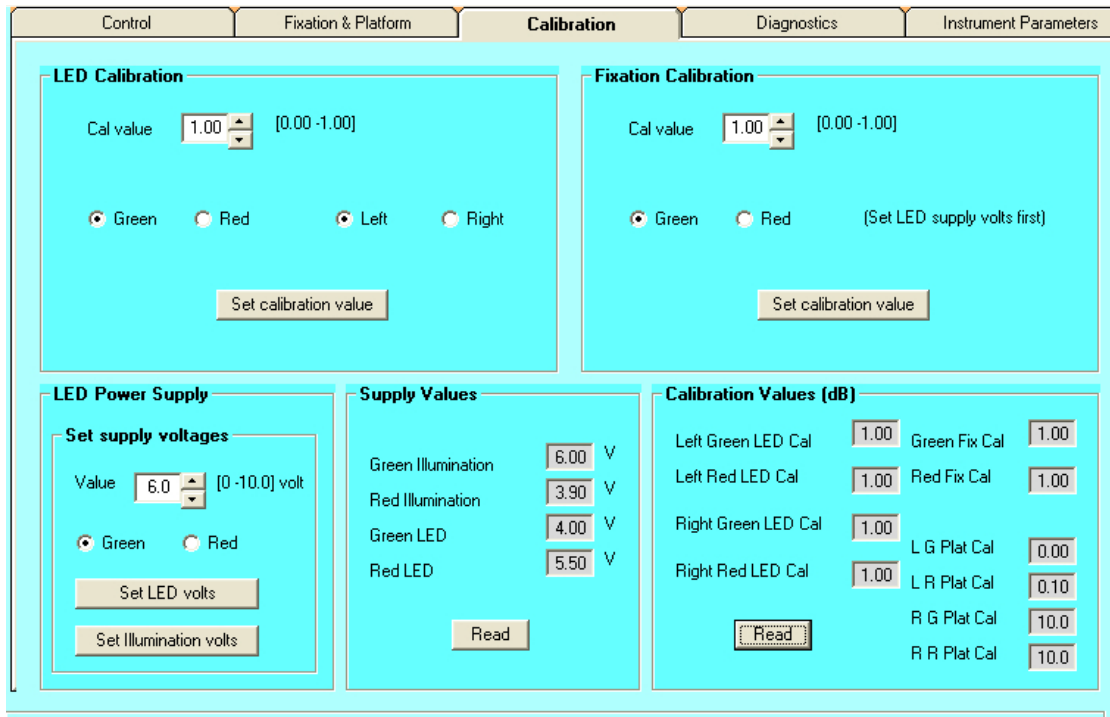


Figure 2.6.4: The calibration screen

2.6.2 Initialisation

In figure 2.6.4 we can see the calibration tab of the GUI. The **LED Power Supply** area is used to adjust the voltage applied to each LED, and is used to give a coarse control of the luminance of each component. The values used are shown in the **Supply Values** portion of the screen. By selecting a radio button in the upper two sections, **LED Calibration** and **Fixation Calibration** fine control of the LED voltage can be made for each LED. Once altered that information is sent to the device by the **Set ...** buttons. Further portions and remaining tabs shown on the screen are legacies from the MPS9000 control software and have no function in the device.

2.6.3 Experimental procedure

The subject was instructed in the procedure as follows; they had to fixate the red central light and when they became aware of the flickering light to the side of their line of sight they should press the hand held button. A series of practice measurements were made without photo-bleach.

Once the subject was comfortable with the task, the left eye was occluded and the right eye, using natural pupils, was exposed to a flash (Speedlight SB800, Nikon, Japan). The flash intensity was one quarter the maximum and bleached the photopigment, dependent upon pupil size, from 23 to 98% (Rushton & Powell 1972). To ensure that accurate fixation could be maintained during the test, care was taken to not expose the fovea to the flash. This meant that the observer experienced a strong after-image which was confined to their temporal visual field.

The observer viewed the fixation point in the centre of the target board illustrated in figure 2.6.2. They were instructed to press the response button as soon as they detected the target in their peripheral field of view. The software recorded the attenuation of the target at this point and there was audible feedback to confirm to the subject correct performance of the task. If the subject failed to see the stimulus or failed to press the button then there was a warning sound and a missing reading was recorded.

Immediately following a button press or a missed reading the stimulus intensity was reduced from the threshold value by the amount indicated in the **Retest step** field of figure 2.6.3, here 9.5dB.

There was a pause set by **Interval** before the stimulus intensity then increased again at a rate defined by the **Ramp rate** until the button was again pressed, signalling that the target has been detected by the observer. This cycle was continued until the end of the test is reached. The intensity of the stimulus was increased at a constant rate, in figure 2.6.3 the **Start** and **Stop** levels are 10dB and 0.0dB respectively, the **Ramp time** shown is the time taken for the equipment to increase from start to stop level.

Notice also that the data returned is in dB, a measure of intensity attenuation, where $10\text{dB} = -1\log_{10}$ unit, rather than absolute luminance. For a fixed source there is a constant factor between intensity and scotopic luminance. This means that constant thresholds measured with this device are reported in dB, but the rate of change of threshold can be reported in $\log_{10}(\text{cd}\cdot\text{m}^{-2})\cdot\text{min}^{-1}$ by dividing the rate of attenuation by -10.

2.6.4 Verification of the digital dark adaptometer

Linear output of LED

In the device the voltage across the LEDs is fixed, it is the current that is varied using pulse width modulation (PWM). PWM means that the voltage across the LED is

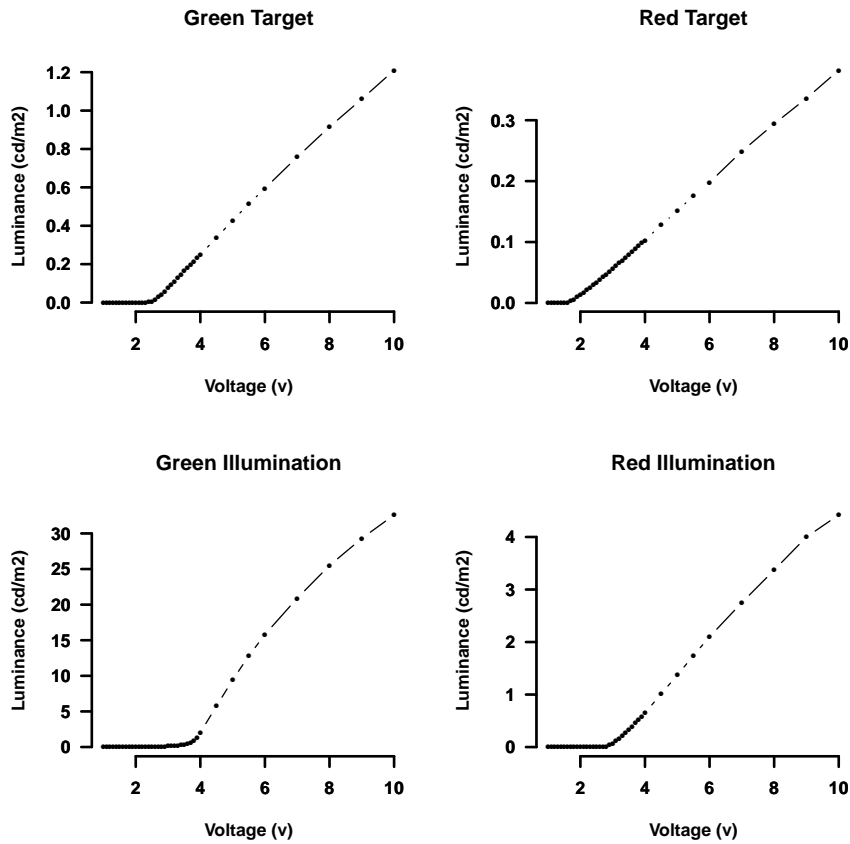


Figure 2.6.5: Linearity of LEDs for varying voltages, green target means the green LED in the target board, similarly, illumination refers to the illumination board.

switched rapidly on and off, the time on compared to the time off determines the current flowing through the LED and hence its intensity. Luminance control using this method has an accuracy better than 0.05 dB (Van Der Veen et al. 2009). If the LED has a linear response over a wide range of applied voltages we can be sure of a uniform change in current if the preset voltage value is in the linear range.

The flicker frequency is controlled by a mask that envelops this modulation so that the intensity increases logarithmically, independent of the flicker frequency chosen.

Method Using Ohm's law a value of resistor in series with the LED was chosen to give a maximum luminance that was usable, e.g the green stimulus LED used $460\text{k}\Omega$ to have a maximum luminance of $0.5\text{ cd}\cdot\text{m}^{-2}$. Linearity was less important for the LEDs

used in the illumination board as they would operate at a constant voltage and hence current.

The PR1500 was used to measure photopic luminance for each LED as the applied voltage varied. The voltage applied came from a power supply unit (EB2025T, TTI, RS Components, UK), and the results are shown in figure 2.6.5

Confirmation of ramp

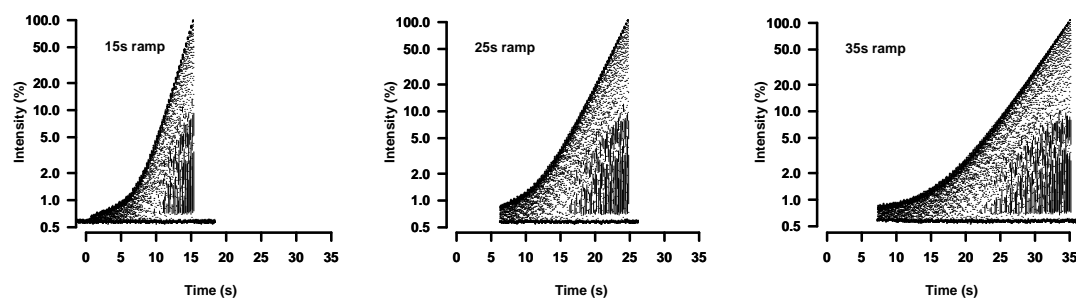


Figure 2.6.6: Change in the LED intensity for a range of ramp times. Note that the Intensity is on a logarithmic scale.

Having ensured that the LEDs respond linearly to changes in current we then need to be aware of the nature of the intensity increase for varying **Ramp time** values. The stimulus increases along a ramp defined by the ramp time and the start and stop levels set in the GUI. In figure 2.6.3, this gives a change of 10dB in 40 seconds.

The ramp was characterised by measuring the radiance of the red target LED, indicated by the voltage at the output jack of the PR1500 see section 2.5.2, over time when sampled by the CED1401, using the ‘Signal’ software (CED version 1.9). The software was set to peri-trigger at 5mV and sampled at 457 Hz so that a sufficiently long epoch could be used, 5 seconds longer than the nominal ramp time was measured.

Figure 2.6.6 shows the relative intensity of the LED ramps for a range of **Ramp times**. We can see that for the three ramp times investigated, the intensity increases logarithmically in the range 2% to 100% of the maximum intensity.

2.7 Psychophysical methods

Psychophysical experiments traditionally use three methods when determining thresholds: the method of limits, the method of constant stimuli and the method of adjustment

2.7.1 Method of limits

The stimulus is increased and when observed the level recorded, then the stimulus is attenuated and when no longer seen this level is also noted and the mean taken, this method was not used in this study.

2.7.2 Constant stimuli

The stimuli are presented at different levels in random order, this method was not used in this study.

2.7.3 Method of adjustment

The stimulus is controlled by the subject and altered until a threshold is set. In this study, the stimulus was presented from unseen to seen, that is the method of adjustment was in one direction only. This was because presenting the stimulus at above threshold levels could have an effect upon the measured threshold due to the exquisite sensitivity of the rod system.

A variant of this is the staircase method, where a stimulus is increased until noticed then reduce by a step and increased again, for static phenomena the mean of a number of reversals is taken. In the work presented here threshold was set at the level of first reversal. Further discussion about tracking thresholds can be found in Von Békésy, Georg and Wever, Ernest Glen (1960). The analogue device and the scotopic contrast measurements used this method.

2.8 Measuring contrast sensitivity at low luminance

2.8.1 Definitions of contrast

Two definitions of contrast are used in this study, Weber and Michelson. Weber contrast is used when the stimulus is small relative to the size of the background or in luminance detection studies and is defined as

$$W = \frac{\Delta L}{L}. \quad (2.8.1)$$

Where ΔL is the change in stimulus luminance and L is the background luminance. Contrast is a dimensionless quantity.

Michelson contrast is used when the object is large when compared to the background and is used to describe contrast for gratings

$$M = \frac{L_1 - L_0}{L_1 + L_0}. \quad (2.8.2)$$

Where L_0 and L_1 are the minimum and maximum luminance respectively. Michelson contrast has fixed mean luminance across the area being considered.

2.8.2 Apparatus

Sinusoidal gratings subtending 10° at 75 cm were presented on a calibrated and gamma-corrected high-resolution CRT monitor (Sony GDM-F500R, Tokyo, Japan). They were generated using the ViSaGe unit (CRS, UK) and a desktop PC (Dell, USA) with Windows XP operating system (Microsoft, USA). The hardware was controlled using Matlab (Nantick, USA) and the psychophysics toolbox (Kleiner, Brainard, Pelli, Ingling, Murray & Broussard 2007, Brainard 1997).

The custom scripts are available in appendix A.1.3 on page 264.

2.8.3 Calibration of the screen

The calibration followed a procedure described by Parry et al.(2006). Initially the screen was auto calibrated using a Colorcal photometer (CRS Ltd, UK) and its associated software, by testing 128 voltages to obtain a gamma correction curve. The software used

for stimulus generation (ViSaGe Desktop, CRS Ltd,UK) allows for correction values to compensate for intrinsic errors in the monitor for the red (R) green (G) and blue (B) phosphors and have default values of one.

CIE coordinates of $x=0.31$ and $y=0.316$ with luminance 12.5 cd.m^{-2} were entered into the software and the chromaticity coordinates at R, G and B were measured using the PR650. The voltages across the R, G and B guns were noted. The correction factors were adjusted until the monitor displayed the luminance required.

Contrast calibration

A script was written in Matlab, `ContrastCalib.m`, that presented two squares on the monitor, each with sides of 100pixels separated by 20 pixels, see figure 2.8.1.

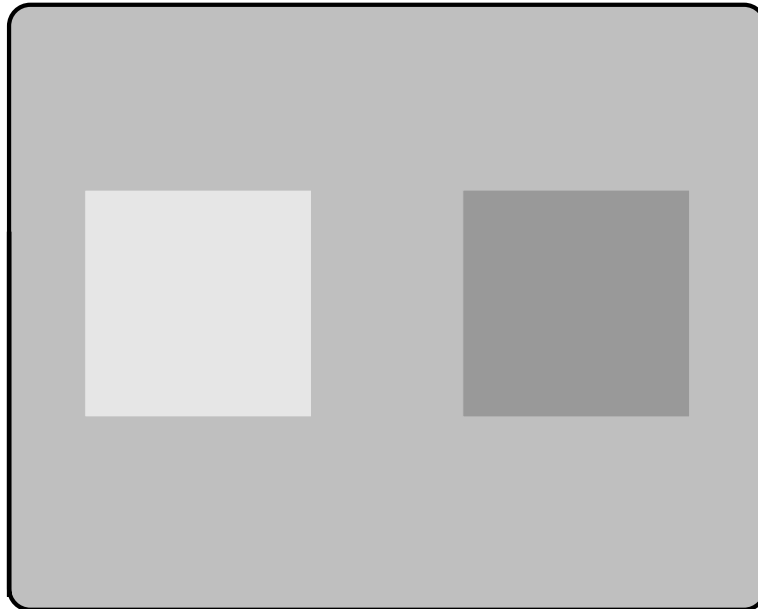


Figure 2.8.1: Contrast calibration screen, not to scale.

The luminance of each square was measured with the PR1500. These squares were generated using a series of look up tables. The look up table number was the independent variable and the measured luminance the dependant variable. For a series of table values the luminance of each square was measured using the PR1500 and the contrast calculated, the results are shown in figure 2.8.2. The $\log(\text{contrast})$ is linear for the look up table number ($R^2=0.9996$).

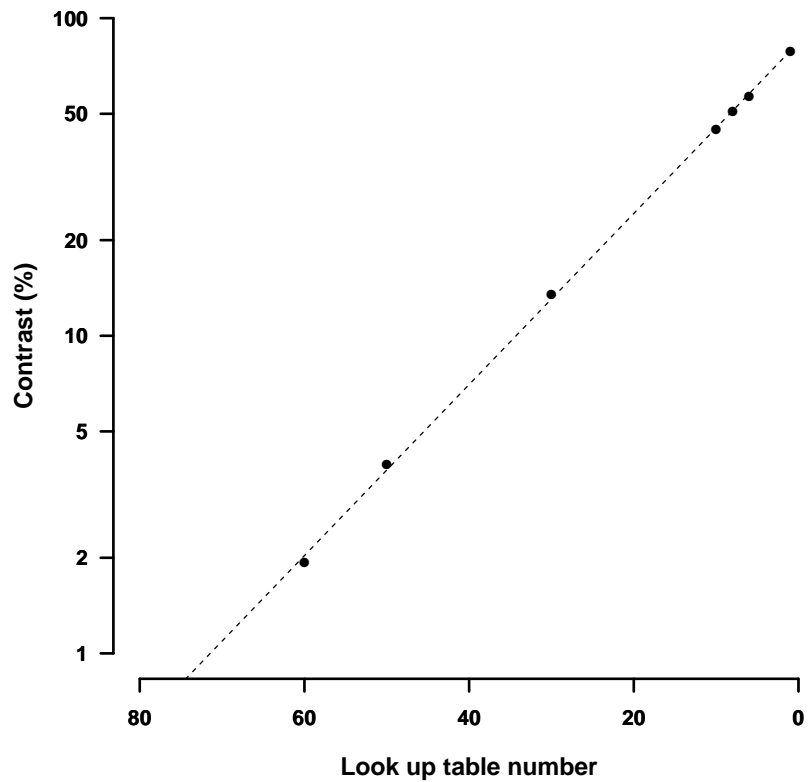


Figure 2.8.2: Contrast as a function of look up table.

2.8.4 Experimental design

Stimuli were horizontal and vertical achromatic sinusoidal gratings displayed in the centre of the monitor in a circular patch subtending 10° at a distance of 75 cm for 340 ms. The spatial frequencies were 0.5, 1, and 2 cycles per degree (cpd) and the Michelson contrast ranged between 0.02 and 0.7. The sinusoidal wave gratings were temporally modulated at 2 Hz.

The mean screen luminance was reduced from 12.5 cd.m^{-2} to $1 \times 10^{-2} \text{ cd.m}^{-2}$ using neutral density filters (LEE Filters, Colorfilter type 211, 0.9 ND [LEE Filters Worldwide, Andover, Hampshire, UK]).

2.8.5 Subjects

A call for volunteers was made within the Optometry department of the Faculty of Life Sciences, University of Manchester. Subjects were required to have best corrected acuity of better than 6/9 (Snellen), no ocular pathology, established by an eye examination within the previous 12 months. Thirteen subjects were recruited (6 female) aged $30.4(\pm 10.7)$ yrs.

2.8.6 Procedure

Principle A method of adjustment was used. At each stimulus presentation, identified by an auditory marker, the subject indicated whether the stimulus gratings were horizontal or vertical, this was entered into the software by the operator. The software scored the result, if correct the threshold was noted and the stimulus extinguished. After 10s the stimulus was represented reduced by 9.5dB, if the response from the subject was incorrect the stimulus was extinguished and represented after 5s increased by 3dB.

An electronic flashgun (Nikon Speedlight SB-800, Tokyo, Japan) was used to produce an estimated 75-95% visual pigment bleach for a pupil size range of 4.5 to 6.5 mm (Rushton & Powell 1972), see table 2.5.2. Spectacles, if worn, were removed and the subject fixated the centre of the flash at a distance that meant the after image generated covered the monitor screen.

The experiment was performed over three visits on different days of the same week. Occasionally measurements were made on the same day and a washout period of at least 45mins was used between measurements. At each session only one spatial frequency was tested. A brief preliminary trial was performed to allow the subject to become familiar with the task. A pilot study found that absolute thresholds were unchanged after 15min, so measurements started at 15min were completed and then the experiment finished. All measurements were completed by 20min.

To isolate the contribution of cone system the experiment was repeated with red sinusoidal wave gratings (0.5, 1 and 2 cpd) and mean luminance 0.01 cd.m^{-2} . The gratings were viewed through a red pass filter (Lee, UK filter 026) mounted in a goggle. The filter had the effect of removing any shorter wavelengths emitted by the red phosphor.

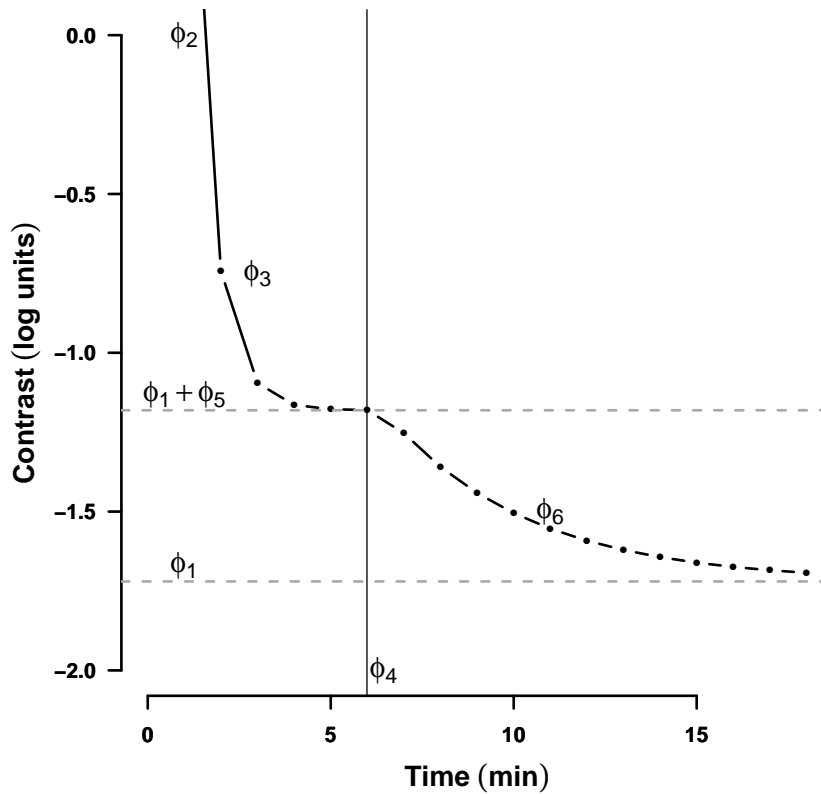


Figure 2.8.3: How the parameters of the bi exponential model relate to the collected data. The parameters are explained in the text. The parameter ϕ_4 is the transition time (vertical black line). The thresholds $\phi_{1,5}$ are labelled with horizontal grey dashed lines. Note the parameter ϕ_5 is the offset from the final phase to the early phase.

2.8.7 Model

The recovery of contrast sensitivity following a photo bleach can be modelled by an exponential function representing a single mechanism

$$CS = \phi_1 + \phi_2 \cdot \exp\left(\frac{-t}{\phi_3}\right) \quad (2.8.3)$$

where ϕ_1 is the absolute threshold, ϕ_2 the threshold at time zero and ϕ_3 the time constant. Alternatively, a bi-exponential model can be fitted, accounting for the possibility of two

systems

$$CS = \phi_1 + \phi_2 \cdot \exp\left(\frac{-t}{\phi_3}\right) + \phi_5 \cdot \exp\left(\frac{-h(t, \phi_4)}{\phi_6}\right) \quad (2.8.4)$$

where the step function $h(t, \phi_4)$ is zero for times less than ϕ_4 and time $t - \phi_4$ for times thereafter. The value of ϕ_1 is the absolute threshold for both phases, ϕ_2 the threshold at time zero and ϕ_3 the time constant value for the first phase, the first phase threshold is given by $\phi_1 + \phi_5$. Figure 2.8.3 shows how the parameters relate to the data.

This model was fitted to the data using a least squares method. A similar model was used by Dimitrov, Guymer, Zele, Anderson & Vingrys (2008) when modelling cone and rod dynamics.

2.9 Summary and outstanding issues

This chapter has described the apparatus and experimental methods used in this study.

An analogue device (figure 2.2.1) to measure the dark adaptation recovery curve has been presented and the characteristics of its components have been considered.

The use of this device and the subsequent digital device require a photo bleach and this is provided by a flashgun. The light emitted by the flashgun at a variety of settings has been investigated and a table produced that relates pupil size to the amount of photopigment bleached (Table 2.5.2).

A second device has been described, which is under digital control and operated using a PC (see figure 2.6.1).

The optimum interval between thresholds being set has yet to be determined and is considered in chapter 6.

The rate at which the stimulus increases in intensity is considered in chapter 7.

A method for measuring contrast sensitivity recovery following a photo bleach is presented.

2.9.1 Detectability of red LED by rods

Both devices used in this study have a red light as a background against which the subject must set a detection threshold for the green stimulus. The background is used to

elevate the cone threshold independently of the rod system, this shortens the cone rod transition time, allowing for earlier measurement of the rod system. It is assumed that the rod system is unaffected by the red light.

An attempt was made to measure the light emitted by the LED at shorter wavelengths (400 – 600 nm). In figure 2.3.9, the shaded area represents the region over which we are unable to dismiss the possibility of there being light. Light that conforms to a narrowband is permissible, since we can compare the findings in this study with other work that also use narrow band sources. The PR650 measurements were ambiguous about the contribution of the red LED to scotopic light. However, using the PR1500 with the narrowband filters the size of this region was markedly reduced.

Other workers have investigated the effect of a background on rod performance. Aguilar and Stiles (1954) used a test light of 520 nm (FWHM 40 nm), against a background of peak wavelength 650 nm (FWHM 120 nm). The linear plot (figure 1 in their 1954 paper) of the light sources used shows no light emitted below 600 nm. They show that over the range of ~ 4 log units of change in field intensity the slope of the rod TVI curve is constant, see figure 1.5.1.

More recently, Sharpe, Fach and Stockman (1992) investigated the effect of changing background intensity and wavelength on rod increment thresholds. Using a Maxwellian view, a test light of 520 nm (FWHM 11.8 nm) and four backgrounds, generated using Schott filters, having wavelengths 450, 520, 560 and 640 nm all with FWHM less than 11 nm, they found that on the long wavelength background (640 nm) the rod threshold increment constant was ~ 1 rather than 0.8 for the other wavelengths and suggest that this is due to quantal absorptions in both cones and rods.

We might expect the background to be detected by the rod system, Wyszecki and Stiles (1967, p104), suggest that light with a wavelength of 655 nm, if narrowband, should have a scotopic luminance of $0.014 \times$ photopic luminance. The standard background of $0.05 \text{ cd.m}^{-2}(\text{phot})$ used in this study converts to $7 \times 10^{-3} \text{ cd.m}^{-2}(\text{scot})$.

The principal aim in this study is the isolation of rod function and it has been shown that it is the measurement of the slope of the recovery of rod function, S2, that is of the most interest clinically. Therefore the questions remaining about the effect of the red background might best be addressed empirically. Chapter 5 considers the effect of the red background.

THE NORMAL DARK ADAPTATION FUNCTION: CURVE
FITTING AND MODELLING

The combination of some data and an aching desire for an answer does not ensure that a reasonable answer can be extracted from a given body of data.

John Tukey 1986

3.1 Introduction

The introductory chapter highlighted the importance of the dark adaptation response when investigating the ageing retina. Special emphasis was placed on the rod phase of sensitivity recovery and how it is affected by ageing. The retinoid deficiency hypothesis was also discussed (see e.g. Jackson, Owsley & Curcio (2002), Lamb & Pugh (2004)).

It was mentioned towards the end of the introduction that a model can attempt to represent the data collected or represent an underlying process (see section 1.5.4 on page 46). The exponential bilinear model (McGwin Jr et al. 1999) first described in section 1.5.3 was shown to be both indicative of biological processes (Mahroo & Lamb

2004, Lamb & Pugh 2004) and representative of the data and is used here. The model is biologically credible and satisfactorily describes the data collected in this study.

When collecting dark adaptation data from young healthy subjects the identification of the essential features of sensitivity recovery is straightforward. This is particularly so in a laboratory environment where the conditions can be freely adjusted. Data collected from a young subject are shown in figure 3.1.1(a), the cone rod transition point, cone threshold and arguably the most important variable, the slope of the rate limited rod recovery (S2 phase), can be identified by eye with little risk of bias in the healthy subject.

A challenge arises when we are presented with data collected from a subject with a compromised retina due to age or disease, e.g. see figure 3.1.1(b). How are we able to objectively identify the components of sensitivity recovery following a bleaching light and determine their magnitude with an unbiased and repeatable method? Furthermore, if such method can be developed we want it to be easily extendable so that it might be used for batch processing of bulk data e.g. data generated in an intervention study.

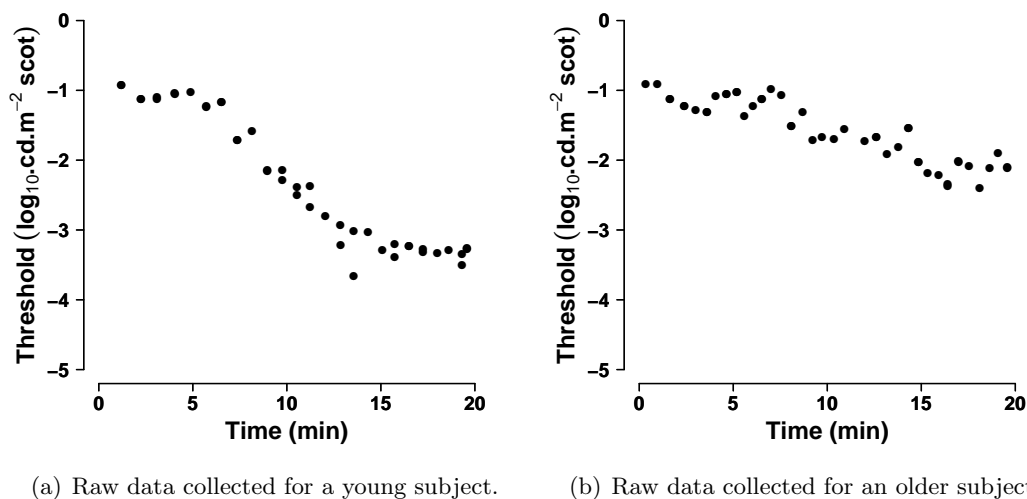


Figure 3.1.1: A comparison of the data collected from a younger subject compared to an elderly or unhealthy subject where the different phases of sensitivity recovery, see section 1.5.4, are less clearly defined or may be absent, their identification is difficult and prone to error at best and bias at worst.

This chapter will discuss the model fitted to the data collected in this study, the parameters that can be extracted from this model and the methods of finding those parameters. Following the model description, there will be a description of the particular methodology used in this work; an algorithm written in the Matlab (Nantick, USA) programming lan-

guage ‘.m’, to extract the parameter values of the dark adaptation recovery curve

Terminology

When considering the parameters of the dark adaptation curve the following terminology will be used; a number is lower if it lies to the left of another on the real number line, but a number is smaller if its absolute value is less, e.g -0.5 is lower than -0.1, but not smaller. This is highlighted because it is the absolute value of the slope of the S2 phase that is indicative of the efficiency of the chorio-rod complex.

Throughout, the following convention is used; vectors are shown as a lowercase bold symbol (\mathbf{p}), matrices uppercase bold symbol (\mathbf{M}) and variables lowercase italic (x). Function names in the body of the text are `typewriter` font and arguments to a function and values returned are presented in **bold sans serif**. Code listings are delineated by a grey line in the left margin and keywords within the listings indicated by **small bold** text.

3.1.1 Fitting a model to experimental data

The dark adaptation response model

Data representing the recovery of sensitivity can be described by two variables; the independent variable, time (min) following a photo bleach and the dependent variable, threshold (log units scotopic luminance) at time t and can be fitted to several different models, these have been discussed in the introduction. The model used in this study has been shown to provide useful insights into the biological processes underpinning the recovery of sensitivity following a photo-bleach (Lamb & Pugh 2004, Mahroo & Lamb 2004, Pugh 1975, Jackson, Owsley & McGwin 1999, Owsley et al. 2001, Owsley, McGwin, Jackson, Kallies & Clark 2007, Leibrock et al. 1998). It is presented here again as a starting point for the discussion. This model relates the change in threshold, measured in log units, to the time following a bleaching light. The energy of this bleach is discussed in the flash calibration, see section 2.5.2 on page 85.

Having collected the thresholds over time from a subject, e.g see figure 3.1.1(a) the main aim is to determine the values of the parameters of the model that best fit the data. The parameters of the model can be usefully represented as a vector, θ . Typical values for the parameters from two methods are shown in table 3.1.1.

Table 3.1.1: Parameter values of the data, taken from McGwin (1999) and Kelly (UoM). Notice the very large θ_2 value in the McGwin data, and the later θ_5 , cone rod transition point. The data in the original paper were presented in log units and have been altered by $/-10$. Luminance is measured in scotopic units

Description	θ	McGwin	UoM	Units
Cone threshold	θ_1 :	-1.47	-1.64	$\log_{10}(\text{cd.m}^{-2} \text{ scot})$
Exponential coefficient	θ_2 :	39.85	1.77	$\log_{10}(\text{cd.m}^{-2} \text{ scot})$
Cone time constant	θ_3 :	1.77	1.77	min
Slope of S2	θ_4 :	-0.154	-0.247	$\log_{10}(\text{cd.m}^{-2}).\text{min}^{-1}$
Rod-cone breakpoint α	θ_5 :	14.2	5.8	min
Sum of S2 and S3	θ_6 :	0.128	0.247	$\log_{10}(\text{cd.m}^{-2}).\text{min}^{-1}$
Rod-rod transition point β	θ_7 :	31.4	12.3	min

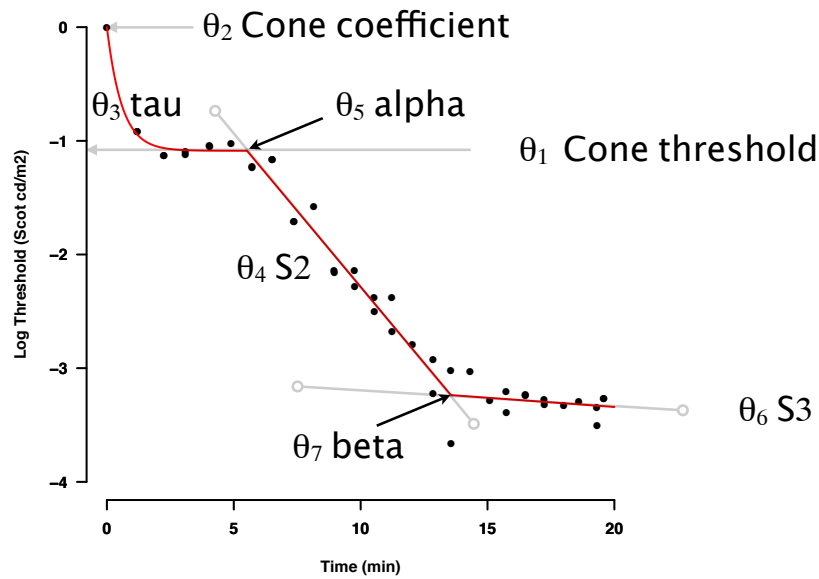


Figure 3.1.2: The seven-parameter model fitted to preliminary data.

The classical three phases of the recovery of sensitivity following a bleach at time zero are shown in figure 3.1.2. The initial phase depicts the cone response, and can be represented by three parameters; the absolute cone threshold (θ_1 , $\log_{10}(\text{cd.m}^{-2})$ scotopic), the cone coefficient (θ_2 , $\log_{10}(\text{cd.m}^{-2})$ scotopic), and the time constant of cone recovery, sometimes

known as tau (θ_3 , min).

The apparatus used in this study returns threshold measurements of the stimulus luminance in either scotopic units ($\log_{10}(\text{cd.m}^{-2} \text{ scot})$) or attenuation (dB). The cone coefficient can be thought of as the cone threshold at the instant following the flash, but as this variable can take non-physiological values it is best perhaps thought of a free variable that aids the fitting process. This phase can be represented as follows;

$$Thrs_c = \theta_1 + \theta_2 \cdot \exp\left(\frac{-t}{\theta_3}\right). \quad (3.1.1)$$

After the cone mediated phase there follows the rod phase, S2, which is defined by its slope, ($\theta_4, \log_{10}(\text{cd.m}^{-2}).\text{min}^{-1}$) and the rod cone transition time or alpha point (θ_5 , min). Similarly the next rod phase, S3, is described by the sum of the slopes of S2 and S3 ($\theta_6, \log_{10}(\text{cd.m}^{-2}).\text{min}^{-1}$) and the rod-rod transition time, occasionally referred to as the beta point (θ_7 , min). The model uses the transition times to control step functions and hence allow each phase to combine. The response threshold $Thrs$ can therefore be summarized as follows:

$$Thrs = Thrs_c + \underbrace{\theta_4 \cdot h(t, \theta_5)}_{\text{S2}} + \underbrace{\theta_6 \cdot h(t, \theta_7)}_{\text{S3}} \quad (3.1.2)$$

where $h(t, \theta_i)$ is a step function

$$h(t, \theta_i) \begin{cases} 0 & \text{if } t - \theta_i \leq 0, \\ t - \theta_i & \text{if } t - \theta_i > 0. \end{cases} \quad i \in (5, 7)$$

Notice that since the threshold data are in log units, when plotted against time the apparently linear phases S2 and S3 describe exponential processes. Further discussion of the model is made in section 3.2 where model selection is considered.

A common assumption in elementary modelling is to assume that the noise component has mean of zero and a constant variance throughout. The alternative, mixed effects modelling, is a method that attempts to model the noise. Although, this adds complexity, it can provide insight to underlying mechanisms, e.g. when used in temporal sensitivity channel models (Mayer, Dougherty & Hu 1995).

Therefore, to summarize, the model can be presented as:

$$Threshold = D(\mathbf{t}, \boldsymbol{\theta}) + M(\mathbf{z}, \sigma_{\mathbf{p}}^2) + \zeta(0, \sigma^2), \quad (3.1.3)$$

where the measured threshold $Thrs$ at time t is the sum of $D(t, \theta)$ the underlying model, $M(z, \sigma_p^2)$ the noise model, described by mean \mathbf{z} , and variance \mathbf{p} , and a residual component, $\zeta(0, \sigma^2)$ with constant variance and mean zero. The algorithm uses the simple model where $M = 0$, i.e. does not attempt to model the noise. The mixed effects model is included here for completeness, and is only considered as far as comparing the variance of the residuals.

3.1.2 Variability in psychophysical data: their cause and effect

When collecting any psychophysical data there are often points that do not lie upon the predicted values calculated by the optimal model. The difference between the observed values and the model predictions is often termed noise, while the vertical distance from the data to the model termed the residual. These variations are occasionally referred to as within or intra-subject variability.

Furthermore, for each subject the parameters of the model may vary between subjects in the same way as many other biological characteristics vary, e.g. height and is known as inter-subject variability. Although there is some information in the literature about inter-subject variability, e.g. how the parameters of dark adaptation vary with age (Jackson et al. 1999), what is not known for the parameters is how these variations are distributed in the population, furthermore, intra-subject variability is poorly understood, e.g. how the parameters vary from day to day.

Noise

When measuring dark adaptation the responses from the subject are likely to have random components. These are due to

- lapses in attention
- anticipating a threshold or guessing
- a change or shift in the criterion used by the subject to set the threshold.

These factors, lapse, guess and shift, are often assumed to be independent of each other and constant but this is not always the case. For a discussion of this point along with possible solutions see Treutwein (1995). In the case of the dark adaptation curve a lapse or guess will elevate or depress the threshold measured, if either of these factors remain

constant throughout a particular phase of the trial then the slope of that phase will be unaffected. A criterion shift during a phase is more complicated, that will introduce a discontinuity in the responses and will have an effect on the slope of that phase. A criterion shift between the phases of the dark adaptation curve, i.e. when changing from the cone dominated phase to the first rod mediated phase (S2), or the two rod phases (S2 and S3), has little effect.

Auto correlated data

Ideally threshold measurements should represent the state of the visual system at the instant the threshold is set. It is important to remark here that the rod system is extraordinarily sensitive, is quickly saturated and adapts to both spatially and temporally modulated stimuli (Masland 2001). Therefore, when a subject has a lapse in concentration the stimulus is at supra threshold levels when it is reported by the subject. This may have the effect of briefly elevating the threshold of the rod system and possibly influencing subsequent thresholds. Alternatively the subject having become aware of a lapse may anticipate the next threshold or adopt an altered criterion. This leads to data that are described as auto correlated, that is, the present threshold is not independent of the previous threshold measurements, but is influenced by them.

Two factors that may lead to a lapse are increasing age and hence reduced reaction time, and the speed of stimulus intensity increase being too rapid. These can be mitigated by selecting a rate of stimulus increase that minimises the auto correlation and a sampling interval that is sufficiently large to allow the briefly raised threshold to fall, yet not so large as to encourage guessing. A guess will have no deleterious effect on the state of rod adaptation and subsequent thresholds, but will affect the estimate of the slope.

To determine whether data are exhibiting auto correlation a model is fitted to the data and the residuals found, this is known as ‘detrending’. The residuals are then correlated to the residuals offset 1, 2, 3... steps, sometimes known as lag. Auto correlated data in this context are data where the threshold measured at time t_n is related to previous threshold measurements at t_{n-k} where $k \in (1 \dots n - 1)$. The count of the number of significant steps informs the level of data interdependence.

Count data, i.e. data only taking positive integer values are usually analysed using a poisson distribution, first described by Poisson (1841). An introductory text on the importance of poisson regression when using count data and a method of calculating

the significance of a general linear model using the natural log link function is given by Coxe, West & Aiken (2009).

Model fitting assumptions

If a threshold measurement can influence a subsequent threshold then the assumptions necessary for accurate curve fitting are violated. Curve fitting relies upon three assumptions:

- normally distributed errors
- constant variance of the error
- independence of errors

These assumptions are usually summarised as the errors being independent and identically distributed (iid). Failure of these assumptions can result in poor fitting of models and inaccurate bootstrap techniques, both of which assume that each data point has either equal validity or has a known weight.

Bootstrap techniques are discussed further in appendix C on page 289.

3.2 Model selection

The primary model used in this study is the seven parameter equation 3.1.2. However, not all subjects have a sensitivity recovery that fits this model, see figure 3.2.1. For subjects with a slow S2 phase the final S3 phase may not be reached and a five parameter model would be more appropriate. Similarly, subjects with an absent or very slow S2 phase might be better modelled by the three phase model in equation 3.1.1. These three models are related, i.e. the models with fewer parameters are simpler forms of those with more and are described as nested, see figure 3.2.1.

A first approach might just compare the residuals squared sum (RSS). This would be mistaken because the more complex model (i.e. having more parameters) is likely to have a lower RSS since it has more inflexion points.

3.2.1 Model selection using the extra sum of squares test

The extra sum of squares test, where the change in the RSS for two models is compared to the change in the degrees of freedom, can be used for nested models determined by least squares methods. When only two models are considered this method is quite straightforward. However, with three or more models the procedure becomes more involved. Although, pairwise F tests for each of the three models or a hierarchical approach could be used, multiple comparisons raise problems regarding confidence levels. This can be addressed with Bonferroni correction but this has been criticised as too conservative (Bland & Altman 1995).

To compare two nested models the test statistic is

$$\frac{(RSS_s - RSS_c)/(p_c - p_s)}{RSS_c/df_c} \sim F(df = p_c - p_s, df_c) \quad (3.2.1)$$

where the subscripts s and c refer to the simple and complex models respectively, df the degrees of freedom and p the parameter count for the models.

3.2.2 Model selection using information theory

An alternative is to use the information criterion (AIC) described by Akaike (1974). This method avoids hypothesis testing and p-values, rather an index of information lost by the model is found and compared to the same index for other models. Nonetheless, the AIC can only tell which of a series of models best fits the data, not whether the models are suitable. The AIC is can be defined as

$$AIC = N \ln \left(\frac{RSS}{N} \right) + 2K \quad (3.2.2)$$

where N is the number of observations and K is the number of parameters in the model fitted plus one (Burnham & Anderson 2004).

An improvement on this measure the corrected AIC, equation 3.2.3, is available and should be used where the number of observations is not many times larger than the number of parameters squared. This applies in this study where the number of observations is of the order of 50 and there are at most 7 parameters (Burnham & Anderson 2004).

The model with the lowest corrected AIC_c value is the most likely. A worked example and further discussion is presented in Motulsky and Christopoulos (1987, pp143)

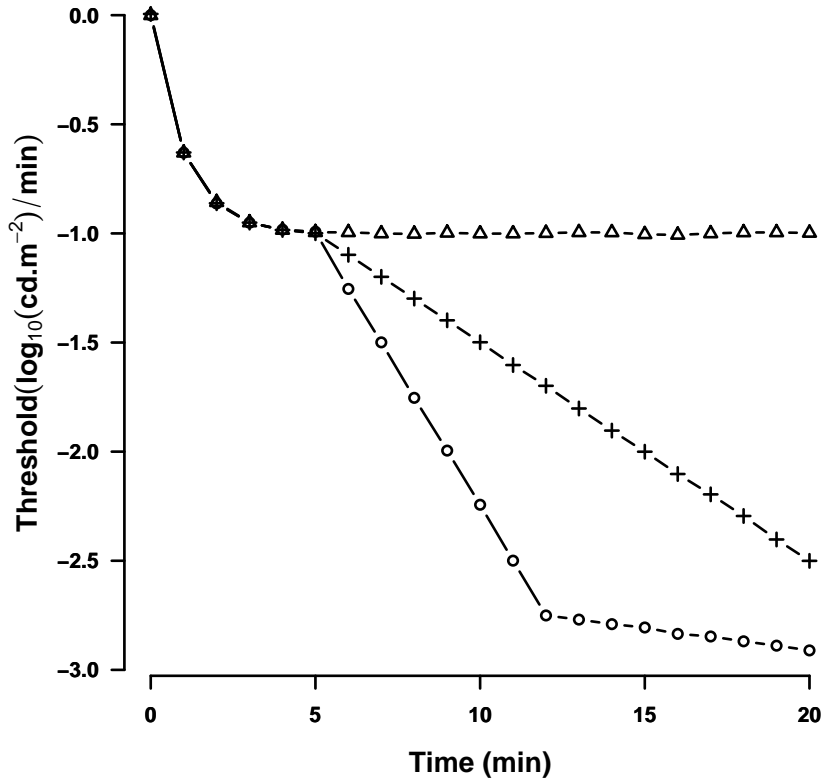


Figure 3.2.1: A series of nested models to represent the recovery of sensitivity. Open circles, seven parameter model (eqn: 3.1.2) an exponential decay and two linear phases; crosses, five parameter model ($Thrs_c + S2$) of exponential decay and one linear phase; open triangles, three parameter model ($Thrs_c$) simple exponential decay.

$$AIC_c = AIC + \frac{2K(K+1)}{N-K-1} \quad (3.2.3)$$

3.3 Methods of parameter extraction

There are many ways of extracting the value of θ . One method would be to subject the data to a transformation to render the relationship between the dependent and independent variables linear. Then simple linear algebra would allow for calculation of θ .

However, there is no obvious way in which the model function presented here could be

transformed. Even if transformation were possible it would not be ideal, as the noise component would also be transformed, with subsequent loss of the constant variance assumption. The seminal text on nonlinear regression (Bates & Watts 1988) advises that without this assumption being held a weighted regression would be necessary to prevent noisy data from excessively biasing parameter estimates.

Least squares

The essence of the linear algebra method of curve fitting is to minimize the vertical distances from the data points to the straight line, the residuals, by altering parameter θ . Nonlinear regression uses the same technique. This is done by forming a function composed of the sum of the squared residuals. This gives rise to a response function with θ as its variable;

$$L(\theta) = \sum_{i=1}^n (Thrs_i^* - Thrs(t_i, \theta))^2 \quad (3.3.1)$$

where n is the number of observations, $Thrs_i^*$ is the i th threshold measurement at time t_i , and $Thrs(t_i, \theta)$ is the model estimate using parameter θ at time t_i .

The $L(\theta)$ function has θ as its variable, since both $Thrs^*$ and t are fixed by the experimental results. The likelihood of the parameter estimates is maximised when $L(\theta)$ is at a global minimum and the resulting values of θ are considered optimal (Bates & Watts 1988, p16).

3.3.1 Analytical methods

Having found a response function $L(\theta)$ we minimize it by adjusting θ . If we think of $L(\theta)$ as a surface then we want to find the lowest point, the global minimum. Many methods (e.g Newton - Raphson) use an initial value and move across the surface by finding the path of steepest descent down that surface. This is done analytically by finding the slope of the response function at the point described by the vector θ . So for an initial parameter $\theta^{(0)}$ we find the partial derivatives of the function $L(\theta)$ with respect to $\theta^{(0)}$, this gives us the slope of the rate of change of the parameter values at this point (Bates & Watts 1988).

Once the direction of steepest descent is found the method takes a step down the slope in this direction to estimate a new $\theta^{(1)}$ and the process of calculating the slope of $L(\theta)$

is repeated until the difference between successive values of L is below a predefined tolerance. This method is at its most efficient when the partial derivatives of the parameters can be found as functions. Here we face a technical difficulty, the step function (see figure 3.3.1b) that is used to switch between the cone and S2 phase and the S2 and S3 phases is difficult to meaningfully differentiate.*

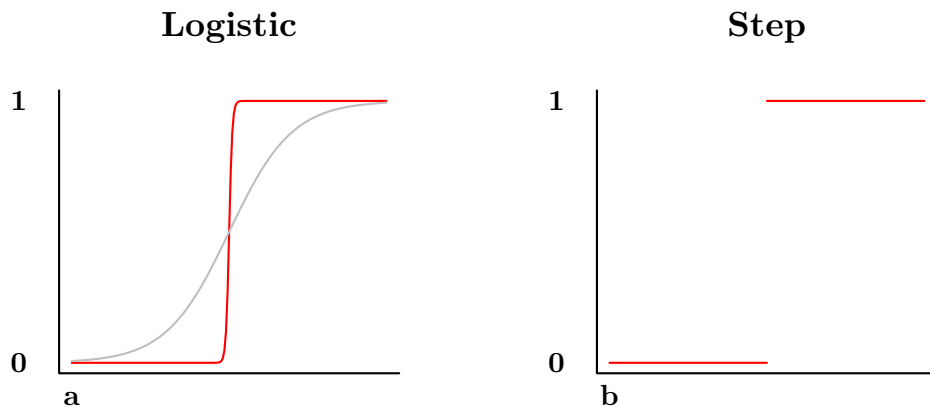


Figure 3.3.1: Comparison of a logistic function (a) and a step (or Heaviside) function (b). The light curve in (a) is for a small value of k the dark is large ($k = 10$)

Short comings of analytic methods when finding DA parameters

Finding the partial derivatives of the function 3.1.2 is not straightforward, due to the step functions. Although they can be differentiated, the result is meaningless in this context. An alternative to the step function in equation 3.1.2 is a logistic function

$$g(t, \theta) \rightarrow \frac{1}{1 + \exp(-k(t - \theta))} \quad (3.3.2)$$

where θ is the transition time and k takes an arbitrarily large constant value or we could allow k (min^{-1}) to be a further variable, one that reflects the rate at which one phase shifts into the next phase. A comparison of the step and logistic functions is shown in

*differentiation of this function yields an impulse or Dirac function and is used in signal detection theory

figure 3.3.1. However, the use of the logistic function makes the model even more complex and although clearly easier to find the partial derivatives, it is still rather cumbersome and difficult to interpret, see equation 3.3.3

$$Thrs_{logi} = \theta_1 + \theta_2 \cdot \exp\left(\frac{-t}{\theta_3}\right) + \theta_4 \cdot \frac{(t - \theta_5)}{1 + \exp(-k \cdot (t - \theta_5))} + \theta_6 \cdot \frac{(t - \theta_7)}{1 + \exp(-k \cdot (t - \theta_7))}. \quad (3.3.3)$$

Moreover, allowing the variable k to become a parameter in the model will improve the ‘goodness of fit’, but may not yield any meaningful insight.

However, it is worth noting here that not all analytic algorithms that use derivative based methods to extract the parameters of a model require them to be supplied. For example, some methods in R approximate derivatives numerically using differencing methods rather than symbolic methods to calculate the partial derivatives required (Fox 2008). That is, the value of the slope of the function $L(\boldsymbol{\theta})$ with respect to $\boldsymbol{\theta}^{(i)}$, the i^{th} estimate, is calculated, rather than derived from a function. So, although analytically distinct, a numerical method of differencing would be unable to distinguish between a step function and a sufficiently abrupt logistic function. In other words, the collected data appear continuous and differentiable at all points. The importance of this is that for well-behaved data, i.e. data for which the model applied is appropriate, analytic methods like `nls` in R might provide quick and meaningful estimates of $\boldsymbol{\theta}$, this will be discussed in detail in appendix D.1 on page 297.

3.3.2 Direct search methods

Since the behaviour of the value of $\boldsymbol{\theta}$ is unknown, the curvature of the response surface $L(\boldsymbol{\theta})$ is difficult to predict and statistical analysis to determine confidence intervals is not possible. The difficulty associated with the unpredictability of these values can be avoided by the use of direct search algorithms. A direct search method is one where test estimates of the parameter $\boldsymbol{\theta}$ are compared, and then new estimates are formed following specified rules. McGwin (1999) used a direct search algorithm that ‘does not use derivatives’ (`dud`), first described by Ralston and Jennrich (1978). Another popular direct search method is a simplex method (Kolda, Lewis & Torczon 2003).

Simplex methodology

The use of simplexes was first proposed in the early 1960's (Spendley, Hext & Himsworth 1962). A widely used simplex method is that described by Nelder and Mead (1965). The Nelder-Mead (NM) method is a popular direct search algorithm (Gao & Han 2010), a search for the 1965 paper by Nelder and Mead on Google Scholar reveals in excess of 13900 citations (search of Google Scholar on 19th April 2012). Its popularity is attributed to two characteristics. Firstly, the NM algorithm is largely independent of the presence or otherwise of first and second derivatives of θ (Lagarias, Reeds, Wright & Wright 1999, McKinnon 1999). Secondly, simplex methods are robust when used on noisy or discontinuous data (Ahmed 2001). A simplex algorithm is available for use by the Solver tool in Microsoft Excel (Fylstra, Lasdon, Watson & Waren 1998), by the `optim` function in 'R' (Nash 1990) and by the `fminsearch` function in Matlab (Lagarias et al. 1999).

The NM algorithm takes an initial $\theta^{(0)}$, the starting point, with n components and creates a simplex of $n+1$ vertices, each vertex is a random multiple of $\theta^{(0)}$. So, for example, if the function to be minimized had a parameter vector θ , with one component, the simplex would be a line segment, two components a triangle, and three components would have a tetrahedron as its simplex.

The two-parameter form is easy to visualize, and will serve to explain the methodology, see figure 3.3.2. As mentioned earlier the function $L(\theta)$ can be considered as describing a surface upon which each θ locates a point or vertex of the simplex on that surface. Each vertex has a corresponding L value analogous to an altitude on a map. The algorithm sorts the vertices and the one with the largest L value, i.e. greatest altitude, is subjected to one of three possible transformations in an attempt to reduce its L value. The possible transformations are; reflection, contraction and dilatation. The first transformation chosen is reflection in the other vertices, if this does not yield a reduced L value, then a contraction is applied, if this is unsuccessful then a dilatation is tried. There are rules also in the event of tied values (Lewis, Torczon & Trosset 2000).

The process, using two reflections and a contraction is illustrated in figure 3.3.2. A simplex of three points has been generated, using a starting point $\theta^{(0)}$, which should be near to the global minimum, the points are random multiples of the starting point, see figure 3.3.2a. The first transformation is a reflection in the axis of the other two estimates, shown in figure 3.3.2b. In this case vertex $\theta^{(3)}$ is reflected in the line $\theta^{(1)} - \theta^{(2)}$, and generates a smaller L value, the algorithm then compares the vertices and $\theta^{(2)}$ now has

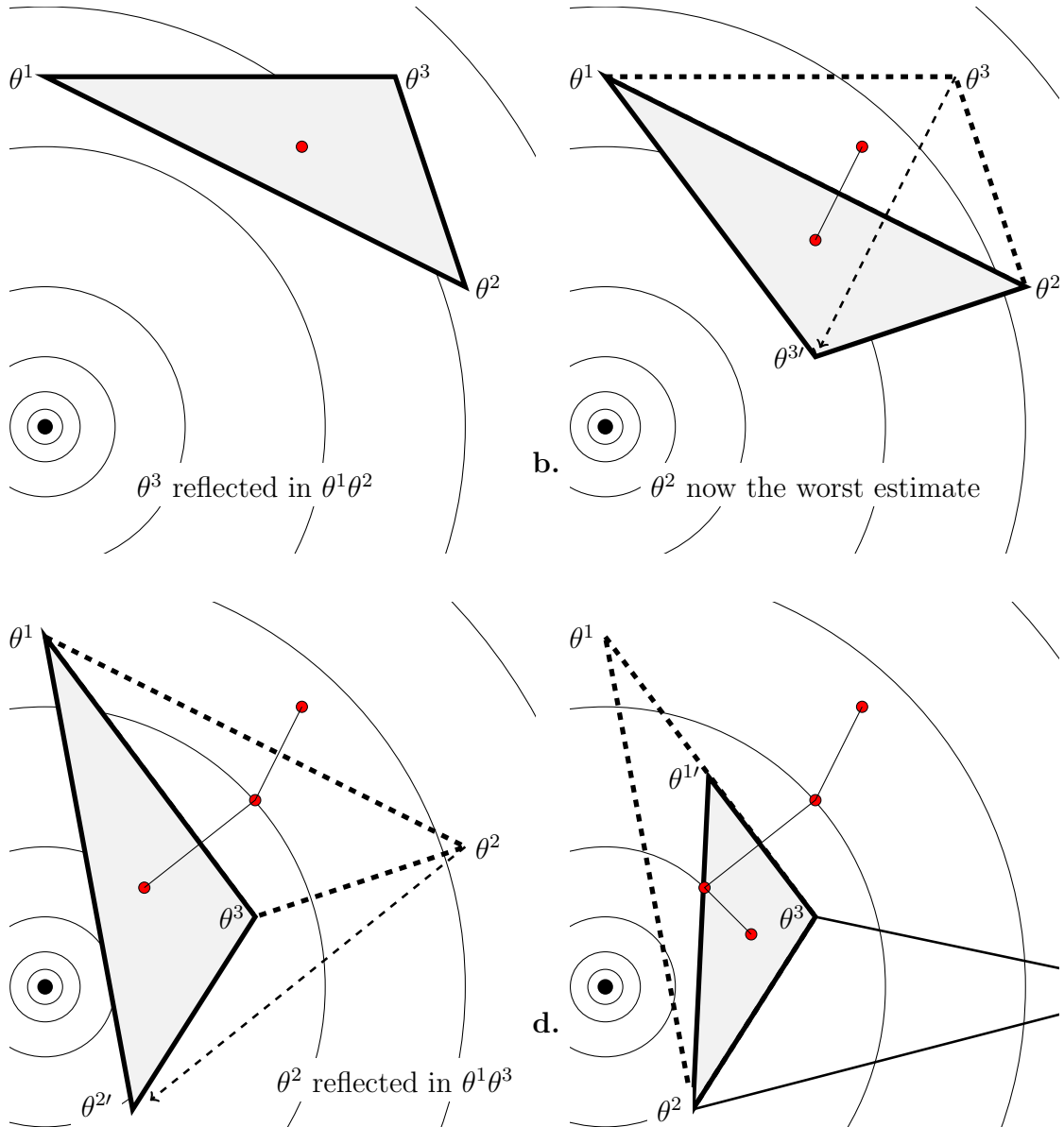


Figure 3.3.2: How the Nelder Mead Simplex parameter search works. Circles centred on the black dot are notional contour lines surrounding the global minimum. The vertices are $\theta^{1,2,3}$. The light grey dots are the centroids of each simplex, showing that although the trend is to the minimum, it is not a direct path. Dashed lines show the position of the previous simplex. For further discussion see the text.

the greatest value and then this too is subjected to a reflection in the other vertices, see figure 3.3.2c. This results in $\theta^{(1)}$ having the largest value, from figure 3.3.2c we can see that reflection in the other two vertices will not reduce the L value for this vertex, the algorithm therefore tries a reflection of half the distance, which also fails to reduce the L value, whereupon a contraction is tried, see figure 3.3.2d. This results in a smaller L value, but does not directly approach the global minimum, as can be seen by the path of the centroid of the simplex.

To summarize, the algorithm subjects the simplex to a succession of transformations with the objective of finding the minimum value of the $L(\theta)$ function, the end point is reached either after a fixed number of iterations or where further transformations yield a reduction in $L(\theta)$ of less than a fixed amount.

Limitations of the Nelder Mead method

The NM algorithm may fail to converge or may converge on a local minima even when the parameter functions are continuous and have third derivatives (McKinnon 1999). To overcome this possibility, many adaptations to the algorithm have been suggested, but the simplest modification is to repeat the algorithm with different initial values (Kolda et al. 2003), sometimes known as a multi start algorithm. This modification was included in the method described below. Although widely used, the theory of the Nelder Mead simplex algorithm convergence is incomplete, in particular it is difficult to predict conditions under which there will be a failure to converge and there are no methods available for assessing the reliability of parameter estimates, e.g. confidence intervals (Gao & Han 2010).

Comparison of direct search and analytic methods

In general analytic methods differentiate the parameters and select the path of steepest descent down the response surface to the global minimum, the direct search method described here selects the highest point of the simplex on the response surface and moves away from it, this subtle difference accounts for direct search method being slower.

The components of the parameter θ in the model used here are not independent, the slope of the S2 phase along with the cone rod transition point and the rod rod transition point are interrelated, a method that treats these components as independent is liable to return nonsensical values.

For both techniques, analytic and direct search, the initial parameter vector θ_0 does not necessarily lead to the global minimum of L , it may instead terminate at a local minimum or at a minimum in a region where the parameters are nonsensical, e.g. a positive slope for the S2 phase ($\theta_4 > 0$) (see section 1.5.4 on page 46), or the transition times ($\theta_{5,7}$) occurring before the measurement began or out of sequence. For direct search methods it is particularly important that the initial starting point is composed of permissible values (Lewis et al. 2000).

3.4 Extraction of the parameters of the dark adaptation curve

Having described the theory behind the method of estimating the parameters of the dark adaptation recovery curve, the following presents the implementation used in this study. An ideal algorithm to estimate the parameters of the dark adaptation recovery curve would have the following attributes:

- return unbiased parameter estimates
- have some measure of the ‘goodness of fit’
- be able to calculate confidence intervals
- multi-platform, i.e. be usable on a variety of computer operating systems and programming languages
- quickly return parameter estimates, CI and any other measures
- capable of batch processing

Two computer languages were employed initially; Matlab (Nantick, MA, USA) and the open source statistical programming language ‘R’ (R Development Core Team 2010). The implementation in R is presented in a later section (D.1). Both are widely used, Matlab is a proprietary software package, that was originally developed to handle matrices (Matrix Laboratory) and is particularly adept at linear algebra, however, at the University of Manchester, it can only be used when on campus or connected via a VPN (Virtual Private Network) client. The statistical programming language R is an open source variant of the commercial software S originally developed at Bell Laboratories. R is described as an environment for statistical computing and graphics, it is a GNU project (Stallman 1999)

and is available as Free Software, it compiles and runs on a wide variety of Unix, *nix, Windows and Mac operating systems.

Table 3.4.1: Comparison of Matlab and R

Feature	Matlab	R
Cost	+++	Free
Toolboxes	+	Free
Licence	On campus only limited number	GNU
Support	Mathworks	Forum
Internet resources	++	++++

3.4.1 Algorithm Implementation in Matlab

In order to extract the parameters of the dark adaptation recovery data collected from a subject a script was written in ‘.m’, the Matlab computer language, `JMKDAParamTest.m`. It uses the Nelder-Mead method as its kernel. The Nelder Mead simplex method is provided by the function `fminsearch` and the script `JMKDAParamTest.m` is essentially a wrapper for this function, multiple starting values are generated by randomly scaling a starting estimate of the parameters, the main features of the script is shown below.

The `JMKDAParamTest.m` function returns up to five values and can accept up to four arguments. The script is invoked with the Matlab program by the line:

```
1 | function [LeastB,Stats,RestB,Count,B] = JMKDAParamTest(data,DBdata, Graph, iter)
```

The first argument **data** was the experimental data presented as a two column array with time in the first column and thresholds in log units in the second. The arguments **DBdata** and **Graph** are switches, i.e. set as on or off. The **DBdata** switch triggers the conversion of **data** provided in deciBels to \log_{10} units. **Graph** draws a figure. The argument **iter** is the number of times that the core of the script is repeated, i.e. the number of starting points used, see below. If only **data** is provided then the other values are set to defaults, **DBdata = off, Graph = off, iter = 50**.

There then follows some checking of the input data for missing values, and the starting or seed parameter $\theta^{(0)}$ is created, denoted as **b** in the script.

```
54 | %% Create the seed parameter
```

```

56 | % Cone phase
    | b(1) = y(1)-2;           % cone threshold
58 | b(2) = 20.0;           % ordinate at time 0
    | b(3) = 1.0;           % time constant
60 | % S2 phase
    | b(4) = -0.6;           % S2 slope
62 | b(5) = 7+7*rand;       % Alpha break?point
    | % S3 phase
64 | b(6) = 0.2;           % S2 + S3 slope
    | b(7) = 15+15*rand;     % Beta break?point

```

Then two functions were created, the first returned the least squares value and has parameter **b** as its variable, equivalent to equation 3.3.1, the second calculated the model threshold values for a series of given times, taken from the first column of **data** and the best estimate of **b** and is equivalent to equation 3.1.2.

```

72 | % define the model functions
74 | funEB = @(b) sum( (y-(b(1)+b(2)*exp(-b(3).*x) ... % to convert to
    |               + b(4).*max(x-b(5),0) ... % exponential time constant
76 |               + b(6).*max(x-b(7),0)).^2); % tau=log10(e)/b(3)
    | % this returns the sum of the residuals squared.
78 |
80 | funEBY = @(b,x) (b(1)+b(2)*exp(-b(3).*x) ...
    |               + b(4).*max(x-b(5),0) ...
82 |               + b(6).*max(x-b(7),0));
    | % this returns the estimated y values at time x, for a given 'b'.

```

The function `fminsearch` takes three arguments, the least squares function to be minimised **funEB**, the initial parameter estimate **b** which is subject to random scaling at each iteration, and a list of **options**. The function then returns two values, the estimates of the parameters **tempB** and the sum of the squared errors **sse**.

The Nelder Mead algorithm is an unconstrained method and it is therefore possible for it to return an estimate of **θ** that is nonsensical. Constrained methods are available in Matlab, but given the preliminary nature of this work they were not used. If nonsensical values were returned, e.g. estimates of the slope of the S2 phase outside the range zero to -0.8 log unit/min, a cone threshold outside the observed range of thresholds, a cone rod transition time with negative value, along with rod rod transition times that precede the cone rod transition point, they were disregarded. Any unreasonable values have their

sse recoded as a number greater than 9000.

```
%% Estimate parameters

ii = 1;
while ii < iter; % calculate ITER estimates of b

    [tempB,sse] = fminsearch(funEB,b*rand,options);

    if not sensible B(ii,8) = 9000;
% Sanity checking, for detail see appendix
else
    B(ii,1:7) = tempB;
    B(ii,8) = sse/(Count);% MSE

end

ii = ii+1;
end
```

This **while** loop creates an array **B** of *iter* rows, with the parameter estimates in the first seven columns and the mean squared error (mse) in the eighth.

A copy of the array is made and then sorted by ascending **mse** value and returned as **RestB**. The first row of which, i.e. lowest **mse**, is chosen as the best estimate of the parameters **LeastB** of the dark adaptation curve 1.5.1.

Finally an index is created of the rows that have **mse** less than 9000, and the index is used to select those values, these are then subjected to some simple statistics. The array **Stats** has three rows, the first contains the means of each parameter, the second row is the standard deviation of the reasonable estimates and the final row is the number of reasonable estimates, **Count**, returned by the **while** loop above.

The full listing of the code can be found in appendix A.1 on page 253

Possible Improvements to the Matlab Algorithm

Setting the value of **iter** to too small a value, means that the likelihood that the algorithm will converge to a local rather than global minimum of the least squares function increases. But too large a value results in the script taking a long time to finish, e.g. 200

iterations complete in about fifteen seconds. For individual results this is not a problem, but when analysing larger data sets of the order of hundreds, or carrying out bootstrap calculations, see below, the time taken becomes a significant factor.

A sanity check of the seed values before they were passed to `fminsearch` did not improve the speed with which the script completed. It seems that the `fminsearch` function is as quick as a series of `if...else` or `switch` statements.

3.5 Summary

This chapter has presented a global model, composed of three nested models that is physiological coherent and fits the data determined in this study. Two methods of model selection have been described.

The importance of iid data and a means to determine auto correlation of data has been presented.

There has been a discussion of the difficulties of nonlinear regression and a proposal of an algorithm to extract the parameters of the model when fitted to the data.

EVALUATION OF AN ALGORITHM BY A SERIES OF
NUMERICAL EXPERIMENTS

Computers are useless. They can only
give you answers

Pablo Picasso

4.1 Introduction

This chapter will investigate the reliability of the algorithm and see what effect noise in the data has on the parameter estimates returned by the algorithm.

This investigation will use test data. Test data have known parameters and for each datum a random element of noise is added. The element is taken from a normal distribution with a known variance and mean of zero. This imitates the effect of noise in real data, assuming that the noise has constant and equal variance in each phase of sensitivity recovery. The parameters of the test data are derived from the literature and preliminary work in this study.

In the final part an application of the algorithm to real data will be presented;

- comparison with estimates found using the ‘Solver’ tool in Excel

This application illustrates both the desirable features of the algorithm and its shortcomings. The first application serves two purposes, firstly to demonstrate the extensibility and cross platform nature of the method used and secondly to verify a method in R (R Development Core Team 2010) using the Matlab method as a benchmark.

The second application illustrates the utility of an objective method when applied to large sets of challenging real data. It also allows a verification of the values extracted by comparison to those found by another method by another worker.

A method of confidence interval calculation is also presented that relies upon model comparison.

4.1.1 Aims

The aim of the work presented here is to verify and investigate the utility of a series of methods of parameter extraction, in particular a multi-start algorithm using a direct search methodology.

4.2 Test data and the effect of noise on parameter estimates

Having produced a script in Matlab that can extract the parameters of the dark adaptation recovery curve, it is important to know how the script will perform when presented with data that reflects reality, that is, has both deterministic and stochastic components.

To this end, two sets of test data were created. One set used the parameters from McGwin's paper (1999) and the other had parameters from preliminary data collected in Manchester. The test sets were composed of a reference array with no random elements, then a series of arrays, each with normally distributed random noise added at each time point, the variance of which increased uniformly for each subsequent array.

The Manchester parameters were collected from a subject aged 46 and therefore unlikely to have rod dysfunction, while McGwin's parameters were from an older subject, aged 75years, and therefore more likely to have a compromised recovery function.

McGwin's parameters were chosen as the model used in their study is the same as the

global model used in this one. The Manchester parameters were collected from the author using the analogue apparatus described in section 2.2 on page 54, from calibration trails and were representative of data collected from other subjects who also took part in early work.

4.2.1 Method

A series of scripts were written in Matlab (see appendix A.1 on page 253 for full details, `TestWrapper.m`, `JMKIdealData.m`, `JMKDAParamTest.m`), using the `fminsearch`, `rand`, and `randn` Matlab functions. The function `TestWrapper.m` controls the verification process, see figure 4.2.1.

Firstly, taking the parameters from McGwin’s paper (1999) where data are presented from measurements lasting 40minutes, the script `JMKIdealData.m` created a data set, with 81 columns and 10,000 rows. For each of the 81 points in the range [0,40] minutes a threshold was calculated with an additional element of noise ξ that varied at each point; the error at each point was drawn from a normal distribution, $\xi \in N(0, \sigma^2)$, with mean zero and standard deviation σ , such that the threshold y for an array was given by;

$$\mathbf{y} = \text{Thres}(\boldsymbol{\theta}) + \boldsymbol{\xi}\sigma.$$

where $\text{Thres}(\boldsymbol{\theta})$ is the ‘true’ threshold or deterministic part and $\boldsymbol{\xi}\sigma$ is the stochastic component or input noise. The standard deviation σ is equivalent of the root mean square (RMS*) of the data.

Across the 10,000 data arrays the variance of the noise σ^2 increased uniformly over the range [0,0.09]. Then script `TestWrapper.m` passed each array of the test data set to `JMKDAParamTest.m`, and using 200 different starting points, estimates of the parameters were made. This created a results array for the parameter estimates that varied as the noise in the data varied. The first data array had no additional noise and was the reference data to which the 9999 other data arrays were compared.

The experiment was repeated using a second data set, using 41 points in the range [0,20] minutes, equivalent to a threshold estimate every thirty seconds. This test data was built using the same method as above, but using parameter values derived from a pilot study at the University of Manchester (UoM). The process of presenting each

*root mean square = $\sqrt{\frac{\text{Sum of Squared Errors}}{\text{number of observations}}}$

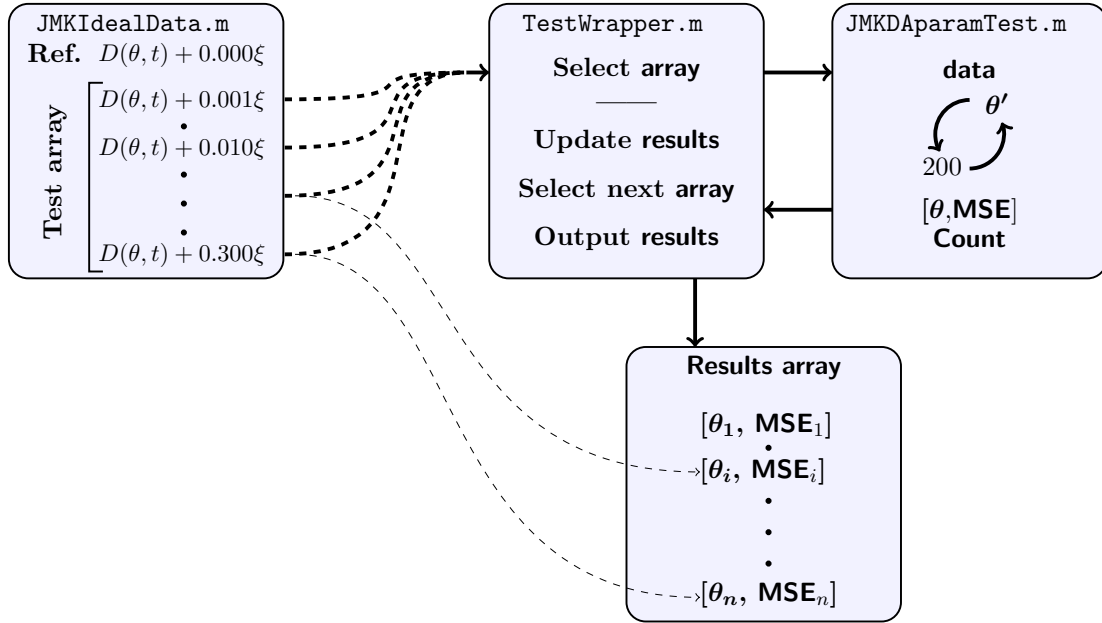


Figure 4.2.1: A summary of the numerical experiment to measure the effect of noise in the observed data on the estimates of the parameters θ . The script `TestWrapper` selects an array and passes it to `JMKDparamTest.m` whereupon an estimate of θ is made and passed back, there to be added to the results array which is output at the end. The thin gray lines shown the link between input data of known noise and the estimated parameter θ .

array to `JMKDparamTest.m` was then repeated and this generated a second results array. Examples of test data at varying input noise levels for the McGwin and UoM parameters are shown in figure 4.2.2, the two sets of parameters are listed in table 3.1.1.

Data were produced on an Apple Macintosh MacBook, operating system OS X 10.6.6 with an Intel Core 2 Duo processor running at 2.16GHz. The range of starting values used is listed in table 4.2.1. These starting values describe the point on the response surface at which the algorithm starts, by randomising the initial values a multiplicity of points on the response surface may be chosen. No constraints were applied to the function and this allowed the method to return values that lay outside the parameter space, therefore the returned parameter estimates were subject to a *post hoc* constraint, see section 3.4.1 for detail.

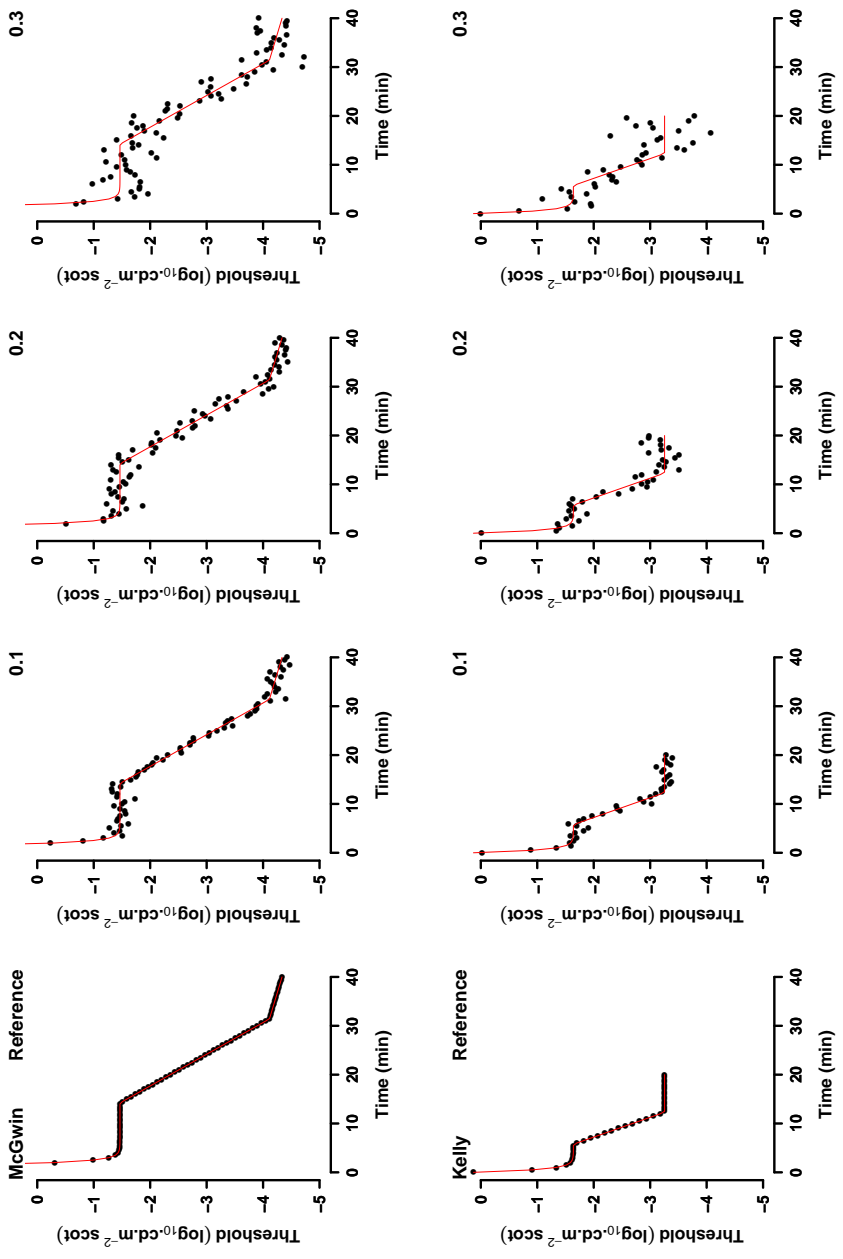


Figure 4.2.2: Illustration of data for varying levels of noise. Each row has the same parameters, the upper from McGwin(1999), the lower preliminary data from Manchester. Each column has the same level of input noise, the square root of the variance of the residuals is indicated by the number in the top right corner of each plot . Notice the smaller dynamic range in the Manchester data, and shorter time scale, hence fewer data points.

Table 4.2.1: Starting parameter values passed to the function `fminsearch`, were randomly chosen from the ranges shown. Where y_1 is the first threshold value. The initial values for α and β are randomly chosen in the range 0 to 7 and 0 to 15. These values provide a starting point for the algorithm.

Description	θ	Range	Units
Cone threshold	θ_1 : 0	$\rightarrow y_1 - 2.0$	$\log_{10}(\text{cd.m}^{-2} \text{ scot})$
Exponential coefficient	θ_2 : 0	$\rightarrow 20.0$	$\log_{10}(\text{cd.m}^{-2} \text{ scot})$
Cone time constant	θ_3 : 0	$\rightarrow 1.0$	min
Slope of S2	θ_4 : 0	$\rightarrow -0.6$	$\log_{10}(\text{cd.m}^{-2}).\text{min}^{-1}$
Rod-cone breakpoint α	θ_5 : 0	$\rightarrow 7(\pm 7)$	min
Sum of S2 and S3	θ_6 : 0	$\rightarrow 0.2$	$\log_{10}(\text{cd.m}^{-2}).\text{min}^{-1}$
Rod-rod transition point β	θ_7 : 0	$\rightarrow 15(\pm 15)$	min

For each noise level the parameters and the value of the minimiser function were stored. This was repeated 9999 times. Each parameter was then compared to the mean squared error of the test data set.

Difference between McGwin's and Kelly's parameter values

The parameters in table 3.1.1, have different values, there are three likely reasons for this

- Experimental set up

It is well known that the size, location and dominant wavelength of the stimulus affects the the cone threshold. Furthermore, the use of dilated pupils or a large bleaching flash would increase the time to the cone rod transition point. McGwin's parameters are taken from a subject presented in Jackson et al. (1999), in this study they used a large photobleach, 98%, dilated pupils, and a small stimulus (1.7°) located in the inferior retina at 12° eccentricity. Furthermore, their threshold measurements were corrected for lens optical density. This would have no effect on the slope of a phase, but will affect the thresholds found. The pilot study in Manchester used a larger stimulus (4°) at a slightly larger eccentricity (15°) in the temporal retina. The difference in cone threshold between the two experimental methods might be due to the smaller stimulus, which is relatively difficult for the cone system to detect.

- Red background

In the Manchester pilot study a red background was used; one effect of the red background is to elevate both the cone threshold and the absolute rod threshold, this also shortens the length of the S2 phase. It is worth noting that the S3 phase in the UoM parameter is rather flat. This has the effect of making the change over point more acute.

- Subject differences

The parameters used in the McGwin data set are reportedly from an elderly subject, aged 75, whereas the subject used in the pilot study was 46years, this might explain the different slopes of the S2 phase.

4.2.2 Results from the verification of the Matlab script

It is important to bear in mind that for these test data the noise element for each threshold calculated is independently and identically distributed. This assumption has not been demonstrated for the data collected from subjects, and is discussed further below

For each of the two test data sets, McGwin and UoM, the parameters θ were estimated at each noise level and are summarised in table 4.2.2. In the Matlab scripts used here each estimate of the parameter θ for each start point is subject to *post hoc* classification, see section 3.4.1.

The skew (or skewness) of a distribution is a dimensionless measure of the size of the tails to one side or another of the distribution, a negative skew indicating a long tail to the left or lower values, positive skew, a longer tail to higher values or the right. Kurtosis is also a dimensionless measure and describes the non normality of a distribution, indicating whether the the distribution is flat (platykurtic) or pointed (leptokurtic). For each parameter estimated, an ideal algorithm would return zero skew and large kurtosis (leptokurtic), this would suggest that the value returned would be as likely be an overestimate as an underestimate and that the values would be very close to the true value.

The parameter of greatest interest in this study is the slope of the S2 phase, therefore estimates of the slope of S2 will be considered, the other parameters are summarised in table 4.2.2, and discussed in detail in appendix B on page 286.

Table 4.2.2: Summary statistics for the two sets of test data. Units are the same as those in table 3.1.1, omitted here for clarity.

McGwin

	Cone			Rod (S2)		Rod (S3+S2)	
Test Value	Threshold	Coeff	Tau	Slope	Alpha	Slope	Beta
Min.	-1.465	39.85	1.77	-0.154	14.21	0.128	31.40
1st Qu.	-1.670	38.91	1.69	-0.587	11.11	0.050	20.62
Median	-1.481	39.78	1.76	-0.157	14.00	0.122	31.00
Mean	-1.465	39.85	1.77	-0.154	14.21	0.129	31.41
3rd Qu.	-1.465	39.85	1.77	-0.155	14.23	0.131	31.35
Max.	-1.448	39.93	1.78	-0.152	14.44	0.138	31.79
	-1.277	40.80	1.87	-0.121	19.09	0.477	37.93
UoM							
Test Value	-1.640	1.77	1.77	-0.247	5.76	0.247	12.30
Min.	-3.065	0.56	0.12	-0.702	0.01	0.056	8.50
1st Qu.	-1.674	1.68	1.57	-0.257	5.50	0.230	12.05
Median	-1.640	1.77	1.78	-0.246	5.75	0.247	12.31
Mean	-1.640	1.76	1.94	-0.246	5.69	0.248	12.36
3rd Qu.	-1.609	1.85	1.98	-0.231	5.99	0.262	12.58
Max.	-0.940	2.68	314.79	-0.135	8.70	0.712	17.94

The S2 phase ($\theta_{4,5}$)

In the Mahroo, Lamb and Pugh model (MLP) this parameter is the rate at which the threshold elevating compound is cleared from the rod outer segment and is dependant upon the rate limited transfer of *cis*-retinal from the RPE to the rod outer segment, as discussed earlier, see section 1.5.4.

In figure 4.2.3 the estimates of the slope of the S2 phase and the alpha points are compared.

The slope of the S2 phase θ_4 : Considering the estimates for the slope of the S2 phase using the McGwin parameters, the true value of S2, $-0.154 \log_{10}(\text{cd.m}^{-2}).\text{min}^{-1}$ was accurately predicted by the median of the values returned and was underestimated by the mean by one thousandth part. The interquartile range of 0.005 suggests a very narrow distribution of values, this is reflected in the very large kurtosis of 564, note that a normal distribution has a kurtosis of zero*. Although extremely leptokurtotic the distribution is also left skewed, -13.24, with a longer tail to lower values, the minimum

*a correction of -3

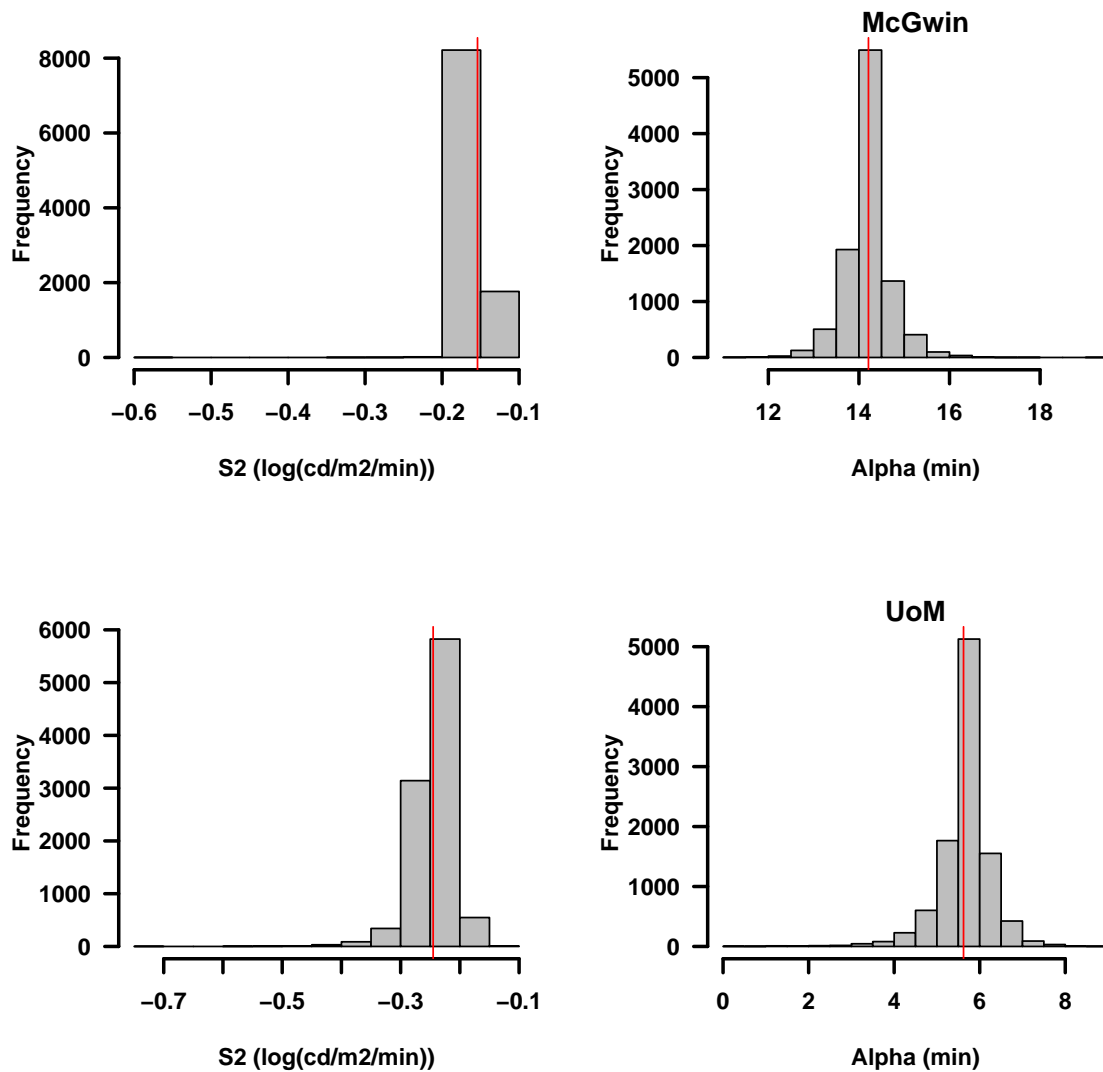


Figure 4.2.3: Histograms of the parameter estimates of the S2 phase for the two data sets true value is shown by the solid vertical line. Upper left the McGwin S2 slope, over 80% are in the interval -0.15 to $-0.2 \log_{10}(\text{cd.m}^{-2}).\text{min}^{-1}$ (true value $-0.154 \log_{10}(\text{cd.m}^{-2}).\text{min}^{-1}$). Upper right McGwin cone rod transition time, over 50% in the interval 14 to 14.5 minutes (14.2min). Lower left the Manchester slope of the S2 phase, $\sim 90\% \pm 0.05$ the true value ($-0.247 \log_{10}(\text{cd.m}^{-2}).\text{min}^{-1}$) lower right Manchester cone rod transition time, over 50% in the interval 5.5 to 6min (5.76min).

value found was $-0.588 \log_{10}(\text{cd.m}^{-2}).\text{min}^{-1}$, suggesting that for large amounts of noise in the data the estimate of S2 can be very difficult to determine. The Manchester pilot study estimate of S2, true value $-0.247 \log_{10}(\text{cd.m}^{-2}).\text{min}^{-1}$ is overestimated by both the

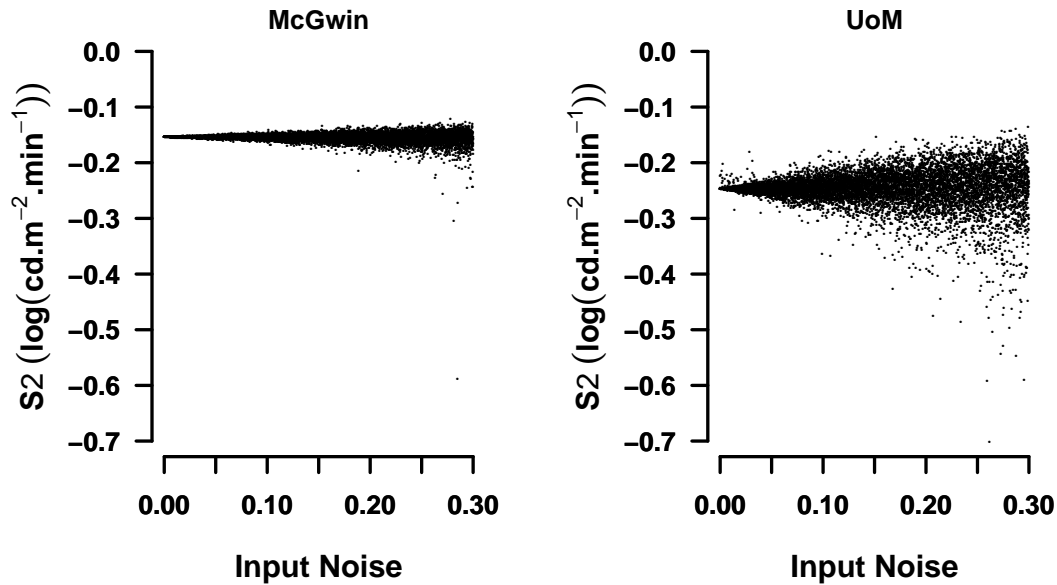


Figure 4.2.4: Changes in the estimate of the slope S2 as input noise varies.

mean and the median by one thousandth part also. The interquartile range is much larger than that for the McGwin parameters at $0.026 \log_{10}(\text{cd.m}^{-2}).\text{min}^{-1}$, this is reflected in a much flatter distribution, kurtosis 16.6 and much less skewed -1.98, minimum value $-0.702 \log_{10}(\text{cd.m}^{-2}).\text{min}^{-1}$. For both sets of test data, the algorithm returns reliable values, but as the noise increases there is a tendency to return lower (more negative) values. Note lower values are values with a greater magnitude. This has the effect of over estimating the performance of the system at delivering *cis*-retinal to the rod outer segment.

This overestimation of the S2 parameter has been reported in the literature. (Ruseckaite, Lamb, Pianta & Cameron 2011) found that estimates fitted by eye tended to be lower than those found objectively

The effect of the different skew and kurtosis is shown in figure 4.2.4. The McGwin parameters are closely constrained to the true value, while the Manchester estimates are more widely dispersed especially for input noise greater than $0.05 \log_{10}(\text{cd.m}^{-2} \text{scot})^2$. It will be shown later that 75% of human subjects have RMS of less than $0.02 \log_{10}(\text{cd.m}^{-2} \text{scot})$, see section 6.3.9.

The cone rod transition time, alpha θ_5 : For both sets of test data the median of the estimates is the more reliable statistic, correctly estimating the value for the McGwin test data and underestimating the value by 0.01minute for the Manchester test data. The interquartile ranges are similar at 0.44min for McGwin and 0.49min for Manchester. Both distributions are leptokurtotic (McGwin 7.37 and Manchester 11.1), suggesting that many of the estimates are close to the true value. The McGwin skew (0.25) is much less than the Manchester skew value (-1.38), suggesting that for the Manchester test data the algorithm is more likely to return a shorter cone rod transition time than the true value.

4.2.3 Discussion of Matlab scripts' parameter estimates

The algorithm `JMKDaparamTest.m` was able to calculate parameter estimates for every data array in the test data set. Table 4.2.2 shows for each test data set the test value and summary statistics for each parameter estimate. The difference between the maximum and minimum returned values gives an indication of the difficulty faced in attempting to objectively derive parameter estimates for the model when fitted to data with large amounts of noise.

As mentioned earlier, an ideal algorithm would have zero skew and large kurtosis, the above numerical experiment has shown that when estimating the slope of the S2 phase, for differing conditions, there remains a possibility that the estimated value is inaccurate. The McGwin test data has a much extended S2 phase and might therefore be more easily estimated and this is reflected in the very high kurtosis (564). However, the maximum and minimum values differ by $0.465 \log_{10}(\text{cd.m}^{-2}).\text{min}^{-1}$ and $0.567 \log_{10}(\text{cd.m}^{-2}).\text{min}^{-1}$ for the McGwin and Manchester test data respectively, this suggests that S2 values should be interpreted cautiously if the data have a large root mean squared error.

4.3 Calculation of confidence intervals for the slope of S2

Having established that the Matlab scripts can return reliable estimates of the dark adaptation recovery curve, interpreted with caution if the data are noisy, a confidence interval for these estimates would be helpful in deciding whether there had been any real change over time following some intervention or treatment.

The direct search method of determining the parameters is unable to calculate confi-

dence intervals for the estimates (Gao & Han 2010), whereas an analytic approach can. However, the use of an analytic method relies on some fundamental assumptions, which are not valid in this case, see section D.1 on page 297. However bootstrap methodology can be used to calculate confidence intervals (Efron 1979) and is discussed below.

An alternative method of confidence interval calculation relies on model comparison methods, see section 3.2.1 on page 115 (Kelly & Murray 2012). The model comparison method holds all parameters fixed except one, which is varied and the probability that the varied model fits the data calculated. This creates a confidence interval for that parameter. The parameter of most interest the slope of the S2 phase is defined by the transition times α and β , therefore confidence intervals were found for these two parameters and the resulting intervals used to calculate the slope of S2. The range of values for the S2 generated by the ranges for α and β is the confidence interval for S2. Further detail can be found in appendix I.3 on page 327

The two approaches were compared, firstly to check if the parameter estimates from a method in R were usable.

4.4 Objective and subjective selection of starting points

As mentioned earlier the Solver tool in Excel (Microsoft, USA) uses a direct search algorithm to compute the values returned for a model (Fylstra et al. 1998). For studies involving many subjects with repeated visits, the analysis of the generated data is no trivial matter.

Batch processing

Dr Makridaki at the University of Manchester in collaboration with another centre measured the dark adaptation recovery curve for 88 subjects, over four visits (PhD Thesis 2011). The data were analysed by Dr Makridaki using the Solver tool. This was a time consuming task and took many days work. For each visit a plot of the data was examined and Dr Makridaki assessed the data by eye and from her interpretation of the data provided a starting point for the Solver tool. From this starting point the Solver tool returned an optimal estimate of the parameters of the dark adaptation recovery curve.

This methodology might be criticised as being prone to bias. However, it is important to remember that it is only the starting point for the algorithm that is provided. As the algorithm progresses random number generators are used to determine the next possible step and an objective assessment of the error for each step determines the direction of the onward search for parameters.

A useful algorithm would be able to process a sequence of data files automatically and return estimates of the parameters of interest, in this case the slope of the S2 phase.

Aim

The first aim of this investigation was to verify the values found using the algorithm used in this study against values found independently. The second aim was to consider whether the use of the algorithm to rapidly investigate a large quantity of information was valid.

4.4.1 Method

Dr Makridaki kindly allowed me access to her data which was stored in Excel (Microsoft, USA) spreadsheet format. A series of scripts in Matlab were written to re-analyse this data. Three scripts were written; the first, `MMJK_data`, stepped through the spreadsheets for the 88 subjects and extracted the raw data and the parameters of the dark adaptation recovery curve fitted to the data found by the solver tool in excel.

The second script `JMK_MM_wrapper.m` was a wrapper function for `JMKDAParamTestMM.m`, and used the raw data held in the structure generated by `MMJK_data` to estimate the parameters of the dark adaptation recovery curve, again subjected to the initial estimates being multiplied by a random factor. The kernel function is similar to `JMKDAParamTest.m` with the defaults set to convert data in dB to log units. The wrapper function cycled through each data set held by the data structure and returned the Matlab estimates of the parameters. Full code details are in appendix A.1.2 on page 262

4.4.2 Comparison of objective and subjective methods

The parameters found by the Solver method and the Matlab method were compared. The most important parameter in this study is the slope of the S2 phase and it is

considered now. The Matlab scripts were able to extract parameter estimates for 300 of the available data sets. By subjectively selecting the initial starting point for the Solver tool Dr Makridaki was able to find parameter estimates for the same 300 plus a further 16 of the 352 available data sets. Note the Matlab script only returns values in the range $[-0.8, 0.0]\log_{10}(\text{cd.m}^{-2}).\text{min}^{-1}$. The two distributions are shown in figure 4.4.1.

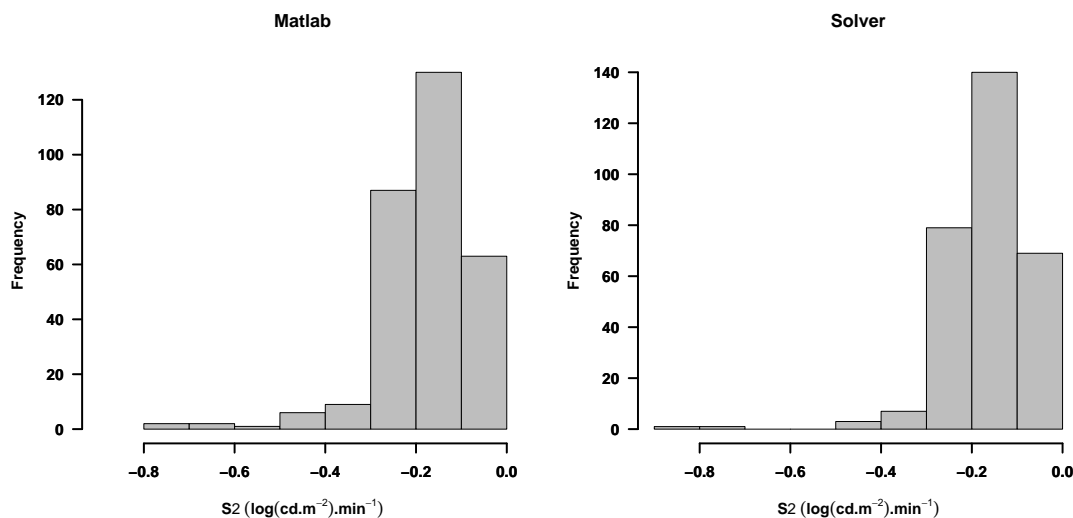


Figure 4.4.1: Comparison of the distribution of the values of S2 found by the Matlab (objective starting point) method and the Solver (subjective starting point)

Considering only those data where values were found by both methods, the Solver method had a mean of $-0.17(\pm 0.09)\log_{10}(\text{cd.m}^{-2}).\text{min}^{-1}$, while the Matlab method had a mean value $-0.18(\pm 0.10)\log_{10}(\text{cd.m}^{-2}).\text{min}^{-1}$. Both estimate distributions, see figure 4.4.1, were negatively skewed, Solver method skew = -2.7198 ($z = -7.6078$, $p\text{-value} < 0.001$), Matlab method skew = -2.1171 ($z = -6.6540$, $p\text{-value} < 0.001$). A non parametric paired test of values (Mann Whitney) found no significant difference between the two methods ($p\text{-value} = 0.86$).

The line of equality plot, figure 4.4.2, shows that for some data sets the Matlab method returns estimates of the slope of the S2 phase that are more negative than the Solver method, i.e. suggestive of better RPE - choroid complex performance than might be justified. The Solver method provides smaller estimates. The Bland Altman plot in figure 4.4.3 shows no systematic effect and reveals 17 points outside the limits of agreement (5.67%) as might be expected.

The data are correlated $\rho = 0.77$ (CI 0.72 – 0.81, $t = 20.81$, $df = 298$, $p\text{-value} < 0.001$),

in agreement $\rho_c = 0.76$ (CI 0.71 – 0.80, $C_b = 0.98$).

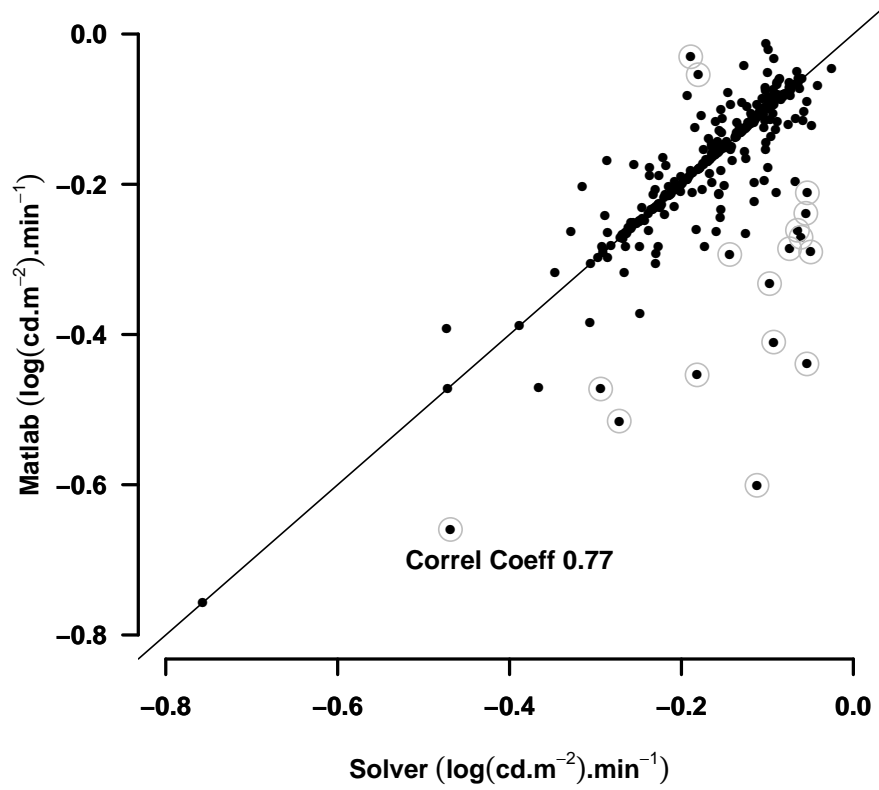


Figure 4.4.2: Measures of agreement. Line of equality plot, potential outliers encircled.

It is well known that the initial starting point should be close to the global minimum of the response surface (Lewis et al. 2000) and this has been demonstrated here. The Solver method where the investigator was able to provide the initial estimate of the parameter values was able to analyse more data sets and found smaller estimates for the slope of the S2 phase when compared to the estimates found by the Matlab method. The difference in the number of data sets successfully analysed is not surprising. A human examining a data set will quickly identify discontinuities and will be able to approximate the starting parameters more efficiently than a random method.

An alternative interpretation is that the seven parameter model over fits the data. This is discussed further below in section 6.4.3 on page 201

The above findings can be summarized as follows;

- subjective selection of starting point

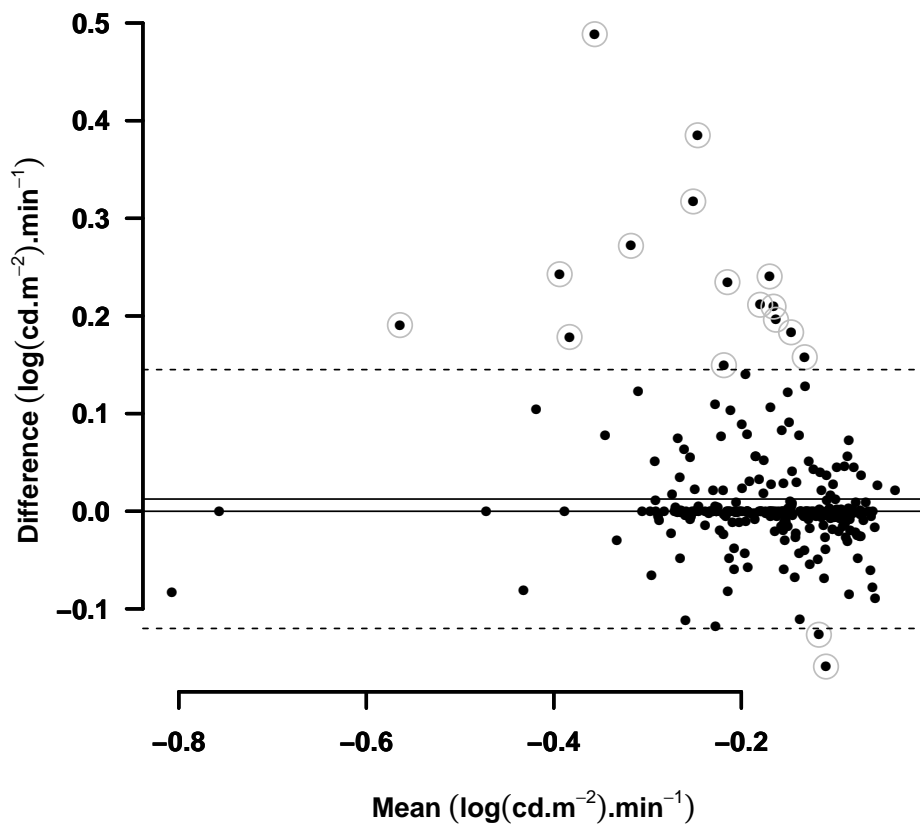


Figure 4.4.3: Measures of agreement. Bland Altman plot, showing that there is no systematic relationship between the measures of the slope of S2 by each method. Dashed lines are the upper and lower limits of agreement. The offset is $0.01 \log_{10}(\text{cd.m}^{-2}).\text{min}^{-1}$.

- gives unbiased estimates of θ
- may be necessary for some data sets
- objective selection of starting point
 - returns values consistent with an item by item approach
 - facilitates batch processing of data
 - allows for large numbers of data sets to be quickly interpreted

4.5 Summary: does the algorithm work?

This chapter along with chapter 3 has described the theory behind parameter estimation for the nonlinear model in equation 3.1.2.

A series of algorithms using direct search methods have been presented and how they extract the parameters of interest discussed.

Furthermore, the methods have been compared and not surprisingly have been found to be consistent in their ability to estimate the parameters of the model used. The Matlab method has been shown to be useful and its weaknesses considered.

Both the Matlab and R methods are adaptable and the Matlab method has been easily modified to account for different data formats and bootstrapping. The methods in R are quicker and available off campus, but grossly underestimate the bootstrap confidence intervals found using HTC. In chapter 6 the assumptions necessary for bootstrapping to be valid are readdressed. That is, identically and independently distributed residuals derived from an appropriate model fit.

As mentioned earlier, an ideal algorithm to estimate the parameters of the dark adaptation recovery curve would have the following attributes:

- unbiased
the numerical experiment using test data in section 4.1 shows that the estimates of the slope of the S2 phase are unbiased when the $\text{RMS} < 0.02 \log_{10}(\text{cd.m}^{-2}).\text{min}^{-1}$, see table 4.2.2
- measure of ‘goodness of fit’
the mean of the squared error (MSE) is returned by the algorithm
- calculate confidence intervals
this is possible, but the method used here is time intensive and only practicable in a research setting. Alternatives, e.g. the method in R, does not provide as much insight as the bootstrap method. Using bootstrap methodology in R without the multi start component allows for a reduction in the time needed for each data set, from ~ 25 hours to ~ 8 , this is still a significant amount of computer processor time and delay. This investigation is not presented here.
- multi-platform
the direct search method described above whether applied in R, Matlab, Excel, and

independent of operating system, returns consistent estimates of the parameters of the dark adaptation recovery curve.

- quick
estimates are returned in 15seconds or less.
- capable of batch processing
the method described above is extensible, that is, it can be modified, or incorporated into wrapper functions to handle data provided in a variety of formats.

The methods described here are effective and their limitations are well understood for the model used in this study.

The parameter estimates, naturally, depend upon the experimental conditions. In an attempt to model the experimental set up used here, test data using parameters from preliminary work suggest that the reduced dynamic range and hence shortened S2 phase results in estimates of the slope of the S2 phase that are liable to error as the noise in the data increases. The algorithm generally returns reliable estimates of S2, but with increasing noise there is a tendency for that estimate to be larger (more negative) than the true value. Suggesting that the retinal system is more efficient, and therefore healthier, than it might be. This is not ideal, in a clinical setting this would have the effect of classifying unhealthy individuals as healthy (false positive), when they are not. Arguably the level of noise in the data could be used as an index of health, but there are too many factors responsible for the generation of noise in a psychophysical measurement for this to be a useful index of retinal health.

The aim therefore is to collect data with as little noise as possible, to be sure a self evident proposition, which will ensure that the assumptions necessary for accurate bootstrap estimates are met. In practise this means that we wish to minimise the auto correlation of data points and understand whether the noise is constant across all phases of dark adaptation recovery. These two conditions are discussed in detail in subsequent chapters.

4.6 Supporting paper

A paper has been submitted to The R Journal proposing a model comparison method of confidence interval determination, see appendix I.3 on page 327

THE EFFECT OF BACKGROUND LUMINANCE ON ROD
SENSITIVITY RECOVERY; LUMINANCE AND CONTRAST
DATA

And the heart that is soonest awake
to the flowers, is always the first to be
touched by the thorns.

Thomas Moore (1779 –1852)

5.1 Introduction

Dark adaptation, the recovery of visual sensitivity when moving from a light to a dark environment, is classically measured by presenting a stimulus against a dark background. The rod recovery is only observable once the cones have reached their minimum threshold. In this study a dim red background is used to elevate the cone threshold. This shortens the cone rod transition time and allows the rod phase to be measured sooner than would be the case otherwise. See figure 5.1.1

However, the background may affect the recovery of rod sensitivity directly if it is detected by the rods or indirectly if the cones detecting the background alter the rod response. The rod response to the background can be understood by considering the

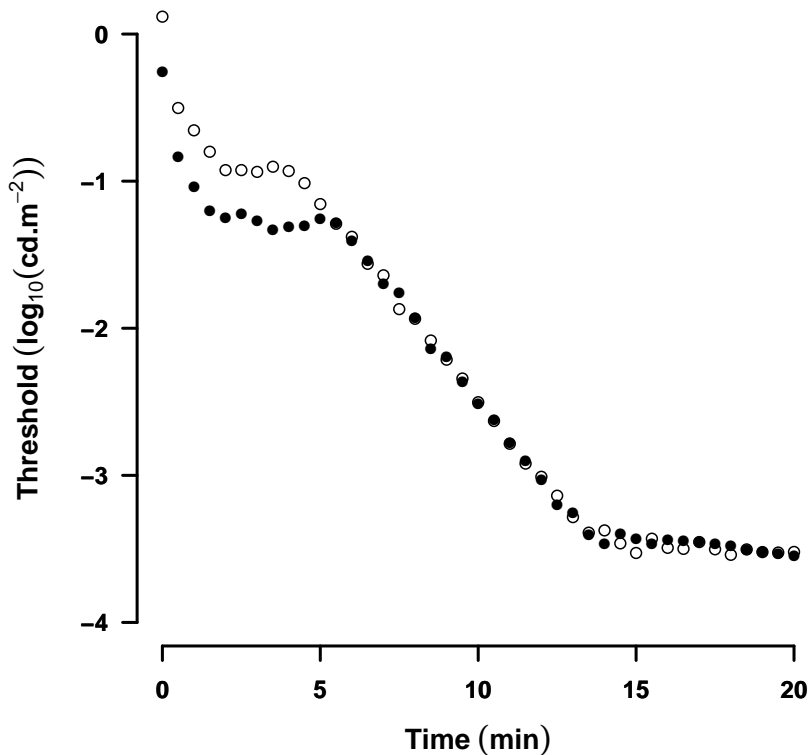


Figure 5.1.1: The effect of the red background. Elevating the cone threshold shortens the cone rod transition time and allows the rod recovery to be measured. This data is simulated. In this case elevating the cone threshold by 0.36 cd.m^{-2} shortened the cone rod transition time by 1.4min

CIE scotopic luminous efficiency curve, which reflects the probability of the rod system detecting light of a particular wavelength, see figure 5.1.2.

The method used in this study to measure dark adaptation has dominant wavelengths of 655nm for the background and 530nm for the stimulus. Light of wavelength 530nm has a relative scotopic luminance of 0.65 while for 655nm light it is 0.0005, therefore 530nm light of equal energy is 1300 times more likely to be detected by the rod system than that of 655nm. But even for this wavelength (655nm), a background with photopic luminance of 0.05 cd.m^{-2} has a scotopic luminance of 0.0007 cd.m^{-2} (p104, Wyszecki & Stiles (1967)) or $-3.15 \log_{10}(\text{cd.m}^{-2})$.

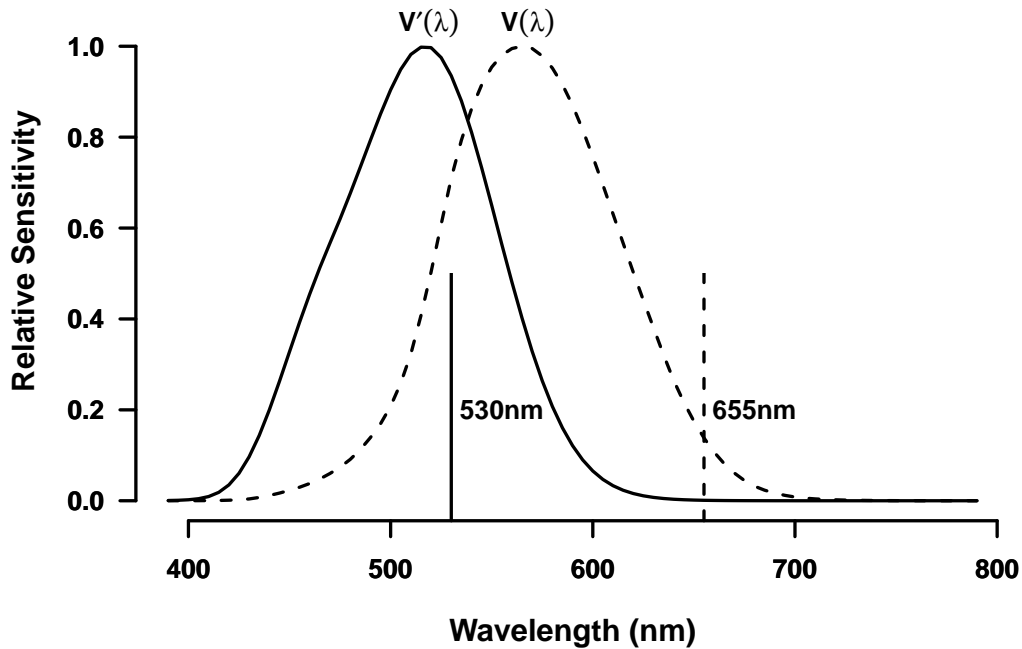


Figure 5.1.2: The principle of the red background. The stimulus (530nm) is near the peak of the scotopic luminous efficiency function ($V'(\lambda)$). The background (655nm) is in a region of poor scotopic sensitivity and reduced photopic sensitivity ($V(\lambda)$)

5.1.1 Changing the background affects the threshold increment

When measuring thresholds it is known that the background influences the measurement. In figure 5.1.3 we can see that the incremental threshold of the rod system is dependent upon the field or background intensity. As the background intensity increases there are four regions of response. The first when the background is below the threshold for the rod system is termed dark light and consists of the random fluctuations in the rod system. As the field intensity increases the deVries region is reached where the incremental contrast threshold is proportional to the reciprocal of the square root of the number of quanta absorbed. Further increase in the field intensity reveals the Weber region, where the ratio of threshold increment to field intensity is constant. Continued increases in the background luminance saturate the rod system and no further response from the rod system is measurable.

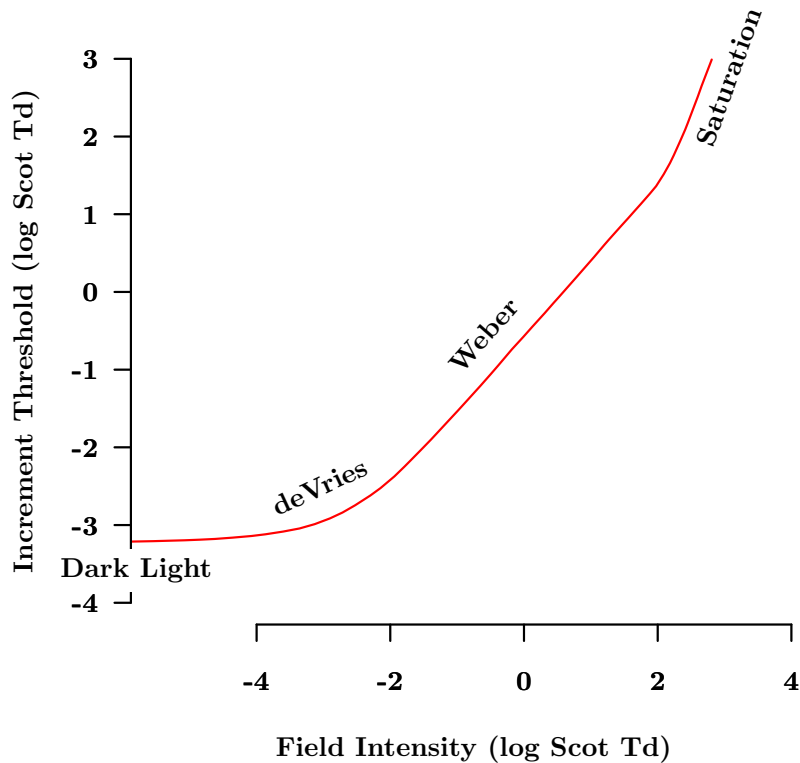


Figure 5.1.3: Threshold versus intensity, taken from Aguilar and Stiles (1956)

5.1.2 How might cones influence rods?

There are two possible mechanisms by which cone threshold elevation could affect rod sensitivity. Firstly, as discussed below, shared pathways mediate the postsynaptic signalling of light. Therefore the baseline signalling of the cone system in the presence of the red background might inhibit or increase the rod activity. It is important to remember that the red background fixes cone activity to a steady state; therefore, inhibitory or excitatory effects will be constant unless further affected by a rod feedback mechanism.

Secondly, the local dynamics of photopigment replenishment may be altered. In section 1.5.4 the Mahroo, Lamb and Pugh model (MLP) of delivery and uptake of the chromophore *cis*-retinal and the retinoid deficiency hypothesis (Mahroo & Lamb 2004, Lamb & Pugh 2004) was described. This hypothesis linked the slope of the S2 phase of sensi-

tivity recovery to the delivery of *cis*-retinal to the rod outer segment.

During the recovery of sensitivity when measured without an adapting background the cone absolute threshold represents the level at which the cones are fully replenished with *cis*-retinal. Their activity is at the level of background random isomerisations, which creates a minimal demand for further *cis*-retinal. However, when the cone threshold is elevated, cones may compete with rods for the available *cis*-retinal as it is presented at the RPE apical surface.

This means that at the threshold fixed by the background the cones will have a constant demand for the available *cis*-retinal. This steady uptake by the cones means that the onset of rod recovery might be delayed and the rate of rod recovery reduced.

5.1.3 Psychophysical evidence of cone-rod interaction

The duplex nature of the retina is long established (Schultze 1866), and there is some evidence that the two systems, rods and cones, can act independently. Flamant and Stiles (1948) have shown that rod adaptation is independent of cones on dim backgrounds undetectable by the cone system.

However, if the cones can detect the background the effect on rod threshold is not straightforward. Benimoff et al.(1982) found that signals from each system combined in an excitatory manner, although to an extent less than might be expected and they found no evidence for inhibitory interactions between rod and cones. In contrast Drum (1981) found that suprathreshold cone activity suppressed rod activity in the parafovea. While Stabell and Stabell (1981) demonstrated that rods make a significant contribution to the brightness of brief suprathreshold lights. Furthermore, the apparent summation of rod and cone signals for conditions found by MacLeod et al.(1972) would seem to contradict the concept of rod cone independence.

This challenge to cone rod independence was supported by Makous and Boothe (1974), who found that as the background luminance increased, i.e. the cone threshold was raised, the assumption of rod cone independence was open to question. When measuring rod incremental thresholds, they used a narrowband stimulus, 491nm, and either a narrowband blue background (491nm) or a broadband red background created using a Wratten filter (No.29, lower cut off 610nm). Although the backgrounds had identical scotopic luminance the photopic luminance was different and they found an elevation in the absolute threshold of between 0.3 and 0.5log units for the red background when com-

pared to the scotopically identical blue background. They concluded that stimulation of the cones prevented detection of a test flash by the rods.

Both inhibitory and excitatory effects were found by Levine et al.(1987) and they suggested that at least two modes of action were available dependent upon the relative density of the two photoreceptor types at the test location; rods may inhibit cones while cones facilitate rods.

The rod-cone independence was also questioned by Sharpe et al.(1992), who used a variety of background wavelengths, 450, 520, 560 and 640nm, to measure rod incremental thresholds. They measured the threshold versus background intensity increment and found that for wavelengths less than 640nm, the slope was identical for normal trichromats and an achromat (cone free retina), but for the longer wavelength background (640nm) the trichromats had a steeper slope, suggesting that the sensitivity of the visual system at these light levels is due to combined rod and cone absorptions.

5.1.4 Anatomical evidence of cone-rod interaction

At maximum cone sensitivity there would be no cone signals above background noise downstream of the cone synapse. However, as the rod signal is carried by the same neuronal pathways as the cone signal, the effect of interaction between the intermediate steady state cone signal and the increasing rod signal should be considered.

Numerous pathways have been described, the differences are mostly in the approach of the investigators. Stockman *et al.*(1991) when considering the speed of impulse transmission as measured by perceptual nulling suggest two pathways. A slow and a fast pathway, the slow pathway is mediated by the rod bipolar cell through the amacrine AII cell that connects to a cone ganglion cell (GC) axon and thence to 'on' and 'off' pathways, a faster pathway is via a gap junction between the rod photoreceptor and the cone pedicle. The authors suggest the faster pathway allows for mesopic vision while the slower path facilitates scotopic vision (Stockman, Sharpe, Zrenner & Nordby 1991). Figure 5.1.4 is from Sharpe & Stockman (1999) and illustrates the rod pathways.

Völgyi et al.(2004) when examining the conversion and segregation of the pathways to the GC, describe three pathways. The primary pathway carries signals with the lowest threshold (dim illumination) to both on-centre and off-centre GCs, while the secondary pathway is less sensitive by $1\log_{10}$ unit than the primary route, and the third pathway using off-signalling is a further $1\log_{10}$ unit less sensitive than the secondary pathway.

They also observe that a class of off-centre cells receive inputs from both the primary and tertiary pathways (Volgyi, Deans, Paul & Bloomfield 2004).

Examination of the anatomy reveals that these two models are compatible. Abd-El-Barr *et al.*(2009) describe the pathway from the rod photoreceptor to the GCs. They outline three principle routes and propose a fourth; the first transmits the rod hyperpolarisation to a depolarising (sign inverting) rod bipolar cell, this bipolar cell sends an excitatory signal to AII amacrine cell. The amacrine cell then connects to a cone depolarising (on) bipolar cell through a gap junction, the amacrine cell also connects through a gap junction to a hyperpolarising (off) cone bipolar cell. These 'on' and 'off' bipolar cells send signals to 'on' and 'off' GCs, respectively.

The second pathway spreads the signal to surrounding cones by gap junctions between rod and the cone pedicle, these cones then signal both 'on' and 'off' bipolar cells.

Two further pathways are described; the third pathway is a direct link between rods and depolarising cone bipolar and the fourth pathway which overlaps the secondary pathway, relaying the hyperpolarising signal to both 'on' and 'off' bipolar cells and subsequently to 'on', 'off' and 'on-off' GCs (Abd-El-Barr, Pennesi, Saszik, Barrow, Lem, Bramblett, Paul, Frishman & Wu 2009).

Evidence of rod-cone interaction

Less importantly for this study, since the interest here is the possible effect of cone stimulation on rod responses, there is electrophysiological and psychophysical evidence that indicates that rods may inhibit cone activity during dark adaptation and thereby cause a rise in the cone threshold (Armington, Johnson & Riggs 1952, Blough 1958, Lie 1963, Stabell & Stabell 1976, Stabell & Stabell 1977, Alexander & Kelly 1984, Arden & Hogg 1985, Alexander, Fishman & Derlacki 1988, Dong, Qian, McReynolds, Yang & Liu 1988, Stabell & Stabell 1990).

Spillmann *et al.*(1971), for example, found a 0.2 log unit increase in the threshold level preceding the cone-rod break. While Arden & Hogg (1985) demonstrated the effect of increasing rod sensitivity on the cone system, illustrated in figure 5.1.5, where it can be clearly seen that as the rod system becomes increasingly sensitive the cone system is less able to detect a flickering stimulus.

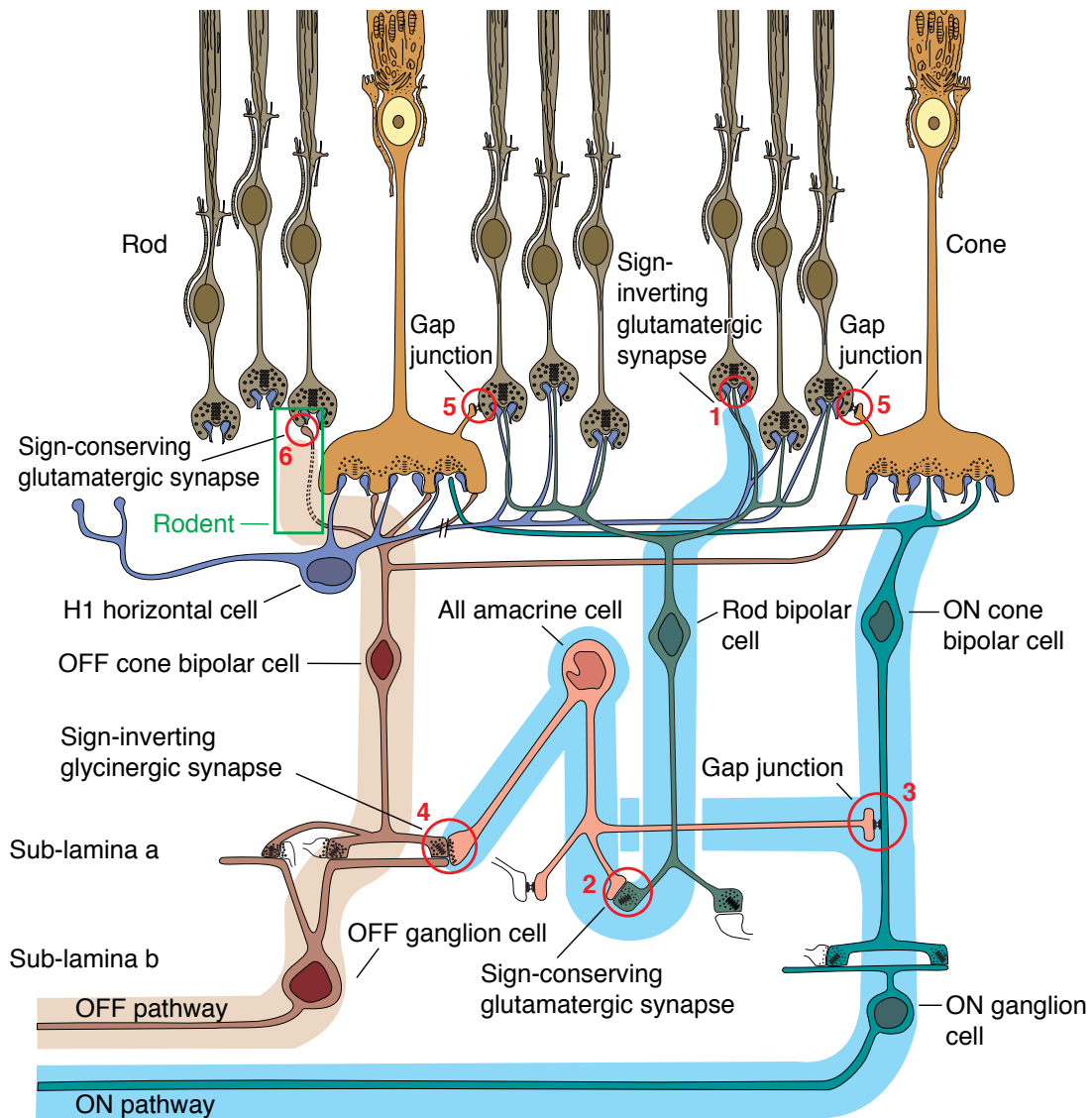


Figure 5.1.4: Summary of the rod pathway: *Rod and cone pathways in the mammalian retina.* The highly schematic retinal diagram depicted here concentrates on the pathways available to the rods, all of which either infiltrate or superimpose upon the cone circuitry. The numbered circles highlight the six so-far identified or inferred regions of rod-signal transmission: (1) the rod-rod bipolar sign-inverting synapse; (2) the rod bipolar-amacrine AII cell sign-conserving synapse; (3) the amacrine I-ON cone bipolar (sign-conserving) electrical gap junction; (4) the amacrine I-OFF cone bipolar (sign-inverting) glycinergic synapse; (5) the rod-cone (sign-conserving) electrical gap junction (shown twice, once each for the ON and OFF pathways); and (6) the inferred rod-OFF cone bipolar (sign-conserving) synapse. Only the parasol ON (light green) and OFF (beige) pathways, which transmit the largest rod signals, are shown. Taken from Sharpe (1999)

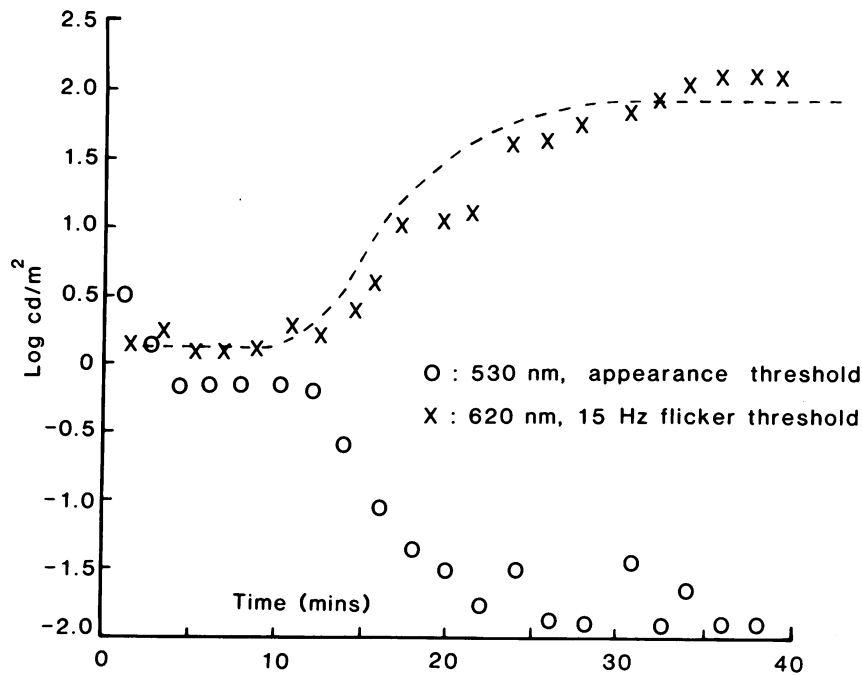


Figure 5.1.5: Rods influence cone flicker thresholds. The red flicker threshold, crosses, begins to rise at about the time rods become more sensitive than cones in the dark adaptation curve shown with open circles. The dashed line is the reciprocal of the rod threshold. Taken from Arden & Hogg (1985)

5.1.5 Effect of cone-rod interaction

The effect of cone stimulation on rod performance seems to be dependant upon many factors, some as yet unexplored; the size of the stimuli, the relative sizes of the test and background fields, the wavelengths used and the test location on the retina. It is clear that for the conditions used in this study a prediction of cone effect on rod performance would be difficult and deserves empirical scrutiny.

5.1.6 Rod cone interaction and contrast sensitivity

In addition to the retinoid deficiency hypothesis, there is an argument that the thickening of Bruch's membrane causes ischaemia of the outer retina and that this reduces the oxygen available to the layers of the retina intermediate to the choroidal and retinal blood supplies. This raises the possibility that the earliest signs of vision loss would be caused by post receptor changes (Feigl et al. 2006).

Ganglion cells are the final output neurones of the retina, collecting signals from a number of bipolar and amacrine cells, in the intermediate layers of the retina. The extent of these inputs is called the receptive field. An important feature of GCs is spatial tuning, this is where the GC response is at a maximum for a stimulus of an optimal size

Spatial tuning is reflected in the contrast sensitivity function (CSF). This is the sensitivity of the visual system to objects, often measured with gratings defined by cycles per degree and contrast, and can be modelled as a linear subtraction of two concentric opposing GC receptive field mechanisms, e.g. 'on' centre and 'off' surround (Rodieck 1965).

Only features detectable by the GC are able to alter the behaviour of the viewer of a scene. The GC are selectively tuned to subtle features in the scene, e.g. colour, size, speed and direction of motion. These signals are passed by the GC to the lateral geniculate nucleus (LGN) and the superior colliculus.

The GC outputs to the LGN have been classified by function as having one of two forms, tonic or phasic (Gouras 1968). Tonic GC have small receptive fields with slow conduction velocity and form the parvocellular pathway. The phasic GC have larger receptive fields than the tonic GC. At the fovea they are 2-3 \times larger while in the periphery they are up to 10 \times larger. They have faster conduction velocities and form the magnocellular pathway. The parvocellular pathway P is best suited to detecting fine, high contrast objects while the magnocellular pathway M is better able to detect larger low contrast objects (Kaplan & Shapley 1986).

Contrast sensitivity at low light Levels

The possibility that a change in the oxygenation of the post receptor cells has an effect on the post receptor processing of an image can be investigated by measuring the contrast sensitivity function. Since the rod system is vulnerable to age change earlier than the cone system a suitable starting point would be to measure CSF under scotopic conditions.

The scotopic contrast sensitivity function measured under static sensitivity conditions is well known, with a characteristic peak sensitivity at lower spatial frequencies and a band pass nature (Van Nes et al. 1967). What is less clear is the dynamic performance of the rod system. It is possible that changes in the RPE choroid complex affect gas transfer before they affect retinoid recycling. This would mean that the CSF could yield useful information about the RPE choroid complex. Little work is published about contrast

sensitivity recovery following a photo-bleach.

5.1.7 In summary

The questions addressed in this chapter are:

- can the rods detect the background ?
- is the rod response to a changing background linear ?
- is the rate of rod recovery during the S2 phase altered ?
- is the recovery of rod sensitivity reflected in contrast sensitivity measurements?

5.1.8 Aims

To investigate the effect of a background luminance on the recovery of rod sensitivity with special reference to the slope of the early phase S2 of rod sensitivity recovery.

The investigation is composed of four experiments.

Experiment 1 will explore the effect of the background wavelength and luminance on the absolute threshold. The absolute thresholds of a dark adapted subject are measured for backgrounds of three wavelengths and four scotopic luminances and compared to the thresholds found when no background illumination is used. This simple ‘on-off’ experiment should reveal the rod response to the background and tests the assumption that the rod system is independent of the background illumination.

Experiment 2 will test whether the threshold measured and the background intensity used have a linear relationship, this is usually known as a threshold versus field intensity measurement. This will allow a comparison between the slope found for the apparatus used here to those found in the literature.

Experiment 3 investigates the effect of changing the background luminance on the slope of the S2 phase of rod sensitivity recovery while keeping the background wavelength constant ($\lambda=655\text{nm}$).

Experiment 4 investigates the recovery of scotopic contrast sensitivity following a photo bleach.

5.2 Method

The first three experiments were undertaken using the analogue apparatus described in chapter 2. This apparatus presents a 4° stimulus 15° temporal to the fovea in the right eye. Each subject has natural pupils and wears an eyepatch over the left eye. The subject sets the threshold by increasing the stimulus luminance from unseen to seen and indicates a threshold by pressing the mark button. See section 2.2 for a more detailed description. An important difference between experiment 3 and the measurements of dark adaptation that came later was that there was no aural prompt to the subject during the twenty minutes.

The method for experiment four is described in section 2.8

5.2.1 Experiment 1: Is the background detectable by the rod system?

To see if a red background had an effect on rod absolute threshold three narrow band sources were used ($\lambda=621, 651$ and 676nm) at a photopic luminance of 0.5 cd.m^{-2} , one wavelength ($\lambda=676\text{nm}$) was also measured at 0.17 cd.m^{-2} (photopic). This gave rise to four scotopic luminances, see table 5.2.1 The scotopic luminance of each background was calculated from the photopic luminance measured with the PR1500 using published conversion factors (Wyszecki & Stiles 1967, p104).

The background light was provided by an ultra bright LED (Lumiled, Phillips, colour temp 5000K) in a custom made housing, driven by a TTI EB2025t (RS components UK) power supply, the light output was then filtered using a narrowband filter to wavelengths $621, 651$ and 676nm , (Schott, Austria).

The subject (JMFK) with natural pupils sat in the dark for 20 minutes, no flash was used. Using the right eye, the left being patched, a threshold was set every ~ 30 seconds, from unseen to seen. Initially thresholds were set for about five minutes with no background then the background was illuminated and thresholds again collected for five minutes this process was repeated for twenty minutes.

Table 5.2.1: Photopic and Equivalent Scotopic Luminances

Wavelength	Luminance (cd.m ⁻²)	
	Photopic	Scotopic
621nm	0.50	0.023
651nm	0.49	0.0076
676nm	0.49	0.0053
676nm	0.17	0.0019

5.2.2 Experiment 2: Linearity of response with dim backgrounds

It is important that measurements of rod recovery vary linearly to changes in background conditions, i.e. are in the Weber region. During dark adaptation the visual system acts as though it is experiencing a ‘background light’ the intensity of which fades as time passes. The state of adaptation is a measure of the intensity of this ‘background light’ (Stiles & Crawford 1932). Dark adaptation measurements therefore, even in the absence of a luminous background, are the increment thresholds against this continually changing background. This experiment will confirm that the rod system is behaving linearly for the luminance used in this apparatus.

Two narrow band sources, produced by filtering a broadband source from a Gnome projector (Gnome, UK) with a narrow band filter (Schott, Lichtenstein). The filters have been described in section 2.3.4 and have peak transmittance at 651 and 676nm. The Gnome projector was housed in a light tight box with baffled ventilation, using an iris diaphragm at the exit aperture to control the background illumination. The third source was a red LED of the same type as used in the apparatus with peak emittance at 655nm, driven by a TTi EB2025t (RS components UK) power supply.

The procedure was as follows: The subject, an experienced observer aged 46 (JMFk) sat in darkness for 20 minutes, the stimulus was increased by the subject turning a potentiometer to increase the voltage across the stimulus, see figure 2.2.1. When the stimulus was detected, the mark button was pressed and the stimulus immediately returned to zero by the observer. This was repeated three times. Then using the PR1500 photometer the background luminance was noted by an assistant who then increased the background luminance while the subject had their eyes closed and covered by a mask. The threshold setting process was repeated at the new background luminance level. The data for each narrowband source was collected in one day, while the LED data was collected over three days. For each wavelength 651nm and 676nm, 15 measurements were made, while for

the LED, 30 measurements were made.

The data in logarithmic units were fitted to a three parameter exponential model using nonlinear regression with the R package `nls` which can return confidence intervals for the parameter estimates (R Development Core Team 2010).

$$Thres = a + b * BG^c, \quad (5.2.1)$$

where $Thres$ is the threshold (cd.m⁻² scot), BG the background luminance (cd.m⁻² scot), a , b , and c , the parameters. The dark light value (a cd.m⁻²) represents random noise in the rod system and straylight, the exponent (c) is the slope $\frac{\Delta L}{L}$ or Weber constant. The isolated rod pathway classically has a slope of 0.8 (Cornsweet 1970).

5.2.3 Experiment 3: The slope of the S2 phase for backgrounds of different luminance

The effect of changing the red background luminance was investigated using six healthy subjects who had their dark adaptation recovery measured for four different background levels of illumination. The subjects were postgraduate students, researchers and lecturers in the department of optometry, aged 28 to 60 years. Four of the subjects were familiar with the work and with psychophysical methods the others were not.

At each trial the subject had a practise run to familiarise themselves with the task and the apparatus. Then they were exposed to a flash to bleach the retina. The same flash setting was used at each trial ‘1/4th’ maximum intensity this gave rise to a bleach of 66% to 96% for pupils of 4 to 7mm, taken from table 2.5.2. Natural pupils were used, and the subjects left eye was occluded. The subject set thresholds at will, without prompt wherever possible from the experimenter.

The background had a wavelength of 655nm and luminance was altered at each visit; the background luminances used were zero, 0.05, 0.1, and 0.2 cd.m⁻²(photopic). Each measurement was taken on a different day and the sequence of background presentations was randomised to counter any possible cumulative effects. The collected data were subjected to the nonlinear curve fitting algorithm described in section 3.4 and the parameters noted.

5.2.4 Experiment 4: The recovery of scotopic contrast sensitivity

Contrast sensitivity is measured by detection of changes in contrast against a background of fixed luminance. Typically sinusoidal gratings are presented to a subject, the gratings in this case had spatial frequencies of 0.5, 1 and 2 cpd. The grating was also modulated temporally at 2Hz. Full details of the method can be found in section 2.8. The main points are repeated here for convenience.

Thirteen naïve subjects were recruited (6 female) aged $30.4(\pm 10.7)$ yrs.

Achromatic sinusoidal gratings were generated using Matlab scripts and the `psycho toolbox` (Brainard 1997, Kleiner et al. 2007) and presented on a gamma corrected high resolution monitor (Sony, GDM-F500R, Japan) using a ViSaGe interface (CED, UK). The gratings subtended 10° at 75cm.

Natural pupils were used and a photo bleach of more than 30% was applied using a flash gun.

Thresholds were set using a one up three down staircase in the following manner. The subject was given an auditory cue and the stimulus presented on the screen for 340ms. The subject indicated whether the grating was vertical, horizontal, or unseen. This response was entered into the computer program, coded by the software and if correctly identified the stimulus was there was a pause of 10 seconds. The next presentation had contrast 9.5dB lower than the threshold just measured. If the subject's response was incorrect the contrast was increased by 3dB and the grating was again presented to the subject.

A preliminary trial indicated that there was no further change in threshold after 15minutes, the measurements ceased if the time at the end of a threshold setting trial was greater than 15min.

Data were analysed using scripts in R and two models were considered. The two models were a simple three parameter exponential and a six parameter bi-exponential. The parameters were determined using nonlinear regression. The ability of the models to fit the data was compared using the extra sum-of-squares F test, see section 3.2.1.

5.3 Results

5.3.1 Experiment 1: Is the red background detectable by the rod system?

If the rods detect the red background we would expect the threshold elevation of the 530nm stimulus to be related to the scotopic luminance of the background and perhaps even be equal to it. Table 5.3.1 shows the equivalent scotopic luminance and the mean elevation in scotopic units against the scotopic luminance of the background for each condition. The raw data are summarised in figure 5.3.1.

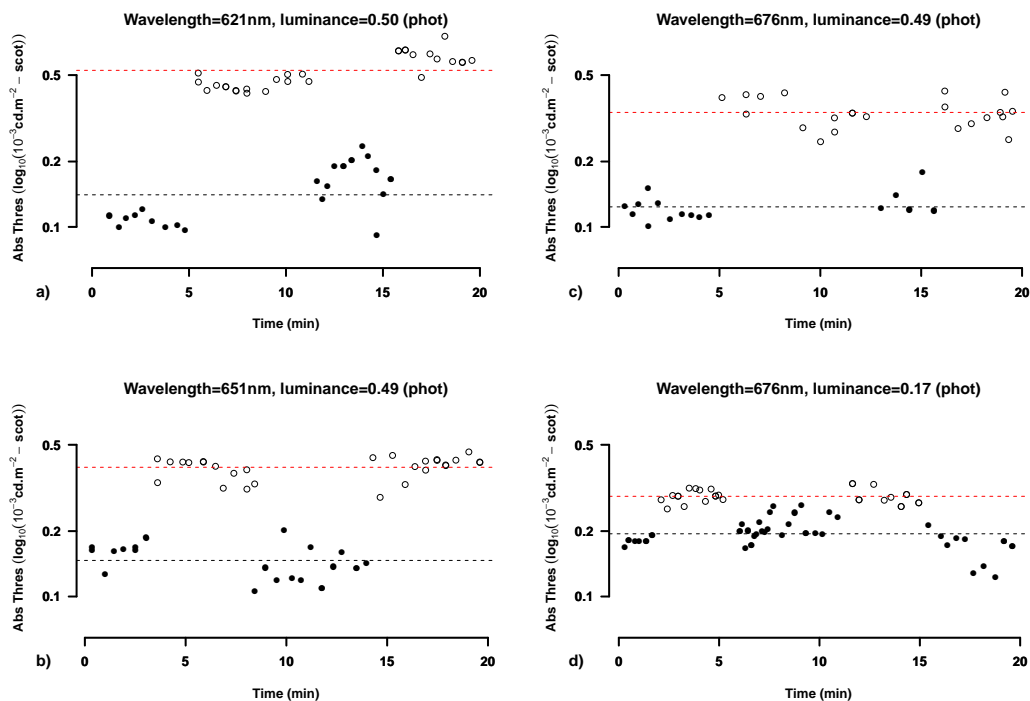


Figure 5.3.1: Threshold elevation in the dark adapted eye for differing wavelengths and scotopic intensities. Open circles are thresholds when the background is on, filled circles the background is off. Upper dashed line is the mean threshold when the background is illuminated, lower dashed line is the mean threshold when no background is used. Note that the ordinate values are scaled by $\times 10^{-3}$.

The background did elevate the absolute threshold but only by a small amount. The measured thresholds were dependant upon the scotopic luminance of the background.

Table 5.3.1: Photopic luminance, equivalent scotopic luminance and the elevation of the rod threshold for each condition

Wavelength	Luminance cd.m ⁻²		
	Photopic	Scotopic	Elevation
621nm	0.50	0.0230	3.9×10 ⁻⁴
651nm	0.49	0.0076	2.1×10 ⁻⁴
676nm	0.49	0.0053	2.5×10 ⁻⁴
676nm	0.17	0.0019	9.5×10 ⁻⁵

An analysis of variance found that the wavelength was not significant ($p=0.14$), however, the presence of an illuminated background ($p<0.001$) along with the scotopic luminance ($p=0.009$) were both significant as was their interaction ($p<0.001$). From this it is reasonable to assume that the rods are capable of detecting the presence of an illuminated background. It is important, nevertheless, to remember that the scotopic luminances used here are larger than those used in the later dark adaptation experiments, where the scotopic luminance of the background is 0.0007 cd.m⁻². These findings suggest that the rod response is being inhibited by the cone detection of the red light.

5.3.2 Experiment 2: Linearity of the rod system response

When measuring the rod system it is important that the responses are within the Weber region. This is a region of linear response and will therefore reflect the underlying processes of the recovery of sensitivity, rather than the dynamics of the photoreceptor to single quantum events.

Furthermore, a question was raised in chapter 3 about the narrowband nature of single colour LEDs, see section 2.3.4 where it was shown that the assumption of the LED being a narrowband source could not be justified. The importance of this can be considered in an alternative way; rather than ask if the source is narrowband, we can ask do the rods respond differently to the LED light source than to the narrowband lights. The narrowband sources bracket the dominant wavelength of the LED and thus provide an opportunity to compare the rod response to the LED to the response elicited by the two narrowband sources.

If the LED light evokes a response that is similar in character to the narrow band sources, in particular, has a Weber constant equal to that evoked by the narrowband source then the assumption of LED light being narrow band becomes tenable.

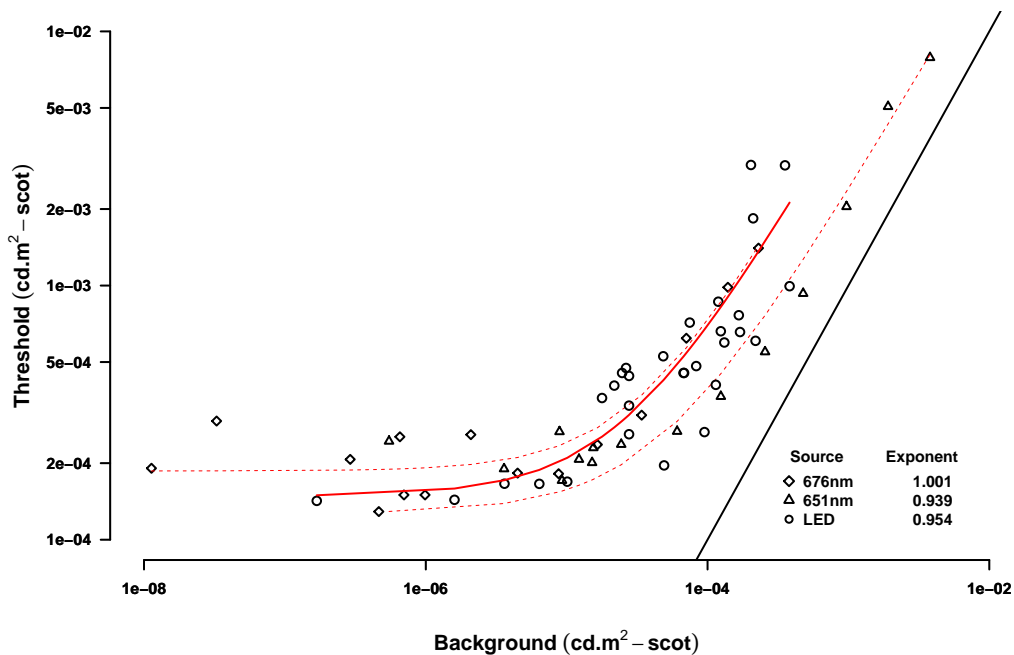


Figure 5.3.2: Threshold versus field intensity for a series of backgrounds. The upper dashed line is the line of best fit for the 676nm background, the lower for 651nm and the solid line fit to the LED.

Table 5.3.2: Summary of the parameter estimates for each background.

Background	Dark light value $\log_{10}(\text{cd.m}^{-2})$	Slope	CI	P value
676nm	1.9e-04	1.0	0.80-1.20	<0.001
LED	1.5e-04	0.95	0.21-1.69	<0.02
651nm	1.3e-04	0.94	0.80-1.08	<0.001

The model equation 5.2.1 was fitted to the collected data. The estimated best fit parameters for each light source are summarised in table 5.3.2. The dark light values are of similar orders of magnitude and probably represent the remaining straylight in the room. The Weber exponent for the rod pathway is usually reported as 0.8 (Sharpe, Stockman & MacLeod 1989). Here the slopes are higher at 0.94 to 1.0, suggesting that there is some cone pathway involvement, this is in agreement with other work. Sharpe et al.(1992) found that for a red background of 640nm the Weber ratio was nearer 1.0

and they explain this as a combined rod and cone response.

The confidence intervals for each estimate of the slopes found here suggest that there is no significant difference between the three backgrounds in terms of cone contribution to rod sensitivity. The wider interval for the LED reflects the noise in the data, recall that these data were collected over three days at differing times of day. However, the significance values (p) associated with each light source suggest that the estimates of the slope are reliable.

In figure 5.3.2 the solid line to the right hand side is the line of equality with slope 1.0 where the increase in threshold is equal to the increase in the field intensity.

The background luminance used for the recovery of red sensitivity experiments later in this study, $0.05 \text{ cd.m}^{-2}(\text{phot})$, has a scotopic luminance of $0.0007 \text{ cd.m}^{-2}(\text{scot})$. From this it follows that the responses measured in the later dark adaptation experiments are in the linear region.

5.3.3 Experiment 3: The slope of the S2 phase as background luminance changes and wavelength remains fixed

The data for the four conditions and six subjects were analysed with the algorithm written in Matlab described in section 3.4. The mean value of the S2 slope was $-0.31 \pm 0.09 \log_{10}(\text{cd.m}^{-2}).\text{min}^{-1}$. The line of best fit of S2 against background luminance had a slope of $-0.03 \text{ min}^{-1} (\pm 0.26, p = 0.9)$ this is not significantly different to zero slope and the intercept $-0.30 \log_{10}(\text{cd.m}^{-2}).\text{min}^{-1} (\pm 0.03, p = 0.01)$ was found to be significant. The change in the background luminance considered here had no effect on the slope of the S2 phase. See figure 5.3.3

The results of one subject (MR) are illustrative of the general findings and show features reported by some of the other subjects. The subject set thresholds at will, rather than being prompted as was the case later in the study.

The closed circle plot in figure 5.3.4 shows the recovery of sensitivity in the absence of any background light. There was a brief pause in threshold setting at 10 minutes. Prior to the lapse and immediately following, the slopes are the same but are offset. This would occur if the subject changed their criterion. The naive subjects in particular found difficulty with the task when there was no background illumination.

The background $0.05 \text{ cd.m}^{-2}(\text{phot})$, filled squares, shows a brief phase of autocorrelated

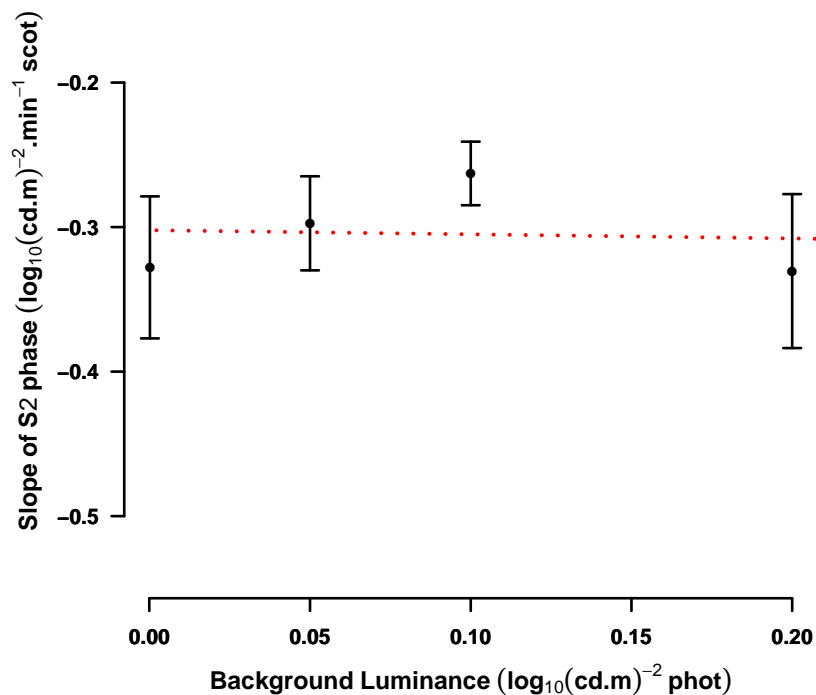


Figure 5.3.3: Slope of the S2 phase against background luminance ($\lambda=655\text{nm}$) for six subjects, error bars are one standard error.

threshold setting half way through the S2 phase, that is, the threshold values set are influenced by earlier thresholds. This leads to discontinuity in the data, where there are four points of rapid descent, this is followed by a correction without a criterion shift.

At the highest luminance, filled diamonds, the S2 phase is shorter and there is some drift as the S2 phase comes to an end. Notice that for each plot the absolute thresholds tend to rise. While the cone threshold hardly rises at all.

5.3.4 Experiment 4: The recovery of scotopic contrast sensitivity

Preliminary investigation of scotopic contrast sensitivity

The aim was to measure contrast sensitivity recovery following a photo bleach and to decide how long to collect data. Earlier experiments (see for example experiment 3 above)

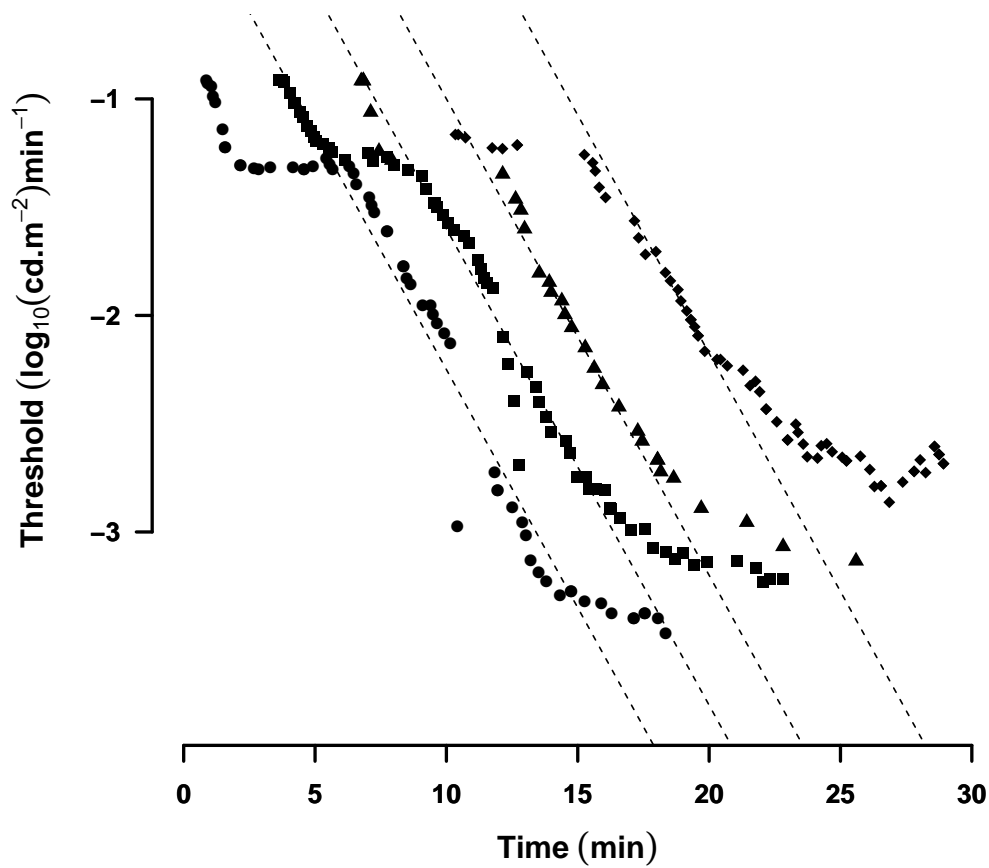


Figure 5.3.4: Slope of the S2 phase for increasing background luminance. Circles are zero background light, squares 0.05 cd.m^{-2} , triangles 0.1 cd.m^{-2} and diamonds 0.2 cd.m^{-2} . The dashed lines are of slope $-0.22 \log_{10}(\text{cd.m}^{-2}).\text{min}^{-1}$. Each plot after the first is offset in time by three minutes.

suggested that the time for rod recovery against a luminous background would reach a plateau after $\sim 12\text{min}$.

The recovery of contrast sensitivity for three spatial frequencies, 0.5, 1.0 and 2.0 cpd, following a photo bleach in excess of 30% was measured using a female subject aged 34 years. The measurements were taken for over twenty five minutes. Initial examination of the data suggested an exponential decay, therefore a three parameter model was fitted to the data, see equation 2.8.3. The parameters of the model of best fit are shown in table 5.3.3. The data is shown in figure 5.3.5 along with the exponential decay model. The horizontal line is the model threshold at 15 minutes. A linear regression of the post fifteen minute thresholds against time found that the slope after this time was not significantly

different from zero (p-value=0.1, 0.8, 0.5 for 0.5, 1.0 and 2.0 cpd respectively)

Table 5.3.3: Parameters of the simple exponential model fitted to the preliminary data. The absolute contrast threshold is ϕ_1 , the threshold at time zero ϕ_2 and the time constant (naperian) of decay ϕ_3 min.

cpd	ϕ_1	ϕ_2	ϕ_3 min
0.5	-1.68	0.99	2.61
1	-1.73	1.09	1.73
2	-1.55	0.88	2.73

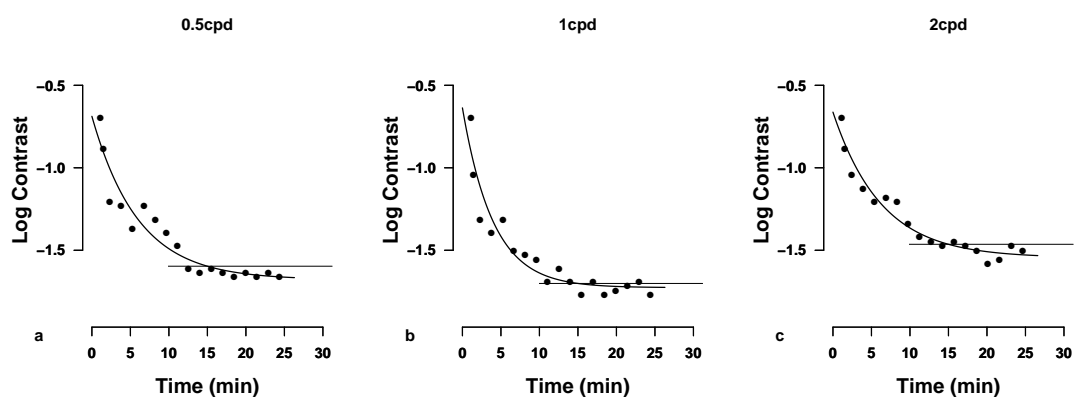


Figure 5.3.5: Contrast sensitivity recovery following photo bleach.

In figure 5.3.5 plots a and c have threshold elevations at ~ 7 minutes. This was investigated further using a larger number of subjects.

Evidence for two phases of contrast sensitivity recovery

Following the preliminary work data was collected for at least fifteen minutes in a series of healthy subjects with normal vision. The data collected from the thirteen subjects are summarised in figure 5.3.6.

To consider whether one or two processes were involved both a simple exponential decay and a bi-exponential model were fitted to the data. An extra sum of squares analysis was applied to the raw data for each spatial frequency and found that the bi-exponential model was a significant improvement over the simple exponential model (F-statistics; 243, 536, 447 on df= 3 and 138, 133, 138 p-value =0.000 for 0.5, 1.0 and 2.0 cpd respec-

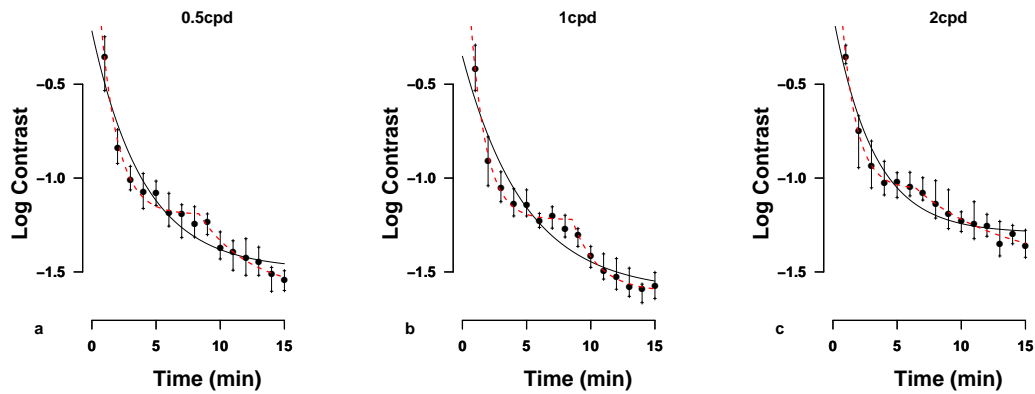


Figure 5.3.6: Contrast sensitivity recovery following photo bleach. Solid curve is the best fit exponential decay model.

tively)*

The bi-exponential model was used to evaluate the data for each subject, the individual results are shown in table F.1.1. Although visual inspection of the pooled data suggests that the offset ($\phi_1 + \phi_5$) or the threshold of the first phase seems to rise with spatial frequency no significant spatial frequency effect was found ($P=0.4$). There was no spatial frequency effect for any parameter against spatial frequency (all p values >0.15).

The time constant for the first phase was $0.35(\pm 0.28)$ min while for the second phase it was $5.15(\pm 4.68)$ min. The difference between the time constants of the two phases was subject to a paired t test and found to be significant ($t = -6.2994$, $df = 38$, p -value <0.001).

5.3.5 Contrast sensitivity recovery using a long wavelength stimulus

The biphasic recovery of contrast sensitivity is suggestive of two processes being involved. To test whether the rod system is responsible for the second phase the experiment was repeated using different conditions. The software was modified so that the gratings were presented on the monitor using the red phosphor alone and the mean luminance was reset to 12.5 cd.m^{-2} . The screen was attenuated by neutral density filters to give a mean

*This was verified by reducing the degrees of freedom by collecting the thresholds into one minute epochs and the median contrast threshold fitted to the two models (F-statistics; 14.88, 33.45, 27.34, $df=3$ and 14, p -value <0.001 for 0.5, 1.0 and 2.0 cpd respectively).

luminance of 1×10^{-2} cd.m⁻² as before.

The same subject who provided the time course data was exposed to a photo bleach and wore goggles with a red pass filter in place (Lee filters) when viewing the monitor. The filter ensured that only long wavelength light was seen by the subject. The results for each spatial frequency are shown in figure 5.3.7. The results are mono phasic and no late change in threshold was seen. The final thresholds are elevated by a factor ~ 0.8 log units, to -0.88, -0.98 and -0.83 log units, when compared to the absolute thresholds for the same subject in figure 5.3.5 where the absolute thresholds were -1.68, -1.73, and -1.54 log units.

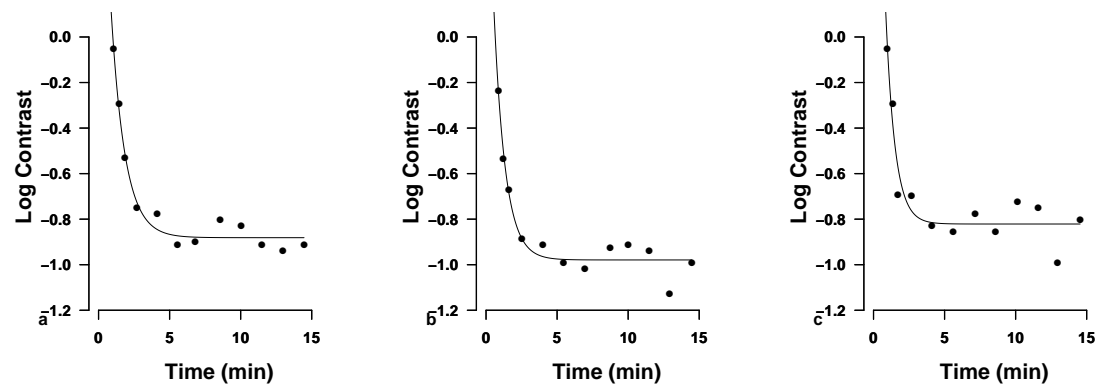


Figure 5.3.7: Recovery of scotopic sensitivity for a red stimulus.

This work is being prepared for publication, a draft as of 18 December 2012 is available in appendix I.3 on page 331.

5.4 Discussion of the four experiments

The first experiment measured the absolute threshold in the presence of a dim long wavelength background and compared these to the absolute threshold in the dark. The results show that rod mediated vision is able to detect the dim red background.

The second experiment compared the threshold increment to the field intensity for rod mediated vision. The results have shown that threshold measurements made with this apparatus while using a background of wavelength greater than 651nm and luminance greater than 0.05 cd.m⁻²(phot) are in the Weber region, furthermore, the slope of this region is in agreement with Sharpe, Fach & Stockman (1992) who suggest the slope of ~ 1 suggest cone input to rod responses.

No evidence was found that the LED light is significantly different from narrowband light.

Crucially, the novel finding of the third experiment that the background illumination and resultant elevation of the rod threshold had no noticeable effect on the rate of the S2 phase of rod sensitivity recovery is reported. Other work regarding sensitivity and background have made measurements of threshold, e.g. Sharpe et al.(1992), but these measurements were of absolute thresholds rather than the rate of recovery. Other workers using variable flash intensity and a zero background found that the value of the slope of S2 remains constant as the amount of photopigment bleached increases beyond 20% (Pugh 1975, Lamb & Pugh 2004).

The question of continued cone photopigment replenishment in the presence of the red background can be understood by considering the cone specific retinoid cycle, for a review see Wang & Kefalov (2011). The cone retinoid cycle uses both the RPE and Müller cells to deliver *cis*-retinal to the outer segment of the cones and the much faster cone recovery is due to the larger outer segment surface area and rôle of the Müller cells. This leads to the possibility that the cones at their intermediate level of activity are relying upon the Müller cells for retinoid recycling and the effect on rod recovery, mediated by the RPE, is unaffected in the healthy normal.

In experiment 3 the subject conducted the trial with little or no input from the author other than time warnings if requested. This was done to reduce bias, it had the unfortunate consequence that the subject occasionally had a lapse in their concentration and attention to the task. The subject was also permitted to set a threshold as they wished, sometimes attempting to set thresholds too frequently. It also became apparent that if the subject overshot the threshold, particularly during the S2 phase, the next threshold was elevated.

Increasing the background illumination had the effect of shortening the S2 phase, see figure 5.3.4 filled diamonds. The numerical experiment in section 4.1 shows that the accuracy of the determination of the slope of S2 is improved the longer the range of data available, with this in mind subsequent experiments were conducted at the minimum background $0.05 \text{ cd.m}^{-2}(\text{phot})$.

The final experiment has shown that the biphasic recovery of rod sensitivity is reflected in the recovery of contrast sensitivity and the time course is independent of spatial frequency. Little work has been done on this subject. Margrain & Thomson (1997) used gratings to measure luminance sensitivity rather than contrast sensitivity and pre-

dictably found that the recovery of luminance sensitivity of bars mirrored the classic dark adaptation response to a circular stimulus. However, Hahn & Geisler (1995) using novel Gabors measured contrast sensitivity at a range of spatial frequencies including 1 and 3 cpd found a simple exponential decay in their uniquely defined measure of contrast. Howard, Tregear & Werner (2000) measured sensitivity recovery to Gabors of 1 and 6 cpd following the offset of an adapting background, this measured the rapid recovery found when the limiting factor is the local *cis*-retinal rather than the rate limited recovery exemplified by the S2 phase discussed here.

A further measurement at 4 cpd would be informative, since the rod resolution limit is 3.5 cpd. This would allow for further discrimination between mechanisms. The thresholds at the change from the first to the second phase will reflect both the contrast sensitivity function for $0.1 \text{ cd}\cdot\text{m}^{-2}$ and the interaction between the cone and rod mechanisms as the rods become dominant in signalling contrast. An interesting further experiment would measure dynamic thresholds and compare them to static thresholds.

5.4.1 Summary

The above experiments provide evidence that the thresholds measured using the analogue dark adaptation apparatus described are reliable. They have demonstrated that rods are able to detect the red background but that the presence of the background has no effect on the slope of the S2 phase, suggesting that the cone mechanisms of retinal replenishment once at a steady state are largely independent of the rods. Although the slope of S2 has been shown to be independent of the luminance of a red background, the question still remains of what effect if any would a different wavelength have on the slope of S2?

Furthermore, evidence of a biphasic contrast sensitivity response has been presented. This opens a further route to understanding rod function.

ANALOGUE DEVICE TO MEASURE DARK ADAPTATION

As your bright and tiny spark,
Lights the traveller in the dark.
Though I know not what you are,
Twinkle, twinkle, little star.

Jane Taylor 1806

6.1 Introduction

The slope of the S2 phase of dark adaptation is a sensitive measure of the health of the outer retina in particular the RPE-rod outer segment complex. This has resulted in growing interest in rod mediated vision.

It is well known that functional night vision facilitates continued independence and ensures high quality of life measures in an ageing population (Kosnik, Winslow, Kline, Rasinski & Sekuler 1988). Further the deleterious effect of some systemic diseases on night vision is well established. The effects of Vitamin A deficiency (Tansley 1931), liver disease (Patek Jr & Haig 1939) and diabetes (Henson & North 1979) on the ability of the retina adapt to a dark environment, mean that measurement of scotopic vision has the potential to provide insights into these systemic diseases.

Furthermore, the recently described role the rods play in preserving cone health (Leveillard

et al. 2004) and the observation that rod function can act as a marker warning of pathological changes in the retina (Dimitrov et al. 2011) have strong relevance to the diagnosis, management and treatment of age related macular degeneration (AMD).

The association between rod function and macula disease is not fully understood. Nevertheless, people with AMD have increased scotopic threshold and prolonged time course for photopigment regeneration (Owsley, Jackson, Cideciyan, Huang, Fine, Ho, Maguire, Lolley & Jacobson 2000, Owsley et al. 2001, Haimovici, Owens, Fitzke & Bird 2002, Scholl et al. 2004).

In those people with AMD scotopic sensitivity decline precedes photopic loss. This change in scotopic sensitivity does not have a clear link to changes in photopic sensitivity, either in time course or magnitude (Jackson, Owsley & Curcio 2002). However, Jackson et al. (1999), have shown a relationship between age and rod function. They found a decrease in the rate of dark adaptation with age, with subjects in their ninth decade having a rate 64% of that of a 20 year old. They also found a three fold rise in the absolute scotopic threshold.

Evidence was presented in the introductory chapter that rod function is dependent upon the regeneration of the photopigment and although rod numbers fall by 30% from middle age to the ninth decade, rhodopsin content remains stable. The effect this change in morphology has on rod function is unclear (Curcio et al. 1993).

Another age dependent change is the thickening of Bruch's membrane, which subsequently becomes more resistant to molecular transport (Curcio, Owsley & Jackson 2000, Ruberti, Curcio, Millican, Menco, Huang & Johnson 2003). The effect of this resistive barrier on RPE cells and their rôle in photopigment replenishment can be linked to the performance of the rod photoreceptor and is characterised by changes in the rate of rod sensitivity recovery during the S2 phase (Lamb & Pugh Jr 2006).

The vulnerability of the rod system and the link between the S2 phase of sensitivity recovery and the physiology of the rod photoreceptor outer segment mean that a method of measurement would be valuable both clinically and in a research setting.

The classical clinical measurement of rod function using the Goldmann Weekers dark adaptometer (Haag-Streit, Liebefeld-Berne, Switzerland) can be time consuming, e.g. see Dieterle & Gordon (1956) and any modification that could shorten this would be an advantage. One possible change would be to try to reduce the cone phase of sensitivity recovery. It has been long known that elevation of the cone threshold allows for study of

rod performance at higher luminance (Aguilar & Stiles 1954).

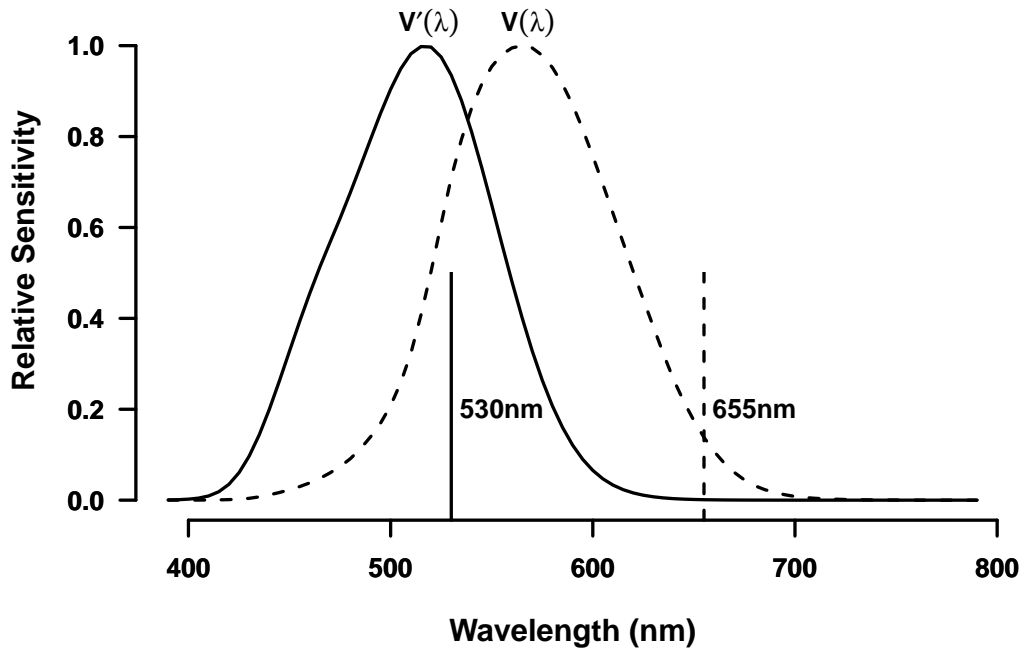


Figure 6.1.1: The principle of the red background. The stimulus (530nm) is near the peak of the scotopic luminous efficiency function ($V'(\lambda)$). The background (655nm) is in a region of poor scotopic sensitivity and reduced photopic sensitivity ($V(\lambda)$)

The apparatus used here has a long wavelength background that elevates the cone threshold and to which the rods are relatively insensitive, see figure 6.1.1. This allows us to examine the recovery of the rod photoreceptor earlier than might be the case otherwise. The sensitivity of the visual system is probed using a mid wavelength stimulus, initially seen by both rods and cones. Once the intensity of the stimulus is below the photopic luminance of the background only the rods can detect the stimulus. Any further change in stimulus threshold is therefore due to the rods response alone.

Aims The aim was to answer the question; could this technique yield useful information about rod function?

In particular:

- Can we measure dark adaptation with this apparatus?
 - is the method reliable?
 - are the parameters found comparable with those in the literature?
 - does the method shorten the cone phase?

Further questions became apparent as data was collected

- What is the optimum threshold setting interval?
- Are the assumptions made for curve fitting held?
 - the residuals are iid
 - the model is appropriate

6.2 Method

The experimental apparatus and method are described in detail in section 2.2.

6.2.1 Subjects

Subjects were recruited by a campus wide call to staff and students for volunteers. Thirty six subjects were recruited and their age distribution is shown in figure 6.2.1 by the grey bars. All subjects gave informed consent and were free to leave at anytime without penalty.

Grounds for inclusion and exclusion

A subject was considered suitable if they had had an eye examination within the last year and a best corrected acuity of better than 6/9 Snellen. A result was considered acceptable if the subject was able to complete the task required. One subject, Sx10, withdrew for personal reasons. The 35 retained subjects (15 female, 20 male) had a mean age of 43.28(\pm 19.6) years, see figure 6.2.1.

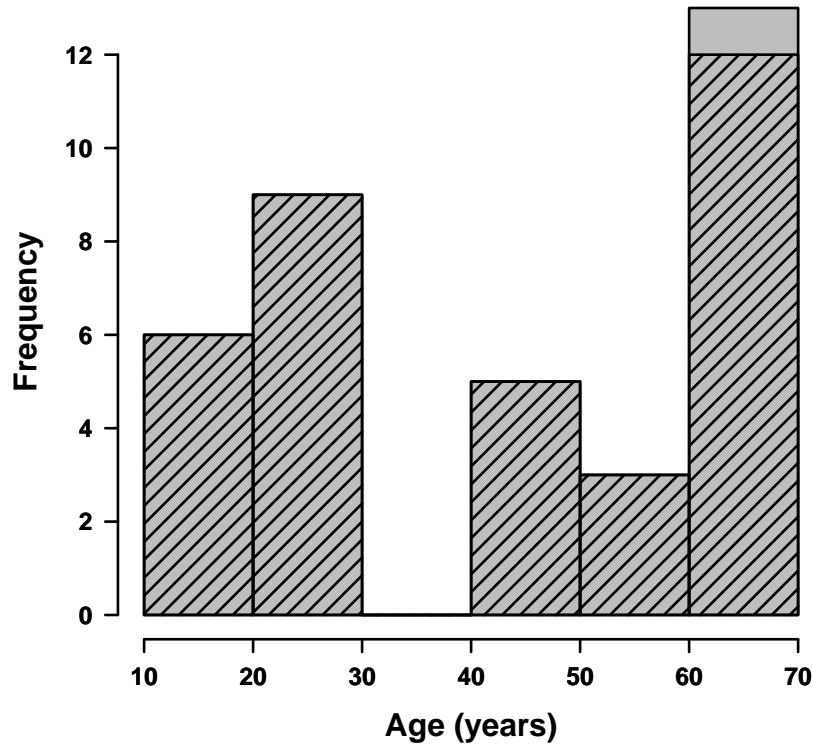


Figure 6.2.1: Age distribution, the initial recruits shown by the solid grey bars, subsequently retained subjects by the shaded bars.

6.3 Results

Following a flash of light the recovery of sensitivity follows a characteristic curve, illustrated in figure 1.5.2. There is an initial cone recovery phase, a break point, often called the alpha point, an early phase of rod recovery, called S2, followed by a slower rod phase S3, approaching absolute threshold.

A summary of the data collected with this device is presented in figure 6.3.1 and table 6.3.1. The data exhibit the typical biphasic recovery found for classical measurements of dark adaptation. The parameter estimates for each subject at each visit are in appendix G on page 308 and detailed description and discussion of individual plots is in appendix G.1.1 on page 308. The data from both visits for all subjects is summarised in figures 6.3.2 and 6.3.3 and detailed discussion of the parameters follows.

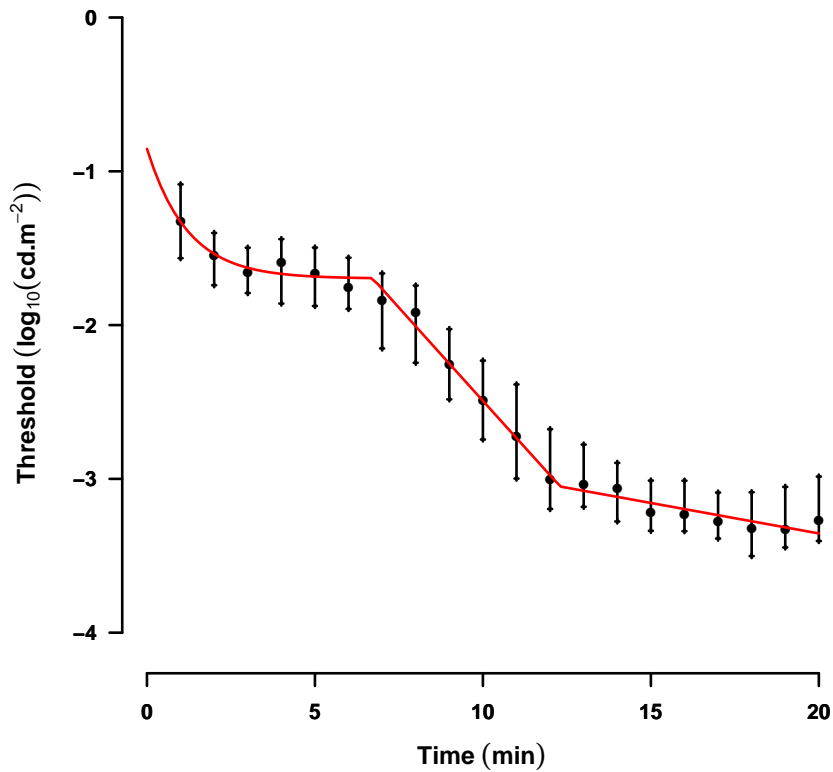


Figure 6.3.1: Summary of the data collected using the analogue device. The pooled data are collected into one minute intervals, the filled circles are the median value for each data bin. The error bars are the interquartile range. The solid line is the line of best fit to the median values.

In this study the parameters of particular interest were the cone threshold since elevation of the cone threshold is the purpose of the red background. The time to rod cone break or α point as the elevation of the threshold would bring this point forward in time. The rate of rod recovery S2 can be considered a marker for the health of the choriocapillaris-rod photoreceptor complex (Lamb & Pugh 2004) and is therefore the characteristic of most interest clinically.

The absolute threshold is also considered as we know from the previous chapter that the rods might be sensitive to the background light. The S3 phase of the rod recovery typically has a very shallow slope ($\sim 0.06 \text{ log.min}^{-1}$) and is dependent upon the flash intensity used and therefore the retinal illuminance (Lamb 1981).

Table 6.3.1: Summary statistics for the parameter values of the dark adaptation curve for 35 subjects' first visit. The left hand column has the parameters, note that θ_6 has not been transformed to S3, see text for this. Q_1 and Q_3 are the lower and upper quartiles. The probability of the distribution being normal using Shapiro-Wilks test is given by N_{SW} , the probability of the kurtosis being that of a normal distribution, using the Anscombe test is given by K_A , and the probability of skewness being from a normal distribution as tested by the D'Agostino test is $S_{D'A}$

θ	mean	sd	Q_1	Median	Q_3	N_{SW}	K_A	$S_{D'A}$
Cone Thres	-1.65	0.46	-1.85	-1.66	-1.41	0.14	0.08	0.97
Cone Coeff	3.06	8.09	0.67	1.23	2.03	<0.001	<0.001	<0.001
Cone TC	0.18	3.40	0.15	0.31	1.163	<0.001	<0.001	0.03
S2	-0.24	0.08	-0.29	-0.23	-0.18	0.61	0.57	0.67
alpha	6.00	2.26	4.96	6.21	7.51	0.08	0.16	0.44
θ_6	0.23	0.08	0.17	0.24	0.29	0.75	0.67	0.89
beta	12.49	2.80	10.46	11.97	13.99	0.53	0.54	0.77
MSE	0.02	0.03	0.01	0.01	0.02	<0.001	<0.001	<0.001

The technique used here aims to minimise the cone phase of the dark adaptation response, for this reason the exponential cone coefficient and cone time constant data can reasonably be expected to be atypical. The repeatability of the measurements was also considered, since a quick but unrepeatable measurement is of less use than a slow repeatable one.

6.3.1 Repeated measures

Of the 35 subjects, 25 returned for a second measurement of their dark adaptation recovery. One of the twenty five returnees withdrew from the experiment after ten minutes. The resulting twenty four subjects' first and second visits are now compared with particular reference to the early rod mediated sensitivity recovery as indicated by the slope of the S2 phase.

The subjects that did return and were able to provide data were aged $38.9(\pm 19.7)$ years and comprised 10 female and 14 male subjects. The subgroup of returning subjects repeated the experiment as described above. The distributions of the two estimates of S2 are shown in figure 6.3.4 a two-sample Kolmogorov-Smirnov test suggests that the two distributions are not significantly distinct (p-value = 0.4). The mean difference between visits was $0.02 \pm 0.07 \log_{10}(\text{cd.m}^{-2}).\text{min}^{-1}$.

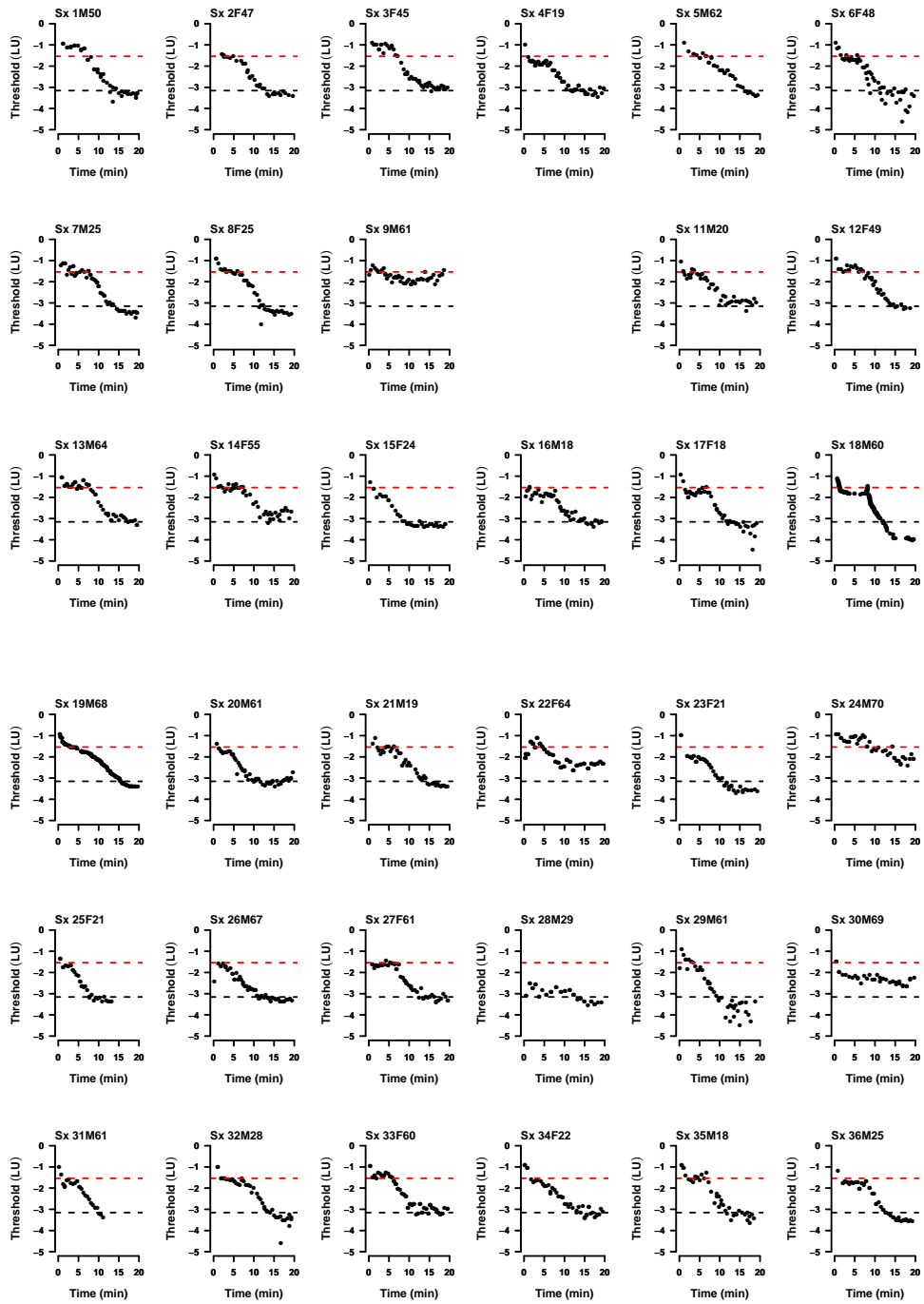


Figure 6.3.2: Individual plots of data collected at the first visit. The upper left key encodes the subject number, sex and age. The upper horizontal dashed line is the luminance of the screen in photopic units, the lower dashed line is the scotopic luminance of the screen. The ordinate axis units are $\log_{10}(\text{cd}\cdot\text{m}^{-2} \text{scot})$ abbreviated as log units (LU).

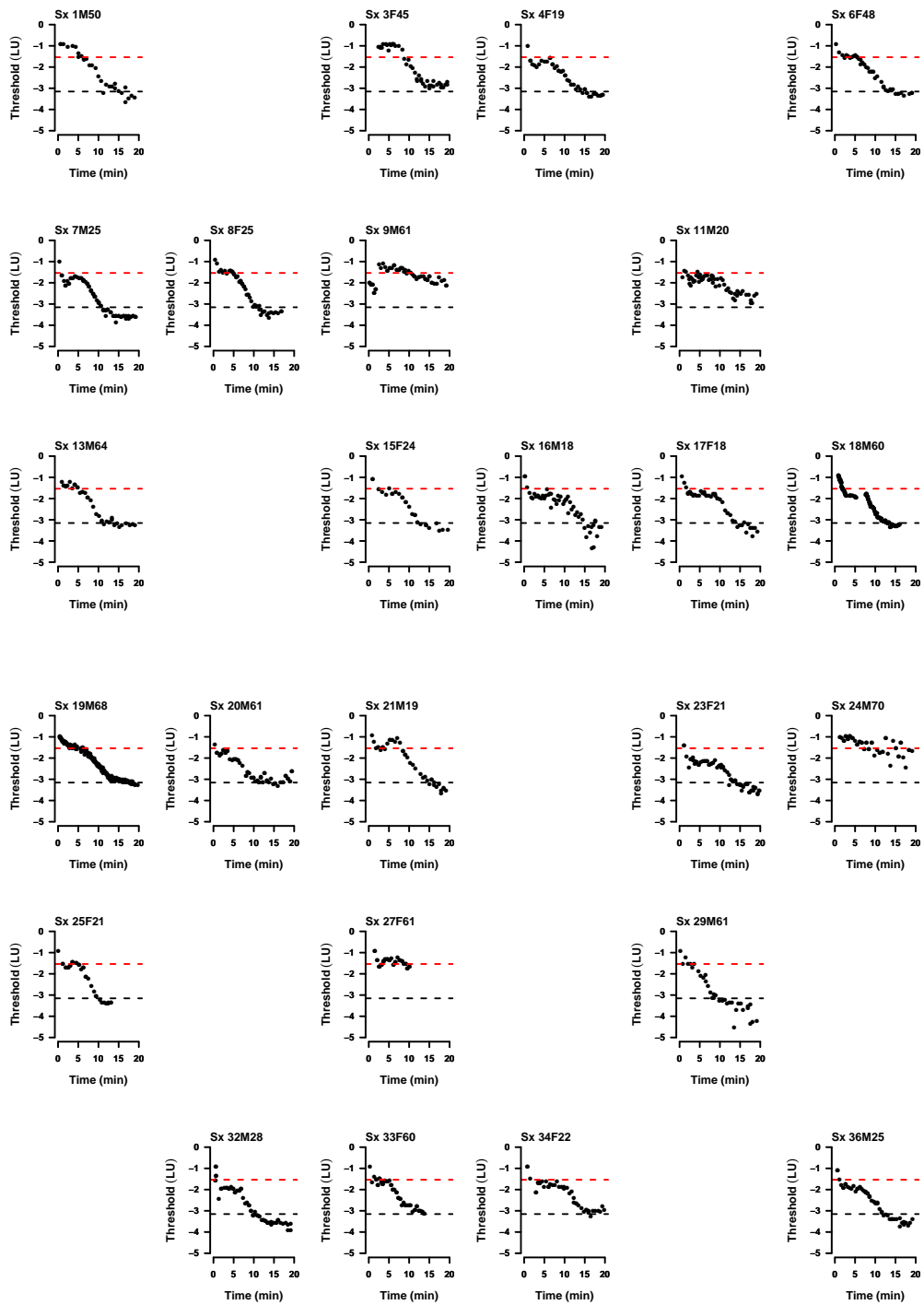


Figure 6.3.3: Data of subjects who returned for a second visit.

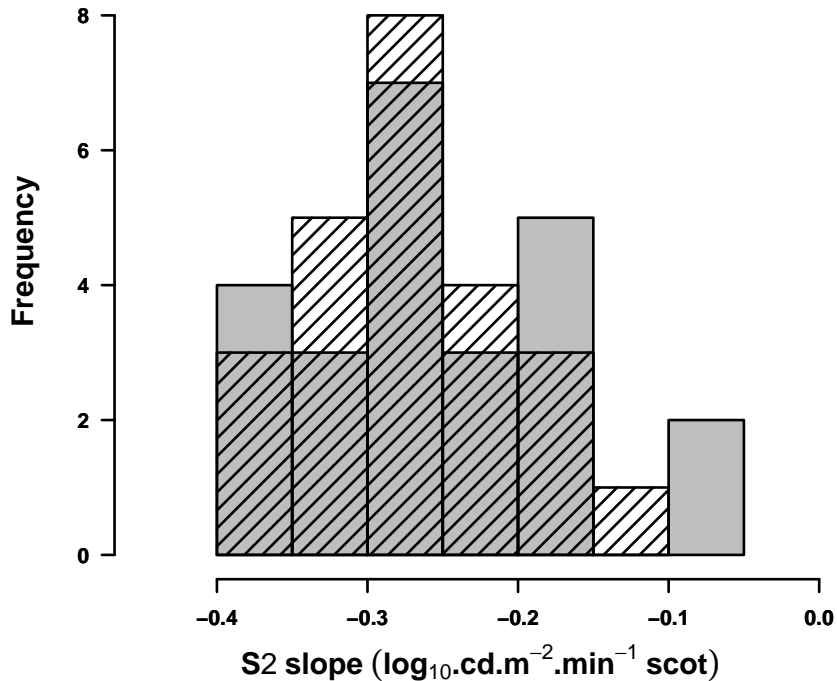


Figure 6.3.4: A histogram of the values of the slope of the S2 phase found at two measurements, the first measurement is shown by the solid grey bars, second visit by the slashed bars. $n=24$.

The two estimates of the S2 component are compared in figure 6.3.5, eight subjects had a smaller S2 slope at their second visits, while 16 had a larger slope. The slopes had a Pearson correlation coefficient of 0.61 ($t = 3.62$, $df = 22$, $p\text{-value} = 0.001$), with a 95% confidence interval of 0.28–0.81. The Lin concordance correlation coefficient was 0.57 with 95% confidence interval of 0.26 to 0.78. The Pearson product moment correlation coefficient measures the linear relationship between the two measurements while the Lin concordance correlation coefficient indicates the disparity between the measurements and the line of equality ($y = x$), further detail can be found in Lin (1989, p258).

A paired t-test found that the differences were not significant ($t = 1.39$, $df = 23$, $p\text{-value} = 0.2$), analysis presented later shows that the slope of the S2 phase for this healthy population is normally distributed. Of the subjects with the greatest difference between visits, subjects 16 and 17 had smaller S2 slopes at their second visit furthermore they had noisier data and poorly defined cone rod breakpoints at their second visit, see figure G.1.6 on page 314, while subject 9 (figure G.1.3 on page 311) had no rod function at either visit and therefore the model was inappropriate. Subjects 21, 32 and 34 had some guessing

at their first visit and poorly defined cone rod transition points, see figures G.1.7 on page 315 and G.1.11 on page 319.

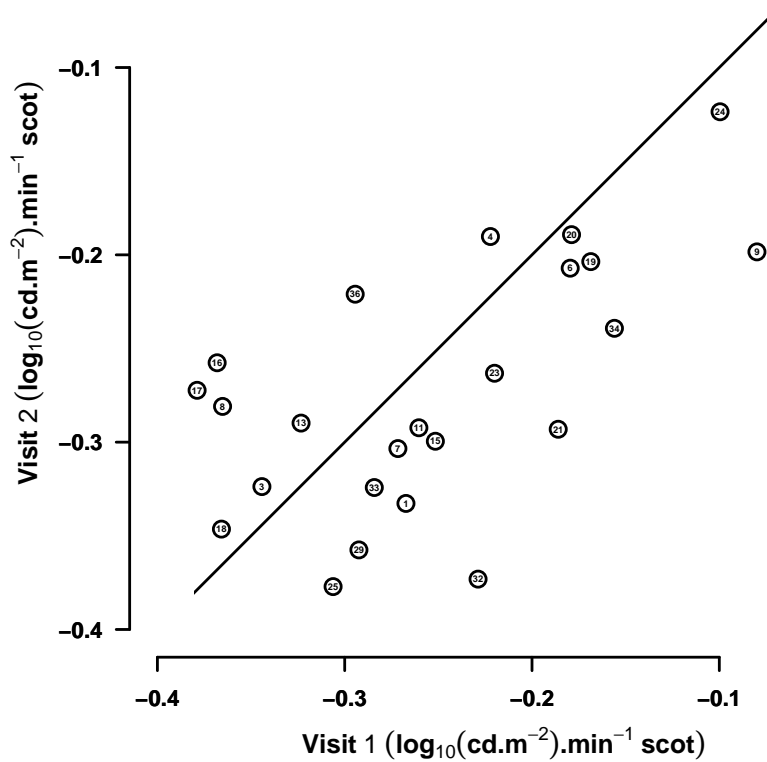


Figure 6.3.5: Comparison of the two estimates of the slope of the S2 phase. The black solid line is the line of equality. The number in the open circles is the subject identification code.

Measures of repeatability have been discussed earlier in section 2.2 on page 58, and are mentioned here to aid the reader. Altman and Bland have presented elementary methods to compare repeated measurements of biological phenomena. They compare the difference between the two measurements to the the mean of the measurements. They also propose the coefficient of repeatability (CoR) as a statistic, which is defined as the standard deviation of the differences multiplied by ± 1.96 and therefore 95% of measurements lie within the interval bounded by $\pm 0.13 \log_{10}(\text{cd.m}^{-2}).\text{min}^{-1}$ (Bland & Altman 1986). Examination of figure 6.3.6 suggests that as the magnitude of the slope falls, the variation in measurements decreases. In other words, subjects with slower rates of recovery have reduced variation between repeated measures.

A systematic relationship between the two measurements can be revealed by regression

analysis of the difference against the mean of the estimates, as described by Maloney & Rastogi (1970) or by regression analysis of the absolute difference against the mean using the Half Normal distribution described by Bland (2005). For the data presented here both methods of analysis failed to achieve statistical significance (MR: F-statistic: 2.16 on 1 and 22 DF, p-value: 0.2. BA: F-statistic: 0.36 on 1 and 22 DF, p-value: 0.6). This suggests that the apparent systematic effect in the measurement of the slope of the S2 phase of rod recovery might be due to chance.

There does not appear to be any significant difference between the two measurements and no general learning effect has been found, the absence of a learning effect has also been reported in the Weekers-Goldman dark adaptometer (Christoforidis & Zhang 2011).

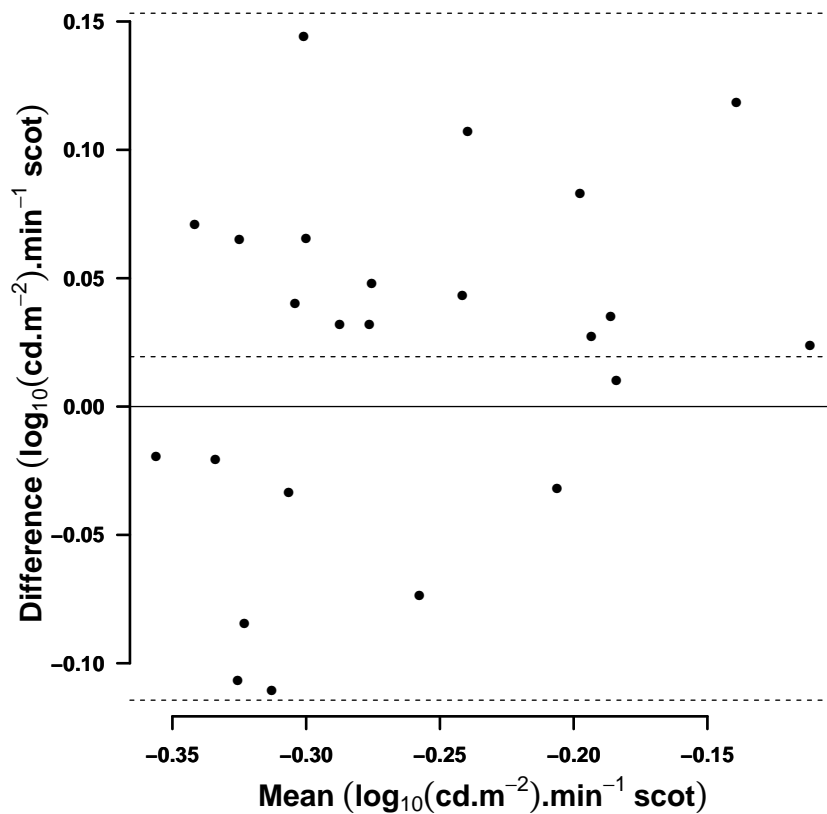


Figure 6.3.6: Bland Altman plot of two estimates of S2. The horizontal lines are from the top; upper limit of agreement, mean difference, abscissa, lower limit of agreement.

6.3.2 Test Retest

There is very little literature on dark adaptation test retest reliability. Both the difference in measurements $0.02(\pm 0.07) \log_{10}(\text{cd.m}^{-2}).\text{min}^{-1}$ and the CoR found in this study $\pm 0.13 \log_{10}(\text{cd.m}^{-2}).\text{min}^{-1}$ were larger than that found by others, for example, Patryas et al.(2012) found a change of $0.004(\pm 0.04) \log_{10}(\text{cd.m}^{-2}).\text{min}^{-1}$ for S2 and CoR for the slope of S2 of $\pm 0.07 \log_{10}(\text{cd.m}^{-2}).\text{min}^{-1}$ measured using a CRT computer controlled system of stimulus presentation.

The group of subjects in the study by Patyras et al. had many members (19) in common with this study. This commonality provides a useful cross check of the values found in this study. The difference in the slope of S2 at first and second visit and in CoR between this study and that of Patyras suggests that it is methodological in nature rather than being a characteristic of the subjects. The main difference in the method here is that in the analogue device the subjects controlled the rate of stimulus increase and to some extent the time between threshold setting.

Christoforidis and Zhang (2011) using the Goldmann Weekers dark adaptometer (Haag-Streit AG, CH) controlled by the experimenter found a change in the rod time constant* of $0.276(\text{CI: } -0.424, 0.976)\text{min}$ this is equivalent to $0.01 \pm 0.03 \log_{10}(\text{cd.m}^{-2}).\text{min}^{-1}$ and a CoR of $0.06 \log_{10}(\text{cd.m}^{-2}).\text{min}^{-1}$ between visits. Surprisingly, given the low CoR in their estimates of the rod time constant, they found little agreement between rod time constant measurements (Lin's concordance 0.375 CI: 0.062 – 0.627). This suggests that the variance in the true value is much less than the measurement error and might be due to the small range of values found, small number of subjects (n=16) and their relative youth (age range 24 to 52 years).

In the present study when setting the threshold the stimulus level was controlled by the subject, the majority of whom were naïve observers. A simple improvement here would have been for the experimenter to prompt the subject and adjust the threshold, waiting for the subject's indication that they were aware of the stimulus

Furthermore, it is important to remember that for this study all data collected were included in the analysis presented here, in other words potential outliers and data to which the seven parameter model was inappropriate were not discounted. This was because until the data were collected it was not possible to know which results might be atypical and a *post hoc* categorisation might introduce bias.

*0.4343 times the reciprocal of the slope in log units

However, in this study there was a significant agreement between visits (Lin: $\rho_c=0.57$ with 95% confidence interval of 0.26 to 0.78).

6.3.3 Summary of dark adaptation recovery parameters

The following summarises the parameters estimates from the 35 subjects at their first visit only. No values found using the algorithm described in section 3.4 are excluded.

Cone threshold: θ_1

The log cone threshold values were normally distributed (SW: $W = 0.95$, p-value = 0.1), with mean $-1.65(\pm 0.46) \log_{10}(\text{cd.m}^{-2} \text{ scot})$. The apparatus is calibrated in scotopic units, therefore, the cone threshold for light with dominant wavelength of 530nm uses a conversion factor of 1.70 to return photopic units (Wyszecki & Stiles 1967, p.104). After conversion to photopic units the mean cone threshold is 0.039 cd.m^{-2} , this is 0.011 cd.m^{-2} higher than the photopic luminance of the background. The stimulus used by Patryas et al. subtended 1° at 11° inferior to the fovea. Comparison with a 4° stimulus 15° eccentric to the fovea in the temporal retina is not trivial, however, we might expect the smaller stimulus to be more difficult to see and this was confirmed by a cone threshold of $-1.32(\pm 0.30) \log_{10}(\text{cd.m}^{-2} \text{ scot})$.

Exponential coefficient θ_2 and cone time Constant θ_3 (τ)

The exponential coefficient or the cone threshold at time zero can take non-physiological values since it represents a notional threshold at the instant of the flashgun discharge. The range of values found was -4.4 to 42.7 cd.m^{-2} , with an inter-quartile range of $0.67-2.03 \text{ cd.m}^{-2}$ and a median value of 1.23 cd.m^{-2} . The values found here were not normally distributed (WS: $W=0.48$, $p < 0.001$).

The cone time constant was not normally distributed (WS: $W=0.79$, $p < 0.001$), being significantly skewed ($p=0.03$) to higher values (D'Agostino 1970). The median value was 0.30 min with IQR 0.17 to 1.12 min . The range of cone time constants for healthy normals has been reported as 0.4 to 1.4 min (Christoforidis & Zhang 2011).

6.3.4 The slope of the rod recovery S2: θ_4

The parameter S2 describes the rate at which the rod system recovers its sensitivity following an adapting light and reflects the performance of the RPE-choroid complex in delivering *cis*-retinal to the rod outer segment. A Shapiro-Wilk test suggests that the data were normally distributed (SW: $W = 0.98$, p -value = 0.6). The mean value of S2 for the 35 subjects was found to be $-0.239(\pm 0.08) \log_{10}(\text{cd.m}^{-2}).\text{min}^{-1}$, the distribution is shown more fully in figure 6.3.7. The values of S2 range from -0.38 to $-0.05 \log_{10}(\text{cd.m}^{-2}).\text{min}^{-1}$.

This range of values of the slope of the S2 phase is in agreement with published values; Owsley et al.(2001) found $-0.23(0.03) \log_{10}(\text{cd.m}^{-2}).\text{min}^{-1}$ for their healthy control group, Lamb (1981) reports the value of the S2 slope as $-0.24 \log_{10}(\text{cd.m}^{-2}).\text{min}^{-1}$ for a young subject (<40), while Dimitrov et al.(2008) with an older group of 22 subjects (66.8 ± 5.9)yrs quotes a mean rate of $0.22 \text{ decades}.\text{min}^{-1}$ and Brown et al.(1986) has a rate of $0.20 \log_{10}(\text{cd.m}^{-2}).\text{min}^{-1}$ for their control group of five healthy subjects mean age 65yrs. An age effect has been described by Jackson et al. (1999) and this possibility is considered below.

The relationship between age and S2

In order to investigate the influence age has on the value of the slope of the S2 phase, a least squares linear regression was carried out between age and S2. The relationship between age and S2 value was found to be;

$$S2 = -0.31 + 0.002.Age \quad (F \text{ 5.16 on 1 and 33 DF, } p = 0.03), \quad (6.3.1)$$

or S2 rises by $0.02 \log_{10}(\text{cd.m}^{-2}).\text{min}^{-1}$ a decade. This is in agreement with other workers (Jackson et al. 1999), who report the same value for the rate at which sensitivity recovery declines with age.

The power of these statistics*, intercept and slope, using a two tailed test and $\alpha=0.05$ on 1 and 33 degrees of freedom was $\beta=0.70$. A 'leave one out analysis' where each data point is omitted in turn showed that no single point was responsible for the relationship between S2 and age being significant.

The raw data and the regression line are shown in figure 6.3.8. The general trend is for

*probability of error ($1-\beta$)

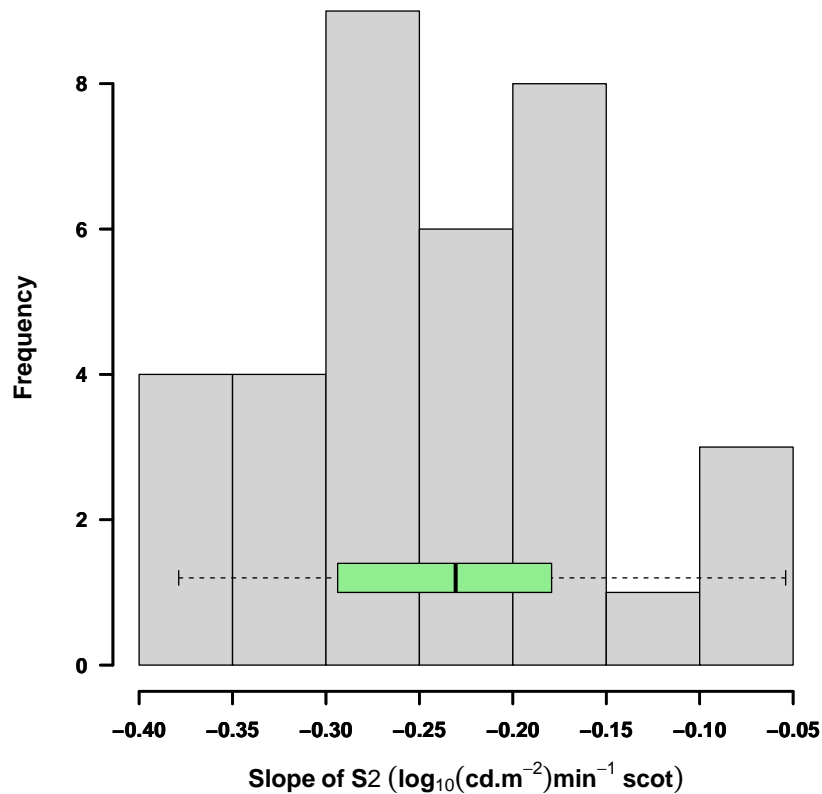


Figure 6.3.7: Distribution of S2 with ‘box and whisker’ plot overlaid.

the value of the slope of the S2 phase to rise, in other words for the rate of recovery of sensitivity to fall with increasing age.

A comparison of the common subjects in this study and the Patryas (2012) study found no significant difference in the paired values ($t = 1.9107$, $df = 18$, $p\text{-value} = 0.07$). However the correlation was not significant ($t = -0.5608$, $df = 17$, $p\text{-value} = 0.6$).

6.3.5 The cone - rod break point: θ_5 (α)

The times to the cone rod breakpoint were normally distributed (SW; $W=0.94$, $p=0.08$) although slightly left skewed to lower values, see figure 6.3.9 with mean $6.00(\pm 2.26)$ min.

In the study by Patryas et al.(2012) using a similar bleach intensity as in this study, the alpha point was found to be $7.96(\pm 2.02)$ min. Significantly longer than the time when

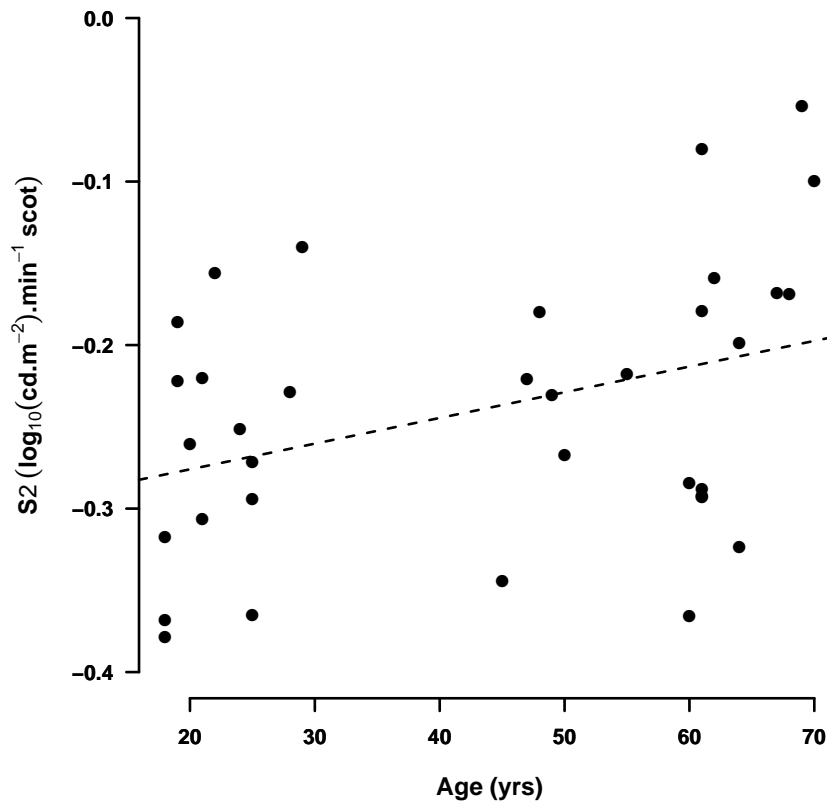


Figure 6.3.8: The effect of age on S2. The dashed line is the linear regression line showing the increase in S2

using the red background ($t = 3.712$, $df = 18$, $p\text{-value} = 0.002$).

Jackson et al.(1999) using a larger sample and conventional method of measurement found the breakpoint to be $14.84(\pm 2.46)$ min following a 98% bleach. Using a similar bleach Owsley et al. (2001) found $15.78(\pm 2.17)$ min. Moreover, Dimitrov et al. (2008) found a mean cone rod break time of $10.40(\pm 2.49)$ min following a 30% bleach, a little over 4minutes longer than in this study. It would seem that the red background reduces the length of the cone phase of recovery.

The relationship between age and alpha point did not reach statistical significance (F-statistic: 1.15 on 1 and 33 DF, $p\text{-value}: 0.3$).

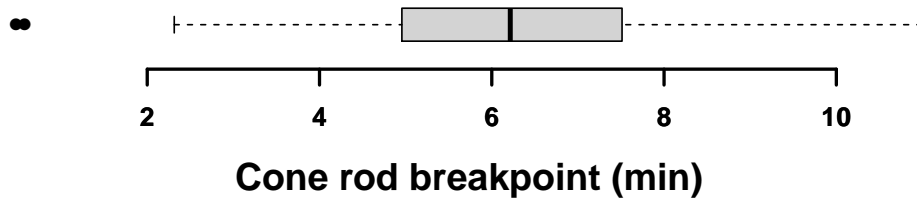


Figure 6.3.9: Box and whisker plots of cone rod breakpoint. Potential outliers, subjects 9 and 29.

6.3.6 The slope of the rod recovery S3: θ_6

The S3 phase, according to Lamb & Pugh (2004), is the result of residual activity of phosphorylated rhodopsin where the slope reflects the removal of phosphate groups from newly regenerated rhodopsin, see section 1.4.1 on page 39. The parameter value θ_6 returned by the algorithm is the sum of the two rod phase slopes, S2 and S3. Therefore the slope of the S3 phase is $\theta_6 - \theta_4(\text{S2})$. The values of S3 were normally distributed (SW: W = 0.96, p-value = 0.3). Mean slope of the S3 phase was $0.47(\pm 0.14) \log_{10}(\text{cd.m}^{-2}).\text{min}^{-1}$. The range was 0.20 to $0.69 \log_{10}(\text{cd.m}^{-2}).\text{min}^{-1}$.

This value is an order of magnitude larger than those in the literature, e.g. Lamb (1981) reports a rate for the S3 phase of $0.06 \log_{10}(\text{units}).\text{min}^{-1}$. This suggests that a different process is at work in this study. A likely candidate is the scotopic luminance of the background and this is considered further in section 6.3.8.

6.3.7 The rod-rod transition point: θ_7 (β)

The rod-rod transition point was normally distributed (SW:W = 0.97, p-value = 0.5) with mean $12.49(\pm 2.80)\text{min}$. These values may not be the β point marking the change from the S2 phase to the S3 phase, but rather the time at which the threshold had fallen to the scotopic luminance of the background and therefore may reflect the S2 distribution rather than the true distribution of β . Further discussion of this point follows.

6.3.8 Absolute threshold

The late phase of rod sensitivity recovery in this study is not comparable with that found by other workers. In this study after the rod-rod transition time, or β point, the rate of sensitivity recovery is much reduced when compared to the recovery during the S2 phase. Flat post β thresholds imply that the slope of S3 = -S2 or $\sim 0.24 \log_{10}(\text{cd.m}^{-2}).\text{min}^{-1}$ this is larger than published values by a factor of four.

This late rod phase may relate to the S3 phase of the typical sensitivity recovery found when dark adaptation recovery is measured without a luminous background. Alternatively the threshold after the β point may relate to the scotopic luminance of the screen.

The photopic luminance of the background (0.05 cd.m^{-2}) with dominant wavelength 655nm can be converted to a scotopic luminance, assuming CIE, using a factor of 0.014 (Wyszecki & Stiles 1967, p104). The scotopic luminance of the background is therefore $-3.15 \log_{10}(\text{cd.m}^{-2} \text{ scot})$.

Threshold at rod-rod transition point

The thresholds at the beta point were found using two methods. In the first method model thresholds were created using the parameters extracted by the algorithm. Then the model threshold at the beta point was selected. This method of calculating the threshold at β uses the best fit model and is influenced by all the data collected. These thresholds were normally distributed (SW = 0.96, p-value = 0.3) with mean $-3.09(\pm 0.44) \log_{10}(\text{cd.m}^{-2} \text{ scot})$ and are shown in figure 6.3.10. The mean is an elevation of 0.06 log units over the background luminance.

The second method used the rod rod transition time parameter extracted by the algorithm to partition the raw data and select the measured threshold at the β point. In figure 6.3.11 this is the first column of thresholds. These values were not normally distributed (SW = 0.88 p-value = 0.004) and had a median value $-3.03 \log_{10}(\text{cd.m}^{-2} \text{ scot})$ and IQR -3.31 to $-2.88 \log_{10}(\text{cd.m}^{-2} \text{ scot})$.

The model thresholds are elevated by 0.06 log units while the measured thresholds are elevated by 0.12 log units at the β point. These findings suggest they there is a small elevation of the rod threshold at the β point.

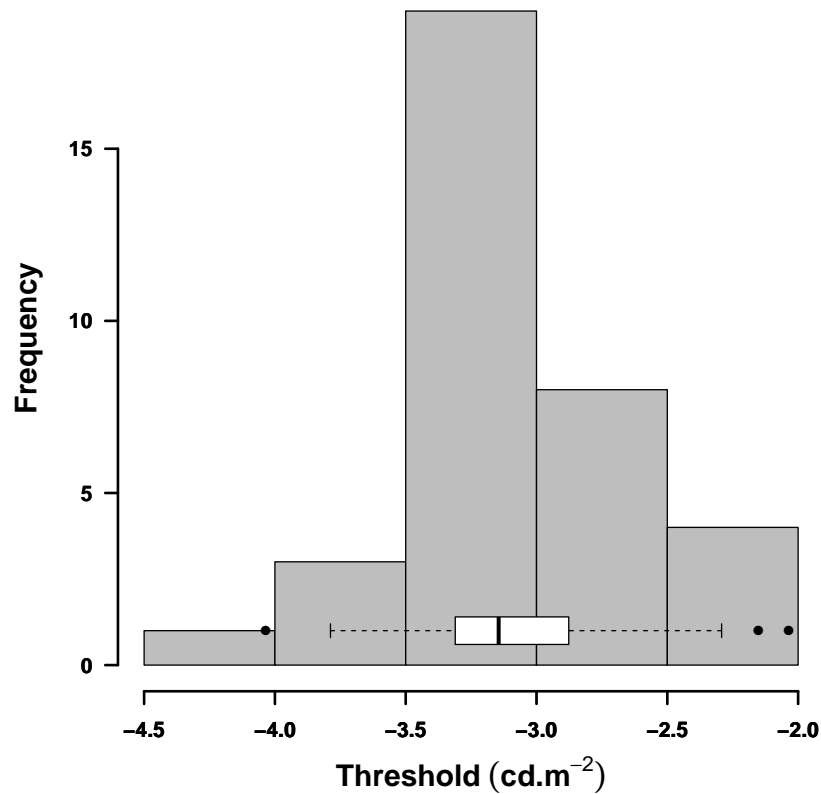


Figure 6.3.10: Distribution of threshold at the rod-rod transition time. Outliers identified as subjects 6, 9 and 24.

Threshold after the rod-rod transition point

The threshold measurements against time after the rod-rod transition (β) point were isolated by partitioning the data as described above. The time after the beta point versus the threshold was subjected to a linear regression and the intercept and slope calculated. In figure 6.3.11 we can see the post β threshold data.

The trend shown by the line of best fit is for the thresholds to approach the scotopic luminance. The linear regression of the pooled data had an intercept at $-2.9 \log_{10}(\text{cd.m}^{-2} \text{scot})$ ($p < 0.001$), the slope of the line of best fit was negative ($-0.01 \log_{10}(\text{cd.m}^{-2}).\text{min}^{-1}$) but not statistically significant ($p=0.2$), the linear model as a whole failed to reach statistical significance (F-statistic: 1.775 on 1 and 559 DF, p-value: 0.2). The null hypothesis that the slope is zero cannot be rejected.

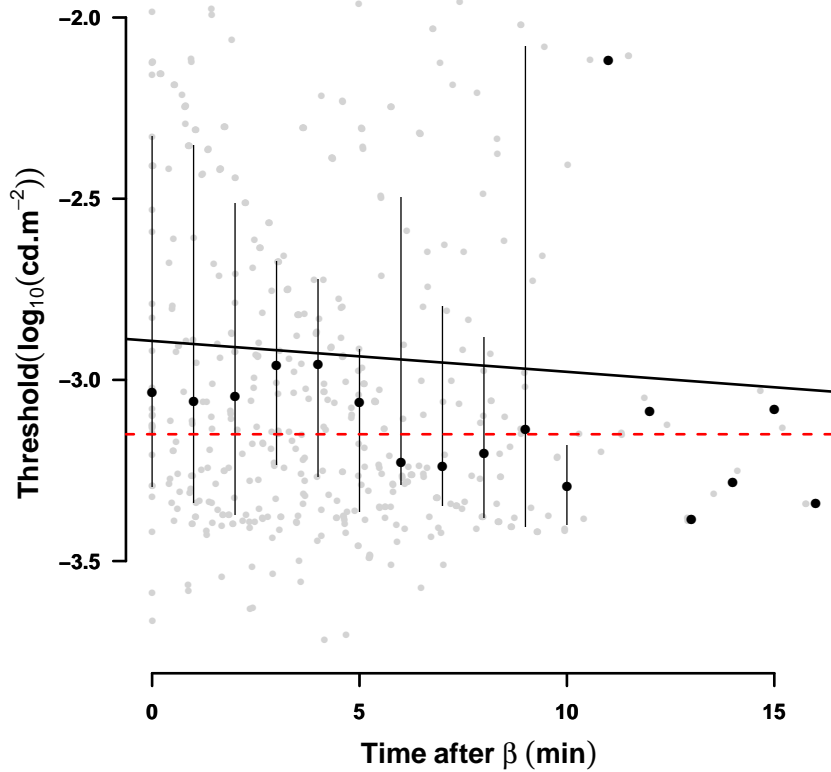


Figure 6.3.11: Post β thresholds. Filled circles are the median values for each minute interval, the vertical lines are the IQR shown for the first 10 minutes only. Upper solid line is the line of best fit to all the data points, the dashed line is the screen scotopic luminance ($3.15 \log_{10}(\text{cd.m}^{-2} \text{ scot})$).

The interquartile range for the data in figure 6.3.11 appears to become smaller with time. There are two possible reasons for this;

- the smaller number of data points with increasing time would lead to smaller IQR.
- the thresholds are converging to some value

The simplest test would be a line of best fit using the number of data points as a weighting factor. This just failed to reach statistical significance (F-statistic: 4.003 on 1 and 15 DF, p-value: 0.06).

To summarise, the threshold after the beta point remains constant with a value offset to the scotopic luminance of the background, this suggests that the post beta phase repre-

sents the screen luminance rather than the S3 phase of rod sensitivity recovery.

The offset may be due to an error of calibration of the apparatus, the CIE values used or a cone rod interaction. An error of calibration of this kind would have an affect on absolute values but not rates of change.

The CIE values used were taken from the 1951 standard and are representative of observers under 30 years. The CIE standard was based on the work of Wald (1945) and Crawford (1949). The two sets of measurements were made using different conditions. Crawford's data, collected by direct visual comparison in a large matching field of low luminance are of particular interest here as a concern is raised by Wyszecki & Stiles (1982, Table I(4.3.2)) that these measurements might be affected by cone activity having an affect upon rod thresholds at long wavelengths.

Cone elevation may in some way be influencing the rod system's sensitivity to the background or to the stimulus. Experiment 1, see section 5.1.8 on page 156, demonstrated that rod elevation was related non-linearly to background luminance.

It is clear however, that the late rod recovery phase in this study is not the S3 phase described by other workers, rather a reflection of the scotopic luminance of the background.

6.3.9 Mean squared error of the data to the fitted model

The mean squared error is the sum of the errors between the data and the best fitting model squared, divided by the number of observations. It was noted in the initial evaluation of the algorithm used to extract the parameter estimates in section 4.1 on page 128 that the range of values for the MSE were unknown. The data collected here provides some insight. The square root of the MSE* is analogous to the input noise in the numerical experiment in section 4.1.

The range of MSE values found for the 35 subjects in this study were 0.002 to 0.18 $\log_{10}(\text{cd.m}^{-2})^2$, the units have no meaning and are omitted from hereon, with an interquartile range of 0.01 to 0.02, see figure 6.3.12. These small values for the majority of subjects (75% < 0.02) are equivalent to input noise less than 0.14 and suggests that the numerical experiment in chapter 4 embraced the full range of possible values.

Potential outliers were identified with a box and whisker plot as subjects 9 and 29.

*the root mean square (RMS)

Subject 9 (see figure G.1.3) has data that the model is inappropriate for, while subject 29 (see figure G.1.10 on page 318) has a poorly defined cone phase and the final rod phase threshold fluctuates markedly.

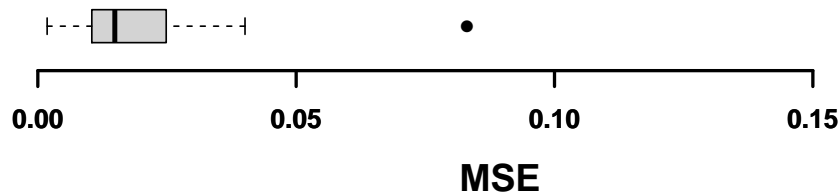


Figure 6.3.12: Box and whisker plots of MSE. Potential outliers, subjects 6 and 29.

6.3.10 Potential outliers

Outliers were identified by comparison to the median and interquartile range. A datum was defined as a potential outlier if it lay outside the range $\text{median} \pm 1.5 \times \text{IQR}$.

Cone phase outliers

Cone threshold outliers

Examination of the distribution of the cone threshold values suggests that subjects 20, 27, 28 and 29 had values that could be considered outliers. These subjects' data are characterised by atypical cone phases and are shown in detail in figure 6.3.13.

Subject 20 has a cone threshold estimated at $-2.63 \log_{10}(\text{cd.m}^{-2})$, this is much lower than the photopic luminance shown by the upper dashed line. In figure 6.3.13 (upper left, a detail taken from G.1.7 on page 315) we can see that there is a small uplift in the cone threshold before the rod phase. The algorithm has fitted a cone threshold much lower than the photopic luminance of the screen and lower than might be fitted by eye. Even by eye the subject has a cone threshold lower than the photopic luminance of the screen. This subject emphasises the point made in section 4.4 on page 139 about the importance of the starting points used in the algorithm and a 'by eye' cross check.

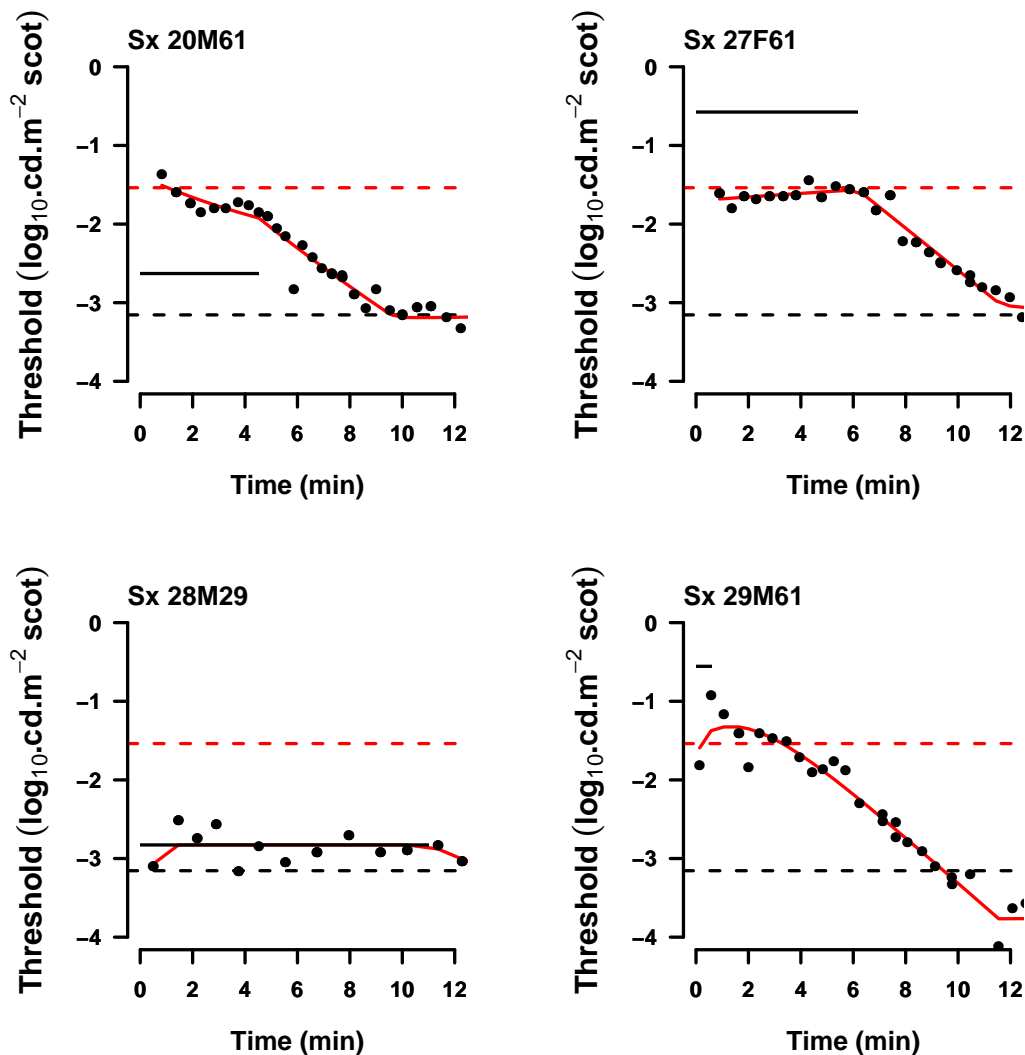


Figure 6.3.13: Detail of cone phase for subjects 20, 27, 28 and 29, whose cone threshold may be outliers. Dashed upper line photopic luminance of background screen, solid line the cone threshold and temporal extent of cone phase. Fitted solid line is the curve of best fit derived using the algorithm, described in section 3.4.1. Lower dashed line the scotopic luminance of the background screen.

Subject 27 (figure 6.3.13, upper right, detail from G.1.9 on page 317) has no cone threshold elevation subsequent to the photo bleach setting thresholds at the photopic luminance at the screen from the beginning of the trial. The algorithm has fitted a negative cone coefficient (-1.3 cd.m^{-2}) to fit the data to the model. A simpler model might be more suitable for this data.

Subject 28 (figure 6.3.13, lower left, detail from G.1.10 on page 318) has experienced no threshold elevation at all, the likely reason for this is that the subject blinked or averted their gaze when exposed to the photo bleach, furthermore, the cone coefficient and time constant returned for this subject are also identified as outliers.

Subject 29 (figure 6.3.13, lower right, detail from G.1.10) has two thresholds that appear to be guesses, at time $t \sim 0$ and $t \sim 2$ minutes. These have the effect of making the cone phase poorly defined. The algorithm returns a very short cone rod breakpoint time.

Cone coefficient outliers

Subjects 12, 13, 25, 26, 28 and 33 were found to have cone coefficient values that could be considered outliers. In figure 6.3.14 the first 12 minutes of each subjects threshold setting is plotted. Subjects 12, 13, 25 and 33 have no cone threshold elevation following the flash apart from the first threshold set. Subject 26 guessed their first threshold and 28 experienced no threshold elevation at all. These subjects' data were fitted by applying either a negative cone coefficient (subject 26 -1.78 cd.m^{-2} see table G.2.1 on page 321) or one larger than $5\log_{10}(\text{ cd.m}^{-2})$ and up to $43\log_{10}(\text{ cd.m}^{-2})$.

Cone time constant outliers

Scrutiny of the time constants suggests that subjects 2,6,16,19,20 and 27 are outliers, their values range from 1.2 to 20.2min.

S2 phase outliers

The slope of the S2 phase was normally distributed and no potential outliers were identified. However, two subjects, 9 and 29, had cone rod transition times of 0.5 and 0.6min respectively and can be described as outliers.

S3 phase outliers

No outliers were identified with the S3 phase of rod recovery.

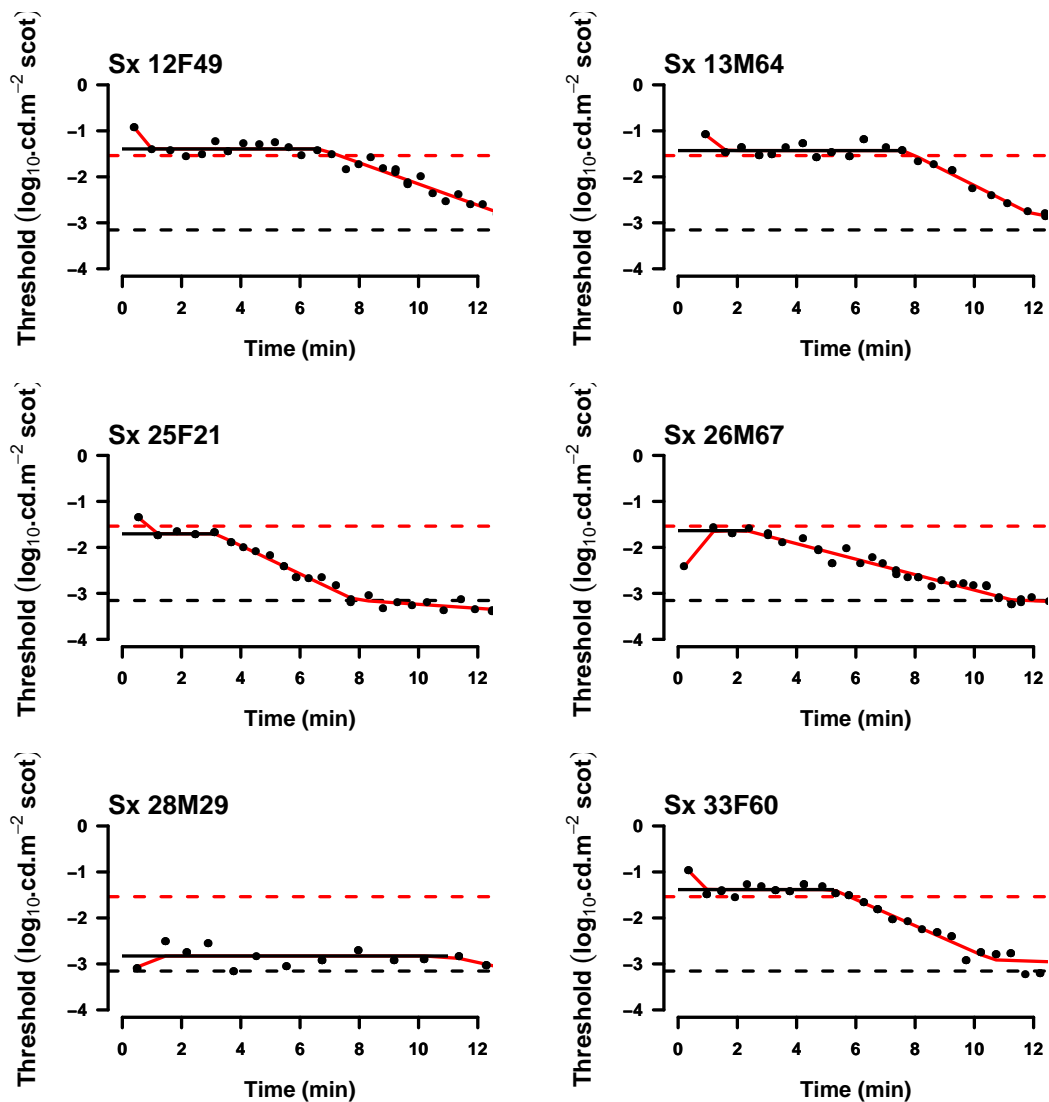


Figure 6.3.14: Detail of cone phase for subjects 12, 13, 25, 26, 28 and 33 with extreme cone coefficient parameters. Dashed upper line photopic luminance of background screen, solid line the cone threshold and temporal extent of cone phase. Fitted solid line is the curve of best fit derived using the algorithm, described in section 3.4.1. Lower dashed line the scotopic luminance of the background screen.

6.4 Variability of data

The test retest values shown in section 6.3.1 reveal no systematic differences between visits, however, there is a large coefficient of repeatability. This means that we cannot say if the values of the S2 slope are different unless they are separated by more than

$0.13 \log_{10}(\text{cd.m}^{-2}).\text{min}^{-1}$. Possible causes for this large CoR fall into two types, methodological failings or physiological unknowns.

There is a possibility that the parameters of dark adaptation fluctuate. Rod physiology is known to vary diurnally (Young 1978). However, this question has not been addressed, neither here nor in the literature. Nevertheless, it has been demonstrated in chapter 5 that the slope of S2 is independent of the background and does not vary significantly between measurements. Other workers have found evidence only of the stability of the rod or S2 phase (Pugh 1975, Christoforidis & Zhang 2011, Dimitrov et al. 2011, Patryas, Parry, Carden, Baker, Kelly, Aslam & Murray 2012). Furthermore, Crawford (1949) found the scotopic system to be stable when repeatedly measured over a year.

Methodological defects include faults in data collection or incomplete photo bleach and have been discussed above. The value of the S2 phase collected in this study and how it changes with age have been shown to be in agreement with other work, suggesting that the technique does measure the recovery of sensitivity following a photo bleach.

The assumptions associated with the model fitting are primarily that the data residuals are identically distributed and independent. In other words the residuals after the model has been fitted have a uniform distribution with constant variance regardless of time and they have no relationship with earlier residuals. Furthermore, it is assumed that the model fitted to the data is valid.

These assumptions are considered below. The data from the first visit only are presented, inclusion of the second visit adds no further information and leaves the analysis open to bias by the characteristics of the returning subset of self selected subjects.

6.4.1 Variance of residuals

The assumptions and suitability of the model can be checked. In chapter 3 the importance of the residuals being independently and identically distributed as well as having constant variance was discussed.

The residuals were found for each subject and the values were coded as belonging to either the cone, S2 or S3 phases based on the estimates for the cone-rod and rod-rod breakpoints. The variances of each phase are summarised in table 6.4.1

Parametric (Bartlett (1937), $p=0.73$) and non parametric (Fligner-Killeen (1981), $p=0.85$) tests of homogeneity of variances found no significant difference in the variance of the

Table 6.4.1: Variance of the residuals as the phase changes

Phase	Cone	S2	S3
Variance	0.171	0.189	0.113

phases. The residuals for each phase were considered, for the cone phase they were not normally distributed (Shapiro $W = 0.79$, p -value = 0.004), however the rod phases S2 and S3 did have normally distributed residuals ($SW = 0.93$, p -value = 0.20). Suggesting that the method of model fitting may have a weakness in the cone phase of measurements. This might be expected since the method of dark adaptation measurement used in this study aims to minimise the cone phase.

Unreliable estimation of the parameters of the cone phase could return unrealistic estimates of the cone threshold, see for example subject 20 in figure 6.3.13, and might affect the estimate of the α point and hence the estimate of the slope of S2.

Possible solutions include; improve the quality of the cone phase data by increasing the dynamic range of the stimulus, assume that the cone threshold is the photopic luminance and set this as a fixed parameter in the model or to use a non parametric model, e.g. one that locates break points, to isolate the S2 phase.

6.4.2 Autocorrelation data

Another assumption used in the nonlinear regression method to determine the parameters of dark adaptation is that the data collected are independent. This can be tested by calculating the correlation between each residual for each threshold measurement and the residual for those 1, 2, 3... prior. The step between residuals is called the lag.

The auto correlation count for each subject was found using the `acf` function in R (Venables & Ripley 2002) and the results are summarised in figure 6.4.1. The method is described fully in section 3.1.2 on page 113.

Count data are expected to have a poisson distribution; a simple test of this would be if the mean equalled the standard deviation of the data, in this case $\mu(1.49) \approx \text{sd}(1.42)$. A Kolmogorov-Smirnov test comparing the count distribution to a poisson distribution found no significant difference ($p=0.6$). A poisson regression is appropriate for count data and was fitted using the `glm` function in R (Chambers, Hastie et al. 1992). The count was plotted against mean time between threshold and found to be statistically significant ($p=0.0002$).

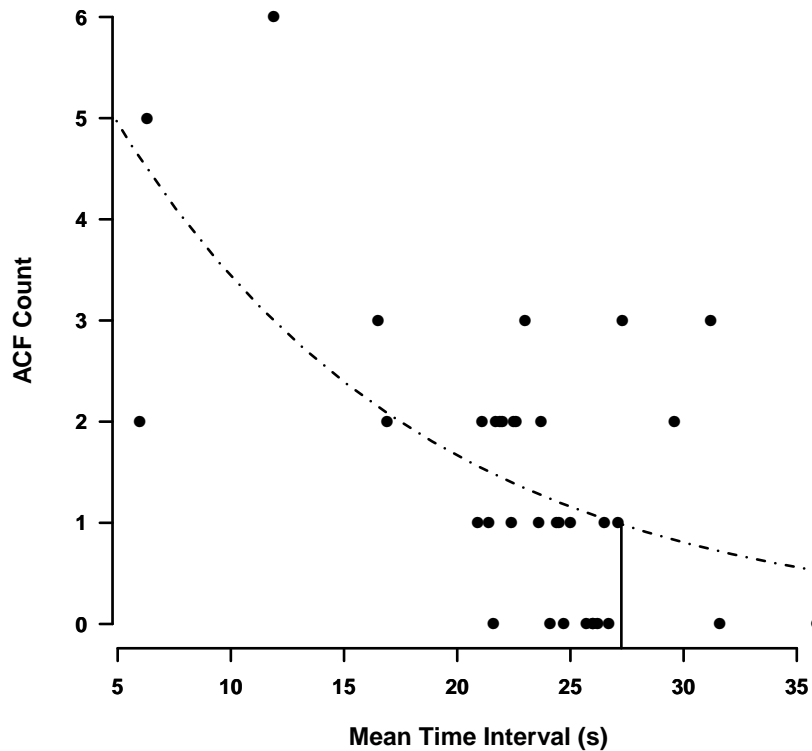


Figure 6.4.1: Auto correlation count against time interval between thresholds. The count falls below one when the interval is greater than ~ 27 s. Dashed line is the poisson regression curve.

Ideally only auto correlation with the residual itself ($\text{lag}=0$) would be preferred, a poisson regression was carried out and the fitted curve was found to return an ACF count ≤ 1 at ~ 27 s. This the time between interval setting rather than the rate of stimulus increase.

This *post hoc* analysis can be criticised since the data were collected without a hypothesis about threshold setting interval. Although subjects were prompted to collect thresholds every thirty seconds, some subjects chose to set thresholds as they wished. Nevertheless, this had the fortunate effect of revealing the phenomenon of auto correlation and suggesting that thresholds should not be set too frequently and providing some indication of how often would be reliable. This question is considered again in section 7.4 on page 225.

6.4.3 Model selection

The appropriateness of the model has been presented as a possible reason for poor estimates of values of the various parameters that describe the recovery of sensitivity, see section 6.3.1. To investigate this the AIC_c was calculated for each subject's data fitted to each member of the family of models described in section 3.2 on page 114. The most appropriate model was defined as the one with the lowest AIC_c score.

If the other models had an AIC_c score within 10 of the best model then they were also considered as candidate models. This rule of thumb for AIC_c values ($\Delta 10$) admits a wide range of candidate models (Burnham & Anderson 2004, p446).

This calculation of AIC_c for each model gave rise to a code for each data set comprised of three numbers, indicating which models could be considered as suitable fits to the data, the codes and their meaning are summarised in table 6.4.2. If no data was available this was coded as '000'.

A tighter criterion of a change of 2 in the AIC_c score was also considered.

Table 6.4.2: Summary of coding for model selection. The columns are described as parameters. The number refers to the complexity of the sub model used.. The left hand column is the code applied to each set of data

	Parameters		
	3	5	7
000			
001			✓
010		✓	
011		✓	✓
100	✓		
101	✓		✓
110	✓	✓	
111	✓	✓	✓

In figures 6.4.2 and 6.4.3 the classification of each data set ($n=72$) from each visit for 36 subjects is summarised for two levels of candidate model selection. In both plots there are 12 data sets, shown in the first column, that were unavailable. The reader will recall that subject 10 withdrew before any measurements could be made, 9 subjects did not return for the second visit and one who did return ceased the experiment early.

Figure 6.4.2 has a liberal criterion for candidate model, i.e. $\Delta 10$. In the second column we see that 43 data sets are best fitted by the seven parameter model alone, however

15 others, columns 3, 4 and 6, can also be reasonably fitted with this model. Fifteen subjects could also be fitted with the five parameter model and 9 could be fitted with the three parameter model. Seventeen datasets could be fitted to more than one model. All three models could be fitted to five subjects.

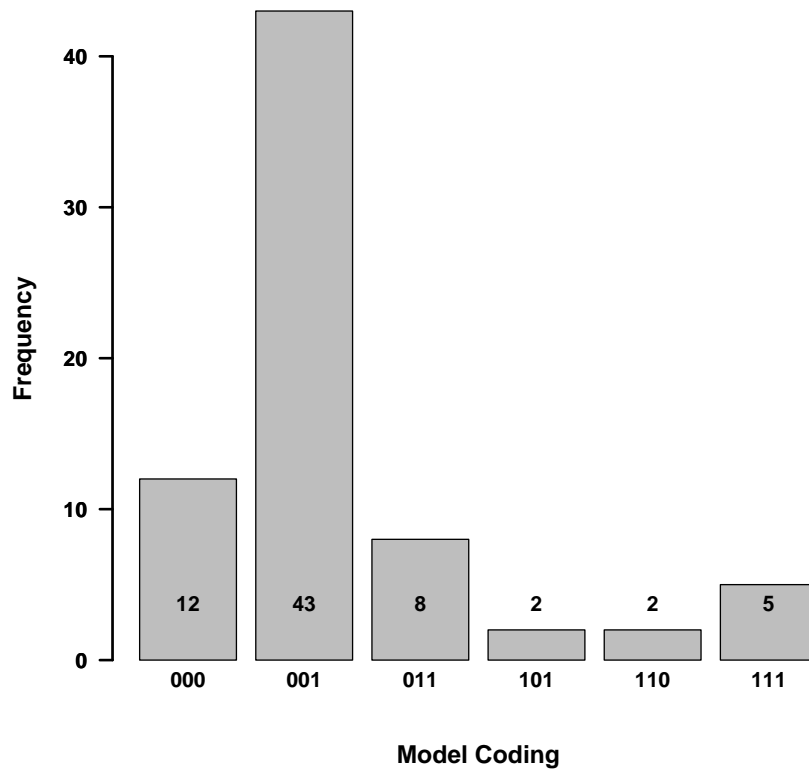


Figure 6.4.2: Frequency plot showing how the data collected can be classified according to which models fit the data, using a liberal criterion, AIC_c difference of less than 10

In figure 6.4.3 a more conservative criterion was used, $\Delta 2$, fifty of the datasets were best fitted with a seven parameter model, a further 8 could be fitted with this model or another. Only one dataset could be fitted with all three models. Ten datasets could be described by more than one model.

This approach can be used to categorise data. Those data labelled by the loose AIC_c comparison as being fitted by only one model might be considered reliable, while those data coded using the conservative criterion as fitting more than one model considered

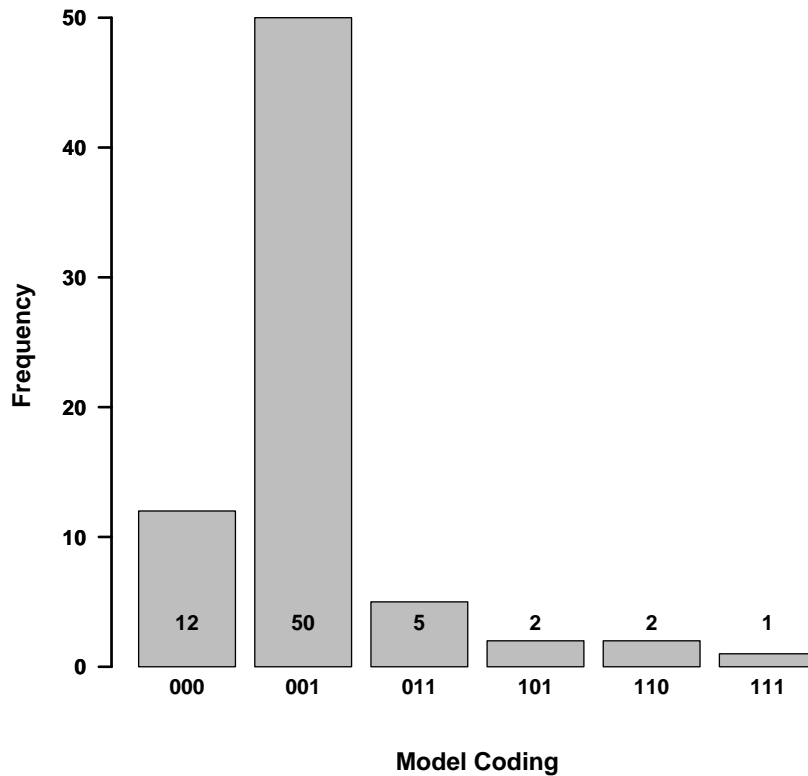


Figure 6.4.3: Frequency plot showing how the data collected can be classified according to which models fit the data, using a conservative criterion, AIC_c difference of less than 2

ambiguous. Using the loose comparison the complex model* only applies to 43 of the 60 available datasets, at best all 58 of the sixty can be fitted by this model. While using the conservative criterion only one data set can be fitted to all three models.

How should this method of model selection be used be used? Consider some data that can be fitted both by the seven and five parameter model. The seven parameter model can be made to fit the data just as well as the five parameter model by allowing the extra two parameters to take exceptional values, e.g any value for the β point and a slope for S3 of zero. Therefore parsimony requires that we select the simplest model that can be fitted to the data.

So for the liberal criterion 43 datasets are best described by a seven parameter model, 8

*seven parameter

by the five parameter model and 9 by the three parameter model. The liberal criterion favours the selection of a simpler model and is to be preferred. The more conservative criterion indicates that 50 datasets are best fit by a seven parameter model, 5 are best fit by the five parameter model and 5 by the three parameter model.

6.5 Discussion and summary

This chapter has described the results of dark adaptation measurements using a red background. The change in threshold with time measured using the techniques described here has a biphasic character. The parameters from the first visit are discussed in detail and the estimates of the slope of the S2 phase are compared for two measurements. The technique presented here of dark adaptation measurement yields useful data about a subject's ability to recover from a photo bleach.

The data found for the slope of the S2 phase are typical of dark adaptation measurements made in the literature, see for example Lamb (1981), McGwin Jr et al. (1999) and Dimitrov et al. (2011). The relationship with age found here is in agreement with that found by other workers. Furthermore, the estimates of the S2 slope are reliable and repeatable and in agreement with other work. The variability in measurements could be reduced by improving the method of threshold setting, in particular making the rate of stimulus increase subject to independent control.

The cone rod breakpoint (α) is shortened by the red background and rod dynamic function can be isolated and examined earlier than has been possible previously.

Analysis of the distributions of the parameter estimates has shown that the cone threshold, cone-rod breakpoint, the slopes of the S2 and S3 phases and rod-rod transition points are normally distributed. The claim in section 3.1.1 on page 111 that the cone coefficient is a fitting variable rather than a physiologic phenomenon is supported by the range of values returned and their distribution.

The cone measurements and the late phase of rod recovery (S3*) are influenced by the red background in a predictable way. The cone threshold and absolute thresholds found reflect the photopic and scotopic luminance of the background respectively rather than physiologic limits.

*in the data presented here it is arguably no longer appropriate to term this phase S3 as it is related to the background luminance rather than a physiologic process in the retinoid cycle

The assumptions made in curve fitting have been discussed. The phenomenon of auto correlated threshold setting was used to tentatively estimate the optimal threshold setting time interval. Moreover, the residuals found after curve fitting were found to have constant variance, with a cautionary note made about the cone phase data.

The purpose of the device is to measure rod function and this has been demonstrated. A further goal is the identification of those subjects with absent or reduced rod function and a method of model selection has been proposed to address this. This also allows for an objective classification of the data and hence description of the rod function.

The description of individual plots in appendix G on page 308 has identified anomalous data. Atypical results have been shown to have at least two causes,

- absent or reduced rod function
 - incorrect model fitted
- incomplete flash

6.5.1 Further work

The apparatus is laboratory based and although many of the experimental conditions are amenable to fine control. Many features are under the control of the subject, e.g. the rate of stimulus increase. A device that allowed for greater control of all the experimental conditions and that was portable would be desirable. This would reduce confounding factors and facilitate the collection of normative data, such a device is described in the next chapter.

The red background allows for the early investigation of rod function. However, it takes 20min to collect the data, which is then subjected to analysis. It is possible that a useful measure of rod function could be found in a shorter time if the data could be analysed as it is collected. This analysis could have two components considered in parallel. An ongoing comparison of the measured thresholds to normative values and fitting of the three nested models described above. The collection of data being halted once some measure of confidence in the fitted model was above a certain level. The halting decision could be either that a value of the slope of the S2 phase has been calculated to a sufficiently accurate tolerance, or that the subject is most likely to have rod function of one of three types: normal, compromised or absent.

From this it follows that collection of normative data is essential if the measurement of dark adaptation is going to be of use clinically.

The problem of incomplete flash is an area for further work. Ideally the photo bleach would be tailored to the subject to provide sufficient light create a rate limited response, i.e. $\approx 20\%$.

A DIGITAL DEVICE TO MEASURE DARK ADAPTATION

When you know better you do better.

Maya Angelou

7.1 Introduction

Conventionally, the kinetics of the change from cone to rod mediated vision are measured by exposing observers to a bright light, called a photo-bleach. The resultant afterimage reduces the sensitivity of the photoreceptors and makes vision difficult. As the afterimage fades, sensitivity recovers and this recovery is measured using a light detected against a dark background. The subject typically pressing a button when the test light is first noticed. The intensity of the test light falls with time.

Some weaknesses were identified in the analogue apparatus; the subject controlled the rate of stimulus increase, was able to set thresholds at intervals of their own choosing and had to control the stimulus control and the mark button at the same time.

The digital apparatus described here as well as being easier for the subject to use offers greater control of stimulus parameters than the analogue apparatus, for example, the interval between measurements and the rate at which the stimulus increases in intensity can be finely controlled. Some features of the device are the same, e.g. the test light is

green flickering at 4Hz against a constant red background. The rods are insensitive to this background but it does have some advantages.

Primarily, the background fixes the level of cone recovery and allows for an accurate estimation of when the switch to rod mediated vision occurs, furthermore, the rate of rod recovery is unaffected by the red background. Once the intensity of the stimulus is below the photopic luminance of the background, only the rods can detect the stimulus. Any further change in stimulus threshold is therefore due to the rod response alone.

7.1.1 Aims

- To test the functionality of the new device using 21 healthy observers
- To compare the data with those obtained from the analogue apparatus
 - the time to the rod cone break
 - slope of the S2 phase
- To examine the effect of stimulus ramp time on the quality of data

7.2 Methods

7.2.1 Description of the device

The device was developed with the help of an industrial partner, Tinsley Instruments and is illustrated in figure 7.2.1. The MPS9000 is normally used to measure macular pigment, but was modified to measure dark adaptation. A detailed description is provided in section 2.6 on page 91.

The instrument is controlled from a PC computer using custom soft- and firmware developed in conjunction with our industrial partner. The software was written in Access (Microsoft, USA) and compiled to machine code to communicate with the main board illustrated in figure 7.2.1. This allows for independent and fine control of the experimental variables. The following parameters of the stimulus and background can be varied;

- background luminance: zero to 0.3 cd.m^{-2}
- background wavelength: either red or green

- initial stimulus intensity
- stimulus luminance range: from zero to 0.5 cd.m^{-2}
- stimulus flicker rate from 1 to 12 Hz
- rate of stimulus increase, or ramp time
- stimulus wavelength; either red or green
- time between stimulus presentations
- stimulus start level following a response.

The parameters of device are controlled by editing a text file either directly or using a graphical user interface (GUI). Further fine control and calibration can be achieved by use of voltage controls and calibration factors accessible through the GUI.

Stimulus intensity (dB) is increased logarithmically from unseen to seen and the rate of increase or ramp time can be varied using the GUI. The software allows for calibration and modification of stimulus, fixation and background intensity, furthermore, the ramp time and test interval can be varied. The full parameter file for this series of measurements is in appendix H.1 on page 325.

The subject looks through the eyepiece at a target board shown in figure 7.2.2. The target had a red (dominant $\lambda = 650 \text{ nm}$) central fixation point and a green (dominant $\lambda = 530 \text{ nm}$) stimulus, the board was illuminated by a red light using the same LED as the fixation point to give a background level of $0.10 \text{ cd.m}^{-2}(\text{phot})$. The stimulus subtended 3° and flickered at 4Hz, when examining the right eye the left hand stimulus was used, this placed the stimulus in the temporal retina, 8° eccentric to the fovea.

At the background used in the analogue device ($0.05 \log_{10}(\text{cd.m}^{-2} \text{ phot})$) the photo bleach was such that stimulus in the digital device was not sufficiently intense for the subject to see the first few presentations and therefore recorded two or three missed thresholds at the beginning of the experiment, by raising the background luminance this shifted the dynamic range. This had two effects; the first few trials were not signalled to the subject as failed and so the subjects were less unsettled, and secondly the opportunity was presented to check that the alpha point was further shortened and that the slope of the S2 phase unaffected.



Figure 7.2.1: The device is seen in the centre of the image and the laptop that drives the controlling software is on the left. The white subject response button is to the right of the device. The main board with control electronics is on the right. Its (red) response button is at the far right.

7.2.2 Measurement technique

The measurement technique is described in detail in section 2.6.3.

7.2.3 Data analysis

Chapters 3 and 4 provide full details of the data analysis. In summary; the apparatus was controlled by custom software written in Access (Microsoft, USA) and installed on a personal computer (Dell, USA) using Windows XP operating system (Microsoft, USA). The software as well as controlling the device recorded the button presses of the subject and created a text file of the time of button press and stimulus attenuation. The text file was subjected to analysis by the algorithm described in section 3.4 on page 123.

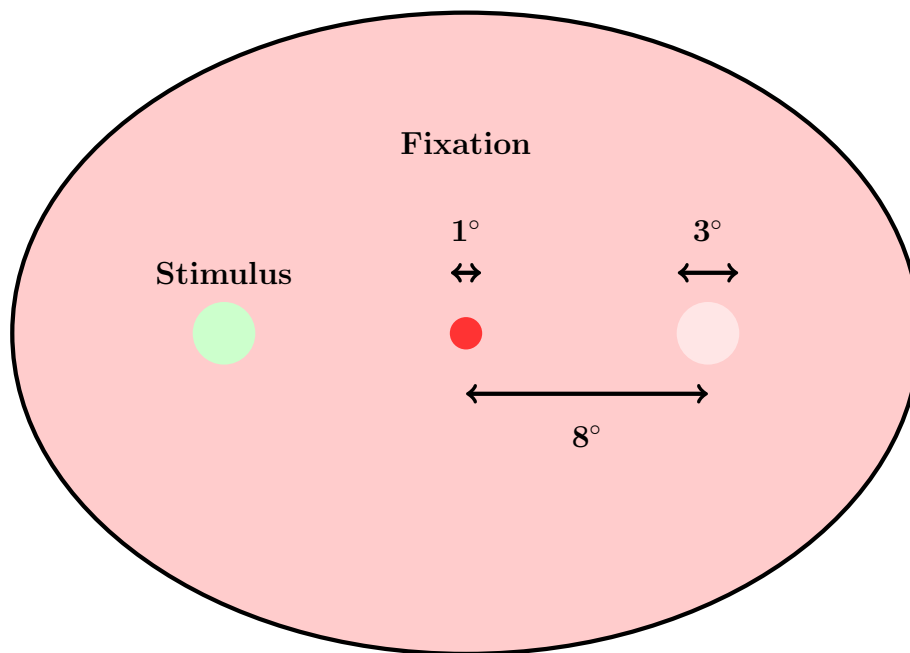


Figure 7.2.2: A schematic view of the target board, the left hand stimulus was used when testing the right eye.

7.2.4 Subjects

Subjects were recruited by a campus wide call for volunteers to staff and students. Twenty one subjects (8 female) were recruited, mean age $38.5(\pm 14.9)$ years the distribution is shown in figure 7.2.3.

There was a disproportionately large number of subjects in the 20 to 30 age group. This was considered acceptable since the aim here was to validate the instrument and a cohort with older subjects may have added age as a confounding factor. Furthermore, the validation of the principle was established with the analogue apparatus.

Grounds for inclusion and exclusion

A subject was considered suitable if they had had an eye examination within the last year and a best corrected acuity of better than 6/9 Snellen. A result was initially considered acceptable if the subject was able to complete the task required, this is discussed further below. A data point more than four standard deviations away from the mean of the remaining group was considered to belong to another distribution.

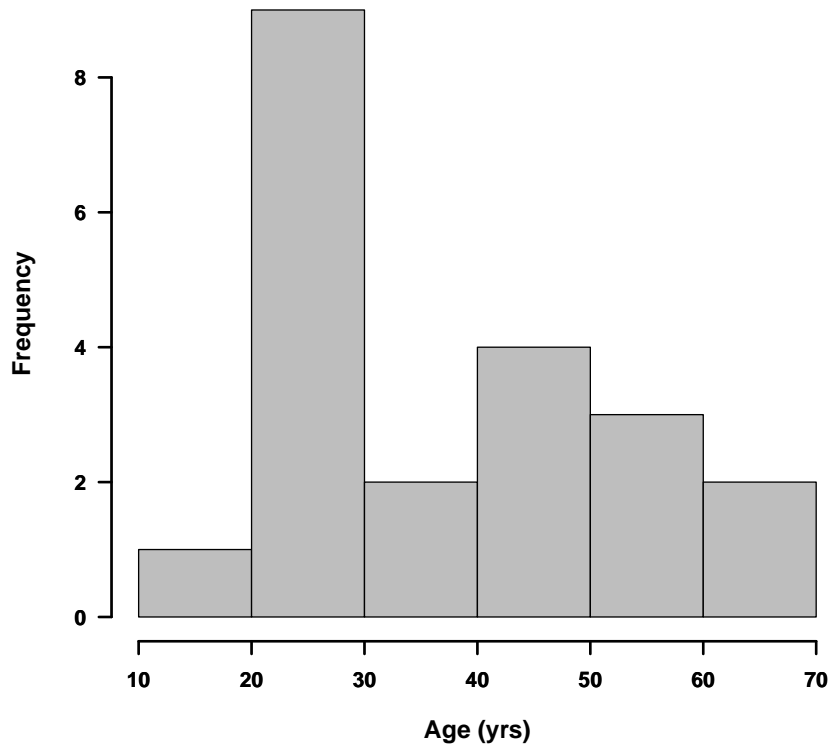


Figure 7.2.3: Age distribution of recruited subjects. Notice the disproportionately large number of subjects in their twenties. It was important that age was not a confounding factor.

Excluded data

Of the twenty one subjects who took part only subject 18 was removed from the analysis. The data returned by this subject, see figure 7.2.4, gave parameters that were non-physiological. The S2 value found was $8 \text{ dB}\cdot\text{min}^{-1}$ this is more than four standard deviations away from the mean of the remaining 20 subjects, the lower bound was $6.36 \text{ dB}\cdot\text{min}^{-1}$ (mean: $2.33 + 4\text{sd}$). Other subjects could perhaps have been excluded but no other parameters for any subject were sufficiently far from the neighbouring values for this to be justified. The data from subject 18 are shown in figure 7.2.4 and suggest that the subject experienced no significant bleach. Thresholds rapidly approached a rod absolute threshold with a period of lapsing after 6min until 8min when threshold setting became more consistent. The parameters found for all the subjects are listed in

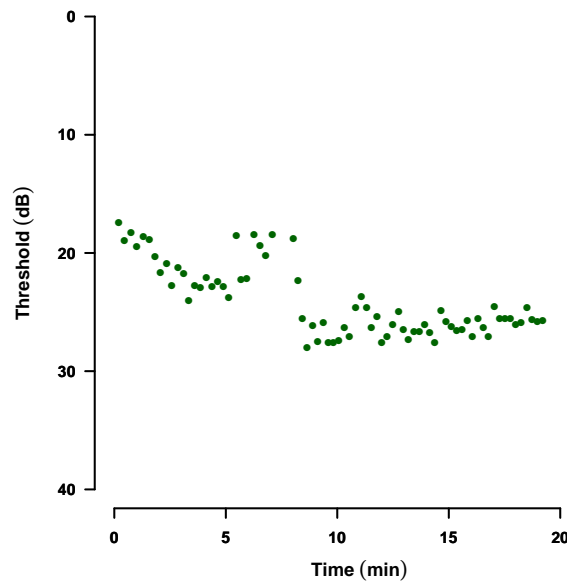


Figure 7.2.4: Data from subject 18, excluded for reasons discussed in the text.

table H.2.1 on page 326

7.3 Results

Following a flash of light the recovery of visual sensitivity follows a characteristic curve and is described elsewhere, for example see chapter 3, where a seven parameter (θ) model is discussed (equation 3.1.2 on page 111) and has been fitted to all the data.

The elements of θ describe various phases of recovery. There is an initial cone recovery phase, encapsulated in elements $\theta_{1,2,3}$, then an early phase of rod recovery called S2 defined by its start time (θ_5), often called the alpha point and by its slope (θ_4). It is this parameter that is of most interest clinically as it reflects the performance and therefore the health of the Choroid-RPE-rod outer segment complex. This is followed by a slower rod phase S3 again defined by its slope, which approaches the absolute threshold and its start time (θ_7) occasionally called the beta point. The value of θ_6 is the sum of the slopes of the S2 and S3 phases.

The pooled data are summarised in figure 7.3.1a and show the characteristic biphasic

appearance found in classic dark adaptation studies. An immediately obvious effect of raising the threshold is the much shortened S2 phase, this will be discussed further below.

Each individual plot is shown in figure 7.3.2. The plots show typical dark adaptation curves and are similar in nature to those found using the analogue apparatus, see figures 6.3.2 and 6.3.3 on page 180.

A few of the plots have features that might be considered anomalous. Cone phase measurements are scarce in subjects 13, 14, 17 and 18. The S2 phase can be easily identified by eye in most subjects with the exception of 18. However, the S2 phase in subject 13 is either delayed following a slow decay in the cone threshold or the S3 phase is faster than the S2 phase.

Not all subjects show a clear late phase of rod recovery, subjects 8, 9 and 20 have S2 phases that were not completed by 20 minutes. Subject 20 has a slow S2 phase rate of recovery $0.7 \text{ dB}\cdot\text{min}^{-1}$. Subjects 3, 17, 19 and 20 have plots that have MSE values greater than 0.02 and examination of the plots verifies this index of noise.

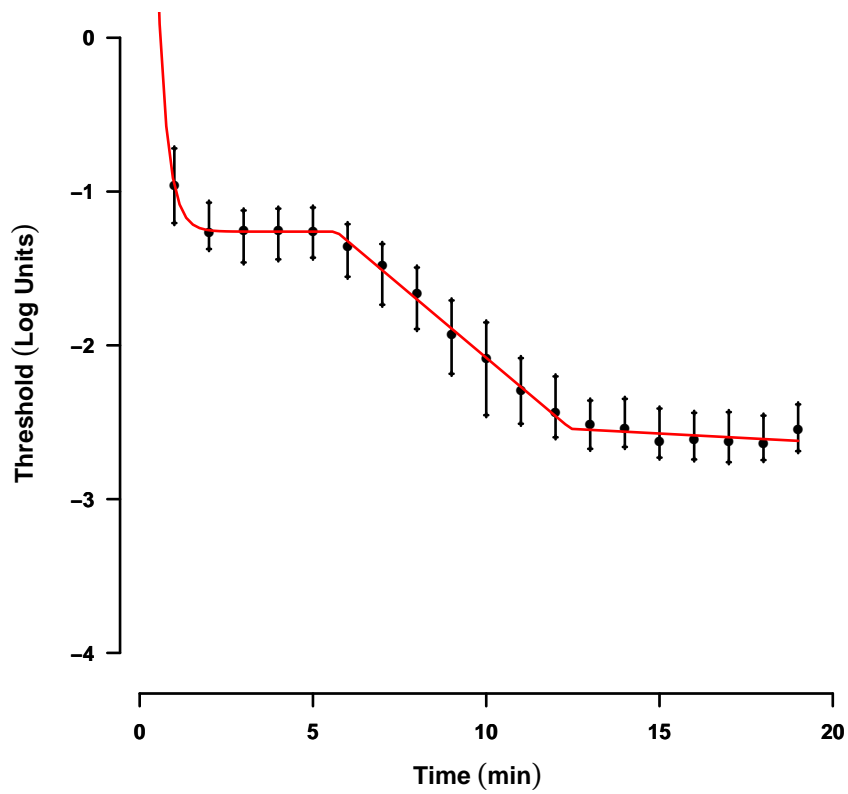


Figure 7.3.1: Summary of all data. The filled circles are the median threshold values for each minute and the vertical bars are the IQR. The solid line is the line of best fit to pooled data.

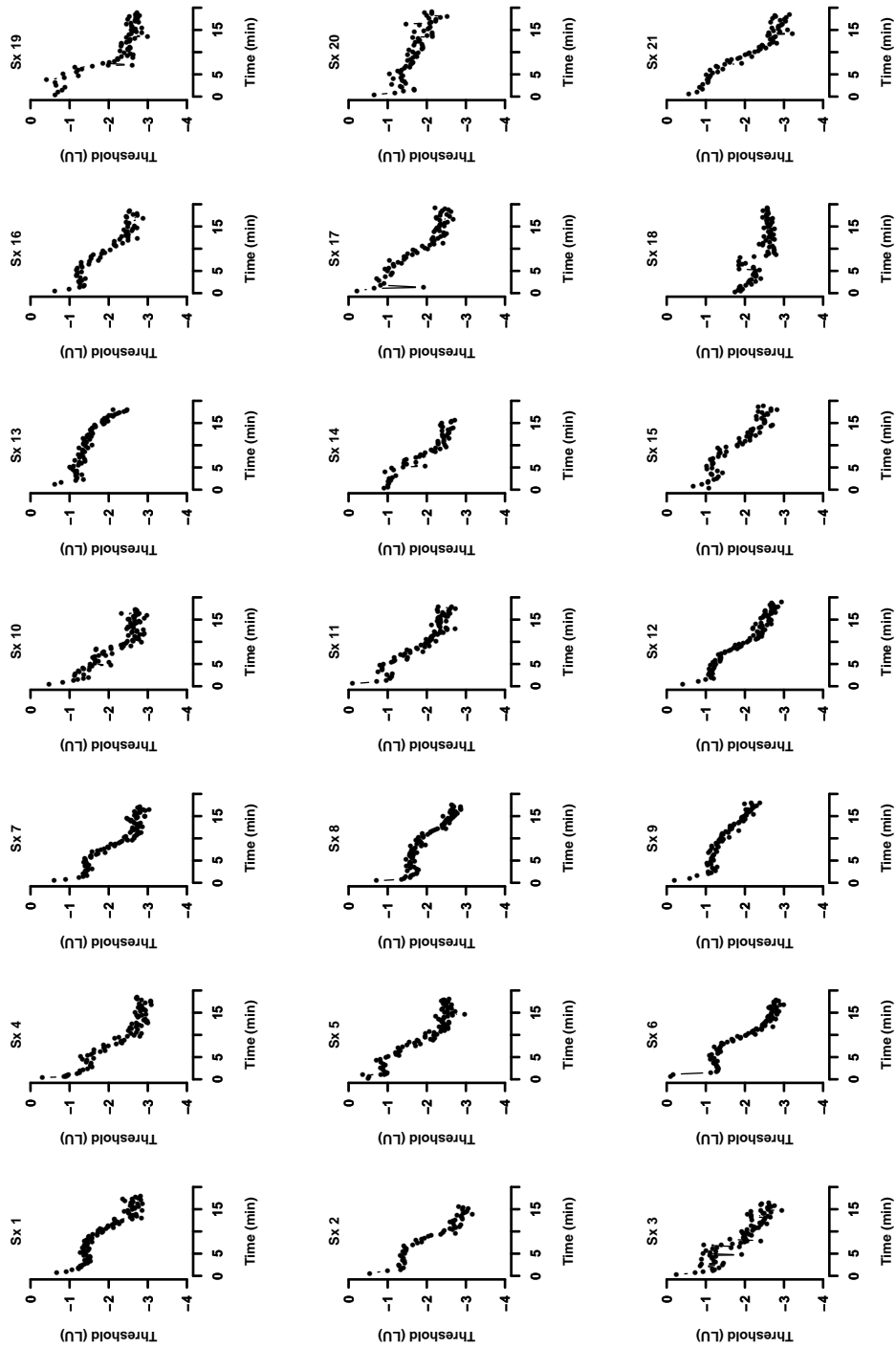


Figure 7.3.2: Individual plots for each subject. Thresholds are in log units (LU = dB/-10)

7.3.1 Parameters of dark adaptation and age

The background has a photopic luminance of 0.10 cd.m^{-2} . The apparatus is calibrated such that thresholds are returned in units of stimulus intensity attenuation (dB)*, rather than scotopic or photopic units. The threshold therefore represents the attenuation required of the stimulus rather than the threshold in units of luminance, because of this it is the distribution of these values that is of interest rather than the absolute values. Absolute values can be assumed by scaling the cone threshold to the photopic luminance of the background.

The values that express a rate of change, the slopes of the two rod phases are independent of the units used and can be converted from one unit to another. In this case $\text{dB.min}^{-1}/-10$ is equivalent to $\log_{10}(\text{cd.m}^{-2}).\text{min}^{-1}$.

Table 7.3.1: Summary of the parameters of dark adaptation of the retained subjects (n=20). The upper three rows describe the distributions. Left column titles; pN, pS, pK are the probabilities that these values came from a normal distribution, with normal skew and kurtosis respectively. The lower six rows describe the central tendency and dispersion of the data. (min minutes, dB deciBels).

pN	0.11	0.00	0.00	0.00	0.26	0.22	0.37	0.90	0.02
pS	0.59	0.03	0.01	0.01	0.99	0.67	0.54	0.78	0.12
pK	0.25	0.00	0.00	0.00	0.79	0.18	0.25	0.93	0.16
	Age	CT	CC	Tau	S2	Alpha	S3	Beta	MSE
	years	dB	dB	min	dB/min	min	dB/min	min	
Min.	18.00	-3.88	-160.00	0.18	0.43	3.99	-8.07	7.90	0.01
1st Qu.	24.00	11.58	-31.99	0.34	1.97	5.14	-5.18	10.57	0.01
Median	35.00	12.46	-20.38	0.56	2.30	5.82	-4.36	11.61	0.02
Mean	38.35	12.19	-31.07	0.84	2.33	6.11	-4.23	11.54	0.02
SD	14.65	4.61	35.53	0.92	1.00	1.43	2.15	1.73	0.01
3rd Qu.	47.75	14.25	-13.50	0.78	2.83	7.41	-3.64	12.36	0.02
Max.	68.00	20.96	-2.56	3.94	4.08	8.59	1.00	14.40	0.04

The distributions are summarised in figure 7.3.3 and table 7.3.1.

*when used for intensity the ratio of powers is in log base ten, when considering amplitude, e.g. contrast it is usual to consider the ratio of the squares hence the 20 multiplier in contrast data (Breitfelder & Messina 2000).

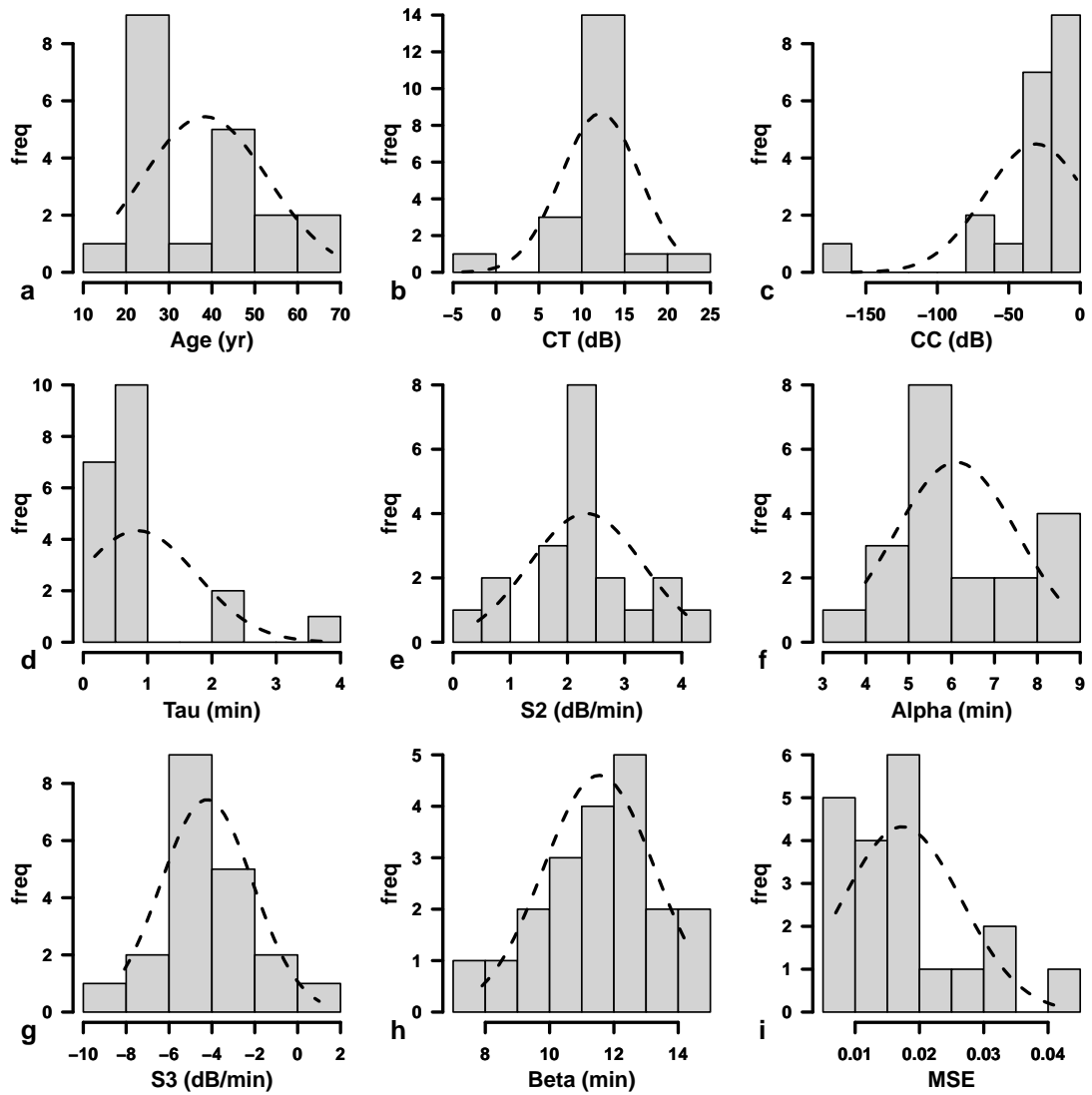


Figure 7.3.3: Summary histograms of the age and parameters of dark adaptation with equivalent normal distributions overlaid from 20 subjects as measured using the digital device.

Age

The distribution of ages was not significantly altered by removal of subject 18, see figure 7.3.3a and compare to figure 7.2.3

Cone threshold θ_1 , Exponential Coefficient θ_2 and Cone Time Constant $\theta_3 \tau$

All the parameters describing the cone phase of sensitivity recovery had non-normal distributions see figures 7.3.3b, c and d. The cone threshold had median 12.46dB and IQR 11.58 to 14.25dB, in section 6.3.3 on page 185 it was shown that the cone threshold is related to the photopic luminance of the background. The leptokurtic distribution suggests that this is the case for the digital device also (kurt = 8.9881, $z = 3.5024$, p-value = 0.001). The analogue apparatus had a cone threshold of $-1.65(\pm 0.46)$ cd.m⁻², figure 7.3.4a compares the two distributions, note the analogue data has been converted to dB.

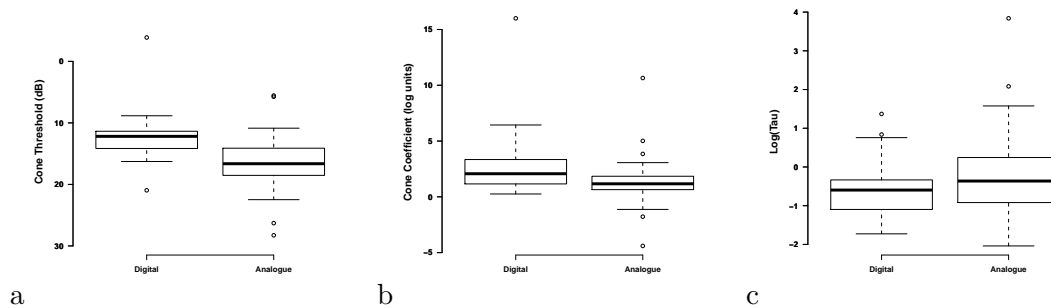


Figure 7.3.4: Boxplot comparison of the cone phase parameters for the digital and analogue apparatus. Plot a, the cone thresholds, plot b, the cone coefficients and plot c the log transformed time constants. Horizontal heavy bar is the median, whiskers are 1.58 times the inter quartile range, shoulders are the 25th and 75th quantiles.

The coefficient of the cone exponent had median -20.dB and IQR of -31.99 to -13.50dB, was left skewed and took non physiological values, see figure 7.3.3c. The analogue device had a median value of 1.23 cd.m⁻²and IQR of 0.67 to 2.03 cd.m⁻². In other words, a threshold elevation of ~ 1.2 to 2 log units. Figure 7.3.4b compares the two distributions. The two distributions are compared in log units, since an elevation of a threshold expressed in log units is more intuitive than dB.

The time constant had median value 0.56min with interquartile range 0.34 to 0.78min, see figure 7.3.3d. The analogue device returned a median value of 0.30 min with IQR 0.17 to 1.12 min. It might be more suitable to transform the time constant data. Time constants of first order biological mechanisms, e.g. the rate of elimination of a compound, which is proportional to the initial concentration, have a log normal distribution (Koch 1966). The values found here are distributed log-normally (after transformation $SW = 0.9287$,

p-value = 0.2). The log transformed values are shown in figure 7.3.4c. The data for the digital device were not significantly different to the time constant values from the analogue apparatus. Whether transformed or not there was no significant difference between the two sets of values ($t = -1.2933$, $df = 35.808$, p-value = 0.2).

The S2 phase: $\theta_{4,5}$

The slope of the S2 phase θ_4 describes the rate at which the rod system recovers its sensitivity following an adapting light. The data were normally distributed, (SW: $W = 0.93$, p-value = 0.3) with a mean value of $2.33 \pm 1.0 \text{ dB} \cdot \text{min}^{-1}$, see figure 7.3.3e. The analogue apparatus found the slope of the S2 phase to be $-0.24 (\pm 0.08) \log_{10}(\text{cd} \cdot \text{m}^{-2}) \cdot \text{min}^{-1}$, see figure 7.3.5a where the two distributes are compared, the analogue data have been converted to dB. There was no significant difference between the two sets of slopes for S2 ($t = 0.2559$, $df = 34.287$, p-value = 0.8).

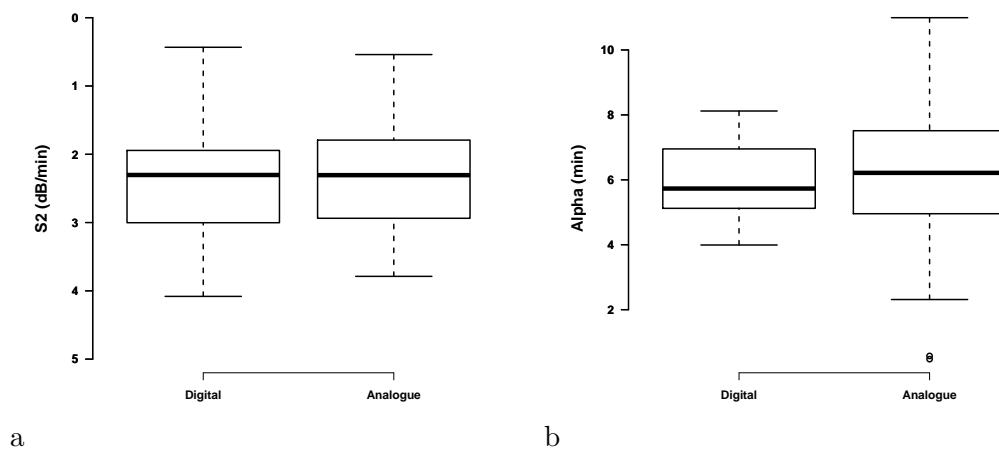


Figure 7.3.5: Boxplot comparison of the S2 phase of rod sensitivity recovery for the digital and analogue apparatus. Plot (a) compares the slopes of the S2 phases, plot (b) compares the cone rod break times.

The values for the slope of S2 for the digital apparatus range from 4.5 to 0.42 $\text{dB} \cdot \text{min}^{-1}$. With subject 18 included subjects 10, 13, 18 and 19 were identified as potential outliers, removal of subject 18 for reasons already discussed, led to subject 3 being identified as an outlier.

The four extreme values for subjects 3, 10, 13, and 19 were 4.0, 4.5, 0.4 and 4.3 $\text{dB} \cdot \text{min}^{-1}$ respectively. The values are within 3 standard deviations of the mean and therefore it would

perhaps be better to classify these values as extrema rather than belonging to another group.

For this small group of 20 subjects the relationship between age and S2 did not reach statistical significance (F-statistic: 1.697 on 1 and 18 DF, p-value: 0.2).

The digital apparatus had a screen luminance of $0.1 \log_{10}(\text{cd.m}^{-2} \text{ phot})$ and the cone rod breakpoint θ_5 data were normally distributed (SW; $W = 0.93$, p-value = 0.2). The mean break point time was $6.11(\pm 1.43)$ min, see figure 7.3.3f. The analogue apparatus had a screen luminance of $0.05 \log_{10}(\text{cd.m}^{-2} \text{ phot})$ and had a cone rod breakpoint time of $6.00(\pm 2.26)$ min. These distributions were not different ($t = 0.2087$, $df = 52.404$, p-value = 0.8) and can be seen in figure 7.3.5b.

The further elevation of the cone threshold for the digital device might reasonably be expected to further reduce the time to the cone rod breakpoint. This has not the case here. A possible reason for this is the youth of the digital group (38.35 ± 14.65 yrs) compared to the analogue apparatus group (43.28 ± 19.6 yrs). Since all subjects were exposed to a uniform flash, 1/4 the maximum intensity, the differences in pupil size and ocular clarity will have an effect on retinal illuminance. A flash through larger pupils with clearer media will admit more light to the retina and effect a more profound photo bleach. This discussed further below.

The S3 phase of recovery: $\theta_{6,7}$

The parameter value θ_6 returned by the algorithm is the sum of the two rod phase slopes, S2 & S3. Therefore $S3 = \theta_6 - \theta_4$. The values of S3 were normally distributed (SW: $W = 0.94$, p-value = 0.37), with mean $-4.23(\pm 2.2)$ dB.min⁻¹ and a range of 1.0 to -8.1 dB.min⁻¹, see figure 7.3.3g. The analogue apparatus returned estimates for the slope of the S3 phase that were normally distributed ($W = 0.9619$, p-value = 0.3) with mean $0.47(\pm 0.14) \log_{10}(\text{cd.m}^{-2}).\text{min}^{-1}$.

The expected range of values for the slope of the S3 phase are from zero to the absolute value of the S2 phase. At the lower end there is no discernible S3 phase, at the higher value the final part of the recovery of sensitivity has a slope of zero. So an S3 value larger than the S2 slope indicates that the threshold is rising, while a negative S3 slope means that the thresholds are falling faster in the S3 phase than they were in the S2 phase. Both situations are physiologically implausible.

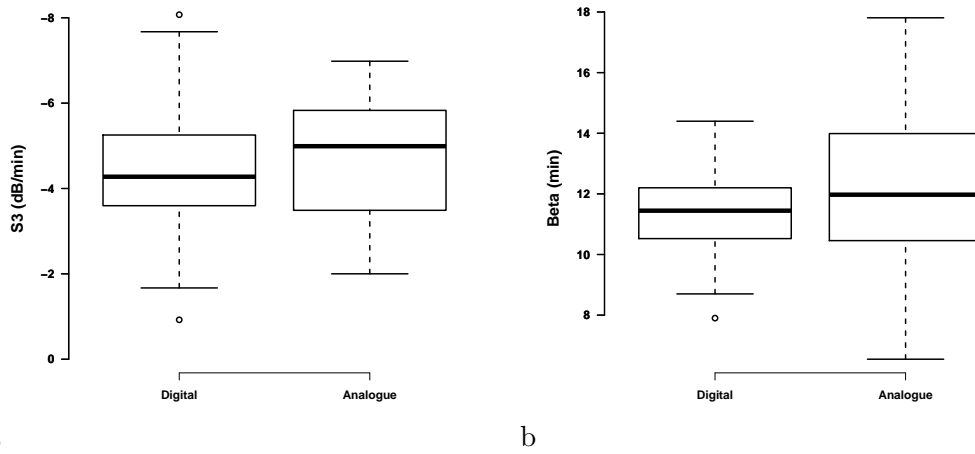


Figure 7.3.6: Boxplot comparison of the S3 phases for the digital and analogue apparatus.

The rod-rod transition point θ_7 was normally distributed (SW:W = 0.96, p-value = 0.9) with mean $11.5(\pm 1.7)$ min, see figure 7.3.3h. The analogue device had β time of $12.5(\pm 2.8)$ min, see figure 7.3.6b for a comparison.

These values may not be the β point marking the change from S2 to S3, but rather the time at which the threshold had fallen to the scotopic luminance of the background and therefore may reflect the S2 distribution rather than the true distribution of β , as was the case in the analogue apparatus mentioned in section 6.3.8 on page 190. Further discussion of this point for the digital data follows.

Threshold after the rod-rod transition point

The threshold measurements against time after the rod-rod transition point θ_7 were subjected to a linear regression and the intercept and slope calculated. See figure 7.3.7

For the pooled data the slope was $0.35 \text{ dB}\cdot\text{min}^{-1}$ and the intercept was 24dB (F-statistic: 41.16 on 1 and 548 DF, p-value: $p < 0.001$). This suggests that the threshold was still changing after the beta point, compare this to the analogue data where no evidence could be found that the threshold varied after the rod rod transition point.

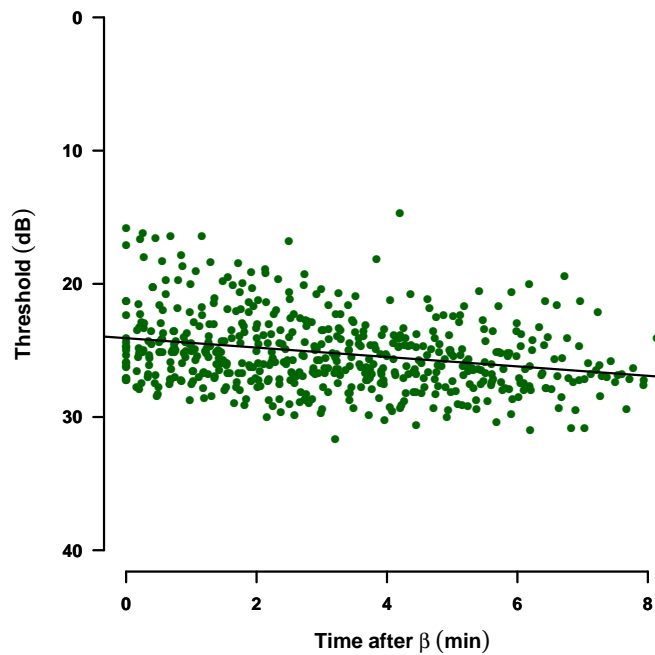


Figure 7.3.7: Threshold after the rod-rod transition point.

7.3.2 Comparison of noise in the data

The mean squared error for the digital device was not normally distributed and had a median value of 0.0159 with IQR of 0.0108 to 0.0204 log units². This is similar to the analogue apparatus median 0.0149 with IQR 0.0105 to 0.0249 log units². A two-sample Kolmogorov-Smirnov* test found that the values of MSE for the analogue and digital methods were drawn from the same population ($D = 0.1857$, $p\text{-value} = 0.7$). The two distributions are shown in figure 7.3.8.

7.3.3 Summary of parameter analysis

The parameters of prime interest in this study are those that reflect rod performance, in particular the slope of the S2 phase of rod recovery. Since this slope can be considered a sensitive marker of retinal health and not just the health of the rod photoreceptor.

*This is a comparison of cumulative distribution functions, and the test statistic (D) is the maximum difference in value.

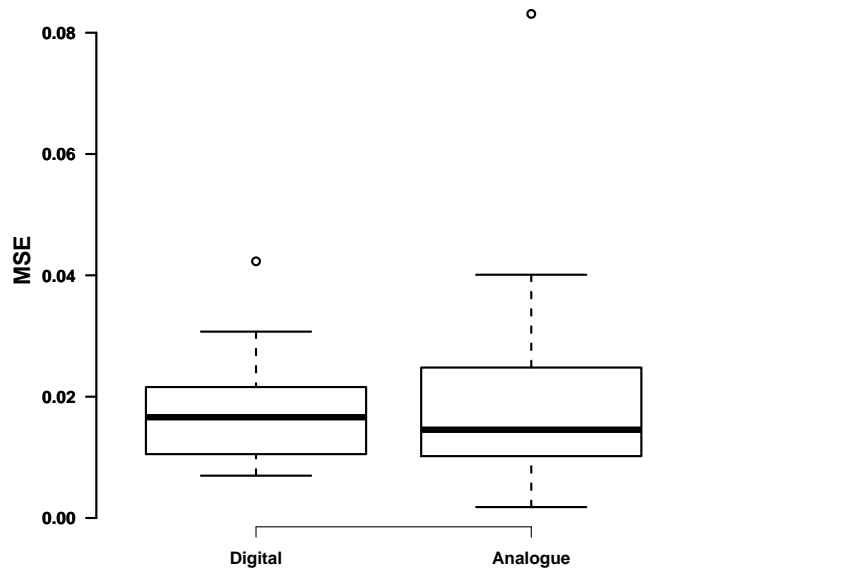


Figure 7.3.8: Comparison of the MSE of the residuals for the data found using the digital and analogue methods.

All the rod parameters had values that were normally distributed and in agreement for both the analogue and digital apparatus. The values for the slope of the S2 phase are similar to those found by the analogue method and values found in the literature, see section 6.3.4. The time to the cone rod breakpoint is not different for the analogue and digital devices, this is followed up in the discussion below. Unlike the analogue data, the post rod rod breakpoint thresholds continued to fall. Suggesting that the thresholds at his breakpoint may be influenced by the activity of the cones, the effect being too small for the dimmer background in the analogue device for it to be seen.

In contrast, the cone parameters of the two devices were not similar. For the analogue apparatus the cone threshold alone was normally distributed, while for the digital device no cone parameters were normally distributed, however, the time constant of the cone recovery was log normally distributed.

The distributions and values of the cone parameters found for the two devices were not equivalent. The differences in the cone threshold can be explained by the increased background intensity used in the digital device. The higher luminance of the background

resulting in less dispersion of the values of the of the cone threshold. The cone coefficient is the theoretical threshold at the instant of the flash discharge and is extrapolated back in time to $t = 0$. It is therefore dependent upon early measurements of cone phase thresholds, however, the methods used here aim to reduce this phase and may contribute to this parameter being unreliable. It is for this reason that no meaning is attached to the differences in the parameter found between the two methods. A similar argument applies to the the time constant, which is dependant upon the value of the threshold at time zero.

Subject 18 has been discussed above, the following considers other possible anomalous data sets. The above analysis has identified subjects 10, 11, 17 and 19 as having cone parameter values that might be outliers. Figure 7.3.2 show the data for all the subjects. Subjects 10 and 11 have very brief cone phases, subject 17 has one point that appears to anticipate the threshold by at least a log unit while subject 19 has a poorly defined cone phase with many random fluctuations.

Subjects 3, 10, 13, and 19 are identified as having rod parameters that might be outliers. In figure 7.3.2 we can see that subjects 3 and 10 have very noisy data. Subject 13 has an S3 phase that appears to recover faster than the S2 phase. The importance of the transition times is emphasised by subject 19, at the cone rod transition (α) there are some elevated points perhaps due to a lapse in concentration, while at the rod-rod transition time (β) there is some anticipation of the threshold.

7.4 Effect of ramp time on data collection

To investigate whether the time taken for the stimulus to increase in intensity had any effect, the dark adaptation curves of the author were measured for six different ramp times, using the standard conditions described above. The ramp time is defined as the time taken for the stimulus to increase from its start value, in this case 10dB to its finish value 0dB.

Measurements were taken using a ramp times of 5, 15, 25, 35, 45 and 55 seconds. The results are summarised in figure 7.4.1.

Auto correlation is the extent to which data are related to each other, in this case the relationship between the residuals of the fitted data to each other is considered. All residual values are compared to those 1, 2, 3.... steps along and if they are related

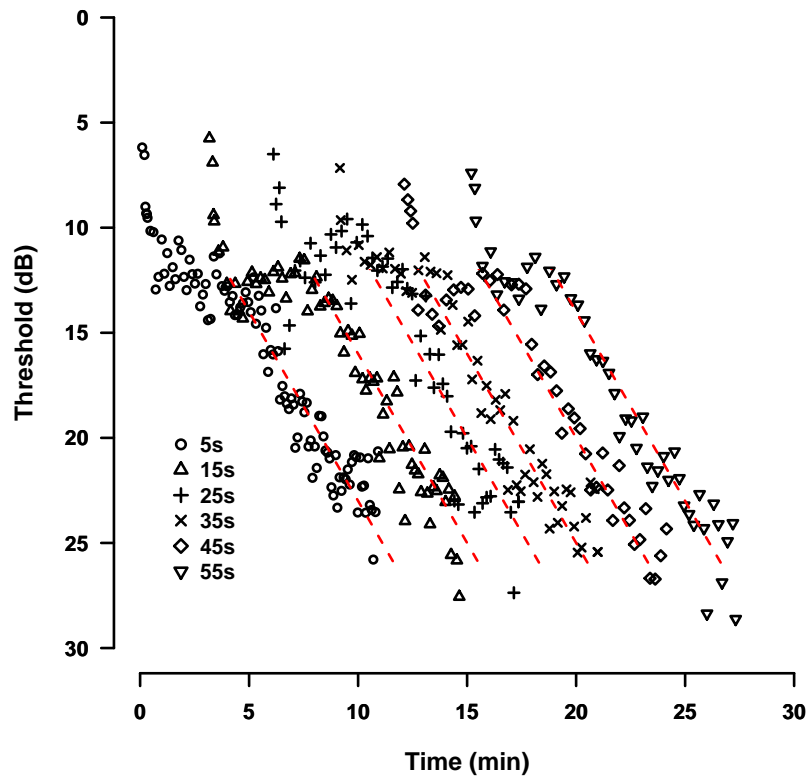


Figure 7.4.1: Dark adaptation curves for different ramp times. The dashed lines are the mean slope of the S2 phase for all the data ($-0.22 \log_{10}(\text{cd.m}^{-2}).\text{min}^{-1}$), fitted to each. Each data set is offset from the next by three minutes.

they yield a correlation coefficient that can have a statistical significance attached to it. Those steps or lags that are significant show how the data measured at one time influence data found at another time. The method is described fully in section 3.1.2. The auto correlation count for each ramp time was found using the `acf` function in R (Venables & Ripley 2002) and the results are summarised in figure 7.4.2. A poisson regression is appropriate for count data (for a discussion of this see Cameron & Trivedi (1998)) and was fitted using the `glm` function in R (Chambers et al. 1992). The model was statistically significant ($p=0.04$).

In figure 7.4.2 the relationship between ramp time and auto correlation count is shown by a dash-dot line, the count falls below 1 when the ramp time is greater than $\sim 11\text{s}$. The analogue data yield a time interval for setting thresholds of $\sim 27\text{s}$. For the analogue

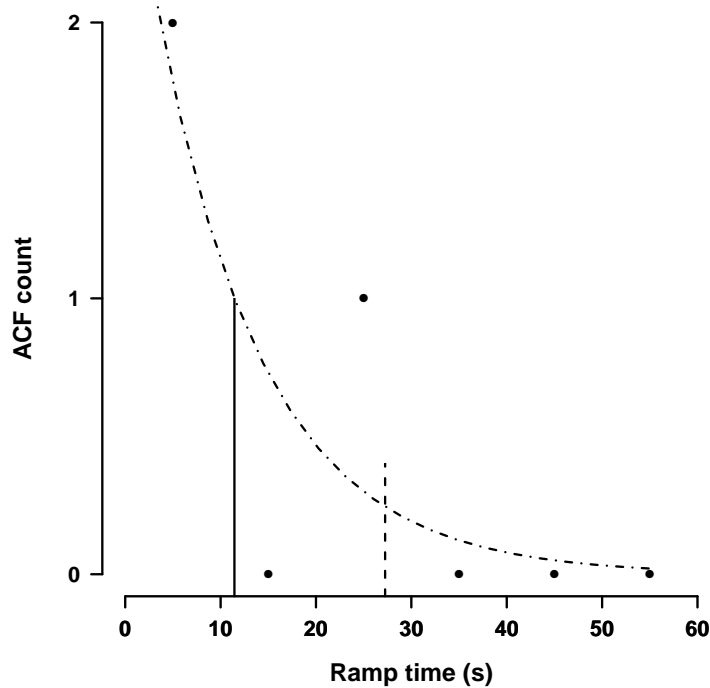


Figure 7.4.2: Poisson regression of the Ramp time to the autocorrelation count data. Solid vertical line at ~ 11.5 s is the ramp time at which the ACF count falls below 1, the dashed vertical line to the right is the same time for the analogue data.

equipment this is the time between measurements not the rate at which the stimulus increases. Furthermore, it is important to remember that the measurements made with the digital apparatus were specifically to investigate the hypothesis that ramp time has no effect. When collecting data with the analogue apparatus the subject was prompted at ~ 30 s intervals, see figure 6.4.1.

7.5 Discussion

It is clear that for this population of observers the instrument performs effectively and yields classical data in agreement with the literature based on conventional techniques, see figure 7.3.2. In some observers, e.g. 9, 13, 18 and 20, the technique did not produce expected data. These subjects have been discussed above.

Only one value of the slope of the S2 phase could be reasonably excluded, the remain-

ing values being normally distributed. Although the relationship between age and S2 rate could not be demonstrated, the values are similar to those found with the analogue device. The digital device had S2 $-0.23(\pm 0.11)$ while the analogue device had S2 $-0.24(\pm 0.08) \log_{10}(\text{cd.m}^{-2}).\text{min}^{-1}$. This is reassuring as the measurements are taken with different sized stimuli in different locations and suggests that a phenomenon that is independent of location is being described, photo-product replenishment.

The dominant wavelength of the background used in this device are slightly different to those used in the analogue apparatus, 650nm here compared to 655nm in the analogue equipment. The change in wavelength will have little effect since the cone threshold is dependent upon the photopic luminance of the background, here set at $0.1 \log_{10}(\text{cd.m}^{-2} \text{ phot})$. Furthermore, sampling the sensitivity of the rod system at a different wavelengths will not yield different rates of recovery, only different absolute values.

The elevation of the background by $0.05 \log_{10}(\text{cd.m}^{-2} \text{ phot})$ will shorten the time to the cone rod breakpoint. Theory suggests by 1.26min, see figure 7.5.1. A further effect is to reduce the dynamic range over which S2 measurements can be made from 1.46 to 1.32 log units, for the analogue ($0.05 \log_{10}(\text{cd.m}^{-2} \text{ phot})$) and digital ($0.10 \log_{10}(\text{cd.m}^{-2} \text{ phot})$) apparatus respectively. The net effect is to shorten the time over which the S2 phase can be measured by ~ 1 minute.

It is worth remarking here that the effect of raising the background from $0.05 \log_{10}(\text{cd.m}^{-2} \text{ phot})$ to $0.1 \log_{10}(\text{cd.m}^{-2} \text{ phot})$ on the time to the cone rod breakpoint is small and to demonstrate a statistically significant change would require a much larger sample*.

Subjects It might be argued that the similarity in the parameter estimates between the analogue and digital data is due to there being common subjects (1,2,5,9,16,17 and 18), however subjects 17 and 18 were identified in the analysis above as having problematic data and 18 was excluded, leaving six common subjects. So of the total cohort of 49 only six were common to both, i.e. 35 in the first group and 20 in the second, less six repeats.

*To obtain a power of 0.8 with a two tailed t test and effect size of 0.2(dz) with the variances found here would require a sample size of 195 (Faul, Erdfelder, Lang & Buchner 2007).

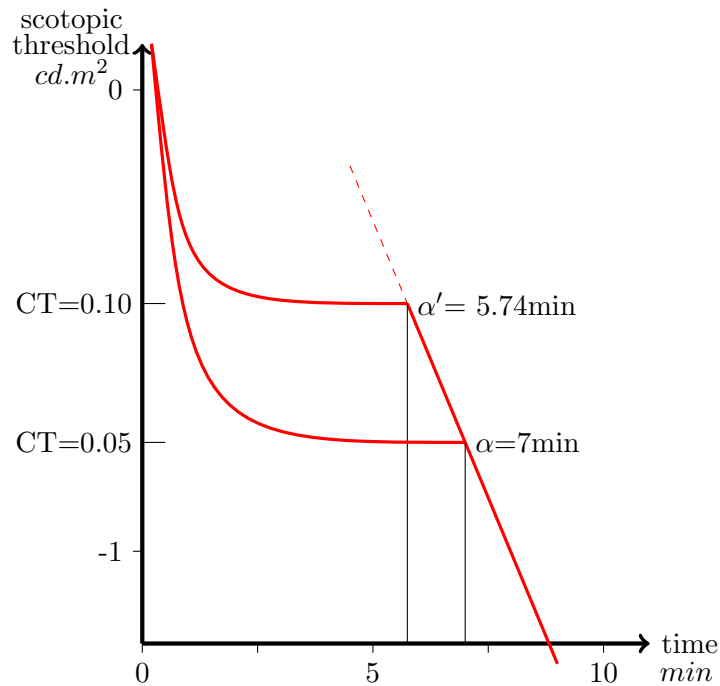


Figure 7.5.1: Detail from the recovery of sensitivity following photo-bleach showing the effect of raising the cone threshold on the cone rod breakpoint, solid curve is the measured threshold, dashed line the underlying rod sensitivity at $-0.24 \log_{10}(\text{cd.m}^{-2}).\text{min}^{-1}$, vertical lines are the cone-rod breakpoint times.

7.5.1 Further work

Directly comparing the cohort that were used to assess the analogue apparatus would have been useful, however, there was a 13 month delay between the two episodes of data collection and although an effort was made to recruit the same subjects this was not always possible.

A larger test group with a uniform age distribution that could be retested would provide normative data and an indication of the repeatability and reliability of the parameter estimates.

The effect of ramp time and the interrelationship between trial intervals and rate of stimulus increase would also be a valuable area of study. The investigation of ramp time and its affect on the auto correlation of threshold measurements suggests that for a healthy subject a ramp time greater than 12s will avoid auto correlation of responses. However, this investigation did not consider the time between threshold setting trials.

The two perhaps should be considered together, since a small elevation in threshold caused by a too rapid increase in stimulus might be countered by an extended time between measurements.

The value of the ramp time used here 30sec, was derived from an arguably flawed *post hoc* analysis of the optimal interval for the analogue data. A shorter ramp time would allow more data to be collected and could need less time to reliably estimate the slope of the S2 phase, however the data collected here was for only one subject with normal rod function. Therefore repeated measurements with a number of subjects with a spread of different ages using different ramp and interval times might yield useful information regarding the optimal set up parameters for a given age.

The possibility that the clearer media and larger pupils of younger subjects leads to a greater photo bleach than in an older subject raises the question of the ideal flash. Is it possible to tailor the flash level to the subject? A step towards this would use normative data about the clarity of the ocular media and pupil size to generate a flash sufficient to bleach more than 20% of the photopigment.

dialectics, as a veteran communist
explained . . . ‘is the art and technique
of always landing on your feet’

Tony Judt

8.1 The aims of the study

Rod mediated dark adaptation is a sensitive marker for the health of the macula and can be summarised by the slope of the S2 phase. This measurement has the potential therefore of being a valuable endpoint in early intervention trails, for example in the treatment of AMD.

To understand rod function within a physiological context, methods of dark adaptation measurement and subsequent model fitting were presented. Once these methods were shown to be robust then the recovery of rod sensitivity was investigated. The aims were as follows:

1. develop a reliable and accurate device to measure rod function in the human
2. derive robust mathematical methods of model selection and parameter extraction

3. investigate methods of confidence interval calculation for parameters derived by numerical methods of non-linear regression
4. calibrate and characterise the components of two devices to measure dark adaptation
5. investigate the parameters of dark adaptation using the above techniques
6. present the results of these investigations

8.2 Main findings

This study has shown that when measuring dark adaptation a dim red background significantly shortens the time to the cone-rod break point. This allows for the examination of the rate of rod mediated dark adaptation sooner than would be the case otherwise. Furthermore the red background has been shown to have no effect on the rate of rod mediated sensitivity recovery.

These two findings can be expected to have a significant impact on the future measurement of dark adaptation. Other workers are trying to shorten the time to a meaningful impaired rod function, for example, by using a conventional method of dark adaptation measurement with a modified protocol (Jackson & Edwards 2008).

8.2.1 Technology

Two novel methods of dark adaptation measurement have been presented. The analogue apparatus is laboratory based and is intrinsically flexible, while the desktop digital device is compact, portable and under computer control. Both can be refined by manipulation of the hardware. The portable desktop device has the potential for generating normative data from population based studies, as well as acting as a clinically useful tool in the evaluation of rod mediated vision.

A population study to generate normative data would be invaluable. Prior knowledge of the parameter distributions would help improve the algorithm used to extract the parameters. While an understanding of the distribution of the S2 phase would be useful in helping to classify subjects as having normal, compromised or absent rod function.

Optimal measurement settings

By considering the noise in the data obtained from these devices a method of determining the optimal rates of stimulus increase and times between presentations has been suggested. The method aims to reduce the auto-correlation between threshold measurements. This has two benefits, firstly, the assumptions required for nonlinear regression are more likely to be met, and secondly any changes in the experimental set up can be tested for their effect in a robust manner.

A further advantage of the digital device is derived from the computer control of the measurement procedure. Since the presentation of the stimulus is defined by the control software, the protocol of stimulus presentation can be reconstructed as a computer model. The benefit of this is that we can test the effect of varying the various parameters of measurement for a ‘standard observer’ (SO). This standard observer can be given a number of characteristics, e.g a threshold function typical of a certain age.

Furthermore, the psychometric performance of the SO can be defined, in other words, the lapse and guess rate, along with the sensitivity to local elevation of threshold can be defined. The parameters of the digital device; ramp rate, step down, interval, etc. can be optimised for each standard observer using Monte Carlo methods, Wichmann & Hill (2001) discuss Monte Carlo methods and the psychometric function further. The stimulus specifications are described in section 2.6 on page 91.

The psychometric function used for the standard observer can, initially, be derived from the measurements already collected, perhaps by using the method described in Treutwein (1995). As the normative data set grows the standard observer can be modified, and hence the utility of the optimal settings for the digital device will improve.

Artefacts of the methodology

In figure 8.2.1 we can see a simulation of measurements made using the digital device. This figure was created by assuming a seven parameter threshold model, the code for this figure is listed in appendix A.2.3 on page 279.

Each plot in the figure represents a different ramp rate, or time for the stimulus luminance to increase by \sim one log unit (9.5dB). The solid line is the ‘true’ threshold, the dashed line is the model of best fit to the threshold estimates indicated by the filled circles, the smaller dots represent the intensity of the stimulus at a given time. The oblique bar at

2min is the slope of the increase in stimulus intensity.

The only variable for each plot is the ramp time. The ramp time is the time taken to increase the stimulus intensity, in this case, by one log unit. The other parameters controlled by the apparatus, start level, stop level, frequency of stimulus flicker, were constant. The lapse rate and guessing rate were also constant with the lapse rate six fold larger than the guessing rate. These rates are arbitrary, but illustrative.

When collecting data the rate of stimulus increase has been indicated as an important factor, due to the exquisite sensitivity of the rod system and the possibility of local adaptation to a lapse in attention by the subject. In the model here there is no modelling of local threshold elevation.

Nevertheless, the very fast ramp time of 5sec in figure 8.2.1a shows signs described in the real data collected; threshold elevation, signs of autocorrelation and increased RMS. The auto correlation is artifactual, since thresholds in this standard observer are independent and identically distributed. Notice that the absolute thresholds are elevated, yet the S2 slope is reliably recorded. The increased noise would have an effect on the confidence interval of the estimate of S2.

A slower ramp time of 55 sec, see figure 8.2.1c allows the rate of lapsing to be come evident, the middle plot 8.2.1b shows the ramp time used in the collection of data in this study. The difference in RMS between 35 and 55 sec is very small and may be insignificant. Further work here though would surely involve the optimisation of the control parameters for a range of lapse and guessing rates. We might expect these rates to have some relationship with age or retinal health.

8.2.2 Data analysis and mathematical methods

To date, analysis of dark adaptation data and classification of recovery curves has relied upon a variety of methods, many chosen for pragmatic rather than theoretical reasons. Principally because computer based methods were inadequate, two examples illustrate this; Jackson et al. (1999) used a four linear model to describe the recovery of sensitivity following a photo-bleach and they excluded data due to the failure of their method to converge. Whereas, Lamb (1981) fitted a series of curves to data from Pugh (1975) by eye.

In this study a group of mathematical methods have been developed. The series of nested

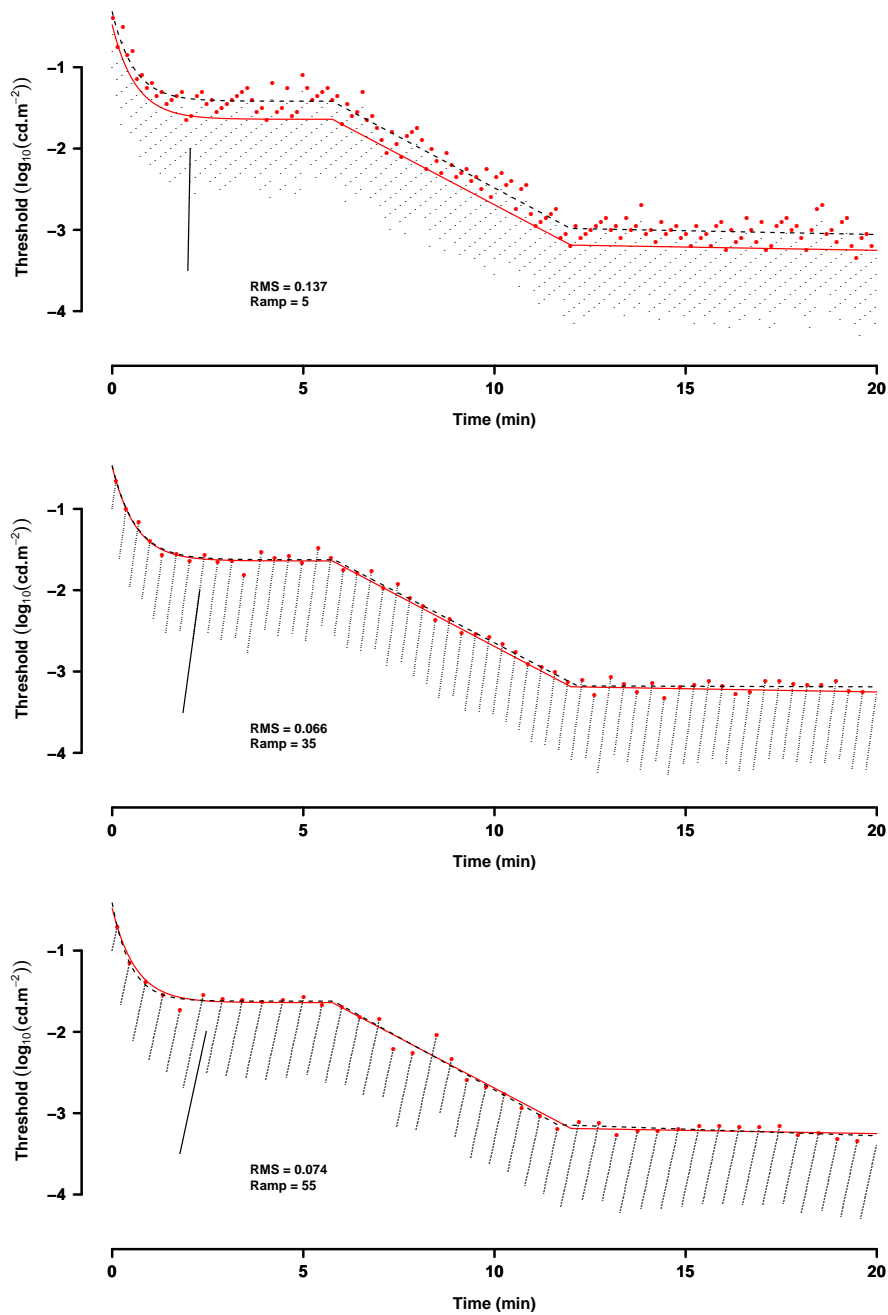


Figure 8.2.1: Simulated data for a standard observer of the digital device. The short oblique bar at 2min shows the rate of stimulus increase. The curve described by a solid line is the 'true' recovery of sensitivity, large filled circles are the threshold estimates at each trial, the dashed line describes the line of best fit to the threshold estimates. The small dots are the time and intensity when the stimulus is on. The simulation tests for each stimulus onset whether the stimulus intensity is greater than the true threshold plus randomly generated confounding factors, lapse and guess.

models and a method of parsimonious selection allow for both subject classification and, in concert with the multi-start algorithm, calculation of a specific value for the early rod phase of recovery. For each subject in a study a method of finding a confidence interval for the estimate of the slope of the S2 phase has also been presented.

None of these methods have been reported, to the authors knowledge, in the dark adaptation literature. Jackson & Edwards (2008) mention differing response curves for subjects with varying levels of macular disease, and suggest that time to threshold is a suitable statistic to classify subjects.

In this study, classification of the subject is based upon the entirety of data collected from the subject. The classification is therefore based on the whole response of the subject rather than one threshold measurement. So, although an arbitrary stopping point may have some merit, a stopping point derived from the multiple datum and having a theoretical basis would be more useful, since it can have an index of reliability, e.g. a level of confidence, attached to it.

Use of test data to evaluate an algorithm

The evaluation of an algorithm using test data and the use of bootstrap methodologies mean that the complexities of nonlinear regression, largely neglected in the literature, can be explored. This will be increasingly important in the future as clinicians become more aware of dark adaptation.

Furthermore, the automated numerical methods of analysis described in this study have shown themselves to be in accordance with values found by labour intensive spreadsheet based methods.

There is still much work to be done on the mathematical methods, in particular unifying the separate elements into one algorithm.

Perhaps, like the apocryphal directions from Hobsbawm (1980) ‘If I were you, I wouldn’t start from here at all’, it might be easier to rewrite the algorithm using all the information learnt about model fitting and selection. As well as the collection of normative data, an investigation of the rates for anticipation and lapse would be important to a future algorithm.

8.2.3 The effect of the red background revisited

The red background as well as elevating the cone threshold, the intended consequence, also has an effect on rod thresholds.

The red background was shown in the ‘on-off’ experiment in chapter four to elevate the absolute rod threshold but not by an amount equivalent to the scotopic threshold, suggesting that the rod response is inhibited by the activity of the cones, see section 5.3.1 on page 161.

However, when looking at the late phase of rod sensitivity recovery, S3, there is a small elevation in the final threshold in the analogue apparatus and in the digital apparatus, which has a higher screen luminance ($0.1 \log_{10}(\text{cd.m}^{-2} \text{ phot})$). This elevation has a relationship with the scotopic luminance and causes the S3 phase for the analogue equipment to be absent while for the digital device it is much reduced.

If the digital data are assumed to have a cone threshold equivalent or lower than the photopic luminance of the background, as was found in the analogue equipment, then the final thresholds of the digital data are elevated by more than the scotopic luminance of the background, see figure 8.2.2a.

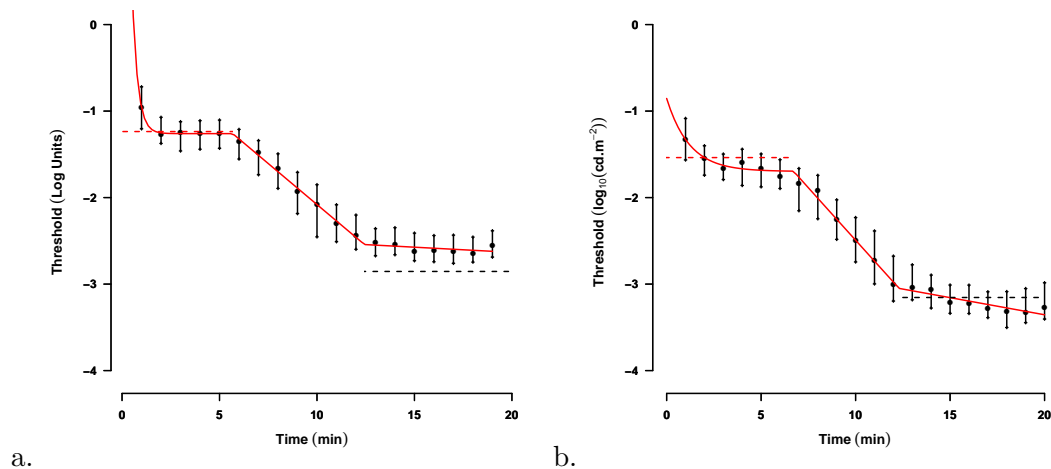


Figure 8.2.2: Comparison of digital (a) and analogue (b) data. The filled circles are the median threshold values for each minute and the vertical bars are the IQR. The solid line is the line of best fit to pooled data. The horizontal dashed lines are the photopic and scotopic luminance of the background, upper line photopic, lower scotopic. Measured for the analogue data and interpolated for the digital. Note that digital thresholds have been converted from dB to log units.

So we have contradictory evidence. The ‘on-off’ experiment was a static assessment of absolute thresholds against a background with two states of luminance and suggests that cones inhibit the rod response. The dynamic measurement of threshold in the continued presence of a red background finds however that there is a summation of response, that is, the threshold suggests that not only do the rods fully see that background but that the cones contribute to the sensation too.

Furthermore, in figure 8.2.2b the cone threshold is below the photopic luminance of the background, suggesting that as the rods recover their sensitivity they contribute to the cone response, before assuming dominance of the sensory percept.

Rod cone interaction mechanisms

What is not clear is whether the rods are detecting the background or the cones are elevating the threshold of the rod photoreceptors, neither is it clear whether rods are contributing to late cone thresholds.

Some things are known however, the reader will recall that the cones are not at their absolute threshold but at some intermediate level. So we have cone signalling at an intermediate level, perhaps even adapting to the background, whilst at the same time rod sensitivity is increasing and using the same post ganglionic pathways as the cones.

The question remains therefore, what, if any interaction is there between the cone and rod mechanisms? The two systems are known to share common neural pathways and have some elements of their retinoid cycles in common. Is it possible psychophysically to investigate this interaction?

BIBLIOGRAPHY

- Abd-El-Barr, M., Pennesi, M., Saszik, S., Barrow, A., Lem, J., Bramblett, D., Paul, D., Frishman, L. & Wu, S. (2009), 'Genetic Dissection of Rod and Cone Pathways in the Dark-Adapted Mouse Retina', *Journal of Neurophysiology* **102**(3), 1945.
- Aguilar, M. & Stiles, W. (1954), 'Saturation of the rod mechanism of the retina at high levels of illumination', *Optica Acta* **1**, 59–65.
- Ahmed, S. (2001), 'Derivative free optimization in higher dimension', *International Transactions in Operational Research* **8**(3), 285–303.
- Akaike, H. (1974), 'A new look at the statistical model identification', *Automatic Control, IEEE Transactions on* **19**(6), 716–723.
- Alexander, K., Fishman, G. & Derlacki, D. (1988), 'Mechanisms of rod-cone interaction: evidence from congenital stationary nightblindness', *Vision research* **28**(5), 575–583.
- Alexander, K. & Kelly, S. (1984), 'The influence of cones on rod saturation with flashed backgrounds', *Vision research* **24**(5), 507–511.
- Alm, A. & Bill, A. (1970), 'Blood flow and oxygen extraction in the cat uvea at normal and high intraocular pressures.', *Acta Physiologica Scandinavica* **80**(1), 19.
- Altman, D. & Bland, J. (1983), 'Measurement in medicine: the analysis of method comparison studies', *The statistician* **32**(3), 307–317.
- Arden, G. & Hogg, C. (1985), 'Rod-cone interactions and analysis of retinal disease.', *British Medical Journal* **69**(6), 404.
- Arden, G., Sidman, R., Arap, W. & Schlingemann, R. (2005), 'Spare the rod and spoil the eye', *British Journal of Ophthalmology* **89**(6), 764.
- Arden, G. & Sivaprasad, S. (2012), 'The pathogenesis of early retinal changes of diabetic retinopathy', *Documenta Ophthalmologica* pp. 1–12.
- Armington, J., Johnson, E. & Riggs, L. (1952), 'The scotopic a-wave in the electrical response of the human retina', *The Journal of Physiology* **118**(3), 289.
- Arshavsky, V. & Burns, M. (2012), 'Photoreceptor signaling: supporting vision across a wide range of light intensities', *Journal of Biological Chemistry* **287**(3), 1620–1626.

- Bartlett, M. (1937), 'Properties of sufficiency and statistical tests', *Proceedings of the Royal Society of London. Series A-Mathematical and Physical Sciences* **160**(901), 268–282.
- Bates, D. & Watts, D. (1988), *Nonlinear regression analysis and its applications*, Vol. 2, Wiley Online Library.
- Baylor, D. (1987), 'Photoreceptor signals and vision', *Invest. Ophthalmol. Vis. Sci.* **28**, 34–49.
- Baylor, D., Lamb, T. & Yau, K. (1979), 'Responses of retinal rods to single photons.', *The Journal of Physiology* **288**(1), 613–634.
- Benimoff, N., Schneider, S. & Hood, D. (1982), 'Interactions between rod and cone channels above threshold: A test of various models', *Vision Research* **22**(9), 1133–1140.
- Bergh, A. & Dean, P. (1972), 'Light-emitting diodes', *Proceedings of the IEEE* **60**(2), 156–223.
- Besharse, J., Hollyfield, J. & Rayborn, M. (1977), 'Turnover of rod photoreceptor outer segments. II. Membrane addition and loss in relationship to light', *Journal of Cell Biology* **75**(2), 507.
- Bill, A., Sperber, G. & Ujiie, K. (1983), 'Physiology of the choroidal vascular bed.', *Int Ophthalmol* **6**(2), 101–107.
- Bland, J. (2005), The half-normal distribution method for measurement error: two case studies. Unpublished talk available on <http://www-users.york.ac.uk/~mb55/talks/halfnor.pdf>.
- Bland, J. & Altman, D. (1986), 'Statistical methods for assessing agreement between two methods of clinical measurement', *The Lancet* **327**(8476), 307–310.
- Bland, J. & Altman, D. (1995), 'Multiple significance tests: the Bonferroni method', *Bmj* **310**(6973), 170.
- Blough, D. (1958), 'Rise in the pigeon's threshold with a red test stimulus during dark adaptation', *Journal of the Optical Society of America* **48**(4), 274.
- Bok, D. (1993), 'The retinal pigment epithelium: a versatile partner in vision.', *Journal of Cell Science. Supplement* **17**, 189–95.
- Booij, J., Baas, D., Beisekeeva, J., Gorgels, T. & Bergen, A. (2010), 'The dynamic nature of Bruch's membrane', *Progress in Retinal and Eye Research* **29**, 1–18.
- Boulton, M. (2008), 'Aging of the retinal pigment epithelium', *Visual Transduction and Non-Visual Light Perception* pp. 403–420.
- Brainard, D. (1997), 'The psychophysics toolbox', *Spatial vision* **10**(4), 433–436.
- Breitfelder, K. & Messina, D. (2000), *IEEE 100: The Authoritative Dictionary of IEEE Standards Terms*, Vol. 879, 7th ed edn, New York : Standards Information Network, IEEE Press,.

- Brown, A. (1986), 'Scotopic sensitivity of the two-month-old human infant.', *Vision research* **26**(5), 707.
- Bürmen, M., Pernuš, F. & Likar, B. (2008), 'LED light sources: a survey of quality-affecting factors and methods for their assessment', *Measurement Science and Technology* **19**.
- Burnham, K. & Anderson, D. (2004), 'Multimodel inference understanding AIC and BIC in model selection', *Sociological methods & research* **33**(2), 261–304.
- Cameron, A. & Trivedi, P. (1998), *Regression analysis of count data*, Vol. 30, Cambridge University Press.
- Campbell, F. & Rushton, W. (1955), 'Measurement of the scotopic pigment in the living human eye', *The Journal of Physiology* **130**(1), 131.
- Carpenter, J. & Bithell, J. (2000), 'Bootstrap confidence intervals: when, which, what? a practical guide for medical statisticians', *Statistics in medicine* **19**(9), 1141–1164.
- Chambers, J., Hastie, T. et al. (1992), *Statistical models in S*, Chapman & Hall London.
- Chhajed, S., Xi, Y., Li, Y., Gessmann, T. & Schubert, E. (2005), 'Influence of junction temperature on chromaticity and color-rendering properties of trichromatic white-light sources based on light-emitting diodes', *Journal of Applied Physics* **97**, 054506.
- Christoforidis, J. & Zhang, X. (2011), 'Learning effect of dark adaptation among normal subjects', *Graefe's Archive for Clinical and Experimental Ophthalmology* pp. 1–8.
- Conover, W., Johnson, M. & Johnson, M. (1981), 'A comparative study of tests for homogeneity of variances, with applications to the outer continental shelf bidding data', *Technometrics* **23**(4), 351–361.
- Cornsweet, T. (1970), *Visual perception.*, Academic Press.
- Cornwall, M. & Fain, G. (1994), 'Bleached pigment activates transduction in isolated rods of the salamander retina.', *The Journal of Physiology* **480**(Pt 2), 261–279.
- Coxe, S., West, S. & Aiken, L. (2009), 'The analysis of count data: A gentle introduction to poisson regression and its alternatives', *Journal of personality assessment* **91**(2), 121–136.
- Crawford, B. (1949), 'The scotopic visibility function', *Proceedings of the Physical Society. Section B* **62**(5), 321.
- Cronin, T., Raffelsberger, W., Lee-Rivera, I., Jaillard, C., Niepon, M., Kinzel, B., Clérin, E., Petrosian, A., Picaud, S., Poch, O. et al. (2010), 'The disruption of the rod-derived cone viability gene leads to photoreceptor dysfunction and susceptibility to oxidative stress', *Cell Death & Differentiation* .
- Cunea, A. & Jeffery, G. (2007), 'The ageing photoreceptor', *Visual neuroscience* **24**(02), 151–155.
- Curcio, C. & Allen, K. (1990), 'Topography of ganglion cells in human retina', *The Journal of Comparative Neurology* **300**(1), 5–25.

- Curcio, C., Bradley, K., Guidry, C., Kirk, M., Wilson, L., Barnes, S., Kruth, H., Chang, C. & Chang, T. (2002), 'A Local Source for Esterified Cholesterol (EC) in Human Bruch's Membrane (BrM)', *Investigative Ophthalmology and Visual Science* **43**(12), 862.
- Curcio, C., Johnson, M., Huang, J. & Rudolf, M. (2009), 'Aging, age-related macular degeneration, and the response-to-retention of apolipoprotein B-containing lipoproteins', *Progress in retinal and eye research* .
- Curcio, C., Millican, C., Allen, K. & Kalina, R. (1993), 'Aging of the human photoreceptor mosaic: evidence for selective vulnerability of rods in central retina', *Investigative Ophthalmology & Visual Science* **34**(12), 3278.
- Curcio, C., Owsley, C. & Jackson, G. (2000), 'Spare the rods, save the cones in aging and age-related maculopathy', *Investigative Ophthalmology & Visual Science* **41**(8), 2015.
- Curcio, C., Sloan Jr, K., Packer, O., Hendrickson, A. & Kalina, R. (1987), 'Distribution of cones in human and monkey retina: individual variability and radial asymmetry', *Science* **236**(4801), 579.
- D'Agostino, R. (1970), 'Transformation to Normality of the Null Distribution of G1', *Biometrika* **57**(3), 679.
- Davison, A. & Hinkley, D. (1997), *Bootstrap methods and their application*, Cambridge Univ Pr.
- Delaey, C. & Van De Voorde, J. (2000), 'Regulatory mechanisms in the retinal and choroidal circulation', *Ophthalmic Research* **32**(6), 249–256.
- Dieterle, P. & Gordon, E. (1956), 'Standard Curve and the Physiological Limits of Dark Adaptation by Means of the Goldmann-Weekers Adaptometer', *The British journal of ophthalmology* **40**(11), 652.
- Dimitrov, P., Guymer, R., Zele, A., Anderson, A. & Vingrys, A. (2008), 'Measuring rod and cone dynamics in age-related maculopathy', *Investigative ophthalmology & visual science* **49**(1), 55.
- Dimitrov, P., Robman, L., Varsamidis, M., Aung, K., Makeyeva, G., Guymer, R. & Vingrys, A. (2011), 'Visual function tests as potential biomarkers in age-related macular degeneration', *Investigative Ophthalmology & Visual Science* **52**(13), 9457–9469.
- Dodabalapur, A. (1997), 'Organic light emitting diodes', *Solid State Communications* **102**(2-3), 259–267.
- Donaldson, J. & Schnabel, R. (1987), 'Computational experience with confidence regions and confidence intervals for nonlinear least squares', *Technometrics* **29**(1), 67–82.
- Dong, C., Qian, H., McReynolds, J., Yang, X. & Liu, Y. (1988), 'Suppression of cone-driven responses by rods in the isolated frog retina.', *Visual neuroscience* **1**(4), 331.

- Dorey, C., Wu, G., Ebenstein, D., Garsd, A. & Weiter, J. (1989), 'Cell loss in the aging retina. Relationship to lipofuscin accumulation and macular degeneration', *Investigative Ophthalmology & Visual Science* **30**(8), 1691.
- Drum, B. (1981), 'Rod - cone interaction in the dark-adapted fovea', *JOSA* **71**(1), 71–74.
- Efron, B. (1979), 'Bootstrap methods: another look at the jackknife', *The annals of Statistics* **7**(1), 1–26.
- Efron, B. & Gong, G. (1983), 'A leisurely look at the bootstrap, the jackknife, and cross-validation', *American Statistician* pp. 36–48.
- Efron, B. & Tibshirani, R. (1986), 'Bootstrap methods for standard errors, confidence intervals, and other measures of statistical accuracy', *Statistical science* **1**(1), 54–75.
- Faul, F., Erdfelder, E., Lang, A. & Buchner, A. (2007), 'G* power 3: A flexible statistical power analysis program for the social, behavioral, and biomedical sciences', *Behavior research methods* **39**(2), 175.
- Feigl, B., Brown, B., Lovie-Kitchin, J. & Swann, P. (2006), 'Functional loss in early age-related maculopathy: the ischaemia postreceptor hypothesis', *Eye* **21**(6), 689–696.
- Felsenstein, J. (1985), 'Confidence limits on phylogenies: an approach using the bootstrap', *Evolution* pp. 783–791.
- Flamant, F. & Stiles, W. (1948), 'The directional and spectral sensitivities of the retinal rods to adapting fields of different wave-lengths', *The Journal of physiology* **107**(2), 187–202.
- Fox, J. (2008), 'Nonlinear regression and nonlinear least squares. Appendix to An R and S-PLUS Companion to Applied Regression', *Retrieved in April*.
- Fridlich, R., Delalande, F., Jaillard, C., Lu, J., Poidevin, L., Cronin, T., Perrocheau, L., Millet-Puel, G., Niepon, M., Poch, O. et al. (2009), 'The Thioredoxin-like Protein Rod-derived Cone Viability Factor (RdCVFL) Interacts with TAU and Inhibits Its Phosphorylation in the Retina', *Molecular & Cellular Proteomics* **8**(6), 1206.
- Fulton, B. & Rando, R. (1987), 'Biosynthesis of 11-cis-retinoids and retinyl esters by bovine pigment epithelium membranes', *Biochemistry* **26**(24), 7938–7945.
- Fylstra, D., Lasdon, L., Watson, J. & Waren, A. (1998), 'Design and use of the Microsoft Excel Solver', *Interfaces* pp. 29–55.
- Gao, F. & Han, L. (2010), 'Implementing the Nelder-Mead simplex algorithm with adaptive parameters', *Computational Optimization and Applications* pp. 1–19.
- Garron, L. (1963), 'The ultrastructure of the retinal pigment epithelium with observations on the choriocapillaris and Bruch's membrane', *Transactions of the American Ophthalmological Society* **61**, 545.
- Gouras, P. (1968), 'Identification of cone mechanisms in monkey ganglion cells', *The Journal of physiology* **199**(3), 533.
- Gozem, S., Schapiro, I., Ferré, N. & Olivucci, M. (2012), 'The molecular mechanism of thermal noise in rod photoreceptors', *Science Signalling* **337**(6099), 1225.

- Guylmer, R., Luthert, P. & Bird, A. (1999), 'Changes in Bruch's membrane and related structures with age', *Progress in retinal and eye research* **18**(1), 59–90.
- Hahn, L. & Geisler, W. (1995), 'Adaptation mechanisms in spatial vision I. Bleaches and backgrounds', *Vision research* **35**(11), 1585–1594.
- Haimovici, R., Owens, S., Fitzke, F. & Bird, A. (2002), 'Dark adaptation in age-related macular degeneration: relationship to the fellow eye', *Graefe's Archive for Clinical and Experimental Ophthalmology* **240**(2), 90–95.
- Ham, W., Mueller, H., Ruffolo, J., Millen, J., Cleary, S., Guerry, R. & Guerry, D. (1984), 'Basic mechanisms underlying the production of photochemical lesions in the mammalian retina', *Current eye research* **3**(1), 165–174.
- Han, M., Giese, G., Schmitz-Valckenberg, S., Bindewald-Wittich, A., Holz, F., Yu, J., Bille, J. & Niemz, M. (2007), 'Age-related structural abnormalities in the human retina-choroid complex revealed by two-photon excited autofluorescence imaging', *Journal of biomedical optics* **12**, 024012.
- Hecht, S., Haig, C. & Chase, A. (1937), 'The influence of light adaptation on subsequent dark adaptation of the eye', *Journal of general Physiology* **20**(6), 831.
- Hecht, S., Haig, C. & Wald, G. (1935), 'The dark adaptation of retinal fields of different size and location', *The Journal of General Physiology* **19**(2), 321–337.
- Hecht, S., Schlaer, S. & Verrijp, C. (1933), 'Intermittent stimulation by light: II. The measurement of critical fusion frequency for the human eye', *The Journal of General Physiology* **17**(2), 237.
- Hendrickson, A. (2005), 'Organization of the adult primate fovea', *Macular Degeneration. Penfold PL, Provis JM, eds. Heidelberg: Springer-Verlag* pp. 1–20.
- Henson, D. & North, R. (1979), 'Dark adaptation in diabetes mellitus.', *British Journal of Ophthalmology* **63**(8), 539–541.
- Ho, M., Massey, J., Pownall, H., Anderson, R. & Hollyfield, J. (1989), 'Mechanism of vitamin A movement between rod outer segments, interphotoreceptor retinoid-binding protein, and liposomes.', *Journal of Biological Chemistry* **264**(2), 928.
- Hobsbawm, E. (1980), 'The revival of narrative: some comments', *Past and present* pp. 3–8.
- Hollyfield, J. (1999), 'Hyaluronan and the functional organization of the interphotoreceptor matrix', *Investigative Ophthalmology & Visual Science* **40**, 12.
- Holm, E. & Fridericia, L. (1925), 'Experimental contribution to the study of the relation between night blindness and malnutrition', *Am. J. Physiol* **73**, 63–78.
- Howard, C., Tregear, S. & Werner, J. (2000), 'Time course of early mesopic adaptation to luminance decrements and recovery of spatial resolution', *Vision research* **40**(22), 3059–3064.
- Jackson, G. & Edwards, J. (2008), 'A short-duration dark adaptation protocol for assessment of age-related maculopathy', *Journal of ocular biology, diseases, and informatics* **1**(1), 7–11.

- Jackson, G., Owsley, C. & McGwin, G. (1999), 'Aging and dark adaptation', *Vision research* **39**(23), 3975–3982.
- Jackson, G. R., Owsley, C. & Curcio, C. A. (2002), 'Photoreceptor degeneration and dysfunction in aging and age-related maculopathy', *Ageing Res Rev* **1**(3), 381–96.
- Johnson, D. (1999), 'The insignificance of statistical significance testing', *The journal of wildlife management* pp. 763–772.
- Jonas, J., Schneider, U. & Naumann, G. (1992), 'Count and density of human retinal photoreceptors', *Graefe's Archive for Clinical and Experimental Ophthalmology* **230**(6), 505–510.
- Kaplan, E. & Shapley, R. (1986), 'The primate retina contains two types of ganglion cells, with high and low contrast sensitivity', *Proceedings of the National Academy of Sciences* **83**(8), 2755–2757.
- Karwatowski, W., Jeffries, T., Duance, V., Albon, J., Bailey, A. & Easty, D. (1995), 'Preparation of Bruch's membrane and analysis of the age-related changes in the structural collagens.', *British Medical Journal* **79**(10), 944.
- Kelly, J. M. F. & Murray, I. J. (2012), Confidence intervals for dark adaptation via model comparison. Submitted for publication.
- Klein, R., Peto, T., Bird, A. & Vannewirk, M. (2004), 'The epidemiology of age-related macular degeneration', *American journal of ophthalmology* **137**(3), 486–495.
- Kleiner, M., Brainard, D., Pelli, D., Ingling, A., Murray, R. & Broussard, C. (2007), 'Whats new in Psychtoolbox-3', *Perception* **36**(14), 1–1.
- Koch, A. (1966), 'The logarithm in biology 1. Mechanisms generating the log-normal distribution exactly', *Journal of theoretical biology* **12**(2), 276–290.
- Kolb, H. & Nelson, R. (1983), 'Rod pathways in the retina of the cat', *Vision Research* **23**(4), 301–312.
- Kolda, T., Lewis, R. & Torczon, V. (2003), 'Optimization by direct search: New perspectives on some classical and modern methods', *SIAM review* **45**(3), 385–482.
- Kosnik, W., Winslow, L., Kline, D., Rasinski, K. & Sekuler, R. (1988), 'Visual changes in daily life throughout adulthood', *Journal of Gerontology* **43**(3), P63–P70.
- LaCour, M. (2008), 'ACTA-EVER lecture 2007 The retinal pigment epithelium: friend or foe?', *Acta Ophthalmologica* **86**(6), 593–597.
- Lagarias, J., Reeds, J., Wright, M. & Wright, P. (1999), 'Convergence properties of the nelder-mead simplex method in low dimensions', *SIAM Journal on Optimization* **9**(1), 112–147.
- Lamb, T. (1981), 'The involvement of rod photoreceptors in dark adaptation', *Vision Research* **21**(12), 1773–1782.
- Lamb, T. D. (1984), 'Effects of temperature changes on toad rod photocurrents.', *J Physiol* **346**, 557–578.

- Lamb, T. & Pugh, E. (2004), 'Dark adaptation and the retinoid cycle of vision', *Progress in retinal and eye research* **23**(3), 307–380.
- Lamb, T. & Pugh Jr, E. (2006), 'Phototransduction, dark adaptation, and rhodopsin regeneration', *Investigative Ophthalmology & Visual Science* **47**(12), 5138.
- Lambert, J. (1758), 'Observationes variae in mathesin puram', *Acta Helvetica* **3**, 128–168.
- Lange, D. (1954), 'Relationship between critical flicker frequency and a set of low frequency characteristics of the eye', *J. opt. Soc. Am.* *44*, 380 **389**.
- Lee, J., Sundar, V., Heine, J., Bawendi, M. & Jensen, K. (2000), 'Full color emission from II-VI semiconductor quantum dot-polymer composites', *Advanced materials* **12**(15), 1102–1105.
- Leibrock, C., Reuter, T. & Lamb, T. (1998), 'Molecular basis of dark adaptation in rod photoreceptors', *Eye* **12**, 511–520.
- Leveillard, T., Mohand-Said, S., Lorentz, O., Hicks, D., Fintz, A.-C., Clerin, E., Simonutti, M., Forster, V., Cavusoglu, N., Chalmel, F., Dolle, P., Poch, O., Lambrou, G. & Sahel, J.-A. (2004), 'Identification and characterization of rod-derived cone viability factor.', *Nat Genet* **36**(7), 755–759.
- Levine, M., Frishman, L. & Enroth-Cugell, C. (1987), 'Interactions between the rod and the cone pathways in the cat retina', *Vision research* **27**(7), 1093–1104.
- Lewis, R., Torczon, V. & Trosset, M. (2000), 'Direct search methods: then and now', *Journal of Computational and Applied Mathematics* **124**(1-2), 191–207.
- Liang, F. & Godley, B. (2003), 'Oxidative stress-induced mitochondrial DNA damage in human retinal pigment epithelial cells: a possible mechanism for RPE aging and age-related macular degeneration', *Experimental eye research* **76**(4), 397–403.
- Lie, I. (1963), 'Dark adaptation and the photochromatic interval', *Documenta Ophthalmologica* **17**(1), 411–510.
- Lin, L. (1989), 'A concordance correlation coefficient to evaluate reproducibility.', *Biometrics* **45**(1), 255.
- Livny, M., Basney, J., Raman, R. & Tannenbaum, T. (1997), 'Mechanisms for high throughput computing', *SPEEDUP journal* **11**(1), 36–40.
- Lorentz, O., Sahel, J., Mohand-Said, S. & Leveillard, T. (2006), 'Cone survival: identification of RdCVF', *Retinal degenerative diseases* pp. 315–319.
- MacLeod, D. (1972), 'Rods cancel cones in flicker.', *Nature* **235**, 173–74.
- Mahroo, O. & Lamb, T. (2004), 'Recovery of the human photopic electroretinogram after bleaching exposures: estimation of pigment regeneration kinetics', *The Journal of Physiology* **554**(2), 417.
- Makous, W. & Boothe, R. (1974), 'Cones block signals from rods', *Vision Research* **14**(4), 285–294.

- Maloney, C. & Rastogi, S. (1970), ‘Significance test for Grubbs’s estimators’, *Biometrics* **26**(4), 671–676.
- Margrain, T. & Thomson, W. (1997), ‘Recovery of spatial vision during dark adaptation in normal subjects’, *Ophthalmic and Physiological Optics* **17**(6), 509–515.
- Marshall, J., Grindler, J., Ansell, P. & Borwein, B. (1979), ‘Convolution in human rods: an ageing process.’, *British Journal of Ophthalmology* **63**(3), 181–187.
- Masland, R. (2001), ‘The fundamental plan of the retina’, *nature neuroscience* **4**, 877–886.
- Mayer, M., Dougherty, R. & Hu, L. (1995), ‘A covariance structure analysis of flicker sensitivity’, *Vision research* **35**(11), 1575–1583.
- McGwin Jr, G., Jackson, G. & Owsley, C. (1999), ‘Using nonlinear regression to estimate parameters of dark adaptation.’, *Behavior research methods, instruments, & computers* **31**(4), 712.
- McKinnon, K. (1999), ‘Convergence of the Nelder-Mead simplex method to a nonstationary point’, *SIAM Journal on Optimization* **9**(1), 148–158.
- Molday, R. (1998), ‘Photoreceptor membrane proteins, phototransduction, and retinal degenerative diseases. The Friedenwald Lecture’, *Investigative Ophthalmology & Visual Science* **39**(13), 2493.
- Motulsky, H. & Ransnas, L. (1987), ‘Fitting curves to data using nonlinear regression: a practical and nonmathematical review’, *The FASEB journal* **1**(5), 365.
- Mustafi, D., Engel, A. & Palczewski, K. (2009), ‘Structure of cone photoreceptors’, *Progress in retinal and eye research* **28**(4), 289–302.
- Nash, J. C. (1990), *Compact Numerical Methods for Computers. Linear Algebra and Function Minimisation.*, Adam Hilger.
- Nelder, J. & Mead, R. (1965), ‘A simplex method for function minimization’, *The computer journal* **7**(4), 308.
- Nelson, R. & Kolb, H. (1985), ‘A17: a broad-field amacrine cell in the rod system of the cat retina’, *Journal of neurophysiology* **54**(3), 592–614.
- Newsome, D., Huh, W. & Green, W. (1987), ‘Bruch’s membrane age-related changes vary by region’, *Current Eye Research* **6**(10), 1211–1221.
- Nilsson, S., Sundelin, S., Wihlmark, U. & Brunk, U. (2003), ‘Aging of cultured retinal pigment epithelial cells: oxidative reactions, lipofuscin formation and blue light damage’, *Documenta ophthalmologica* **106**(1), 13–16.
- Ohno-Matsui, K., Yoshida, T., Uetama, T., Mochizuki, M. & Morita, I. (2003), ‘Vascular endothelial growth factor upregulates pigment epithelium-derived factor expression via vegfr-1 in human retinal pigment epithelial cells’, *Biochemical and biophysical research communications* **303**(3), 962–967.
- Østerberg, G. (1935), ‘Topography of the layer of rods and cones in the human retina’, *Acta Ophthalmol. (Copenh.)* **6**, 1–103.

- Owsley, C., Jackson, G., Cideciyan, A., Huang, Y., Fine, S., Ho, A., Maguire, M., Lolley, V. & Jacobson, S. (2000), ‘Psychophysical evidence for rod vulnerability in age-related macular degeneration’, *Investigative ophthalmology & visual science* **41**(1), 267.
- Owsley, C., Jackson, G., White, M., Feist, R. & Edwards, D. (2001), ‘Delays in rod-mediated dark adaptation in early age-related maculopathy’, *Ophthalmology* **108**(7), 1196–1202.
- Owsley, C., McGwin, G., Jackson, G., Heimbürger, D., Piyathilake, C., Klein, R., White, M. & Kallies, K. (2006), ‘Effect of short-term, high-dose retinol on dark adaptation in aging and early age-related maculopathy’, *Investigative ophthalmology & visual science* **47**(4), 1310–1318.
- Owsley, C., McGwin, G., Jackson, G., Kallies, K. & Clark, M. (2007), ‘Cone-and rod-mediated dark adaptation impairment in age-related maculopathy’, *Ophthalmology* **114**(9), 1728–1735.
- Parry, N., McKeefry, D. & Murray, I. (2006), ‘Variant and invariant color perception in the near peripheral retina’, *JOSA A* **23**(7), 1586–1597.
- Patek Jr, A. & Haig, C. (1939), ‘The occurrence of abnormal dark adaptation and its relation to vitamin A metabolism in patients with cirrhosis of the liver’, *Journal of Clinical Investigation* **18**(5), 609.
- Patryas, L., Parry, N., Carden, D., Baker, D., Kelly, J., Aslam, T. & Murray, I. (2012), A computer-based technique for assessing rod dark adaptation; age changes, data quality and reproducibility. Submitted for publication.
- Pelli, D. (1997), ‘The videotoolbox software for visual psychophysics: Transforming numbers into movies’, *Spatial vision* **10**(4), 437–442.
- Pierce, K., Premont, R. & Lefkowitz, R. (2002), ‘Seven-transmembrane receptors’, *Nature Reviews Molecular Cell Biology* **3**(9), 639–650.
- Poisson, S. & Schnuse, C. (1841), *Recherches sur la probabilité des jugements en matière criminelle et en matière civile*, Meyer.
- Poole, C. (2001), ‘Low p-values or narrow confidence intervals: which are more durable?’, *Epidemiology* **12**(3), 291.
- Pugh, E. (1975), ‘Rushton’s paradox: rod dark adaptation after flash photolysis.’, *The Journal of Physiology* **248**(2), 413.
- Pugh, E. & Lamb, T. (2000), ‘Phototransduction in vertebrate rods and cones: molecular mechanisms of amplification, recovery and light adaptation’, *Handbook of biological physics* **3**, 183–255.
- R Development Core Team (2010), *R: A Language and Environment for Statistical Computing*, R Foundation for Statistical Computing, Vienna, Austria.
- Ralston, M. & Jennrich, R. (1978), ‘Dud, a derivative-free algorithm for nonlinear least squares’, *Technometrics* **20**(1), 7–14.

- Ramrattan, R., van der Schaft, T., Mooy, C., De Bruijn, W., Mulder, P. & De Jong, P. (1994), 'Morphometric analysis of bruch's membrane, the choriocapillaris, and the choroid in aging', *Investigative Ophthalmology & Visual Science* **35**(6), 2857–2864.
- Rieke, F. & Baylor, D. (1998), 'Origin of reproducibility in the responses of retinal rods to single photons', *Biophysical Journal* **75**(4), 1836–1857.
- Robinson, S. & Hendrickson, A. (1995), 'Shifting relationships between photoreceptors and pigment epithelial cells in monkey retina: implications for the development of retinal topography', *Visual neuroscience* **12**(04), 767–778.
- Rodieck, R. (1965), 'Quantitative analysis of cat retinal ganglion cell response to visual stimuli', *Vision research* **5**(12), 583–601.
- Ruberti, J., Curcio, C., Millican, C., Menco, B., Huang, J. & Johnson, M. (2003), 'Quick-freeze/deep-etch visualization of age-related lipid accumulation in Bruch's membrane', *Investigative Ophthalmology & Visual Science* **44**(4), 1753.
- Ruseckaite, R., Lamb, T., Pianta, M. & Cameron, A. (2011), 'Human scotopic dark adaptation: Comparison of recoveries of psychophysical threshold and erg b-wave sensitivity', *Journal of Vision* **11**(8).
- Rushton, W. (1956), 'The difference spectrum and the photosensitivity of rhodopsin in the living human eye', *The Journal of Physiology* **134**(1), 11.
- Rushton, W. & Powell, D. (1972), 'The rhodopsin content and the visual threshold of human rods', *Vision Research* **12**(6), 1073–1081.
- Sakuragawa, M. & Kuwabara, T. (1976), 'The pigment epithelium of the monkey: Topographic study by scanning and transmission electron microscopy', *Archives of Ophthalmology* **94**(2), 285.
- Scholl, H., Bellmann, C., Dandekar, S., Bird, A. & Fitzke, F. (2004), 'Photopic and scotopic fine matrix mapping of retinal areas of increased fundus autofluorescence in patients with age-related maculopathy', *Investigative Ophthalmology & Visual Science* **45**(2), 574.
- Schultze, M. (1866), 'Zur anatomie und physiologie der retina', *Archiv für Mikroskopische Anatomie* **2**(1), 175–286.
- Sharpe, L., Fach, C. & Stockman, A. (1992), 'The field adaptation of the human rod visual system.', *The Journal of Physiology* **445**(1), 319.
- Sharpe, L. & Stockman, A. (1999), 'Rod pathways: the importance of seeing nothing', *Trends in Neurosciences* **22**(11), 497–504.
- Sharpe, L., Stockman, A. & MacLeod, D. (1989), 'Rod flicker perception: scotopic duality, phase lags and destructive interference', *Vision Research* **29**(11), 1539–1559.
- Singh-Hayreh, S. (1974), 'The choriocapillaris', *Graefe's Archive for Clinical and Experimental Ophthalmology* **192**(3), 165–179.
- Smith, S. (2010), 'Structure and Activation of the Visual Pigment Rhodopsin.', *Annual Review of Biophysics* **39**(in press).

- Spendley, W., Hext, G. & Himsworth, F. (1962), ‘Sequential application of simplex designs in optimisation and evolutionary operation’, *Technometrics* **4**(4), 441–461.
- Spillmann, L., Hendershot, G. & Nowlan, A. (1971), ‘Dark adaptation in rod homologous loci’, *Graefe’s Archive for Clinical and Experimental Ophthalmology* **182**(3), 206–213.
- Stabell, U. & Stabell, B. (1976), ‘Absence of rod activity from peripheral vision’, *Vision Research* **16**(12), 1433 – 1437.
- Stabell, U. & Stabell, B. (1977), ‘Wavelength discrimination of peripheral cones and its change with rod intrusion’, *Vision Research* **17**(3), 423–426.
- Stabell, U. & Stabell, B. (1981), ‘Spectral sensitivity of the dark-adapted extrafoveal retina at photopic intensities’, *JOSA* **71**(7), 841–844.
- Stabell, U. & Stabell, B. (1990), ‘Dark adaptation of foveal cones during the cone-plateau period’, *Scand. J. Psychol* **31**, 212–219.
- Stallman, R. (1999), ‘The gnu operating system and the free software movement’.
- Stiles, W. & Crawford, B. (1932), ‘Equivalent adaptation levels in localized retinal areas’, *Report of a joint discussion on vision* pp. 194–211.
- Stockman, A., Sharpe, L., Zrenner, E. & Nordby, K. (1991), ‘Slow and fast pathways in the human rod visual system: electrophysiology and psychophysics’, *J. Opt. Soc. Am. A* **8**, 1657–1665.
- Strader, C., Fong, T., Tota, M., Underwood, D. & Dixon, R. (1994), ‘Structure and function of G protein-coupled receptors’, *Annual review of biochemistry* **63**(1), 101–132.
- Strauss, O. (2005), ‘The retinal pigment epithelium in visual function’, *Physiological reviews* **85**(3), 845.
- Tansley, K. (1931), ‘The regeneration of visual purple: its relation to dark adaptation and night blindness’, *The Journal of physiology* **71**(4), 442–458.
- Treutwein, B. (1995), ‘Adaptive psychophysical procedures’, *Vision research* **35**(17), 2503–2522.
- Ts’o, M. & Friedman, E. (1968), ‘The Retinal Pigment Epithelium: III. Growth and Development’, *Archives of Ophthalmology* **80**(2), 214.
- Van Der Veen, R., Berendschot, T., Hendrikse, F., Carden, D., Makridaki, M. & Murray, I. (2009), ‘A new desktop instrument for measuring macular pigment optical density based on a novel technique for setting flicker thresholds’, *Ophthalmic and Physiological Optics* **29**(2), 127–137.
- Van Nes, F., Bouman, M. et al. (1967), ‘Spatial modulation transfer in the human eye’, *JOSA* **57**(3), 401–406.
- Venables, W. & Ripley, B. (2002), *Modern applied statistics with S*, Springer.

- Volgyi, B., Deans, M., Paul, D. & Bloomfield, S. (2004), 'Convergence and segregation of the multiple rod pathways in mammalian retina', *Journal of Neuroscience* **24**(49), 11182.
- Von Békésy, Georg and Wever, Ernest Glen (1960), *Experiments in hearing*, Vol. 8, McGraw-Hill New York.
- Wald, G. (1945), 'Human vision and the spectrum.', *Science* .
- Wang, J. & Kefalov, V. (2011), 'The cone-specific visual cycle', *Progress in retinal and eye research* **30**(2), 115–128.
- Wark, B., Lundstrom, B. & Fairhall, A. (2007), 'Sensory adaptation', *Current opinion in neurobiology* **17**(4), 423–429.
- Wichmann, F. & Hill, N. (2001), 'The psychometric function: II. Bootstrap-based confidence intervals and sampling', *Attention, Perception, & Psychophysics* **63**(8), 1314–1329.
- Wright, M. (1995), 'Direct search methods: Once scorned, now respectable', *Numerical analysis* pp. 191–208.
- Wyszecki, G. & Stiles, W. (1967), *Color science*, Wiley New York.
- Wyszecki, G. & Stiles, W. (1982), *Color science*, 2nd edn, Wiley New York.
- Yang, Y., Mohand-Said, S., Danan, A., Simonutti, M., Fontaine, V., Clerin, E., Picaud, S., Léveillard, T. & Sahel, J. (2009), 'Functional cone rescue by RdCVF protein in a dominant model of retinitis pigmentosa', *Molecular Therapy* **17**(5), 787–795.
- Young, R. (1967), 'The renewal of photoreceptor cell outer segments', *Journal of Cell Biology* **33**(1), 61.
- Young, R. (1971), 'Shedding of discs from rod outer segments in the rhesus monkey', *Journal of ultrastructure research* **34**(1), 190–203.
- Young, R. (1978), 'The daily rhythm of shedding and degradation of rod and cone outer segment membranes in the chick retina', *Investigative Ophthalmology & Visual Science* **17**(2), 105.

Appendices

COMPUTER CODE

A.1 Matlab code

A full listing of the algorithm used to extract the parameters of a dark adaptation model.

```
1 function [LeastB,Stats,RestB,Count,B]=JMKDAparamTest(data,DBdata, Graph, BoxP, iter)
3 %% Background
5 % JMF Kelly
6 % March 2011
7 % University of Manchester
9 % reset(RandStream.getDefaultStream);
10 % ensures repeatability of the code.
11 FileName=datestr(now,30); ##ok<NASGU>
12 % used to name figures and to estimate time taken
13 %% Create a series of default values for switches
15 if nargin<5
16     iter =100;
17 end
18 if nargin<4
19     BoxP=0;
20 end
21
22 if nargin<3
23     Graph=0;
24 end
```

```

25 if nargin<2
26     DBdata=0;
27 end
28
29 LeastB=[]; %#ok<NASGU>
30 RestB=[];
31 Stats=[];
32
33 %% Prepare the data
34 % This allows the author to visualise the data while writing the
35 % code.
36 Ind=data(:,1)>=0; % deselect NaN
37
38 x = data(Ind,1);
39 y = data(Ind,2);
40 Count=sum(Ind);
41
42 if DBdata
43     y=y/-20; % converts from dB to log units
44 end
45
46
47 if numel(y)==0; % manage empty data set
48     % important when batch processing real data
49     LeastB=zeros(1,8);
50 elseif sum(y)==0;
51     LeastB=zeros(1,8);
52 else % calculate the values
53
54 %% Create the seed parameter
55 %
56 % Cone phase
57 % b(1) = y(1)-2;      % cone threshold
58 % b(2) = 2.0;        % abscissa
59 % b(3) = 1.0;       % time constant
60 % S2 phase
61 % b(4) = -0.6;      % S2 slope
62 % b(5) = 7+7*rand;  % Alpha break-point
63 % S3 phase
64 % b(6) = 0.2;       % S2 + S3 slope
65 % b(7) = 15+15*rand; % Beta break-point
66 %% The parameters of the model
67 % arbitrarily set using McGwin (1999) values
68 % use JMK value from DPOD type setup
69
70 b(1) = -1.465; % -1;      % cone threshold 20dB
71 b(2) = 19.8; % 1.0;      % abscissa -20
72 b(3) = 1.77; % 0.9;      % time constant

```

```

75 % S2 phase
b(4) = -0.154; % -.105; % S2 slope 2.10
b(5) = 14.21; % a; % Alpha break-point
77 % S3 phase
b(6) = 0.128; % puts slope at zero, S2 + S3 slope 0.4
79 b(7) = 31.4; % 23;

81 %% The models
% pre allocate the variable B
83 B = ones(50,8);

85 % define the model functions

87 funEB = @(b) sum( (y-(b(1)+b(2)*exp(-b(3).*x) ...
89 + b(4).*max(x-b(5),0) ...
+ b(6).*max(x-b(7),0))).^2);
% this returns the sum of the residuals squared.

91 funEBY = @(b,x) (b(1)+b(2)*exp(-b(3).*x) ...
93 + b(4).*max(x-b(5),0) ...
+ b(6).*max(x-b(7),0));
95 % this returns the estimated y values, for a given 'b'.

97 % set some values for 'fminsearch'
99 options = optimset('Display','none');
% ensures that no messages are written
101 % to the command screen and sets all
% others to default

103 %% Estimate parameters

105 ii=1;
107 while ii<iter; % calculate ITER estimates of b
[tempB,sse]=fminsearch(funEB,b*rand,options);
109
111 if tempB(1)<y(end) % indicates cone threshold is
% less than absolute
% rod threshold
113 B(ii,8)=99999;

115 elseif tempB(4)>0 || tempB(4)<-.8; % nonsense value for S2

117 B(ii,8)=99998;

119 elseif tempB(5)>tempB(7)

121 B(ii,8)=99997; % nonsense values for alpha and beta

```

```

123     elseif tempB(5)<0
125         B(ii,8)=99996; % nonsense – Ve value for alpha
127         elseif tempB(3)<0;
129             B(ii,8)=99995; % nonsense – Ve value for time constant
131         else
132             B(ii,1:7)=tempB;
133             B(ii,8)=sse/(Count-7);% MSE corrected for number of parameters
135         end
136         % this coding allows for the data to be
137         % collected and retained. The
138         % SSE can be calculated if necessary.
139
140         ii = ii+1;
141
142     end
143 %% Select optimal estimate of the parameters
144
145     RestB=sortrows(B,8); % sort by ascending SSE
146     RestB=round(RestB*10000)/10000; %round to 4 decimal places
147     LeastB=RestB(1,:); % select best estimate
148
149     Ind2=B(:,8)<1000; % Select all sane values
150     Count=sum(Ind2); % count them,
151     % overloading of the Count variable
152
153
154
155     Stats(1,:)=mean(B(Ind2,:));
156     Stats(2,:)=std(B(Ind2,:));
157     Stats(3,:)=Count;
158     % we now have two estimates,
159     % a lowest MSE and a range for this data set
160
161 %% The figures
162
163 if Graph
164     close all
165     %Fid=figure('Visible ',' Off '); % allows for figure to be saved
166     % without
167     % drawing to the screen
168
169     X=min(x):.1:max(x);
170     plot(x,y,'+', X, funEBY(LeastB,X),'r');

```



```

173 hold on;
plot(X,LeastB(1),'r- ');
plot(LeastB(5),funEBY(LeastB,LeastB(5)), 'sr' );
175 plot(LeastB(7),funEBY(LeastB,LeastB(7)), 'sr' );
title ('Exp and Bi-Lin');
177 xlabel('Time (min)');
ylabel('Log Threshold (scot cd.m{-2})');
179 xlim ([0,60])
ylim ([-7 0]);

181 box off
183 hold off
    % saveas(Fid, FileName, 'eps ');
185 % saveas(Fid, FileName, 'fig ');

187 end
    %% Boxplot
189 % this is a legacy from early development,
    % but retained to allow other programs to still call this function

191 if BoxP
193 % Fid2=figure(' Visible ',' Off ');
    % FileName=datestr(now,30);
195 % subplot (1,3,1)
    % boxplot(B(Ind2,1));
197 % title ('Cone Threshold');
    %
199 % subplot (1,3,2)
    % boxplot ([B(Ind2,5), B(Ind2,7)])
201 % title (' Alpha & Alpha2');
    %
203 % subplot (1,3,3)
    % boxplot(B(Ind2,4))
205 % title ('S2');
    % saveas(Fid2, FileName, 'eps ');
207 % saveas(Fid2, FileName, 'fig ');

209 end

211 end

```

A.1.1 Numerical Experiment Code

Generate Test Data

```

function [data]=JMKIdealData(a,Points)
2 %% Create default values

```

```

4  if nargin<1
    a=14.21;
6  end

8
10 if nargin<2
    Points=100; % number of test data sets
12 end
14 rand('twister',5489)
    % reset(RandStream.getDefaultStream); % uses same random numbers each time

16 x=0:5:40; % twenty minutes worth of data rather than 40;
    [r c]=size(x);
18 y=ones(r,c);

20 %% The parameters of the model
    % arbitrarily set using McGwin (1999) values
22 % use JMK value from DPOD type setup

24 b(1) = -1.465; % -1; % cone threshold 20dB
    b(2) = 39.854; % 1.0; % abscissa -20
26 b(3) = 1.77; % 0.9; % time constant
    % S2 phase
28 b(4) = -0.154; % -.105; % S2 slope 2.10
    b(5) = 14.21; % a; % Alpha break-point
30 % S3 phase
    b(6) = 0.128; % puts slope at zero, S2 + S3 slope 0.4
32 b(7) = 31.4; % 23;

34 %% Initialise the model

36 Signal = (b(1)+b(2)*exp(-b(3).*x) ...
38           + b(4).*max(x-b(5),0) ...
           + b(6).*max(x-b(7),0));

40 %% Create the data
42 EndPoint=0.3;
    r=1;
44     for ii=linspace(0,EndPoint,Points);
        y(r,1:c)=Signal+ii*randn(1,c);
46         r=r+1;
    end

48
50 data=[x;y];

```

```

52 %% Calculate Signal to Noise Ratio
[r c]=size(data);
54 Signal=data(2,2:c);

56     for jj=1:r
        Response=data(jj,2:c);
58         Noise=Response-Signal;
        if jj < 3

60             data(jj , c+1)=NaN;

62         else
64             SNR=10*log10((Signal./Noise).^2); % power dB
            data(jj , c+1)=mean(SNR);
66             data(jj , c+2)=sum(Noise.^2)/41; % should bne sum of the noise over 81

68         end
        end

70

72 % N=linspace(0,EndPoint,Points)';
% SNR=data(2:end,end-1);

74

76 % %% Draw a figure
% figure1 = figure('XVisual ',...
%     '0x24 (TrueColor, depth 24, RGB mask 0xff0000 0xff00 0x00ff)',...
78 %     'PaperSize',[20.98404194812 29.67743169791]);
%

80 % %% First graph
%

82 % % Create axes
% axes1 = axes('Parent', figure1 ,...
84 %     'Position',[0.0679425837320574 0.11 0.469856459330144 0.815],...
%     'LineWidth ',2,...
86 %     'FontWeight','bold ',...
%     'FontSize ',12);
88 % hold(axes1,' all ');
%

90 % plot(x,y,'Parent', axes1 ,...
%     'MarkerSize ',5,...
92 %     'Marker ',';',...
%     'LineStyle ',' none ');
94 %

96 % plot(x,y (1:),' LineWidth ',2,...
%     'Color',[0 0 0],...
%     'MarkerSize ',6,...
98 %     'Marker',' none ',...
%     'LineStyle ','-');
100 %

```

```

102 % % plot(x,y (20,:), 'k+', 'LineWidth',3)
%
% % Create title
104 % title ('Test data ', 'FontWeight', 'bold ', 'FontSize', 20);
%
% % Create xlabel
106 % xlabel('Time (min)', 'FontWeight', 'bold ', 'FontSize', 16);
%
% % Create ylabel
110 % ylabel('Log-10 Threshold', 'FontWeight', 'bold ', 'FontSize', 16);
%
% %% Second graph
%
% % Create axes
114 % axes2 = axes('Parent', figure1 ,...
116 %     'Position', [0.623929425837321 0.107840172786177...
%     0.334659090909091 0.815],...
118 %     'LineWidth', 2,...
%     'FontWeight', 'bold ',...
120 %     'FontSize', 12);
% % Uncomment the following line to preserve the Y-limits of the axes
122 % % ylim(axes2, [0 110]);
% hold(axes2, 'all ');
124 %
% % Create plot
126 % plot(N, SNR, 'Parent', axes2, 'Marker', 'o ',...
%     'LineWidth', 2.5, 'LineStyle', 'none ',...
128 %     'Color', [0 0 0]);
%
% % Create title
% title ('Signal to Noise ratio v input noise ', 'FontWeight', 'bold ',...
132 %     'FontSize', 20);
%
% % Create xlabel
134 % xlabel('Input noise (log units) ', 'FontWeight', 'bold ', 'FontSize', 16);
%
% % Create ylabel
136 % ylabel('S/N ratio (dB)', 'FontWeight', 'bold ', 'FontSize', 16);
138

```

Wrapper Code

```

function [LeastB, Stats, RestB]=TestWrapper(Test)
2 %% Create test data
if nargin<1
4     Test=JMKIdealData(5.76,10000);
end
6
[r , ~, L]=size(Test);
8

```

```

10 %% Pre allocate memory
LeastB=ones(r,9,L); % The parameters with the lowest SSE
12 Stats=ones(3,8,r-1); % Brief statistics of the sane values returned
RestB=ones(200,8,r-1); % The whole of the raw data
14 % returned by JMKDAparamTest
save 'RealTestParamsApril2012.txt' LeastB -ascii
16
17 %% Calculate for a range of data sets
18 for ii=1:L
disp(num2str(ii))
20 for jj=1:r-1;
disp(num2str(jj));
22 data=[Test(1,1:end-2,ii);Test(jj+1,1:end-2,ii)];
dB=Test(jj+1,end-1,ii);
24 %[LeastB(jj,1:8), Stats (:,:, jj ), RestB (:,:, jj)]=JMKDAparamTest(data,0,0,0);
[LeastB(jj,1:8, ii)]=JMKDAparamTest(data,0,0,0);
26 LeastB(jj,9, ii)=dB;
save 'RealTestParamsApril2012.txt' LeastB -ascii
28 %save 'realStats.mat' Stats
%save 'RealRestB.mat' RestB
30
end
32 end

```

Bootstrap

```

1 function [PARAM]=BSWrapper(infile,No)
3 No = str2double(No); % shell only passes characters
5 %% Establish file path to data
[pathstr, name, ext, ~] = fileparts ( infile );
7 outfile = fullfile ( pathstr, strcat (name, '.out' ));
9 %% Check for file existence
% and handle error
11 try
D=importdata(infile);
13 catch ME
disp('Oops, there is no file by that name Michael');
15 D=[0,0];
%create dummy variable that can be handled later
17 end
19 if isstruct (D)
data=D.data;
21 else
data=D;

```

```

23 end
25 %% Import data
26 % check size of imported data if three cols then use col 1 and col 3 o/w
27 % use cols 1 and 2
29
30 [r,c]=size(data);
31 x=data(:,1);
33 if c==3
34     y=data(:,3);
35 else
36     y=data(:,2);
37 end
39 DATA=[x,y];
41
42 %% Pass data to Bootstrap
43 PARAM=zeros(No,8);
45 if sum(D)==0
46     save( file {1}, 'PARAM','-ascii')
47 else
48     for ii =1:No
49         disp(num2str(ii))
50         idx=randsample(r,r, true);
51         PARAM(ii,:)=JMKDAParamTest(DATA(idx,:),0,0,0);
52     end
53 end
55 save( outfile , 'PARAM','-ascii')

```

A.1.2 Batch Processing

Preprocessing

```

1 function [Data]=MMJK_data
3 HH=pwd;
5 Do1{1}=('~/Dropbox/JMFK-MM/Manchester Data');
5 Do1{2}=('~/Dropbox/JMFK-MM/Maastricht Data');
7
7 Data=zeros(50,100,44,2); % bit too big
9
9 for nn=1:2
11

```

```

13     cd(Dol{nn});
15     files = dir('*.xls');
15     Len = length(files);
17
19     warning('off') %#ok<WNOFF>
19     for ii = 1:Len
21         fil = files(ii).name;
23         [r,c] = size(xlsread(fil));
23         if c > 100
25             Data(:, :, ii, nn);
25         else
27             Data(1:r, 1:c, ii, nn) = xlsread(fil);
27         end
29
31     end
31 end
33 warning('on') %#ok<WNON>
35
37 %TestData=
39 cd(HH);
39 save MM_Data2

```

Batch

```

function Raw = JMK_MM_wrapper
2
4 [Data] = MMJK_data;
6
6 [M, Res, V] = MMDataStr(Data);
6 [~, Co, Sx, Lo] = size(Res);
8
8 Raw = zeros(size(M.Summ));
10
10 C = [1, 2, 3, 4; 5, 6, 7, 8];
12
14 arr = zeros(11, 1);
16
16 for ii = 1:Lo

```

```

18   for jj=1:Sx
19       for kk=1:Co/2
20           T=(Res(:, :, jj , ii ));
21           z=sum(T);
22
23           if sum(isnan(z))>4
24               arr(1:44)=0;
25               break
26
27           else
28
29               temp=(Res(:,C(kk,:), jj , ii ));
30
31               ln=temp(:,1)>=0;
32               temp=[temp(ln,1),temp(ln,2)/-20];
33               if sum(temp(ln,1))<10;
34                   arr (1:8, kk)=0;
35               else
36                   [LeastB,Count]=JMKDAparamTestMM(temp);
37                   arr (1:8, kk)=LeastB;
38                   arr (9, kk)=Count(end,1);
39
40               end
41           end
42       end
43
44       Raw(:,1, jj , ii )=reshape(arr,44,1);
45   save /Users/jeremiahkelly /Dropbox/JMFK-IJM/Year-3/2012_04/MM/RawSmall.mat Raw
46       disp( strcat ( {' Subject ' }, num2str(jj) ));
47   end
48 end

```

A.1.3 Scotopic Contrast Sensitivity

JMKDALinearCSF.m

This script controls the experiment

```

function [IterSum,InterimRes]=JMKDALinearCSF(SubjectData)
2
3   if nargin<1;
4       SubjectData=1; % sets default to collect subject data
5   end
6   SubjectString=('xxxx'); %#ok<NASGU>
7
8   if SubjectData
9       [SubjectString,Sub]=CollectSubjectInfo; %#ok<NASGU>
10  end

```



```

12 clc
13 HH=pwd;
14 %% the experiment to measure CSF
15 global CRS;
16 vsgInIt ();
17
18 crsSetVideoMode(CRS.EIGHTBITPALETTEMODE);
19 crsSetDrawMode(CRS.CENTREXY + CRS.SOLIDFILL);
20 %% Open the response box
21 errorCode = crsResponseBoxOpen(CRS.respCB6); ##ok<NASGU>
22 %% initialise the exp
23 [Clevels dB]=JMKDrawLutsBinS(128,0.0990); ##ok<NASGU>
24 [Cycles, m]=JMKDrawRampsBinS;
25 crsSetDisplayPage(m);
26 %% start calculating variables
27 SFs=length(Cycles);
28 j=(1:SFs)';
29 i=2*j-1;
30 PageArray=[j i i+1 i+2*SFs i+2*SFs+1];
31
32 page_numbers=[1 2*SFs+1];% a cross check ;)
33 Rate=crsGetFrameRate;% number of frames each page is displayed
34 page_times=[Rate Rate];
35 crsPageCyclingSetup( page_numbers,page_times);
36 crsSetCommand(CRS.CYCLEPAGEENABLE);
37 pause; % makes script halt until subject ready and provides a check of screen display.
38
39 % crsSetDisplayPage(4*length(Cycles)+1);
40 %% perform exp
41 Trial_Time=10;
42 Start=cputime;
43 End=Start+60*Trial_Time;
44 Repeats=1;
45 display=3;% the time the grating should be displayed
46 lterSum=zeros(10,9,Repeats,SFs);
47 % might use Clevels/2 later
48 while cputime<End;% continue for Trial_Time minutes
49     for k=1:SFs; %selects each SF
50         % audible warning of new sf
51         Spat= strcat(' Spatial Frequency ', num2str(Cycles(k)));
52         disp(Spat);
53
54         lter=zeros(1,9);
55         lter(1)=1;
56
57         lter(end)=Start;
58         if Repeats > 1
59             pen=InterimRes(k,2,Repeats-1)+19;

```

```

60         % the last threshold for this frequency less 9.5db say, 19
        % pen steps
62         if pen > 128; pen=128; end
        if pen < 1; pen=1; end
64         lter(3)=pen;

66     else
        lter(3)=64;% start contrast level
68     end

70     while lter(end,2)==0;

72         pen=lter(end,3);
        crsLUTBUFFERtoPalette(pen);
74         % internally randomises the orientation
        n=floor(2*rand)+1;
76         if n==1;
            pageseed=PageArray(k,2);
78         else
            pageseed=PageArray(k,4);
80         end
        % start pagecycling

82         page_numbers=[pageseed:pageseed+1]; %#ok<NBRAK>
84         pause(0.05);
        crsPageCyclingSetup(page_numbers,page_times);

86         crsResponseBoxBuzzer(CRS.respSEC01,CRS.respTONE1);
88         [RT, Response,Event] = JMKDALinExpKb(pageseed,k, display);
        [ lter ] = MMBSLinCSFDA(Response,lter,RT, Event);
90         disp( lter )
        page_numbers=[m:m+1]; %#ok<NBRAK>
92         pause(0.05);
        crsPageCyclingSetup(page_numbers,page_times);
94     end

96

98     % Save as experiment procedes
    %     [a,ss]= fileparts ( SubjectString );
100    %     ResFilePath=strcat('C:\Documents and Settings\mqbxgjk2\My Documents\MATLAB\Scripts\Eclipse\Result');
    %     if isdir (ResFilePath)<1;
102    %         mkdir(ResFilePath);
    %     end
104    %     cd(ResFilePath);
    %     SS=strcat(' Trial ', num2str(r), '- ', ' SF', num2str(k), '- ', ss, ' eclipse ', '- CSF', '. txt ');
106    %     save (SS, ' lter ', '- ASCII ');
    % Create summary file
108    [Row,c]=size( lter ); %#ok<NASGU>

```

```

110     IterSum(1:Row, :, Repeats, k) = Iter;
112     Pen = Iter(end, 3); % using a 128 contrast array not
114     %                               % 64 as originally written; i.e. a half dB graduation
116     %
118     InterimRes(k, 1, Repeats) = Cycles(k);    % #ok < AGROW >
120     InterimRes(k, 2, Repeats) = Pen;         % #ok < AGROW >
122     InterimRes(k, 3, Repeats) = Iter(end, 8); % #ok < AGROW >
124     InterimRes(k, 4, Repeats) = Start;      % #ok < AGROW >
126
128     end
130     Repeats = Repeats + 1;
132     pause(10);
134     crsResponseBoxBuzzer(CRS.respSEC01, CRS.respTONE1);
136 end
138
140 cd(HH);
142 JMKChirrup;
144 Summ = mean(InterimRes, 3);
146 plot(Summ(:, 1), Summ(:, 2))
148
150 if SubjectData == 1;
152     [a, b] = fileparts(SubjectString);
154     save(b);
156 end

```

MMBSLinCSFDA.m

This script receives keyboard input and calculates nest threshold

```

1  %% Manchester Modified Binary Search for the CSF only, has reduced number
2  %% of 'PENS@
3  % this function comes after the stimulus to calculate the next stimulus
4  % definition sets the initial stimulus or provides a final estimate of
5  % threshold. In the CSF exp estimates threshold, in the Toric exp sets the
6  % initial contrast of the letter C
7
8  function [ Iter ] = MMBSLinCSFDA(Response, Iter, RT, Event) % Response is the correct
9  % response, Pen is the estimated contrast threshold, receives the last
10 % estimate and returns the new estimate.
11 %% initialize
12 if nargin < 4
13     Event = cputime;
14 end
15 if nargin < 3
16     RT = NaN;

```

```

17 end
    Trial=lter(end,1);
19
21 Pen=lter(end,3);
    Correct=lter(end,4);%#ok<NASGU> % mod 3, collates three correct responses.
    Turn=lter(end,5);
23 Start=lter (1,9);

25 %% ascending pen
27
    if Response==0;% incorrect
29         Pen=Pen-6;% makes pen darker
        if Pen<1;
31             Pen=1;
        end
    end
33
35
37 %% Define 'lter' the returned array
39
n=Triall+1;
41 lter (n,1)=n;% next trial
    lter (n,2)=Response; % blank carrier for response
43 lter (n,3)=Pen; % pen
    lter (n,4)=mod(sum(lter(:,2)),3); % cumulative correct responses
45 lter (n,5)=Turn;% just a toggle
    lter (n,6)=sum(lter (:,5)); % counts the number of turns
47 lter (n,7)=RT;

49 lter (n,8)=Event;
    lter (n,9)=Start;

```

DA_CallBoxKb.m

Keyboard interaction script

```

function [RT,Button,KeyNum]=DA_CallBoxKb(display)
2 global CRS;
    if nargin<1,
4         display=3;
    end
6

8 %% [RT, Button]=CallBoxKb; the function call will return RT and the
    %% button pressed using PsychToolBox Keyboard Commands

```

```

10 Event=cputime;
12 End=Event+display;
   FlushEvents('keyDown');
14 % this now presents the stimulus
   ListenChar(2); % switches off the keyboard
16 KbName('UnifyKeyNames');

18 % escapeKey = KbName('ESCAPE');
   startSecs = GetSecs;

20 while KbCheck; end % Wait until all keys are released .

22 while cputime<End;
   % Check the state of the keyboard.
   [ keylsDown, seconds, keyCode ] = KbCheck;

26   % If the user is pressing a key, then display its code number and name.
28   if keylsDown
       Button=KbName(keyCode);
30       RT=seconds-startSecs;
       KeyNum=find(keyCode);
32       break;
   end

34 end

36 ListenChar(0); % this line returns the keyboard to MATLAB
   if keylsDown~=1
38       Button=KbName(6553); %Undefined
       RT=NaN;
40       KeyNum=NaN;
   end

42

44 %crsResponseBoxBuzzer(CRS.respSEC01,CRS.respTONE10);
   pause(0.05);

```

JMKDrawLutsBinS.m

Define look up tables

```

1 function [ Clevels dB]=JMKDrawLutsBinS(Levels, BGLum)
   global CRS; %#ok<NUSED>

3

5   if nargin<2;
       BGLum=0.0990; % sets background luminance to ~12.5cdm^2
   end
7   if nargin <1;

```

```

    Levels=128;
9  end

11  %This function writes the pens to each LUT for differing contrast levels as
12  %defined by CONTRAST, there are three parts to each LUT; The first 90
13  %values are used in the outer portion of the target and represent the
14  %contrast of interest , the next 90 create a central occluder which is a
15  %half the contrast of the surround. Then finally two pens, one for a
16  %fixation cross and the other to set the background luminance
17
18
19  myLut=BGLum.*ones(256,3); % sets all to BGLum
20  dB=linspace(1,64,Levels);
21  Contrast=10.^(-dB./20);
22  Clevels=length(Contrast);
23
24
25  initPhase=0;
26  for j=1:Clevels;
27
28      for i=1:90;
29          phase=2*pi*((i-1)/90);
30          phase =phase + initPhase;
31          sp=Contrast(j)*sin(phase);
32          val=(sp+1)*BGLum;
33          myLut(i,1:3)=[val , val , val ];
34      end
35
36      for i=91:180;
37          phase=2*pi*((i-1)/90);
38          phase =phase + initPhase;
39          sp=.15*Contrast(j)*sin(phase);
40          val=(sp+1)*BGLum;
41          myLut(i,1:3)=[val , val , val ];
42      end
43
44      myLut(255,1:3)=[0,0,0];           % a black pen
45      myLut(256,1:3)=[BGLum,BGLum,BGLum]; % background screen luminance
46
47      crsLUTBUFFERWrite(j,myLut);
48
49
50
51 end
52
53 crsLUTBUFFERtoPalette(Levels);% acts as a check that we have loaded a lut
54 % plot(myLut(1:250,:));%used to check the continuity and profile of the LUT.
55

```

JMKDrawRampsBinS.m

Define the display screens

```
1 function [Cycles,m]=JMKDrawRampsBinS
3 % draws a horizontal and vertical ramps and their reverse for each spatial
4 % frequency
5
7 global CRS;
8 ErrorCode = crsSetViewDistMM(3000); ##ok<NASGU>
9 subtense=4;% size of the grating overall
10 Radius=floor(3000*atan(subtense*pi/180));
11 OuterRad=Radius+5;
12 DiscRad=1;%floor(3000*atan(subtense*pi/(4*180)));
13
15 %Cycles =[6 12 18 24]; %measures the linear part of the CSF
16 % Cycles = [1 4 8 16];
17 % Cycles=16;
18 Cycles= [2 4 8]; % EQUIVALENT TO [0.5 1 2] AT 75CM
19 Len=length(Cycles);
20 m=0;
21 for n=1:2;% draws a horizontal and a vertical ramp
22     for j=1:Len;
23
24         m=m+1;% obverse
25         crsSetDrawPage(CRS.VIDEOPAGE,m,256);%6;
26
27         for i=-OuterRad:OuterRad;
28             % draws a ramp, OuterRad pixels wide
29
30             pen=floor(1+subtense*Cycles(j)*89*(i-Radius)/(2*Radius));
31             pen=mod(pen,90)+1;
32             crsSetPen1(pen+90);
33
34             Ht=sqrt(OuterRad^2-i^2);
35             if n > 1;
36                 crsDrawLine([i,-Ht],[i,Ht]); % 150 pixels high
37             else
38                 crsDrawLine([-Ht,i],[Ht,i]); % 150 pixels high
39             end
40         end
41
42
43         for i=-Radius:Radius; % draws a ramp Radius, is the radius, pixels wide
44
45             pen=floor(1+subtense*Cycles(j)*89*(i-Radius)/(2*Radius));
```

```

47     pen=mod(pen,90)+1;
    crsSetPen1(pen);
    Ht=sqrt(Radius^2-i^2);
49     if n > 1;
        crsDrawLine([i,-Ht],[i,Ht]); % 150 pixels high
51     else
        crsDrawLine([-Ht,i],[Ht,i]); % 150 pixels high
53     end
55
    end
57
    for i=-DiscRad:DiscRad; % draws a ramp Radius, is the radius, pixels wide
59
        pen=floor(1+subtense*Cycles(j)*89*(i--Radius)/(2*Radius));
        pen=mod(pen,90)+1;
        crsSetPen1(pen+90);
        Ht=sqrt(DiscRad^2-i^2);
63         if n > 1;
            crsDrawLine([i,-Ht],[i,Ht]); % 150 pixels high
65         else
            crsDrawLine([-Ht,i],[Ht,i]); % 150 pixels high
67         end
69     end
71
    crsSetPen1(128); %draw a black fixation target
    crsDrawOval([0,0], [20,20]);
73
    % draw reverse ramps
75     m=m+1; %reverse
77
    crsSetDrawPage(CRS.VIDEOPAGE,m,256);
    for i=-OuterRad:OuterRad;
79         % draws a ramp, OuterRad pixels wide
81
            pen=floor(1+subtense*Cycles(j)*89*(i--Radius)/(2*Radius));
            pen=mod(pen,90)+1;
            crsSetPen1(181-pen);
            Ht=sqrt(OuterRad^2-i^2);
85             if n > 1;
                crsDrawLine([i,-Ht],[i,Ht]); % 150 pixels high
87             else
                crsDrawLine([-Ht,i],[Ht,i]); % 150 pixels high
89             end
91         end
93
        for i=-Radius:Radius; % draws a ramp Radius, is the radius, pixels wide

```



```

95     pen=floor(1+subtense*Cycles(j)*89*(i--Radius)/(2*Radius));
96     pen=mod(pen,90)+1;
97     crsSetPen1(91-pen);
98     Ht=sqrt(Radius^2-i^2);
99     if n > 1;
100         crsDrawLine([i,-Ht],[i,Ht]); % 150 pixels high
101     else
102         crsDrawLine([-Ht,i],[Ht,i]); % 150 pixels high
103     end
104
105
106     end
107
108     for i=-DiscRad:DiscRad; % draws a ramp Radius, is the radius, pixels wide
109
110         pen=floor(1+subtense*Cycles(j)*89*(i--Radius)/(2*Radius));
111         pen=mod(pen,90)+1;
112         crsSetPen1(181-pen);
113         Ht=sqrt(DiscRad^2-i^2);
114         if n > 1;
115             crsDrawLine([i,-Ht],[i,Ht]); % 150 pixels high
116         else
117             crsDrawLine([-Ht,i],[Ht,i]); % 150 pixels high
118         end
119     end
120
121     crsSetPen1(128); %draw a black fixation target
122     crsDrawOval([0,0], [20,20]);
123
124
125     end
126
127 end
128 m=m+1;
129 crsSetDrawPage(CRS.VIDEOPAGE,m,256);
130 % crsSetPen1(255); %draw a black fixation target
131 % crsDrawLine([0,-5;-5,0], [0,5;5,0]);
132
133 crsSetDrawPage(CRS.VIDEOPAGE,m+1,256);
134 % crsSetPen1(255); %draw a black fixation target
135 % crsDrawLine([0,-5;-5,0], [0,5;5,0]);
136 %

```

A.2 R code

A script loads the data, in the example shown here the data is from the first visit of subjects in the N36 study (see chapter 6). The data is passed to the script as an array of two columns. These two columns are converted to a list structure for the `nls` function.

```
##### Get data
2   DATA<-Get36Data(N) # function to load the data from experiment N36
   x = DATA[,1]
4   y = DATA[,2]
6   DATAlist = list(x,y)
```

these two variables x, y are taken by subsequent functions by default if not specified. Then two further scripts are called, the first defines the least squares function, `modelFn` with parameter **a** this is equivalent to equation 3.3.1, and the second, `DAest` that uses the best estimate of the parameter **a** and the original time values **x** to enable plotting of the fitted function;

```
modelFn<- function (a){# the least squares function
2   Yest<-a[1]+a[2]*exp(-x*a[3])+ a[4]*ifelse(x<a[5],0, x-a[5]) + a[6]*ifelse (x<a[7],0, x-a[7])
4   return(sum((y-Yest)^2))
}
6
8   DAest <- function(a,x){# the model estimates of the threshold
   Y<-a[1]+a[2]*exp(-x*a[3])+ a[4]*ifelse(x<a[5],0, x-a[5]) + a[6]*ifelse (x<a[7],0, x-a[7])
10  return(Y)
}
```

The script then creates an initial estimate of the parameters **tmp**, in R the NM algorithm is provided by the function `optim` which initially takes two arguments, **tmp**, the first estimate of the parameters and **modelFn**, the least squares function to be minimised, notice that this function has become an argument, similar to the situation in the Matlab scripts.

```
##### Seven Param Nelder Mead
1   tmp<-c(y[1]-2,2,1,-0.3,5,0.2,15)
3   OPT1<-optim(tmp, modelFn)
   for(i in 1:5){
5     OPT1<-optim(OPT1$par, modelFn, hessian = TRUE)
   }
```

The recycling of the parameter estimates in the **for** loop allows for rapid convergence, however the concern regarding convergence to a local rather than global minimum remains. The new parameters estimates are held in **OPT1\$par** and are passed to the next

part of the script that uses the `nls` function and the **port** algorithm. Firstly the model has to be defined in a slightly different manner, and the parameter estimates have to be presented as a list rather than a vector.

```

##### Seven Param port search
2 Thres<-y~(a1+a2*exp(-x*a3)+ a4*ifelse(x<a5,0, x-a5) + a6*ifelse(x<a7,0, x-a7))

4 Param<- list(a1 = OPT1$par[1],a2 = OPT1$par[2],a3 = OPT1$par[3],
              + a4 = OPT1$par[4],a5 = OPT1$par[5],
              + a6 = OPT1$par[6],a7 = OPT1$par[7])
6 mod<-nls(formula = Thres,data = DATAlist, start = Param,
           + trace = T, alg = 'port',
           + control = list(warnOnly = TRUE, tol = 1e-06, minFactor = 1/2048))
8

##### CI data from nls
12 summary(mod)$p[,1:2] #returns the estimate and SE of the parameters

```

Then the object **mod** is interrogated and the estimates of the parameter and the standard error of the estimates is returned as an array. See table D.1.1.

A.2.1 Code listing

```

##### Initialise
1

3 source("~/Dropbox/RScripts/Functions/modelFn.R")
  source("~/Dropbox/RScripts/Functions/DAest.R")
5
7 source("~/Dropbox/RScripts/Functions/Get21Data.R")
  source("~/Dropbox/RScripts/Functions/Get36Data.R")
  source("~/Dropbox/RScripts/Functions/Get36bData.R")
9
##### Get data
11 DATA<-Get36bData(N)

13 x=DATA[,1]
  y=(DATA[,2])
  DATAlist=list(x,y)
15

##### Seven Param model Nelder Mead
17 tmp<-c(y[1]-2,2,1,-0.3,5,0.2,15)
19
21 OPT1<-optim(tmp, modelFn)
  for(i in 1:5){
    OPT1<-optim(OPT1$par, modelFn, hessian=TRUE)
23 }

25 Par7=sum((Yest1-y)^2)/length(x-7)

```

```

27     Yest1<- DAest(OPT1$par,x)
29     ##### Draw Figure
31     par(las=1, font=2, font.axis=2, font.lab=2, lwd=2, bty='n', mfrow=c(1,1))
33     plot(x,y,xlim=c(0,20), ylim=c(-4,0),xlab='Time (min)',
35     ylab='Threshold (scot cd/m2)', main='Parametric models')
37     Yest1<- DAest(OPT1$par,x)
39     lines(x, Yest1, col='red', lty=1)
41     Bold()
43     ##### Seven Param Newton Raphson search model
45     Thres<-y~(a1+a2*exp(-x*a3)+ a4*ifelse(x<a5,0, x-a5) + a6*ifelse(x<a7,0, x-a7))
47     Param<- list(a1=OPT1$par[1],a2=OPT1$par[2],a3=OPT1$par[3],
49     a4=OPT1$par[4],a5=OPT1$par[5],a6=OPT1$par[6],a7=OPT1$par[7])
51     mod<-nls(formula=Thres,data=DATAlist, start=Param, trace=T, alg='port',
53     control=list(warnOnly=TRUE, tol=1e-06, minFactor=1/2048))
55     Nest<-coef(mod)
57     ResN=sum((Yest-y)^2)/length(x-7)
59     ##### CI data from nls
61     summary(mod)
63
65 modelFn<- function (a){
67     Yest<-a[1]+a[2]*exp(-x*a[3])+ a[4]*ifelse(x<a[5],0, x-a[5]) + a[6]* ifelse (x<a [7],0, x-a[7])
69     return(sum((y-Yest)^2))
71 }
73
75 DAest <- function(a,x){
77     Y<-a[1]+a[2]*exp(-x*a[3])+ a[4]*ifelse(x<a[5],0, x-a[5]) + a[6]*ifelse (x<a [7],0, x-a[7])
79     return(Y)
81 }

```

A.2.2 A method of model selection based on AIC_c values

This code fits the data to a series of models, calculates the AIC_c values.

```

# which model fits the data best
2
4     source("~/Dropbox/JMFK-IJM/Year-3/2012_09/CurveFitting/Models.R")
6     source("~/Dropbox/RScripts/Functions/Bold.R")
8     par(las=1, font=2, font.axis=2, font.lab=2, bty='n')#, bg='lightgrey')
10
12 xT<-0:20
14     source("~/Dropbox/RScripts/Functions/Get36Data.R")
16     source("~/Dropbox/RScripts/Functions/Get36bData.R")
18     source("~/Dropbox/RScripts/Functions/Get21Data.R")
20     source("~/Dropbox/RScripts/Functions/GetSparse.R")

```

```

14      source('~ /Dropbox/RScripts/Functions/TestData.R')
16      #Data<-Get36bData(1)
16      Tx<-TestData(x=xT,SSE=0.0071)
18      Data<-cbind(xT,Tx)
18      x=Data[,1]
20      y=Data[,2]
20      Time=x
22      Thres=y
22      plot(Time,Thres, ylim=c(-4,0),xlim=c(0,22), pch=16, col='darkgreen')
24      Bold()
24      N<-length(x)
26
26      ##### Two Param model Nelder Mead
28      #tmp<-c(-1.0660, 1.2695,1.7565,-0.2966,4.9232)
28      tmp<-c(-4,2)
30
30      OPT2<-optim(tmp, P2)
32      for(i in 1:7){
32      OPT2<-optim(OPT2$par, P2, hessian=TRUE)
34      }
36
36      X<-seq(0,max(x),0.01)
38
38      Yest1<- Pest2(OPT2$par,X)
38      lines(X, Yest1, col=2, lty=1)
40
40      N<-length(x)
40      K1<-2+1
42      MSE1<-OPT2$value
42      AIC2<- N*log(MSE1/N)+2*K1 + 2*K1*(K1+1)/(N-K1-1)
44
44      Score<-AIC2
46      ##### Three Param model Nelder Mead
46      #tmp<-c(-1.0660, 1.2695,1.7565,-0.2966,4.9232)
48      tmp<-c(-4,2,1)
50
50      OPT3<-optim(tmp, P3)
52      for(i in 1:7){
52      OPT3<-optim(OPT3$par, P3, hessian=TRUE)
54      }
56
56      X<-seq(0,max(x),0.01)
58
58      Yest1<- Pest3(OPT3$par,X)
58      lines(X, Yest1, col=3, lty=1)
60
60      K1<-3+1
60      MSE1<-OPT3$value
60      AIC3<-N*log(MSE1/N)+2*K1 + 2*K1*(K1+1)/(N-K1-1)

```

```

62 Score<-c(Score,AIC3)

64 ##### Four Param model Nelder Mead
   #tmp<-c(-1.0660, 1.2695,1.7565,-0.2966,4.9232)
66   tmp<-c(-4,-2,10,-.25)

68   OPT4<-optim(tmp, P4)
   for(i in 1:7){
70     OPT4<-optim(OPT4$par, P4, hessian=TRUE)
   }

72   X<-seq(0,max(x),0.01)

74   Yest1<- Pest4(OPT4$par,X)
   lines(X, Yest1, col=4, lty=1)

76 K1<-4+1
MSE1<-OPT4$value
78 AIC4<-N*log(MSE1/N)+2*K1 + 2*K1*(K1+1)/(N-K1-1)
Score<-c(Score,AIC4)

80 xmu<-mean(X)
82 ymu<-mean(Yest1)
   #lines(X,(ymu+OPT4$p[4]*(X-xmu)), lwd=3)

84 ##### Five Param model Nelder Mead
86   tmp<-c(-1.8,1.7,1.6, -0.249,4.9232)
   #tmp<-c(-1.6523,1.1609,0.4659,-0.2248,7.3498)

88   OPT5<-optim(tmp, P5)
   for(i in 1:7){
90     OPT5<-optim(OPT5$par, P5, hessian=TRUE)
   }

92   X<-seq(0,max(x),0.01)

94   Yest1<- Pest5(OPT5$par,X)
96   lines(X, Yest1, col=5, lty=1, lwd=3)

98 K1<-5+1
MSE1<-OPT5$value
100 AIC5<-N*log(MSE1/N)+2*K1 + 2*K1*(K1+1)/(N-K1-1)
Score<-c(Score,AIC5)

102 ##### Six Param model Nelder Mead
104   #tmp<-c(-1.0660, 1.2695,1.7565,-0.2966,4.9232,0.3092)
   tmp<-c(-2.500,-12.500, 0.489, 5.410, 89.200, 0.354)

106   OPT6<-optim(tmp, P6)
108   for(i in 1:7){
   OPT6<-optim(OPT6$par, P6, hessian=TRUE)
110   }

```

```

112                                     X<-seq(0,max(x),0.01)
114     Yest1<- Pest6(OPT6$par,X)
114     lines(X, Yest1, col=6, lty=1)

116 K1<-6+1
116 MSE1<-OPT6$value
118 AIC6<-N*log(MSE1/N)+2*K1 + 2*K1*(K1+1)/(N-K1-1)
118 Score<-c(Score,AIC6)

120 ##### Seven Param model Nelder Mead
122 tmp<-c(-1.0660, 1.2695,1.7565,-0.2966,4.9232,0.3092,6.3982)
124 #tmp<-c(-1.6523,1.1609,0.4659,-0.2248,7.3498,0.2046,13.4566)
124 tmp<-c(-1, 1,1,-0.25,5,0.2,12)

126 OPT7<-optim(tmp, P7)
128 for(i in 1:7){
128     OPT7<-optim(OPT7$par, P7, hessian=TRUE)
130     }

132                                     X<-seq(0,max(x),0.01)
134     Yest1<- Pest7(OPT7$par,X)
134     lines(X, Yest1, col=7, lty=1)

136 K1<-7+1
136 MSE1<-OPT7$value
138 AIC7<-N*log(MSE1/N)+2*K1 + 2*K1*(K1+1)/(N-K1-1)
138 Score<-c(Score,AIC7)

140 Idx<-which(Score==min(Score))
142 Idx+1

144 round(exp((Score[Idx]-Score)/2),3)
144 #1/exp((Score[Idx]-Score)/2) # this number @, means that models chosen is @ times more likely than the alternative
146 UpBound<-Score[Idx]+10
146 LoBound<-Score[Idx]-10

148 idx<-Score<=UpBound & Score>=LoBound
148 0+idx

```

A.2.3 A standard observer of the digital device

This script both creates the response of a standard observer to three different measurement protocols.

```

1 # a model of a standard observer
3 #pdf("~/Dropbox/JMFK-IJM/Year-3/Thesis/Chapter8/Figs/SimulatedDPOD.pdf",

```

```

height=0, width=0, paper='a4')
5
library ( plotrix )
7 source("~/Dropbox/JMFK-IJM/Year-3/2012_09/CurveFitting/Models.R")
source("~/Dropbox/RScripts/Functions/Bold.R")
9 par(las=1, font=2, font.axis=2, font.lab=2, bty='n', mar=c(4,5,0.1,1),
cex.lab=1.3, cex.axis=1.2, mfrow=c(3,1))
11
set.seed(1234)# ensures same figure is drawn
13 ## Parameters
LL=1
15 for (Rt in c(5,35,55)){
Freq = 4 / 2 # Hz of the stimulus, halved to reduce number of points plotted
17 Stepdown = 9.5 # dB
TimeMax = 20 # Time data collected minutes
19 RampTime = Rt # seconds
Start = 10 # dB
21 Stop = 0 # the initial cone threshold
Interval = 5 # seconds
23
b<-numeric(8)
25
b[1]= -1.64
27 b[2]= 1.16
b[3]= 1.63
29 b[4]= -0.248
b[5]= 5.76
31 b[6]= 0.24
b[7]= 12
33
35 X=seq(0,TimeMax,length.out=60*TimeMax*Freq) # the time
Len=length(X)
37 Y<-numeric(Len)
39 ## Model
# this is the idealised response of the retina, the rod and cone response
41 # combined.
Thrs = Pest7(b,X)
43
45 plot(X,Thrs,col='red', type='l', ylim=c(-4.5,-.2), xlab='Time (min)',
ylab=expression(bold(Threshold~(log[10]*(cd*.m^{-2}))))))
47 Bold()
mtext(letters[LL], side=1, adj=-0.18)
49 LL=LL+1
51 ## Stimulus
# this is how the stimulus varies over time

```



```

53 delta=(Start-Stop)/(10*RampTime)
55 jj=1
   ii=1
57 kk=1
   xest=numeric(10)
59 yest=numeric(10)

61 ACF=0

63 while( ii < Len){
   Y[ii]=delta*(kk-1)-0.1*Start # changes START from dB to log
65
   Guess=abs(rnorm(1,0,0.1))
67 Lapse=abs(rnorm(1,0,0.3))
   Mod=Pest7(b, X[ii])-Guess+Lapse +ACF #(guess, lapse, criterion shift)
69 points(X[ii ], Y[ii ], pch=16, cex=.2)
   kk=kk+1
71 if (Y[ii ]>Mod){
73     Start=(-10*Y[ii]+Stepdown)
       xest [ jj ]=X[ii ]
75     yest [ jj ]=Y[ii ]
       jj =jj+1
77     kk=1
       ii =ii+1*Freq*Interval
79     }

81     ii =ii+1 # steps through the array of X values,
}

83

85 points(xest, yest, pch=16, col='red', cex=.7)
87
## fit model
89 data=cbind(xest, yest)
91 Ind=data[,1]>=0 # deselect NaN

93 x = data[Ind,1]
   y = data[Ind,2]
95 Count=sum(Ind)

97

99 ## Estimate parameters
101 Opt<-optim(b,P7)

```

```

103 for ( ii in 1:5){
105     Opt<-optim(Opt$p,P7)
    }
107 a<-Opt$p
    Tx<-rbind(paste('RMS =',round(sqrt(Opt$v/Count),3),sep=' '),paste('Ramp =',RampTime, sep=' '))
109
    lines(X,Pest7(a,X), lty=2)
111 M<-(Y[2]-Y[1])/(X[2]-X[1])
    xb=2
113 yb= -3
    Int=-xb*M+yb
115 ablineclip (Int,M, y1=-3.5,y2=-2)
    legend(3,-3.5,Tx,bty='n')
117 #rm(list=ls())
    }
119 #dev.off()

```

A.3 Shell Scripts and Condor

Procedure

```
1  #log in to submitter and do the following  
   #Unzip the file  
3  unzip kelly_reply.zip  
  
5  #compile up the MATLAB script. It will pull in JMKDAparamTest.m  
   automatically  
7  cd kelly_reply  
   mcc -m BSWrapper.m  
9  #Note that the important output is BSWrapper and run_BSWrapper.sh  
  
11 #submit this job to condor  
   condor_submit submit.txt
```

This script submits all the jobs to the condor system

```
   #!/bin/bash  
2  line_num=0;  
   iters=10;  
  
4  #read through list of files  
6  while read fullpath  
   do  
8  folder='dirname $fullpath'  
   filename='basename $fullpath'  
10 #enter directory corresponding to current file  
   cd $folder  
12 #create submit.txt in this directory  
   echo "Universe = vanilla  
  
14 requirements = (Opsys == \"LINUX\" && Arch == \"X86_64\" && HAS_MATLAB=?=True && Memory>0)  
16 rank = Memory  
  
18 Log = $filename.log  
   Output = $filename.out  
20 Error = $filename.err  
   notification = error  
  
22 WhenToTransferOutput = ON_EXIT  
24 ShouldTransferFiles = Yes  
  
26 executable = ../run_BSWrapper.sh  
   arguments = /opt/MATLAB/MATLAB_Compiler_Runtime/v713/ $filename $iters  
  
28 transfer_input_files = ../BSWrapper,$filename  
  
30
```

```

Queue 1
32 " > submit.txt
   #submit this job to the pool
34 condor_submit submit.txt

36 #move back to base directory
   cd ..
38
40 line_num='expr $line_num + 1';
   done < $1

```

An example of a submit file for subject 2 second visit.

```

Universe = vanilla
2
requirements = (Opsys == "LINUX" && Arch == "X86_64" && HAS_MATLAB=?=True && Memory>0)
4 rank = Memory

6 Log = sx2b.txt.log
  Output = sx2b.txt.out
8  Error = sx2b.txt.err
  notification = error
10
WhenToTransferOutput = ON_EXIT
12 ShouldTransferFiles = Yes

14 executable = run_BSWrapper.sh
  arguments = /opt/MATLAB/MATLAB_Compiler_Runtime/v713/ sx2b.txt 1500
16
  transfer_input_files = BSWrapper,sx2b.txt
18
Queue 1

```

This is the shell script that calls for the compiled files

```

#!/bin/sh
2 # script for execution of deployed applications
  #
4 # Sets up the MCR environment for the current $ARCH and executes
  # the specified command.
6 #
exe_name=$0
8 exe_dir='dirname "$0"'
echo "-----"
10 if [ "$1" = "x" ]; then
  echo Usage:
12   echo $0 \<deployedMCRroot\> args
else
14   echo Setting up environment variables

```

```

MCRROOT="$1"
16 echo ----
LD_LIBRARY_PATH=.{MCRROOT}/runtime/glnxa64 ;
18 LD_LIBRARY_PATH=${LD_LIBRARY_PATH}:${MCRROOT}/bin/glnxa64 ;
LD_LIBRARY_PATH=${LD_LIBRARY_PATH}:${MCRROOT}/sys/os/glnxa64;
20     MCRJRE=${MCRROOT}/sys/java/jre/glnxa64/jre/lib/amd64 ;
LD_LIBRARY_PATH=${LD_LIBRARY_PATH}:${MCRJRE}/native_threads ;
22     LD_LIBRARY_PATH=${LD_LIBRARY_PATH}:${MCRJRE}/server ;
LD_LIBRARY_PATH=${LD_LIBRARY_PATH}:${MCRJRE}/client ;
24     LD_LIBRARY_PATH=${LD_LIBRARY_PATH}:${MCRJRE} ;
XAPPLRESDIR=${MCRROOT}/X11/app-defaults ;
26 export LD_LIBRARY_PATH;
export XAPPLRESDIR;
28 echo LD_LIBRARY_PATH is ${LD_LIBRARY_PATH};
shift 1
30 "${exe_dir}"/BSWrapper $*
fi
32 exit

```

FURTHER RESULTS FROM NUMERICAL EXPERIMENT

The Cone Phase ($\theta_{1,2,3}$)

The cone phase is described by three parameters, the cone threshold (cd.m⁻²), the cone coefficient(cd.m⁻²) and the cone time constant(τ (min)) the distributions for each parameter estimate are shown in figure B.0.1. For the McGwin test data each parameter is accurately estimated by both the median and the mean of values. The Manchester test data cone threshold is accurately estimated by both the mean and the median, the cone coefficient is accurately described by the median and underestimated by the mean by 0.01 cd.m⁻². The time constant of the Manchester data is closely estimated by the median, however it is overestimated by the mean.

Considering the cone threshold, both data sets have low skew values (McGwin 0.0013, Manchester -0.375) and moderately large kurtosis (McGwin 5.5, Manchester 18.8), these two together suggest that the estimates of cone threshold are robust for increasing noise level. Similarly the cone coefficient is reliably estimated with low skew (McGwin 0.115, Manchester -0.141) and moderate kurtosis (McGwin 5.5, Manchester 5.6).

The estimate of the cone time constant for the McGwin parameters is robust (skew = 0.000, kurtosis = 5.3) but for the Manchester test data the high skew value (82) results in the mean overestimating the true value by 0.16min.

The S3 Phase ($\theta_{6,7}$)

The slope of the S3 phase is slightly overestimated, for the McGwin data, by both the mean and the median, by 0.001 and 0.003 log₁₀(cd.m⁻²).min⁻¹respectively. While the Manchester estimate is correct for the median and overestimated the mean by

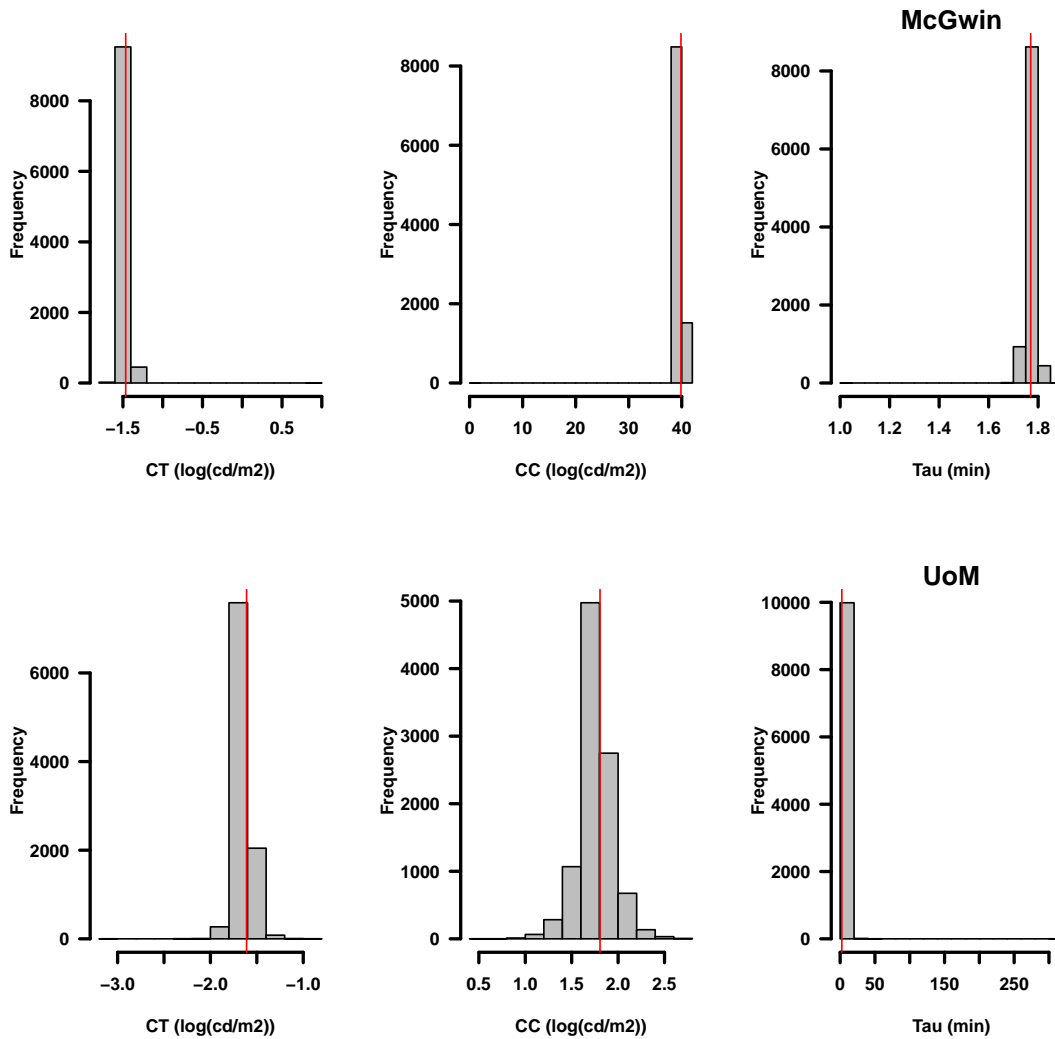


Figure B.0.1: Changes in cone parameter estimates; for each parameter in the McGwin test data, the bar enclosing over 80% of estimates, contains the true value. For the Manchester values, over 70% of the cone threshold estimates are enclosed by the bar that encloses the true value (-1.640 cd.m^{-2}). For the cone coefficient nearly 80% are within $\pm 0.02 \text{ cd.m}^{-2}$ of the true value. The time constant estimates for Manchester are heavily skewed by an outlier.

$0.001 \log_{10}(\text{cd.m}^{-2}).\text{min}^{-1}$. The estimates of the slope of S3 are both positively skewed to the right with McGwin being more skewed than Manchester (2.70 and 1.06), suggesting that for noisy data the McGwin estimate is more likely to exceed the true value.

The rod rod transition time is best estimated by the median in both test data sets, the mean underestimating the true value in the McGwin test data and overestimating the

value for the Manchester test data. This is reflected in the skew values, with the McGwin test data (-1.38) being negatively skewed and the Manchester test data (0.88) positively skewed. For both test data sets the kurtosis for each parameter is moderately large and in the range 8.85 to 29.7.

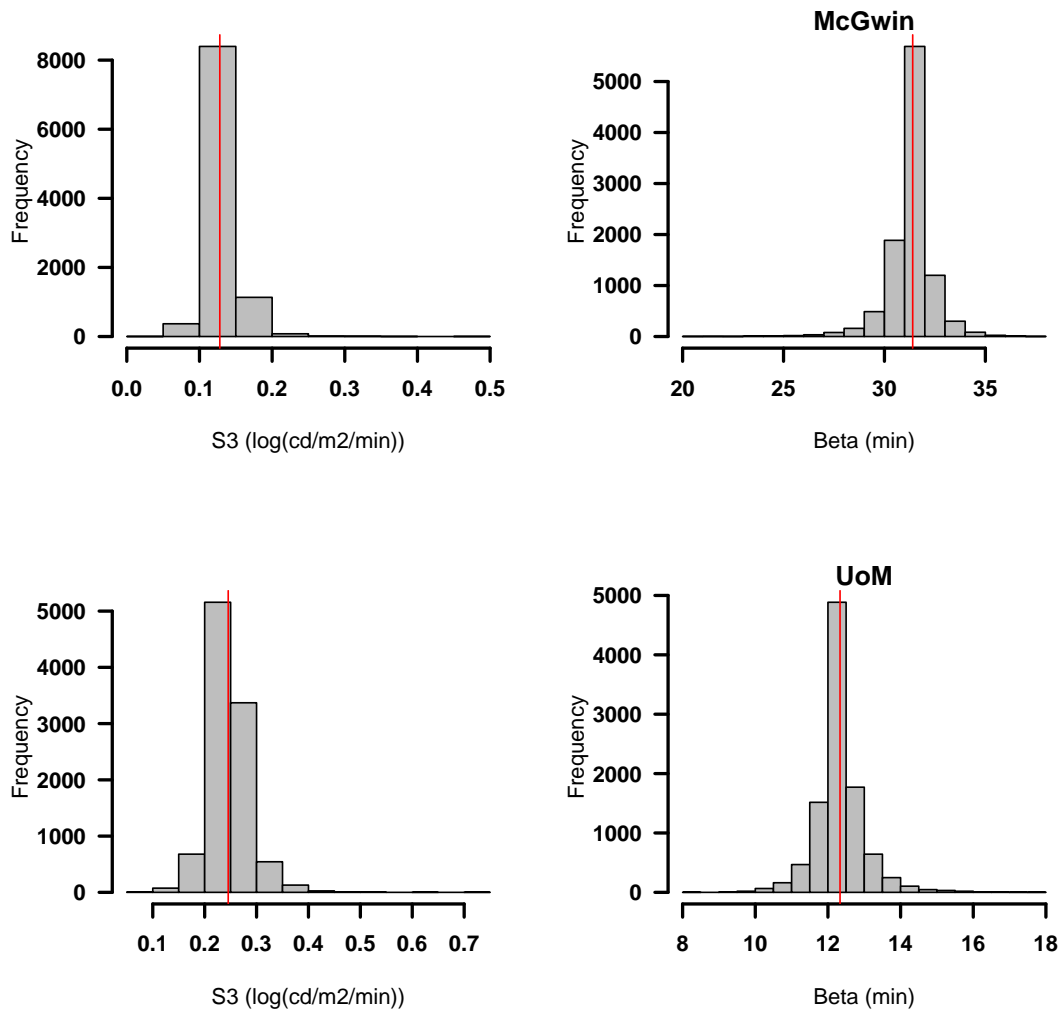


Figure B.0.2: Histograms of the parameters defining the second phase of rod sensitivity recovery, S3. The vertical red line is the test value. The slope returned by the algorithm is the sum of the slopes of the S2 and S3 phases. For the McGwin data over 80% of the estimates are within $\pm 0.025 \log_{10}(\text{cd}\cdot\text{m}^{-2})\cdot\text{min}^{-1}$ of the true value, for the Manchester data over 80% are within $\pm 0.05 \log_{10}(\text{cd}\cdot\text{m}^{-2})\cdot\text{min}^{-1}$ of the true value. For both the McGwin and Manchester test data more than 80% of the estimates are within $\pm 1.5\text{min}$.

BOOTSTRAP METHODOLOGY AND APPLICATION

C.1 Bootstrap calculation of confidence intervals

As has been mentioned there is no theoretical route from the Nelder Mead method to confidence intervals, unlike analytical methods and therefore an alternative approach is needed. Efron (1979) proposed a method of determining the underlying distribution of a data set and in particular, estimating the underlying statistics, termed ‘bootstrapping’. The method repeatedly estimates the values of a parameter, in this case θ for equation 3.1.2, by using a subset of the data available. The mean of the series of estimates then provides an indication of the true mean of the parameter, and the standard deviation of the estimates is the standard error (SE) of the parameter being considered. If the estimates are not symmetrically distributed then a quantile range can be used (Carpenter & Bithell 2000).

In general the method produces robust confidence intervals for the parameters estimates, with some conditions (Efron 1979, Efron & Tibshirani 1986, Davison & Hinkley 1997, Carpenter & Bithell 2000). The most important condition is that the sampled data should be identically and independently distributed. This means there should be no correlation between data points and that the noise in the observed data should have constant variance. If this correlation condition is not true then we have fewer data points than we believe. For example, if there are correlations between 40 observations say, with maybe only 25 independent, then the variability in the parameter estimates will be too small, since we will have related values over represented in the bootstrap sample, a further discussion of this can be found in Felsenstein (1985). Furthermore, if the variance is not constant over the entire data set, then some values will have a greater influence than others on the estimate of the underlying distribution. The problem of autocorrelated data and constant variance are addressed in chapter 6.

Procedure The collected data are sampled with replacement, creating a subset of equal size to the original data. The term ‘with replacement’ means that a data point may be selected more than once for inclusion in the sample. The statistic of interest, i.e. θ , is calculated for the sample and the process repeated. A great many repeats are needed, Efron suggests that for a complex non-linear problem 1500 repeated samples should be sufficient (Efron & Gong 1983). However, the parameter estimates only became asymptotic in this study when bootstrap repetitions exceeded 5000. In figure C.1.1 the estimated value for each component of θ approaches a fixed point after 5000 repetitions.

Each estimation takes approximately 15seconds, therefore for 6000 repeats the total time required to calculate the mean and dispersion of the parameter θ was ~ 25 hours, clearly this method is limited in its usefulness and an alternative method of calculating confidence intervals would be preferred. One way of dealing with such long processing time would be to use distributed computing, that is, use a cluster of computer cores to calculate the parameter estimates in parallel. This approach was used to find bootstrap estimates of the mean and 95% confidence interval for data collected from 35 subjects. The method relies upon high throughput computing (HTC) and is described below.

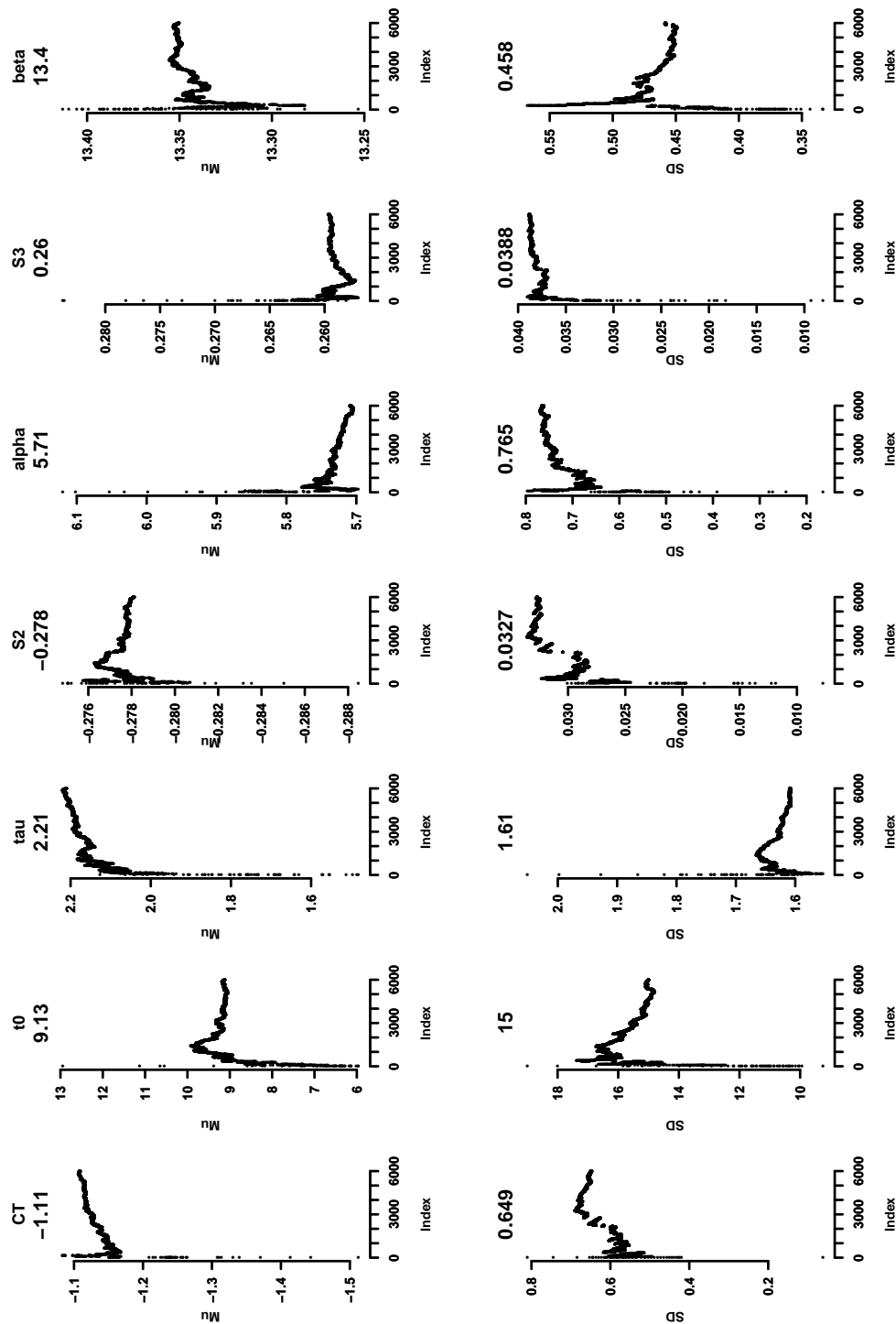


Figure C.1.1: Bootstrap estimates of the mean and standard error of each parameter component for one subject as the number of samples selected increases. Where CT , cone threshold; t_0 is the threshold at time zero, and τ is the time constant of the cone phase, these parameters are the first three in equation 3.1.2. S_2 is the slope of the S2 phase, α the cone rod transition time. The S_3 parameter is the sum of the slopes of the S2 and S3 phases, β is the rod rod transition time.

Condor High Throughput Computing (HTC) is the term given to computing environments that can deliver large amounts of processing capacity over extended periods of time. Central to HTC is the exploitation of all available resources rather than having high processor speeds (Livny, Basney, Raman & Tannenbaum 1997). The University of Manchester has many computer clusters, each composed of several desktop machines. These are provided for students to use; once logged in the student has access to a wide variety of resources for document preparation and research. However, for long periods of time and in particular after 5pm until 8am the following day and during vacations many of the available computers are unused. When the computer is unused it reverts to its standby status as a UNIX workstation.

Since the mid 1980's the Condor Team at the Computer Sciences Department of the University of Wisconsin-Madison have developed software to enable the exploitation of this surplus capacity. The software, Condor, manages a queue of jobs, monitors their progress and reports that progress and advises of completion, furthermore, error capture and reporting mechanisms are also available. The Condor Team internet home page can be found at <http://research.cs.wisc.edu/condor/>.

Method

In this study, the simplest method was to send the 35 data sets to the system and allow 35 cores to run for 25hours. The computer code could have been restructured to distribute the data sets over a much larger number of cores, but the time needed to rewrite and more importantly test the code could not be justified.

Using the script `JMKDAParamTest.m` as its kernel a wrapper function `BSWrapper.m` was written. The wrapper function created a bootstrap sample with replacement and passed the sample to the kernel, see appendix A.1.1 on page 261. This process was repeated 6000 times, using a different bootstrap sample each time. This process was repeated for each subject's data across 35 cores.

In order for the Condor system to be able to process the data the Matlab code had to be compiled, this attaches the Matlab site licence so that the code acts as a stand alone application on each workstation, this prevents the University's available Matlab licences from all being used by the Condor system. The process is summarised in figure C.1.2

Data analysis The HTC process resulted in 6000 estimates of the dark adaptation parameters for each subject. These estimates were summarised by the mean, median and 95% interquartile range.

C.1.1 Results

The bootstrap method takes 25 hours, this could be shortened significantly by altering the wrapper code, however it still relies on the HTC facility available from the University of Manchester. The model comparison method in R takes less than 10 seconds if a figure is drawn.

Confidence intervals A significant relationship between bootstrap CI and model comparison CI was found

$$MC = 0.05 + 0.08BS \quad (\text{C.1.1})$$

where MC is the confidence interval for model comparison and BS is the bootstrap CI, (F-statistic: 8.166 on 1 and 33 DF, p-value: 0.007).

From this we can see that the model comparison CI is a gross under estimate of the bootstrap CI by a factor of ~ 10 , however relative model comparison values can provide information about the bootstrap CIs for a series of measurements. Figure C.1.4 shows the relationship between the methods, a linear relationship with systematic differences.

Discussion of comparison results

All the data used here is presented later in chapter 6. In that chapter some of the data are found to be atypical, either because the seven parameter model is inappropriate, an inadequate photo bleach was applied or the data were excessively noisy. The analysis presented here used all the datasets available, since until collected and subject to this investigation it is difficult to characterise any dataset as anomalous. Nevertheless, the two methods return parameter estimates in agreement with each other, with some exceptions.

Discussion of the CI results

The confidence intervals for each method are attached to their $S2 \log_{10}(\text{cd.m}^{-2}).\text{min}^{-1}$ estimates in figure C.1.3. The bootstrap estimates are restricted to the range $[-0.8, 0]$ by the algorithm, see section 3.4 on page 123. Without this restriction the bootstrap intervals if symmetric would be much larger.

We are now left with the challenge of identifying, objectively, anomalous data sets.

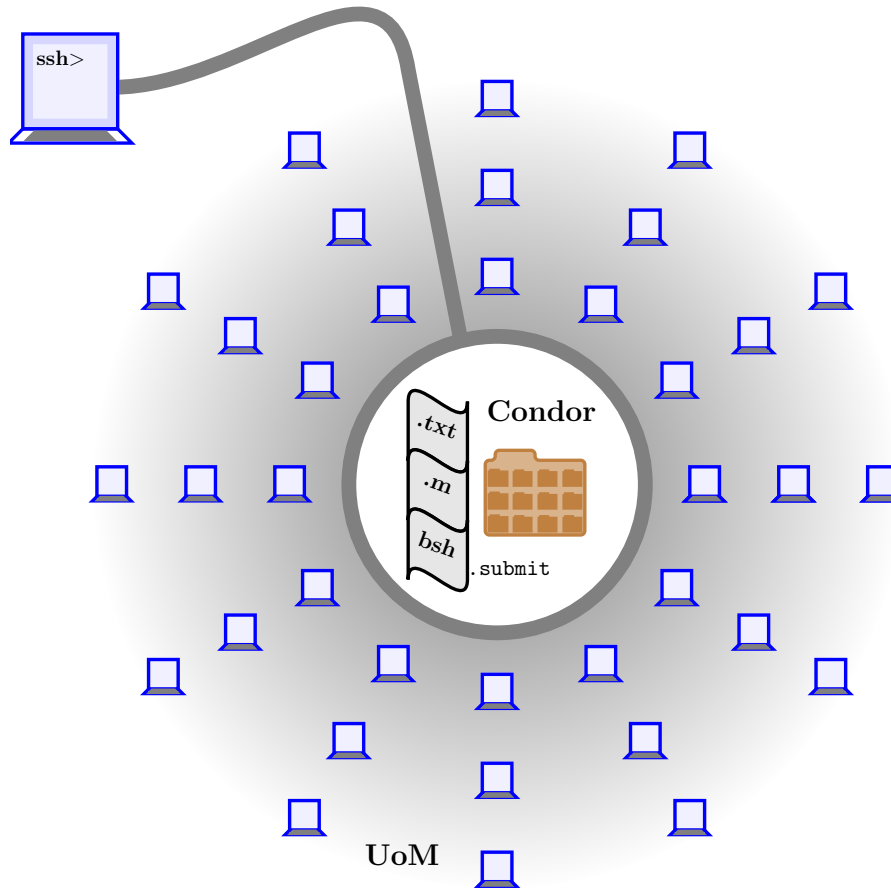


Figure C.1.2: The process of HTC to calculate the confidence intervals of dark adaptation data. A folder was prepared; containing the source data and a text file (**.txt**) listing the path for each data file for all the subjects, the wrapper code and subsidiary functions (**.m**) and the shell script (**bsh**) that would control the process (**.submit**). This file was uploaded from the author's desktop computer using a secure shell (**ssh**), once uploaded the Matlab scripts were compiled and the **.submit** script executed. The **Condor** software recruits unused computer cores from the University of Manchester (**UoM**) cluster, and uses them to process each data file. Should a student log in to a workstation, then Condor halts the processing, recruits another workstation and resumes the processing. Recovery of the processed data is through the secure shell (**ssh**)

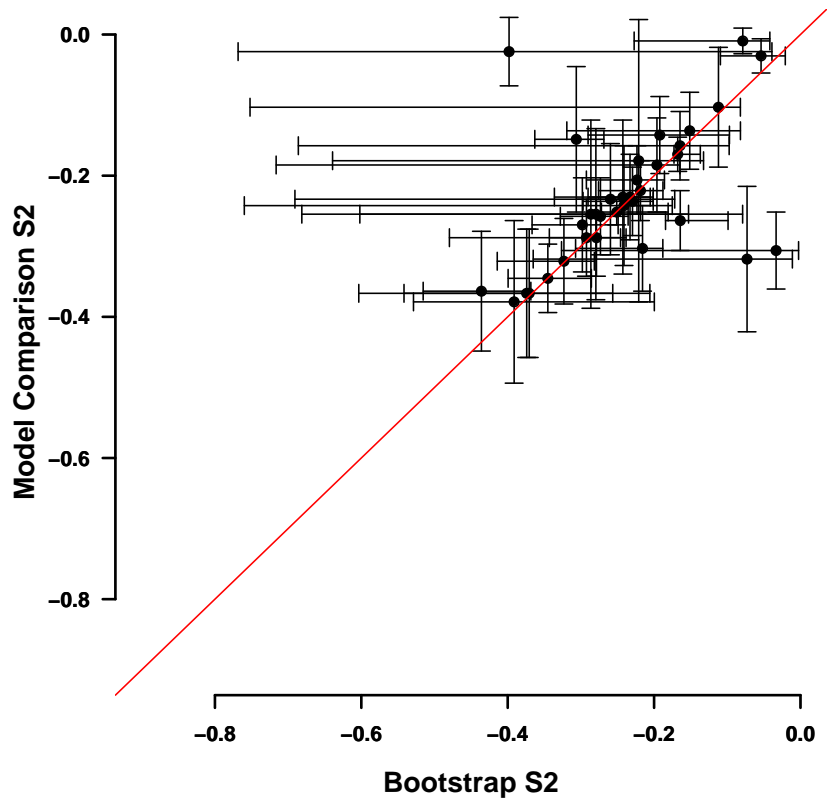


Figure C.1.3: Comparison of parameter estimates and confidence intervals for bootstrap and model comparison methods. Points are the estimates of the S2 value (units $\log_{10}(\text{cd.m}^{-2}).\text{min}^{-1}$ omitted for clarity). Vertical and horizontal bars are the 95% confidence intervals for the model comparison and bootstrap methods respectively

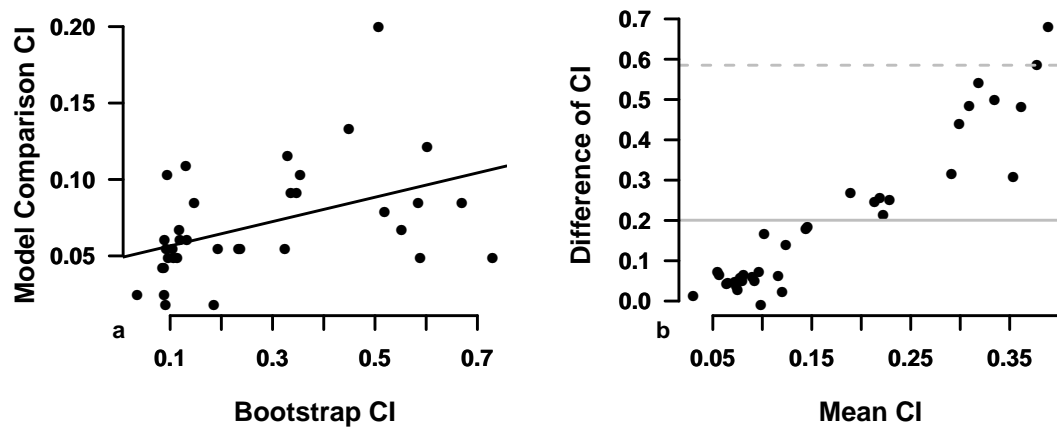


Figure C.1.4: Plot a shows the linear relationship between the confidence intervals found by the two methods, units omitted ($\log_{10}(\text{cd.m}^{-2}).\text{min}^{-1}$) for clarity. Plot b is a Bland Altman plot showing that the bootstrap values are much greater than those found by model comparison.

ANALYTICALLY DERIVED CI ARE WRONG

D.1 A pragmatic approach in R

A method in R that was initially used to estimate the parameters of the dark adaptation recovery curve and confidence intervals, uses a single starting point and the `optim` function's implementation of the Nelder Mead algorithm. Then once an initial estimate of the parameters has been made another function `nls` was used. The `nls` function was developed by Bates & Watts (1988), and is available from the CRAN servers and their mirrors.

The `nls` function returns estimates of the parameters, standard errors for those estimates, 't' values and probabilities for each parameter, e.g. see table D.1.1. The detail of how the standard errors are calculated is outside the scope of this work. However, in brief, the method uses the hessian matrix of the second partial derivatives of the parameters; using this function `nls` and the derived standard errors requires an assumption about the behaviour of the second partial derivatives that may not be justified. The function assumes that the response surface is linear at or near the global minimum. The function also reports whether it has been able to converge to a satisfactory solution. This option was disabled so that only a warning was issued.

I have described the method as 'pragmatic' because a result can be coerced from the method, even when convergence criteria are not met and to account for the assumptions made regarding continuity of the model function and the uniformity the noise variance, see section 3.3.1. Furthermore the multi start option is not included, and so the likelihood of a local rather than global minimum is higher than in the Matlab method.

The structure of the script is similar to that in Matlab and is discussed in detail in appendix A.2.

Table D.1.1: An example of the summary statistics returned for the estimates of the parameter values using `nls` function.

	Estimate	Std. Error	t value	Pr(> t)
$\hat{\theta}_1$	-1.01	0.23	-4.40	0.00
$\hat{\theta}_2$	0.21	0.81	0.26	0.79
$\hat{\theta}_3$	1.11	7.45	0.15	0.88
$\hat{\theta}_4$	-0.24	0.02	-10.44	0.00
$\hat{\theta}_5$	3.94	0.93	4.22	0.00
$\hat{\theta}_6$	0.15	0.03	4.60	0.00
$\hat{\theta}_7$	11.27	0.99	11.43	0.00

D.2 Comparison of Matlab bootstrap quantiles with R standard errors

The main reason for using the bootstrap method here was that we have no analytical route to determine the variability of the elements of the parameter θ and we have no knowledge of its underlying distribution. Therefore it is prudent to use quantiles to describe the variance of parameter estimates (Carpenter & Bithell 2000). The 95% confidence intervals from the `nls` method were compared to the 95% quantile range from the bootstrap. The parameter of most interest in this study is the slope of the S2 phase; confidence intervals for this value, using data collected from 35 subjects, is shown in figure D.2.1.

The aim when comparing the robust bootstrap method with the coerced R method is to discover in what circumstances can the much faster method in R be reliably used.

When can we use the R method? The method in R was initially unable to return parameter estimates for two of the data sets, subjects 25, and 31. If the seed parameters provided to the R script were those found using the Matlab script then every dataset was able to be analysed with the R script. This emphasises the importance of the starting values when using a direct search algorithm. The Matlab method was able to return values for all 35 of the data sets.

Parameter estimates The `nls` method and bootstrap median estimates, see figure D.2.1a, are in reasonable agreement, however, five data sets are not in agreement (subjects: 9, 22, 28, 35 and 36). The possible reasons for these data being anomalous are discussed in chapter 6 when the analogue data are discussed in detail. The Bland-Altman plot (Bland & Altman 1986) highlights these data points, see figure D.2.1b, and shows that there is no systematic relationship between the estimates from both methods.

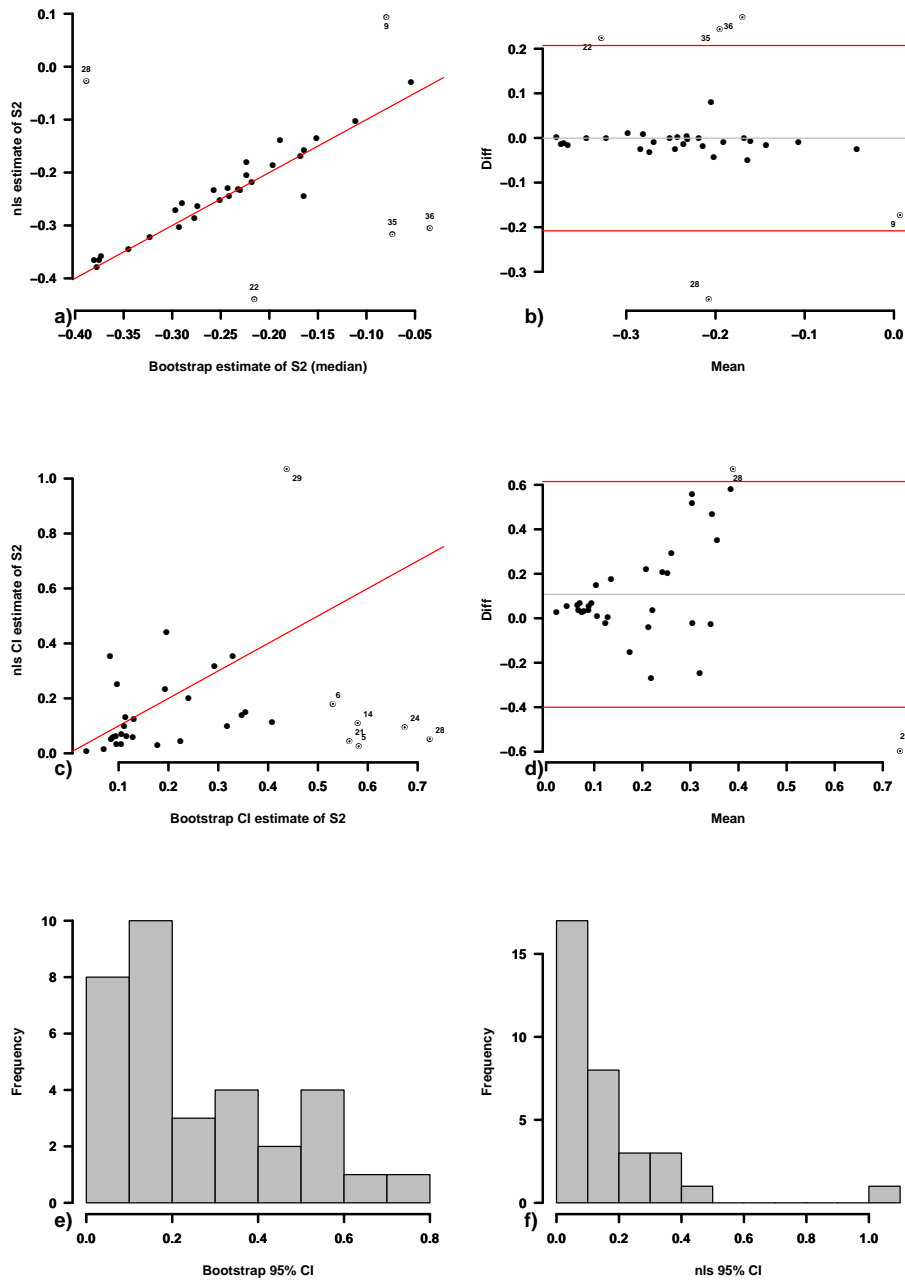


Figure D.2.1: A comparison of the estimates for the value of S2 and the 95% confidence intervals calculated by nls and the bootstrap method. Plot (a) shows the direct comparison, and the line of equality, of the S2 estimates. (b), is a mean against difference plot (Altman & Bland 1983) (BA) for the two methods. Plot (c) compares the two confidence intervals, (d) is a BA plot for the size of the confidence intervals. Figures (e) and (f) show the distribution of the confidence intervals. Units for S2 are $\log_{10}(\text{cd.m}^{-2}).\text{min}^{-1}$ scotopic.

For all the data the Pearson correlation coefficient of $\rho = 0.49$ (CI 0.18 – 0.72, p-value = 0.003). A further measure of agreement between continuous methods of measurement is the Lin concordance correlation coefficient $\rho_c = 0.49$ (CI 0.18 – 0.71), (Lin 1989). This is a conservative measure of agreement that as well as giving information about the agreement or otherwise of a pair of measurements, also indicates how far a data pair are from the line of equality, compare this to the Pearson product moment correlation coefficient which measures how far each data pair is from the line of best fit. From this we can infer that the small differences between the two methods when comparing all points are due to the extreme values, since $\rho = \rho_c$ occurs if and only if the means and variances of the two measurements are equal (Lin 1989, p258).

Confidence intervals The confidence intervals were not in close agreement. In figure D.2.1c the `nls` values are consistently smaller than the values found by bootstrapping. In particular the `nls` method returns very small confidence intervals for data from subjects 5, 6, 14, 24 and 28, and a much larger interval for subject 29. There is no correlation between the values $\rho = 0.12$ (CI: -0.23 to 0.45, $t = 0.68$, $df = 31$, p-value = 0.5). The Bland Altman plot D.2.1d, reiterates the disparity between the values returned by the two methods in calculating confidence intervals. This discrepancy between numerical and analytic methods has been described in the literature, and has been ascribed to a failure of linearisation, see for example (Donaldson & Schnabel 1987).

In figure D.2.1 e and f, we can see that the distributions of the confidence intervals returned by each method are very different. The bootstrap returns a more uniform range of values and is less skewed. It would seem therefore that we can use the R script for rapid determination of parameter values. But that the more intensive process of bootstrapping is required to obtain confidence intervals.

A method of model comparison to calculate a confidence interval for the S2 phase of rod recovery is presently awaiting reviewers comments. This novel application of an established method first fits the model to the data, then the values of the cone rod breakpoint and rod rod breakpoint are varied. When the new value is significantly different to the initial value this is taken as the upper or lower confidence limit. The pairs of possible α and β points are used to find possible values for the slope of S2. The maximum and minima values found represent a confidence interval for the slope. The draft paper is in appendix I.3.

In chapter 6 the characteristics of the data that gave rise to the anomalous points will be discussed, see section 6.5. Furthermore the assumptions central to bootstrapping will be examined, that is, that the data are independent and identically distributed.

D.3 The assumption of linearity of the parameters in the response surface at the global minimum

Analytical methods of calculating confidence intervals assume that the function being minimised has parameters that are linear at the global minimum. This assumption may not be valid. One way of investigating this validity for the seven parameter model used in this study is to hold six of the parameters constant and calculate a confidence interval for one parameter at a time. The results of this process are summarised in figures D.3.1 and D.3.2.

In figure D.3.1 , the noise free data, we can see that the cone parameters and the rod cone break point and the sixth parameter are linear (labelled a1,2,3, a5 and a6 in the figure). The sixth parameter is the sum of the S2 and S3 slopes. The parameter a7 the rod rod transition time is slightly irregular However, even for this ideal data the estimate of the S2 slope (a4) is not linear.

Introducing a small amount of noise into the data causes quite marked changes in the linearity of the parameter estimates. The parameter a4 the slope of the S2 phase is undefined for values greater than the best estimate. Similarly the estimates for the rod cone breakpoint and the sum of the S2 and S3 phases are unbounded.

This behaviour accounts for the failure of the `nls` method to calculate the confidence intervals in section D.2 with any reliability. Further discussion of the difficulties of approximating bootstrap methods with linear approximations is discussed by Donaldson & Schnabel (1987).

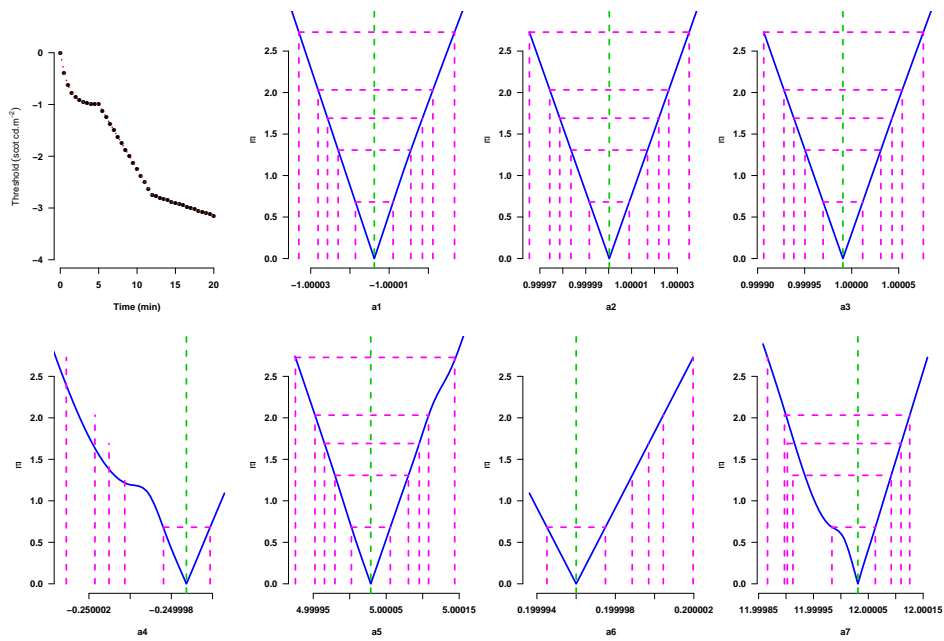


Figure D.3.1: Linearity of parameter estimates for noise free data. Upper left plot is the data being considered. Each subsequent plot from left to right considers the absolute t value against the change in the parameter for each each of the seven parameters.

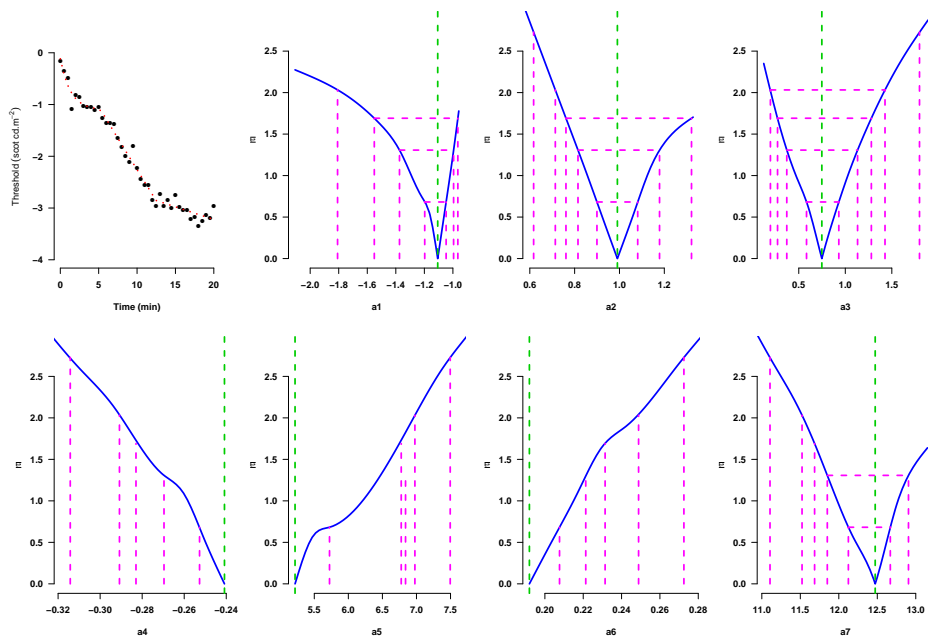


Figure D.3.2: Linearity of parameter estimates for data with very little noise. Upper left plot is the data being considered. Each subsequent plot from left to right considers the absolute t value against the change in the parameter for each each of the seven parameters.

ELECTRONIC CIRCUIT DIAGRAMS

E.1 Analogue Dark Adaptometer

E.2 Digital Dark Adaptometer

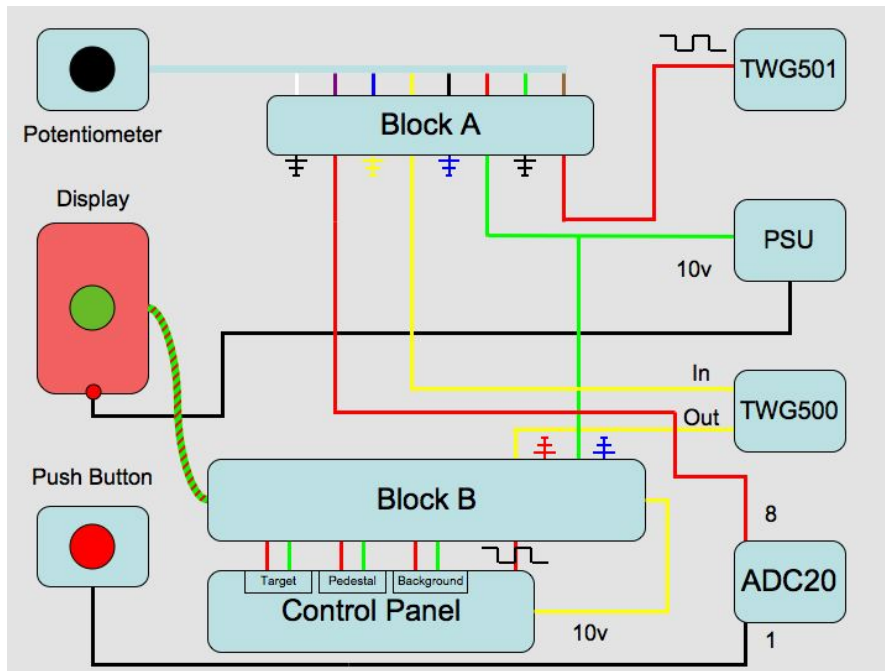


Figure E.2.1: Block diagram of Analogue Apparatus. Blocks A and B are connector blocks. The wires are colour coded to facilitate reassemble if necessary. TWG501, a signal generator. PSU, power supply unit (10v). TWG 500 signal generator acting as an amplifier. ADC20, precision data logger. Control panel, switches between pre set background levels and wavelengths chosen.

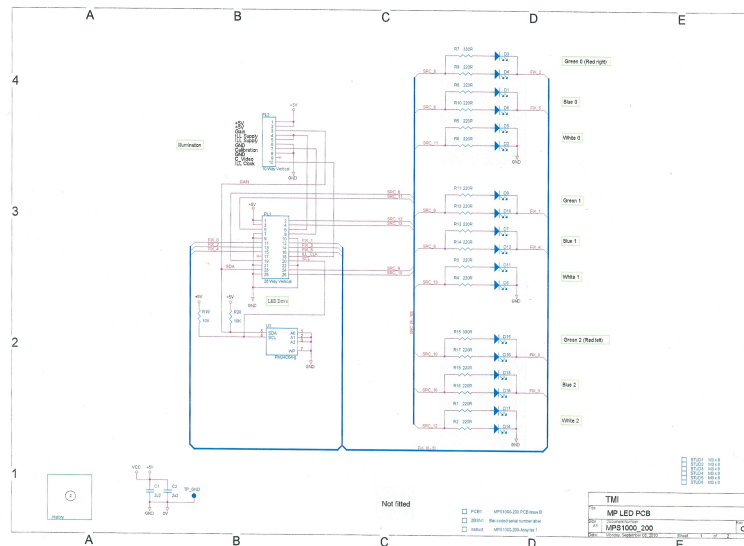


Figure E.2.2: Circuit Diagram of the Target Board, LEDs D1 to D15 were altered to provide red and green targets and fixation points. Resistors R1 to R18 were altered to bring the linear range and luminance to the desired values.

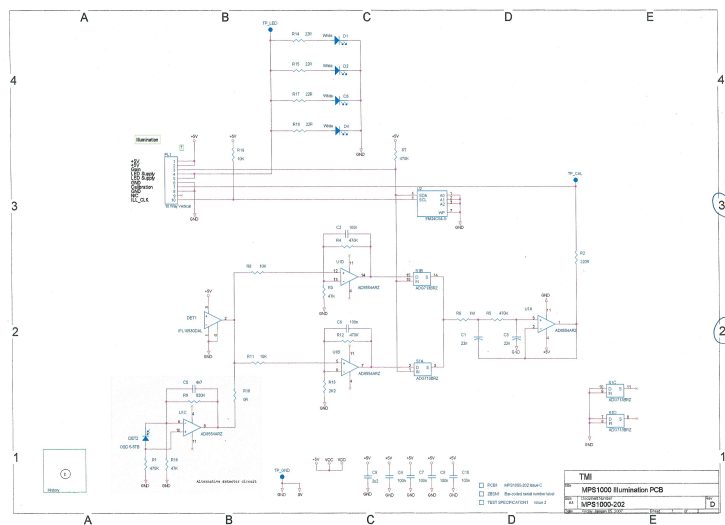


Figure E.2.3: Circuit Diagram of the Illumination Board. LEDs D1 to D4 were removed and replaced with red or green LEDs.

SCOTOPIC CONTRAST SENSITIVITY RESULTS

F.1 Parameter values from a bi exponential model

Table F.1.1: Parameters of the bi-exponential model fitted to the data from 13 subjects, measured for three spatial frequencies (0.5, 1, 2cpd). Sx is the subject code, units for $\phi_{1,2,6}$ are $\log_{10}(\text{contrast})$ and for $\phi_{3,4,6}$ are minutes. SSE is the sum of squares of the errors and SF is the spatial frequency of the grating (cpd).

Sx	ϕ_1	ϕ_2	ϕ_3	ϕ_4	ϕ_5	ϕ_6	SSE	SF
1	-1.54	1.95	0.5	8.16	0.35	0.33	0.37	0.5
	-1.78	4.24	1.33	6.02	0.62	0.2	0.6	1
	-1.38	3.19	0.94	8.37	0.23	0.5	0.74	2
2	-1.56	3.16	0.77	7.57	0.57	0.06	0.43	0.5
	-1.41	2.71	0.24	5.48	-0.62	1.13	0.69	1
	-1.63	4.94	1.3	2.33	0.85	0.04	0.31	2
3	-1.66	5.59	1.7	4.83	0.45	0.29	0.57	0.5
	-2.23	2.08	0.95	5.8	0.96	0.08	0.54	1
	-1.49	8.97	2.72	4.93	0.52	0.28	0.62	2
4	-1.73	5.52	2.1	2.22	0.71	0.16	0.35	0.5
	-1.96	2.92	1.24	8.84	0.49	0.23	0.6	1
	-1.68	5.12	1.44	7.24	0.52	0.15	0.2	2
5	-1.74	4.37	1.56	6.61	0.89	0.19	0.38	0.5
	-3.61	205.38	4	5.24	2.73	0.04	0.23	1
	-1.36	12.38	3.06	9.08	0.37	0.53	0.51	2
6	-1.97	4.82	1.8	4.59	0.77	0.07	0.19	0.5
	-2.51	16.23	3.36	1.53	1.48	0.04	0.11	1
	-2.5	1.67	1.15	7.5	1.21	0.04	0.18	2
7	-1.89	6.58	1.78	5.93	0.92	0.12	0.16	0.5
	-1.92	4.72	1.35	5.47	0.97	0.09	0.2	1
	-1.44	2.9	1.11	5.75	0.48	0.13	0.16	2
8	-1.69	6.96	1.78	9.39	0.34	0.68	0.22	0.5
	-2.02	1.83	1.33	1.63	1.02	0.06	0.3	1
	-1.51	6.34	2.25	7.75	0.52	0.12	0.33	2
9	-1.89	1.19	1.43	2.93	0.74	0.09	0.12	0.5
	-2.73	5.41	2.37	3.54	1.68	0.03	0.14	1
	-2.23	2.79	2.99	3.54	1.61	0.03	0.58	2
10	-1.6	2.46	0.93	10.25	0.31	0.76	0.14	0.5
	-2.08	3.01	1.33	7.31	0.7	0.08	0.13	1
	-1.48	2.03	1.1	6.68	0.33	0.26	0.18	2
11	-2.15	9.1	2.23	5.89	1.22	0.1	0.4	0.5
	-1.54	4.13	1.38	9	0.37	24.12	0.07	1
	-1.07	3.12	1.42	5.87	0.29	0.92	0.11	2
12	-1.91	6.01	1.61	9.23	0.73	0.18	0.46	0.5
	-1.98	19.06	3.65	1.62	1.03	0.06	0.37	1
	-2.48	4.93	1.66	2.71	1.42	0.02	0.56	2
13	-2.1	1.76	0.84	8.4	1.27	0.05	0.23	0.5
	-2.53	2.49	1.02	5.93	1.48	0.05	0.36	1
	-1.45	5.82	1.54	2.15	0.47	0.2	0.36	2

RAW DATA FROM ANALOGUE APPARATUS

G.1 Plots of raw data, with fitted curves

G.1.1 Comments on individual plots

Twelve pages of results, each with visit one and two, along with parameter estimates.

G.2 Parameter Values for each Subject at each Visit

G.3 Model Fitting using Information Theory

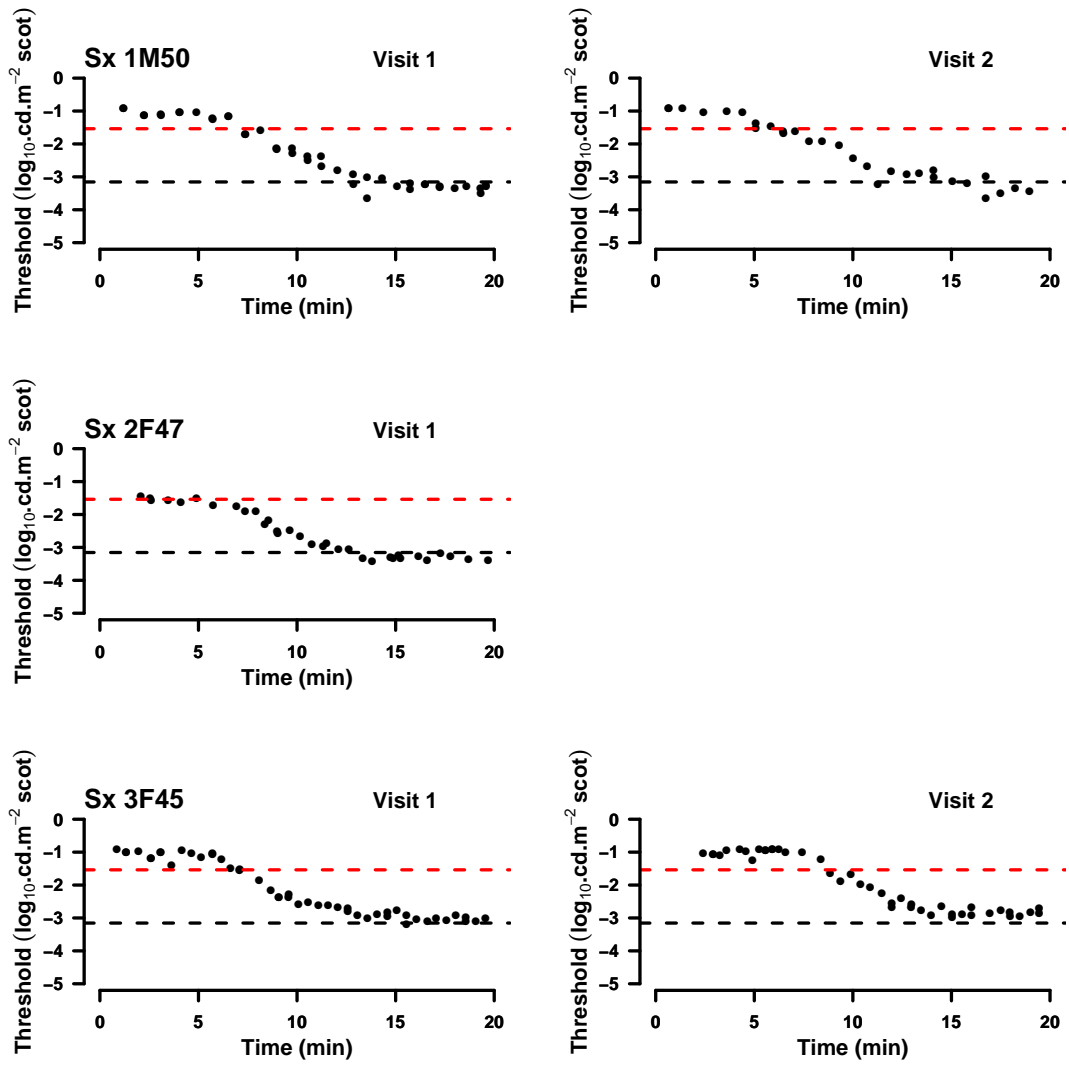


Figure G.1.1: Subjects 1 to 3. Subjects 1 and 3 have elevated cone thresholds at both visits. Subject 2 has no thresholds recorded above cone threshold.

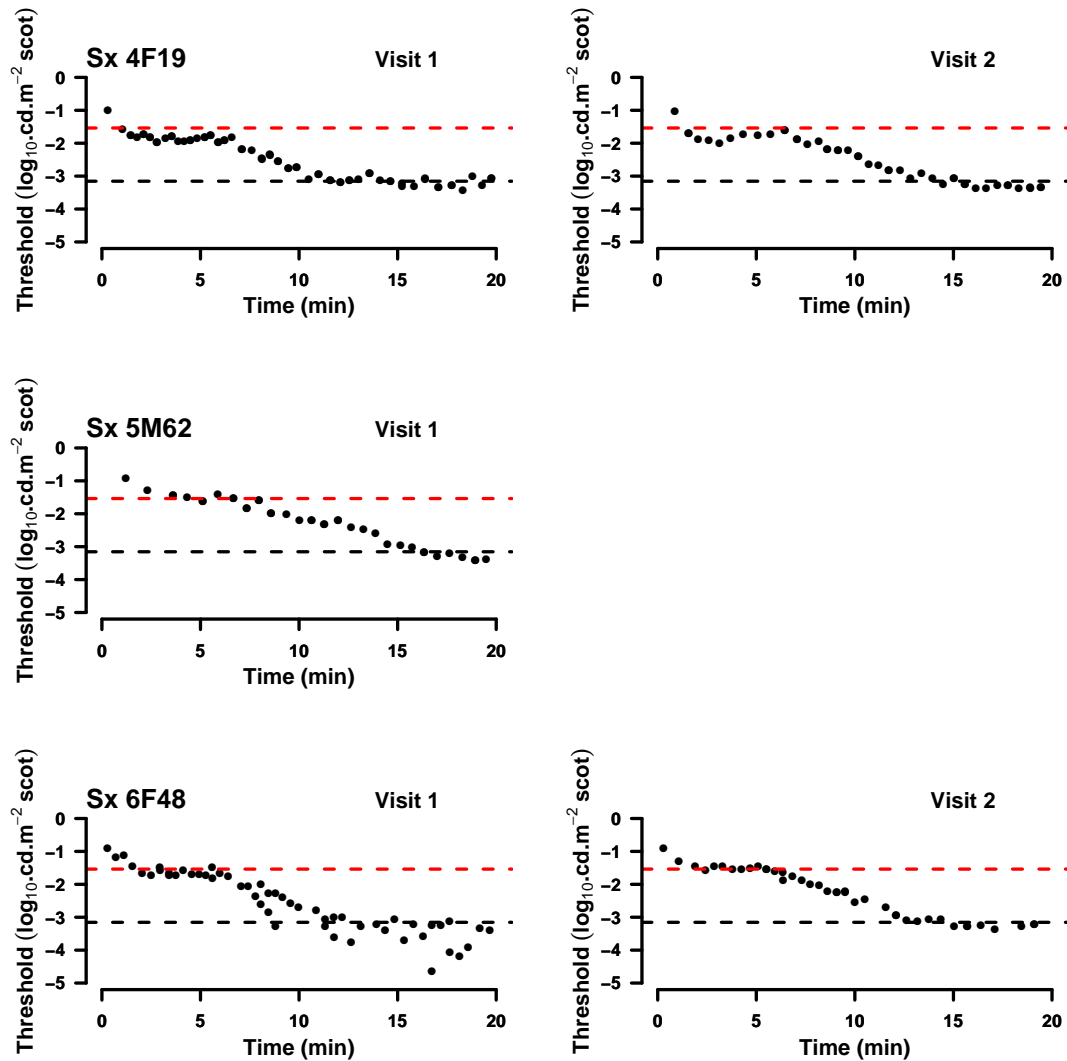


Figure G.1.2: Subjects 4 to 6. Subject 4 has cone threshold slightly below the photopic luminance of the background with some auto-correlation of the thresholds at the first visit. At the second visit thresholds were set less frequently. Both visits show some elevation in cone threshold just before the rod sensitivity recovery phase S2. Subject 5 has a poorly defined cone rod breakpoint. Subject 6 is prone to guessing during the S2 phase and the rod threshold phase, this subject's absolute threshold is a potential outlier. At the second visit this tendency is absent, suggesting a learning effect of this subject.

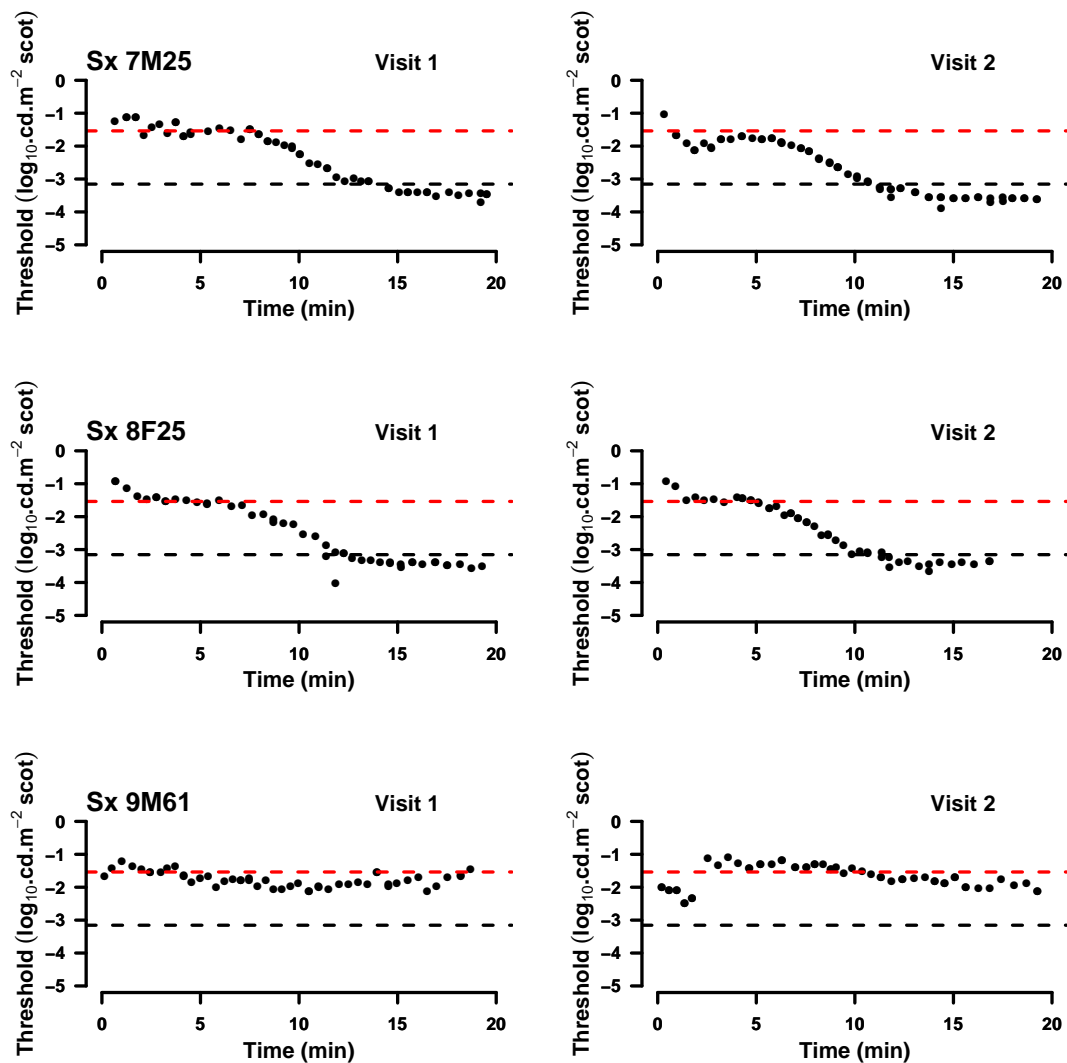


Figure G.1.3: Subjects 7 to 9. Subject 7 demonstrates a tendency to guess during the early cone dominated phase at both visits, with rod threshold just below the scotopic luminance of the background. Subject 8 only guesses once at the rod rod transition point on their first visit. Subject 9 appears to have no rod recovery in the twenty minutes following the photo-bleach, and is identified as an outlier for many parameters, see text for further detail.

Sx 10

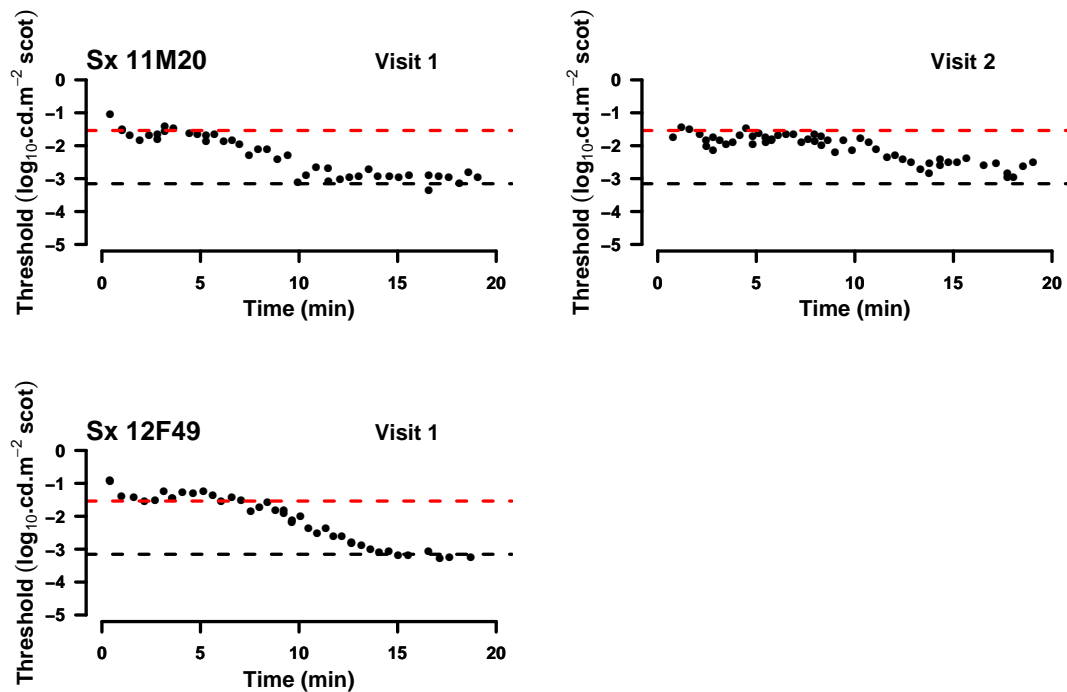


Figure G.1.4: Subjects 10 to 12. Subject 10 withdrew for personal reasons before any data could be collected. Subject 11 has a short cone phase at the first visit, with a tendency to guess during the S2 phase, at the second visit the cone rod transition point is later with erratic thresholds at the transition time, the final rod phase is elevated suggestive of delayed responses. Subject 12 has cone and rod thresholds at the photopic and scotopic luminances respectively, of the background screen

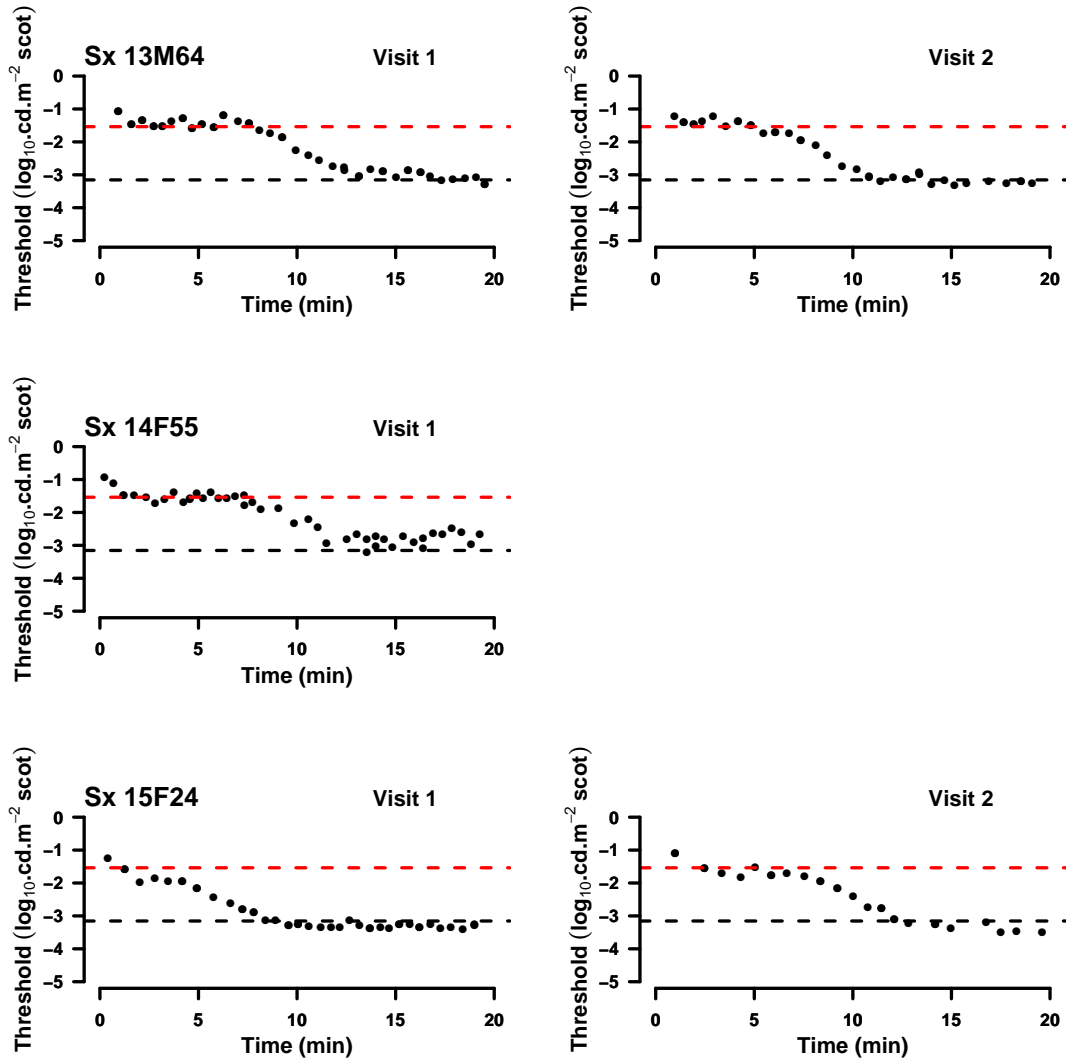


Figure G.1.5: Subjects 13 to 15.

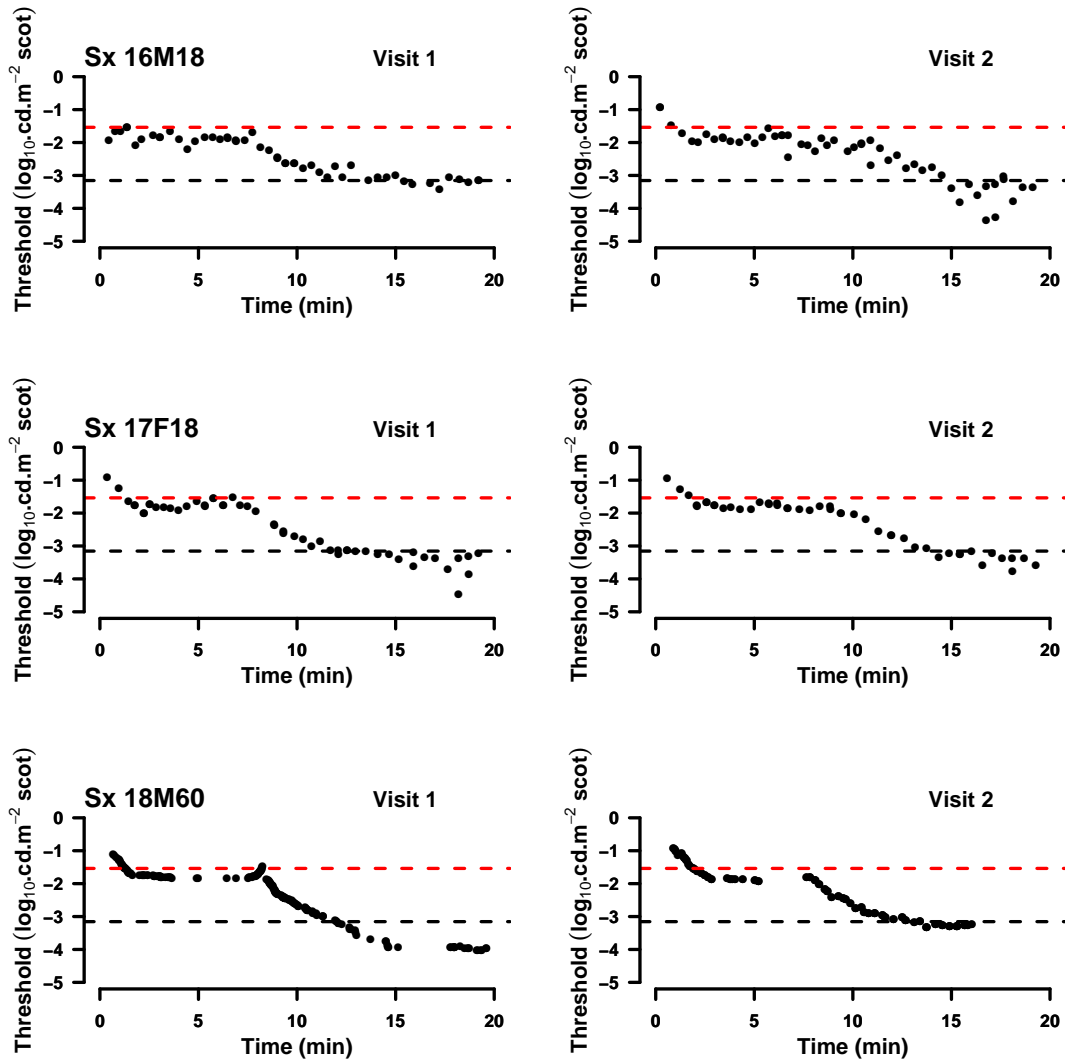


Figure G.1.6: Subjects 16 to 18. Subject 16 had a poorly defined cone phase, with thresholds that increase in short phases. Suggesting that the subject either had a tendency to guess or that they had a lower threshold than the screen luminance and that subsequent thresholds were influenced by earlier measurements. Their second visit had a better defined cone phase, but a very noisy rod phase, reflected in their MSE of 0.07 (see table G.2.2). Subject 17 had cone threshold just below screen luminance with a slight elevation before the cone phase, their absolute threshold was subject to some fluctuation more noticeable at their first visit than the second. Subject 18 was an experienced psycho-physicist and set their thresholds at will. The first visit has a cone threshold just below screen luminance and an absolute threshold nearly a log unit below the scotopic screen luminance. At their second visit cone threshold was similar (1.8 against 1.9 cd.m^{-2}), but the absolute threshold related to screen luminance. At both visits the subject became distracted during the late cone phase, at the first visit returning a series of increasing threshold and at the second failing to mark their threshold.

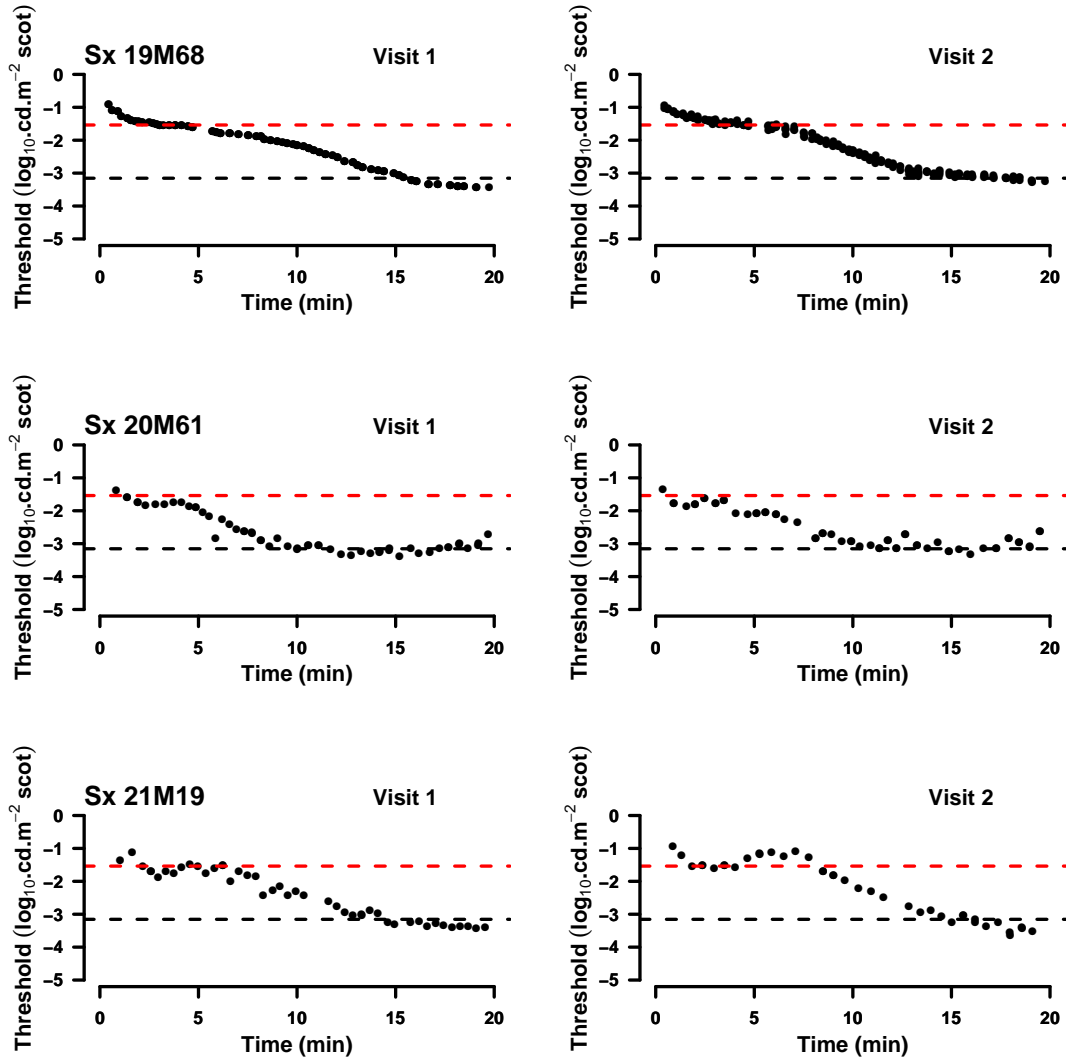


Figure G.1.7: Subjects 19 to 21. Subject 19 was an experienced participant of psychophysical experiments and set thresholds at will. Both cone and absolute thresholds are closely related to the luminance of the screen. Subject 20 had cone threshold just below photopic screen luminance, absolute threshold at scotopic luminance. Subject 21 had thresholds rallied to screen luminance, but the estimates fluctuated slightly, suggesting that threshold measurements were influencing subsequent thresholds. On their second visit there is noticeable elevation in the the threshold just before the first rod phase begins.

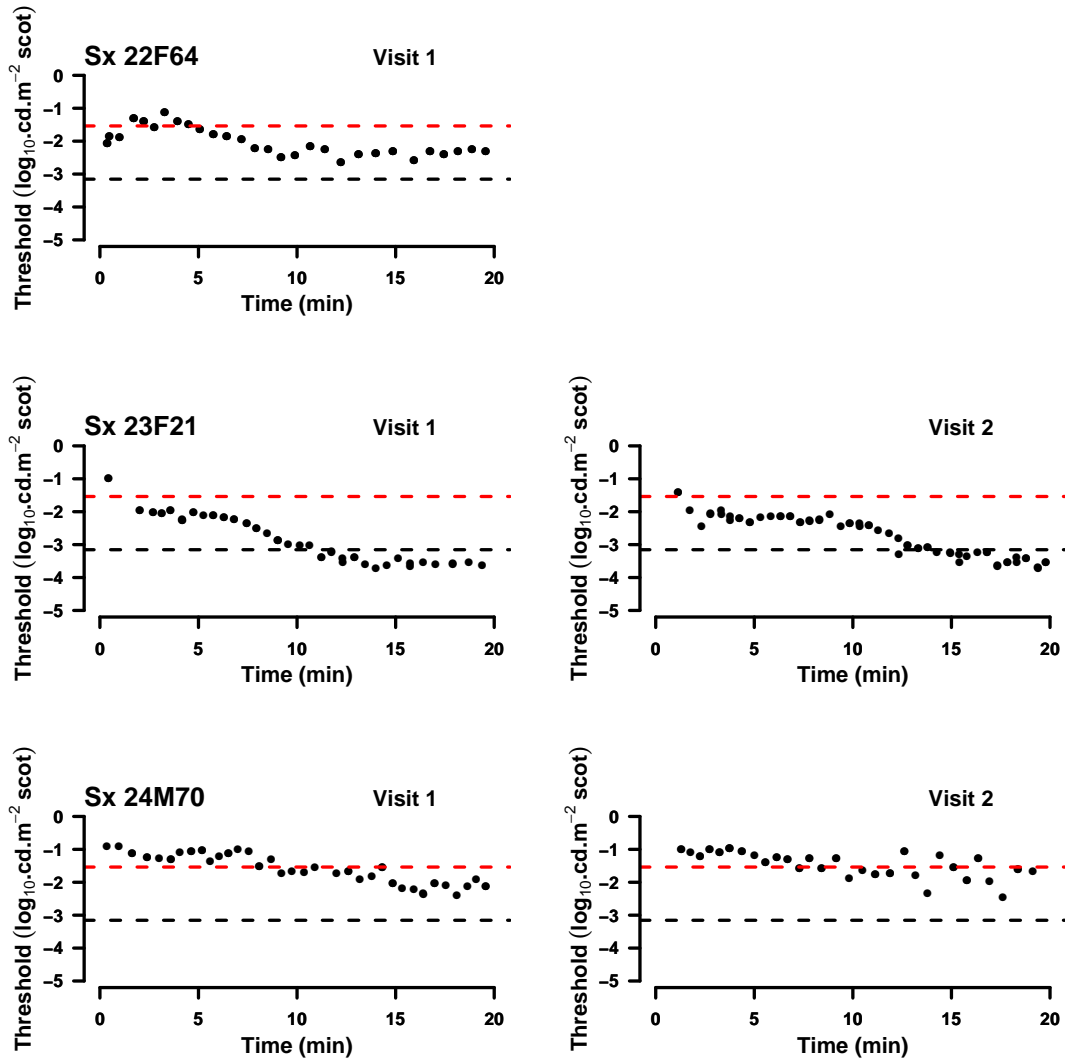


Figure G.1.8: Subjects 22 to 24. Subject 22 has elevated rod threshold apparent at 10 minutes followed by a sinusoidal fluctuation in the threshold. Subject 23 has a cone threshold below the photopic luminance of the screen, the absolute threshold is slightly below the scotopic luminance of the screen for both visits. Subject 24, a 70 year old male, has no apparent rod recovery phase in the time they were measured. Subject 24's absolute threshold at the first visit is identified as a potential outlier.

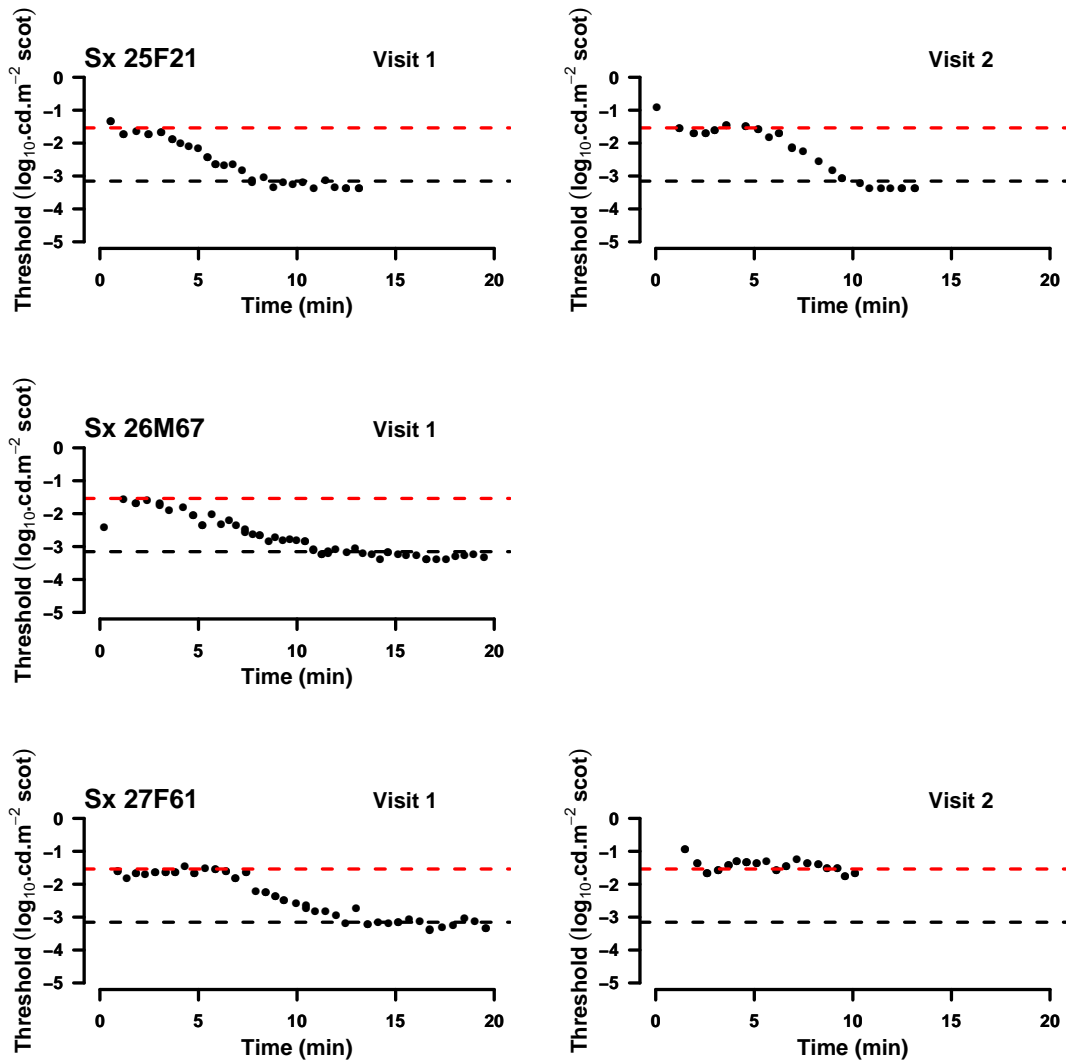


Figure G.1.9: Subjects 25 to 27. Subject 25 presents data with a defined cone phase and accurate rod phases, each phase at the luminance of the screen. Subject 26 has an early guess then in the rod phase settles to non noisy estimates of threshold at the scotopic luminance of the screen. Subject 27 provided non noisy data at their first visit, but chose to withdraw after ten minutes of their second visit.

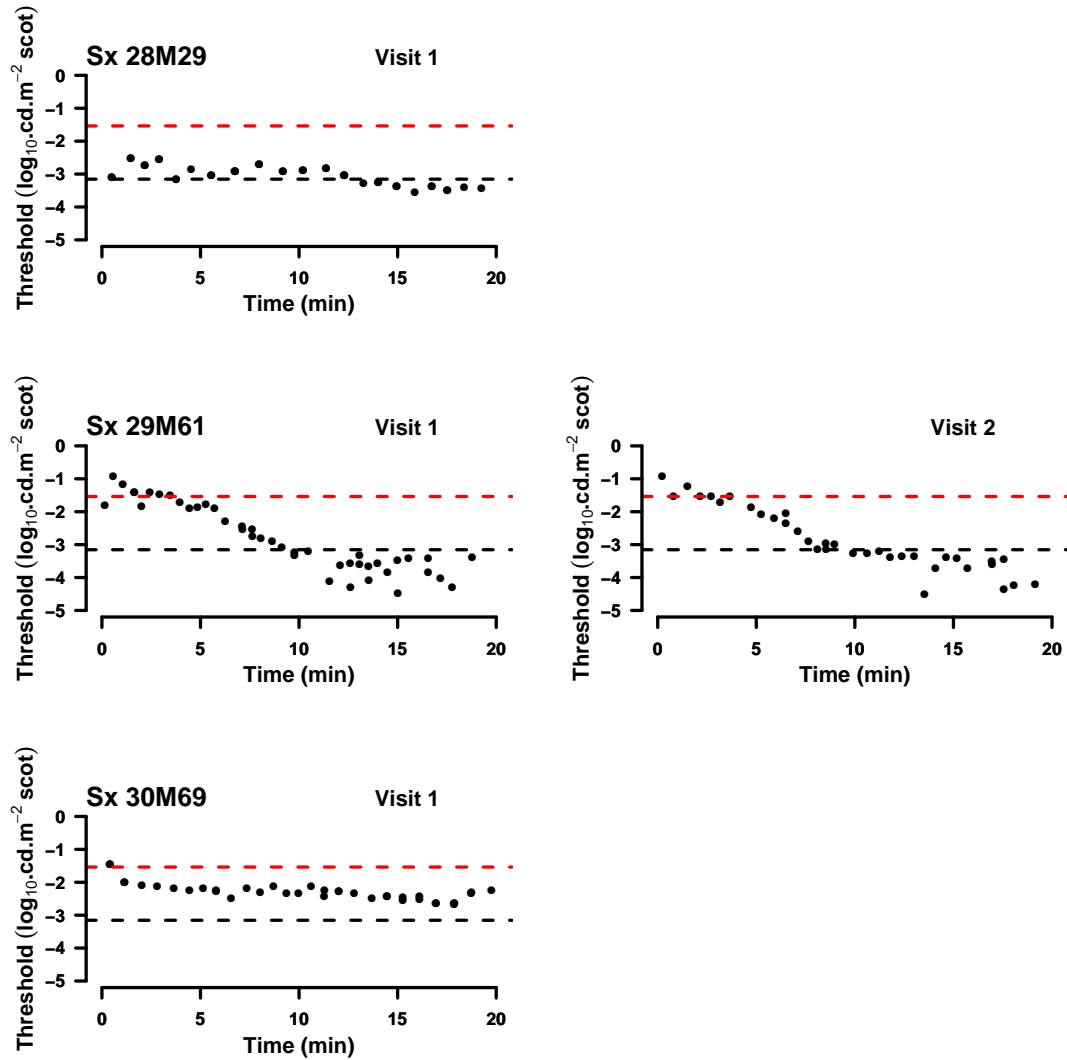


Figure G.1.10: Subjects 28 to 30. Subject 28 has no elevation of the their threshold most likely due to misalignment of the flashgun or a blink just prior to the flash. Subject 29 is prone to guessing during the final rod phase, and is identified as an outlier when the MSE error of the model fit is considered. Subject 30 has a threshold midway between the photopic and scotopic luminance of the screen. Suggestive of some rod function and perhaps no photo bleach, alternatively the instructions may have been poorly given.

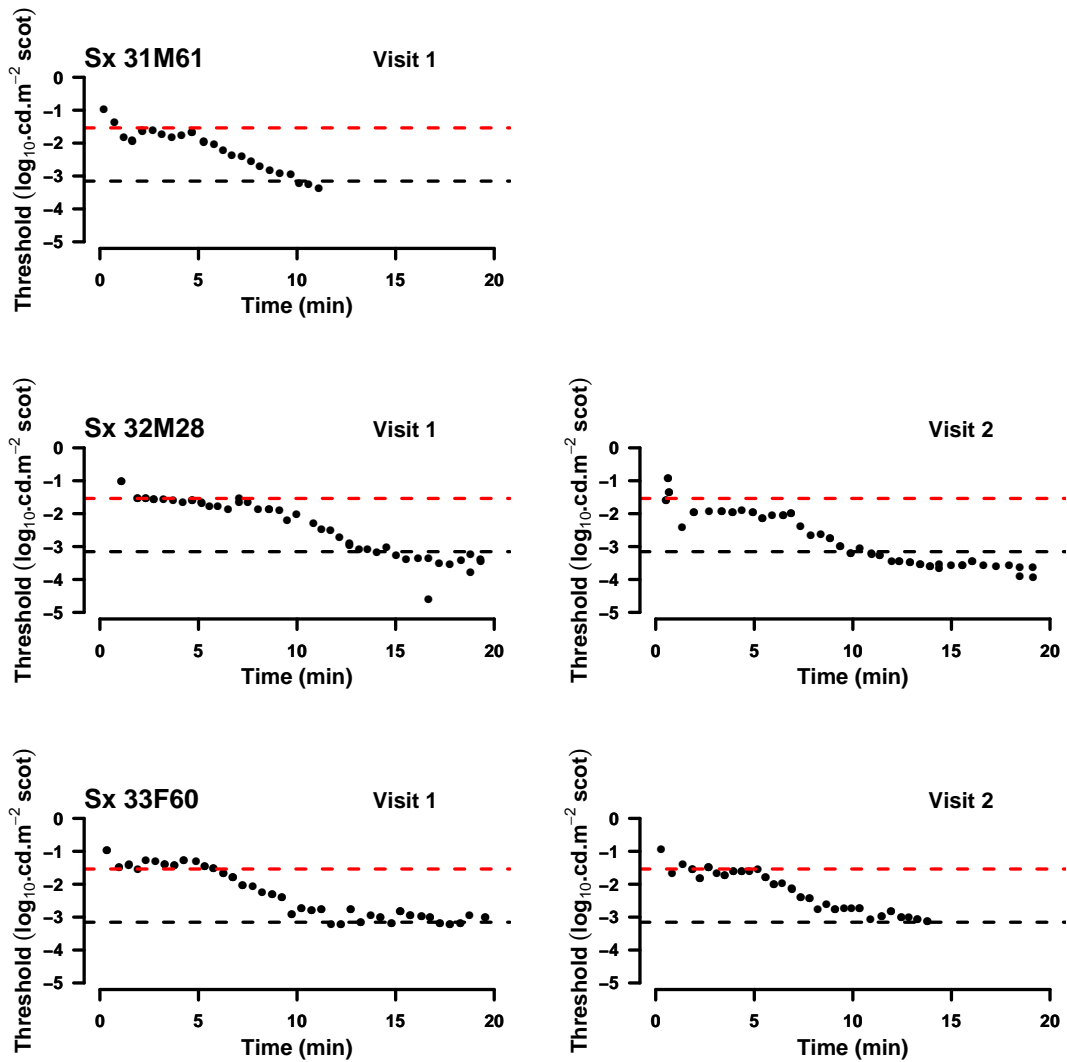


Figure G.1.11: Subjects 31 to 33. Subject 31 male age 61, did not continue beyond 12minutes. Cone threshold at or just below photopic luminance of the screen. Subject 32 male aged 28, On first visit absolute threshold just below scotopic screen luminance, on second visit both cone and rod thresholds below screen luminance. Subject 33 female age 60 thresholds closely related to screen luminance.

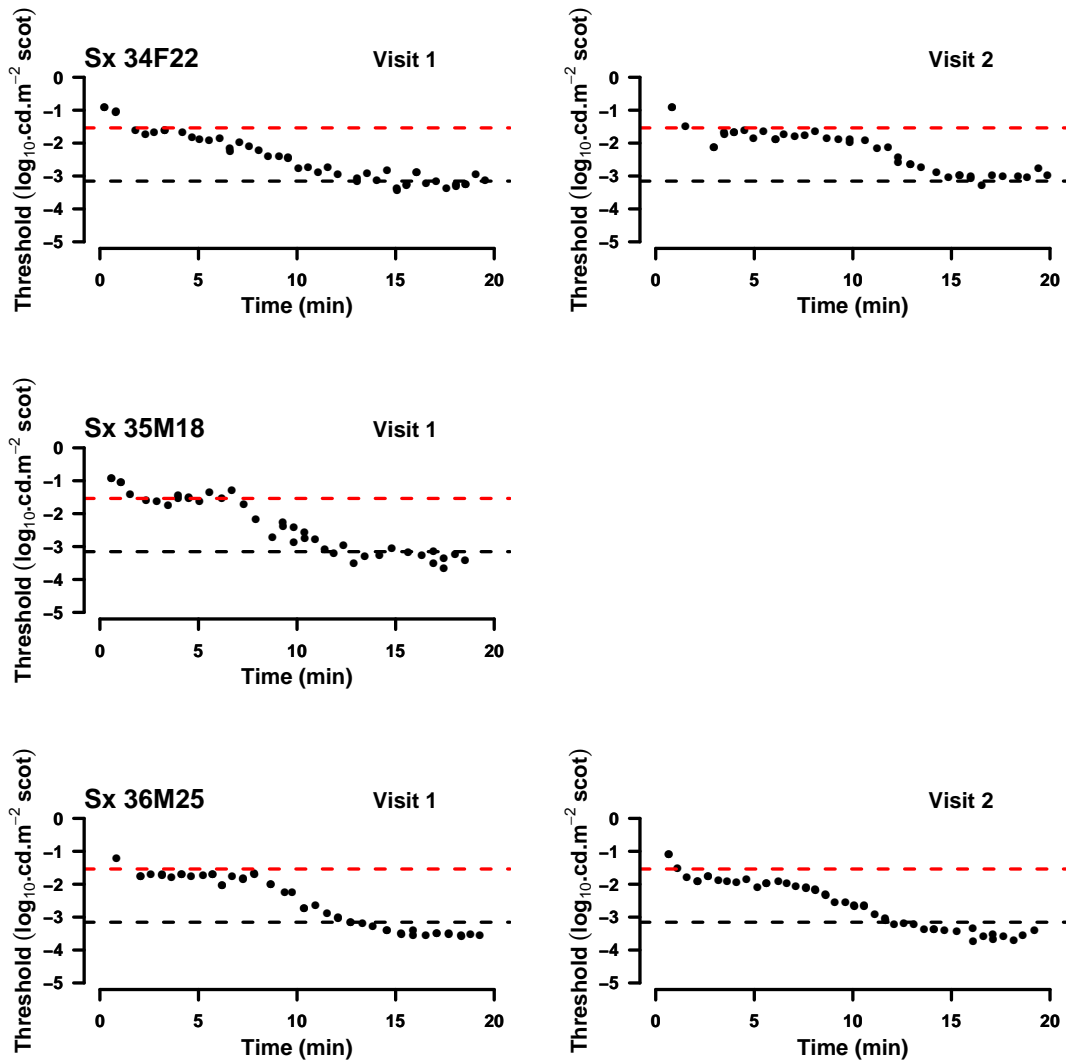


Figure G.1.12: Subjects 34 to 36. Subject 34 female age 22 cone threshold just below photopic luminance of the background, absolute threshold at scotopic luminance of background. Subject 35 male age 18 completed one visit shows slight threshold elevation before rod phase some guessing during S2 phase and during absolute threshold at scotopic luminance of screen. Subject 36 male age 25, both cone and rod thresholds just below luminance of the screen.

Table G.2.1: Summary of parameters from the first visit, CT cone threshold cd.m^{-2} , CC cone coefficient cd.m^{-2} , Tau cone time constant min, S2 slope of S2 phase $\log_{10}(\text{cd.m}^{-2}).\text{min}^{-1}$, Alpha, cone rod breakpoint min, S3 slope of S3 phase $\log_{10}(\text{cd.m}^{-2}).\text{min}^{-1}$, Beta, rod rod breakpoint min

	CT	CC	Tau	S2	Alpha	S3	Beta	MSE
1	-1.09	3.85	0.16	-0.27	5.52	0.25	8.04	0.02
2	-1.88	0.64	2.10	-0.22	6.38	0.22	6.71	0.01
3	-1.09	0.69	0.29	-0.34	5.72	0.29	4.48	0.01
4	-1.86	1.39	0.27	-0.22	5.78	0.21	5.68	0.01
5	-1.54	1.96	0.46	-0.16	6.50	0.07	10.51	0.01
6	-1.95	1.03	1.30	-0.18	5.59	0.44	11.60	0.18
7	-1.61	0.71	0.93	-0.27	7.67	0.24	6.28	0.01
8	-1.61	1.17	0.57	-0.37	7.37	0.32	4.48	0.03
9	-1.31	-0.51	0.14	-0.08	0.48	0.12	9.03	0.02
10								
11	-1.66	2.10	0.15	-0.26	5.81	0.24	4.55	0.03
12	-1.39	10.65	0.06	-0.23	6.70	0.19	7.33	0.01
13	-1.43	42.70	0.08	-0.32	7.65	0.28	4.32	0.01
14	-1.55	0.98	0.26	-0.22	6.88	0.27	6.49	0.02
15	-2.00	1.07	0.50	-0.25	4.19	0.25	5.09	0.00
16	-1.97	0.29	1.97	-0.37	7.73	0.32	2.36	0.02
17	-1.76	1.76	0.24	-0.38	7.34	0.30	3.22	0.04
18	-1.80	2.53	0.25	-0.37	7.99	0.33	5.42	0.01
19	-1.85	0.96	1.20	-0.17	7.84	0.13	8.80	0.00
20	-2.63	1.24	3.49	-0.18	4.52	0.22	5.19	0.02
21	-1.67	1.27	0.39	-0.19	6.21	0.15	8.43	0.02
22	-1.24	-1.12	0.47	-0.20	3.29	0.21	5.82	0.01
23	-2.11	1.84	0.39	-0.22	6.07	0.20	6.29	0.01
24	-1.17	0.55	0.25	-0.10	6.53	0.12	9.88	0.03
25	-1.71	22.21	0.06	-0.31	3.16	0.26	4.70	0.01
26	-1.64	-1.78	0.11	-0.17	2.31	0.14	8.94	0.01
27	-0.58	-1.13	20.20	-0.29	6.17	0.24	5.48	0.01
28	-2.83	-4.40	0.08	-0.14	10.99	0.15	4.59	0.02
29	-0.56	-1.12	0.80	-0.29	0.58	0.29	10.97	0.08
30	-2.25	1.29	0.35	-0.05	10.65	0.30	7.16	0.01
31	-1.74	1.23	0.19	-0.29	4.68	0.05	1.87	0.01
32	-1.66	3.07	0.30	-0.23	7.67	0.35	9.00	0.03
33	-1.38	5.02	0.06	-0.28	5.24	0.26	5.37	0.02
34	-1.74	1.06	0.54	-0.16	4.47	0.14	8.64	0.02
35	-1.56	1.39	0.37	-0.32	6.62	0.28	5.05	0.03
36	-1.78	2.64	0.24	-0.29	7.83	0.25	5.18	0.01

Table G.2.2: Summary of parameters from the second visit, CT cone threshold cd.m^{-2} , CC cone coefficient cd.m^{-2} , Tau cone time constant min, S2 slope of S2 phase $\log_{10}(\text{cd.m}^{-2}).\text{min}^{-1}$, Alpha, cone rod breakpoint min, S3 slope of S3 phase $\log_{10}(\text{cd.m}^{-2}).\text{min}^{-1}$, Beta, rod rod breakpoint min

	CT	CC	Tau	S2	Alpha	S3	Beta	MSE
1	0.87	-2.07	2.04	-0.33	0.65	0.22	10.35	0.03
2								
3	4.14	-5.28	72.38	-0.32	6.90	0.30	6.50	0.01
4	-1.78	20.66	0.11	-0.19	6.67	0.15	7.06	0.01
5								
6	-1.51	0.93	0.28	-0.21	5.45	0.18	7.93	0.01
7	-1.87	2.18	0.15	-0.30	6.59	0.27	5.13	0.01
8	-1.48	1.20	0.27	-0.28	4.91	0.29	7.06	0.01
9	0.71	-3.13	3.86	-0.20	3.87	0.10	8.73	0.04
10								
11	-1.82	0.49	0.47	-0.29	10.28	0.26	2.41	0.03
12								
13	-2.65	1.43	8.15	-0.29	6.51	0.30	4.22	0.01
14								
15	-1.74	1.59	0.48	-0.30	7.72	0.26	4.89	0.01
16	-1.95	1.39	0.31	-0.26	9.93	0.46	6.84	0.07
17	-1.82	1.76	0.39	-0.27	8.92	0.21	5.04	0.01
18	-1.91	2.69	0.43	-0.35	7.90	0.27	3.05	0.00
19	-1.62	0.76	0.94	-0.20	6.46	0.16	6.53	0.00
20	-1.75	1.47	0.11	-0.19	3.47	0.20	7.00	0.02
21	-1.37	12.01	0.11	-0.29	7.58	0.17	4.68	0.02
22								
23	-2.21	9.93	0.20	-0.26	9.62	0.19	3.40	0.02
24	-1.05	0.40	0.20	-0.12	4.08	0.10	3.20	0.07
25	-1.59	0.79	0.15	-0.38	5.62	0.34	4.52	0.01
26								
27	1.57	-3.39	2.80	-0.75	1.50	0.52	1.12	0.01
28								
29	-1.51	6.41	0.04	-0.36	3.98	0.26	4.29	0.08
30								
31								
32	-2.01	2.20	0.22	-0.37	6.70	0.32	3.31	0.03
33	-1.61	16.41	0.04	-0.32	5.07	0.24	3.16	0.01
34	-1.79	4.86	0.21	-0.24	9.57	0.27	5.36	0.02
35								
36	-1.93	2.49	0.26	-0.22	6.80	0.18	6.60	0.01

Table G.3.1: Classification of data using a liberal AIC_c criterion according to model fit, highlighted data are fitted by the seven parameter model alone at both first and second visits.

Sx	Visit 1			Vist2		
	m3	m5	m7	m3	m5	m7
1			1	1		1
2			1			
3			1			1
4			1			1
5	1	1	1			
6	1	1	1			1
7			1			1
8			1			1
9			1		1	1
10						
11			1	1	1	1
12			1			
13			1			1
14			1			
15			1			1
16			1		1	1
17			1			1
18			1			1
19			1			1
20		1	1			1
21			1			1
22			1			
23			1		1	1
24	1	1	1	1	1	
25			1			1
26			1			
27			1	1	1	
28		1	1			
29			1	1		1
30		1	1			
31		1	1			
32		1	1			1
33			1			1
34	1	1	1			1
35			1			
36			1			1

Table G.3.2: Classification of data according to model fit, using a conservative AIC_c criterion, highlighted data are fitted by the seven parameter model alone at both first and second visits.

Sx	m3	m5	m7	m3	m5	m7
1			1			1
2			1			
3			1			1
4			1			1
5		1				
6			1			1
7			1			1
8			1			1
9			1		1	
10						
11			1		1	1
12			1			
13			1			1
14			1			
15			1			1
16			1			1
17			1			1
18			1			1
19			1			1
20		1	1			1
21			1			1
22			1			
23			1			1
24	1		1	1		
25			1			1
26			1			
27			1		1	
28		1				
29			1	1		
30			1			
31		1				
32			1			1
33			1			1
34			1			1
35			1			
36			1			1

SUPPLEMENTARY DATA FOR THE DIGITAL APPARATUS

H.1 Experimental Parameter Files

The default test parameters for the digital dark adaptometer.

— Parameters —

Start dB = 40.0 dB

End dB = 0.0 dB

Retest reduction dB = 9.5 dB

Flicker frequency = 4.0 Hz

Ramp time = 45 s

Repeat interval = 5 s

Stimulus colour = Green

Test side = Right

Green fixation dB = 0.0 dB

Red fixation dB = 0.0 dB

Left red calibration dB = 1.00 dB

Left green calibration dB = 1.00 dB

Right red calibration dB = 1.00 dB

Right green calibration dB = 1.00 dB

Red fixation calibration dB = 0.50 dB

Green fixation calibration dB = 1.00 dB

Left green platform calibration dB = 30.00 dB

Left red platform calibration dB = 30.00 dB

Right green platform calibration dB = 10.00 dB

Right red platform calibration dB = 10.00 dB

Green illumination voltage = 2.7 V

Red illumination voltage = 2.7 V

Green target voltage = 3.4 V

Red target voltage = 3.4 V

H.2 Dark Adaptation Parameter Estimates

Table H.2.1: Summary of the parameters for the data found using the digital device. LU is log units.

	Age years	CT LU	CC LU	Tau min	S2 $\frac{LU}{min}$	Alpha min	S3 $\frac{LU}{min}$	Beta min	MSE LU ²
1	62	-1.45	1.90	0.79	-0.24	8.6	-0.03	13.4	0.01
2	30	-1.41	2.49	0.56	-0.32	6.6	-0.07	10.6	0.01
3	18	-1.20	2.09	0.40	-0.39	5.9	-0.08	7.9	0.04
4	30	-1.47	1.89	0.64	-0.24	5.3	-0.02	10.4	0.02
5	30	-0.88	0.78	0.55	-0.23	4.5	-0.02	11.5	0.02
6	24	-1.28	3.06	0.66	-0.28	7.4	-0.05	11.8	0.01
7	24	-1.44	2.01	0.55	-0.24	5.6	-0.03	10.7	0.01
8	23	-1.63	3.63	0.32	-0.16	8.1	-0.06	14.4	0.01
9	68	-1.18	2.07	0.77	-0.09	7.6	-0.09	12.1	0.01
10	46	-2.10	1.54	3.93	-0.40	8.1	0.01	9.9	0.02
11	47	-0.96	6.44	0.28	-0.20	4.6	-0.03	11.3	0.02
12	22	-1.21	1.77	0.65	-0.22	6.2	-0.05	11.1	0.01
13	54	-1.19	6.27	0.53	-0.04	5.1	-0.18	13.7	0.01
14	40	-1.09	0.26	0.84	-0.22	4.1	-0.03	9.8	0.02
15	24	-1.42	0.57	2.31	-0.28	8.0	-0.02	12.6	0.02
16	47	-1.27	2.51	0.35	-0.19	6.0	-0.03	12.3	0.01
17	51	-1.00	16.00	0.18	-0.21	5.7	-0.03	12.0	0.03
18	62	-2.16	0.56	1.00	-0.80	8.0	-0.22	8.8	0.02
19	47	0.39	0.26	0.24	-0.41	4.0	-0.05	8.7	0.03
20	30	-1.37	5.84	0.21	-0.07	5.2	0.03	14.4	0.03
21	50	-1.22	0.77	2.13	-0.23	5.7	-0.03	12.1	0.02

SUPPORTING PAPERS

- I.1 Confidence Intervals for Dark Adaptation via Model Comparison
- I.2 Recovery of spatial contrast thresholds following a bleach; cone and rod components
- I.3 A computer-based technique for assessing rod dark adaptation; age changes, data quality and reproducibility

Confidence Intervals for Dark Adaptation via Model Comparison

by Jeremiah MF Kelly and Ian J Murray

Abstract Dark adaptation is the ability of the human visual system to recover its sensitivity when moving into a dark environment. It is a sensitive measure of the health of the retina and an area of increasing clinical and research interest (Dimitrov et al., 2011). Dark adaptation is measured using psychophysical techniques to determine the change in visual threshold over time. The data collected are intrinsically noisy and there is large inter-observer variability. However, there is no published method of calculating confidence intervals (CI) for models fitted to the recovery function.

A method described by Motulsky and Christopoulos (2004, p112) is modified for the calculation of confidence intervals for one parameter of a seven-parameter non-linear model of dark adaptation.

The recovery of visual sensitivity on moving from a bright to a dark environment is described as dark adaptation. There are two mechanisms in the visual system. One is based on cone photoreceptors and is responsible for detail and colour vision at higher light levels. The other is mediated by rod photoreceptors and is specialised to detect very low levels of light. The range over which the human visual system can operate is of the order of 8 log units, from a bright sunny day to starlit night time.

The change in threshold (1/sensitivity) with time is shown in figure 1. The recovery of sensitivity can be described by a seven parameter model shown below (McGwin et al., 1999). This model has three phases; the first is the recovery of the cone system, followed by two rod phases, referred to as S2 and S3.

$$\text{Threshold} = a_1 + a_2 * \exp(-x * a_3) + a_4 * \max(0, x - a_5) + a_6 * \max(0, x - a_7)$$

The threshold of the cone system is given by a_1 , the value a_2 is the threshold at time zero and can take non physiological values. The time constant of the cone recovery is given by a_3 . The rod phase can be divided in to two parts, an early phase defined by two parameters, the rod-cone transition time a_5 or α and its slope a_4 , classically known as S2. The later rod phase is defined by the rod-rod transition time a_7 or β with slope S3. The parameter a_6 is the sum of the slopes of the two rod phases, S2 + S3.

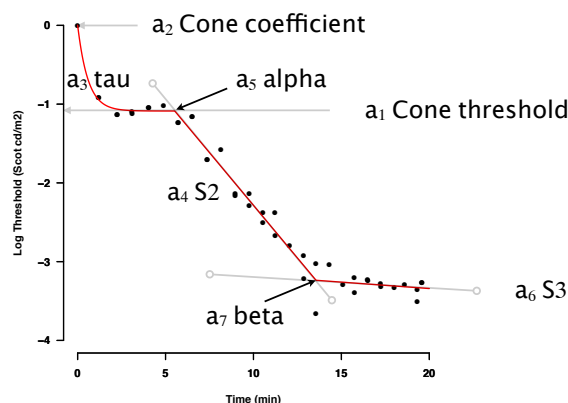


Figure 1: An explanation of the parameters in the model.

The early rod recovery phase S2 is of most interest clinically as it represents the rate at which the recycled visual pigments are restored to the light sensitive layer of the eye, the retina (Lamb and Pugh, 2004). This rate of recovery is known to be compromised in many diseases, e.g. the sight threatening condition age related macula degeneration (AMD), diseases of the liver and diabetes.

Finding the best fit model

The best fit model is found by minimising the sum of the square residuals. A least squares function is created with the variable \mathbf{a} , a seven element array.

```
P7<-function(a){
  Yest<-a[1]+a[2]*exp(-x*a[3])
  + a[4]*pmax(0, x-a[5])
  + a[6]*pmax(0, x-a[7])
  return(sum((y-Yest)^2))
}
```

The best estimate of the parameters in \mathbf{a} is found using the `optim` function. The start values are dependant upon the conditions under which the data are collected, the array `Start` was found to be useful for the conditions used in Manchester.

```
Start<-c(-1.65,1.16,2.2,-0.23,7.3,0.20,13)
```

```
OPT7<-optim(Start, P7)
for(i in 1:5){
  OPT7<-optim(OPT7$par, P7)
}
```

The parameter estimates (`OPT7$par`) are recycled using the `for` loop, this helps if the `Start` values are

a poor initial fit. The seven elements of `OPT7$par` are the best estimate of \mathbf{a} and are used to create a fixed model with $N=\text{length}(x)$ observations. The fixed model sum of residuals squared is given by $SS_{fixed} = \text{OPT7\$value}$.

Creating a range of possible α and β values

Having found a best fit model, we are curious to know by how much the parameters in \mathbf{a} can be varied before they no longer fit the data. The parameter of most interest clinically is the slope S_2 , which is geometrically related to the α and β times. The α point is the time when the rod system becomes more sensitive than the cone system. Due to variability in the data, the β point is weakly defined for some subjects, therefore the two transition points are varied.

A range of α and β values are created as follows;

```
Steps=30
tmp=OPT7$par # best fit values,
# changed to tmp for ease of typing

alpha <- tmp[5]
# extract the best alpha fit value
beta <- tmp[7]
# the best fit beta value

A <- seq(alpha-3, alpha+3, length.out=Steps)
B <- seq(beta-3, beta+3, length.out=Steps)
```

A matrix, \mathbf{SS} is initialised to receive the calculated sum of squares for each pair of α and β values

```
SS<-matrix(0,Steps,Steps)
```

Then the sum of squares for all possible pairs of α and β times is calculated;

```
for(ii in 1:Steps){
  tmp[5]<-A[ii]
  for(jj in 1:Steps){
    tmp[7]<-B[jj]
    Yest1<-Pest7(tmp, x)
    SS[ii, jj]<-sum((y-Yest1)^2)
  }
}
```

Where the function `Pest7()` returns the threshold values for the given parameter \mathbf{a} , for times \mathbf{x} and is defined as:

```
Pest7
function(a, x){
  a[1]+a[2]*exp(-x*a[3])
  + a[4]*pmax(0, x-a[5])
  + a[6]*pmax(0, x-a[7])
}
```

When is a model different?

For each pair of possible values of α and β the sum of residuals squared is calculated. The region of acceptable α and β values is obtained by finding the F ratio that gives a 1-p value of ≤ 0.05 . The F statistic for a given p value is returned by the `qf()` function with N observations and P=2 parameters since only two parameters are being varied.

```
F<- qf(0.95, P,N-P)
```

This F value is used to calculate the upper bound of the sum of residuals squared using equation 1

$$SS_{vary} = SS_{fixed} \left(F \cdot \frac{P}{N-P} + 1 \right) \quad (1)$$

```
SSbf<-OPT7$val
# sum of residuals squared for best fit model
SSaf<-SSbf*(F*P/(N-P)+1)
# the upper bound of the sum of residuals squared
```

The upper bound, SS_{vary} , is used to select the pairs of values for the transition times for which the sum of residuals squared is not significantly different to that of the fixed model. The values of SS less than the fixed model are used to create an index which is then used to find the acceptable pairs of transition times.

```
idxCI<- SS<=SSaf
```

The selected pairs of transition times α and β are coerced into a 2 column array.

```
Lims<-cbind(matrix(A,Steps,Steps)[idxCI],
+ matrix(B,Steps,Steps,byrow=TRUE)[idxCI])
```

Each of these pairs are then used to find the CI for the slope S_2 .

Calculation of the CI of slope of the S_2 phase

Each pair of transition times is then used in a model with only one parameter S_2 keeping the other six parameters fixed, the value of this parameter is found with the `optimise` function. The function makes a call to a variable outside the function environment.

```
SolveS2<-function(S2){
  a<-tmp
  # the call to environment outside the function
  Yest <- a[1]+a[2]*exp(-x*a[3])
  + S2*pmax(0, x-a[5])
  + a[6]*pmax(0, x-a[7])
  return(sum((y-Yest)^2))
}
```

The function `SolveS2(S2)` calls four parameters `a[1,2,3,6]` from the best fit model `OPT7$par`. The values of `a[4,6]` for each pair of α and β values calculated above and held in the array `Lims` and are provided at each iteration of a loop.

An array `Res` is created to hold the resultant `S2` values. Then the loop calculates the optimal `S2` value for each transition time pair.

```
L<-length(Lims[,1])
Res<-numeric(L)

for(ii in 1:L){
  tmp<-OPT7$par
  tmp[5]<-Lims[ii,1]
  tmp[7]<-Lims[ii,2]
  Mod<-optimize(SolveS2,interval=c(-0.8,0))
  Res[ii]<-Mod$minimum
}
c(max(Res),min(Res))
```

The maximum and minimum values of `Res` are taken as the lower (2.5%) and upper (97.5%) limits since the selected transition times are selected from within the 95% two tailed confidence interval.

Summary

Calculation of confidence intervals in multi-parameter nonlinear models is a non trivial task. The slope of the `S2` phase is a sensitive marker of retinal health. It is known to be reduced in people with liver disease and diabetes and in particular it is affected in AMD. Interest is growing in the potential of `S2` as a biomarker for early intervention or treatment.

The approach presented here is intended as an easily understood method of calculating confidence intervals that will allow for an objective and meaningful interpretation of the reliability of the estimated value of `S2`.

Bibliography

- P. Dimitrov, L. Robman, M. Varsamidis, K. Aung, G. Makeyeva, R. Guymer, and A. Vingrys. Visual function tests as potential biomarkers in age-related macular degeneration. *Investigative Ophthalmology & Visual Science*, 52(13):9457–9469, 2011.
- T. Lamb and E. Pugh. Dark adaptation and the retinoid cycle of vision. *Progress in retinal and eye research*, 23(3):307–380, 2004.
- G. McGwin, G. Jackson, and C. Owsley. Using non-linear regression to estimate parameters of dark adaptation. *Behavior Research Methods*, 31(4):712–717, 1999.
- H. Motulsky and A. Christopoulos. *Fitting models to biological data using linear and nonlinear regression: a practical guide to curve fitting*. Oxford University Press, USA, 2004.

JMF Kelly
University of Manchester
Carys Bannister Building
Dover Street
Manchester
M13 9PL
UK
jeremiah.kelly@manchester.ac.uk

IJ Murray
University of Manchester
Carys Bannister Building
Dover Street
Manchester
M13 9PL
UK
ian.j.murray@manchester.ac.uk

Recovery of spatial contrast thresholds following a bleach; cone and rod components

M.Cinta Puell¹, Jeremiah MF Kelly², Ian J. Murray²

1 Applied Vision Research Group, Complutense University, Av. Arcos de Jalón 118, Madrid 28037, Spain.

2 The Vision Centre, Carys Bannister Building, Faculty of Life Sciences, University of Manchester, Manchester, UK

WORD COUNT:

GRANT INFORMATION:

Spanish Ministry of Education, ref PR2011-0203

UK College of Optometrists

CORRESPONDENCE

María Cinta Puell

Faculty of Optics and Optometry, Complutense University, Av. Arcos de Jalón 118, Madrid 28037, Spain.

Phone: +34913946863

Fax: +34913946885

e-mail: puellma@fis.ucm.es

Abstract (250 W)

Purpose: To characterize the recovery of contrast thresholds for sine-wave gratings of low spatial frequencies and low mean luminance as function of time in darkness after photo pigment bleaching.

Methods: 13 subjects took part in the study. Contrast thresholds were measured for 15 minutes following almost complete photo pigment bleaching. The stimuli were achromatic sine-wave gratings of 0.5, 1 and 2 c/deg, and mean luminance 0.01 cd/m² that were generated in the centre (10°) of a CRT monitor. Dynamics of the recovery at each spatial frequency were modelled using a 5-parameter non-linear regression curve.

Results: The first phase of the sensitivity recovery was exponential. There was a distinct transition point around 6 min after the bleach. A second phase of recovery followed a linear trend with slope (ψ_2) -0.05 log₁₀ units. min⁻¹. After 15 min the sensitivity recovery was complete and the contrast threshold remained constant. The mean recovery rates (T1) and mean contrast thresholds (CT1) of the first phase and the mean transition points (α) did not differ significantly between the three spatial frequencies. The mean ψ_2 slopes of the second phase were significantly higher (-0.05 log₁₀ units. min⁻¹) for 0.5 and 1 c/deg and lower (-0.04 log₁₀ units. min⁻¹) for 2 c/deg and the mean time constant (T2) was 3 min more (p<0.01) for 2 c/deg than for 0.5 and 1 c/deg. The mean final contrast threshold (CT2) was 0.3 log₁₀ units significantly higher at 2 c/deg than at 0.5 and 1 c/deg.

Conclusions: The dynamics of contrast sensitivity recovery after a bleach follow two phases and these may be attributed to the cone and rod systems.

Key Words: Four to nine key words for indexing purposes must be given.

Dark adaptation, recovery sensitivity, contrast threshold, bleach, mesopic luminance, cones, rods

Introduction

The recovery of visual sensitivity that occurs following exposure to a phot bleach is now well known (Lamb & Pugh 2004; Lamb & Pugh 2006; Reuter 2011). It has been described as being composed of several “components” that are kinetically distinct. Classically this so-called dark adaptation curve is divided into cone- and rod-mediated sections (Lamb 1981). The kinetics of this recovery are adversely affected by many systemic and ophthalmic diseases. Sensitivity recovery is slowed in later life (Jackson et al. 1999) and has been shown to be abnormal in the presence of ocular diseases such as AMD and diabetic retinopathy (Henson & North 1979; Brown et al. 1986; Owsley et al. 2000). Specifically, kinetic aspects of the second, rod-mediated dark adaptation component (referred to as S2) are vulnerable in AMD, particularly in the early stage of the disease phases (Owsley et al. 2001; Owsley et al. 2007).

The speed of dark adaptation is dependent on the retinoid cycle (Lamb & Pugh 2004). However, it is still not clear whether functional deficits in early AMD are primarily caused by a reduced sensitivity of photoreceptors, by post-receptoral abnormalities or by damage to other tissues involved in AMD, such as the RPE/Bruch's membrane complex or the choroid. Feigl et al. (2007) reviewed this issue and based on psychophysical and electrophysiological findings, they proposed that most functional impairment in early AMD is postreceptoral. Bearing in mind this ischemia/postreceptoral hypothesis it could be interesting to examine the recovery of the visual system to stimuli that depend on the activity of postreceptoral processing rather than the recovery of simple luminous thresholds as in the classical dark adaptation curve. Spatial contrast threshold detection is a good candidate. Contrast

detection involves postreceptoral processing through parvocellular (P) and magnocellular (M) pathways (see Lee et al, 2011)(Lee 2011) for a contemporary review.

It is thought the M pathway dominates detection of spatial patterns in the mesopic (rod- and cone-mediated) and scotopic (rod-dominated) ranges of retinal illumination.

According to Purpura et al. 1988 (Purpura et al. 1988) M cells, but not P cells were sensitive to sine gratings temporally modulated at 4 Hz when the spatial frequency was 0.6-1.6 cycles per degree and the mean retinal illumination lower than 0.43 td equivalent to 0.6 td (low mesopic range) in the human. Previous studies have demonstrated that magnocellular (M) pathways receive rod and cone input (Lennie & Fairchild 1994) (Gouras & Link 1966; D'Zmura & Lennie 1986; Purpura et al. 1988; Lee et al. 1997; Sun et al. 2001) (Enroth-Cugell et al. 1977). Using a technique to isolate rod and cone system it was found that over most of the mesopic range the spatial contrast sensitivity of the cone system was lower than that of the rod system at low spatial frequencies (1 – 3 c/deg) (D'Zmura & Lennie 1986). If this is so, then it could be expected that the recovery in contrast sensitivity for sine-wave gratings, would have a different time course for rod and cone-mediated components.

To our knowledge there are very few studies that have used sine-wave gratings to measure contrast threshold recovery. In one case recovery of the luminance mechanism required to resolve sinusoidal gratings (0.6-14 c/deg) was determined following a full bleach throughout the course of dark adaptation. Threshold (log td) for the lowest spatial frequency was qualitatively similar to a classical dark adaptation function, showing discrete rod and cone phases and for spatial frequencies above the rod spatial resolution limit (3.5 c/deg) the rod phase was absent (Margrain & Thomson 1997). In a further investigation Hahn and Geisler (Hahn & Geisler 1995) reported recovery of luminance sensitivity (log td) for sine-wave gratings targets (250 ms flash) ranging from 1 to 15 c/deg during long-term dark adaptation following full bleaches. They found that

the dark adaptation curves were similar in shape and time course throughout the course of long-term dark adaptation. Due to the experimental design measurements were confined to the cone system. The recovery of contrast threshold for a “rod-isolating” grating (1.38 c/deg and mean illumination 9.3 td) after a bleach showing cone and rod phases were also presented in a control experiment (D'Zmura & Lennie 1986).

Little is known about recovery of contrast thresholds following a photo bleach using sine wave-gratings in the low mesopic range. The aim of this study was to characterize the recovery of contrast thresholds for sine-wave gratings of low spatial frequencies and low mean luminance as function of time in darkness after photopigment bleaching. We address this issue by measuring the time course of recovery of spatial contrast thresholds for 15 minutes after photopigment bleaching.

Methods

Contrast sensitivity is measured by detection of changes in contrast against a background of fixed luminance. Typically sinusoidal gratings are presented to a subject, the gratings in this case had spatial frequencies of 0.5, 1 and 2cpd. The grating was also modulated temporally at 2Hz.

Achromatic sinusoidal gratings were generated using Matlab scripts and the `psychtoolbox` \cite{Brainard:1997,Kleiner:2007} and presented on a gamma corrected high resolution monitor (Sony, GDM-F500R, Japan) using a ViSaGe interface (CED, UK). The gratings subtended 10° at 75cm.

Natural pupils were used and a photo bleach of more than 30% was applied using a flash gun.

Thresholds were set using a one up three down staircase in the following manner. The subject was given an auditory cue and the stimulus presented on the screen for 340ms.

The subject indicated whether the grating was vertical, horizontal, or unseen. This response was entered into the computer program, coded by the software and if correctly identified the stimulus was there was a pause of 10 seconds. The next presentation had contrast 9.5dB lower than the threshold just measured. If the subject's response was incorrect the contrast was increased by 3dB and the grating was again presented to the subject.

A preliminary trial indicated that there was no further change in threshold after 15minutes, the measurements ceased if the time at the end of a threshold setting trial was greater than 15min.

Data were analysed using scripts in R and two models were considered. The two models were a simple three parameter exponential and a six parameter bi-exponential. The parameters were determined using nonlinear regression. The ability of the models to fit the data was compared using the extra sum-of-squares F test.

Apparatus

Sinusoidal gratings subtending 10° at 75cm were presented on a calibrated and gamma-corrected high-resolution CRT monitor (Sony GDM-F500R, Tokyo, Japan). They were generated using the ViSaGe unit (CRS, UK) and a desktop PC (Dell, USA) with Windows XP operating system (Microsoft, USA). The hardware was controlled using Matlab (Nantick, USA) and the psychophysics toolbox [\cite{Kleiner:2007,Brainard:1997}](#). The custom scripts are available from the author (JMK).

Calibration of the screen

The calibration followed a procedure described by Parry [\etal \citeyear{Parry:2006}](#). Initially the screen was auto calibrated using a Colorcal photometer (CRS Ltd, UK) and its associated software, by testing 128 voltages to obtain a gamma correction curve.

The software used for stimulus generation (ViSaGe Desktop, CRS Ltd,UK) allows for correction values to compensate for intrinsic errors in the monitor for the red (R) green (G) and blue (B) phosphors and have default values of one.

CIE coordinates of $x=0.31$ and $y=0.316$ with luminance 12.5cdm were entered into the software and the chromaticity coordinates at R, G and B were measured using the PR650. The voltages across the R, G and B guns were noted. The correction factors were adjusted until the monitor displayed the luminance required.

Contrast calibration

A script was written in Matlab, that presented two squares on the monitor, each with sides of 100 pixels separated by 20 pixels. The luminance of each square was measured with the PR1500. These squares were generated using a series of look up tables. The look up table number was the independent variable and the measured luminance the dependant variable. The $\log(\text{contrast})$ was linear for the look up table number ($R^2=0.9996$).

Experimental design

Stimuli were horizontal and vertical achromatic sinusoidal gratings displayed in the centre of the monitor in a circular patch subtending 10 degrees at a distance of 75 cm for 340 ms. The spatial frequencies were 0.5, 1, and 2 cycles per degree (cpd) and the Michelson contrast ranged between 0.02 and 0.7. The sinusoidal wave gratings were temporally modulated at 2 Hz. The mean screen luminance was reduced from 12.5cd.m^{-2} to 1×10^{-2} using neutral density filters (LEE Filters, Colorfilter type 211, 0.9 ND [LEE Filters Worldwide, Andover, Hampshire, UK]).

Subjects

A call for volunteers was made within the Optometry department of the Faculty of Life Sciences, University of Manchester. Subjects were required to have best corrected acuity of better than 6/9 (Snellen), no ocular pathology, established by an eye examination within the previous 12 months. Thirteen naïve subjects were recruited (6 female) aged 30.4(10.7) yrs. Subjects were given written and verbal information about the experiment and possible consequences of their participation. Informed consent was obtained and the study was carried out in agreement with the tenets of the Helsinki agreement.

Procedure

A criterion free method of adjustment was used. At each stimulus presentation, identified by an auditory marker, the subject indicated whether the stimulus gratings were horizontal or vertical, this was entered into the software by the operator. The software scored the result, if correct the threshold was noted and the stimulus extinguished. After 10s the stimulus was represented reduced by 9.5dB, if the response from the subject was incorrect the stimulus was extinguished and represented after 5s increased by 3dB.

An electronic flashgun (Nikon Speedlight SB-800, Tokyo, Japan) was used to produce an estimated 75-95% visual pigment bleach for a pupil size range of 4.5 to 6.5 mm (Rushton:1972). Spectacles, if worn, were removed and the subject fixated the centre of the flash at a distance that meant the after image generated covered the monitor screen.

The experiment was performed over three visits on different days of the same week. Occasionally measurements were made on the same day and a washout period of at least 45mins was used between measurements. At each session only one spatial

frequency was tested. A brief preliminary trial was performed to allow the subject to become familiar with the task. A pilot study found that absolute thresholds were unchanged after 15min, so measurements started at 15min were completed and then the experiment finished. All measurements were completed by 20min.

To isolate the contribution of cone system the experiment was repeated with red sinusoidal wave gratings (0.5, 1 and 2 cpd) and mean luminance 0.01 cdm . The gratings were viewed through a red pass filter (Lee, UK filter 026) mounted in a goggle. The filter had the effect of removing any shorter wavelengths emitted by the red phosphor.

Model

The recovery of contrast sensitivity following a photo bleach can be modelled by an exponential function representing a single mechanism

$$CS = \psi_1 + \psi_2 \cdot \exp\left(-\frac{t}{\psi_3}\right)$$

where ψ_1 is the absolute threshold, ψ_2 the threshold at time zero and ψ_3 the time constant. Alternatively, a bi-exponential model can be fitted, accounting for the possibility of two systems

$$CS = \psi_1 + \psi_2 \cdot \exp\left(-\frac{t}{\psi_3}\right) + \psi_5 \cdot \exp\left(-\frac{h(t, \psi_4)}{\psi_6}\right)$$

where the step function $h(t, \psi_4)$ is zero for times less than ψ_4 and time $t - \psi_4$ for times thereafter. The value of ψ_1 is the absolute threshold for both phases, ψ_2 the threshold at time zero and ψ_3 the time constant value for the first phase, the first phase threshold is given by $\psi_1 + \psi_5$.

Figure \ref{fig:modelMCP} shows how the parameters relate to the data. This model was fitted to the data using a least squares method of nonlinear regression. A similar model was used by \citeasnoun{Dimitrov:2008} when modelling cone and rod dynamics.

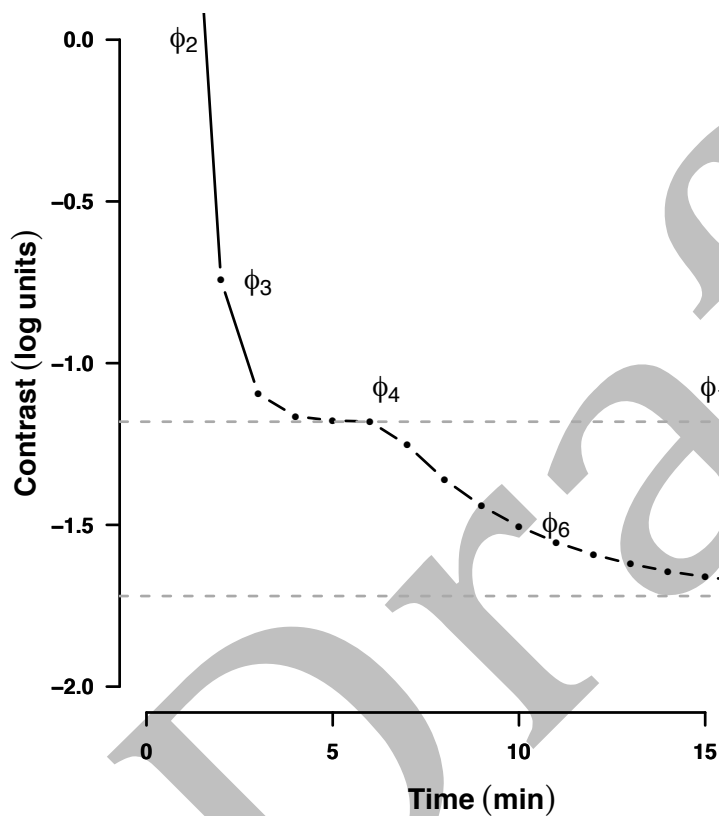


Figure 1 How the parameters of the bi exponential model relate to the collected data. The parameters are explained in the text. Note the parameter ϕ_5 is the offset from the final phase to the early phase. MCPfirst.pdf

Results

Preliminary investigation of scotopic contrast sensitivity

The aim was to measure contrast sensitivity recovery following a photo bleach and to decide how long to collect data. Earlier experiments suggested that the time for rod recovery against a luminous background would reach a plateau after ~12min.

The recovery of contrast sensitivity for three spatial frequencies, 0.5, 1.0 and 2.0cpd, following a photo bleach in excess of 30% was measured using a female subject aged 34years. The measurements were taken for over twenty-five minutes. Initial examination of the data suggested an exponential decay, therefore a three parameter model was fitted to the data, see equation \ref{eqn:MCP}. The parameters of the model of best fit are shown in table \ref{tab:LongTime}. The data is shown in figure \ref{fig:LongTime} along with the exponential decay model. The horizontal line is the model threshold at 15minutes. A linear regression of the post fifteen minute thresholds against time found that the slope after this time was not significantly different from zero (p-value=0.1, 0.8, 0.5 for 0.5, 1.0 and 2.0cpd respectively)

Table 1 Parameters of the simple exponential model fitted to the preliminary data. The absolute contrast threshold is ϕ_1 , the threshold at time zero ϕ_2 and the time constant (naperian) of decay ϕ_3 min.

cpd	ϕ_1	ϕ_2	ϕ_3
			min
0.5	-1.68	0.99	2.61
1	-1.73	1.09	1.73
2	-1.55	0.88	2.73

\label{tab:LongTime}

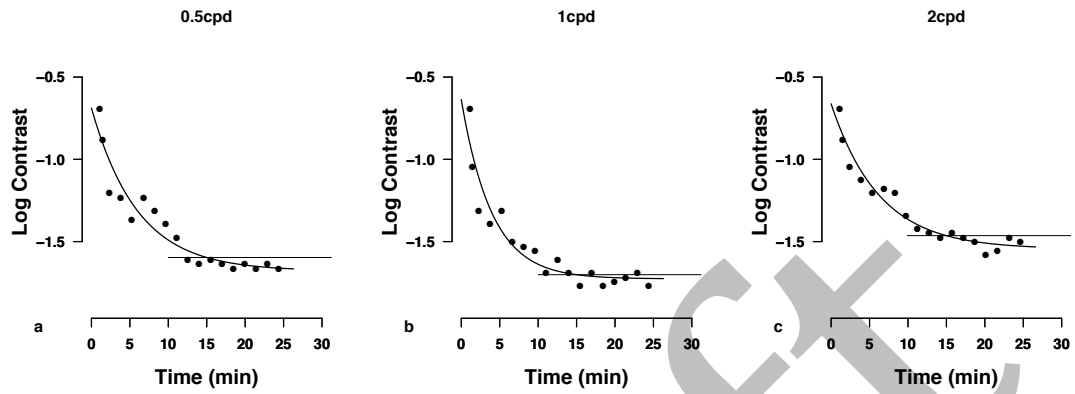


Figure 2 Contrast sensitivity recovery following photo bleach.

LongTime.pdf fig:LongTime

In figure [\ref{fig:LongTime}](#) plots a and c have threshold elevations at ~ 7 minutes. This was investigated further using a larger number of subjects.

Evidence for two phases of contrast sensitivity recovery

Following the preliminary work data was collected for at least fifteen minutes in a series of healthy subjects with normal vision. The data collected from the thirteen subjects are summarised in figure [\ref{fig:SEffect}](#).

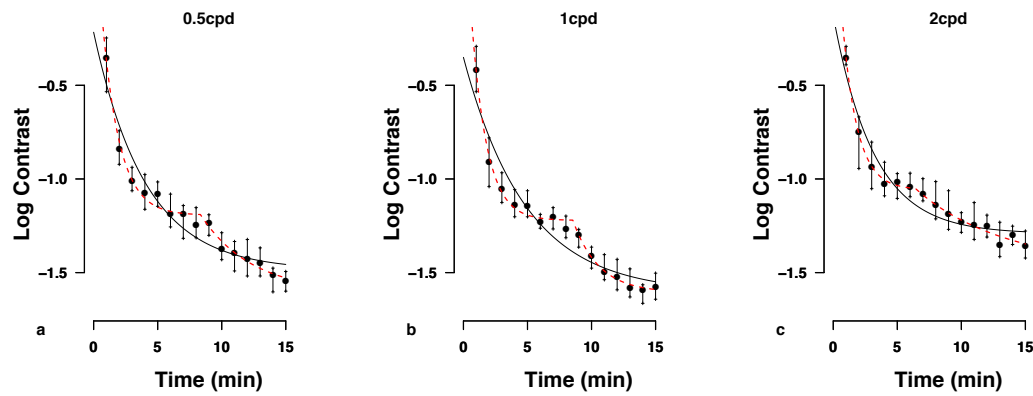


Figure 3 Contrast sensitivity recovery following photo bleach. Solid curve is the best-fit exponential decay model, the horizontal line is the threshold of the model at 15min.

`\includegraphics[width=\textwidth]{../2012_08/MCP/MCPModelComparisonUnsmoothed3a.pdf}`

`\label{fig:SFEffct}`

To consider whether one or two processes were involved both a simple exponential decay and a bi-exponential model were fitted to the data.

An extra sum of squares analysis was applied to the raw data for each spatial frequency and found that the bi-exponential model was a significant improvement over the simple exponential model (F-statistics; 243, 536, 447 on $df= 3$ and 138, 133, 138 p -value =0.000 for 0.5, 1.0 and 2.0cpd respectively)\footnote{ This was verified by reducing the degrees of freedom by collecting the thresholds into one minute epochs and the median contrast threshold fitted to the two models (F-statistics; 14.88, 33.45, 27.34, $df= 3$ and 14, p -value \leq 0.001 for 0.5, 1.0 and 2.0cpd respectively).}

The bi-exponential model was used to evaluate the data for each subject, the individual results are shown in table \ref{tab:Res6}. Although visual inspection of the pooled data suggests that the offset ($\phi_1 + \phi_5$) or the threshold of the first phase seems to rise with spatial frequency no significant spatial frequency effect was found ($P=0.4$). There was no spatial frequency effect for any parameter against spatial frequency (all p values >0.15).

The time constant for the first phase was 0.35(0.28)min while for the second phase it was 5.15(4.68)min. The difference between the time constants of the two phases was subject to a paired t test and found to be significant ($t = -6.2994$, $df = 38$, $p\text{-value} < 0.001$).

Contrast sensitivity recovery using a long wavelength stimulus

The biphasic recovery of contrast sensitivity is suggestive of two processes being involved. To test whether the rod system is responsible for the second phase the experiment was repeated using different conditions. The software was modified so that the gratings were presented on the monitor using the red phosphor alone and the mean luminance was reset to 12.5 cdm . The screen was attenuated by neutral density filters to give a mean luminance of $1 \times 10^{-2} \text{ cdm}$ ~as before.

The same subject who provided the time course data was exposed to a photo bleach and wore goggles with a red pass filter in place (Lee filters) when viewing the monitor. The

filter ensured that the subject saw only long wavelength light. The results for each spatial frequency are shown in figure \ref{fig:RedonlyCSF}. The results are mono phasic and no late change in threshold was seen. The final thresholds are elevated by a factor ~ 0.8 log units, to -0.88, -0.98 and -0.83 log units, when compared to the absolute thresholds for the same subject in figure \ref{fig:LongTime} where the absolute thresholds were -1.68, -1.73, and -1.54 log units.

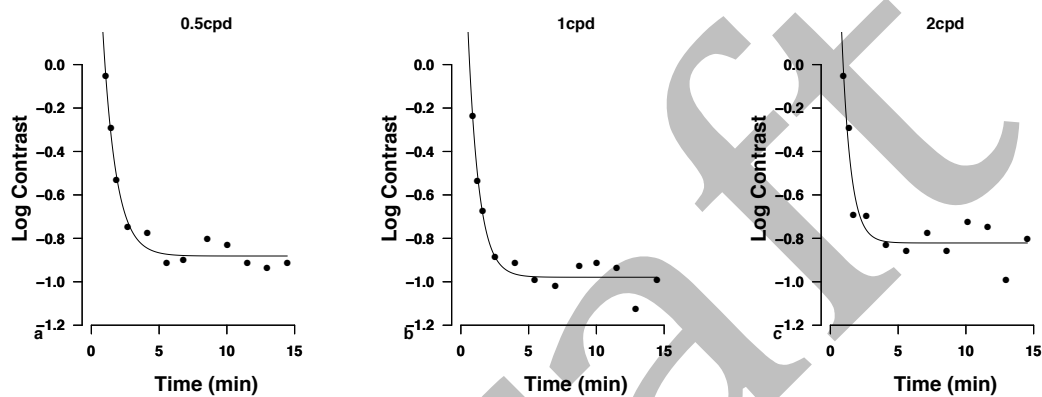


Figure 4 Recovery of scotopic sensitivity for a red stimulus.

\includegraphics[trim = 05mm 05mm 15mm 25mm, clip,
width=\textwidth]{../2012_11/OnlyRed.pdf} label{fig:RedonlyCSF}

Discussion

The final experiment has shown that the biphasic recovery of rod sensitivity is reflected in the recovery of contrast sensitivity and the time course is independent of spatial frequency. Little work has been done on this subject. \citeasnoun{Margrain:1997} used gratings to measure luminance sensitivity rather than contrast sensitivity and predictably found that the recovery of luminance sensitivity of bars mirrored the classic dark adaptation response to a circular stimulus. However, \citeasnoun{Hahn:1995} using novel Gabors measured contrast sensitivity at a range of spatial frequencies

including 1 and 3cpd found a simple exponential decay in their uniquely defined measure of contrast. \citeasnoun{Howard:2000} measured sensitivity recovery to Gabors of 1 and 6cpd following the offset of an adapting background, this measured the rapid recovery found when the limiting factor is the local cis-retinal rather than the rate limited recovery exemplified by the S2 phase discussed here.

Draft

Graefe's Archive for Clinical and Experimental Ophthalmology
A computer-based technique for assessing rod dark adaptation; age changes, data quality and reproducibility
 --Manuscript Draft--

Manuscript Number:	
Full Title:	A computer-based technique for assessing rod dark adaptation; age changes, data quality and reproducibility
Article Type:	Medical Ophthalmology
Keywords:	CRT; Dark adaptometry; Rods; Ageing; Repeatability
Corresponding Author:	Laura Patryas UNITED KINGDOM
Corresponding Author Secondary Information:	
Corresponding Author's Institution:	
Corresponding Author's Secondary Institution:	
First Author:	Laura Patryas
First Author Secondary Information:	
Order of Authors:	Laura Patryas Neil Parry David Carden Daniel Baker Jeremiah Kelly Tariq Aslam Ian Murray
Order of Authors Secondary Information:	
Abstract:	<p>Purpose To characterize the rate of scotopic sensitivity decline with age using a PC-driven cathode ray tube (CRT) monitor. To provide data regarding the repeatability of the technique and its ability to identify early photoreceptor degeneration in the presence of normal fundus and normal photopic vision.</p> <p>Methods Rod dark adaptation was monitored for 30 minutes following a minimum 30% pigment bleach, using a white 1° stimulus (modulated at 1 Hz), presented 11° below fixation on a CRT monitor. A VSG system was used to generate the stimuli and control the experiment. 33 subjects with no ocular pathology and normal fundus photographs were divided into two groups: older (≥45, n = 16) and younger (<45, n = 17).</p> <p>Results Rod recovery was assessed using component S2 of dark adaptation. S2 was 0.04 log₁₀.min⁻¹ slower in the older (0.19 ± 0.03 log₁₀.min⁻¹) compared with the younger group (0.23 ± 0.03 log₁₀.min⁻¹, p < 0.001), despite no difference in visual acuity and fundus appearance. Faster rates of S2 recovery were correlated with lower threshold at 30 minutes (T30) (r = 0.49, p < 0.005). Correlation coefficients between first and second measurements for S2 and T30 were 0.49 (p < 0.009) and 0.84 (p < 0.0001), respectively. The coefficient of repeatability was 0.07 log₁₀.min⁻¹ for S2 and 0.35 log cd.m⁻² for T30. The coefficients of variation for S2 and T30 were 15% and 10%, respectively.</p> <p>Conclusions Dark adaptation is slowed in normal ageing. CRT-based dark adaptometry is highly</p>

sensitive, easily implemented, non-invasive and highly repeatable. The technique described in this article would be useful for documenting visual changes in future clinical trials assessing retinal health in the older eye with and without ocular pathology.

Authorship Form: Graefes Archive for Clinical and Experimental Ophthalmology

Title:- _____

I, _____ hereby confirm that all named authors meet the ICMJE

(corresponding author)

requirement of authorship and meet all three criteria as mentioned below:

1) substantial contributions to conception and design, or acquisition of data, or analysis and interpretation of data;

2) drafting the article or revising it critically for important intellectual content; and

3) final approval of the version to be published.

Authors should meet conditions 1, 2, and 3.

*signed: _____ date: _____

signed: _____ date: _____

signed: _____ date: _____

signed: _____ date: _____

signed: _____ date: _____

signed: _____ date: _____

signed: _____ date: _____

signed: _____ date: _____

signed: _____ date: _____

*First signature should be of corresponding author

The acknowledgment section includes contributors who provided purely technical help, writing assistance, or a department chair who provided only general support. Medical Writers; Financial and material support should also be acknowledged.

Groups of persons who have contributed materially to the paper but whose contributions do not justify authorship may be listed under a heading such as 'clinical investigators' or 'participating investigators,' and their function or contribution should be described—for example, 'served as scientific advisors,' 'critically reviewed the study proposal,' 'collected data,' or 'provided and cared for study patients.'

I confirm that this paper is not being submitted simultaneously elsewhere.

signed: _____ date: _____

(corresponding author)



<http://www.springer.com/journal/417>

Graefe's Archive for Clinical and Experimental
Ophthalmology
Incorporating German Journal of Ophthalmology
Editors-in-Chief: A.M. Jousseaume; D. Wong
ISSN: 0721-832X (print version)
ISSN: 1435-702X (electronic version)
Journal no. 417

1
2
3
4
5
6
7
8
9
10
11
12
13
14
15
16
17
18
19
20
21
22
23
24
25
26
27
28
29
30
31
32
33
34
35
36
37
38
39
40
41
42
43
44
45
46
47
48
49
50
51
52
53
54
55
56
57
58
59
60
61
62
63
64
65

A computer-based technique for assessing rod dark adaptation; age changes, data quality and reproducibility

Laura Patryas¹, Neil R.A. Parry^{2,3}, David Carden¹, Daniel H. Baker⁴, Jeremiah M.F. Kelly¹, Tariq Aslam^{2,3} and Ian J. Murray¹

1. The Vision Centre, Carys Bannister Building, Faculty of Life Sciences, University of Manchester, Manchester, UK

2. Vision Science Centre, Manchester Royal Eye Hospital, Manchester, UK

3. University of Manchester Academic Health Science Centre, Manchester, UK

4. School of Life & Health Sciences, Aston University, Birmingham, UK

Corresponding author: Laura Patryas, The Vision Centre, Carys Bannister Building, Faculty of Life Sciences, University of Manchester, Manchester, M13 9PL, UK;
laura.patryas@manchester.ac.uk.

Word count: 4081

Keywords: CRT, dark adaptometry, Rods, Ageing, Repeatability

Abstract

Purpose

To characterize the rate of scotopic sensitivity decline with age using a PC-driven cathode ray tube (CRT) monitor. To provide data regarding the repeatability of the technique and its ability to identify early photoreceptor degeneration in the presence of normal fundus and normal photopic vision.

Methods

Rod dark adaptation was monitored for 30 minutes following a minimum 30% pigment bleach, using a white 1° stimulus (modulated at 1 Hz), presented 11° below fixation on a CRT monitor. A VSG system was used to generate the stimuli and control the experiment. 33 subjects with no ocular pathology and normal fundus photographs were divided into two groups: older (≥ 45 , $n = 16$) and younger (< 45 , $n = 17$).

Results

Rod recovery was assessed using component S2 of dark adaptation. S2 was $0.04 \log_{10} \cdot \text{min}^{-1}$ slower in the older ($0.19 \pm 0.03 \log_{10} \cdot \text{min}^{-1}$) compared with the younger group ($0.23 \pm 0.03 \log_{10} \cdot \text{min}^{-1}$, $p < 0.001$), despite no difference in visual acuity and fundus appearance. Faster rates of S2 recovery were correlated with lower threshold at 30 minutes (T_{30}) ($r = 0.49$, $p < 0.005$). Correlation coefficients between first and second measurements for S2 and T_{30} were 0.49 ($p < 0.009$) and 0.84 ($p < 0.0001$), respectively. The coefficient of repeatability was $0.07 \log_{10} \cdot \text{min}^{-1}$ for S2 and $0.35 \log \text{cd} \cdot \text{m}^{-2}$ for T_{30} . The coefficients of variation for S2 and T_{30} were 15% and 10%, respectively.

Conclusions

Dark adaptation is slowed in normal ageing. CRT-based dark adaptometry is highly sensitive, easily implemented, non-invasive and highly repeatable. The technique described in this article would be useful for documenting visual changes in future clinical trials assessing retinal health in the older eye with and without ocular pathology.

Introduction

Dark adaptometry is considered a useful tool for investigating a variety of systemic and ocular diseases including vitamin A deficiency¹, liver disease², diabetes^{3,4}, age-related macular degeneration (AMD)⁵⁻¹⁰ and retinitis pigmentosa¹¹. It has also been used to assess non-pathological mechanisms of ageing^{12,13}. The term dark adaptation refers to the gradual recovery of visual sensitivity in total darkness following exposure to a bright light. The light bleaches the photoreceptor visual pigment resulting in its inactivation and a profound (~5 log units) loss of sensitivity. Classically, the dark adaptation function has been described as biphasic and comprises an initial rapid phase served by the cones, followed by a slower phase served by the rods. In recent years, significant advances have been made in our understanding of the biological processes underpinning rod recovery¹⁴. In terms of analysing and modelling dark adaptation data to obtain clinically useful parameters, the rod recovery can be partitioned into three partly overlapping components: S1, S2 and S3¹⁵. Normally, S1 is obscured by cone recovery so that, in the standard dark adaptation curve, S2 is the first measurable sign of rod recovery.

Slowed dark adaptation, particularly the rate of S2, is characteristic of ageing and AMD, and precedes retinal changes and cone-mediated visual function changes such as reduced visual acuity (VA)^{8,9,13,16,17}. Dark adaptometry is, therefore, likely to become the test of choice for investigating ageing and assessing efficacy of therapies and management strategies for early stage AMD. To that end, an inexpensive, readily available and repeatable technique for measuring dark adaptation kinetics will be essential if functional, as well as structural, features form part of the clinical outcomes.

There have been many studies aimed at using dark adaptation to assess age-related ocular pathology, but few have provided data regarding the repeatability of the slope of S2. Accurate determination of this parameter repeatability is important because detecting small changes in the slope of S2 is of clinical significance. The problem of accurate determination of dark adaptation parameters is compounded by the fact that data obtained from elderly subjects, who may or may not have ocular pathology, are usually more variable than those produced by young, healthy individuals. Repeatability and reliability of any technique will, therefore, be paramount to its applicability. In the main, studies published so far have used traditional, non-digital equipment such as the Goldman-Weekers adaptometer (GWA) or custom-built methods that are not at present widely available.

Two recent studies employed cathode ray tube (CRT) technology to assess dark adaptation kinetics^{17,18}. CRTs are ideally suited to, and used extensively in, visual psychophysics research. Their temporal and spatial characteristics are well documented and they are easily controlled by a computer. A major limitation of using computer monitors for dark adaptation, however, is that they have a limited dynamic range, but this problem is easily avoided by the use of neutral density (ND) filters¹⁷.

As far as we are aware, the coefficient of reliability (CoR) for the rod parameters measured by CRT dark adaptometry has not yet been established. The CoR is important when evaluating the performance of an instrument that is to detect clinically significant changes over the course of an intervention trial¹⁹. In this study we use a customized version of commercially available software to investigate the ability of CRT-based dark adaptometry to quantify delays in rod-mediated recovery in ageing. We also provide data regarding the repeatability of this technique.

We chose to focus on the measurement of the slope of S2 since rods are more vulnerable than cones in ageing and AMD^{8,9,20}.

Methods

Subjects

Thirty three normal volunteers participated in this study and were divided into two groups. The older group (≥ 45 years old, age range 45-68, mean 57.44 ± 7.98 , $n = 16$) consisted of 8 males and 8 females. The younger group (< 45 years old, age range 15-36, mean 25.12 ± 6.08 , $n = 17$) consisted of 10 males and 7 females.

Younger subjects were primarily recruited from the University of Manchester undergraduate population and older subjects from university staff. Informed consent was obtained. The tenets of the Declaration of Helsinki were followed. This study was approved by the University of Manchester Committee on the Ethics of Research on Human Beings.

All subjects had had a recent eye examination (up to 12 months before recruitment), were free from any ocular disease (e.g. glaucoma, AMD, cataract) and were not taking nutritional supplements. Subjects with diabetes or liver disease, current smokers, and those using systemic medications known to be retinotoxic were excluded from the study.

On the day of testing all subjects underwent assessment of VA and dark adaptation. Fundus photographs were taken with a TRC-NW6S Non-Mydriatic Retinal Camera (Topcon, Tokyo, Japan). All the participants from the present study were also participants in a study that examined the relationship between dark adaptation parameters and macular pigment optical density, which was measured in the same time period.

The VA was measured using an internally illuminated Early Treatment of Diabetic Retinopathy Study (ETDRS) chart (166.3 ± 3.92 cd.m⁻²), and expressed as logarithm of the minimum angle of resolution (logMAR). VA in the test eye was at least 0.2 or better in all cases. There was no difference in VA between the two groups ($t = 1.00$, $p = 0.3$).

The fundus photographs were processed using IMAGE Net 2000 software (Topcon, Tokyo, Japan) and viewed on a 20-inch monitor (1600 × 1200 pixels, 32 bits). The fundus images of all participants were graded by one of the authors (LP) according to a macular grading scale¹³. No subject had a grade beyond 1, thus all were classified as being normal.

Procedure

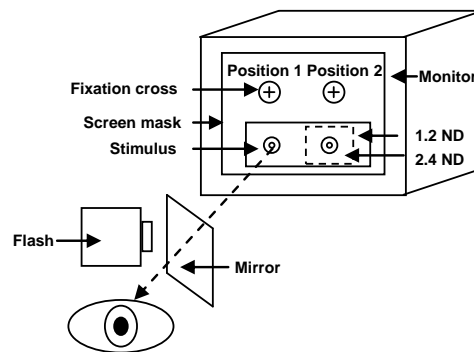
The stimuli were generated using a VSG 2/5 card (Cambridge Research Systems, Rochester, UK) running the Visual Psychophysics Engine (customized by its author, NRAP, who is one of the authors of this paper) and presented on a calibrated and gamma-corrected high-resolution CRT monitor (Sony GDM-F500R, Tokyo, Japan). A black cardboard mask with four apertures corresponding to the stimuli and fixation cross was placed over the monitor screen. One or more 1.2 log unit ND filters (#299; Lee Filters, Andover, UK) were placed in front of the test stimulus in the configuration illustrated in Figure 1.

The observer fixated a red cross (0.3°) at position 1 and responded to a 1° circular test spot (1931 CIE $x = 0.31$, $y = 0.316$), temporally modulated with a 1 Hz square wave and presented at 11° in the inferior field. The stimulus intensity was attenuated by a 1.2 log unit ND filter that extended over both stimulus locations. When the absolute filtered intensity of the stimulus was below -2.3 log cd.m⁻² (usually after about 12-15 minutes), the fixation cross shifted to position 2 and the observers responded to the stimulus at 11° below this new position. At this location the stimulus was further attenuated by a 2.4 log unit ND filter, so that total attenuation for the latter stages of the procedure was 3.6 log units. The dynamic range was sufficient (approximately 5.5 log units) to enable the measurement of the entire scotopic recovery function. A similar approach has been used previously with the filters

1 mounted on goggles worn by the observer^{17,18}. In our procedure, the expansion of the
2 dynamic range by addition of further ND filters is fully automatic. In the absence of other
3 visual cues (as the subject is in total darkness), the shift in location of the targets is rarely
4 noticed.

5 All subjects were dark adapted for 5 minutes followed by a practice session for a further 5
6 minutes. A localised 30-98% visual pigment bleach²¹ was then performed using an
7 electronic 0.9 ms flash of white light (Nikon Speedlight SB-800, Tokyo, Japan). The
8 maximum flash intensity was $6.08 \log \text{cd.s.m}^{-2}$ as measured using a PR1500 spot
9 photometer (Photo Research, Burbank, Ca, USA).

10 The flashgun was positioned 15 cm from the eye and at this distance subtended an angle of
11 20.9° wide by 13.3° high. The flash and the bleach area were precisely aligned so that
12 location of the test stimulus was centred on the bleached area of the retina. This was
13 achieved by using a calibrated semi-silvered mirror, as illustrated in Figure 1, so that the
14 subject observed the fixation mark when the flash was fired. An adjustment of 0.3 log units
15 was made to all thresholds to compensate for the absorption characteristics of the mirror,
16 which remained in place throughout the experiment.



17
18
19
20
21
22
23
24
25
26
27
28
29
30
31
32
33
34
35
36
37
38 Figure 1: The experimental set up. A mask with four apertures corresponding to the stimuli and fixation cross
39 locations covered the entire screen. A 1.2 log unit ND filter was attached to the back of the mask at stimulus
40 positions 1 and 2. When the filtered screen luminance fell below $-2.3 \log \text{cd.m}^{-2}$, the fixation cross and the
41 stimulus moved to position 2 where an additional smaller 2.4 log unit ND filter (attached to the back of the mask)
42 exposed the remaining region of rod recovery. The retinal area to be tested was accurately bleached by aligning
43 the flash with the stimulus (at position 1) through the use of a semi-silvered mirror.

44 Monocular thresholds were measured with natural pupils immediately after bleaching using
45 the method of adjustment (controlled by the experimenter) and were set at approximately
46 twice per minute for a duration of 30 minutes. The non-stimulated eye was patched during
47 testing and the subjects wore their best optical correction (where necessary) for the test
48 distance. The subject's head was positioned in a chin/head rest. All participants repeated the
49 dark adaptation measurement twice, separated by at least one week. These data were used
50 to determine test-retest reliability, but all the other data presented here are the means of two
51 visits.

52 53 *Data analysis*

54 Dark adaptation curves were plotted as \log_{10} threshold in cd.m^{-2} versus time in minutes.
55 These were fitted with a single exponential component to the cone phase and two linear
56 components to the rod phase, as described by McGwin et al²². The non-linear regression
57 technique was implemented in Matlab (Mathworks, MA, USA) and yielded the following
58
59
60
61
62
63
64
65

parameters of the dark adaptation curve: cone recovery rate, cone threshold, the rod-cone break (RCB), the slopes of the first (S2) and second (S3) rod components, the transition point between the two, and the threshold 30 minutes after the bleach (T_{30}). Of these parameters, we were primarily interested in component S2 and T_{30} . The latter was corrected for pre-retinal absorption (pupil diameter and media opacity) based on previous work²³⁻²⁶.

Kolmogorov-Smirnov tests were used to determine that the distributions of S2 and T_{30} did not differ from normal. Origin[®] (Northampton, MA, USA) and Matlab were used for statistical analysis and graph plotting. Repeatability was assessed using the standard correlation coefficient (Pearson's r) and by calculating the CoR (1.96 multiplied by the standard deviation of the differences between test and retest data) and coefficients of variation (CoV, the ratio of the standard deviation to the mean multiplied by 100).

Results

Preliminary data

Figure 2a depicts a classic dark adaptation function obtained with our CRT-based technique for a young, healthy observer (LP, one of the authors). An exponential-bilinear model partitioned the curve into three distinct phases of sensitivity recovery: a cone-mediated phase, followed by a rod-mediated phase divided into two linear regions. The two components of rod dark adaptation, S2 and S3, had negative slopes of $0.24 \log_{10} \cdot \text{min}^{-1}$ and $0.06 \log_{10} \cdot \text{min}^{-1}$, respectively.

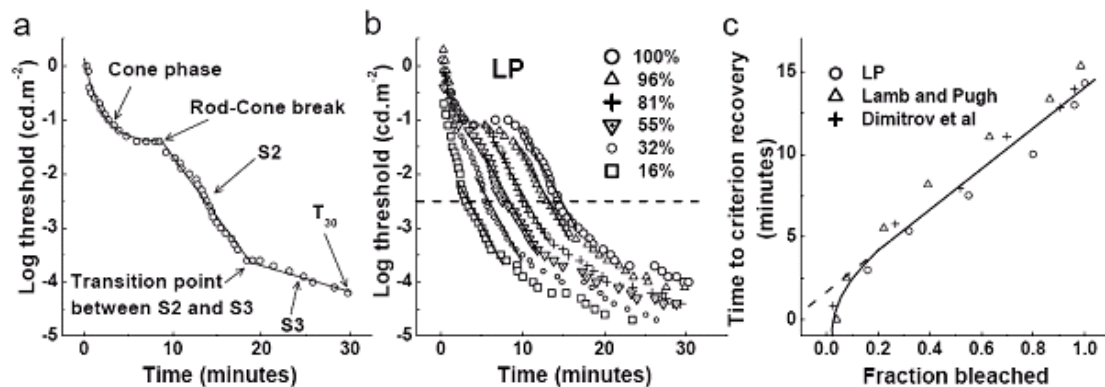


Figure 2: a) Typical dark adaptation data measured with our CRT-based technique for a young, healthy observer (LP) measured inferiorly at 11° degrees eccentricity, using a 1° white light stimulus following an 82% bleach. The data points were fitted with an exponential-bilinear model. S2 is the second rod component, S3 is the third rod component and T_{30} is the threshold 30 minutes after the bleach. $\text{SSE} = 0.3$, $r^2 = 0.9$. b) Dark adaptation curves for the same observer using the same technique following a range of bleaches (16 – 100%). The parallel solid lines plot component S2 and demonstrate a constant rate of rod recovery across bleaches. The horizontal dashed line is an arbitrary criterion (-2.5 log units) used to plot the graph in panel c. c) Linear relationship between fraction bleached (above 20%) and the time required to reach a criterion recovery level for our data (LP) and those from previous studies^{14,17}.

The parallel lines in Figure 2b plot component S2 for different bleach intensities. There was no significant correlation between bleach and slope of S2 ($r = 0.65$, $p > 0.23$) confirming that this phase of rod recovery is independent of the bleach magnitude provided the bleach is greater than 10-20%¹⁴. In Figure 2c, the time taken to reach an arbitrary threshold of -2.5 log units (extracted from Figure 2b) was re-plotted against the fraction bleached. The straight line fit when plotted in semi-logarithmic co-ordinates for bleaches greater than 10 - 20%

reveals the rate-limited behaviour of S2¹⁴. Our data are in good agreement with previous studies^{14,17}.

Repeatability

In order to quantify measurement error, repeated measurements were obtained on different days. Correlation coefficients between first and second measurements for S2 and T₃₀ were 0.49 ($p < 0.009$) and 0.84 ($p < 0.0001$), respectively. The average absolute change between sessions (dotted line in Figure 3) was 0.004 (± 0.04) for S2 and 0.05 (± 0.23) for T₃₀ indicating only minimal bias. The CoR was 0.07 log₁₀.min⁻¹ for S2 and 0.35 log cd.m⁻² for T₃₀. The CoV was 15% for S2 and 10% for T₃₀.

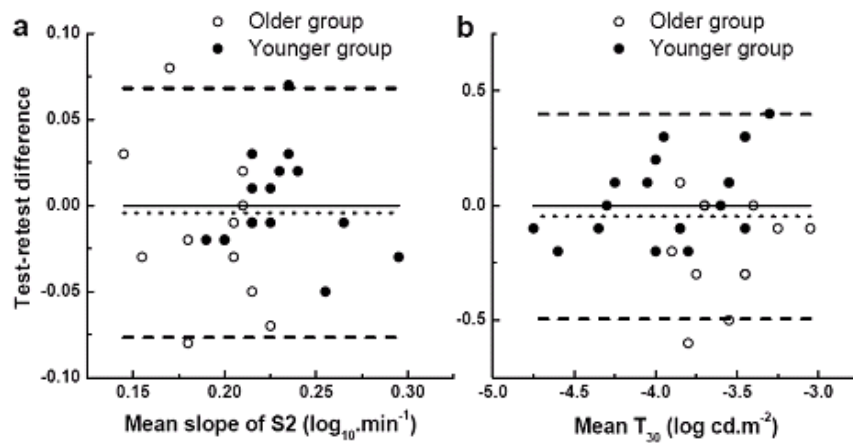


Figure 3: Test-retest differences versus means to assess the repeatability of dark adaptation curve parameters S2 (panel a) and T₃₀ (panel b). The dotted line represents the bias (test-retest mean differences) and the dashed lines represent 95% limits of agreement.

Dark adaptation in older and younger eyes

Figure 4 depicts rod dark adaptation kinetics (components S2 and S3), after the RCB, for the younger and the older group. Each subject's curve was linearly shifted in x and y directions so that their individual RCBs were coincident. The group data were fitted with a bilinear function. The older group (solid line, panel b) had a shallower slope of S2 compared with the younger group (dashed line) indicating slower rate of recovery. The vertical (upward) shift in the older group along the y-axis indicates threshold elevation across the entire rod-dominated region of sensitivity recovery.

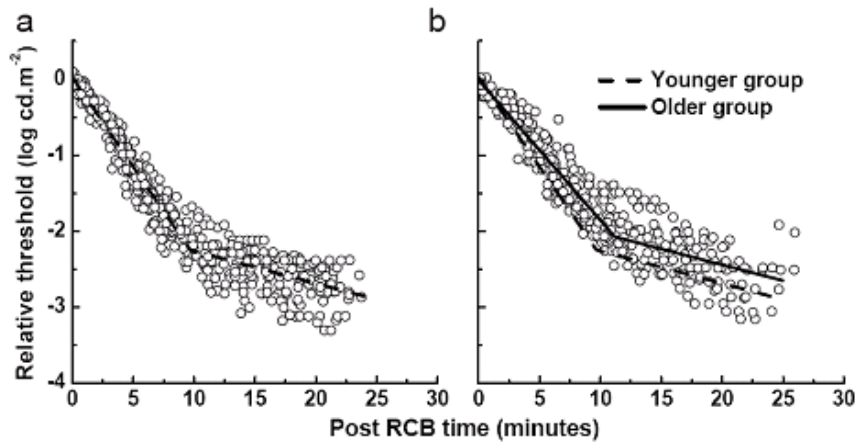


Figure 4: Group data showing the S2 and S3 regions of rod recovery for younger (panel a) and older (panel b) subjects. A bilinear function was fitted to each data set. The younger group model (dashed line) is superimposed onto the older group data in panel b to demonstrate slowing of the S2 region and elevated thresholds in the older group. Data have been shifted along the x and y axes so that the individual RCBs were coincident.

Figure 5a shows the slope of S2 as a function of age. The younger group had an average S2 of $0.23 \pm 0.03 \log_{10} \cdot \text{min}^{-1}$ with a time constant (τ) of 1.9 minutes ($\log_{10}(e) / \text{S2}$). The older group was significantly slower than the younger group ($t = 13.08, p < 0.0002$) with an average S2 of $0.19 \pm 0.03 \log_{10} \cdot \text{min}^{-1}$ ($\tau = 2.3$ minutes). The rate of recovery over the S2 region decreased $0.01 \log$ units/min per decade in our population.

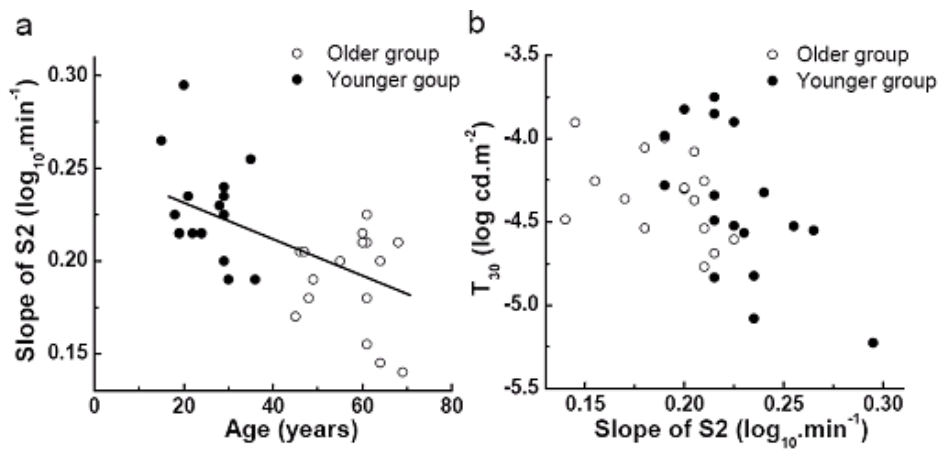


Figure 5: a) Scatter plot of S2 as a function of age. The line represents linear regression fitted to the data ($r = 0.62, p < 0.0002$). b) Scatter plot illustrating the significant relationship between T_{30} and S2 ($r = 0.49, p < 0.005$). All data points are means of two sessions. Thresholds were corrected for lens density and pupil miosis.

We found a correlation between S2 and T_{30} after corrections for media changes. Figure 5b shows that, for our cohort, lower thresholds were associated with faster rod-mediated recovery (larger S2 values) for the whole group ($r = 0.49, F[1, 32] = 9.57, p < 0.005$).

Discussion

The data presented in this paper demonstrate that our CRT-based dark adaptometry produces results that agree with previous studies^{14,17}. The slowing of component S2 with increasing age found in this study was $0.01 \log$ units/decade and reflects reduced rhodopsin

1 regeneration rate, in agreement with other psychophysical¹³ and rod densitometry²⁷ data.
2 The technique proved capable of differentiating between younger and older eyes, despite no
3 differences in VA and fundus appearance between the two groups. The power in this study
4 to detect a difference between old and young eyes was 0.96 (calculated using G*Power
5 3.0.10). This is a good indicator of the ability of the technique to detect small changes in the
6 slope of S2, either between two groups or in individuals in a longitudinal study.

7
8 It is thought that the reduced rhodopsin regeneration rate with age is likely to be a result of
9 progressive thickening of Bruch's membrane which acts as a resistive barrier to metabolic
10 exchange¹³. In particular, it may limit the amount of vitamin A reaching the retinal pigment
11 epithelium (RPE) and reduce the transport of 11-cis retinal to the outer rod segment from the
12 RPE. Compelling evidence for this hypothesis is the observed delay in dark adaptation
13 kinetics in subjects with vitamin A deficiency and its amelioration following vitamin A
14 supplementation^{1,28}. Furthermore, even in healthy subjects without vitamin A deficiency and
15 either early AMD or normal retinal health, retinol supplementation improves the rate of rod
16 recovery²⁹.

17
18 The correlation between the rate of rod-mediated recovery (slope of S2) and T₃₀ is at odds
19 with one previous study³⁰. In that study the absolute threshold was measured which may not
20 be directly comparable to our measure of threshold after 30 minutes. Our correlation can be
21 explained by geometry of the dark adaptation function and by the cellular model of recovery
22 kinetics presented by Lamb and Pugh¹⁴. If the slope of S2 is steeper then the threshold at
23 30 minutes will be lower. Although the measurements were restricted to 30 minutes and
24 some observers would have reached lower thresholds had the time been extended, it seems
25 likely that the rate of S2 and T₃₀ share the same cellular and molecular mechanisms¹⁴.

26
27
28 Prolonged dark adaptation kinetics in older adults lead to difficulties with vision-oriented
29 tasks in dim lighting and increase the risk of night-time falls and road traffic accidents. These
30 problems have been confirmed in self-reporting surveys such as that described by Scilley et
31 al³¹ who used a questionnaire designed specifically for assessing low light visual problems.
32 Difficulties arise, however, in establishing the exact contribution of impaired night vision to
33 accidents because of the absence of a satisfactory test which can be used routinely under
34 clinical conditions. It seems likely that those older observers with a healthy lifestyle and good
35 nutrition, can be expected to have relatively good scotopic recovery, but confirming such a
36 hypothesis might be difficult because a technique for measuring the slope of S2 precisely is
37 not generally available. The method described here could be used to quantitatively assess
38 patient night vision with excellent reproducibility, enabling researchers to use scotopic
39 recovery as a realistic outcome measure.

40
41
42 The CRT method has previously been compared with the conventional GWA showing good
43 agreement between the two methods on almost all parameters of the dark adaptation curve
44 including cone recovery rate, RCB and S2¹⁷. The general problem with the GWA is its poor
45 repeatability for cone recovery. Gaffney et al³² have shown a clinically unacceptable CoR for
46 cone recovery time constant and concluded that the GWA would not be a useful instrument
47 for documenting visual changes in future clinical trials. Christoforidis and Zhang³³ also used
48 GWA in a test-retest paradigm. They showed no learning effects and no statistically
49 significant differences on repeated measures for any of the parameters of the scotopic
50 recovery curve. Although their group mean S2 recovery rate of 0.15 log₁₀.min⁻¹ is
51 significantly slower than ours and that typically reported in the literature for healthy subjects,
52 their CoR for S2 of 0.06 log₁₀.min⁻¹ is very similar to ours.

53
54
55 Dimitrov et al¹⁷ used a similar method to the one described in this article. However, in that
56 study, which also investigated AMD patients, the CoV for the rod parameters was not given.
57 Their CoV for the RCB was 32% for normal and 44% for AMD subjects which is relatively
58 large. This could be due to the fact that the RCB is largely dependant on the magnitude of
59
60
61
62
63
64
65

1 the bleach and highlights the importance of precise and uniform bleaching between visits for
2 longitudinal clinical trials. In the present study we were able to accurately bleach the area to
3 be tested by using a semi-silvered mirror. Although, we did not dilate the pupils because we
4 were only interested in the rod parameters, we would highly recommend pupil dilation in any
5 future clinical trials investigating cone dynamics. This is because dilation of pupils allows
6 tighter control over the bleach. Finally, our technique readily elicited the third rod component
7 (S3) unlike the protocol suggested by Dimitrov et al ¹⁷ using a single 2.6 log unit ND filter.
8 Such a narrow range may pose problems in evaluating dark adaptation in ageing,
9 particularly in subjects with good scotopic sensitivity due to its ceiling effect.
10

11
12 In summary, the present study makes two key contributions. First, we demonstrate the
13 validity of using an easily implemented computer-based technique to explore scotopic
14 sensitivity recovery in ageing using an automated and inexpensive method of expanding the
15 luminance range with ND filters. Second, we provide data on the repeatability of rod-
16 mediated dark adaptation parameters measured with this technique. Because of its sound
17 physiological basis, S2 is of particular interest. It seems likely that given its many
18 advantages, dark adaptometry based on digital methods will become the method of choice
19 for future work in assessing retinal health in the older eye with and without ocular pathology.
20
21
22
23
24

25 Acknowledgements

26 Supported by BBSRC grant (BB/F017227/1) and Vitabiotics. NRAP and TA are supported by
27 the NIHR Manchester Biomedical Research Centre. DHB was supported by EPSRC grant
28 (EP/H000038/1).
29
30
31
32
33

34 NRAP has a proprietorial interest in the software described here.
35

36 References

- 37 1. Russell RM, Multack R, Smith VC, Krill A, Rosenberg IH. Dark-adaptation testing for
38 diagnosis of subclinical vitamin-A deficiency and evaluation of therapy. *Lancet*.
39 1973;302(7839):1161–1164.
- 40 2. Abbott-Johnson WJ, Kerlin P, Abiad G, Clague AE, Cuneo RC. Dark adaptation in vitamin
41 A-deficient adults awaiting liver transplantation: improvement with intramuscular vitamin A
42 treatment. *British Journal of Ophthalmology*. 2010;544–548.
- 43 3. Henson DB, North RV. Dark adaptation in diabetes mellitus. *British Journal of*
44 *Ophthalmology*. 1979;63(8):539–541.
- 45 4. Phipps JA. Rod Photoreceptor Dysfunction in Diabetes: Activation, Deactivation, and Dark
46 Adaptation. *Investigative Ophthalmology & Visual Science*. 2006;47(7):3187–3194.
- 47 5. Brown B, Adams AJ, Coletta NJ, Haegerstrom-Portnoy G. Dark adaptation in age-related
48 maculopathy. *Ophthalmic and Physiological Optics*. 1986;6(1):81–84.
- 49 6. Steinmetz R, Haimovici R, Jubb C, et al. Symptomatic abnormalities of dark adaptation in
50 patients with age-related Bruch's membrane change. *Br J Ophthalmol*. 1993;77(9):549–54.
51
52
53
54
55
56
57
58
59
60
61
62
63
64
65

- 1 7. Owsley C, McGwin G, Jackson G., Kallies K, Clark M. Cone- and rod-mediated dark
2 adaptation impairment in age-related maculopathy. *Ophthalmology*. 2007;114(9):1728–1735.
- 3 8. Owsley C, Jackson GR, White M, Feist R, Edwards D. Delays in rod-mediated dark
4 adaptation in early age-related maculopathy* 1. *Ophthalmology*. 2001;108(7):1196–1202.
- 5 9. Owsley C, Jackson GR, Cideciyan AV, et al. Psychophysical evidence for rod vulnerability
6 in age-related macular degeneration. *Investigative ophthalmology & visual science*.
7 2000;41(1):267.
- 8 10. Jackson G., Aleman TS, Owsley C. The Scotopic Sensitivity Tester-1 and the detection
9 of early age-related macular degeneration. *Ophthalmic Physiol Opt*. 2006;26(4):431–437.
- 10 11. Omar R, Herse P. Quantification of dark adaptation dynamics in retinitis pigmentosa
11 using non-linear regression analysis. *Clin Exp Optom*. 2004;87(6):386–389.
- 12 12. Coile DC, Baker HD. Foveal dark adaptation, photopigment regeneration, and aging. *Vis*.
13 *Neurosci*. 1992;8(1):27–39.
- 14 13. Jackson GR, Owsley C, McGwin Jr G. Aging and dark adaptation. *Vision research*.
15 1999;39(23):3975–3982.
- 16 14. Lamb TD, Pugh EN. Phototransduction, dark adaptation, and rhodopsin regeneration the
17 proctor lecture. *Investigative ophthalmology & visual science*. 2006;47(12):5138.
- 18 15. Lamb TD. The involvement of rod photoreceptors in dark adaptation. *Vision Research*.
19 1981;21(12):1773–1782.
- 20 16. Curcio CA, Owsley C, Jackson GR. Spare the rods, save the cones in aging and age-
21 related maculopathy. *Investigative ophthalmology & visual science*. 2000;41(8):2015.
- 22 17. Dimitrov PN, Guymer RH, Zele AJ, Anderson AJ, Vingrys AJ. Measuring rod and cone
23 dynamics in age-related maculopathy. *Investigative ophthalmology & visual science*.
24 2008;49(1):55.
- 25 18. Dimitrov PN, Robman LD, Varsamidis M, et al. Visual function tests as potential
26 biomarkers in age-related macular degeneration. *Invest. Ophthalmol. Vis. Sci*.
27 2011;52(13):9457–9469.
- 28 19. Bland JM, Altman DG. Statistical methods for assessing agreement between two
29 methods of clinical measurement. *Lancet*. 1986;1(8476):307–310.
- 30 20. Jackson GR, Owsley C, Curcio CA. Photoreceptor degeneration and dysfunction in
31 aging and age-related maculopathy. *Ageing research reviews*. 2002;1(3):381–396.
- 32 21. Rushton WAH, Powell DS. The rhodopsin content and the visual threshold of human
33 rods. *Vision Research*. 1972;12(6):1073–1081.
- 34 22. McGwin G, Jackson GR, Owsley C. Using nonlinear regression to estimate parameters
35 of dark adaptation. *Behavior Research Methods, Instruments, & Computers: A Journal of the*
36 *Psychonomic Society, Inc*. 1999;31(4):712–717.
- 37 23. Birren JE, Shock NW. Age changes in rate and level of visual dark adaptation. *J Appl*
38 *Physiol*. 1950;2(7):407–411.

- 1
2
3
4
5
6
7
8
9
10
11
12
13
14
15
16
17
18
19
20
21
22
23
24
25
26
27
28
29
30
31
32
33
34
35
36
37
38
39
40
41
42
43
44
45
46
47
48
49
50
51
52
53
54
55
56
57
58
59
60
61
62
63
64
65
24. Pulos E. Changes in rod sensitivity through adulthood. *Invest. Ophthalmol. Vis. Sci.* 1989;30(8):1738–1742.
 25. Sturr JF, Zhang L, Taub HA, Hannon DJ, Jackowski MM. Psychophysical Evidence for Losses in Rod Sensitivity in the Aging Visual System. *Vision Research.* 1997;37(4):475–481.
 26. Pokorny J, Smith VC, Lutze M. Aging of the human lens. *Appl. Opt.* 1987;26(8):1437.
 27. Liem AT, Keunen JE, van Norren D, van de Kraats J. Rod densitometry in the aging human eye. *Investigative ophthalmology & visual science.* 1991;32(10):2676.
 28. Russell RM, Morrison SA, Smith FR, Oaks EV, Carney EA. Vitamin-A reversal of abnormal dark adaptation in cirrhosis. Study of effects on the plasma retinol transport system. *Ann. Intern. Med.* 1978;88(5):622–626.
 29. Owsley C, McGwin G, Jackson GR, et al. Effect of short-term, high-dose retinol on dark adaptation in aging and early age-related maculopathy. *Investigative ophthalmology & visual science.* 2006;47(4):1310.
 30. Jackson GR, Owsley C. Scotopic sensitivity during adulthood. *Vision Research.* 2000;40(18):2467–2473.
 31. Scilley K, Jackson GR, Cideciyan AV, et al. Early age-related maculopathy and self-reported visual difficulty in daily life. *Ophthalmology.* 2002;109(7):1235–1242.
 32. Gaffney AJ, Binns AM, Margrain TH. The repeatability of the Goldmann-Weekers adaptometer for measuring cone adaptation. *Doc Ophthalmol.* 2011;122(2):71–75.
 33. Christoforidis J, Zhang X. Learning effect of dark adaptation among normal subjects. *Graefes Arch. Clin. Exp. Ophthalmol.* 2011;249(9):1345–1352.

ETHICAL APPROVAL

J.1 Application for Ethical Oversight

J.2 Subject Information

J.3 Subject Consent

J.4 Subject Advertisement

UNIVERSITY OF MANCHESTER

COMMITTEE ON THE ETHICS OF RESEARCH ON HUMAN BEINGS

Application form for approval of a research project

This form should be completed by the Chief Investigator(s), after reading the guidance notes.

1. Title of the research

Full title: **Temporal characteristics of photoreceptor function in older eyes**

2. Chief Investigator

Title: Dr

Forename/Initials: Ian

Surname: Murray

Post: Faculty of Life Sciences, Moffat Building, University of Manchester,
Manchester, M60 1QD, UK

Qualifications: BSc, MSc, PhD, FBCO

School/Unit: Faculty of Life Sciences

E-mail: ian.j.murray@manchester.ac.uk

Telephone: 01613063886

3. Details of Project

3.1 Proposed study dates and duration

Start date: 01/08/2009

End date: 31/07/2013

3.2 Is this a student project?

Yes/No

If so, what degree is it for?

PhD

3.3. What is the principal research question/objective? *(Must be in language comprehensible to a lay person.)*

There are two main types of photoreceptors in the human retina called rods and cones. Cones operate in light (photopic) conditions and rods in dark (scotopic) conditions. Cones are concentrated in the central (macular) retina, whereas rods are more numerous in the peripheral retina. The objectives of the research are as follows:

- i) to develop a technique for separating the tiny electrical signal (ERG) generated by rods from that generated by cones. .
- ii) to investigate the effects on the retina of normal aging by measuring cone-specific and rod-specific ERGs in a population of older observers.
- iii) to investigate the effects on the retina of normal aging by measuring thresholds for the detection of cone-specific flicker or rod-specific flicker sensitivity.

3.4. What is the scientific justification for the research? What is the background? Why is this an area of importance / has any similar research been done? *(Must be in language comprehensible to a lay person.)*

In the normal human retina there are three sub-types of cones, each tuned to different regions of the visible spectrum. S-cones (Short-wavelength cones) have their peak spectral absorbance in the short-wave region ($\lambda_{\text{max}} = 450\text{nm}$), M-cones (Medium-wavelength cones) in the medium-wave region ($\lambda_{\text{max}} = 535\text{nm}$) and L- cones (Long-wavelength cones) in the long-wave region ($\lambda_{\text{max}} = 590\text{nm}$) (these spectra are illustrated in figure 2).

The cones allows us to see fine details and colours and are capable of following fast trains of impulses. As stated above they rely on relative high levels of illumination.

The ability to see in low illumination relies on vast numbers (~120 million in normals) of rod photoreceptors. In almost complete darkness, the rod system increases its sensitivity so as to allow us to detect objects and this process normally takes around 20 minutes. This so-called dark adaptation process has been shown to be impaired in older eyes and in those affected by age-related macular degeneration, a common disorder of central vision in older people.

It is well known that the ability to process dynamical information declines with age in all visual systems. It is thought that this phenomenon is due either to reduced numbers of photoreceptors or to impaired ability of the photoreceptors to absorb light (Curcio et al. 2000). Rods in particular are thought to be susceptible to age-related impairment (Owsley et al 2007).

The new techniques will allow us to contribute to the literature on the age-related decline in photoreceptor performance. This is important for three

reasons. First, we will be able to establish, as suggested from other types of research, whether rods are more susceptible to aging than cones. One study, (Curcio et al. 1993) suggests a 30% decline in numbers of rods but that cone numbers are relatively stable with age. Second, donor eye studies have shown that rods are impaired in a particular region of the aging retina, an annular zone at around 15 degrees of eccentricity. It would be extremely valuable to be able to confirm this in living eyes. Finally, a technique capable of separating rod activity from cone activity in vivo would be helpful in establishing the borderline between normal photoreceptor aging and the degenerative disease processes such as Age Related Macular Degeneration (ARMD). This disease leads to extensive visual impairment and is by far the leading reason for vision loss in the older populations of the developed countries. Some studies have suggested that up to 30% of the older 65s have the early stage of the disease (Klein et al. 1997). Due to demographics, ARMD is due to become a real clinical problem in the next decade.

3.5. How has the scientific quality of the research been assessed? *(Tick as appropriate)*

- Independent external review**
- Review within a company
- Review within a multi-centre research group
- Internal review (e.g. involving colleagues, academic supervisor)**
- None external to the investigator
- Other, e.g. methodological guidelines *(give details below)*

If relevant, describe the review process and outcome. If the review has been undertaken but not seen by the researcher, give details of the body which has undertaken the review:

Part of this research was reviewed by referees acting for the British College of Optometrists (BCOO) who have awarded a PhD stipend, starting in September 2009. The technical aspects have been discussed in detail with Dr Neil Parry who is a Senior Electrophysiologist at the Manchester Royal Eye Hospital and with David Carden who is an electronics engineer and has many years experience of recording from the human retina in vivo.

3.6. Give a full summary of the purpose, design and methodology of the planned research, including a brief explanation of the theoretical framework that informs it. It should be clear exactly what will happen to the research participant, how many times and in what order. Describe any involvement of research participants, patient groups or communities in the design of the research. (This section must be completed in language comprehensible to the lay person).

Purpose

The overall purpose of this study is to develop new techniques for recording the electrical impulses (ERG), generated exclusively by cones or exclusively by rods. There are two novel features to the research: first, we will use a sequence of

stimuli (illustrated below in figure 1, and called Centre Surround Sweep) capable of activating different regions of the retina. Second, a method called silent substitution (see figure 2) will be used to separate the signal generated by L-cones from that generated by M-cones. This method has been described by us previously (Murray et al. 2004) combined with Centre Surround Sweep stimulation using only a small group of subjects (details on the two methods follow below).

A secondary purpose is to study the sensitivity to flicker with a new stimulus which is designed to isolate rod- and cone- activity using different principles from the above. This psychophysical procedure, in which observers will adjust the luminance of flicker until the stimulus appears stable, called the flicker threshold, will enable us to compare data from the two techniques. There is substantial literature suggesting that flicker detection in the human visual system is intimately linked to the performance and integrity of photoreceptors. Comparing the two sets of data will provide additional knowledge on this notion and at the same time may lead to the development of a rapid clinical procedure capable of assessing the healthiness of rods and cones.

ERG – theoretical design

The centre-surround sweep technique.

ERGs are recorded when a sequence of 15 stimuli are each presented for a 4 second period on a computer monitor, as shown in figure 1. The first is a blank, seen in the top left of the diagram. The second is a small, 10 degree region of flicker, seen by the subject in the centre of their field of view. The second is a 20 degree region of flicker, again centred around a fixation point in the middle of the screen. The flickering zones continue to increase in 10 degree steps until 70 degrees (stimulus 7) after which a central 10 degree zone of non-flicker appears. This central zone gradually increases, again in the 10 degree steps, until the flicker in the 14th stimulus is confined only to the outer 10 degrees. During this sequence, signals are recorded from the retina as outlined below. The averaging technique requires 2 repeats and so, with computer ‘dead-time’, each recording takes around 2.5 minutes.

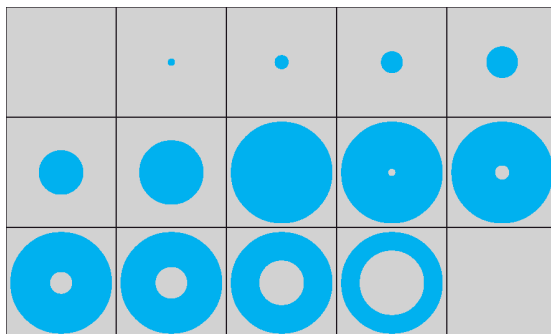


Figure 1. The centre-surround sweep sequence.

The amplitude of the signal generated from each stimulus was compared with the photoreceptor count in donor eyes using interference contrast microscopy (Curcio et al. 1990; Murray et al. 2008). The data suggest a close association between the two methods ($r^2 = 0.99$) indicating that the technique can accurately estimate the number of functioning photoreceptors in the average human retina as discussed in Murray et al. (2004).

The silent substitution technique

As described above the peak absorption of the L- and M-cones are quite similar as are their absorption spectra. This complicates the problem of recording L- or M- cone specific ERGs. The technique of silent substitution was developed in order to exclusively stimulate either one of the two cone types. The principle is illustrated in figure 2. A pair of wavelengths is selected which will activate one cone type whilst at the same time producing zero modulation in the other. The two lights are then presented in alternate phase (one appears as the other disappears and vice versa). The signal obtained can then be attributed to the activated cone. In the case illustrated, M-cones are 'silenced' and L-cones are activated. A different pair of lights is selected to 'silence' L-cones and activate M-cones.

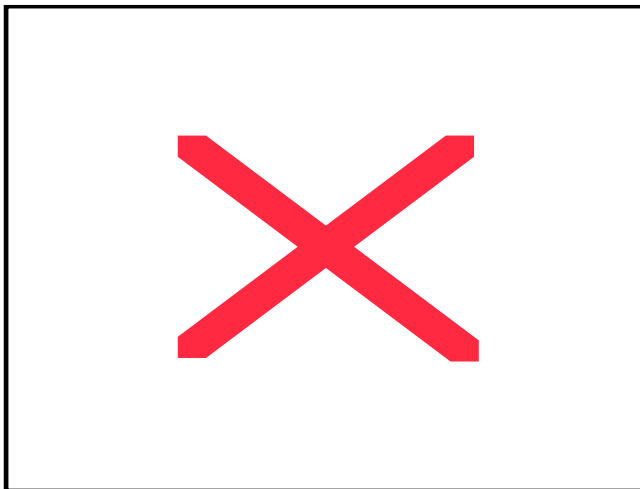


Figure 2. Silent substitution for M-cones. The excitation values for the three cone-types are from Stockman and Sharp 2000 cone-fundamentals using a 2 degree stimulus.

Methodology

Electroretinography - Rod- and cone-specific ERG

Electroretinography (ERG) is a well established technique used to study normal and abnormal retinal function. It is used on a daily basis in eye clinics. It is usually necessary to dilate the pupil with mydriatic drops (tropicamide 1%) in order to ensure adequate stimulation of the photoreceptors. Typically a small electrode is placed on the skin below the eyelid (called a skin electrode) or underneath the lower eyelid. The latter is composed of extremely fine fibre, just visible to the human eye and is placed in the lower canthus between the eye and

the lower eyelid where 'foreign bodies' such as dust sometimes accumulate (when such a 'foreign body' is sufficiently large it induces a 'foreign body' reaction and discomfort is experienced). When fibre electrodes are correctly located, observers are entirely unaware of their presence and there is no 'foreign body' reaction. Placing of the electrode is not regarded as an invasive procedure. The fibre electrode is called the active electrode. Additional electrodes are positioned on the forehead to act as an earth and the other (reference) on the temporal forehead. The skin, the reference and the earth electrodes are placed on the skin using a water-soluble paste to maintain good contact. After the electrodes are placed and the pupil is dilated (about 10-15 minutes after the instillation of the drops) the observer views a computer monitor on which the various stimuli are present. The signals generated by the retina are transmitted via the electrodes to an amplifier (x5000) and subsequently to a smart interface for signal analysis. Depending on the presentation rate, signals are extracted from noise and plotted in Fourier components or, for slow presentation they are plotted as a function of time. The entire procedure, including the placing of the electrodes and the administration of the drops will be conducted either by Dr Murray or by the PhD student, who will be a qualified optometrist (as required by the funding organisation (British College of Optometrists)).

Psychophysics - Rod-and cone-specific flicker thresholds

This psychophysical technique will be based on the principle, first described by Aguilar and Stiles (1954) of suppressing the activity of the cones with a long wavelength (650nm) pedestal of light and testing sensitivity of the rods with a green (520nm) light superimposed on the red light. In a pilot study, funded by Manchester University, we have established that this technique of isolating rod activity allows the integrity of rods to be assessed without prolonged periods of dark adaptation. In this procedure observers are presented with a small (8 degrees) narrow band red (610nm) or green (595nm) flickering light. The lights will be superimposed on either a red or green background. Observers have control of the luminance of one of the lights and set thresholds for the detection of flicker.

Control Experiments

Two control experiments are required. First, the only way to ensure isolation of the either L or M cones, congenitally colour defective observers who are known to have only one of the two cones types will be tested. By recording L-cone specific ERGs in an observer who is known to have only either M-cones or L-cones the isolating technique can be validated. Subjects with an x-linked loss of L or M cones are quite common (~8%) in the male Caucasian population. Absence of S-cones is extremely rare.

Second, in order to confirm isolation of rod activity a bleaching method is frequently used. Here subjects look at a bright light for a 5 minute period prior to

performing the rod isolating tests. It is known that this temporarily 'bleaches' the rods, leaving only the cones (which unlike rods, do not saturate) to respond. The light is not of excessive intensity (~1000cd/m²) which is approximately the intensity of a white surface under moderate sunlight. Bleaching can also be achieved with a conventional photographic flash light. Both methods induce dazzle which lasts the duration of photoreceptor recovery which is 1 to 2 minutes. Bleaching will be performed in a small number (between 3 and 6) of observers.

Overall Experimental Design

Three groups of observers will participate in the study. There will be a small group of observers having a colour vision defect such that they have only either L-cones or M-cones (5 observers). Recording ERGs from these subjects is the standard technique for confirming that the silent substitution method is successfully isolating the two different cone types. The second group will consist of young observers who have normal colour vision (20 observers, age range 18-40 years) and in whom we will establish the range of normal electrophysiological and psychophysical data, the third group will be composed of normal elderly observers (20 observers, age-range 50-70 years).

Protocol

The subjects will be asked to take part in two experimental sessions. During the first session an eye test examination and a colour vision test will be performed. After, the flicker threshold experiment will follow. During the second visit, the ERGs experiment will take place. The schedule for the observers' visits will be as follow:

First Visit

- 1) The subject will be given the information sheet of this study and he/she will have as much time he/she wants to read it and ask questions. If he/she agree to participate in the study will sign the consent form.
- 2) First, the visual acuity of the participant will be assessed using a Snellen chart. Snellen chart is a self illuminated panel of letters of different sizes, viewed at a standard distance. This test takes less than 2 minutes.
- 3) Next, the health of the eye will be assessed by a qualified optometrist using an ophthalmoscope to examine the ocular fundus. The Intra-Ocular pressure (IOP) will be measured, using a non-contact tonometer While the observer looks at a light spot, the instrument introduces a sharp pulse of air, on the centre of the cornea. The pulse of air distorts the cornea and by measuring the time taken to recover an estimate of IOP is derived The device is used world wide for routine IOP measurements and it is completely painless. This procedure should take about 10 minutes.
- 4) The colour vision of the participant will be tested, using the Nagel Anomaloscope. The participant has to match a mix of red (620nm) and

green (535nm) wavelengths with a third yellow (555nm) wavelength. This test would take less than 10 minutes.

- 5) The last step of the first visit will be the main flicker-threshold experimental procedure. In this procedure, an optical system will be used to present observers a small (8 degrees) narrow band red (610nm) or green (595nm) flickering light. The lights will be superimposed on either a red or green background. Observers have control of the luminance of one of the lights and set it until the stimulus appears stable. This is the so called flicker-threshold. The experiment will last approximately an hour.

The first visit is expected to have duration of approximately 2 hours including breaks and time for explanations of the various tests.

Second Visit.

- 1) On arrival, the first step will be the instillation of the 1% tropicamide drops. These drops are used to dilate the participants' pupil and a single drop will be administered on the one eye. The effect of tropicamide will reach its maximum about 20 minutes after the instillation.
- 2) Next, the electrodes will be placed around the eye. Four electrodes will be used. Two active electrodes will be placed, one underneath the lower eyelid and one on the skin under the lower eyelid. The two additional electrodes are positioned on the forehead to act as an earth and the other (reference) on the temporal forehead. Participants will not feel any discomfort.
- 3) The subject will view a monitor where the rod-only and cone-only stimuli will be presented. A chin rest will be used to keep the distance from the monitor constant. The averaging technique requires 2 to 4 repeats and so with computer 'dead-time' each recording takes around 2.5 minutes. This will be repeated for the rod-only and two cone-only stimuli. If necessary, further sampling will be performed, but the overall recording time will not exceed 20 minutes. Regular breaks will be provided. .

The second visit is expected to have duration of approximately 2 hours including breaks and time for explanation of the procedure.

References:

- Curcio C.A., Leigh Millican C., Allen K.A., Kalina R.E., 1993. Aging of the human photoreceptor mosaic: evidence for selective vulnerability of rods in central retina. *Invest Ophthalmol Vis Sci*, **34**, 3278-96.
- Curcio C.A., Sloan K.R., Kalina R.E., Hendrickson A.E., 1990. Photoreceptor topography. *J Compar Neurol*, **292**, 497-23.
- Curcio C.A., Owsley C., Jackson G.R., 2000. Spare the rods, save the cones in aging and age-related maculopathy. *Invest Ophthalmol Vis Sci*, **41**, 2015-8.
- Murray I.J., Parry N.R.A., Kremers J., Stepien M., Schild A., 2004. Photoreceptor topography and cone-specific electroretinograms. *Vis Neurosci*, **21**, 231-35.
- Murray I.J., Kremers J., Parry N.R.A., 2008. L- and M-cone isolating ERGs: LED versus CRT stimulation. *Vis Neurosci*, **25**, 327-31.
- Klein R., Klein B.E., Jensen S.E., Meuer S.M., 1997. The five-year incidence and progression of age-related maculopathy: The Beaver Dam Eye Study. *Ophthalmology*, **104**, 7-21.
- Owsley C., McGwin G.Jr., Jackson G.R., Kallies K., Klark M., 2007. Cone and rod mediated dark-adaptation impairment in age-related maculopathy. *Ophthalmology*, **114**, 1728-35.

3.6.1. Has the protocol submitted with this application been the subject of review by a statistician independent of the research team?(Select one of the following)

- Yes – copy of review enclosed
- Yes details of review available from the following individual or organisation (give contact details below)
- No – justify below**

The overall experimental design is straightforward. The protocol allows the comparison of results from young and older eyes. As the data do not require complex statistical manipulation and the experimental design is not elaborate, independent review of the analysis is thought unnecessary.

3.6.2. If relevant, specify the specific statistical experimental design, and why it was chosen?

Observations will be compared from two groups of subjects. Each participant will be tested using rod- and cone-specific electrophysiological and psychophysical techniques. See below for details

3.6.3. How many participants will be recruited?

If there is more than one group, state how many participants will be recruited in each group. For international studies, say how many participants will be recruited in the UK and in total.

Three groups of observers are required as described above. The first group will be composed of 5 colour defective subjects (see overall experimental design, p7). The second group will be 20 young observers (18-40 years). The third group will be 20 older observers (50-70 years). All members of group one will be males, because colour abnormalities are x-linked and rarely seen in females. We will attempt to recruit equal numbers of males and females in groups 2 and 3.

3.6.4. How was the number of participants decided upon?

If a formal sample size calculation was used, indicate how this was done, giving sufficient information to justify and reproduce the calculation.

The psychophysical technique is totally novel. In general signal/noise ratios are less in this form of measurement compared with electrophysiology. The

a priori calculations are therefore based on the rod and cone count data only. As there is a very strong correlation ($r^2=0.99$) between the ERG amplitude and the donor eye study based on physiological data of Curcio (1990), we have used the Curcio data to calculate the numbers of participants required in groups 2 and 3. The mean rod count was 91.96M ($n=7$) $SD = \pm 14.75M$. Histologic data suggest there is said to be a loss of 30% of rods, but not cones, with age (Curcio et al 1993). The standard deviation of cone count is smaller than that for rods and, according to Curcio et al (1993), there is no age-related loss of cones. Hence, in order to establish any difference between old and young eyes for rods more observers will be required than for cones. So *a priori* statistics were performed on the rod count data only.

Formally the statistics were set out as follows assuming the above values:

H_0 : no difference in rod count between young and older observers. A priori Independent samples t-test (1 tailed) showed that in order to detect a difference with $\alpha = 0.05$ and with power of 0.85 we will need $n_1=19$ and $n_2 = 19$.

3.6.5. Describe the methods of analysis (statistical or other appropriate methods, e.g. for qualitative research) by which the data will be evaluated to meet the study objectives.

Histologic data indicate that there is a 30% loss of rods in older eyes. To test this observation *in vivo* we will perform two independent samples t-tests, comparing ERGs in older and young subjects in i) rod-specific ERGs and ii) cone-specific ERGs. A regression analysis to establish whether there is association between age and rod count, and age and cone count, based on the ERG data.

ERGs

- 1) Test h_0 : no difference in rod count between young and older observers. Post-hoc Independent samples T-test. $\alpha = 0.05$.
- 2) Test h_0 ; no difference in cone count between young and older observers. Post-hoc Independent samples T-test. $\alpha = 0.05$.
- 3) Test h_0 ; there is no association between rod-count and age. Regression analysis/Bland Altman plots
- 4) Test h_0 :there is no association between cone count and age. Regression analysis/Bland Altman plots

Flicker thresholds

- 1) Test h_0 : no difference in rod-specific flicker thresholds between young

and older observers. Post-hoc Independent samples T-test. $\alpha = 0.05$.
2) Test h_0 ; no difference in cone-specific flicker thresholds between young and older observers. Post-hoc Independent samples T-test. $\alpha = 0.05$.

Overall comparison of two methods:

Test h_0 : no correlation between rod specific ERGs and rod specific flicker thresholds

Test h_0 : no correlation between cone-specific ERGs and cone-specific flicker thresholds

3.7. Where will the research take place?

The research will take place in University of Manchester, Faculty of Life sciences (Moffat Building).

3.8. Names of other staff involved.

Athanasios Panorgias, 2nd year PhD student, Faculty of Life Sciences

Second PhD student (to be recruited).

3.9. What do you consider to be the main ethical issues which may arise with the proposed study and what steps will be taken to address these?

The proposed techniques (ERGs and psychophysics) are used routinely in ophthalmic clinics. There are therefore no particular ethical issues arising from the methodology. The technical and personal data will be held on secure, password protected computers, therefore there are no ethical issues concerning confidentiality. Though not strictly an ethical issue, the experimenters should be concerned about the possibility of fatigue, particularly in the older subjects. In previous studies involving older people this problem has been avoided by repeatedly offering tea breaks and careful observation of the participant for signs of discomfort. This strategy will be followed in the proposed project.

3.9.1. Will any intervention or procedure, which would normally be considered a part of routine care, be withheld from the research participants?

Yes No

If yes, give details and justification

4. Details of Subjects.

4.1. Total Number

We propose to recruit a total of 45 participants.

4.2 Sex and Age Range

Approximately equal numbers of males and females. Age range from 18yrs to ~70yrs

4.3 Type

40 colour normal participants aged 18 to 70.
5 dichromats

4.4. What are the principal inclusion criteria? *(Please justify)*

For the dichromats, the inclusion criteria will be; normal visual acuity. Nagel anomaloscope values which will clearly establish whether or not colour vision is normal and if not allow its categorisation. (Nagel Anomaloscope is a matching technique in which observers adjust a red-green mix to match a standard yellow light. It takes around 10 minutes).

For the colour normal observers, the inclusion criteria will be normal Visual Acuity no ophthalmological disease..

4.5. What are the principal exclusion criteria? *(Please justify)*

For the dichromats, the exclusion criteria will be any systemic pathology affecting the eyes and any ocular disease, reduced visual acuity .

The exclusion criteria for colour normals will be any ocular disease. Reduced visual acuity. Any systemic pathology which may affect the eyes, such as diabetes,. Abnormal colour vision according to the Nagel Anomaloscope. Intra-Ocular pressure greater than 20mmHg.

4.6. Will the participants be from any of the following groups? *(Tick as appropriate)*

- Children under 16
- Adults with learning difficulties
- Adults who are unconscious or very severely ill
- Adults who have a terminal illness
- Adults in emergency situations
- Adults with mental illness (particularly if detained under mental health legislation)
- Adults with dementia
- Prisoners
- Young offenders

- Adults in Scotland who are unable to consent for themselves
- Healthy volunteers
- Those who could be considered to have a particularly dependent relationship with the investigator, e.g. those in care homes, medical students.
- Other vulnerable groups

Justify their inclusion

4.7. Will any research participants be recruited who are involved in existing research or have recently been involved in any research prior to recruitment?

- Yes **No** Not known

If Yes, give details and justify their inclusion. If Not Known, what steps will you take to find out?

4.8 How will potential participants in the study be (i) identified, (ii) approached and (iii) recruited?

Where research participants will be recruited via advertisement, please append a copy to this application

The potential participants will be recruited via an advertisement at the university website, in the UoM magazine and in local newspapers (see attached document).

4.9 Will individual research participants receive *reimbursement of expenses* or any other *incentives* or *benefits* for taking part in this research?

- Yes** No

If yes, indicate how much and on what basis this has been decided

The participants will receive reimbursement of travel expenses up to £12.00 for each visit

5 Details of risks

5.1 Drugs and other substances to be administered

Indicate status, eg full product licence, CTC, CTX. Attach: evidence of status of any unlicensed product; and Martindales Pharmacopoeia details for licensed products

DRUG	STATUS	DOSAGE/FREQUENCY/ROUTE
------	--------	------------------------

1.0% tropicamide (mydriatic). 1 drop 20mins before the ERG recordings. Information sheet of the drug is attached.

5.2 Procedures to be undertaken

Details of any invasive procedures, and any samples or measurements to be taken. Include any questionnaires, psychological tests etc. What is the experience of those administering the procedures?

As stated above, placement of the electrodes is not an invasive procedure. All those involved in the attachment of the electrodes and in the administration of eye drops will be professionally qualified optometrists.

5.3 Or Activities to be undertaken

Please list the activities to be undertaken by participants and the likely duration of each

Details of all activities are outlined above and in the protocol

5.4 What are the potential adverse effects, risks or hazards for research participants, including potential for pain, discomfort, distress, inconvenience or changes to lifestyle for research participants?

Overall none. However the following should be taken in to account.

Fatigue levels of the participant, particularly the older observers

Mild discomfort associated with the electrodes, which is easily alleviated.

The Tropicamide drops sting most eyes for a maximum of 30 seconds following instillation .

Historically there have been concerns that mydriatics may induce an attack of acute glaucoma. It was thought that, as the pupil dilates it restricts the flow of aqueous humour in to the anterior angle (between back surface of cornea and front surface of iris). This has been extensively investigated in the last few decades (Pandit and Taylor, 2000) and the risk has been established as close to zero. See appendix for additional details.

Pandit R.J. and Taylor R, 2000. Mydriasis and glaucoma: exploring the myth. A systematic review. *Diabetic Medicine*, **17**, 693-699.

5.5 Will individual or group interviews/questionnaires discuss any topics or issues that might be sensitive, embarrassing or upsetting, or is it possible that criminal or other disclosures requiring action could take place during the study (e.g. during interviews/group discussions, or use of screening tests for drugs)?

Yes No

If yes, give details of procedures in place to deal with these issues:

5.6 What is the expected total duration of participation in the study for each participant?

The participants will attend the clinic twice. At the first visit, consent forms will be signed and the preliminary tests will be conducted, i.e Visual Acuity, eye examination, colour vision tests. At this visit the observer will perform the cone- and rod-specific flicker threshold measurement. . Previous experience suggests

a 15 minute tea/coffee break half way through the session, and constant offers of 'rest periods' are greatly appreciated by the participants. Accounting for breaks, the visit will last approximately two hours.

During the second visit the ERGs will be recorded. This will take approximately two hours, including preparation and breaks. We anticipate the two visits will occur within two to three weeks of each other

5.7 What is the potential benefit to research participants?

Participants will be given a thorough examination of their eyes including colour vision, free of charge. They are invariably interested in the healthiness of the eye and to take part in unusual forms of eye testing procedures.

5.8 What is the potential for adverse effects, risks or hazards, pain, discomfort, distress, or inconvenience to the researchers themselves? (If any)

None but see section 5.4 above

6. Safeguards

6.1 What precautions have been taken to minimise or mitigate the risks identified above?

As described above there is a very low risk of inducing an attack of acute closed angle glaucoma when dilating the pupil. To ensure this will not occur, we will measure the Intra-Ocular pressure of all our participants during the first visit. Intra-ocular pressure greater than 20mmHg will be excluded. The main issue with respect to the comfort of our subjects is fatigue. How we will minimise the effect of this is outlined above. Mainly they will be encouraged to take breaks during the measurements and will be given a tea/coffee break half way through the visit. Regarding discomfort associated with the electrodes, this can be minimised by using modern electrode paste and small, unobtrusive electrodes. We cannot mitigate against the stinging, experienced by some observers. This is of a short duration (maximum 30 seconds) and is readily tolerated by patients in ophthalmic clinics.

6.2 Will informed consent be obtained from the research participants?

Yes No

If Yes, give details of who will take consent and how it will be done. Give details of the experience in taking consent and of any particular steps to provide information (in addition to a written information sheet) e.g. videos, interactive material.

Consent will be taken by either Dr Murray or Mr Panorgias. Both have extensive experience of taking consent. Mr Panorgias is associated with a separate study approved by this committee (Colour in the peripheral visual field ref 08279)

If participants are to be recruited from any of the potentially vulnerable groups listed in Question 4.6, give details of extra steps taken to assure their protection. Describe any arrangements to be made for obtaining consent from a legal representative.

N/A

If consent is not to be obtained, please explain why not.

Consent will be obtained

Where relevant the committee must have a copy of the information sheet and consent form.

Information sheet and consent form are attached

6.3 Will a signed record of consent be obtained?

Yes No

If not, please explain why not.

6.4 How long will the participant have to decide whether to take part in the research?

The participant will be given at least two weeks to decide.

6.5 What arrangements have been made for participants who might not adequately understand verbal explanations or written information given in English, or who have special communication needs? (e.g. translation, use of interpreters etc.)

Unfortunately, the budget for this project does not allow us to provide translators.

6.6 What arrangements are in place to ensure participants receive any information that becomes available during the course of the research that may be relevant to their continued participation?

As subjects will be involved in the study for less than one month, it is unlikely that any information that becomes available will be relevant to their continued participation.

6.7 Will the research participants' General Practitioner be informed that they are taking part in the study?

Yes No

If No, explain why not

We do not envisage contacting the participants' GP because their health will not be affected by taking part in the study. However, if the initial eye examination

reveals any abnormality of which the participant was unaware then they will be referred in the usual way by the qualified optometrist

6.8 Will permission be sought from the research participants to inform their GP before this is done?

√Yes No

If No, explain why not

6.9 What arrangements have been made to provide indemnity and/or compensation in the event of a claim by, or on behalf of, participants for (a) *negligent* harm and (b) *non-negligent* harm?

It is anticipated that Manchester University will provide this indemnity

7. Data Protection and Confidentiality

7.1 Will the research involve any of the following activities at any stage (including identification of potential research participants)? (Tick as appropriate)

- Examination of medical records by those outside the NHS, or within the NHS by those who would not normally have access
- Electronic transfer by magnetic or optical media, e-mail or computer networks
- Sharing of data with other organisations
- Export of data outside the European Union
- Use of personal addresses, postcodes, faxes, e-mails or telephone numbers
- Publication of direct quotations from respondents
- Publication of data that might allow identification of individuals
- Use of audio/visual recording devices
- Storage of personal data on any of the following:
 - Manual files including X-rays
 - NHS computers
 - Home or other personal computers
 - √University computers**
 - Private company computers
 - Laptop computers

Further details:

7.2 What measures have been put in place to ensure confidentiality of personal data? Give details of whether any encryption or other anonymisation procedures have been used and at what stage?

Confidentiality of research records will be rigorously maintained. The data will be stored in a password protected PC, in MS Excel files using the subjects'

initials and the date. Subjects' name will not appear in files containing any data. After the completion of the study the data will be destroyed.

7.3 Where will the analysis of the data from the study take place and by whom will it be undertaken?

The analysis of the data from the study will take place at the University of Manchester and it will be undertaken by Athanasios Panorgias, Dr Ian Murray and the as yet not appointed PhD student under the supervision of the principal investigator Dr Ian Murray.

7.4 Who will have control of and act as the custodian for the data generated by the study?

The principal investigator Dr Ian Murray

7.5 Who will have access to the data generated by the study?

The principal investigator, Athanasios Panorgias and the PhD student.

7.6 For how long will data from the study be stored?

4 Years

Give details of where they will be stored, who will have access and the custodial arrangements for the data:

The data will be stored in password protected University computer, where only the principal investigator, Athanasios Panorgias and the PhD student will have access.

8. Reporting Arrangements

8.1 Please confirm that any adverse event will be reported to the Committee

We confirm that any adverse event will be reported to the committee

8.2. How is it intended the results of the study will be reported and disseminated?
(Tick as appropriate)

- Peer reviewed scientific journals**
- Internal report
- Conference presentation**
- Thesis/dissertation**
- Written feedback to research participants
- Presentation to participants or relevant community groups
- Other/none e.g. Cochrane Review, University Library

8.3 How will the results of research be made available to research participants and communities from which they are drawn?

From time to time we may provide small articles to the University News magazine and other lay publications.

8.4 Has this or a similar application been previously considered by a Research Ethics Committee in the UK, the European Union or the European Economic Area?

- Yes
 No

If Yes give details of each application considered, including:

Name of Research Ethics Committee or regulatory authority:
Decision and date taken

Research ethics committee reference number:

8.5 What arrangements are in place for monitoring and auditing the conduct of the research?

Will a data monitoring committee be convened?

- Yes
 No

What are the criteria for electively stopping the trial or other research prematurely?

There are no circumstances under which it will be necessary to end the research prematurely.

9. Funding and Sponsorship

9.1 Has external funding for the research been secured?

- Yes No

If Yes, give details of funding organisation(s) and amount secured and duration:

Organisation: British College of Optometrists

UK contact:
Therasa Murtagh. Theresa@bcoo.org.uk

Amount (£): 62,000

Duration: 36 Months

9.2 Has the external funder of the research agreed to act as sponsor as set out in the Research Governance Framework?

Yes No Not Applicable

9.3 Has the employer of the Chief Investigator agreed to act as sponsor of the research?

Yes No. PI employed by UoM

9.4 Sponsor *(must be completed in all cases where the sponsor is not the University)*

Name of organisation which will act as sponsor for the research:

10. Conflict of interest

10.1 Will individual researchers receive any personal payment over and above normal salary and reimbursement of expenses for undertaking this research?

Yes No

If Yes, indicate how much and on what basis this has been decided:

10.2 Will the host organisation or the researcher's department(s) or institution(s) receive any payment of benefits in excess of the costs of undertaking the research?

Yes No

If Yes, give details:

10.3 Does the Chief Investigator or any other investigator/collaborator have any direct personal involvement (e.g. financial, share-holding, personal relationship etc.) in the organisation sponsoring or funding the research that may give rise to a possible conflict of interest?

Yes No

If Yes, give details:

11. Signatures of applicant(s)

.....

.....

Signed

Date

.....
Signed

.....
Date

12 Signature by or on behalf of the Head of School

The Committee expects each School to have a pre-screening process for all applications for an ethical opinion on research projects. The purpose of this pre-screening is to ensure that projects are scientifically sound, have been assessed to see if they need ethics approval and, if so, go to the relevant ethics committee. It is **not** to undertake ethical review itself, which must be undertaken by a formal research ethics committee.

The form must therefore be counter-signed by or on behalf of the Head of School to signify that this pre-screening process has been undertaken

I approve the submission of this application

.....
Signed by or on behalf of the Head of School

.....
Date

Temporal characteristics of photoreceptor function in older eyes

Participant Information sheet

You are being invited to take part in a research study to investigate subtle vision changes with age. This study is part of Jeremiah MF Kelly's PhD research. Before you decide it is important for you to understand why the research is being done and what will be involved. Please take time to read the following information carefully and discuss it with others if you wish. Please ask if there is anything that is not clear or if you would like more information. Take time to decide whether or not you wish to take part. Thank you for reading this.

Who will conduct the research?

The research will be conducted by :

Insert PhD student HERE

Dr Ian Murray, Senior Lecturer. Faculty of Life Sciences, Moffat Building,
University of Manchester, M60 1QD, Manchester

Athanasios Panorgias, PhD student. Faculty of Life Sciences, Moffat Building,
University of Manchester, M60 1QD, Manchester

Title of the research.

Temporal characteristics of photoreceptor function in older eyes.

What is the aim of the research?

In the retina there are four types of cells responsible for vision. We plan to investigate whether the number of these cells changes with the age.

Why have I been chosen?

For the study 45 volunteers are required, all will have healthy eyes. The age range for the participants is 18-70 years old. Also, 5 observers with healthy eyes and congenital colour dysfunction will be recruited. If you fall in that age range and your eye are healthy you can take part in the study.

What would I be asked to do if I took part?

The health of your eye will be assessed by a qualified optometrist. A conventional test will be used to establish whether or not your colour vision is normal. During your first visit you will be asked to view some flickering lights and adjust the luminance to eliminate flicker. A series of different conditions will be tested. During your second visit we will first instil drops in your eye to dilate the pupil. Small electrodes will be placed near your eye. An electrode, composed of extremely fine fibre, just visible to the human eye, is placed in the lower canthus between the eye and the lower eyelid where 'foreign bodies' such as dust sometimes accumulate (when such a 'foreign body' is sufficiently large it induces a 'foreign body' reaction and discomfort is experienced). When fibre electrodes are correctly located, observers are entirely unaware of their presence and there is no 'foreign body' reaction. You will then watch a computer monitor, while a recording system will record the activity generated in your eye.

Are there any potential dangers, discomfort or inconvenience?

These techniques are used on a daily basis in all ophthalmic clinics. The following should be taken in to account. Fatigue levels, particularly at the older observers Mild discomfort associated with the electrodes, which is easily alleviated. The drops sting most eyes for a maximum of 30 seconds following instillation . Historically there have been concerns that mydriatics may induce an attack of acute glaucoma. It was thought that, as the pupil dilates it restricts the flow of aqueous humour in to the anterior angle (between back surface of cornea and front surface of iris). This has been extensively investigated in the last few decades and the risk has been established

as close to zero. There is slight inconvenience because you will not be able to drive until the pupil is back to its normal size after having the dilating drops, which takes around 2 hours. You also may need to wear sunglasses, if the weather is very sunny when you leave the building, because lights will appear bright. The drops have no long-term adverse effects on the eye.

In the highly unlikely event that you experience i) painful red eye, ii) misty vision, iii) sickness or nausea you should contact one of the research team immediately and look for advice at the card that will be handed to you at the end of the experiments.

What happens to the data collected?

Once the study is completed the data will be analysed to determine the difference in the number of light sensitive cells (photoreceptors) in the retina, between young and elderly observers.

How is confidentiality maintained?

The data will be stored in a password protected PC, in MS Excel files using the subjects' initials and the date. Subjects' name will not appear in files containing any data. After the completion of the study the data will be destroyed.

What happens if I do not want to take part or if I change my mind?

It is up to you to decide whether or not to take part. If you decide to take part you will be given this information sheet to keep and be asked to sign a consent form. If you decide to take part you are still free to withdraw at any time without giving a reason and without detriment to yourself.

Will I be paid for participating in the research?

Reasonable travelling or other expenses up to £12.00 will be available for each visit.

What is the duration of the research?

You will have as much time as you want to ask any questions and read this information sheet. Once you decide to participate you will sign a consent form. A series of tests to assess the health of your eyes and your colour vision will then be conducted. These tests will last about 15 minutes. After that you will perform the first experiment where you have to set the flicker threshold and this will last about 45mins. So, the total duration of the first visit will not be more than 2 hours including questions, discussion and breaks. The second visit, during which we will record the activity of your eye, will last approximately 2 hours including breaks. You are expected to attend the clinic twice for 2 hours each time.

Where will the research be conducted?

The research will be conducted at the University of Manchester, Faculty of Life Sciences, Moffat Building, M60 1QD, Manchester.

Will the outcomes of the research be published?

The outcomes of the research will be published in scientific peer reviewed journals and will be part of PhD student NAME insert HERE thesis.

Contact for further information.

If you have further questions concerning matters related to this research or you would like to know about the findings of this research, please contact:

PhD student contact details here.

Dr Ian J. Murray, Faculty of Life Sciences, Moffat Building, Room C , University of Manchester

e-mail: ian.j.murray@manchester.ac.uk tel: 01613063886

Athanasios Panorgias, PhD student, Faculty of Life Sciences, Moffat Building, Room A12, University of Manchester, Manchester.

e-mail: athanasios.panorgias@postgrad.manchester.ac.uk tel: 01613063878

What if something goes wrong?

In the event of you having any major concerns regarding this project, you are welcome to contact the supervisor Dr Ian Murray at any time.

If there are any issues regarding this research that you would prefer not to discuss with members of the research team, please contact the Research Practice and Governance Co-ordinator by either writing to 'The Research Practice and Governance Co-ordinator, Research Office, Christie Building, The University of Manchester, Oxford Road, Manchester M13 9PT', by emailing: Research-Governance@manchester.ac.uk, or by telephoning 0161 275 7583 or 275 8093

Committee on the ethics of research on human beings reference number:

CONSENT FORM FOR PARTICIPATING SUBJECT

Title: Temporal characteristics of photoreceptor function in older eyes

Principle investigators: Dr Ian J. Murray, Jeremiah MF Kelly, Athanasios Panorgias

If you are happy to participate please complete and sign the consent form below

- 1) I confirm that I have read and understand the information sheet for the above study and have had the opportunity to ask questions.

- 2) I understand that my participation is voluntary and that I am free to withdraw at any time without giving any reason.

- 3) I understand that this study is for the purpose of research and not for the treatment of any visual condition that I may have.

- 4) I have been informed that any information I provide will be confidential.

- 5) I agree to take part in the above study.

- 6) I agree my GP being informed for my participation in the study.

Name of participant

Signature

Date

Name of person taking consent

Signature

Date

Committee on the Ethics of Research on Human Beings reference No:

Proposed advertisement.

Volunteers required to take part in an aging eye study.

You are being invited to take part in a research study to investigate subtle vision changes with age. In our eyes there are photosensitive cells, called photoreceptors, responsible for the vision sensation. We want to know how the number of these cells is changing with the age and if there are any changes in visual sensitivity. You will be expected to attend the clinic twice. At the first visit, a thorough eye test will be performed by a qualified optometrist and your colour vision will be assessed. In the main experiment you will be asked to watch a flickering disk and adjust the luminance until you see no flicker. The duration of the whole procedure will be no longer than 2 hours, including the preliminary tests and breaks. At your second visit we will first instil drops in your eye to dilate the pupil. Small electrodes will be placed near your eye. You will then be asked to watch a computer monitor, while a recording system will record the activity generated in your eye.

The study is part of my PhD research, supervised by Dr Ian J. Murray.

Reasonable travelling or other expenses up to £12.00 will be offered to all participants for each visit.

For any questions and details please feel free to contact me.

Ethics committee number:

Jeremiah MF Kelly

Room 4.008

Carys Bannister Building

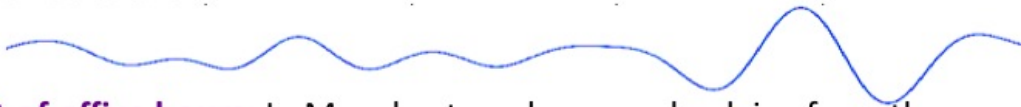
Dover Street

M13 9PL

Jeremiah.kelly@manchester.ac.uk

Call us during office hours on one of the following numbers

- 0161 3063886 (Dr Ian Murray, Principal Investigator)
- 0161 3063862
- 0161 3063878



Out of office hours: In Manchester, please seek advice from the Acute Referral Centre at the Royal Eye Hospital or the Emergency Eye clinic at the Royal Infirmary. Both facilities are on Oxford Road. If you are not within easy reach of central Manchester, please seek advice from your GP or nearest A&E Unit.

Information for the examining clinician: This card holder is a current or former volunteer taking part in a study conducted at the Faculty of Life Sciences at the University of Manchester (please see phone numbers above).

Figure J.4.1: Emergency Information card for subjects